frontiers | Research Topics

Gut microbiota modulation to mitigate stress-induced functional changes

Edited by
LinShu Liu, Aarti Gautam, Michael Stephen Goodson, Rasha Hammamieh, Camilla Mauzy, Adrienne Narrowe and Jason W. Soares

Published in
Frontiers in Microbiology
Frontiers in Microbiomes

FRONTIERS EBOOK COPYRIGHT STATEMENT

The copyright in the text of individual articles in this ebook is the property of their respective authors or their respective institutions or funders. The copyright in graphics and images within each article may be subject to copyright of other parties. In both cases this is subject to a license granted to Frontiers.

The compilation of articles constituting this ebook is the property of Frontiers.

Each article within this ebook, and the ebook itself, are published under the most recent version of the Creative Commons CC-BY licence. The version current at the date of publication of this ebook is CC-BY 4.0. If the CC-BY licence is updated, the licence granted by Frontiers is automatically updated to the new version.

When exercising any right under the CC-BY licence, Frontiers must be attributed as the original publisher of the article or ebook, as applicable.

Authors have the responsibility of ensuring that any graphics or other materials which are the property of others may be included in the CC-BY licence, but this should be checked before relying on the CC-BY licence to reproduce those materials. Any copyright notices relating to those materials must be complied with.

Copyright and source acknowledgement notices may not be removed and must be displayed in any copy, derivative work or partial copy which includes the elements in question.

All copyright, and all rights therein, are protected by national and international copyright laws. The above represents a summary only. For further information please read Frontiers' Conditions for Website Use and Copyright Statement, and the applicable CC-BY licence.

ISSN 1664-8714
ISBN 978-2-8325-7459-1
DOI 10.3389/978-2-8325-7459-1

Generative AI statement
Any alternative text (Alt text) provided alongside figures in the articles in this ebook has been generated by Frontiers with the support of artificial intelligence and reasonable efforts have been made to ensure accuracy, including review by the authors wherever possible. If you identify any issues, please contact us.

About Frontiers

Frontiers is more than just an open access publisher of scholarly articles: it is a pioneering approach to the world of academia, radically improving the way scholarly research is managed. The grand vision of Frontiers is a world where all people have an equal opportunity to seek, share and generate knowledge. Frontiers provides immediate and permanent online open access to all its publications, but this alone is not enough to realize our grand goals.

Frontiers journal series

The Frontiers journal series is a multi-tier and interdisciplinary set of open-access, online journals, promising a paradigm shift from the current review, selection and dissemination processes in academic publishing. All Frontiers journals are driven by researchers for researchers; therefore, they constitute a service to the scholarly community. At the same time, the *Frontiers journal series* operates on a revolutionary invention, the tiered publishing system, initially addressing specific communities of scholars, and gradually climbing up to broader public understanding, thus serving the interests of the lay society, too.

Dedication to quality

Each Frontiers article is a landmark of the highest quality, thanks to genuinely collaborative interactions between authors and review editors, who include some of the world's best academicians. Research must be certified by peers before entering a stream of knowledge that may eventually reach the public - and shape society; therefore, Frontiers only applies the most rigorous and unbiased reviews. Frontiers revolutionizes research publishing by freely delivering the most outstanding research, evaluated with no bias from both the academic and social point of view. By applying the most advanced information technologies, Frontiers is catapulting scholarly publishing into a new generation.

What are Frontiers Research Topics?

Frontiers Research Topics are very popular trademarks of the *Frontiers journals series*: they are collections of at least ten articles, all centered on a particular subject. With their unique mix of varied contributions from Original Research to Review Articles, Frontiers Research Topics unify the most influential researchers, the latest key findings and historical advances in a hot research area.

Find out more on how to host your own Frontiers Research Topic or contribute to one as an author by contacting the Frontiers editorial office: frontiersin.org/about/contact

Gut microbiota modulation to mitigate stress-induced functional changes

Topic editors

LinShu Liu — Eastern Regional Research Center, Agricultural Research Service (USDA), United States

Aarti Gautam — Walter Reed Army Institute of Research, United States

Michael Stephen Goodson — Air Force Research Laboratory, United States

Rasha Hammamieh — Walter Reed Army Institute of Research, United States

Camilla Mauzy — Air Force Research Laboratory, Wright-Patterson Air Force Base, United States

Adrienne Narrowe — Agricultural Research Service (USDA), United States

Jason W. Soares — Combat Capabilities Development Command United States Army, United States

Citation

Liu, L., Gautam, A., Goodson, M. S., Hammamieh, R., Mauzy, C., Narrowe, A., Soares, J. W., eds. (2026). *Gut microbiota modulation to mitigate stress-induced functional changes*. Lausanne: Frontiers Media SA. doi: 10.3389/978-2-8325-7459-1

Table of contents

frontiers | Frontiers in Microbiomes

TYPE Editorial
PUBLISHED 20 January 2026
DOI 10.3389/frmbi.2025.1731851

Check for updates

OPEN ACCESS

EDITED AND REVIEWED BY
Franck Carbonero,
Washington State University Health Sciences Spokane, United States

*CORRESPONDENCE
Ruoting Yang
ruoting.yang.civ@health.mil

RECEIVED 24 October 2025
REVISED 23 December 2025
ACCEPTED 29 December 2025
PUBLISHED 20 January 2026

CITATION
Yang R and Hammamieh R (2026) Editorial: Gut microbiota modulation to mitigate stress-induced functional changes.
Front. Microbiomes 4:1731851.
doi: 10.3389/frmbi.2025.1731851

COPYRIGHT
© 2026 Yang and Hammamieh. This is an open-access article distributed under the terms of the Creative Commons Attribution License (CC BY). The use, distribution or reproduction in other forums is permitted, provided the original author(s) and the copyright owner(s) are credited and that the original publication in this journal is cited, in accordance with accepted academic practice. No use, distribution or reproduction is permitted which does not comply with these terms.

Editorial: Gut microbiota modulation to mitigate stress-induced functional changes

Ruoting Yang* and Rasha Hammamieh

Walter Reed Army Institute of Research, Silver Spring, MD, United States

KEYWORDS

gut-brain axis, microbiome, modulation of microbiota, stress pathophysiology, stress therapeutic

Editorial on the Research Topic
Gut microbiota modulation to mitigate stress-induced functional changes

The gut-brain axis and stress

The gut-brain axis is a complex, bidirectional signaling network involving the central, autonomic, and enteric nervous systems, alongside endocrine, immune, and metabolic mediators. Its equilibrium is essential for health. Stress, defined as a state of threatened homeostasis, activates the hypothalamic-pituitary-adrenal (HPA) axis, leading to sustained elevations of glucocorticoids (e.g., cortisol) during chronic exposure. Environmental perturbations in endocrine signaling can also lead to microbial changes; for example, altered photoperiod reduces melatonin and reshapes the cecal microbiota and breast muscle inflammation in broilers [Yu et al.].

The gastrointestinal (GI) tract is a primary target of these stress hormones. Preclinical and clinical studies show that these hormones can significantly alter the composition and function of the gut microbiota, linking stress-induced physiological changes directly to conditions such as anxiety, depression, and irritable bowel syndrome (IBS). In this Research Topic, this theme is evident across models of exertional heat stroke [Xuan et al.], traumatic brain injury [Rusling et al.], and chronic stress-induced obesity with cognitive decline [Liu et al.].

Stress-induced dysbiosis and its consequences

HPA axis activation releases signaling molecules (e.g., CRF and glucocorticoids) that directly alter intestinal motility, secretion, and visceral sensitivity. These alterations modulate the growth conditions for commensal microbes, favoring certain taxa and leading to dysbiosis.

Perhaps the most critical consequence—and one of the most studied—is the impairment of intestinal barrier function. Reduced expression of tight junction proteins leads to increased intestinal permeability, or "leaky gut". This allows microbial components, notably lipopolysaccharides (LPS), to translocate from the gut lumen in the bloodstream. This triggers a pro-inflammatory cascade. Because these circulating

cytokines can cross the blood-brain barrier, they are directly implicated in promoting neuroinflammation, which in turn contributes to mood and cognitive disturbances.

The mechanistic roles of the microbiota

Gut microbes influence the brain and behavior through several interconnected pathways; however, it is worth asking which of these are truly significant. Much attention has been given to the production of neuroactive metabolites. For instance, certain Lactobacillus species can produce GABA, and some Clostridium species can stimulate serotonin (5-HT) synthesis. However, it is still a matter of intense debate whether this microbial GABA or 5-HT significantly impacts central neurotransmitter pools, rather than just acting locally in the gut.

A more robust pathway appears to be through short-chain fatty acids (SCFAs), especially butyrate, which is produced by the microbial fermentation of dietary fiber. Butyrate is fascinating because it functions as a histone deacetylase (HDAC) inhibitor. This is not just a biochemical curiosity; it means that butyrate can epigenetically modulate gene transcription in colonocytes and immune cells, thereby directly reducing inflammation. Butyrate also appears crucial for the integrity of both the intestinal and blood-brain barriers. Interest in SCFA-related pathways is also reflected in clinical meta-analyses of putative SCFA-producing taxa in spinal cord injury [Zhong et al.].

Additionally, the vagus nerve acts as a direct, non-hormonal communication highway. Microbial metabolites can stimulate its afferent pathways, sending signals straight to the brainstem. This pathway is compelling, but it is notoriously difficult to study in humans, leaving many questions about its relative importance unanswered.

Microbiota-targeted interventions

This flurry of mechanistic data has, understandably, led to a boom in "psychobiotic" interventions. Probiotics (live microorganisms) are the most direct example, and their reputation has often outpaced the empirical data. Nevertheless, specific strains of Lactobacillus (e.g., L. helveticus) and Bifidobacterium (e.g., B. longum) have shown promise in reducing psychological distress in some clinical trials. In line with this, probiotic supplementation has prevented stress-impaired spatial learning in rats and amplified the effects of environmental enrichment [Flynn et al.]. Beyond classical psychobiotics, several studies in this Research Topic evaluate nutritional and feed-based approaches that reshape microbial communities and host physiology in animal models [Jiang et al., Li et al., Yang et al.].

Prebiotics (e.g., FOS/GOS) offer a more subtle approach by feeding the beneficial bacteria we already have to enhance endogenous SCFA production. Of course, all these points go back to diet. Fiber-rich and fermented food diets support a diverse ecosystem, whereas the typical Western diet, which is processed and high in fat, appears to be almost designed to promote dysbiosis. Diet composition can modify stress responses itself; for example, omega-6 enrichment altered microbiome dynamics and physiological outcomes in rodent models of acute traumatic psychological stress and blast traumatic brain injury (TBI) [3].

Challenges and future directions

Despite these promising results, the field is struggling with significant hurdles. The high inter-individual variability in microbiota composition means that a "one-size-fits-all" probiotic is unlikely to be effective for everyone. Furthermore, trial outcomes are wildly inconsistent, and the mechanisms by which these probiotics work (or fail to work) are poorly understood. What the field desperately needs, in our view, is a move beyond simple correlational studies. We need longitudinal, multi-omics studies to establish causal links. Simply put, progress will depend on developing personalized approaches that tailor interventions to an individual's unique microbial and physiological profile. Contributions to this Research Topic also point toward stratification and controllability. For example, baseline gut microbiota features predicted chemotherapy-induced neutropenia duration in leukemia patients [Huang et al.], while conceptual and experimental work argues for host-controllable healthy microbiomes and tractable, multi-strain model systems for testing mechanisms [Bouchez et al., Maloney et al.].

Conclusion

In conclusion, the gut microbiota is unequivocally a key regulator of the host stress response. Its disruption is a direct contributor to the physiological and psychological sequelae of chronic stress. Modulating the microbiota is therefore a compelling therapeutic strategy. While significant challenges in personalization remain, continued investigation into these mechanisms holds immense potential for novel therapeutics for stress-related disorders.

Author contributions

RY: Writing – original draft. RH: Writing – original draft, Writing – review & editing.

Conflict of interest

The author(s) declared that this work was conducted in the absence of any commercial or financial relationships that could be construed as a potential conflict of interest.

Generative AI statement

The author(s) declared that generative AI was used in the creation of this manuscript. Gemini 2.5 was used to assist with grammatical corrections and stylistic enhancements. All technical content and conclusions remain the original work of the author(s) and were manually verified for accuracy.

Any alternative text (alt text) provided alongside figures in this article has been generated by Frontiers with the support of artificial intelligence and reasonable efforts have been made to ensure accuracy, including review by the authors wherever possible. If you identify any issues, please contact us.

Publisher's note

All claims expressed in this article are solely those of the authors and do not necessarily represent those of their affiliated organizations, or those of the publisher, the editors and the reviewers. Any product that may be evaluated in this article, or claim that may be made by its manufacturer, is not guaranteed or endorsed by the publisher.

frontiers | Frontiers in Microbiomes

TYPE Original Research
PUBLISHED 11 September 2024
DOI 10.3389/frmbi.2024.1430340

Check for updates

OPEN ACCESS

EDITED BY
David C. B. Taras,
Boehringer Ingelheim, Germany

REVIEWED BY
Firas H. Kobeissy,
Morehouse School of Medicine, United States
Jessica Weaver,
University of California, San Diego, United States
Robin Michelle Voigt,
Rush University, United States

*CORRESPONDENCE
Aarti Gautam
aarti.gautam.civ@health.mil

RECEIVED 09 May 2024
ACCEPTED 26 July 2024
PUBLISHED 11 September 2024

CITATION
Rusling MR, DeMar JC, Chakraborty N, Hoke AV, Miller SA, Rosenberger JG, Batuure AB, Wilder DM, Sajja VS, Long JB, Hammamieh R and Gautam A (2024) The effect of dietary omega-6 fatty acid enrichment in rodent models of military-relevant acute traumatic psychological stress and traumatic brain injury.
Front. Microbiomes 3:1430340.
doi: 10.3389/frmbi.2024.1430340

COPYRIGHT
© 2024 Rusling, DeMar, Chakraborty, Hoke, Miller, Rosenberger, Batuure, Wilder, Sajja, Long, Hammamieh and Gautam. This is an open-access article distributed under the terms of the Creative Commons Attribution License (CC BY). The use, distribution or reproduction in other forums is permitted, provided the original author(s) and the copyright owner(s) are credited and that the original publication in this journal is cited, in accordance with accepted academic practice. No use, distribution or reproduction is permitted which does not comply with these terms.

The effect of dietary omega-6 fatty acid enrichment in rodent models of military-relevant acute traumatic psychological stress and traumatic brain injury

Matthew R. Rusling[1], James C. DeMar[1], Nabarun Chakraborty[1], Allison V. Hoke[1], Stacy Ann Miller[1], John G. Rosenberger[2], Andrew B. Batuure[2], Donna M. Wilder[2], Venkatasivasai Sujith Sajja[2], Joseph B. Long[2], Rasha Hammamieh[1] and Aarti Gautam[1]*

[1]Medical Readiness Systems Biology Branch, Center for Military Psychiatry and Neuroscience, Walter Reed Army Institute of Research (WRAIR), Silver Spring, MD, United States, [2]Blast-Induced Neurotrauma Branch, Center for Military Psychiatry and Neuroscience, Walter Reed Army Institute of Research (WRAIR), Silver Spring, MD, United States

Introduction: Sequelae from traumatic brain injuries (TBIs) and post-traumatic stress disorder (PTSD) are major career-limiting factors for combat soldiers. Overlap between TBI and PTSD symptoms alongside other common comorbidities complicate the diagnosis and treatment. Systems-level and high-throughput approaches are key in understanding the underlying biomolecular mechanisms and differentiating these conditions.

Methods: The present study identifies dietary factors and proposes mechanisms behind psychological stress and TBI, using established preclinical animal models and a multi-omics approach. Here, we used microbiome characterizations of rats exposed to simulations of blast-induced TBI and underwater trauma (UWT)-induced psychological stress. We further studied the effect of dietary omega-6 versus omega-3 polyunsaturated fatty acid (n-6, n-3 PUFA) enrichment on the insult responses. The use of excess n-6 PUFA was chosen due to its high prevalence in the Western diet and pro-inflammatory nature. Prior to TBI or UWT, animals were maintained for 6 weeks and continued thereafter on either a standard diet or two customized chows imbalanced and diminished in omega-3 content. Corresponding shams were carried out for all groups. Fecal bacterial microbiome populations were assessed using 16S rRNA gene sequencing.

Results: Physiologic outcome modeling identified that dietary status affected post-TBI lactate dehydrogenase (LDH) and triglyceride levels, with n-3 PUFA having a large attenuating influence. The UWT model showed similar trends, with diet significantly altering LDH, terminal corticosterone (14 days post-exposure), and a fear behavior susceptibility. Fecal microbiome alpha diversity was significantly reduced by high levels of n-3 PUFA. Likewise, beta diversity of the microbiome was significantly affected by both diet and time but not exposure to TBI or UWT. Compositionally, temporal effects on the microbiome were more likely to be observed with the diets. The most affected features fell within the

Proteobacteria phyla, in which n-3 PUFA enrichment significantly reduced *Alphaproteobacteria* in the TBI model and increased *Gammaproteobacteria* in the UWT group.

Discussion: All these observations can influence the vulnerability or resilience of the warfighter to blast-induced TBI and acute psychological stress. The microbiome mechanisms facilitate and provide a knowledge-driven unbiased panel of signatures to discriminate between the two insults and is an essential tool for designing precise care management.

KEYWORDS

omega-3, omega-6, microbiome, traumatic brain injury, post-traumatic stress disorder, linoleic acid, alpha-linolenic acid, rat

1 Introduction

During Operations Iraqi Freedom and Enduring Freedom, there were significant increases in hospitalizations among service members due to traumatic brain injury (TBI) as well as mental disorders such as post-traumatic stress disorder (PTSD) and major depressive disorder (Staff, 2018). Many of these disorders coexist (Bryant, 2011; Weckle, 2013) because brain injuries are frequently sustained during psychologically traumatic situations, especially those faced in combat operations. There is an overlap between symptoms accompanying each condition, and the range of other comorbid problems that commonly coexist in the two conditions further complicates the diagnosis. Discrimination between psychological stress and TBI using a knowledge-driven unbiased panel of biomarker signatures would be extremely valuable in designing precise health care managements.

TBI involves damage to the brain from an external force, e.g., skull impact concussions, and the severity of TBI is typically described in terms of mild, moderate, or severe. the major source of closed-head TBI to soldiers in combat operations is blast exposure from bomb explosions, which results from three basic types of strikes to the skull and propagation of the kinetic energy forces to the brain: primary from overpressure waves, e.g., rapid air expansion; secondary from projectiles, e.g., thrown rocks; and tertiary from body displacement, e.g., falls against hard objects. These events mainly cause diffusive axonal shearing and compressive contusions to the brain's neuronal cell layers, with accompanying tearing of blood vessels and subsequent triggering of deep neuroinflammation processes, e.g., macrophage infiltration as well as microglial and astrocyte overactivation (e.g., cytokine release). The extreme size and proximity of many bomb explosions leads to most victims experiencing all three types of blast-related insults to the head, often despite wearing protective body armor (e.g., goggles and helmet). Thus, we have chosen to combine the first two exposures (i.e., primary and secondary) in our animal model as they are the easiest to stepwise simulate and are highly relevant. Likewise, we have found that the combined insult readily produces an enhanced TBI compared with blast wave or projectile strike (weight drop) alone exposure, having marked pathophysiological and behavioral changes that can manifest both in the acute and chronic phase (Arun et al, 2024). This TBI model, however, can be easily adjusted (i.e., via attenuating the blast wave pressure and weight drop height) within a range of mild to moderate severity that has low mortality and allows for potential full neurological recovery when studying the efficacy of nutritional interventions and drug therapeutics.

Delayed onset of many of the symptoms along with overlap with those of other disorders can lead to diagnosis issues for those affected by TBI (Bramlett and Dietrich, 2015). Thus, clinical and preclinical studies are crucial for assessing the extent of behavioral and molecular changes associated with the diseases to advance studies in this field. Our current study focused on the use of standardized rodent models mimicking human disease state(s) to advance studies in this field. The TBI resulting from simulated blast exposures in these animals is currently being used to mimic blast-related injuries sustained in field-like conditions by soldiers (Rama et al., 2018; Sajja et al., 2018). Blast TBI is the leading cause of combat casualties in which the primary blast overpressure (BOP) waves generated by high intensity explosives lead to diffuse axonal brain injury (Yarnell et al., 2013; Zhou et al., 2018; Bryden et al., 2019). The overpressure energy produced causes concussive damage (e.g., propagated shear forces) to the brain and associated structures within the cranium.

On the other hand, the animal model known as underwater trauma (UWT) exposure is a brief but significant psychological stressor (Richter-Levin, 1998) that produces an acute stress reaction (ASR) and may develop into an acute stress disorder (ASD) or PTSD-like condition if not alleviated or especially repeated. UWT, as predominantly applied when using rats, causes acute and lasting consequences of "anxiety-like" behaviors (e.g., restlessness and weight loss) (Ardi et al., 2014; Ritov and Richter-Levin, 2014). In humans, if symptoms of an ASR or ASD persist for longer than 1

month, individuals can develop PTSD, which presents with an anxiety component characterized by re-experiencing similar sensory input, leading to avoidance and hypervigilance behaviors.

In the second part of our studies, we focused on a nutrition-based approach as a countermeasure for prevention of TBI and PTSD-related debilitations in warfighters. We understand that any trauma to the brain initiates a complex cascade of internal events that can lead to vascular damage, ischemia, excitotoxicity, inflammation, and neuronal cell loss (Lu et al., 2019). Dietary n-3 polyunsaturated fatty acids (PUFAs) are crucial building blocks of neuronal membranes and can be converted to potent anti-inflammatory metabolites (Bazan et al., 2011; Mayurasakorn et al., 2011; Dyall and Michael-Titus, 2008). Nutritional deficiency of n-3 PUFA has been identified as a risk factor for neurocognitive performance and neuropsychiatric disorders. The n-6 and n-3 PUFAs strongly compete in shared biochemical pathways, as based upon their respective ratios and levels in the diet (Lands et al., 1992; Blasbalg et al., 2011).

Previous work suggests that the n−3 polyunsaturated fatty acids α-linolenic acid (ALA), eicosapentaenoic acid (EPA), docosapentaenoic acid (DPA), and docosahexaenoic acid (DHA) are relatively deficient in the present-day Western diet (e.g., from a lack of seafood consumption), including that of the USA, and is instead very high in n-6 PUFAs (e.g., from overconsumption of seed oils and red meat) such as linoleic acid (LA), i.e., 10–30:1 (Blasbalg et al., 2011). This imbalance can lead to adverse consequences as n-3 PUFAs have potent anti-inflammatory, inflammation resolving, and neuroprotective properties, whereas n-6 PUFAs (e.g., arachidonic acid) primarily stimulate inflammation responses. Diet-induced changes in PUFA composition can also modify neuronal cell membrane fluidity and signal transduction (Calder, 2011), and DHA, with the highest degree of polyunsaturation, plays a central role in influencing these neuronal states. All these mechanisms can influence the relative vulnerability or resilience to TBI and traumatic stress. Such diet-derived susceptibilities should be readily and safely correctible through dietary supplements (e.g., ocean fish oil); therefore, the results of this research are highly translatable. Here, we explored the possibility of whether feeding adult rats a n-3 and n-6 PUFA-enriched diet increases their vulnerability to TBI and traumatic stress, in part by influencing the composition of the gut bacterial microbiome.

Additionally, physical and psychological insults to the brain, i.e., TBI and PTSD, can cause the release of HPA-axis-driven stress hormones (e.g., glucocorticoids) that circulate in the bloodstream and then trigger changes to the architecture and function of gut tissues. This in turn leads to loss of the intestinal lumen-epithelium barrier and dysbiosis and leakage of the gut microbiota, which sets off a cascade of immune cell processes (George et al., 2021). Not only does this promote exposure of the brain to elevated circulating inflammation factors (e.g., cytokines) but it also deprives it of important metabolites facilitated by normal gut microbial activity, i.e., nutrient (e.g., short chain fatty acids: acetate, propionate, and butyrate) and neurotransmitter (e.g., dopamine and serotonin) production. Dietary n-3 PUFAs can increase intestinal lumen integrity and likewise decrease gut inflammation (Durkin et al., 2021). Thus, we sought to further identify the intersection as well as unique molecular patterns associated between these two brain insults, with an emphasis on the influence of PUFA nutrition and the gut microbiome.

2 Methods

All animal experiments were conducted in accordance with the Animal Welfare Act and other federal statutes and regulations relating to animals and experiments involving animals, and adhered to principles stated in the Guide for the Care and Use of Laboratory Animals (NRC Publication 2011 edition), as performed under an Institutional Animal Care and Use Committee (IACUC)-approved protocol in an AAALAC International accredited facility with a Public Health Services Animal Welfare Assurance. Young adult male 8–9 week-old Sprague Dawley rats that weighed 270–290 g (Charles River Laboratories, Wilmington, MA, USA) were housed at 20–22°C (12 h light/dark cycle) with free access to food and water *ad libitum*.

2.1 Subjects and diets

In our study, 72 rats were equally divided into two intervention arms (TBI arm: n = 18 sham, n = 18 TBI exposure. UWT arm: n = 18 sham, n = 18 forced underwater submersion). Groups were equally assigned to one of three diets, with six rats per diet exposure group. Two experimental diets consisted of isocaloric rodent chows, i.e., containing 1% or 8% of energy (en%) as derived from linoleic acid (n-6 PUFA); 1 en% as α-linolenic acid (n-3 PUFA); and no other n-3 PUFAs, which have been used by others to produce in rodents a tissue deficiency of DHA and related physiological disturbances, including brain function (Alvheim et al., 2012). These diets were custom made for the study and followed the National Institutes of Health guidelines for the general nutritional requirements of rodents by using an AIN-93G formulation starting base (modified formula #s: 181161 and 181162, Dytes Inc., Bethlehem, PA, USA). The total protein, carbohydrate, and fat content of both diets is stated by the manufacturer as 18, 46, and 35 en%, respectively. Thus, they are characterized as medium fat diets. A separate group of rats were given a standard animal-facility provided diet (house chow), which is well-balanced in all PUFAs, including EPA and DHA as 0.5 en% combined (Prolab RHM 3000, LabDiet, Purina/PMI Nutrition International, Richmond, IN, USA). The total protein, carbohydrate, and fat content of this diet is stated as 25, 49, and 15 en%, respectively, with 4 and 0.5 en% coming from linoleic and α-linolenic acid, respectively. Thus, the house chow is higher in protein and lower in fat, especially n-6 PUFAs, compared with the other two diets. We confirmed manufacturer-reported fatty acid compositions of the three diets as being accurate within 10% for random food samples (n = 4 each; data not shown), using total lipid extraction, methyl ester derivative, and gas chromatography methods (DeMar et al., 2008). Likewise, preliminary experiments on sham animals verified that moderately prolonged feeding (1–2 months) of the two n-3 PUFA-deficient diets versus house chow (n = 6 each) leads to significant imbalances of n-6 to n-3 PUFA and/

or decreases in DHA content (approximately two-fold; $p < 0.05$) in their livers, a primary organ for the storage of PUFA reserves; however, as reported by others (DeMar et al., 2004), this was protected against within the brains by DHA conservation mechanisms (data not shown).

To create military-relevant pathological changes in the brain that can in turn impact gut integrity, the animals are then exposed to high-fidelity simulated blast waves plus a weight drop-induced concussion (Marmarou et al., 1994; Sajja et al., 2018), i.e., a traumatic brain injury (TBI), or an underwater trauma (UWT) psychological stressor (Richter-Levin, 1998; Moore et al., 2012), to be described below in the methods section. Both TBI- and UWT-exposed animals were fed one of the three different diets for 6 weeks prior to insult and continued thereafter: standard house chow (HC) and chows enriched with 1 or 8% of calories/energy as linoleic acid (1 or 8 en% LA diet). The experimental plan is shown as Figure 1.

2.2 Diet and intervention validation

To broadly validate the effects of diet and exposure on the models, collected tissues were quick-frozen fresh and reserved for future studies on related changes in gene expression, abundances, and activities of proteins (i.e., transcriptomics, proteomics, and metabolomics), as for within the brain, retina, and plasma. This was carried out to identify novel biomarkers of TBI and acute psychological stress, especially under an exacerbating nutritional deficiency of omega-3 fatty acids. In the beginning stages of the planning of this current study, when we were testing the efficiency of the three diets to produce changes in the brain, we subjected the brains of four animals on each diet that were exposed to blast-TBI, along with age-matched shams, to coronal sectioning and colloidal silver staining to detect axonal degeneration by bright field light microscopy.

2.3 Exposures

2.3.1 Primary and secondary blast model

A closed head TBI model consisting of blast overpressure (BOP) wave exposure (primary blast injury) coupled with a weight drop concussion (Marmarou method) (secondary blast injury) was used on a group of adult male rats (n=8 each diet). Isoflurane inhalation (2–3%) anesthetized animals were subjected once to BOP (18 psi) inside an Advanced Blast Simulator (ABS) that generates a shock wave following the rapid rupture of a canvas membrane by compressed air. This was immediately followed by dropping a 500 g metal weight from 125 cm above onto a stainless-steel disc affixed to the rat's skull midway between the lambda and bregma, whereas equivalent diet groups of shams (SH; n=8 each) received handling and anesthesia alone.

2.3.2 Underwater trauma

In parallel, a group of rats were subjected to an UWT stressor model (Richter–Levin method) that consisted of 30 s of swimming and habituation in a 20-gallon tank half-filled with room temperature 0.1% (w/v) saline to help prevent lung inflammation

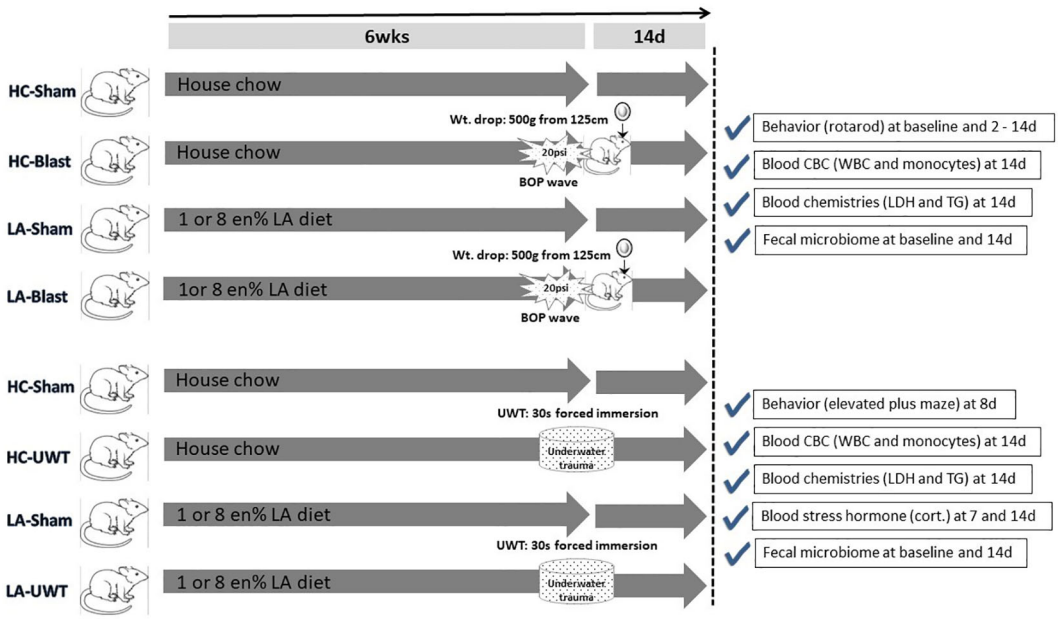

FIGURE 1
Experimental timeline showing the entire study design. In brief, rats were raised for 6 weeks on one of three diets: house chow, enriched with 1 energy (en)% as linoleic acid (LA), or enriched with 8 en% LA. The latter two diets are thus elevated in n-6 PUFA content (i.e., LA) but contain no long chain n-3 PUFAs, e.g., EPA or DHA. The animals were then exposed to blast-plus-weight-drop-induced TBI (top four arrows) or UWT-induced acute stress (bottom four arrows), along with their respective shams. At baseline and out to 14 d post-insult, the animals were behavior tested and subjected to blood and fecal microbiome assessments, which are further described within the accompanying check marked boxes.

from any aspiration, followed by 30 s of forced whole-body immersion using a perforated plunger. This triggers in the animals the extreme fear response associated with the sensation of near drowning. Shams (SH) received 1 min of free swimming.

2.3.3 Brain histopathology by silver and senescence detector staining

At 14 days following TBI or UWT exposure, animals were deeply anesthetized by 5% isoflurane inhalation for 6 min, and then they were gravity line perfused transcardially with physiological saline to cause blood exsanguination, followed by phosphate-buffered 4% paraformaldehyde saturated with picric acid to fix the tissues. Prior to saline perfusion, blood was taken by cardiac puncture via a syringe and placed in chilled EDTA and heparin vacuum collection tubes. Some blood was centrifuged at 3,000 × g for 10 min to obtain the plasma fraction. Whole blood and plasma were then used for blood work assessments, as to be described. Brains were removed and post-fixed by immersion for up to 6 h in phosphate-buffered 4% paraformaldehyde, and then were switched overnight to buffered 20% sucrose solution followed by one change to fresh sucrose, for cryopreservation purposes. Fixed brains were sectioned, stained, and mounted on microscope slides by submission to FD Neurotechnologies, Inc. (Ellicott City, MD, USA). Brains were cut into serial coronal sections (30–50 μm) at 11 evenly spaced positions (bregma 1.0 mm to −8.3 mm), and mounted in triplicate. These sections cover the entire regions of the cortex, hippocampus, optic tracts, amygdala, thalamus, hypothalamus, mid-brain, and cerebellum. Silver staining, which is highly reactive toward exposed cellular proteins, was performed on the sections derived from the TBI-exposed animals to reveal, as a brown to black color, the presence of any degenerating axonal fiber tracts of the neurons (DeMar et al., 2016). Likewise, floating brain sections from the UWT-exposed animals were provided to us and then slide mounted and stained to reveal as a blue coloration the presence of any prematurely aged neurons, using a senescence detection kit (BioVision, Mipitas, CA, USA) according to the manufacturer's instructions (Arun et al., 2020). Senescence detector staining is highly reactive toward aging neurons, which overexpress the enzyme β-galactosidase, but not to presenescent, quiescent, or immortal cells. For all prepared slides, mosaic (12 × 14) pictures of the different brain regions of interest were taken using an Olympus BX61 microscope (Olympus Corporation, Center Valley, PA, USA) and the Stereo Investigator virtual image tool (MBF Biosciences, Williston, VT, USA). The intensity of the silver or sequence staining in the captured images was quantified using densitometry (lumens/mm2), as assessed by Image-Pro Premier software (Media Cybernetics Inc., Rockville, MD, USA). For the densitometry measurements, those cells that stained intensely were included and those cells that showed <50% of maximum staining intensity were excluded. A total of four shams and four TBI or four UWT-exposed animals were evaluated for each diet, i.e., house chow, 1 en% LA, and 8 en% LA; however, three, two, and three animals, respectively, were used for the corresponding shams of the TBI-exposed group and their values combined as expected neutral controls for background signal determination. Group comparisons of the averaged staining densities were carried out for sham versus TBI- or UWT-exposed animals using a Kruskal–Wallis one way analysis with a *post-hoc* Dunn's test, and between the diets alone using ANOVA.

2.4 Behavioral, blood, and microbiome assessments

2.4.1 Rotarod

Rats were pretrained for 2 days on a rotarod device (Rotamex-5; Columbus Instruments, Columbus, OH, USA), on which they had to walk on a rotating spindle set at 10 rpm for 45 s. Animals were then tested at 5–35 rpm over 60 s at baseline and then at 2–14 days post-TBI. Latency to fall is reported. This tests for brain impairments (e.g., motor cortex) in balance and coordination.

2.4.2 Elevated plus maze

Animals were placed in the center of an elevated plus maze (EPM) device (Model #: LE840, Harvard Apparatus/Panlab, Holliston, MA, USA) consisting of a raised platform with double intersecting open and closed arms (i.e., risky and safe) and allowed to freely explore it for 5 min, at 8 days post-UWT. The time spent on the arms is reported. This tests for brain (e.g., amygdala) impairments in composure (fear-control) and exploration.

2.4.3 Blood markers

At 7 and 14 days following UWT exposure only, animals were lightly anesthetized through the brief inhalation of 2–3% isoflurane; a blood sample (approximately 200 μl) was collected by lateral tail vein draw, using a 1cc syringe and 27G butterfly needle catheter, and then placed in ice-chilled microfuge tubes containing sodium heparin as an anticoagulant. The blood was immediately centrifuged to obtain the plasma, which was stored at −80°C. Animals were allowed to recover from anesthesia in their home cages. Alternatively, at 14 days post-TBI and -UWT, animals were deeply anesthetized through the prolonged inhalation of 4–5% isoflurane and then euthanized by terminal blood exsanguination followed by decapitation. Exsanguination was carried out by heart puncture with a 10cc syringe and 18G needle, after surgically opening the thorax. Whole-blood draws (approximately 3 ml) were placed inside tubes (Vacutainer, Becton Dickinson, Franklin Lakes, NJ, USA) containing anticoagulant, i.e., di-potassium (K2) EDTA or sodium heparin, that were then gently hand-mixed and kept chilled on ice.

Corticosterone levels (Cort; ng/ml) of plasma samples from tail vein blood taken at 7- and 14-days post-UWT were determined within the investigator's lab (i.e., BINT Branch) using a species-specific multiplex immunoassay array (MILLIPLEX MAP Rat Stress Hormone Magnetic Bead Panel, Millipore Sigma, Burlington, MA, USA). After loading the samples and then developing the assay, the arrays were read on a multiplexing imaging platform (Luminex MAGPIX–xPONENT®; Bio-

Techne/R&D Systems, Minneapolis, MN, USA), which calculates the results from a standard curve. In brief, the instrument scans for the specific binding of tagged (e.g., fluorescent nano-bead) antibodies to register and quantify the corticosterone.

Terminal whole-blood samples taken at 14 days post-TBI and -UWT were submitted on the same day to the WRAIR Clinical Pathology Department for a chemistry panel and complete blood count assessment, with processing undertaken within 24 h post-collection. Chemistries (heparin-treated samples) for lactate dehydrogenase (LDH; U/L) and triglyceride (TG; mg/dl) levels were performed on plasma, as isolated by blood centrifugation, using a clinical chemistry analzyer (VITROS 350 System; Ortho-Clinical Diagnostics/Quidel Ortho, San Diego, CA, USA). In brief, the instrument uses colorimetric reactions to quantify the two analytes. Likewise, complete blood counts (ETDA-treated samples) for levels (density per μl) of total white blood cells (WBC) and monocyte fraction were performed on whole blood, using a clinical hematology analyzer (XT-2000iV; Sysmex America, Lincolnshire, IL, USA). In brief, the instrument uses fluorescent dye-based flow cytometry to identify and count the immune cell populations.

2.4.4 Fecal microbiome

Fecal pellets were collected directly from the animals in the morning 1–2 days before and 14 days after blast plus weight drop or underwater trauma exposure, by holding the subject over a new absorbent under pad until a fresh stool sample (1–2 droppings) was deposited on it, which was immediately transferred with tweezers to a cryotube and then quick frozen on dry ice and stored at −80°C. Massaging of the animals was used to promote defecation. A fresh area of the under pad was used each time and the tweezers were cleaned with isopropyl alcohol wipes between animals. Microbial DNA was isolated from the fecal pellets using a bacterial nucleic acid extraction kit (QIAamp PowerFecal Pro DNA, Qiagen, Germantown, MD, USA). The quality and quantity of the prepared DNA was checked by UV spectrometry (NanoDrop 8000, Thermo Fisher Scientific), dye fluorometry (Qubit 4, Invitrogen/Thermo Fisher Scientific), and capillary gel-electrophoresis (2200 TapeStation, Agilent Technologies, Santa Clara, CA, USA). The DNA was fragmented and then analyzed on a metagenomic sequencing machine (MiSeq, Illumina, San Diego, CA, USA) using primers for the V3 and V4 regions of the prokaryote-ubiquitous 16S rRNA gene, which are variable according to the bacterial type and absent in the mammalian host cells, for amplification (Karl et al., 2023). In brief, amplified DNA was sequenced, producing 300 bp paired-end reads in a single run. Pairs were merged with q2-vsearch, were quality checked, had chimeras removed, and were de-multiplexed using q2-demux and DADA2 (Callahan et al., 2016), using QIIME2 v.2020.82 (Bolyen et al., 2019). Amplicon sequence variants (ASV) were aligned with MAFFT (Katoh and Standley, 2013) via q2-alignment and used to construct a phylogeny with FastTree2 via q2-phylogeny (Price et al., 2010). To assign taxonomy, a naïve Bayes Classifier was trained on the 16S rRNA V3–V4 region with the specific primers and the Greengenes v13.8 (McDonald et al., 2012) 99% operational taxonomic unit database of reference sequences using the q2-feature-classifier via Classify-Sklearn.

2.5 Data analysis

2.5.1 Physiologic outcomes

Outcome measures were sampled after either sham or experimental exposure. Outcomes were analyzed within each experiment using linear modeling of continuous diet compositions testing $Outcome \sim [ALA] + [LA] + Condition$. Tables were formatted with *stargazer* (Hlavac, 2022). Categorical comparisons using t-tests were made within diets comparing sham vs. treatment, and between diets comparing treatment-exposed models. Power analysis was performed for each significant outcome using Cohen's D to quantify effect size with alpha = 0.05, n = 36 using *pwr* (Champely, 2020), and *effsize* packages in R (Torchiano, 2020).

2.5.2 Preparation

The 16S OTU tables were prepared in QIIME. Relative abundance tables were exported into R for downstream analysis. Features observed in fewer than half of the samples were removed, and data were not interpreted below the family level as OTUs at this classification level could not be further classified. Relative abundance data are available in Appendix A.

2.5.3 Alpha diversity

Alpha diversity is defined as reflecting the number or relative abundances of bacteria taxa within the averaged samples. Shannon-, Chao1-, and Simpson-based alpha diversities were calculated using QIIME and exported into R for analysis and visualization. The effects of diet were evaluated using linear modeling of $diversity\ metric \sim [ALA] + [LA] + Time + Treatment\ exposed$ to characterize the continuous effects of dietary components on outcome. Diet group differences were compared within and across diets using a t-test and ANOVA. Within diets, alpha diversity was compared before and after exposure. Across diets, treatment (not sham)-exposed models were compared against other diet alpha diversity.

2.5.4 Beta diversity

Beta diversity is defined as reflecting the variability in identities of bacteria taxa among the individual samples. Beta diversity was calculated in R using the *vegan* package (Oksanen et al., 2022). Distance matrices were produced from relative abundance tables at the family level. Bray distances were calculated using relative abundance and Jaccard distances were calculated using a binary-transformed dataset. All beta diversity comparisons were performed using an ADONIS test, which under brain insult conditions (TBI vs. UWT) showed a significant distance between experiments; therefore, each experiment was independently analyzed. Within experiment analysis was performed by testing $Distance \sim [ALA] + [LA] + Time + Treatment\ exposed$ with both Jaccard and Bray distances.

2.5.5 Composition

Effects of experimental treatments on fecal microbiome composition were evaluated across the measured taxonomic levels

using linear modeling of *scale* (*Abundance*) ~ [*ALA*] + [*LA*] + *Time* + *Treatment exposed*. Microbiome abundances were centered and scaled to reduce the effect of non-normal feature distribution on modeling and to enable interpretation of the results between features with different abundances. Categorical comparisons were made within and between diet groups following the same strategy as outlined in alpha diversity above; however, Kruskal–Wallis was chosen due to the non-normal distribution of the microbiome abundances.

2.5.6 Microbiome feature selection

The process described in 2.4.1 identified outcomes that were significantly affected by either experimental exposure or dietary status. Outcomes with models that had at least a moderate effect size (>0.2 for adjusted R2) were used to build stepwise microbiome models. Exhaustive feature selection is a method that rationally identifies predictors that balance model fit with error rate to conclude what combination of possible predictors best explains a target outcome, balancing both positive and negative effects on the target (Chowdhury and Turin, 2020). Stepwise selection was limited to the same number of predictors (3) as in the diet + exposure models. The *leaps* package was used to perform exhaustive predictor selection (Miller, 2020). Once predictors were identified, they were centered and scaled to aid in interpretation given the wide difference in the magnitude of relative abundance between predictors. The final model was run using stepwise predictors using the base R package lm() function. The distribution of residuals was checked for homoscedasticity using *lmtest* (Achim and Torsten, 2002). All outcome measure models were homoscedastic.

3 Results

3.1 Diet and intervention validation

We observed a significant presence of degenerated axons in the blast-TBI exposed animals above shams, especially in the white matter rich optic tracts, with the highest tendency in those fed the omega-3-deficient diet containing 1 en% of LA. There were, however, no significant differences found between the three diets, and thus, it was only a verification that the model was producing a robust brain injury (Supplementary Figure S1). As for the UWT-exposed animals, it is known that this model mainly produces HPA-axis-driven neurochemical/hormonal imbalances in the brain that at an acute exposure stage do not result in readily observed physical changes to the neuronal cells; however, there are reports of microglia overactivation in other animal models of acute and especially chronic psychological stress (Enomoto and Kato, 2021). Likewise, we tried looking at brain sections obtained from UWT-exposed pilot animals on each diet (n = 6) with a highly sensitive immuno-stain for detecting senescent/aged neurons (i.e., β-galactosidase expression), but did not find any significant increases over shams of dysfunctional cells within the hippocampus and amygdala in the primary fear memory centers. Independent of UWT exposure, interestingly, there was across the board a significantly greater number of prematurely aging neurons in both omega-3-deficient diets (Supplementary Figure S2).

Power analysis described in 2.5.1 for UWT (Appendix B) and TBI models (Appendix C) found that future studies could be improved by larger sample sizes. UWT model power was calculated as 0.052 for 7-d

TABLE 1 LM results of UWT outcomes.

UWT outcome measures								
	WBC***	Monocyte***	LDH***	TG***	Open***	Closed***	Cort 7d***	Cort 14d***
LA	40.59	**14.24*** **	**-129.11*** **	**-8.28***	1.30	**-17.05*** **	**10,487.75** **	**12,269.80*** **
	(36.38)	**(2.99)**	**(16.97)**	**(3.30)**	(1.19)	**(2.02)**	**(3,267.85)**	**(2,773.15)**
ALA	364.67	**238.87*** **	**-2,380.89*** **	-117.08	33.25	**-340.90*** **	**230,474.10*** **	**283,320.40*** **
	(674.32)	**(55.49)**	**(314.51)**	(61.25)	(21.97)	**(37.45)**	**(60,328.32)**	**(51,401.74)**
UWT	**683.54*** **	-13.02	**-244.93*** **	**-17.05**	**-16.11*** **	**19.11***	3,479.03	**-52,173.16*** **
	(143.42)	(11.80)	**(66.89)**	**(13.03)**	**(4.67)**	**(7.97)**	(13,197.91)	**(10,932.20)**
Constant	3,565.78	**-1,120.24*** **	**15,135.35*** **	**855.16***	**-126.90**	**2,083.04*** **	**-1,051,995.00** **	**-1,324,956.00*** **
	(3,914.10)	**(322.11)**	**(1,825.58)**	**(355.55)**	**(127.50)**	**(217.39)**	**(350,498.40)**	**(298,360.10)**
Observations	245	245	245	245	245	245	231	245
R^2	0.13	0.11	0.23	0.08	0.08	0.30	0.11	0.29
Adjusted R^2	0.12	0.10	0.22	0.07	0.07	0.29	0.10	0.28
Residual Std. Error	1,120.95	92.25	522.83	101.82	36.51	62.26	100,157.20	85,446.79
F Statistic	12.48***	10.28***	24.40***	7.42***	6.90***	33.69***	9.20***	32.40***

*p<0.05; **p<0.01; ***p<0.001.
Bolded values highlight significant results corresponding to p-values <0.05.

corticosterone, 0.63 for 14-d corticosterone, 0.48 for LDH, 0.53 in open arm EPM, and 0.31 in closed arm EPM. TBI models were powered at 0.59 for LDH, 0.75 for 6 d rotarod, and 0.38 for 14-d rotarod.

3.2 UWT physiologic effects

Linear modeling the effects of UWT using linear regression of *outcome measure* ~ [*LA*] + [*ALA*] + *condition* found that these predictors explained only 10–30% of the outcome measures (Table 1). Given that blood samples were only collected in the post-exposure, condition time was not included as a factor. With this approach, all measured outcomes were found to produce statistically significant models, although only LDH, time in the EPM closed arm, and 14-d corticosterone had a moderate effect size. Across outcomes, [ALA] had a greater effect size than [LA]. Notably, [ALA] had greater negative effects on the EPM closed arm and LDH. UWT, at 14 d post-exposure, was not found to cause significant neuronal cell perturbations in brain regions, i.e., the hippocampus and amygdala, controlling the formation of fear-memory-related behaviors (e.g., elevated plus maze impairments), as assessed by histopathology using senescence detection staining.

Using a t-test to evaluate categorical within-diet differences between sham and UWT, we found that WBC count, LDH, TGs, and corticosterone 14-d post exposure were significantly different between UWT and sham (Figure 2). WBC count was significantly higher in UWT (HC), whereas LDH was significantly reduced in the UWT group (HC and 8% LA). Corticosterone was significantly reduced in UWT models at 7 and 14 d within the HC and 1% LA diets (Figure 2).

Across diets, behavioral testing shows that across UWT-exposed diet groups, both LA-enriched diets spent significantly more time in both elevated plus maze (EPM) open and closed arms than the HC diet. Within diets, when comparing sham and UWT, there was a significant decrease in the time spent in EPM closed arms within the UWT-exposed model in every diet. Linear modeling found that these categorical observations of across-diet differences were most attributable to [ALA], not [LA] in the diet.

3.3 TBI physiologic effects

Linear models of TBI outcomes found that [LA] and [ALA] had significant positive effects on monocyte and TG levels, but a negative effect on LDH. For these outcomes, [ALA] showed a greater magnitude of effect (Table 2). TBI exposure significantly increased monocytes and LDH and reduced TG and day 6 rotarod behaviors of balance and coordination. [ALA] had greater effect sizes than [LA] in these TBI models. Of the outcomes that were measured in the TBI and

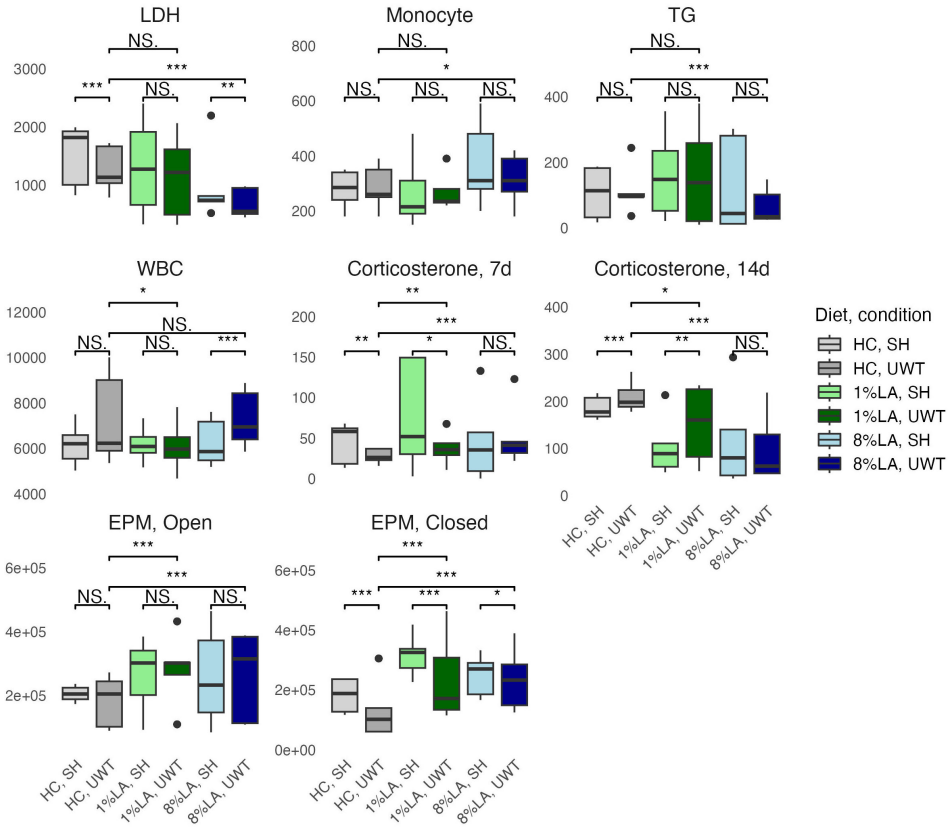

FIGURE 2
Physiologic outcomes of UWT exposure comparing shams with matched UWT-exposed models using a t-test (n=6 per group). LDH, lactate dehydrogenase; TG, triglyceride; WBC, white blood cell; EPM, elevated plus maze; HC, house chow, 1%LA, 1%en LA diet; 8%LA; 8%en LA diet; SH, Sham; UWT, underwater test. NS = $p>0.05$, *$p<0.05$, **$p<0.01$, ***$p<0.001$.

10.3389/frmbi.2024.1430340

TABLE 2 LM results of TBI outcomes.

TBI outcome measures						
	WBC	Monocyte***	LDH***	TG***	Rotarod, 6d*	Rotarod, 14d**
LA	-38.27	**9.51***	**-101.34*****	**17.18*****	0.31	-0.42
	(56.33)	**(3.95)**	**(12.24)**	**(2.38)**	(0.40)	(0.43)
ALA	-975.95	**205.84****	**-2,207.95*****	**364.43*****	5.00	-11.59
	(1,049.67)	**(73.65)**	**(228.05)**	**(44.27)**	(7.46)	(7.92)
TBI	364.40	**50.51****	**314.75*****	**-28.15****	**-4.34****	-1.96
	(222.28)	**(15.60)**	**(48.29)**	**(9.38)**	**(1.58)**	(1.68)
Constant	11,395.81	**-859.77***	**13,381.75*****	**-1,888.32*****	**2.16**	**98.17***
	(6,085.68)	**(426.98)**	**(1,322.17)**	**(256.69)**	**(43.23)**	**(45.94)**
Observations	238	238	238	238	238	238
R^2	0.02	0.10	0.46	0.32	0.04	0.05
Adjusted R^2	0.01	0.09	0.45	0.31	0.02	0.04
Residual Std. Error	1,704.47	119.59	370.31	71.89	12.11	12.87
F Statistic	1.90	8.85	66.16	36.52	2.90	4.48

*p<0.05; **p<0.01; ***p<0.001.
Bolded values highlight significant results corresponding to p-values <0.05.

UWT models, effect magnitudes were nearly identical. Adjusted R2 values found that only LDH and TGs had moderate effect sizes.

A t-test comparison of TBI and sham groups within diets found that TBI had significantly higher levels of monocytes (HC), LDH (8% LA), and TGs (HC) but lower levels of TGs in the 1% LA diet (Figure 3). Rotarod testing at day 6 showed no between diet differences and that TBI had significantly lower balance times in the 8% LA only. At day 14, balance times were significantly lower in the TBI group within the HC and 8% LA but were higher in the 1% LA.

Between diets comparisons in TBI models found that terminal LDH was significantly lower in both LA-enriched diets compared with HC. Terminal TGs were elevated in LA-enriched diets. Rotarod latency to fall times were not significantly different between diets.

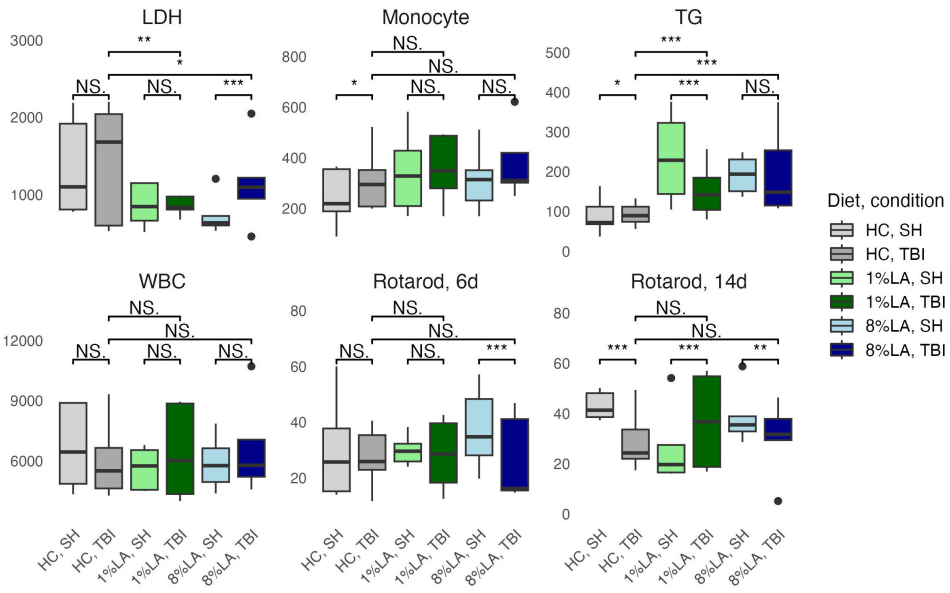

FIGURE 3
Physiologic outcomes of TBI exposure comparing shams with matched TBI-exposed models using a t-test (n=6 per group). LDH, lactate dehydrogenase; TG, triglyceride; WBC, white blood cell, HC, house chow, 1%LA, 1%en LA diet; 8%LA, 8%en LA diet; SH, Sham; TBI, traumatic brain injury. NS = p>0.05, *p<0.05, **p<0.01, ***p<0.001.

TABLE 3 Effects of diet and condition on Shannon and Simpson alpha diversity.

	Shannon		Simpson	
	TBI*	UWT*	TBI***	UWT***
LA	-0.06	-0.05	-0.01	**-0.06****
	(0.08)	(0.13)	(0.02)	**(0.02)**
ALA	-1.94	-1.21	-0.51	**-1.39*****
	(1.56)	(2.33)	(0.42)	**(0.33)**
Time	0.37	**-2.20****	-0.07	-0.05
	(0.43)	**(0.64)**	(0.12)	(0.09)
Treatment Exposed	0.25	0.33	0.10	-0.01
	(0.39)	(0.57)	(0.10)	(0.08)
Constant	**22.26***	21.27	**6.48***	**11.71*****
	(9.09)	(13.56)	**(2.46)**	**(1.95)**
Observations	48	48	48	48
R^2	0.25	0.24	0.39	0.47
Adjusted R^2	0.18	0.17	0.33	0.42
F Statistic (df = 4; 43)	3.60*	3.45*	6.76***	9.37***

*p<0.05; **p<0.01; ***p<0.001.
Bolded values highlight significant results corresponding to p-values <0.05.

3.4 Microbiome alpha diversity

Simpson diversity was significantly reduced by dietary [LA] and [ALA] in the UWT models (Table 3). Treatment exposure was not significant for either model. Only time was significant for the Shannon diversity of the UWT models. The UWT and TBI models had a small to moderate effect size.

Categorically, within TBI diets, alpha diversity was significantly decreased by sham exposure in the 1% LA models (Figure 4). Within the UWT group, alpha diversity was significantly decreased by sham exposure in the 8% LA group and by UWT exposure in the 1% LA UWT group. Alpha diversity was only disrupted in LA-supplemented models.

3.5 Microbiome beta diversity

We found a significant difference between TBI and UWT when comparing all samples in both Bray (ADONIS: p<0.01, R2 = 0.09, Residual = 0.91) and Jaccard (ADONIS: p<0.001, R2 = 0.08, Residual = 0.92); therefore, analysis proceeded within TBI and within UWT models.

Diet effects were not observed in the UWT model (Table 4) but were present in TBI (Table 5). Within-experiment distances were tested with ADONIS controlled against the HC diet, baseline condition, and SH condition by $\beta \sim Diet + Time + Treatment\ exposed$ (Figure 5).

Within the TBI model, only time was significant (Bray ADONIS, P<0.01, R2 = 0.09, Residuals = 0.8; Jaccard P<0.001, R2 = 0.8, Residuals = 0.84). The 8% LA diet was nearly significant (Jaccard ADONIS, P=0.08, R2 = 0.03, Residuals = 0.84). TBI exposure was not significant (Table 5).

In contrast, within the UWT model (Table 4), diet was highly significant for 8% LA (Bray ADONIS, P<0.01, R2 = 0.06, Residuals = 0.83) and 1% LA (Bray ADONIS, P=0.01, R2 = 0.06). Brain insult exposure by either model did not have a significant effect on microbiome beta diversity.

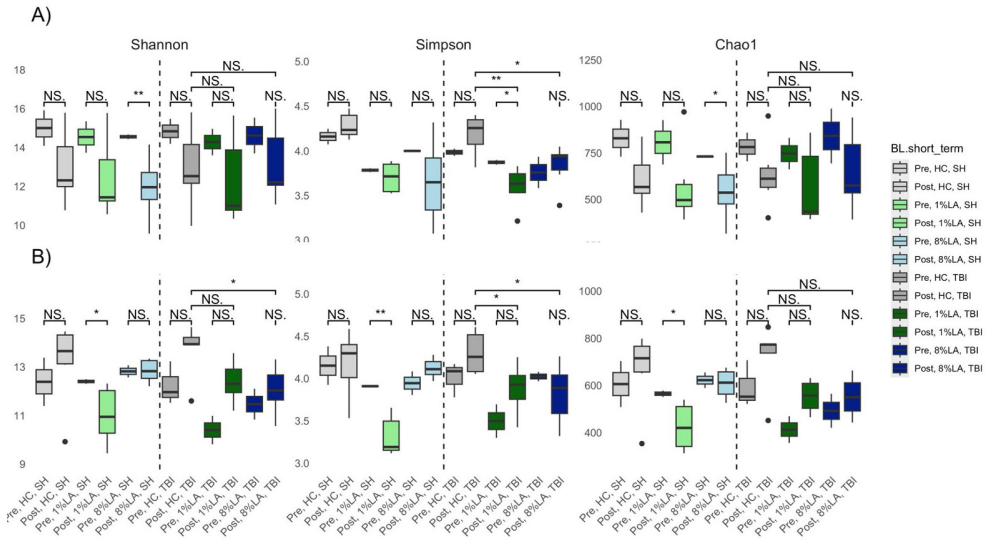

FIGURE 4
Effect of diet and brain insult exposure on three measures of alpha diversity (Shannon, Simpson and Chao1) of UWT **(A)** and TBI **(B)** models using a t-test (n=6 per group). HC, house chow; 1%LA, 1%en LA diet; 8%LA, 8%en LA diet, SH, sham; UWT, underwater test; TBI, traumatic brain injury. NS = p>0.05, *p<0.05, **p<0.01, ***p<0.001.

TABLE 4 ADONIS beta diversity results within the UWT model.

Effect	Bray					Jaccard			
	Df	Sum of Sq.	R2	F	P	Sum Of Sq.	R2	F	P
1 % LA	1	0.29	0.06	3.13	***	0.44	0.06	2.91	***
8 % LA	1	0.27	0.06	2.88	**	0.42	0.05	2.73	***
Time	**1**	**0.18**	**0.04**	**2.00**	*	**0.29**	**0.04**	**1.92**	*
Tx Exposure	1	0.06	0.01	0.6	NS	0.1	0.01	0.63	NS
Residual	*43*			*NA*	*NA*			*NA*	*NA*

p<0.01; **p*<0.05; ***p*<0.01; ****p*<0.001.
NA, Not Applicable; NS, Not Significant.
Bolded values highlight significant results corresponding to p-values <0.05.

TABLE 5 ADONIS beta diversity results within the TBI model.

Effect	Bray					Jaccard			
	Df	Sum of Sq.	R2	F	P	Sum Of Sq.	R2	F	P
1 % LA	1	0.12	0.02	1.04	NS	0.21	0.02	1.15	NS
8 % LA	1	0.18	0.03	1.55	NS	0.30	0.03	1.62	.
Time	**1**	**0.56**	**0.09**	**4.80**	***	**0.79**	**0.08**	**4.30**	***
Tx Exposure	1	0.11	0.02	0.90	NS	0.16	0.02	0.90	NS
Residual	*43*	*5.05*	*0.84*	*NA*	*NA*	*7.88*	*0.84*	*NA*	*NA*

p<0.01; **p*<0.05; ***p*<0.01; ****p*<0.001.
NA, Not Applicable; NS, Not Significant.
Bold values highlight significant findings (p < 0.05).

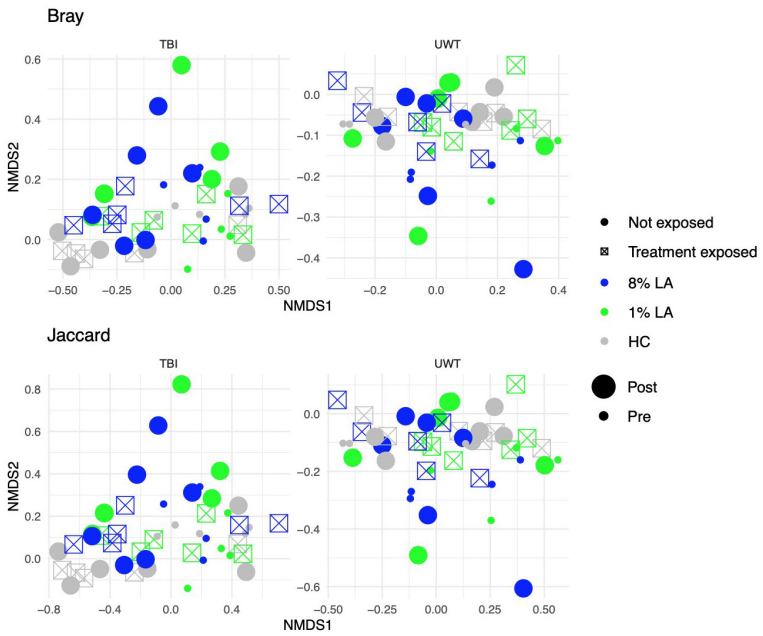

FIGURE 5
Effect of diet and brain insult exposure on beta diversity within TBI (left panels) and UWT (right panels) models. The top row of panels shows beta diversity measured by Bray–Curtis distances, whereas the bottom row displays beta diversity measured by Jaccard distances. Each panel compares the impact of diet and brain insult on the microbial communities, highlighting differences in community composition (Bray–Curtis) and the presence/absence of taxa (Jaccard).

3.6 Compositional effects of diet and time

3.6.1 Phyla level

Linear modeling found that there were different effects of the LA-enriched diets between experimental groups. At the phyla level, [ALA] and [LA] only affected *Proteobacteria* abundance in the UWT model, in which [ALA] had a larger effect size than [LA]. Exposure was not significant for any phyla (Figure 6).

Pre-post Kruskal–Wallis within TBI groups found *Proteobacteria* (1% LA) and *Bacteroidetes* (HC) were significant increased by TBI exposure, whereas *Firmicutes* (HC) were significantly decreased. These findings were not observed in the sham models. Within the UWT model, there were significant increases in *Actinobacteria* (1% LA), *Firmicutes* (HC), and *Tenericutes* (HC), and a decrease in *Bacteroidetes* (HC). These effects were also not observed in the sham controls.

3.6.2 Class level

Linear modeling found that [ALA] and [LA] had a significant effect on two *Proteobacteria* subclasses. Within the TBI model (Figure 7, top panel), *Alphaproteobacteria* was significantly decreased by [ALA], with a small effect observed by [LA]. Within the UWT model (Figure 7, bottom panel), *Gammaproteobacteria* was significantly increased by [ALA], while [LA] had a much smaller effect size (Figure 7).

A Kruskal–Wallis test within diets and between timepoints showed that class level changes within the TBI model were more likely to occur in the [LA] (n-6 PUFA)-enriched diets, whereas the opposite was observed in the UWT model. Within the TBI model, there were significant increases in *Bacilli* (1% LA), *Bacteroidia* (HC), and *Betaproteobacteria* (HC and 1% LA), and decreases in *Clostridia* (1% LA and 8% LA) and *Erysipelotrichi* (HC). Only one of these effects *(Clostridia)* was also shared with its matched sham control. Within the UWT models, there was an exposure-related increase in *Actinobacteria* (8% LA), *Clostridia* (HC), and *Mollicutes* (HC), and a decrease in *Bacteroidales* (HC).

3.6.3 Order level

Modeling showed that at the order level, [ALA] and [LA] only had a significant effect on *Enterobacteriales* abundance. TBI or UWT exposure was not significant for any order (Figure 8).

Observed changes in *Alphaproteobacteria* were attributable to the RF32 order in the UWT and TBI models. TBI-associated increases in *Betaproteobacteria* were attributable to *Burkholderiales*, which was found to significantly increase post-TBI in the 1% LA and was nearly significant in the 8% LA diet (p=0.07), but not for the HC. The *Bacilli* TBI effect was not significant for any sub-assignment of that class, although this trend appeared to be split between a non-significant post-exposure increase in *Lactobacillales* and *Turicibacterales*. Furthermore, within the TBI diets, there were significant pre-post increases in *Bacteroidales* (HC) and *RF32* (8% LA, nearly significant in 1% LA p=0.07), and decreases in *Clostridiales* (1% LA and 8% LA), *Erysipelotrichales* (HC), and *RF39* (1% LA). Within UWT diets, there were significant increases in *Actinomycetales* (1% LA), *Clostridiales* (HC), and *RF39*, (HC) and decreases in *Bacteroidales* (HC). Notably, *Verrucomicrobiales* was nearly significantly increased in both sham (p=0.053) and UWT (p=0.07) HC groups.

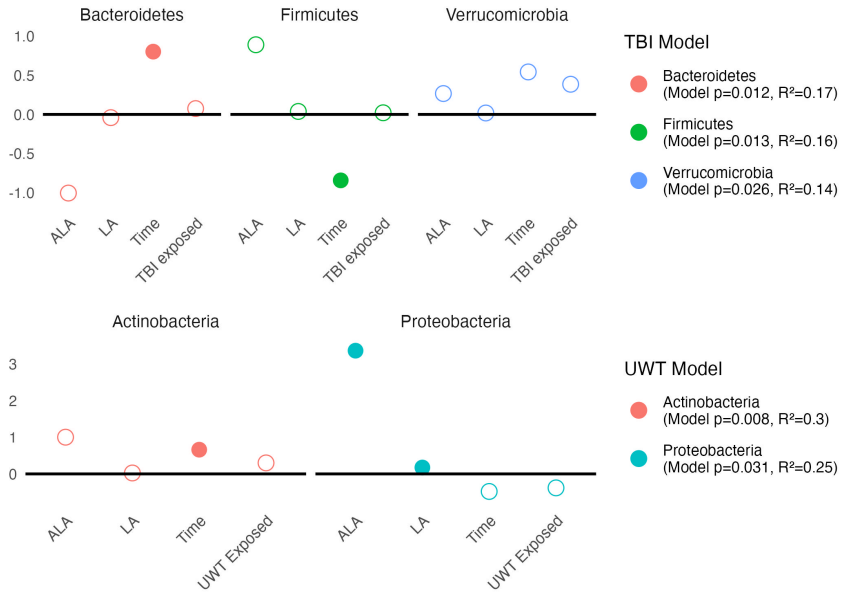

FIGURE 6
Estimates of phyla-level linear models of *scale(abundance) ~ [ALA]+[LA]+Time+Treatment exposed*$_{yes/no}$. Estimate values of the TBI (top panel) and UWT (bottom panel) models are shown. Open circles represent non-significant predictors. Filled circles identify significant model predictors. Model R2 and *p*-values are shown in the legend. ALA, alpha linolenic acid; LA, linoleic acid; TBI, traumatic brain Injury; UWT, underwater test.

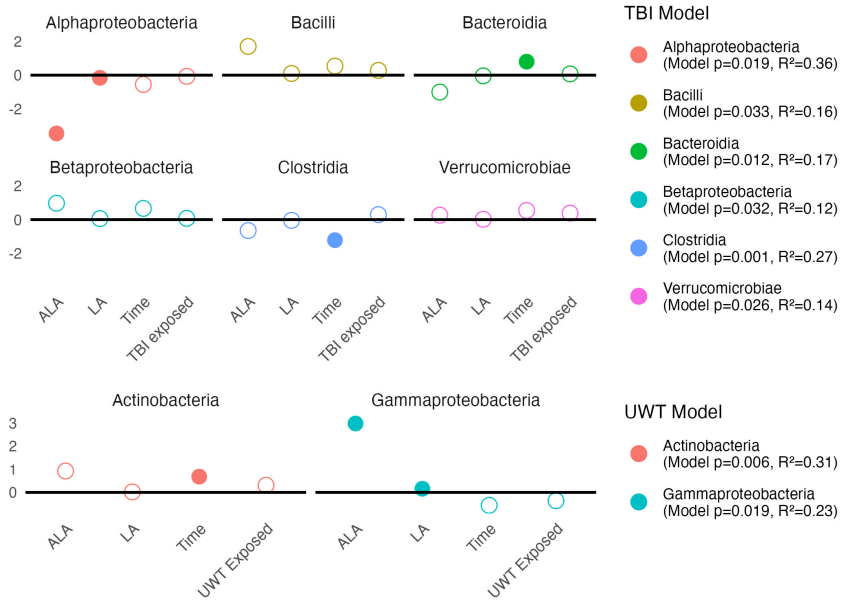

FIGURE 7
Estimates of class-level linear model *scale(abundance) ~ [ALA]+[LA]+Time+Treatment exposed*$_{yes/no}$. Estimate values of the TBI (top panel) and UWT (bottom panel) models are shown. Open circles represent non-significant predictors. Filled circles identify significant model predictors. Model R2 and *p*-values are shown in the legend. ALA, alpha linolenic acid; LA, linoleic acid; TBI, traumatic brain injury; UWT, underwater test.

3.7 Effect of microbiome composition on outcome measures

3.7.1 Phyla level

At the phyla level, *Actinobacteria* exerted a negative effect on the time spent in the EPM closed arms and corticosterone levels at day 14 (Table 6). *Verrucomicrobia* reduced LDH levels within the UWT model and in time spent in the EPM closed arms. *Bacteroidetes* were associated with an increase in LDH in the TBI model. *Tenericutes* were associated with significantly reduced 14-d corticosterone levels. *Cyanobacteria* was associated with increased LDH only in the TBI model. Between the UWT and TBI models, different

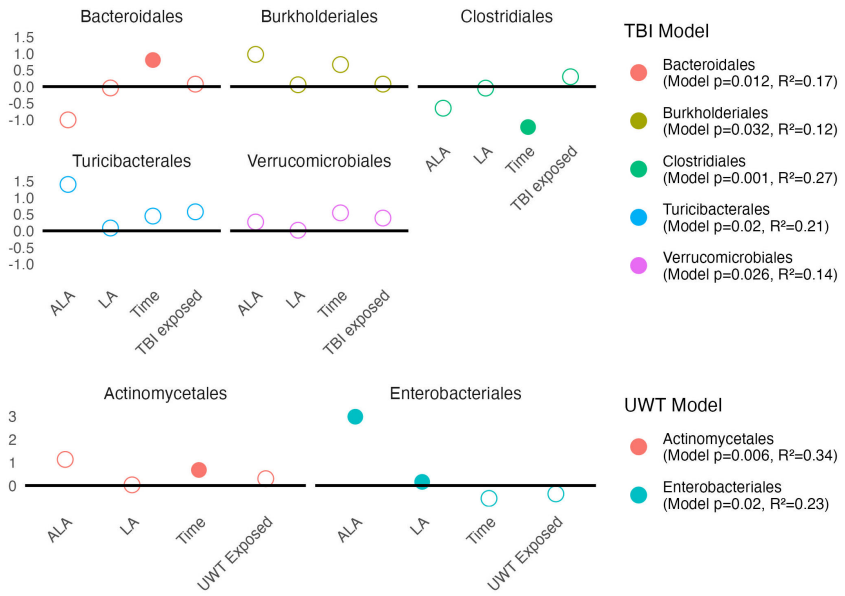

FIGURE 8
Estimates of order-level linear model *scale(abundance) ~ [ALA]+[LA]+Time+Treatment exposed*$_{yes/no}$. Estimate values of the TBI (top panel) and UWT (bottom panel) models are shown. Open circles represent non-significant predictors. Filled circles identify significant model predictors. Model R2 and *p*-values are shown in the legend. ALA, alpha linolenic acid; LA, linoleic acid; TBI, traumatic brain injury; UWT, underwater test.

TABLE 6 Stepwise feature selection of microbiome predictors of outcome measures.

	UWT			TBI	
	LDH *	EPM, closed ***	Cort. 14d (10^{-3}) ***	LDH ***	TG NS
Firmicutes	-16.44 (10.52)			18.16 (18.85	19.07 (15.37)
Actinobacteria		**-28.47** (11.01)**	**-41.52** (16.09)**		-23.72 (14.24)
Verrucomicrobia	**-24.74** (9.93)**	**-24.12** (10.71)**			
Bacteroidetes			24.39 (14.80)	**37.92** (17.99)**	
Tenericutes	11.83 (10.25)		**-62.90** (15.70)***		
Cyanobacteria		14.39 (10.79)		**20.47** (7.73)**	-17.87 (15.35)
Constant	**115.11** (9.46)***	**140.73** (10.21)***	**227.21** (14.20)***	**105.95** (6.78)***	**158.33** (13.81)***
Observations	35	35	35	36	36
R2	0.21	0.40	0.38	0.36	0.09
Residual Std. Error	55.98	60.42	84.00	40.66	82.88
F Statistic	2.72	6.96	6.33	7.46	2.13`

*p<0.05, **p<0.01, ***p<0.001.
Outcome measures affected by experimental interventions were evaluated for UWT (left) and TBI (right) to observe the effects of bacterial phyla on outcomes. The selection was limited to a maximum of three predictors, mirroring the number of predictors incorporated in the diet (three levels) and condition outcome models. Predictors were centered and scaled so that the effects of taxa with different abundances could be better compared.
Bold values highlight significant findings ($p < 0.05$).

predictors were selected between the same outcomes. Effect sizes on the microbiome were small to moderate, and R2 values were like the diet + condition models.

4 Discussion

4.1 Physiologic outcomes

Analysis of WBC, monocyte, LDH, and TG blood levels across experiments found that diet but not treatment exposure had a small but significant effect on outcome measures. Of the regression models testing experimental variables that reached significance, the effect sizes of diet and exposure were small to moderate. The three experimental diets showed higher sensitivity to disruptions in WBCs, LDH, corticosterone elevation, and rotarod behavioral impairments in balance and coordination. These findings across both experiments suggest that n-6 PUFA enrichment may increase susceptibility to cellular and immunologic dysfunction independent of brain insult exposure. Within the UWT model, the greatest behavioral effect of dietary n-6 PUFA enrichment was increased time spent in closed arms of the elevated plus maze. This suggests that fear, or in essence, anxiety-like behaviors, as noted in these animals, may be especially sensitive to this dietary feature. Biologically, corticosterone at 14 d post-exposure was also significantly affected by dietary n-6 PUFA intake. The longitudinal changes in cortisol, the analog of corticosterone that is present in humans, is complex in PTSD. Classically, immediately after the initial trauma in human subjects, cortisol spikes and falls over time; the degree of hypocortisolemia may be associated with symptom severity and PTSD development (Heim et al., 2000). A review of the evidence emphasizes that the development of a hypocortisol state following traumatic exposure may be an important factor in at least some PTSD biotypes (Meewisse et al., 2007). The corticotropin-releasing hormone receptors (CRH-Rs), which regulate cortisol and corticosterone production, are highly susceptible to sensitization. Typically, a strong CRH negative feedback signal will *de-sensitize* the receptor; however, if certain circumstances are met, the receptor can instead become sensitized to the presence of cortisol (or corticosterone), which leads to chronically low basal levels of cortisol in individuals suffering from trauma disorders. This has been suggested as a factor in how childhood trauma causes persistent phenotypic changes (Toth et al., 2015), and further studies have shown that CRH-Rs variants may be associated with susceptibility to trauma disorders (White et al., 2013). Our finding that n-6 PUFA experimental diets significantly reduced day 14 corticosterone levels may be clinically important because it identifies a potential modifiable dietary factor that contributes to hypocortisolemia, a PTSD risk factor. We hypothesize that n-6 PUFA is a dietary factor that might increase the risk of developing PTSD, potentially through

a cortisol or CRH-R sensitizing mechanism. As measured values of 7-d corticosterone were significantly lower in the UWT-exposed models than in the sham swim rats, this hypothesis could be further explored. Higher frequency sampling may be important in the post-trauma exposure to capture post-traumatic corticosterone increases as this may have resolved within 7 d post-exposure.

TBI and trauma occur unpredictably with variable time from event to medical care (Mohamadpour et al., 2019). It has been difficult to develop acute phase post-injury interventions that have been effective in blunting the biologic cascade that occurs after these exposures (Bramlett and Dietrich, 2015). Previous work has identified that the acute period is of extreme biological importance in determining the severity of long-term injury (Prins et al., 2013). Delay from exposure to point of care may reduce the efficacy of post-exposure treatments given the speed of the biologic response immediately after exposure. Populations with a high incidence of TBI and psychologic trauma (especially the military) may benefit most from prophylactic interventions, in which even those with small effect sizes could have a high population level benefit.

Owing to the relatively small group sizes (n = 8) used in this study, it was difficult to consistently detect behavioral deficits in the animals on the three diets under the two brain insult conditions, i.e., blast-TBI and UWT. Likewise, the TBI model used in the study is mild to moderate in intensity and its duration of effect. Thus, it is not surprising that significant behavioral deficits on the rotarod were absent 6 d post-exposure. Typically, our other behavioral studies require at least 16 animals per group to overcome the variances in individual animal intrinsic-performance capabilities on the rotarod. Likewise, in a separate study that used 10 animals, we found at 2 d post-TBI that house-chow-diet-fed animals showed a 30% decrease ($p < 0.05$) in latency times on the rotarod, which resolved by day 6. Thus, we could try reanalyzing the rotarod data at 2 days out and/or as normalized to the animal's baseline performance scores. The elevated plus maze testing for the UWT-exposed animals was also likely underpowered, leading to an inability to detect behavioral deficits in increased exaggerated fear response ("anxiety") as characterized by avoidance of the high-risk environment represented by the open arms. In other studies, however, we have noted that animals under acute psychological stress more readily show signs of increased exploratory hyperactivity on all arms of the elevated plus maze (i.e., distance traveled), which in this case with the small powering may have led to an overall tendency to spend less time in the closed arms. The non-concurrent increase in open arm time can be partially explained by the animals frequently hesitating to move while in the central zone of the maze (i.e., the intersection of the arms), which was not counted as part of the time scoring. To help eliminate some of these issues, which reflect the complexity of even occupancy exchanges between the arms of the maze, the data are often processed by other investigators (Mazor et al., 2009) using the following "anxiety" index formula: 1 − [((open arm time/300-s) + (open arm entries/total entries))/2]. Unfortunately, in our study, we only recorded arm time and not the number of arm entry events.

4.2 Alpha diversity

Alpha diversity disruption was only observed in experimental diets across both studies. This suggests that the presence of dietary n-6 PUFA may negatively affect microbiome diversity. These effects were observed in both sham- and brain-insult-exposed experimental diet groups, suggesting that despite the 6-week period of diet acclimation before the intervention, there was still a temporal effect as a confounding variable. Previous research has suggested that the post-TBI microbiome state contributes to the development of TBI sequelae (Simon et al., 2020). Little research has been carried out associating alpha diversity with trauma or TBI outcomes. Premorbid n-6 PUFA dietary status should be further evaluated as a risk factor for developing trauma and TBI-related disorders.

4.3 Beta diversity

The TBI and UWT groups were analyzed independently. There was a large degree of residual variability when accounting for all interventions. Across experiments, the 8% LA diet and time showed the greatest effect on beta diversity with condition being non-significant in both experiment's ADONIS. This suggests that between group differences reached significance because of both sham and experimental exposure, but neither experimental condition itself significantly affected beta distances. High levels of n-6 PUFA intake, observed in the 8% LA diet, exerted significant and nearly significant effects on the UWT and TBI exposures, respectively. This suggests that a high n-6 PUFA diet supported a microbiome that was compositionally distinct from standard house chow, with a better balance of n-3 to 6 n-6 PUFA. Cumulatively, these beta diversity effects show that there was significant variance in microbiome composition between the measured groups, especially between diets.

4.4 Composition and effects on physiologic outcomes

There were a host of TBI-, UWT-, and diet-related effects. The main observed compositional changes were *Bacteroidetes* and *Proteobacteria*, which were both decreased by UWT exposure. In the TBI group, *Proteobacteria* increased over time. Other studies of traumatic exposures have found prominent increases in *Proteobacteria* and *Firmicutes* post-TBI (Nicholson et al., 2019). Studies evaluating how phyla abundance affects TBI outcomes suggest that some clinically relevant observations, such as lesion size, may be significantly predicted by microbiome composition. *Proteobacteria* abundance has been suggested to be positive correlated with magnetic resonance imaging lesion size in TBI patients, whereas *Firmicutes* has been shown to be inversely correlated using single-feature phyla level linear models (Nicholson et al., 2019). This further suggests that the observation

of n-6 PUFA enrichment potentially exposing models to *Proteobacteria* upregulation may be biologically relevant and attenuating increases in *Proteobacteria* changes post-TBI could have the potential to improve outcomes.

Increases in bacteria taxa with a n-6 PUFA-enriched diet suggests that premorbid n-6 PUFA intake may contribute to this change. Likewise, as microbiome suppression by antibiotics has been found to ameliorate TBI sequelae, when given in the subacute period (Uckun et al., 2015), increases in taxa prevalence (possibly *Proteobacteria)* may be more likely to contribute to TBI sequelae than taxa that are decreased by TBI, although this hypothesis needs more evidence.

Deeper classification analysis attributed *Proteobacteria*'s enhancement to *Betaproteobacteria* in the TBI-exposure model across diets. The biological relevance of the *Betaproteobacteria* includes sulfur oxidation into sulfate and the acidification of its environment via hydrogen ion production (Watanabe et al., 2019), as well as environmental nitrification, with studies finding associations between *Betaproteobacteria* population levels and ammonia and phosphorous concentrations with R2 >90% in environmental samples (Martínez-García et al., 2022). It is unknown how TBI affects neuronal cell ammonia levels; however, evidence from other organ systems shows that disrupting circulating ammonia elimination has a strong association with brain concentrations and, thus, the extent of cerebral edema, seizure development, and encephalopathic symptoms (Sharma et al., 2024). Although this is a highly interpretive conclusion, it strongly identifies *Betaproteobacteria* as a potential candidate for contributing to TBI sequelae. This may be worth further research toward a better understanding of the relationship between blood ammonia levels and TBI explicitly.

Within the UWT model, exposure significantly increased *Alphaproteobacteria* and *Actinobacteria* by linear modeling. *Alphaproteobacteria* has an unclear ecological function, especially as we were unable to further subclassify this class given the limitations of only carrying out 16S rRNA analysis and not looking at other characterizing bacterial genes. Although *Proteobacteria* subgroups were somewhat classified with conserved ecological roles, that was not the case with *Actinobacteria*. This phylum has been suggested as a potent modulator of secondary metabolites almost acting as a regulatory promoter of the metagenome (Hoskisson and Fernández-Martínez, 2018); therefore, extrapolations about its potential role in our model microbiomes cannot be reasonably made.

The resulting models included the same number of variables from our initial evaluation of how diet (which was treated as three degrees of n-6 to n-3 PUFA balance) and brain insult condition influenced outcomes. The notable difference in models was that variability in microbiome composition had similar or higher R2 values than the effects of diet and brain condition alone. As feature selection allows the model to find the most suitable variables, it is unknown whether results represent a biologic relevance or overfitting.

However, features identified by this method are largely consistent with previous research. We want to highlight the associations found with *Verrucomicrobia* and reducing both LDH and time spent in the elevated closed arm. *Verrucomicrobia* is a mucin-dependent anaerobe that thrives on mucosa membranes. Previous studies have shown that *Verrucomicrobia* is inversely correlated with the severity of metabolic disease, lipopolysaccharide translocation into circulation, and inflammation status (Derrien et al., 2004). Across studies, *Verrucomicrobia* has presented itself as a candidate microbiome feature for which upregulation could improve host resilience. It has been shown to have immune modulatory effects and is associated with increased IL-10 expression in the gut, which is a cytokine known to markedly suppress inflammation processes (Lindenberg et al., 2019). Given the consistent finding of the benefit of this phyla, future interventional research is warranted regarding specifically upregulating this target. Culture for this microbe is challenging given its specific mucin and anaerobic requirements; therefore, prebiotics, such as the glucose-absorption-reducing drug metformin (Pavlo et al., 2023), may be more effective in increasing *Verrucomicrobia* abundance.

Tenericutes (subclassified as *RF39* and *RF32)* were shown to have a strong association with reduced corticosterone levels at 14 d in this study. *Tenericutes* typically exist at low levels in the microbiome but exert an outsized ecological role. Biologically, *Tenericutes* are butyrate producers (Vital et al., 2014), with a high representation of acetate-producing genes but lacking the somewhat common ability of other microbial species to synthesize the mucosal irritant hydrogen peroxide from glycerol (Wang et al., 2020). *RF39* and *RF32* are also notable for their gene content encoding cardiolipin production (Wang et al., 2020), a metabolite (di-phosphatidylglycerol lipid) that has been shown to enhance oxidative processes within the mitochondria, especially under glutamatergic stress (Głombik et al., 2021). Given the large effect size of *Tenericutes* on corticosterone levels, further investigation into its effect on known metabolites, such as cardiolipin, is warranted. Unsurprisingly, there was little overlap in the microbiome features associated with the TBI and UWT models. The UWT model was designed to induce neuroendocrine dysfunction, whereas the TBI model was designed to induce physical axonal and inflammatory injury in the brain. Taken collectively, these results illustrate that in two military-relevant models n-3 to n-6 PUFA intake may affect (even if only to a small magnitude) traumatic sequelae.

Finally, the application of stepwise feature selection to relate microbiome composition with outcome measures may also play an important role in understanding which collection of taxonomies in combination best explains a phenotype. A key limitation of our study was that a testing dataset was not available for validation. Future microbiome studies by others in rats using alternative established traumatic stressor (e.g., inescapable foot shocks) or closed head TBI (e.g., lateral fluid percussion injury) methods may clarify our results by testing our stepwise models against their own. Another limitation of this work was the small sample size per group (n=6) and evaluation of only male models, as females often show sex-specific microbiome responses. Repetition of this study would likely yield different taxonomic changes due to baseline compositional variance between cohorts, especially as our results were produced from a single cohort. However, we would anticipate similar findings that dietary PUFA significantly affects both alpha and beta diversity. Likewise, the blast-

TBI and acute traumatic stress exposures would have been translationally better to that occurring in humans if they were instead performed in a ferret or mini-pig model, which also possess a structurally higher-ordered brain, i.e., gyrencephalic (folded cerebral cortex), with better behavioral capabilities; and thus, might also have more similar systemic communication effects on the microbiome. It is also known that the rat gut microbiome composition does not mirror the human equivalent well, whereas mice are considered a better rodent model for these types of studies (Nagpal et al., 2018). Thus, an interesting extension of our work would be to stay with rats as a model, as opposed to using less neurologically advanced mice, but to oral dose some of them prior to the two brain insults with probiotic bacterial strains that are known to reside and maintain gut health in humans.

We are currently in pursuit of two projects that are utilizing the tissues that were collected from the same animals used in this study. The first project is looking at the transcriptomic (gene expression) changes that occurred in the whole retinas, as an indicator of neurosensory (visual system) impairment, and has found that numerous proteins and associated signaling pathways specific to retinal neurons, e.g., photoreceptor cells and endocannabinoid signaling, were significantly altered by both the blast-TBI and UWT exposures, with the highest degree of inhibition found in the animals on the omega-3-deficient diet containing 8 en% of LA. Likewise, we are now pursuing transcriptomic analysis of the whole brain and plasma samples that were collected from these same animals to look at the central nervous system and systemic changes. Overall, it is our desire to eventually perform correlation analysis between the changes found in the gut microbiome and the transcriptome in brain, retina, and/or plasma, as a means of identifying biomarkers (proteins and bacteria) that tightly associate with the occurrence of the blast-TBI and UWT exposures and severity of the behavioral impairments. We also want to support these data in the future by conducting total proteomic and metabolomic assessments of these tissues, using LC/MS-MS methods, as a means of identifying changes in the abundances of the expressed proteins and their enzymatic products (e.g., energy metabolism), including site-specific amino acid shifts in post-translation modifications that can greatly modulate the protein's function and ability to cause pathological states, e.g., phosphorylation patterns.

This project identified that premorbid dietary composition has a potential role in influencing hypocortisolemia, a risk factor for developing PTSD. To date, there are only limited methods to influence cortisol levels that could reasonably be used in a military deployment. Reducing dietary n-6 PUFA may be a promising method. The gut microbiome appeared to be significantly disrupted by dietary status more so than exposure to TBI or UWT, highlighting that diet has a profound effect on modulating microbiome signaling. Thus further work needs to be undertaken in identifying microbiome features associated with positive outcomes of TBI and PTSD.

Data availability statement

Normalized data files have been uploaded as Supplementary material. The raw data supporting the conclusions of this article will be made available by the authors, without undue reservation.

Ethics statement

The animal study was approved by Walter Reed Army Institute of Research. The study was conducted in accordance with the local legislation and institutional requirements.

Author contributions

MR: Formal analysis, Writing – original draft. JD: Conceptualization, Investigation, Writing – review & editing. NC: Investigation, Writing – review & editing. AH: Methodology, Writing – review & editing. SM: Methodology, Writing – review & editing. JR: Methodology, Writing – review & editing. AB: Data curation, Methodology, Writing – review & editing. DW: Methodology, Writing – review & editing. VS: Data curation, Writing – review & editing. JL: Funding acquisition, Project administration, Resources, Writing – review & editing. RH: Funding acquisition, Project administration, Resources, Writing – review & editing. AG: Data curation, Project administration, Supervision, Writing – review & editing.

Funding

The author(s) declare financial support was received for the research, authorship, and/or publication of this article. This work was supported by DoD grants from the US Army Medical Research Development Command (USAMRDC)/Military Operational Medicine Research Program (MOMRP) (e.g., project #: 19250).

Acknowledgments

Marti Jett, Bintu Sowe, Ross J. Campbell, Raina Kumar, William B. Rittase, Micheal J. Covell, and Arshiya Dutta.

Conflict of interest

The authors declare that the research was conducted in the absence of any commercial or financial relationships that could be construed as a potential conflict of interest.

Publisher's note

All claims expressed in this article are solely those of the authors and do not necessarily represent those of their affiliated organizations, or those of the publisher, the editors and the reviewers. Any product that may be evaluated in this article, or claim that may be made by its manufacturer, is not guaranteed or endorsed by the publisher.

Author disclaimer

Material has been reviewed by the Walter Reed Army Institute of Research. There is no objection to its presentation and/or publication. The opinions or assertions contained herein are the private views of the author, and are not to be construed as official, or as reflecting true views of the US Department of the Army or the US Department of Defense. Research was conducted under an IACUC-approved animal use protocol in an AAALAC International - accredited facility with a Public Health Services Animal Welfare Assurance and in compliance with the Animal Welfare Act and other federal statutes and regulations relating to laboratory animals.

Supplementary material

The Supplementary Material for this article can be found online at: https://www.frontiersin.org/articles/10.3389/frmbi.2024.1430340/full#supplementary-material

References

Achim, Z., and Torsten, H. (2002). Diagnostic checking in regression relationships. *R News* 2, 7–10. Available at: https://CRAN.R-project.org/doc/Rnews/.

Alvheim, A. R., Malde, M. K., Osei-Hyiaman, D., Lin, Y. H., Pawlosky, R. J., Madsen, L., et al. (2012). Dietary linoleic acid elevates endogenous 2-AG and anandamide and induces obesity. *Obesity (Silver Spring).* 20 (10), 1984–1994. doi: 10.1038/oby.2012.38

Ardi, Z., Ritov, G., Lucas, M., and Richter-Levin, G. (2014). The effects of a reminder of underwater trauma on behaviour and memory-related mechanisms in the rat dentate gyrus. *Int. J. Neuropsychopharmacol.* 17 (4), 571–580. doi: 10.1017/S1461145713001272

Arun, P., Krishnan, J. K. S., Govindarajulu, M., Wilder, D. M., and Long, J. B. (2024). Repeated mild concussive events heighten the vulnerability of brain to blast exposure. *J. Neurotrauma.* 41 (7-8), 1000–1004. doi: 10.1089/neu.2023.0367

Arun, P., Rossetti, F., Wilder, D. M., Sajja, S., Van Albert, S. A., and Wang, Y. (2020). Blast exposure leads to accelerated cellular senescence in the rat brain. *Front. Neurol.* 11, 438. doi: 10.3389/fneur.2020.00438

Bazan, N. G., Molina, M. F., and Gordon, W. C. (2011). Docosahexaenoic acid signalolipidomics in nutrition: significance in aging, neuroinflammation, macular degeneration, Alzheimer's, and other neurodegenerative diseases. *Annu. Rev. Nutr.* 31, 321–351. doi: 10.1146/annurev.nutr.012809.104635

Blasbalg, T. L., Hibbeln, J. R., Ramsden, C. E., Majchrzak, S. F., and Rawlings, R. R. (2011). Changes in consumption of omega-3 and omega-6 fatty acids in the United States during the 20th century. *Am. J. Clin. Nutr.* 93 (5), 950–962. doi: 10.3945/ajcn.110.006643

Bolyen, E., Rideout, J. R., Dillon, M. R., Bokulich, N. A., Abnet, C. C., Al-Ghalith, G. A., et al. (2019). Reproducible, interactive, scalable and extensible microbiome data science using QIIME 2. *Nat. Biotechnol.* 37 (8), 852–857. doi: 10.1038/s41587-019-0209-9

Bramlett, H. M., and Dietrich, W. D. (2015). Long-term consequences of traumatic brain injury: current status of potential mechanisms of injury and neurological outcomes. *J. Neurotrauma.* 32 (23), 1834–1848. doi: 10.1089/neu.2014.3352

Bryant, R. (2011). Post-traumatic stress disorder vs traumatic brain injury. *Dialogues Clin. Neurosci.* 13, 251–262. doi: 10.31887/DCNS.2011.13.2/rbryant

Bryden, D. W., Tilghman, J. I., and Hinds, S. R. (2019). 2nd, blast-related traumatic brain injury: current concepts and research considerations. *J. Exp. Neurosci.* 13, 1179069519872213–1179069519872213. doi: 10.1177/1179069519872213

Calder, P. C. (2011). Fatty acids and inflammation: The cutting edge between food and pharma. *Eur. J. Pharmacol.* 668, S50–S58. doi: 10.1016/j.ejphar.2011.05.085

Callahan, B. J., McMurdie, P. J., Rosen, M. J., Han, A. W., Johnson, A. J., and Holmes, S. P. (2016). DADA2: High-resolution sample inference from Illumina amplicon data. *Nat. Methods* 13 (7), 581–583. doi: 10.1038/nmeth.3869

Champely, S. (2020). *_pwr: basic functions for power analysis* (R package version 1.3-0). Available at: https://CRAN.R-project.org/package=pwr.

Chowdhury, M. Z. I., and Turin, T. C. (2020). Variable selection strategies and its importance in clinical prediction modelling. *Fam. Med. Community Health* 8, e000262. doi: 10.1136/fmch-2019-000262

DeMar, J. C. Jr, DiMartino, C., Baca, A. W., Lefkowitz, W., and Salem, N. Jr. (2008). Effect of dietary docosahexaenoic acid on biosynthesis of docosahexaenoic acid from alpha-linolenic acid in young rats. *J. Lipid Res.* 49, 1963–1980. doi: 10.1194/jlr.M800117-JLR200

DeMar, J. C. Jr, Ma, K., Bell, J. M., and Rapoport, S. I. (2004). Half-lives of docosahexaenoic acid in rat brain phospholipids are prolonged by 15 weeks of nutritional deprivation of n-3 polyunsaturated fatty acids. *J. Neurochem.* 91, 1125–1137. doi: 10.1111/j.1471-4159.2004.02789.x

DeMar, J. Jr, Sharrow, K., Hill, M., Berman, J., Oliver, T., and Long, J. (2016). Effects of primary blast overpressure on retina and optic tract in rats. *Front. Neurol.* 7, 59. doi: 10.3389/fneur.2016.00059

Derrien, M., Vaughan, E. E., Plugge, C. M., and de Vos, W. M. (2004). Akkermansia muciniphila gen. nov., sp. nov., a human intestinal mucin-degrading bacterium. *Int. J. Syst. Evol. Microbiol.* 54, 1469–1476. doi: 10.1099/ijs.0.02873-0

Durkin, L. A., Childs, C. E., and Calder, P. C. (2021). Omega-3 polyunsaturated fatty acids and the intestinal epithelium-A review. *Foods* 10, 199. doi: 10.3390/foods10010199

Dyall, S. C., and Michael-Titus, A. T. (2008). Neurological benefits of omega-3 fatty acids. *NeuroMolecular Med.* 10, 219–235. doi: 10.1007/s12017-008-8036-z

Enomoto, S., and Kato, T. A. (2021). Involvement of microglia in disturbed fear memory regulation: Possible microglial contribution to the pathophysiology of posttraumatic stress disorder. *Neurochem. Int.* 142, 104921. doi: 10.1016/j.neuint.2020.104921

George, A. K., Behera, J., Homme, R. P., Tyagi, N., Tyagi, S. C., and Singh, M. (2021). Rebuilding microbiome for mitigating traumatic brain injury: importance of restructuring the gut-microbiome-brain axis. *Mol. Neurobiol.* 58, 3614–3627. doi: 10.1007/s12035-021-02357-2

Głombik, K., Detka, J., and Budziszewska, B. (2021). Hormonal regulation of oxidative phosphorylation in the brain in health and disease. *Cells* 10, 2937. doi: 10.3390/cells10112937

Heim, C., Ehlert, U., and Hellhammer, D. H. (2000). The potential role of hypocortisolism in the pathophysiology of stress-related bodily disorders. *Psychoneuroendocrinology.* 25 (1), 1–35. doi: 10.1016/s0306-4530(99)00035-9

Hlavac, M. (2022). *stargazer: well-formatted regression and summary statistics tables* (R package version 5.2.3). Available at: https://CRAN.R-project.org/package=stargazer.

Hoskisson, P. A., and Fernández-Martínez, L. T. (2018). Regulation of specialised metabolites in Actinobacteria - expanding the paradigms. *Environ. Microbiol. Rep.* 10, 231–238. doi: 10.1111/1758-2229.12629

Karl, J. P., Whitney, C. C., Wilson, M. A., Fagnant, H. S., Radcliffe, P. N., Chakraborty, N., et al. (2023). Severe, short-term sleep restriction reduces gut microbiota community richness but does not alter intestinal permeability in healthy young men. *Sci. Rep.* 13, 213. doi: 10.1038/s41598-023-27463-0

Katoh, K., and Standley, D. M. (2013). MAFFT multiple sequence alignment software version 7: Improvements in performance and usability. *Mol. Biol. Evol.* 30, 772–780. doi: 10.1093/molbev/mst010

Lands, W. E., Libelt, B., Morris, A., Kramer, N. C., Prewitt, T. E., Bowen, P., et al. (1992). Maintenance of lower proportions of (n – 6) eicosanoid precursors in phospholipids of human plasma in response to added dietary (n – 3) fatty acids. *Biochim. Biophys. Acta (BBA) - Mol. Basis Dis.* 1180 (2), 147–162. doi: 10.1016/0925-4439(92)90063-S

Lindenberg, F., Krych, L., Fielden, J., Kot, W., Frøkiær, H., van Galen, G., et al. (2019). Expression of immune regulatory genes correlate with the abundance of specific

Clostridiales and Verrucomicrobia species in the equine ileum and cecum. *Sci. Rep.* 9, 12674. doi: 10.1038/s41598-019-49081-5

Lu, M., Yan, X. F., Si, Y., and Chen, X. Z. (2019). CTGF triggers rat astrocyte activation and astrocyte-mediated inflammatory response in culture conditions. *Inflammation.* 42 (5), 1693–1704. doi: 10.1007/s10753-019-01029-7

Marmarou, A., Foda, M. A., van den Brink, W., Campbell, J., Kita, H., and Demetriadou, K. (1994). A new model of diffuse brain injury in rats. *Part I: Pathophysiology and biomechanics. J. Neurosurg.* 80 (2), 291–300. doi: 10.3171/jns.1994.80.2.0291

Martínez-García, S., Bunse, C., Pontiller, B., Baltar, F., Israelsson, S., Fridolfsson, E., et al. (2022). Seasonal dynamics in carbon cycling of marine bacterioplankton are lifestyle dependent. *Front. Microbiol.* 13, 834675. doi: 10.3389/fmicb.2022.834675

Mayurasakorn, K., Williams, J. J., Ten, V. S., and Deckelbaum, R. J. (2011). Docosahexaenoic acid: brain accretion and roles in neuroprotection after brain hypoxia and ischemia. *Curr. Opin. Clin. Nutr. Metab. Care* 14 (2), 158–167. doi: 10.1097/MCO.0b013e328342cba5

Mazor, A., Matar, M. A., Kaplan, Z., Kozlovsky, N., Zohar, J., and Cohen, H. (2009). Gender-related qualitative differences in baseline and post-stress anxiety responses are not reflected in the incidence of criterion-based PTSD-like behaviour patterns. *World J. Biol. Psychiatry* 10, 856–869. doi: 10.1080/15622970701561383

McDonald, D., Price, M. N., Goodrich, J., Nawrocki, E. P., DeSantis, T. Z., Probst, A., et al. (2012). An improved Greengenes taxonomy with explicit ranks for ecological and evolutionary analyses of bacteria and archaea. *ISME J.* 6 (3), 610–618. doi: 10.1038/ismej.2011.139

Meewisse, M. L., Reitsma, J. B., de Vries, G. J., Gersons, B. P., and Olff, M. (2007). Cortisol and post-traumatic stress disorder in adults: systematic review and meta-analysis. *Br. J. Psychiatry* 191, 387–392. doi: 10.1192/bjp.bp.106.024877

Miller, A. (2020). *Leaps: regression subset selection* (R package version 3.1). Available at: https://CRAN.R-project.org/package=leaps.

Mohamadpour, M., Whitney, K., and Bergold, P. J. (2019). The importance of therapeutic time window in the treatment of traumatic brain injury. *Front. Neurosci.* 13. doi: 10.3389/fnins.2019.00007

Moore, N. L. T., Gauchan, S., and Genovese, R. F. (2012). Differential severity of anxiogenic effects resulting from a brief swim or underwater trauma in adolescent male rats. *Pharmacol. Biochem. Behav.* 102, 264–268. doi: 10.1016/j.pbb.2012.05.002

Nagpal, R., Wang, S., Solberg Woods, L. C., Seshie, O., Chung, S. T., Shively, C. A., et al. (2018). Comparative microbiome signatures and short-chain fatty acids in mouse, rat, non-human primate, and human feces. *Front. Microbiol.* 9. doi: 10.3389/fmicb.2018.02897

Nicholson, S. E., Watts, L. T., Burmeister, D. M., Merrill, D., Scroggins, S., Zou, Y., et al. (2019). Moderate traumatic brain injury alters the gastrointestinal microbiome in a time-dependent manner. *Shock* 52, 240–248. doi: 10.1097/SHK.0000000000001211

Oksanen, J., Simpson, G., Blanchet, F., Kindt, R., Legendre, P., Minchin, P., et al. (2022). *_vegan: community ecology package_* (R package version 2.6-4). Available at: https://CRAN.R-project.org/package=vegan.

Pavlo, P., Kamyshna, I., and Kamyshnyi, A. (2023). Effects of metformin on the gut microbiota: A systematic review. *Mol. Metab.* 77, 101805. doi: 10.1016/j.molmet.2023.101805

Price, M. N., Dehal, P. S., and Arkin, A. P. (2010). FastTree 2—Approximately maximum-likelihood trees for large alignments. *PloS One* 5, e9490. doi: 10.1371/journal.pone.0009490

Prins, M., Greco, T., Alexander, D., and Giza, C. C. (2013). The pathophysiology of traumatic brain injury at a glance. *Dis. Model. Mech.* 6, 1307–1315. doi: 10.1242/dmm.011585

Rama Rao, K. V., Iring, S., Younger, D., Kuriakose, M., Skotak, M., Alay, E., et al. (2018). A single primary blast-induced traumatic brain injury in a rodent model causes cell-type dependent increase in nicotinamide adenine dinucleotide phosphate oxidase isoforms in vulnerable brain regions. *J. Neurotrauma* 35 (17), 2077–2090. doi: 10.1089/neu.2017.5358

Richter-Levin, G. (1998). Acute and long-term behavioral correlates of underwater trauma — potential relevance to stress and post-stress syndromes. *Psychiatry Res.* 79 (1), 73–83. doi: 10.1016/S0165-1781(98)00030-4

Ritov, G., and Richter-Levin, G. (2014). Water associated zero maze: a novel rat test for long term traumatic re-experiencing. *Front. Behav. Neurosci.* 8. doi: 10.3389/fnbeh.2014.00001

Sajja, V. S., Arun, P., Van Albert, S. A., and Long, J. B. (2018). "Rodent Model of Primary Blast-Induced Traumatic Brain Injury: Guidelines to Blast Methodology," in *Pre-Clinical and Clinical Methods in Brain Trauma Research*. Eds. A. K. Srivastava and C. S. Cox (Springer New York, New York, NY), 123–138.

Sharma, B., Schmidt, L., Nguyen, C., Kiernan, S., Dexter-Meldrum, J., Kuschner, Z., et al. (2024). The effect of L-carnitine on critical illnesses such as traumatic brain injury (TBI), acute kidney injury (AKI), and hyperammonemia (HA). *Metabolites.* 14 (7), 363. doi: 10.3390/metabo14070363

Simon, D. W., Rogers, M. B., Gao, Y., Vincent, G., Firek, B. A., Janesko-Feldman, K., et al. (2020). Depletion of gut microbiota is associated with improved neurologic outcome following traumatic brain injury. *Brain Res.* 1747, 147056. doi: 10.1016/j.brainres.2020.147056

Staff, A. (2018). Hospitalizations, active component, U.S. Armed Forces. Available online at: https://health.mil/News/Articles/2019/05/01/Hospitalizations?page=4#pagingAnchor. (accessed May 01, 2024).

Torchiano, M. (2020). *Effsize: efficient effect size computation* (R package version 0.8.1). Available at: https://CRAN.R-project.org/package=effsize. doi: 10.5281/zenodo.1480624

Toth, S. L., Sturge-Apple, M. L., Rogosch, F. A., and Cicchetti, D. (2015). Mechanisms of change: Testing how preventative interventions impact psychological and physiological stress functioning in mothers in neglectful families. *Dev Psychopathol.* 27 (4 Pt 2), 1661–1674. doi: 10.1017/S0954579415001017

Uckun, O. M., Alagoz, F., Secer, M., Karakoyun, O., Ocakcioglu, A., Yildirim, A. E., et al. (2015). Neuroprotective effects of tetracyclines on blunt head trauma: An experimental study on rats. *J. Neurosci. Rural Pract.* 6, 27–32. doi: 10.4103/0976-3147.143186

Vital, M., Howe, A. C., and Tiedje, J. M. (2014). Revealing the bacterial butyrate synthesis pathways by analyzing (meta)genomic data. *mBio* 5, e00889. doi: 10.1128/mBio.00889-14

Wang, Y., Huang, J. M., Zhou, Y. L., Almeida, A., Finn, R. D., Danchin, A., et al. (2020). Phylogenomics of expanding uncultured environmental Tenericutes provides insights into their pathogenicity and evolutionary relationship with Bacilli. *BMC Genomics* 21, 408. doi: 10.1186/s12864-020-06807-4

Watanabe, T., Kojima, H., Umezawa, K., Hori, C., Takasuka, T. E., Kato, Y., et al. (2019). Genomes of neutrophilic sulfur-oxidizing chemolithoautotrophs representing 9 proteobacterial species from 8 genera. *Front. Microbiol.* 10. doi: 10.3389/fmicb.2019.00316

Weckle, F. A. (2013). Traumatic brain injury vs. *post-traumatic Stress disorder Nebr. Nurse* 46, 8.

White, S., Acierno, R., Ruggiero, K. J., Koenen, K. C., Kilpatrick, D. G., Galea, S., et al. (2013). Association of CRHR1 variants and posttraumatic stress symptoms in hurricane exposed adults. *J. Anxiety Disord.* 27, 678–683. doi: 10.1016/j.janxdis.2013.08.003

Yarnell, A. M., Shaughness, M. C., Barry, E. S., Ahlers, S. T., McCarron, R. M., and Grunberg, N. E. (2013). Blast traumatic brain injury in the rat using a blast overpressure model. *Curr. Protoc. Neurosci.* 62, 9.41.1–9.41.14. doi: 10.1002/0471142301.ns0941s62

Zhou, Y., Wen, L. L., Wang, H. D., Zhou, X. M., Fang, J., Zhu, J. H., et al. (2018). Blast-induced traumatic brain injury triggered by moderate intensity shock wave using a modified experimental model of injury in mice. *Chin. Med. J.* 131 (20), 2447–2460. doi: 10.4103/0366-6999.243558

frontiers | Frontiers in Microbiology

TYPE Original Research
PUBLISHED 28 October 2024
DOI 10.3389/fmicb.2024.1439481

Check for updates

OPEN ACCESS

EDITED BY
Jason W. Soares,
Combat Capabilities Development Command, United States Army, United States

REVIEWED BY
Yafei Duan,
South China Sea Fisheries Research Institute, China
Bochen Song,
Shandong Agricultural University, China

*CORRESPONDENCE
Yuguang Guo
guoyuguang@vtrbio.com

RECEIVED 28 May 2024
ACCEPTED 14 October 2024
PUBLISHED 28 October 2024

CITATION
Jiang Z, Huang Z, Du H, Li Y, Wang M, Chen D, Lu J, Liu G, Mei L, Li Y, Liang W, Yang B and Guo Y (2024) Effects of high-dose glucose oxidase on broiler growth performance, antioxidant function, and intestinal microbiota in broilers. *Front. Microbiol.* 15:1439481. doi: 10.3389/fmicb.2024.1439481

COPYRIGHT
© 2024 Jiang, Huang, Du, Li, Wang, Chen, Lu, Liu, Mei, Li, Liang, Yang and Guo. This is an open-access article distributed under the terms of the Creative Commons Attribution License (CC BY). The use, distribution or reproduction in other forums is permitted, provided the original author(s) and the copyright owner(s) are credited and that the original publication in this journal is cited, in accordance with accepted academic practice. No use, distribution or reproduction is permitted which does not comply with these terms.

Effects of high-dose glucose oxidase on broiler growth performance, antioxidant function, and intestinal microbiota in broilers

Zipeng Jiang[1,2], Zhiyi Huang[1], Hongfang Du[1], Yangyuan Li[1], Min Wang[1], Dandie Chen[1], Jingyi Lu[1], Ge Liu[1], Liang Mei[1], Yuqi Li[1], Weifan Liang[1], Bo Yang[2] and Yuguang Guo[1]*

[1]Guangdong VTR Bio-tech Co., Ltd., Zhuhai, China, [2]South China University of Technology, School of Biology and Biological Engineering, Guangzhou, China

Glucose oxidase (GOD) has been investigated as a potential additive for enhancing intestinal health and growth performance in poultry. However, limited research exists on the effects of ultra-high doses of GOD in practical poultry production. This study aimed to investigate the impact of high dietary GOD levels on broiler growth performance, antioxidant capacity, and intestinal microbiota. A total of 400 healthy, 1-day-old, slow-growing broiler chickens were randomly assigned to four treatment groups. The control group was fed a standard basal diet, while the other groups (G1, G2, and G3) were fed the basal diet supplemented with 4 U/g, 20 U/g, and 100 U/g of VTR GOD, respectively. The results showed that a dose of 100 U/g GOD significantly improved the final body weight and average daily feed intake (ADFI) ($p < 0.05$). Additionally, the G3 group exhibited a marked increase in glutathione peroxidase (GSH-Px) activity ($p < 0.05$), reflecting enhanced antioxidant function. Gut morphology remained intact across all groups, indicating no adverse effects on intestinal barrier integrity. Microbiota analysis revealed significant increases ($p < 0.05$) in Firmicutes and Verrucomicrobiota abundance at the phylum level in the GOD-supplemented groups. Moreover, GOD treatments significantly increased the abundance of *Faecalibacterium*, *Mucispirllum*, and *CHKCI001* at the genus level. Metabolic function predictions suggested that high-dose GOD supplementation enriched carbohydrate metabolism, particularly starch and sucrose metabolism. Correlation analysis indicated that *Faecalibacterium* and *CHCKI001* were two bacteria strongly influenced by GOD supplementation and were associated with enhanced growth performance and improved gut health. In conclusion, high-dose GOD supplementation had no adverse effects and demonstrated significant benefits, promoting both growth performance and gut health in broilers.

KEYWORDS

glucose oxidase, ultra-high doses, broilers, antioxidant ability, gut microbiota

1 Introduction

Glucose Oxidase (GOD) is an aerobic dehydrogenase enzyme that uses a non-covalently bound coenzyme, flavin adenine dinucleotide (FAD). As an oxidoreductase, the flavoprotein catalyzes the oxidation of β-D-glucose into D-glucono-δ-lactone and hydrogen peroxide (H_2O_2), with molecular oxygen serving as the electron acceptor (Bankar et al., 2009). Due to its catalytic properties, GOD has gained significant commercial value and is widely used in various industries, including food processing, medical diagnostics, oral hygiene products, the chemical industry, and biotechnology (Mano, 2019; Tu et al., 2019; Zhao et al., 2017).

GOD plays a crucial role in neutralizing free oxygen radicals (Ding et al., 2022; Zhang et al., 2020). It catalyzes the oxidation of glucose to produce gluconolactone, using molecular oxygen as an electron acceptor (Yue Wang et al., 2023), which helps reduce oxidative tissue damage, preserve health, and promote growth. Due to these beneficial properties, GOD is considered an effective alternative to antibiotics (Liang et al., 2023; Zhao et al., 2023). GOD has emerged as a novel and promising feed additive in animal husbandry, with the majority of studies focusing on its effects as a feed additive aimed at maintaining animal health (Sun et al., 2022; Wang et al., 2018), enhancing growth performance (Tang et al., 2016; Zhao et al., 2021), and preventing pathogens (Liu et al., 2020; Wang et al., 2022; Wang et al., 2020) or mycotoxin infection (Qu and Liu, 2021; Gao et al., 2022; Zhao et al., 2022). Typically, 0–4 U/g of GOD is added to feed as an efficient and environmentally friendly additive (Wang et al., 2018; Tang et al., 2016; Wang et al., 2022; Zhao et al., 2022; Meng et al., 2021; Wang et al., 2022). One study found that 12 U/g of GOD could replace antibiotics and improve broiler growth performance (Zhao et al., 2023), while another used 100 U/g of GOD to improve the growth performance of pigs (Dang et al., 2021). However, the optimal dosage of GOD and the impact of excessively high doses on broiler production remain underexplored. Many users focus on the effects of adding lower concentrations of GOD to achieve practical production without fully considering the maximum effective limit at which GOD can exert its benefits. Therefore, this study experimentally investigated the effects of several high concentrations of GOD on broilers.

Growth performance is critical to all animal farming operations as it directly impacts economic returns. The gut microbiota plays a vital role in animal health, significantly influencing nutrition, digestion, absorption, and immune function (Li et al., 2023; Novoa Rama et al., 2023; Shi et al., 2019). During its catalytic process, GOD generates hydrogen peroxide, which has led some researchers to hypothesize that it might be detrimental to gut health. However, there is currently a lack of direct evidence to support the notion that GOD could negatively affect intestinal health or growth performance in animals. Furthermore, the optimal maximum additive amount of GOD has not been clearly established, limiting its potential and value in practical applications. Therefore, it is essential to conduct further animal experiments to determine whether high doses of GOD affect gut microbiota, antioxidant status, or growth performance, and to confirm its safety and efficacy.

In this study, based on our previous results, we aimed to investigate whether supplementing broiler chickens with high doses of GOD could positively impact growth performance, antioxidant status, and gut microbiota. This was accomplished through a series of animal experiments and various analytical techniques.

2 Materials and methods

All experimental procedures were approved by the Institutional Animal Care and Use Committee of Guangdong VTR Biotech and were conducted in strict accordance with the guidelines established by the National Institute of Animal Health.

2.1 Animals experimental design and diets

A total of 400 healthy one-day-old slow-growing broiler chickens (female chicks, purchased from Guangzhou Shunxin Agriculture and Animal Husbandry) were randomly assigned into four treatment groups, with 10 replicates per group and 10 broilers per replicate. The control was fed a basal diet, while G1, G2, and G3 were supplemented with 4 U/g, 20 U/g, and 100 U/g of VTR GOD in the basal diet, respectively (Figure 1).

The experiment was conducted in three stages: 1–21 days, 22–56 days, and 57–119 days of age. At the beginning and end of the experiment, the fasting weight of the broilers was measured per replicate group. The trial took place at the animal testing facility of Guangdong VTR Biotechnology Co., Ltd., where the broilers were housed in cages and managed under standard production practices, with free access to feed and water.

For the starter phase (10 broilers per cage), cage dimensions were 60 cm in length, 66 cm in width, and 44 cm in height. For the grower and finisher phases (two broilers per cage), cage dimensions length 43 cm in length, 40 cm in width, and 42 cm in height. Temperature control was maintained using infrared lamps and fans, with the first week's temperature set at 31–33°C, the second week at 29.5°C, and a gradual reduction starting in the third week. Relative humidity was maintained at 60–65%, and the flock was vaccinated according to a routine immunization schedule.

The immunization procedures were as follows:

- 1-day old: Neck subcutaneous injection of Marek's vaccine
- 7 days old: Newcastle Disease IV, branch 120, double vaccine drops in the nose and eyes 14 days old: Infectious bursa vaccine drops in the nose or eyes
- 21 days old: Second drinking water immunization with the infectious bursa vaccine
- 28 days old: Second drinking water immunization with Newcastle Disease IV, branch 120, double vaccine

The ingredient composition and calculated nutrient content of the experimental diets are shown in Supplementary Tables S1, S2. Throughout the experiment, daily feed intake, remaining feed, and mortality were meticulously recorded. At the beginning and end of the trial, the fasting weight of the broilers was measured for each replicate group to calculate key performance indicators, including average daily gain (ADG), average daily feed intake (ADFI), feed conversion ratio (FCR), and survival rate.

2.2 Sample collection

At the end of the experiment, six broilers from each group were randomly selected for sampling and euthanized using CO_2. Serum was then obtained by centrifuging the blood at 3,000 g for 10 min at

10.3389/fmicb.2024.1439481

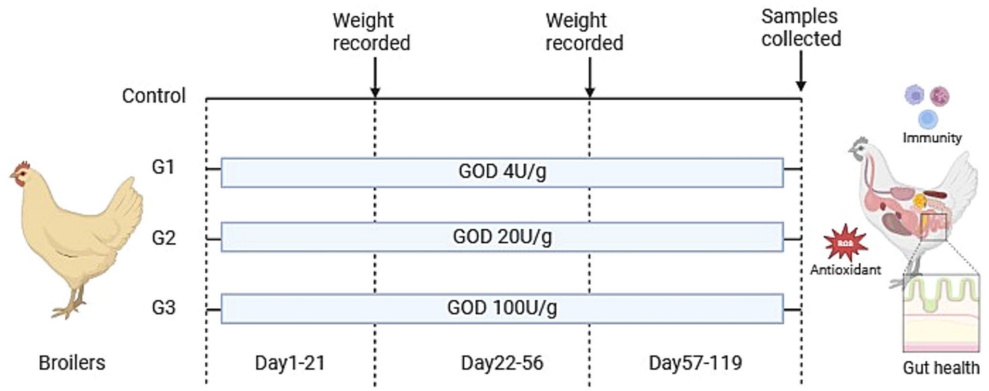

FIGURE 1
Experimental design and scheme of the animal treatments. (Created in BiorRender.com).

4°C. After exsanguination, mid-segments (approximately 1 cm) of the jejunum from one broiler per replicate were collected and fixed in a 10% paraformaldehyde solution for morphology analysis. Additionally, jejunal segments were collected for mRNA or protein determination. Cecal contents were collected and stored at −80°C for microbiota composition analysis.

2.3 Intestinal morphology

After fixation in 4% paraformaldehyde, gut samples were stained with hematoxylin and eosin (H&E). Intestinal morphology was analyzed following previously established methods (Hao et al., 2021). The measurements included villus height, intestinal crypt depth, and the villus-to-crypt (V/C) ratio to assess intestinal structure.

2.4 Serum antioxidant ability

Serum antioxidant indices, including superoxide dismutase (SOD), glutathione peroxidase (GSH-Px), and the damage index malondialdehyde (MDA), were measured using ELISA kits (provided by Jiangsu Meibiao Biotechnology Co., Ltd., China).

2.5 Quantitative real-time PCR

Total RNA was extracted using an RNA kit (Invitrogen, United States). RNA concentration was measured using the NanoDrop 2000 spectrophotometer. Quantitative real-time PCR was then performed using a CFX96 Real-Time System (Bio-Rad Laboratories). Primer sequences used for qPCR are shown in Supplementary Table S3. The reference gene *GAPDH* was used as a housekeeping gene. Relative mRNA expression levels were calculated using the $2^{-\Delta\Delta Ct}$ method.

2.6 Microbial analysis

Genomic DNA from the cecal contents was extracted using the PowerSoil DNA isolation kit (MoBio Laboratories Inc., USA) following the manufacturer's protocol. Subsequently, the V3-V4 region of the bacterial 16S rRNA gene (primers 515F: ACTCCTACGGGAGGCAGCAG, 806R: GGACTACHVGGGT-WTCTAAT) was amplified through PCR. Sequencing was conducted using the Illumina Hiseq2500 platform, which was conducted according to previous studies (Su et al., 2022; Jiang et al., 2021). The clean sequences were classified into identical amplicon sequence variants (ASVs). Chao, Simpson, Shannon, and Good's coverage indices were calculated using the QIIME2 (http://qiime2.org/) pipeline, with DADA2 (Version 1.8) used for denoising sequences (Edgar and Flyvbjerg, 2015). UniFrac-based principal coordinate analysis (PCoA) was conducted to visualize the microbial community differences. Linear discriminant analysis effect size (LEfSe) was used to identify the main differentially abundant genera. Tax4Fun was used to predict the functional profile of the gut microbiota. The sequence data were deposited in the Sequence Read Archive (SRA) under accession number PRJNA1116544.

2.7 Spearman correlation analysis of gut bacteriome, growth performance, antioxidant parameters, tight junction protein mRNA, and V/C

We conducted a Spearman correlation analysis to identify key microorganisms associated with the potential gut health benefits of GOD supplementation. This analysis assessed the relationship between changes in gut microbiota composition, growth performance, antioxidant markers, mRNA expression levels of tight junction proteins, and the V/C ratio. Spearman's correlation was conducted using R (version 4.2), considering an absolute value of correlation coefficients >0.45 and a p-value of <0.05 as statistically significant.

2.8 Statistical analysis

Data analysis was conducted using SPSS 22.0 software (IBM Company, Armonk, NY). Significant differences between groups were

determined using one-way ANOVA followed by Duncan's multiple range test, with a p-value of < 0.05 considered statistically significant. The results are expressed as mean ± SD. In addition, data visualization and graphing were conducted using GraphPad Prism version 9.0 (San Diego, CA, USA) and R version 4.2.

3 Results

3.1 Growth performance of broilers

Table 1 shows that incorporating GOD into the diet at levels of 4 U/g and 20 U/g had no significant impact on the broilers' daily feed intake throughout each week ($p < 0.05$). In contrast, supplementation with 100 U/g GOD significantly increased weekly daily feed intake from weeks 13 to 17 in the G3 group. Table 2 shows that, compared to the control group, GOD supplementation at various doses enhanced the growth performance of broilers, leading to an increase in ADG and a reduction in FCR during days 1–21. The improvement in growth appears to be directly proportional to the amount of GOD added.

During days 22–56, compared to the control group, ADFI increased significantly ($p < 0.05$) in the G1, G2, and G3 groups, although this did not result in a corresponding improvement in ADG or a reduction in FCR. In the Finisher phase (days 57–119), GOD improved final body weight, increased the ADFI of the yellow-feathered broilers, and reduced FCR. The 100 U/g GOD was the most effective, significantly improving ADFI ($p < 0.05$), increasing ADG by 15.63%, and reducing FCR by 8.86%.

Throughout the entire experimental period, an increasing trend was observed in the G1, G2, and G3 groups for final weight, ADG, and ADFI. The 100 U/g GOD dose significantly increased the final weight by 3.44% ($p < 0.05$) and ADFI by 3.88% ($p < 0.05$). The effect of GOD on enhancing growth performance appeared to be directly proportional to the amount of GOD added.

3.2 GOD improved antioxidant function

The results for the serum antioxidant ability are presented in Table 3. Compared to the control group, SOD levels showed a gradual increase in the G1, G2, and G3 groups, though the differences were not statistically significant among these groups. Similarly, the MDA concentration in the serum decreased in the G2 and G3 groups, but no significant reduction was observed between them. Notably, GSH-Px levels significantly increased in the G3 group ($p < 0.05$).

3.3 GOD improved intestinal barrier function

Figure 2 shows the jejunum villus and crypt morphology analysis. Compared to the control group, the GOD addition groups exhibited continuous brush borders and intact villi, suggesting that the gut structure and gut physical barrier were normal. Specifically, Table 4 presents the villus height, crypt depth, and the V/C ratio. The G1 group showed that the GOD significantly increased the villus height and the V/C ratio ($p < 0.05$) in the duodenum segment. In the jejunum and ileum sections, compared to the control group, the GOD groups showed an increase in the villus height and the V/C ratio in the ileum and villus height in the jejunum. The G2 group exhibited a noticeable reduction in crypt depth in the jejunum.

TABLE 1 Weekly daily feed intake (g/d).

Treatment[1]	Control	G1	G2	G3	p- value
Week 1	14.78 ± 0.53	15.24 ± 0.40	15.46 ± 0.80	15.03 ± 0.60	0.121
Week 2	18.31 ± 0.26	18.14 ± 0.83	18.17 ± 0.69	18.22 ± 0.61	0.649
Week 3	34.49 ± 2.27	34.50 ± 1.17	34.49 ± 1.17	34.15 ± 2.55	0.953
Week 4	45.24 ± 1.33	45.69 ± 1.41	45.73 ± 1.35	45.96 ± 1.78	0.910
Week 5	63.19 ± 0.85	63.21 ± 1.12	62.79 ± 0.85	63.34 ± 1.20	0.840
Week 6	68.59 ± 1.40	68.45 ± 1.58	68.76 ± 1.10	69.00 ± 1.33	0.932
Week 7	72.47 ± 1.71^{c}	75.65 ± 2.66^{ab}	74.21 ± 1.75^{bc}	76.49 ± 2.35^{a}	0.000
Week 8	78.77 ± 2.70^{b}	81.95 ± 3.30^{ab}	83.57 ± 1.71^{a}	83.79 ± 3.50^{a}	0.005
Week 9	88.37 ± 4.48	91.69 ± 3.78	89.54 ± 3.61	90.66 ± 3.61	0.208
Week 10	95.81 ± 3.23^{b}	99.51 ± 6.60^{ab}	95.67 ± 2.93^{b}	101.30 ± 2.56^{a}	0.020
Week 11	101.23 ± 1.87	104.37 ± 8.09	100.86 ± 3.23	101.05 ± 3.91	0.542
Week 12	96.91 ± 3.75^{a}	98.46 ± 3.40^{a}	92.86 ± 5.73^{b}	96.98 ± 3.44^{a}	0.003
Week 13	114.37 ± 11.24	111.46 ± 8.93	110.05 ± 8.39	116.03 ± 7.38	0.233
Week 14	103.58 ± 7.58^{b}	104.74 ± 4.68^{b}	105.02 ± 7.34^{b}	112.68 ± 5.96^{a}	0.005
Week 15	120.24 ± 11.07	121.75 ± 7.28	118.40 ± 6.28	124.33 ± 6.41	0.520
Week 16	119.40 ± 6.85^{b}	120.92 ± 8.06^{b}	123.02 ± 7.76^{ab}	127.65 ± 7.50^{a}	0.042
Week 17	118.83 ± 6.77^{b}	120.83 ± 5.95^{b}	123.67 ± 5.62^{b}	131.07 ± 6.21^{a}	0.000

[1]Control, no additives; G1-3: GOD 4 U/g, 20 U/g, and 100 U/g. ^{a,b,c}Values within a row with different letters differ significantly ($p < 0.05$).

10.3389/fmicb.2024.1439481

TABLE 2 Effect of GOD on the Growth performance of Broilers in starter to finisher Phases.

Treatment[1]	Control	G1	G2	G3	*p*- value
Starter phase (d0-21)					
ADG (g/d)	11.39 ± 0.92	11.40 ± 0.66	11.61 ± 0.64	11.78 ± 0.65	0.523
ADFI (g/d)	22.53 ± 0.66	22.63 ± 0.41	22.70 ± 0.57	22.47 ± 0.75	0.885
FCR	1.99 ± 0.17	1.99 ± 0.09	1.96 ± 0.11	1.91 ± 0.10	0.357
Survival rate (%)	100	100	100	100	1
Grower phase (d22-56)					
ADG (g/d)	23.50 ± 0.97	22.74 ± 0.83	22.74 ± 0.44	23.29 ± 0.80	0.246
ADFI (g/d)	65.65 ± 0.90^{b}	66.99 ± 1.01^{a}	67.01 ± 0.52^{a}	67.72 ± 0.63^{a}	0
FCR	2.80 ± 0.12^{b}	2.95 ± 0.09^{a}	2.95 ± 0.06^{a}	2.91 ± 0.10^{a}	0.036
Survival rate (%)	100	100	100	100	1
Finisher phase (d57-119)					
ADG (g/d)	12.92 ± 1.68	13.93 ± 1.73	14.04 ± 1.36	14.94 ± 1.78	0.119
ADFI (g/d)	112.22 ± 5.41^{b}	113.03 ± 4.08^{b}	112.17 ± 4.61^{b}	118.12 ± 3.73^{a}	0.003
FCR	8.80 ± 1.01	8.22 ± 1.04	8.06 ± 0.82	8.02 ± 1.05	0.462
Survival rate (%)	100	98.90 ± 3.48	99.00 ± 3.16	97.90 ± 4.43	0.61
Starter to finisher phase (d0-119)					
Initial weight (g)	30.50 ± 0.33	30.45 ± 0.28	30.45 ± 0.28	30.40 ± 0.39	0.967
Final weight (g)	2270.49 ± 66.84^{b}	2274.31 ± 41.12^{b}	2291.06 ± 48.45^{b}	2348.53 ± 85.29^{a}	0.0499
ADG (g/d)	18.82 ± 0.56	18.86 ± 0.34	19.00 ± 0.41	19.48 ± 0.72	0.0502
ADFI (g/d)	79.68 ± 1.52^{b}	80.89 ± 2.07^{b}	80.13 ± 1.82^{b}	82.77 ± 1.57^{a}	0.001
FCR	4.24 ± 0.13	4.29 ± 0.15	4.22 ± 0.11	4.25 ± 0.17	0.856
Survival rate (%)	100	98.90 ± 3.48	99.00 ± 3.16	97.90 ± 4.43	0.61

ADG, Average daily gain; ADFI, average daily feed intake; FCR, feed conversion ratio. [1]Control, no additives; G1-3: GOD 4 U/g, 20 U/g, and 100 U/g. [a,b,c]Values within a row with different letters differ significantly ($p < 0.05$).

TABLE 3 Effect of GOD on the antioxidant ability of broilers (Serum).

Treatment[1]	Control	G1	G2	G3	*p*- value
SOD (U/mL)	444.61 ± 160.73	495.15 ± 67.17	574.58 ± 77.82	526.09 ± 42.99	0.468
MDA (nmol/mL)	3.78 ± 1.65	3.78 ± 0.19	3.22 ± 1.17	2.67 ± 0.67	0.552
GSH-Px (U)	2371.43 ± 318.16^{b}	2447.62 ± 280.43^{b}	3419.05 ± 847.73^{ab}	4361.90 ± 554.27^{a}	0.007

[1]Control, no additives; G1-3: GOD 4 U/g, 20 U/g, and 100 U/g. [a,b,c]Values within a row with different letters differ significantly ($p < 0.05$).

3.4 GOD improved gut microbiota

Microbial analysis was conducted using 16 s rRNA sequencing. Table 5 shows that Good's coverage for all samples was 0.99, indicating that the sequencing depth was sufficient for further analysis. The total number of ASVs and Chao1 increased by the GOD treatment. However, the number of observed ASVs, Chao1 index, and Shannon index had no differences among the four groups. The Simpson index decreased significantly ($p < 0.05$) in the G3 group compared to the other groups.

Figure 3A shows that the number of observed ASVs in the G2 group was higher ($p < 0.05$) than in other groups. Figure 3B shows that the 83 ASVs were shared by all treatments, and the G2 group had unique microbes (326). Furthermore, PCoA analysis in Figure 3C shows that bacterial community structure in GOD treatment groups was visibly separated from the control group, suggesting GOD treatment made a substantial impact on microbiota β diversity. The bar chart illustrates the compositions of microbiota at the phylum level in Figure 3D. The predominant phylum in the digest of the four groups was Firmicutes and Bacteroidetes. Compared to the control group, Firmicutes significantly increased in the GOD treatment groups ($p < 0.05$). The G3 group was distinguishable from the others because it had the highest relative abundance of Verrucomicrobiota, which could help the host maintain gut health. The relative abundance of Actinobacteriota was higher in the control and G2 groups than in the G1 and G3 groups.

At the genus level, Figure 4A shows GOD treatment increased the abundance of *Bacteroides*, *Faecalibacterium*,

10.3389/fmicb.2024.1439481

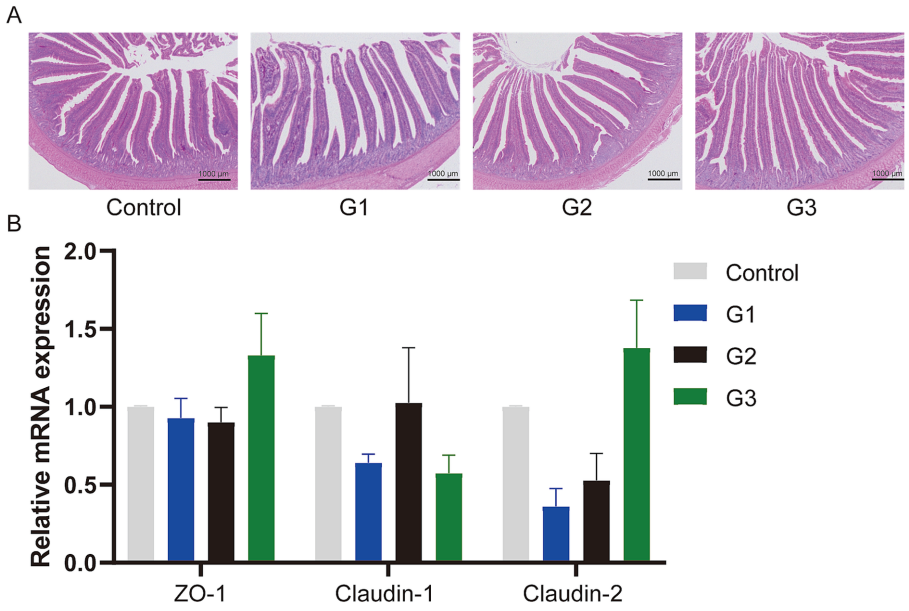

FIGURE 2
GOD enhanced the gut barrier function. (A) Jejunum tissue stained with hematoxylin and eosin (H&E) (microscope magnification 20×, bars = 1,000 μm). (B) The relative mRNA expression of Jejunum tissue. The results are presented as mean ± SD ($n = 6$).

TABLE 4 Effect of GOD on intestinal morphology of broilers (Jejunum).

Treatment[1]	Control	G1	G2	G3
Villus Height (μm)				
Duodenum	1447.02 ± 157.89[b]	1985.97 ± 195.10[a]	1624.01 ± 199.22[b]	1570.92 ± 171.09[b]
Jejunum	1292.42 ± 241.35	1480.32 ± 185.52	1394.97 ± 257.50	1561.05 ± 61.98
Ileum	1083.59 ± 86.20	1146.88 ± 62.20	1153.21 ± 232.83	1333.68 ± 57.82
Intestinal Crypt (μm)				
Duodenum	268.19 ± 67.49	283.50 ± 5.97	247.52 ± 36.04	325.12 ± 69.43
Jejunum	197.13 ± 68.01	197.33 ± 10.41	187.09 ± 54.72	253.48 ± 80.74
Ileum	153.99 ± 9.66	156.40 ± 16.55	157.81 ± 17.61	161.18 ± 41.95
V/C				
Duodenum	5.93 ± 0.92[b]	7.90 ± 1.25[a]	6.85 ± 0.20[ab]	5.21 ± 1.10[b]
Jejunum	7.41 ± 1.19	7.93 ± 1.19	8.16 ± 1.15	6.85 ± 2.14
Ileum	7.41 ± 0.22	8.36 ± 0.17	8.05 ± 1.18	9.36 ± 1.96

[1]Control, no additives; G1-3: GOD 4 U/g, 20 U/g, and 100 U/g. [a,b,c]Values within a row with different letters differ significantly ($p < 0.05$).

Methanocorpusculum, *Megamonas*, *Mucispirllum*, and *CHKCI001* while reducing the abundance of *Olsenella*, *Enorma*, and *Candidatus Vestibaculum*. Figure 4B shows the significant differences in bacteria from the phylum to the species level. Notably, we found that the G2 group increased the abundance of Clostridia at class level, Oscillospiraceae, Butyricicoccaceae at family level, *Omithinibacillus*, *V9D2013 group*, *Oscillospia*, *CHCKI001*, *Butyricicoccus*, *Sellimonas* in genus level, and *Bacteroides* sp. *Marseille P3166* in species level. Figure 4C uses a cladogram to visualize the specific difference between the four groups. Red represented the control group, and green, blue, and orange represented the G1, G2, and G3 groups, respectively.

3.5 GOD improved gut microbiota metabolic function

The metabolic functions of the gut microbiota were predicted using the KEGG pathway database with the Tax4Fun tool. Figures 5A,B show that the cecal bacterial metabolic functions (Level 1 and Level 2) in the G3 group were enriched in cellular processes (transport and catabolism, cell growth and death), genetic information processing (folding, sorting, and degradation), metabolism (carbohydrate metabolism, amino acid metabolism, glycan biosynthesis, and metabolism, enzyme families, lipid metabolism, and biosynthesis of other secondary metabolites), and the organismal system (endocrine system).

The results of the predicted function at Level 3 (Figure 5C) further showed that the high doses of GOD treatment enriched pathways related to starch and sucrose metabolism, amino sugar and nucleotide sugar metabolism, chaperones and folding catalysts, exosome function, alanine, aspartate, and glutamate metabolism, and peptidases. However, GOD also led to a reduction in ABC transporters, butanoate metabolism, cysteine and methionine metabolism, and ribosome biogenesis metabolic function in the G3 group.

TABLE 5 Effect of GOD on the α-diversity of intestinal microbiota in broilers (Cecal contents).

Item	Control	G1	G2	G3
Good's coverage	0.99 ± 0	0.99 ± 0	0.99 ± 0	0.99 ± 0
ASVs	356.0 ± 17.64	382.66 ± 23.06	443.50 ± 39.17	423.30 ± 34.43
Chao 1	400.92 ± 21.34	432,32 ± 31.41	483.72 ± 39.95	491.96 ± 33.24
Shannon	5.93 ± 0.13	5.99 ± 0.08	6.14 ± 0.20	5.74 ± 0.19
Simpson	0.96 ± 0.00 [a]	0.96 ± 0.00 [a]	0.96 ± 0.00 [a]	0.94 ± 0.00 [b]

[a,b]Values within a row with different letters differ significantly ($p < 0.05$).

3.6 Spearman correlation analysis revealed the relationship between the microbiota and basic index

To identify the main gut microorganisms for GOD to improve gut health, spearman correlation analysis was conducted to study the relationship among differential gut microbiota, growth performance, antioxidant parameters, tight junction protein mRNA expression, and V/C ratio. Figure 6 shows that *Methanobrevibacter* ($p < 0.01$) and *Megasphaera* ($p < 0.05$) were positively correlated with *Claudin-2* expression, and these two bacteria were enriched in the G2 and G3 groups. Meanwhile, the *Faecalibacterium* was positively correlated with the final weight, ADG, ADFI, *ZO-1*, and V/C of the ileum ($p < 0.05$). *Mucispirillum*, which was enriched in the G2 group, was positively correlated with the SOD ($p < 0.05$). *Enorma* had a negative relationship with ADFI, ADG, V/C ratio of ileum, and final weight of broilers in the control group ($p < 0.05$). Moreover, the *CHCKI001*, which was enhanced in the G3 group, showed a positive relationship with the ADG and the final weight ($p < 0.01$) and maintained a positive correlation with *ZO-1* expression ($p < 0.05$). These findings suggest these microorganisms play a significant role in improving gut health and the overall performance of the animals.

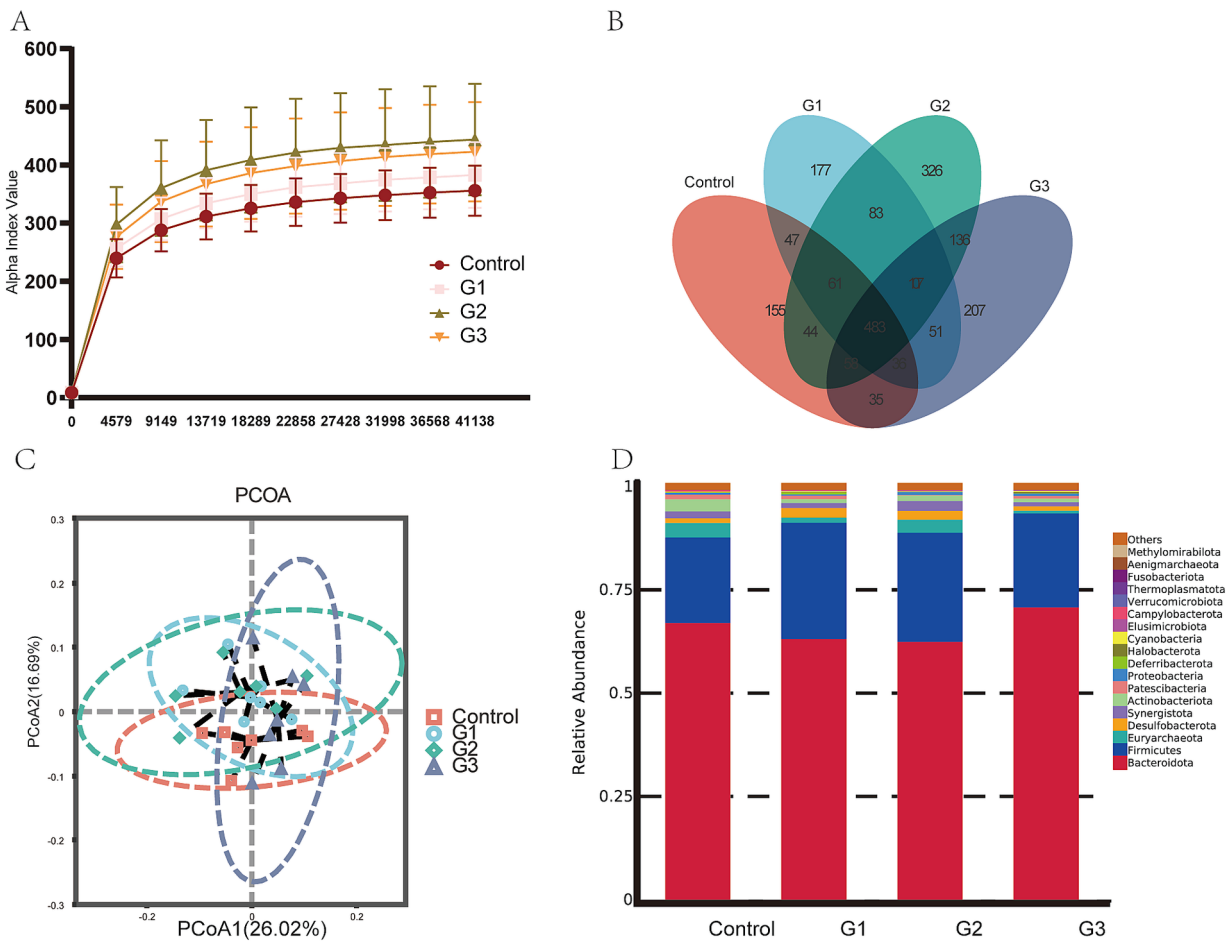

FIGURE 3
GOD influenced the gut microbiota in broilers (cecal contents) ($n = 6$). (A) Observed ASV line chart. (B) Venn diagram. (C) Principal coordinated analysis (PCoA). (D) Relative abundance bar chart in Phylum-level.

10.3389/fmicb.2024.1439481

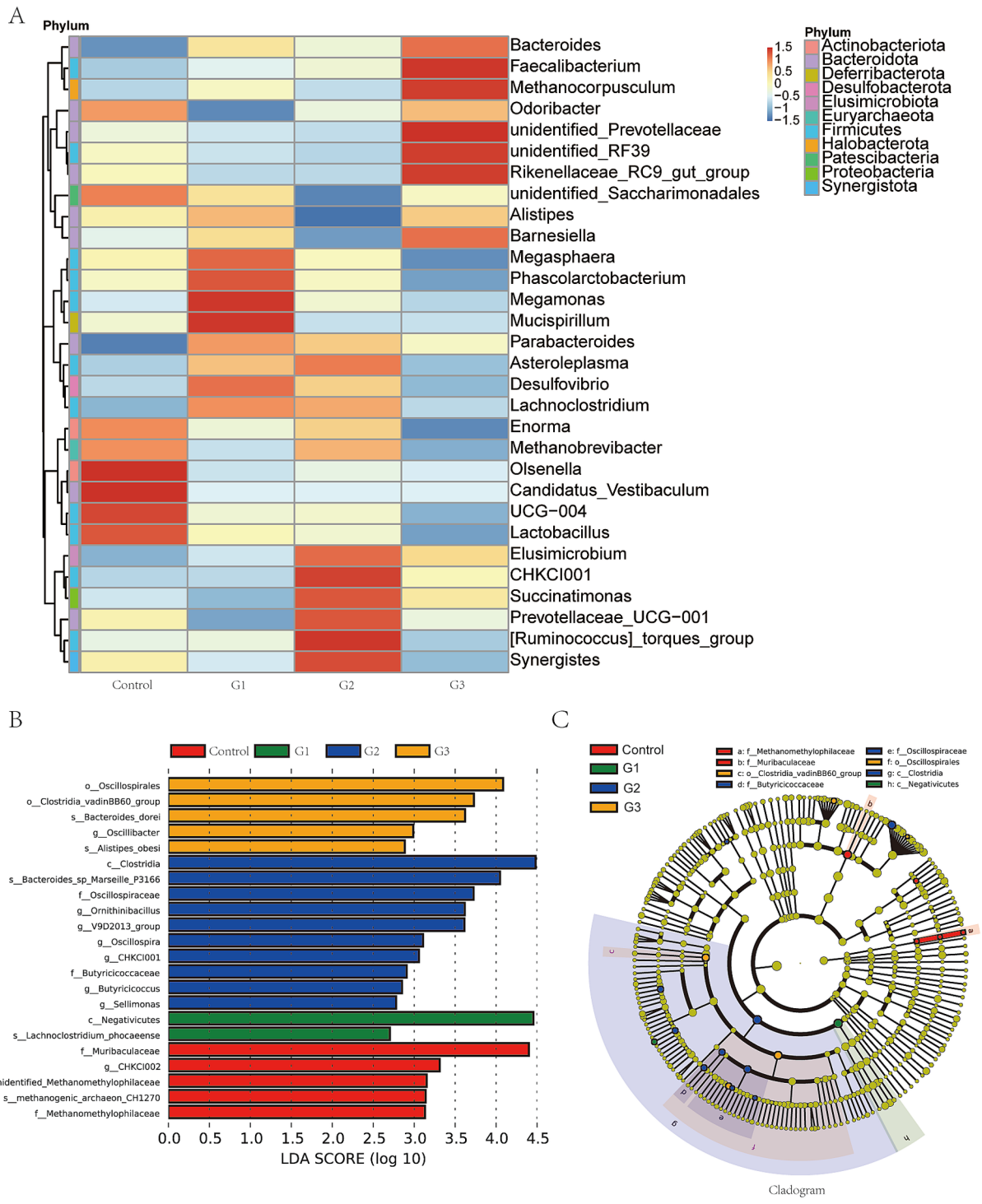

FIGURE 4
GOD altered the intestinal microbial community structure in broilers (cecal contents). (A) Heatmap in genus level. (B) Linear discriminant analysis LDA scores (> 2.5) were calculated for features at the amplicon sequence variance (ASV) level. Letters represented the taxonomy of the bacteria: p, phylum; c, class; o, order; f, family; g, genus. (C) Cladogram in genus level.

4 Discussion

GOD catalyzes the oxidation of β-D-glucose into gluconic acid, using atomic oxygen as the electron acceptor. This process concurrently generates hydrogen peroxide, which can enhance intestinal health. Some studies suggest that when GOD enters the gut with feed, it consumes oxygen (Kundu et al., 2013), creating a relatively anaerobic environment in the gut that eliminates pathogens. This environment increases villus height, decreases crypt depth, and enhances the surface area available for digestion and absorption in the intestinal tract. Relevant studies have proven that GOD can inhibit the growth and spore production of *Fusarium*

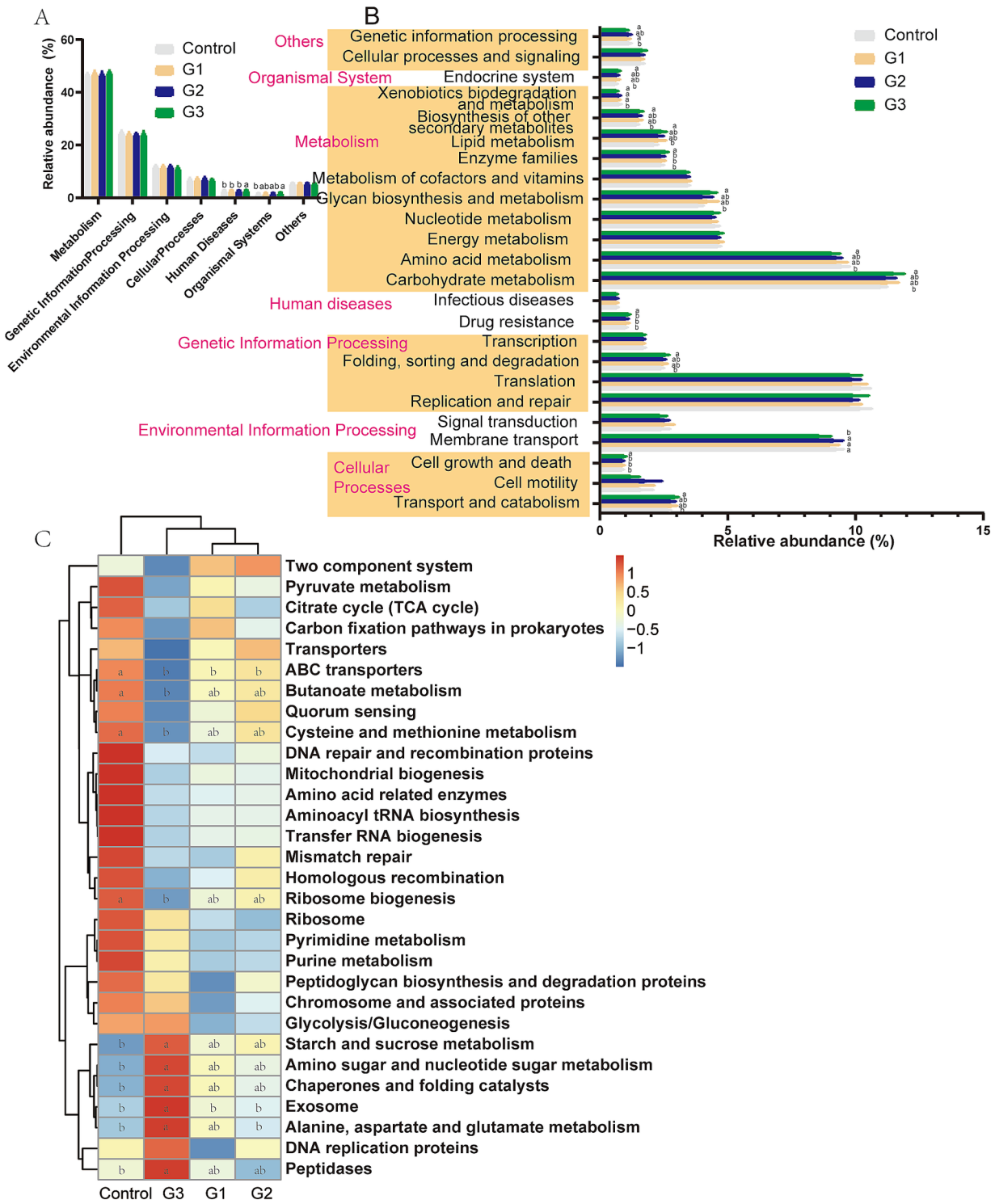

FIGURE 5
Dynamic bacterial functional profiles were analyzed by Tax4Fun (Cecal contents) ($n = 6$). (A) Metabolic pathways in level 1. (B) Metabolic pathways in level 2. (C) Functional predictions of the relative abundances of the top 30 metabolic functions (Level 3). a, b Means with a row with different superscripts significantly differ ($p < 0.05$).

solani (Kriaa et al., 2015). Additionally, another study confirmed that GOD could completely eliminate mastitis pathogens, with the exception of *Ps. aeruginosa* (Sandholm et al., 2010). Furthermore, due to the reduction in pathogens, the secretion of diamine oxidase and D-lactate decreased, which subsequently alleviated inflammation in intestinal epithelial cells caused by pathogens (Liu et al., 2020; Zhao et al., 2022). The increased villi height-to-crypt depth ratio also contributed to improved intestinal epithelial cell proliferation. Evidence shows that the gene expression of tight junction proteins (ZO-1, claudin-1, and claudin-2) was enhanced

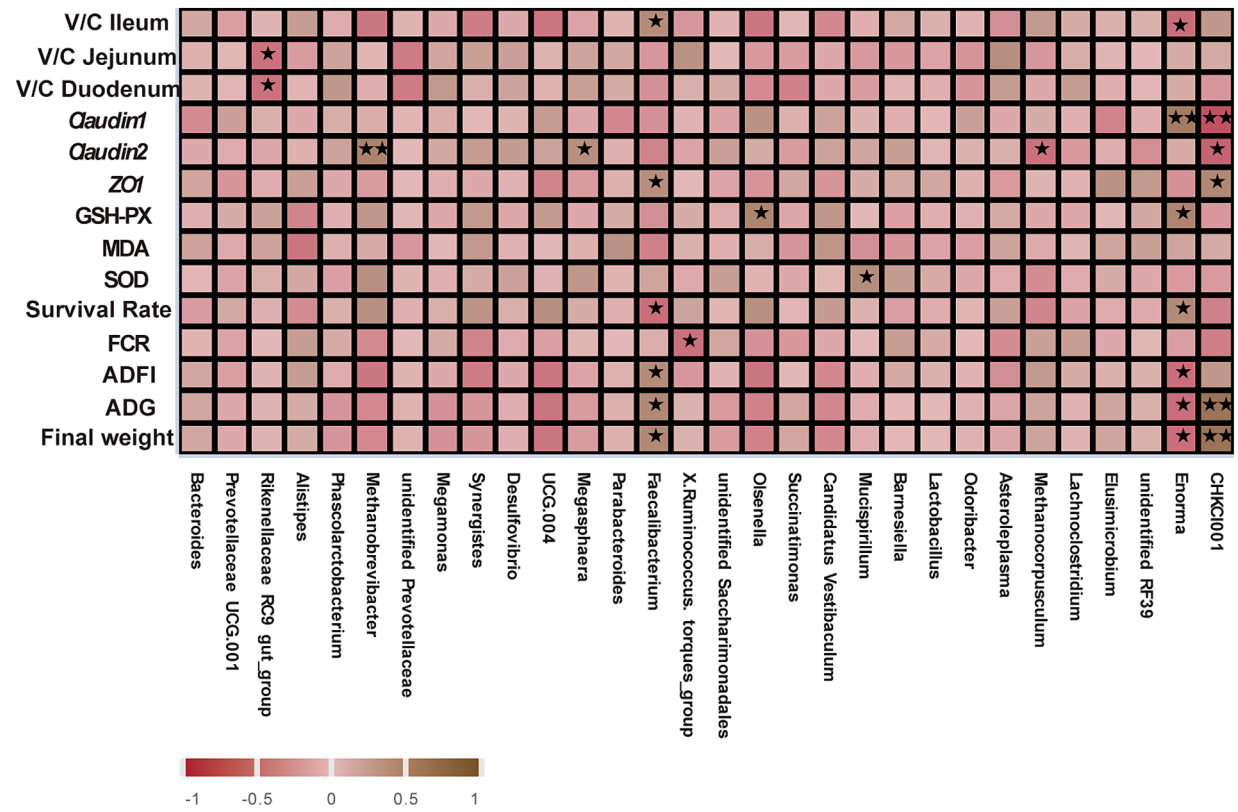

FIGURE 6
Spearman correlation analysis of gut bacteriomes (cecal contents), growth performance, antioxidant parameters, tight junction protein mRNA expression, and V/C. Significant correlation is represented by $^{**}0.001 < p < 0.01$, $^{*}0.01 < p < 0.05$, respectively. All the values contained six repetitions.

by the addition of GOD (Teng et al., 2020). The physical barrier of the gut is crucial for maintaining intestinal health (Wang et al., 2024), and GOD effectively maintains the expression of tight junction proteins and protects the integrity of intestinal villi. These findings suggest that GOD has the potential to improve digestive and absorptive functions by enhancing gut health.

Additionally, GOD's effectiveness at the macro level is reflected in the improved growth performance in animals. Numerous studies have reported that GOD treatment could increase growth performance, including ADG, ADFI, and the final weight. Zhao et al. found that the feed-to-gain ratio significantly decreased in the group supplied with 1,200 U/kg GOD (GOD1200) compared to the antibiotic group (Zhao et al., 2023). Wu et al. showed that the GOD-P treatment group, by modulating the intestinal microbiota, significantly increased ng ADG and ADFI in broiler chickens, improving meat quality at 21 and 42 days of age (Wu et al., 2020). Research has shown that the addition of 250 units of GOD per kilogram of feed can enhance weight gain in broiler chickens from 22 to 42 days of age, as well as increase the apparent ileal digestibility of certain amino acids (Meng et al., 2021). Wu et al. also found that broilers supplemented with GOD exhibited increased ADG, improved meat quality, and enhanced digestive capacity, with positive effects comparable to those observed in the group supplemented with antimicrobial growth promoters (AGPs) (Wu et al., 2019). However, some studies have reported no significant effects of GOD on growth performance in broilers. Meng et al. found that adding 500 or 1,000 units of GOD per kilogram of feed did not significantly affect ADG, ADFI, or other growth parameters (Meng et al., 2021). Similarly, Wang et al. reported that supplementing broiler diets with 75 U/kg of GOD did not have a significant impact on broilers' growth performance (Wang et al., 2018).

Other studies also presented that GOD could prevent the *Clostridium perfringens*, *E.coli*, or mycotoxin infection. 200 U/kg GOD in the diet has been shown to improve the growth performance of ducks infected with 3×10^9 CFU/mL *E.coli* O88 (Liu et al., 2020). GOD supplementation (150 U/kg) alleviated the decrease in the ADG and ADFI triggered by *Clostridium perfringens* infection (Zhao et al., 2022). Gao et al. discovered that exposure to Aflatoxin B1 (AFB1) and lipopolysaccharide (LPS) can lead to a reduction in the final body weight, ADG, and ADFI of broiler chickens, while supplementation with GOD or *Bacillus subtilis* has been shown to counteract the adverse effects of these toxins on the growth performance and FCR of broiler chickens (Gao et al., 2022). These studies demonstrate that appropriate doses of GOD can improve growth performance and prevent pathogen or mycotoxin infections in animals. However, they do not address the effects of excessive doses of GOD on animals. In the present study, we focused on growth performance and found that dietary supplementation with 100 U/g GOD significantly increased the final weight, ADG, and ADFI in broilers, a finding that has not been previously reported. Similarly, the G2 group with GOD supplementation of 25 U/g also showed the potential to increase broilers' growth performance.

Because of their high lipid content, broilers are susceptible to the generation of reactive oxygen species (ROS) (Bai et al., 2017). To counteract the excess ROS, two key antioxidant enzymes, SOD and GSH-Px, were utilized to neutralize the harmful effects of these

reactive molecules (Hasko et al., 2004). MDA was a metabolite from lipid peroxidation and a biomarker for oxidative stress (Cordiano et al., 2023). One study reported that 1,200 U/kg of GOD significantly increased SOD activity and decreased MDA levels (Zhao et al., 2023). Another study confirmed the same results, stating that GOD treatment significantly increased the activity of GSH-Px in the jejunal mucosa (Wang et al., 2022). In this study, we demonstrated that GOD could effectively alleviate oxidative stress induced by ROS, and 100 U/g GOD significantly increased GSH-Px concentration in broilers, confirming that high doses of GOD had positive effects on animals.

Enhancements in the nutritional quality of diets can significantly impact intestinal morphology and the functionality of the intestinal barrier (Schoultz and Keita, 2020). Intestinal morphology is primarily reflected in the villus height, crypt depth, and microvilli integrity. The intestinal mucosal barrier serves as the first line of defense against pathogens, with the core tight junction proteins complex, including ZO proteins (Zonula occludens) and claudin, playing an important role in maintaining this barrier's function (Chelakkot et al., 2018; König et al., 2016). *Enterotoxigenic Escherichia coli* (ETEC) challenges have been shown to increase serum alanine transaminase activity, leading to intestinal morphological damage and inflammation. However, GOD has been found to counteract these harmful effects (Wang et al., 2022). Meng et al. reported that the addition of 250 U/kg GOD improved intestinal morphology by increasing villus height and enhancing the villus height to crypt depth ratio, both key indicators of intestinal health (Meng et al., 2021). Regarding tight junction protein mRNA expression, Wang et al. showed that 75 U/kg GOD increased the expression of tight junction protein genes (Wang et al., 2018). Similarly, Liu et al. found that 200 U/kg GOD increased the expression of *ZO-1*, *Claudin-1,* and *Claudin-2* genes (Liu et al., 2020). Our current study corroborates these findings, showing that GOD helps maintain intestinal integrity by increasing villus height, reducing crypt depth, and promoting dense and intact microvilli while also upregulating the expression of tight junction protein-related genes. These results suggest that high doses of GOD do not cause adverse side effects in broilers and contribute to maintaining intestinal health. These studies demonstrate that GOD is a key factor in maintaining gut health. The main reasons can be summarized as follows: First, GOD consumes oxygen, creating an anaerobic gut environment that reduces the prevalence of pathogens, such as *Escherichia coli O88* and *Clostridium perfringens*, thereby preserving the gut's biological barrier function (Liu et al., 2020; Wang et al., 2022; Zhao et al., 2022). Second, GOD enhances the physical barrier of the gut by enhancing the integrity of intestinal villi, stimulating intestinal cell proliferation, and increasing the expression of tight junction proteins (Meng et al., 2021; Teng et al., 2020). Third, GOD supports immune function and reduces oxidative stress in intestinal cells by decreasing the release of inflammatory factors (IFN-γ, IL-1β, IL-6, and TNF-α) (Wang et al., 2018; Liu et al., 2020; Wang et al., 2022), promoting the secretion of anti-oxidative enzymes, including SOD, CAT, and GSH-Px, and reducing MDA concentrations, all of which contribute to the fundamental functions of the gut (Zhao et al., 2023; Qu and Liu, 2021). Inflammatory factors can cause significant intestinal damage, and maintaining a balance between pro-inflammatory and anti-inflammatory factors is crucial for the homeostasis of intestinal cells (Li et al., 2020; de et al., 2021; Wang et al., 2024). Enzymes such as SOD and GSH-Px are essential for removing excess ROS (Ko et al., 2004), and they have demonstrated significant benefits in animal models (Pamplona and Costantini, 2011).

Then, we show how GOD promotes gut microbial homeostasis. The cecal microbiota of broilers can influence the host's health and productivity, as the gut microbiota plays an essential role in maintaining gut health. Therefore, analyzing the microbiota could help identify its core components (Stanley et al., 2014). Analysis of microbial community alpha (α) and beta (β) diversity revealed significant differences in the cecal microbiota between the moldy corn group and the 0.01% GOD groups (Qu and Liu, 2021). Alpha diversity (Chao1, Shannon, Simpson index) often represents the species diversity of intestinal microorganisms. In our study, using 100 U/g GOD improved the diversity of microbiota by reducing the Simpson index. PCoA analysis revealed differences in beta diversity among these groups. There was a significant difference in the GOD treatment group compared to the control group, which indicated that the high doses of GOD reshape the gut microbiota in broilers. Wu et al. revealed significant alterations in the abundance of the phylum Firmicutes, the families Ruminococcaceae and Rikenellaceae, and the genus *Faecalibacterium*, specifically the species *F. prausnitzii* (Wu et al., 2019). Wang et al. found that treatment with GOD significantly increased the relative abundance of the *Bacteroides* genus, which play a crucial role in the breakdown of complex carbohydrates in the gut (Wang et al., 2022). 250 U/kg GOD treatment resulted in elevated relative abundances of the phylum Firmicutes, known for their role in digestion and energy homeostasis, and the genus *Lactobacillus*. These beneficial bacteria contribute to gut health. In contrast, the relative abundance of *Escherichia-Shigella* decreased (Meng et al., 2021). Similarly, the relative abundance of the Firmicutes phylum, another major group of gut bacteria, was observed to increase with the present GOD treatment. The alteration in microbiota composition may impact gut health and digestive efficiency. In the group treated with the GOD, the ratio of Bacteroidetes to Firmicutes was higher compared to the control group (Kim et al., 2021). In the group raised on thick bedding material with added 200 U/kg of GOD, the relative abundance of the Firmicutes and Bacteroidetes phyla in the gut microbiota was significantly higher at 42 days of age (Zhao et al., 2021). These findings suggest that GOD can promote a balanced and diverse gut microbiota, which is essential for maintaining optimal gut health and enhancing digestive efficiency in broilers.

Furthermore, *Akkermansia muciniphila* is the predominant member in the Verrucomicrobiota, which proves that it had a strong positive correlation with gut health (Han and Zhuang, 2021), and Verrucomicrobiota significantly increased in the high doses GOD treatment group. *Actinobacillus* spp., associated with causing abortion, metritis, and reduced litter sizes in animals, notably decreased in the GOD group (Rycroft and Garside, 2000). The *Faecalibacterium* enriched in the G3 group is a potential novel probiotic bacterium for human diseases such as inflammatory bowel disease (IBD) (Miquel et al., 2013). *Olsenella* has a high positive relationship with obesity (Kong et al., 2019), which is reduced in the present GOD treatment groups, proving that normal or high doses of GOD addition could modulate the gut microbiota. *Enorma* is a bacterial genus often found in groups receiving long-term AGP supplements, but its abundance was reduced in the GOD-supplemented group (Dubourg et al., 2014). Chen et al. researched the fact that fermented feed groups increase the abundance of *CHCKI001* and *Faecalibacterium* in laying hens (Chen et al., 2023). The evidence confirms that the supplementation of GOD, whether at a normal or high level, effectively modulates the gut microbiota in broilers, causing no adverse effects during the farming process.

GOD-induced changes in the hindgut microbiota also led to alterations in microbial metabolic function. Jiang et al. used the

same method to introduce the metabolic function of bacteria and understand the main pathway affected by probiotics (Jiang et al., 2021). Su et al. also used the metabolic function prediction to illustrate the dynamic changes of fermented feed during a two-stage solid-state fermentation process (Su et al., 2021). Enhanced carbohydrate metabolism (starch and sucrose metabolism), amino acid metabolism (amino sugar and nucleotide sugar metabolism, alanine aspartate and glutamate metabolism), glycan biosynthesis and metabolism, enzyme families (peptidases), lipid metabolism and exosome, and biosynthesis of other secondary metabolites presented that the 100 U/g GOD treatment effectively improved the metabolism function in broilers. An explanation for these metabolic function predictions is that GOD promotes probiotic proliferation and inhibits pathogens, enhancing nutrient digestibility and absorption.

A correlation analysis was conducted to identify the main gut microorganisms that GOD can use to improve gut health. Su et al. conducted a correlation analysis and discovered that the fermented feed produced butyric acid, which plays an essential role in maintaining gut immune function (Su et al., 2022). Jiang et al. utilized a specific methodological approach to demonstrate that the probiotic strain BA40 improved the growth performance of piglets, and this improvement was found to be positively correlated with the abundance of *Phascolarctobacterium*, a genus of bacteria known to be beneficial in the gastrointestinal tract (Jiang et al., 2023). Correlation analysis suggested that GOD-driven *Faecalibacterium*, *CHKCI001,* and *Mucispirllum* improved the gut health of broilers. At the genus level, *Mucispirllum* abundance was decreased significantly in response to DSS-induced colitis (Jiang et al., 2024). *Faecalibacterium* is a promising anti-inflammatory bacterium that colonizes the gut and plays an important role in the pathogenesis of IBD (Zhou et al., 2021). The correlation analysis suggested that the *Enorma*, which decreased with GOD treatment, was negatively correlated with growth performance. These findings imply that high doses of GOD can also benefit the microbial community and enhance gut health by modulating microbiota functions. Researchers utilized the Spearman correlation coefficient to explore the relationships between specific bacterial species and various outcomes. This approach helped to elucidate the complex interactions between gut microbiota and host health, providing valuable insights into the mechanisms by which GOD enhances gut health and overall performance in broilers.

5 Conclusion

In this study, the results of the broilers model, along with the assessment of antioxidant ability and intestinal morphology, demonstrated that GOD supplementation benefited ADG, ADFI, FCR, antioxidant function, and gut morphology. Additionally, GOD enhanced the abundance of beneficial gut probiotics, such as *Faecalibacterium*, and promoted microbial carbohydrate metabolism, particularly in starch and sucrose pathways. Correlation analysis identified *Faecalibacterium* and *CHCKI001* as two key microbial effectors contributing to the improvements in growth performance and gut health induced by GOD. These beneficial outcomes were achieved with a 100 U/g GOD supplementation, which did not exhibit any adverse effects. Notably, the high-dose GOD supplementation had a significant positive impact on broiler health and performance. Consequently, applying higher GOD doses could be advantageous in poultry and livestock farming. This foundational evidence offers valuable guidance for the practical use of high-dose GOD as an effective feed additive.

Data availability statement

The datasets presented in this study can be found in online repositories. The names of the repository/repositories and accession number(s) can be found in the article/Supplementary material.

Ethics statement

The animal studies were approved by the Institutional Animal Care and use Committee of Guangdong VTR Biotech. The studies were conducted in accordance with the local legislation and institutional requirements. Written informed consent was obtained from the owners for the participation of their animals in this study.

Author contributions

ZJ: Conceptualization, Formal analysis, Investigation, Methodology, Software, Visualization, Writing – original draft, Writing – review & editing, Data curation, Validation. ZH: Funding acquisition, Methodology, Resources, Writing – review & editing. HD: Funding acquisition, Methodology, Resources, Writing – review & editing. YaL: Data curation, Project administration, Resources, Writing – review & editing. MW: Data curation, Methodology, Software, Writing – review & editing. DC: Data curation, Formal analysis, Investigation, Writing – review & editing. JL: Formal analysis, Investigation, Writing – review & editing. GL: Methodology, Writing – review & editing. LM: Formal analysis, Investigation, Methodology, Software, Writing – review & editing. YuL: Methodology, Software, Writing – review & editing. WL: Investigation, Resources, Supervision, Writing – review & editing. BY: Investigation, Supervision, Writing – review & editing. YG: Formal analysis, Funding acquisition, Methodology, Project administration, Resources, Writing – review & editing.

Funding

The author(s) declare that financial support was received for the research, authorship, and/or publication of this article. This research was supported by the Zhuhai Science and Technology Programme Key Funding Projects in the Social Development Field——Research on Quantitative Feed enzyme preparations for Improving Livestock and Poultry culture benefit (Project number: 2320004000138), Enzyme-probiotics combination on the pre-digestion treatment of feed ingredients and its effect on the intestinal health of piglets and the mechanism research (Project number: 2420004000196).

Conflict of interest

ZJ, ZH, HD, YaL, MW, DC, JL, GL, LM, YuL, WL, and YG were employed by Guangdong VTR Bio-tech Co., Ltd.

The remaining author declares that the research was conducted in the absence of any commercial or financial relationships that could be construed as a potential conflict of interest.

Publisher's note

All claims expressed in this article are solely those of the authors and do not necessarily represent those of their affiliated organizations, or those of the publisher, the editors and the reviewers. Any product that may be evaluated in this article, or claim that may be made by its manufacturer, is not guaranteed or endorsed by the publisher.

Supplementary material

The Supplementary material for this article can be found online at: https://www.frontiersin.org/articles/10.3389/fmicb.2024.1439481/full#supplementary-material

References

Bai, K., Huang, Q., Zhang, J., He, J., Zhang, L., and Wang, T. (2017). Supplemental effects of probiotic *Bacillus subtilis* fmbJ on growth performance, antioxidant capacity, and meat quality of broiler chickens. *Poult. Sci.* 96, 74–82. doi: 10.3382/ps/pew246

Bankar, S. B., Bule, M. V., Singhal, R. S., and Ananthanarayan, L. (2009). Glucose oxidase--an overview. *Biotechnol. Adv.* 27, 489–501. doi: 10.1016/j.biotechadv.2009.04.003

Chelakkot, C., Ghim, J., and Ryu, S. H. (2018). Mechanisms regulating intestinal barrier integrity and its pathological implications. *Exp. Mol. Med.* 50, 1–9. doi: 10.1038/s12276-018-0126-x

Chen, X., Zhou, X., Li, S., Zhang, H., and Liu, Z. (2023). Effects of tea residues-fermented feed on production performance, egg quality, antioxidant capacity, caecal microbiota, and ammonia emissions of laying hens. *Front. Vet. Sci.* 10:1195074. doi: 10.3389/fvets.2023.1195074

Cordiano, R., di Gioacchino, M., Mangifesta, R., Panzera, C., Gangemi, S., and Minciullo, P. L. (2023). Malondialdehyde as a potential oxidative stress marker for allergy-oriented diseases: an update. *Molecules* 28:979. doi: 10.3390/molecules28165979

Dang, D. X., Hoque, M. R., Liu, Y., Chen, N., and Kim, I. H. (2021). Dietary glucose oxidase supplementation improves growth performance, apparent nutrient digestibility, and serum antioxidant enzyme parameters in growing pigs. *Ital. J. Anim. Sci.* 20, 1568–1574. doi: 10.1080/1828051x.2021.1984853

de, A., Chen, W., Li, H., Wright, J. R., Lamendella, R., Lukin, D. J., et al. (2021). Bacterial Swarmers enriched during intestinal stress ameliorate damage. *Gastroenterology* 161, 211–224. doi: 10.1053/j.gastro.2021.03.017

Ding, Y., Wang, C., Ma, Y., Zhu, L., Lu, B., Wang, Y., et al. (2022). Tumor microenvironment responsive polypeptide-based supramolecular nanoprodrugs for combination therapy. *Acta Biomater.* 146, 396–405. doi: 10.1016/j.actbio.2022.04.027

Dubourg, G., Lagier, J. C., Robert, C., Armougom, F., Hugon, P., Metidji, S., et al. (2014). Culturomics and pyrosequencing evidence of the reduction in gut microbiota diversity in patients with broad-spectrum antibiotics. *Int. J. Antimicrob. Agents* 44, 117–124. doi: 10.1016/j.ijantimicag.2014.04.020

Edgar, R. C., and Flyvbjerg, H. (2015). Error filtering, pair assembly and error correction for next-generation sequencing reads. *Bioinformatics* 31, 3476–3482. doi: 10.1093/bioinformatics/btv401

Gao, S., Zhang, L., Zhu, D., Huang, J., Yang, J., Jiang, J., et al. (2022). Effects of glucose oxidase and *Bacillus subtilis* on growth performance and serum biochemical indicexs of broilers exposed to aflatoxin B1 and endotoxin. *Anim. Feed Sci. Technol.* 286:115186. doi: 10.1016/j.anifeedsci.2021.115186

Han, W., and Zhuang, X. (2021). Research progress on the next-generation probiotic *Akkermansia muciniphila* in the intestine. *Food Front.* 2, 443–448. doi: 10.1002/fft2.87

Hao, L., Cheng, Y., Su, W., Wang, C., Lu, Z., Jin, M., et al. (2021). *Pediococcus pentosaceus* ZJUAF-4 relieves oxidative stress and restores the gut microbiota in diquat-induced intestinal injury. *Appl. Microbiol. Biotechnol.* 105, 1657–1668. doi: 10.1007/s00253-021-11111-6

Hasko, G., Sitkovsky, M. V., and Szabo, C. (2004). Immunomodulatory and neuroprotective effects of inosine. *Trends Pharmacol. Sci.* 25, 152–157. doi: 10.1016/j.tips.2004.01.006

Jiang, Z., Li, W., Su, W., Wen, C., Gong, T., Zhang, Y., et al. (2021). Protective effects of *Bacillus amyloliquefaciens* 40 against *Clostridium perfringens* infection in mice. *Front. Nutr.* 8:733591. doi: 10.3389/fnut.2021.733591

Jiang, N., Liu, Z., Wang, H., Zhang, L., Li, M., Li, G., et al. (2024). Alterations in metabolome and microbiome: new clues on cathelicidin-related antimicrobial peptide alleviates acute ulcerative colitis. *Front. Microbiol.* 15:1306068. doi: 10.3389/fmicb.2024.1306068

Jiang, Z., Su, W., Li, W., Wen, C., du, S., He, H., et al. (2023). *Bacillus amyloliquefaciens* 40 regulates piglet performance, antioxidant capacity, immune status, and gut microbiota. *Anim. Nutr.* 12, 116–127. doi: 10.1016/j.aninu.2022.09.006

Kim, D., Yu, J., Wang, E. K., Lee, S., Kim, J. S., Hwang, J., et al. (2021). Potential of an enzyme mixture of glucose oxidase, Glucosyl transferase, and Fructosyl transferase as an antidiabetic medicine. *Biomedicines* 9:745. doi: 10.3390/biomedicines9070745

Ko, Y. H., Yang, H. Y., and Jang, I. S. (2004). Effect of conjugated linoleic acid on intestinal and hepatic antioxidant enzyme activity and lipid peroxidation in broiler chickens. *Asian Australas. J. Anim. Sci.* 17, 1162–1167. doi: 10.5713/ajas.2004.1162

Kong, C., Gao, R., Yan, X., Huang, L., and Qin, H. (2019). Probiotics improve gut microbiota dysbiosis in obese mice fed a high-fat or high-sucrose diet. *Nutrition* 60, 175–184. doi: 10.1016/j.nut.2018.10.002

König, J., Wells, J., Cani, P. D., García-Ródenas, C. L., MacDonald, T., Mercenier, A., et al. (2016). Human intestinal barrier function in health and disease. *Clin. Transl. Gastroenterol.* 7:e196. doi: 10.1038/ctg.2016.54

Kriaa, M., Hammami, I., Sahnoun, M., Azebou, M. C., Triki, M. A., and Kammoun, R. (2015). Biocontrol of tomato plant diseases caused by *Fusarium solani* using a new isolated aspergillus tubingensis CTM 507 glucose oxidase. *C. R. Biol.* 338, 666–677. doi: 10.1016/j.crvi.2015.05.007

Kundu, N., Yadav, S., and Pundir, C. S. (2013). Preparation and characterization of glucose oxidase nanoparticles and their application in dissolved oxygen metric determination of serum glucose. *J. Nanosci. Nanotechnol.* 13, 1710–1716. doi: 10.1166/jnn.2013.7102

Li, S., Li, X., Wang, K., Li, Y., Nagaoka, K., and Li, C. (2023). Gut microbiota intervention attenuates thermogenesis in broilers exposed to high temperature through modulation of the hypothalamic 5-HT pathway. *J. Anim. Sci. Biotechnol.* 14:159. doi: 10.1186/s40104-023-00950-0

Li, T., Wang, C., Liu, Y., Li, B., Zhang, W., Wang, L., et al. (2020). Neutrophil extracellular traps induce intestinal damage and thrombotic tendency in inflammatory bowel disease. *J. Crohn's Colitis* 14, 240–253. doi: 10.1093/ecco-jcc/jjz132

Liang, Z., Yan, Y., Zhang, W., Luo, H., Yao, B., Huang, H., et al. (2023). Review of glucose oxidase as a feed additive: production, engineering, applications, growth-promoting mechanisms, and outlook. *Crit. Rev. Biotechnol.* 43, 698–715. doi: 10.1080/07388551.2022.2057275

Liu, J., Liu, G., Chen, Z., Zheng, A., Cai, H., Chang, W., et al. (2020). Effects of glucose oxidase on growth performance, immune function, and intestinal barrier of ducks infected with *Escherichia coli* O88. *Poult. Sci.* 99, 6549–6558. doi: 10.1016/j.psj.2020.09.038

Mano, N. (2019). Engineering glucose oxidase for bioelectrochemical applications. *Bioelectrochemistry* 128, 218–240. doi: 10.1016/j.bioelechem.2019.04.015

Meng, Y., Huo, H., Zhang, Y., Bai, S., Wang, R., Zhang, K., et al. (2021). Effects of dietary glucose oxidase supplementation on the performance, apparent Ileal amino acids digestibility, and Ileal microbiota of broiler chickens. *Animals (Basel)* 11:909. doi: 10.3390/ani11102909

Miquel, S., Martín, R., Rossi, O., Bermúdez-Humarán, L. G., Chatel, J. M., Sokol, H., et al. (2013). *Faecalibacterium prausnitzii* and human intestinal health. *Curr. Opin. Microbiol.* 16, 255–261. doi: 10.1016/j.mib.2013.06.003

Novoa Rama, E., Bailey, M., Kumar, S., Leone, C., den Bakker, H. C., Thippareddi, H., et al. (2023). Characterizing the gut microbiome of broilers raised under conventional and no antibiotics ever practices. *Poult. Sci.* 102:102832. doi: 10.1016/j.psj.2023.102832

Pamplona, R., and Costantini, D. (2011). Molecular and structural antioxidant defenses against oxidative stress in animals. *Am. J. Phys. Regul. Integr. Comp. Phys.* 301, R843–R863. doi: 10.1152/ajpregu.00034.2011

Qu, W., and Liu, J. (2021). Effects of glucose oxidase supplementation on the growth performance, Antioxidative and inflammatory status, gut function, and microbiota composition of broilers fed moldy corn. *Front. Physiol.* 12:646393. doi: 10.3389/fphys.2021.646393

Rycroft, A. N., and Garside, L. H. (2000). *Actinobacillus* species and their role in animal disease. *Vet. J.* 159, 18–36. doi: 10.1053/tvjl.1999.0403

Sandholm, M., Ali-Vehmas, T., Kaartinen, L., and Junnila, M. (2010). Glucose oxidase (GOD) as a source of hydrogen peroxide for the Lactoperoxidase (LPO) system in Milk:

antibacterial effect of the GOD-LPO system against mastitis pathogens. *J. Veterinary Med. Ser. B* 35, 346–352. doi: 10.1111/j.1439-0450.1988.tb00506.x

Schoultz, I., and Keita, A. V. (2020). The intestinal barrier and current techniques for the assessment of gut permeability. *Cells* 9:909. doi: 10.3390/cells9081909

Shi, D., Bai, L., Qu, Q., Zhou, S., Yang, M., Guo, S., et al. (2019). Impact of gut microbiota structure in heat-stressed broilers. *Poult. Sci.* 98, 2405–2413. doi: 10.3382/ps/pez026

Stanley, D., Hughes, R. J., and Moore, R. J. (2014). Microbiota of the chicken gastrointestinal tract: influence on health, productivity and disease. *Appl. Microbiol. Biotechnol.* 98, 4301–4310. doi: 10.1007/s00253-014-5646-2

Su, W., Jiang, Z., Hao, L., Li, W., Gong, T., Zhang, Y., et al. (2021). Variations of soybean meal and corn mixed substrates in physicochemical characteristics and microbiota during two-stage solid-state fermentation. *Front. Microbiol.* 12:688839. doi: 10.3389/fmicb.2021.688839

Su, W., Jiang, Z., Wang, C., Xu, B., Lu, Z., Wang, F., et al. (2022). Dynamics of defatted rice bran in physicochemical characteristics, microbiota and metabolic functions during two-stage co-fermentation. *Int. J. Food Microbiol.* 362:109489. doi: 10.1016/j.ijfoodmicro.2021.109489

Su, W., Jiang, Z., Wang, C., Zhang, Y., Gong, T., Wang, F., et al. (2022). Co-fermented defatted rice bran alters gut microbiota and improves growth performance, antioxidant capacity, immune status and intestinal permeability of finishing pigs. *Anim. Nutr.* 11, 413–424. doi: 10.1016/j.aninu.2022.07.008

Sun, X., Piao, L., Jin, H., Nogoy, K. M. C., Zhang, J., Sun, B., et al. (2022). Effects of dietary supplementation of glucose oxidase, catalase, or both on reproductive performance, oxidative stress, fecal microflora and apoptosis in multiparous sows. *Anim Biosci* 35, 75–86. doi: 10.5713/ab.20.0839

Tang, H., Yao, B., Gao, X., Yang, P., Wang, Z., and Zhang, G. (2016). Effects of glucose oxidase on the growth performance, serum parameters and faecal microflora of piglets. *S. Afr. J. Anim. Sci.* 46:14. doi: 10.4314/sajas.v46i1.2

Teng, P.-Y., Yadav, S., Castro, F. L. S., Tompkins, Y. H., Fuller, A. L., and Kim, W. K. (2020). Graded Eimeria challenge linearly regulated growth performance, dynamic change of gastrointestinal permeability, apparent ileal digestibility, intestinal morphology, and tight junctions of broiler chickens. *Poult. Sci.* 99, 4203–4216. doi: 10.1016/j.psj.2020.04.031

Tu, T., Wang, Y., Huang, H., Wang, Y., Jiang, X., Wang, Z., et al. (2019). Improving the thermostability and catalytic efficiency of glucose oxidase from aspergillus Niger by molecular evolution. *Food Chem.* 281, 163–170. doi: 10.1016/j.foodchem.2018.12.099

Wang, Y., Wang, J., Leng, F., Ma, J., and Bagadi, A. (2020). Expression of aspergillus Niger glucose oxidase in Pichia pastoris and its antimicrobial activity against *Agrobacterium* and *Escherichia coli*. *PeerJ* 8:e9010. doi: 10.7717/peerj.9010

Wang, Q., Wang, F., Tang, L., Wang, Y., Zhou, Y., Li, X., et al. (2024). *Bacillus amyloliquefaciens* SC06 alleviated intestinal damage induced by inflammatory via modulating intestinal microbiota and intestinal stem cell proliferation and differentiation. *Int. Immunopharmacol.* 130:111675. doi: 10.1016/j.intimp.2024.111675

Wang, Y., Wang, Y., Xu, H., Mei, X., Gong, L., Wang, B., et al. (2018). Direct-fed glucose oxidase and its combination with *B. amyloliquefaciens* SC06 on growth performance, meat quality, intestinal barrier, antioxidative status, and immunity of yellow-feathered broilers. *Poult. Sci.* 97, 3540–3549. doi: 10.3382/ps/pey216

Wang, Y., Wang, B., Zhan, X., Wang, Y., and Li, W. (2022). Effects of glucose oxidase and its combination with *B. amyloliquefaciens* SC06 on intestinal microbiota, immune response and antioxidative capacity in broilers. *Animal* 16:100473. doi: 10.1016/j.animal.2022.100473

Wang, W., Xie, R., Cao, Q., Ye, H., Zhang, C., Dong, Z., et al. (2022). Effects of glucose oxidase on growth performance, clinical symptoms, serum parameters, and intestinal health in piglets challenged by enterotoxigenic *Escherichia coli*. *Front. Microbiol.* 13:994151. doi: 10.3389/fmicb.2022.994151

Wang, Z., Xie, N., Liang, X., Shu, Q., Hong, Y., Shi, H., et al. (2024). Gut mechanoimmunology: shaping immune response through physical cues. *Phys Life Rev* 50, 13–26. doi: 10.1016/j.plrev.2024.05.003

Wu, S., Chen, X., Li, T., Ren, H., Zheng, L., and Yang, X. (2020). Changes in the gut microbiota mediate the differential regulatory effects of two glucose oxidases produced by aspergillus Niger and Penicillium amagasakiense on the meat quality and growth performance of broilers. *J. Anim. Sci. Biotechnol.* 11:73. doi: 10.1186/s40104-020-00480-z

Wu, S., Li, T., Niu, H., Zhu, Y., Liu, Y., Duan, Y., et al. (2019). Effects of glucose oxidase on growth performance, gut function, and cecal microbiota of broiler chickens. *Poult. Sci.* 98, 828–841. doi: 10.3382/ps/pey393

Yue Wang, X. C., Jiang, S., Gao, L., Han, X., Qu, J., Jiang, X., et al. (2023). Engineering the substrate preference of glucose oxidase for the enzymatic oxidation of xylose. *Green Chem.* 26, 4851–4859. doi: 10.1039/d3gc04981g

Zhang, J., Liu, Y., Yang, Z., Yang, W., Huang, L., Xu, C., et al. (2020). *Illicium verum* extracts and probiotics with added glucose oxidase promote antioxidant capacity through upregulating hepatic and jejunal Nrf2/Keap1 of weaned piglets. *J. Anim. Sci.* 98:77. doi: 10.1093/jas/skaa077

Zhao, Y., Fu, J., Li, P., Chen, N., Liu, Y., Liu, D., et al. (2022). Effects of dietary glucose oxidase on growth performance and intestinal health of AA broilers challenged by *Clostridium perfringens*. *Poult. Sci.* 101:101553. doi: 10.1016/j.psj.2021.101553

Zhao, W., Huang, Y., Cui, N., Wang, R., Xiao, Z., and Su, X. (2023). Glucose oxidase as an alternative to antibiotic growth promoters improves the immunity function, antioxidative status, and cecal microbiota environment in white-feathered broilers. *Front. Microbiol.* 14:1100465. doi: 10.3389/fmicb.2023.1100465

Zhao, Y., Li, P., Chen, N., Liu, Y., Liu, D., and Guo, Y. (2021). Effects of housing systems and glucose oxidase on growth performance and intestinal health of Beijing you chickens. *Poult. Sci.* 100:100943. doi: 10.1016/j.psj.2020.12.040

Zhao, L., Wang, L., Zhang, Y., Xiao, S., Bi, F., Zhao, J., et al. (2017). Glucose oxidase-based glucose-sensitive drug delivery for diabetes treatment. *Polymers* 9:255. doi: 10.3390/polym9070255

Zhou, Y., Xu, H., Xu, J., Guo, X., Zhao, H., Chen, Y., et al. (2021). *F. prausnitzii* and its supernatant increase SCFAs-producing bacteria to restore gut dysbiosis in TNBS-induced colitis. *AMB Express* 11:33. doi: 10.1186/s13568-021-01197-6

frontiers | Frontiers in Microbiology

TYPE Original Research
PUBLISHED 30 October 2024
DOI 10.3389/fmicb.2024.1453145

Check for updates

OPEN ACCESS

EDITED BY
Jason W. Soares,
Combat Capabilities Development Command United States Army, United States

REVIEWED BY
Yafei Duan,
South China Sea Fisheries Research Institute, China
Jordan Whitman,
Combat Capabilities Development Command United States Army, United States

*CORRESPONDENCE
Yuxiang Shi
✉ hbyxshi@126.com

RECEIVED 22 June 2024
ACCEPTED 04 October 2024
PUBLISHED 30 October 2024

CITATION
Yang S, Huo M, Su Z, Wang F, Zhang Y, Zhong C and Shi Y (2024) The impact of dietary supplementation of Quercetagetin on growth, antioxidant capacity, and gut microbiota of diquat-challenged broilers. *Front. Microbiol.* 15:1453145. doi: 10.3389/fmicb.2024.1453145

COPYRIGHT
© 2024 Yang, Huo, Su, Wang, Zhang, Zhong and Shi. This is an open-access article distributed under the terms of the Creative Commons Attribution License (CC BY). The use, distribution or reproduction in other forums is permitted, provided the original author(s) and the copyright owner(s) are credited and that the original publication in this journal is cited, in accordance with accepted academic practice. No use, distribution or reproduction is permitted which does not comply with these terms.

The impact of dietary supplementation of Quercetagetin on growth, antioxidant capacity, and gut microbiota of diquat-challenged broilers

Shuo Yang, Min Huo, Zixuan Su, Fangfang Wang, Yongying Zhang, Cuihong Zhong and Yuxiang Shi*

College of Life Science and Food Engineering, Hebei University of Engineering, Handan, China

This experiment aimed to investigate the effects of Quercetagetin (QG) on the growth performance, antioxidant capacity, and cecal microbiota of broilers. Two hundred and forty 21-day-old WOD168 broilers with similar body weights were randomly divided into five groups of six replicates each with eight chickens. The control group was fed a basal diet composed of corn and soybean meal, while the experimental groups received basal diets supplemented with 0, 10, 20, and 40 mg/kg QG, along with intraperitoneal injection of 20 mg/kg body weight Diquat (DQ). The experiment lasted for 21 days. The results showed that: (1) QG significantly alleviated the decrease in average daily feed intake and average daily gain induced by Diquat, reduced the elevation of serum ACTH content, and significantly increased GH content ($P < 0.05$); (2) QG supplementation significantly mitigated the decrease in serum CAT activity and duodenal GSH-Px activity induced by Diquat ($P < 0.05$), as well as the increase in MDA content ($P < 0.05$); additionally, QG significantly increased the gene expression levels of *GSH-Px*, *Nrf2*, and *Keap1* ($P < 0.05$); (3) Alpha and Beta diversity analysis revealed that QG supplementation significantly increased the cecal microbial OTUs and Chao1 index of broilers ($P < 0.05$). At the phylum level, compared with the Diquat group, the LQG group significantly decreased the relative abundance of Firmicutes ($P < 0.05$) and significantly increased the relative abundance of Bacteroidota ($P < 0.05$). At the genus level, compared with the CON group, the Diquat group significantly decreased the abundance of *Lactobacillus* and *Alistipes* ($P < 0.05$), while QG supplementation significantly alleviated the decrease in the abundance of *Lactobacillus* and *Alistipes* ($P < 0.05$). In conclusion, the addition of an appropriate amount (20 mg/kg) of QG to the diet can promote the growth of broilers, enhance antioxidant capacity, and improve intestinal health.

KEYWORDS

Quercetagetin, broilers, growth performance, antioxidant capacity, microbial community

1 Introduction

In recent years, the intensification of poultry production systems has introduced a range of health challenges, with oxidative stress becoming a central issue. This condition arises from an imbalance between reactive oxygen species (ROS) production and the antioxidant defense mechanisms within the organism. The resulting oxidative stress impairs the health, growth performance, and overall productivity of poultry, particularly in high-density, intensive farming environments. Addressing the underlying mechanisms of oxidative stress and developing effective mitigation strategies are vital steps toward improving animal welfare and ensuring the long-term sustainability of poultry production systems.

The scale and intensification of breeding models has become the norm in modern animal husbandry. However, this approach has also led to the increasing emergence of various poultry health issues (Estévez, 2015). In intensive breeding environments, multiple factors such as pathological agents, unbalanced nutritional supply, and deficiencies in management can collectively trigger oxidative stress in poultry, leading to intestinal dysfunction and suboptimal gut health (Kong et al., 2022; Zheng et al., 2020). These issues not only affect the production performance of poultry but also result in a decline in the quality of livestock products, causing significant economic losses. To investigate oxidative stress in poultry, diquat (DQ), a bipyridyl herbicide, is commonly used to establish stress models due to its potent ability to generate ROS and induce oxidative damage across various tissues, including the liver and intestines (Chen et al., 2020). DQ toxicity is characterized by the production of highly reactive free radicals, such as superoxide anions ($O_2^{\cdot-}$), through single-electron reduction and redox cycling. When the body's antioxidant defenses are overwhelmed, these excess free radicals lead to oxidative stress, resulting in mitochondrial dysfunction, disruption of intracellular homeostasis, inflammation, cell cycle arrest, and ultimately, cell death (Yu et al., 2022). Previous studies have demonstrated that intraperitoneal injection of 20 mg/kg body weight of DQ can successfully establish an oxidative stress model in broilers (Wu F. et al., 2023; Chen et al., 2020). This suggests that the selected dose effectively induces oxidative stress, providing a reliable experimental framework for further investigations into the physiological responses and underlying mechanisms of oxidative damage in poultry. Such a model is crucial for evaluating interventions aimed at mitigating oxidative stress, including nutritional strategies and antioxidant treatments, which may enhance poultry health and production efficiency under stress conditions. Numerous studies have confirmed that factors such as mycotoxins, pesticide compounds, high fat diets, nutrient deficiencies, and intestinal ischemia can all trigger severe oxidative stress in the poultry intestine, causing significant harm to animal health (Chen et al., 2022; Wang et al., 2022). The generation of oxidative stress can primarily be attributed to two key mechanisms: first, an imbalance between oxidative products and the antioxidant defense system within cells, disrupting the redox balance (Li et al., 2019); and second, the overproduction of ROS triggered by internal or external stressors. Under normal physiological conditions, animals have the ability to regulate the balance between oxidation and antioxidation, mitigating oxidative stress. However, when ROS scavenging mechanism fail to act promptly, excessive ROS can severely damage cell lipids, proteins, and DNA, disrupting cell signaling pathways and physiological functions, ultimately leading to a series of health problems (Chen et al., 2020). Thus, understanding and addressing oxidative stress-related intestinal health issues in poultry, particularly in intensive breeding environments, is therefore of significant importance for improving the productivity and product quality of livestock products.

The intestinal microbiota, as a dynamic and complex ecosystem, is influenced by numerous interactions among microbes, host, diet, and environment. These microbial communities play a crucial role in the development of host organ morphology, immune responses, metabolic processes, and overall health (Waite and Taylor, 2015). The functions of the gut microbiota extend beyond nutrient metabolism and absorption; it also plays a central role in maintaining intestinal barrier integrity, modulating immune system, and providing resistance against pathogen invasion (Bhagat et al., 2023). By regulating gut homeostasis, the microbiota helps prevent the occurrence of intestinal diseases in animals (Polansky et al., 2015). The balance of the gut flora is closely linked to the host's ability to resist pathogens, and plays a critical role in protecting the host from harm. Research has shown that incorporating plant-derived feed additives into poultry diets is an effective strategy for enhancing animal health and production performance (Li et al., 2022). Rich in a various of bioactive components, these additives not only improve animal growth performance but also to boost immune function, enhance antioxidant status, and stabilize the gut microbiota. Therefore, the inclusion of plant-derived feed additives in animal nutrition strategies that leverage their bioactive components to optimize gut microbiota, is an effective approach to improve animal health and production efficiency. This strategy also holds significant promise for promoting the sustainable development of the livestock industry.

Recently, natural plant extracts have garnered significant attention for maintaining the intestinal health of livestock and poultry due to their safety, stability, and lower potential for resistance development. Particularly, flavonoid compounds, as secondary metabolites of plants, have become a focus of research due to their abundant resources, diverse origins, and their potent anti-inflammatory, antibacterial, antioxidant, and gastrointestinal function-regulating properties (Wan et al., 2024). In livestock and poultry production, flavonoids positively impact intestinal health by promoting digestive and absorptive functions, enhancing intestinal structure integrity, regulating mucosal layers, boosting the expression of tight junction proteins, and reducing epithelial cell permeability. Quercetagetin (QG), chemically known as 3,3′,4′,5,6,7-hexahydroxyflavone (chemical formula $C_{15}H_{10}O_8$), is one of the main active components extracted from marigold and belongs to the flavonol category of flavonoids (Wu F.

Abbreviations: DQ, Diquat; QG, Quercetagetin; BW, Body weight; ADFI, Average daily feed intake; ADG, Average daily gain; F:G, Feed-to-Gain ratio; ACTH, Adrenocorticotropic hormone; CORT, Corticosterone; GH, Growth hormone; GSH-Px, Glutathione peroxidase; CAT, Catalase; SOD, Superoxide dismutase; MDA, Malondialdehyde; Nrf2, Nuclear factor erythroid 2-related factor 2; Keap1, Recombinant kelch like ECH associated protein 1.

Y. et al., 2023). Due to its structure containing six phenolic hydroxyl groups, it exhibits excellent antioxidant and antibacterial properties. Previous studies have shown that QG has a strong capability to scavenge DPPH·, ·OH, and O_2.– radicals (Fuentes et al., 2021). Supplementing broiler diets with QG has been shown to significantly improve apparent digestibility, enhance the structural morphology of the duodenum and ileum, and enhance immune function. However, research on the effects of QG as a feed additive on the antioxidant function of the chicken intestine and gut microbiota remains limited (Wu et al., 2022). This study utilizes a DQ-induced oxidative stress model in broilers to investigate the effects of QG on growth performance, intestinal antioxidant capacity, and gut microbiota diversity. The objective is to elucidate its potential applications in livestock and poultry production, providing a scientific foundation and practical insights for improving production efficiency and promoting animal health.

2 Materials and methods

2.1 Experimental materials

QG was procured from the Chenguang Biotech Group Co., Ltd., with a purity exceeding 85%. Diquat (Diquat Dibromide Monohydrate, Aladdin, Lot#b2327176) was obtained from Shanghai Aladdin Biochemical Technology Co., Ltd. Glutathione peroxidase (GSH-Px), Catalase (CAT), Superoxide Dismutase (SOD), and Malondialdehyde (MDA) assay kits were purchased from Nanjing Jiancheng Bioengineering Institute. RNAiso Plus, SYBR Green qPCR Master Mix, and the SYBR Green PCR kit were obtained from Takara Biotechnology Co., Ltd. in Dalian.

2.2 Animal ethics statement

The experimental protocol was approved by the Animal Care and Use Committee of Hebei University of Engineering (Handan, China). The animal experiments were conducted in strict adherence to the guidelines outlined in the Care and Use of Animals (BER-YXY-2024006).

2.3 Experimental design, animal, and management

The experiment utilized a single-factor randomized design. A total of 240 21-day-old WOD168 broilers were selected and randomly assigned to five treatment groups, ensuring similar body weight across groups. The groups were as follows: the control group (CON), which was fed a basal diet and intraperitoneally injected with 0.9% saline; the Diquat group (DQ), which was fed a basal diet and intraperitoneally injected with Diquat; the low-dose QG group (LQG), which received 10 mg/kg QG added to the basal diet and was intraperitoneally injected with Diquat; the medium-dose QG group (MQG), which received 20 mg/kg QG added to the basal diet and was intraperitoneally injected with Diquat; and the high-dose QG group (HQG), which received 40 mg/kg QG added to the basal diet and was intraperitoneally injected with Diquat. Each treatment group had six replicates, with eight chickens per replicate. The experiment lasted for 21 days, with a pre-feeding period from days 1 to 14. On the 15th day, broilers in the Diquat treatment groups were intraperitoneally injected with a Diquat solution at 2 mL/kg body weight (Diquat solution concentration was 10 mg/mL in saline), while the control group received an equivalent volume of saline. The experimental design is referenced in Figure 1.

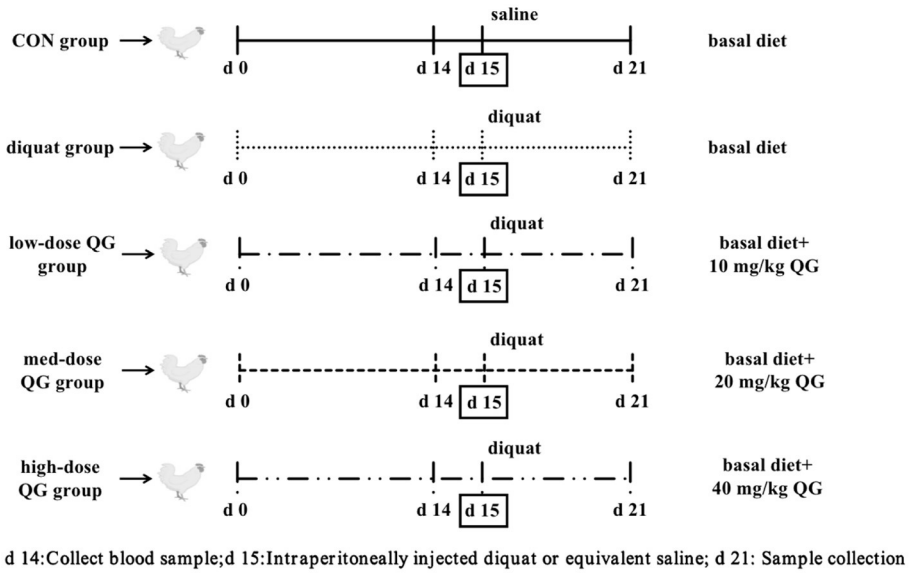

FIGURE 1
Broiler experiment flow diagram. DQ, Diquat; QG, Quercetagetin.

TABLE 1 Composition and nutrient level of the basal diet (as-feed basis), %.

Items	Content
Ingredients	
Corn	58.80
Soybean meal	33.80
Soybean oil	3.00
Dicalcium phosphate	1.80
Limestone	1.22
Salt	0.37
L-Lysine	0.03
DL-Methionine	0.07
Premix[a]	0.80
Choline	0.11
Total	100.0
Nutrient levels[b]	
Metabolizable energy (MJ/kg)	12.62
Crude protein	19.65
Calcium	1.02
Available phosphorus	0.42
Lys	1.15
Met	0.40
Cys	0.36

[a]Premix provided the following per kilogram of diet: vitamin A: 9,000 IU, vitamin D3: 3,000 IU, vitamin E: 26 mg, vitamin K3: 1.20 mg, vitamin B: 13.00 mg, vitamin B2: 8.00 mg, vitamin B6: 4.40 mg, vitamin B12: 0.012 mg, nicotinic acid: 45 mg, folic acid: 0.75 mg, biotin: 0.20 mg, choline: 1,100 mg, calcium pantothenate: 15 mg, Fe: 100 mg, Cu: 10 mg, Zn: 108 mg, Mn: 120 mg, I: 1.5 mg, and Se: 0.35 mg.
[b]Crude protein is a measured value, while the others are all calculated values.

During the experimental period, all broilers were housed in fully automated, standardized poultry houses with *ad libitum* access to feed and water. The housing was structured as a three-tier cage system. The basal diet was a corn-soybean meal type, formulated into pelleted feed according to the nutritional recommendations of the NRC (1994) and the Chinese Nutrient Requirements of Poultry (NY/T 33-2004). The composition and nutritional levels of the basal diet are detailed in Table 1. All groups were managed under uniform husbandry and environmental conditions to ensure consistency throughout the experiment.

2.4 Sample collection and preparation

On day 21 of the trial, a broiler with an average weight representative of its group was selected from each replicate for blood collection. Blood samples were collected from the wing vein using vacuum blood collection tubes without anticoagulant. After allowing the samples to sit at room temperature for 30 min to facilitate clot formation, they were centrifuged at 3,000×*g* for 15 min at 4°C. The resulting serum samples were then carefully collected and stored at −20°C for subsequent analysis of serum hormone levels and antioxidant indicators. Following blood collection, the chickens were euthanized by exsanguination from the neck, and the small intestine (duodenum, jejunum, and ileum) was harvested. A segment from the middle of each intestinal section was cleaned of its contents with saline, surface moisture was absorbed with filter paper, and the mucosa was scraped onto a slide, collected into 2 mL sterile tubes, and stored at −20°C for antioxidant indicator analysis. Another portion of the small intestinal tissue was rinsed with pre-chilled sterile saline solution to remove blood contamination, quickly frozen in liquid nitrogen, and then stored at −80°C for RNA extraction. Additionally, 2 g of cecal contents were collected into cryovials, flash-frozen in liquid nitrogen, and stored at −80°C for the analysis of microbial diversity.

2.5 Determination indexes and methods

2.5.1 Growth performance

The broilers were weighed on days 14 and 21 of the trial. Feed intake was evaluated by measuring the total amount of feed supplied and the remaining feed at the end of each day, which facilitated the calculation of daily feed consumption. Key performance metrics, including Average Daily Gain (ADG), Average Daily Feed Intake (ADFI), and Feed-to-Gain ratio (F/G), were subsequently derived from these measurements for each experimental period. The health status of the broilers was observed daily, and the mortality rate was also recorded.

2.5.2 Serum stress hormone indicators

The serum levels of ACTH, CORT and GH were determined using commercial ELISA kits from Genway Biotech, Inc., strictly following the procedures provided in the kit manuals.

2.5.3 Serum and tissue sample antioxidant indexes

Following the method described by Shi et al. (2022), antioxidant indicators, including SOD, CAT, and GSH-Px, as well as the oxidative stress damage marker MDA, were measured in the samples using commercial assay kits (Nanjing Jiancheng Bioengineering Institute, Nanjing, China). The specific procedures were conducted strictly according to the instructions provided in the kit manuals.

2.5.4 Expression level of antioxidant-related genes in small intestine

Total RNA from the small intestine was extracted using the Trizol method. RNA purity and concentration were assessed spectrophotometrically at 260 and 280 nm, and RNA integrity was evaluated by 1.5% agarose gel electrophoresis. Reverse transcription was performed using the TaKaRa Reverse Transcription Kit according to the manufacturer's instructions. Quantitative fluorescence PCR was conducted using Gen Star qPCR PreMix and the 7500 Real-Time PCR

TABLE 2 Genes and their primer sequences.

Genes	Gene bank No.	Primer sequences, 5′-3′	Length (bp)
β-Actin	NM_205518	F-GCCAACAGAGAGAAGATGACAC	118 bp
		R-GTAACACCATCACCAGAGTCCA	
Nrf2	NM_205117.1	F-GATGTCACCCTGCCCTTAG	215 bp
		R-CTGCCACCATGTTATTCC	
SOD	NM_205064.1	F-TTGTCTGATGGAGATCATGGCTTC	98 bp
		R-TGCTTGCCTTCAGGATTAAAGTGA	
CAT	NM_001031215.1	F-GTTGGCGGTAGGAGTCTGGTCT	182 bp
		R-GTGGTCAAGGCATCTGGCTTCTG	
GSH-Px	NM_001163245.1	F-CAAAGTTGCGGTCAGTGGA	136 bp
		R-AGAGTCCCAGGCCTTTACTACTTTC	
Keap1	XM_015274015.1	F-TGCCCCTGTGGTCAAAGTG	104 bp
		R-GGTTCGGTTACCGTCCTGC	

F, forward primer; R, reverse primer; β-Actin, beta-actin; Nrf2, nuclear factor erythroid-2-related factor 2; SOD, superoxide dismutase; CAT, catalase; GSH-Px, glutathione peroxidase; Keap1, kelch like ECH associated protein 1.

System. The total reaction volume was 20 μL, consisting of 10 μL 2×RealStar Fast SYBR PCR Mix, 0.5 μL of each primer, 8 μL ddH_2O, and 1 μL cDNA template. The reaction conditions were set as follows: pre-denaturation at 95°C for 30 s, denaturation at 95°C for 5 s, annealing at 60°C for 30 s, and extension at 72°C for 20 s, for a total of 45 cycles. In this experiment, *β-actin* served as the internal reference gene, and the relative expression levels of the *GSH-Px*, *CAT*, *SOD*, *Nrf2*, and *Keap1* genes were calculated using the $2^{-\Delta\Delta Ct}$ method. Primers for the relevant genes were synthesized by Sangon Biotech Co., Ltd., with the primer sequences presented in Table 2.

2.5.5 Cecal microbiota

Following the method described by Li et al. (2021), cecal microbial DNA was extracted, the V3-V4 variable regions of the 16S rDNA were amplified, libraries were constructed, sequencing and species annotation were performed, and analyses were conducted to calculate the relative abundance of cecal microbial phyla and genera based on operational taxonomic units (OTUs), as well as Alpha and Beta diversity.

2.6 Statistical analysis of data

After being organized in Excel 2016, all data were subjected to one-way ANOVA using the SPSS 21.0 software for the analysis of variance. When significant differences in treatment effects were observed, Duncan's multiple range test was applied for *post-hoc* comparisons. Differences were considered significant at $P < 0.05$. The results of the experiment are presented as mean values with standard error of the mean (SEM).

3 Results

3.1 Growth performance

The effects of different concentrations of QG on the growth performance of broiler chickens are presented in Table 3. On the 14th day of the experiment, there were no significant differences among the groups in BW, ADFI, ADG, and F:G ($P > 0.05$). On the 21st day of the experiment, compared to the DQ group, both the LQG and MQG groups significantly increased the BW of broiler chickens ($P < 0.05$). Compared to the CON group, the DQ group significantly decreased ADFI ($P < 0.01$), while the QG treatment groups (LQG, MQG, and HQG) were significantly higher in ADFI than the DQ group ($P < 0.01$), and there were no significant differences in ADFI compared to the CON group ($P > 0.05$). Compared to the CON group, the DQ group significantly decreased ADG ($P < 0.05$), while the MQG and HQG groups were significantly higher than the DQ group ($P < 0.05$), with no significant differences compared to the CON group ($P > 0.05$). Furthermore, compared to the CON group, both the LQG and MQG groups significantly decreased F:G ($P < 0.05$).

3.2 Serum stress hormone indicators

The effects of different concentrations of QG on the serum stress hormone indicators of broiler chickens are presented in Table 4. On the 14th day of the experiment, there were no significant differences among the groups in ACTH, CORT, and GH ($P > 0.05$). On the 21st day of the experiment, compared to the CON group, the DQ group significantly increased the ACTH content ($P < 0.05$), while the ACTH content in the MQG group was significantly lower than that in the DQ group ($P < 0.05$), with no significant differences compared to the CON group ($P > 0.05$). Furthermore, compared to the CON group, the DQ group

TABLE 3 Effects of different concentrations of QG on growth performance of broilers.

	Item	CON	DQ	LQG	MQG	HQG	SEM	*P*-value
14 d	BW (g)	1,108.85 ± 187.48	946.94 ± 21.46	1,221.50 ± 53.23	1,235.33 ± 58.23	1,198.00 ± 51.30	44.49	0.17
	ADFI (g)	87.19 ± 9.33	90.76 ± 18.35	89.83 ± 13.04	99.34 ± 8.93	93.72 ± 5.58	2.74	0.22
	ADG (g)	42.43 ± 8.59	36.53 ± 17.65	47.98 ± 2.29	49.51 ± 2.79	45.82 ± 2.53	2.41	0.47
	F:G	2.00 ± 0.08	2.02 ± 0.09	1.97 ± 0.08	1.95 ± 0.03	2.01 ± 0.11	0.02	0.70
21 d	BW (g)	1,537.67 ± 61.60^{bc}	1,492.00 ± 69.66^{c}	1,646.67 ± 40.61^{ab}	1,674.67 ± 63.26^{a}	1,510.33 ± 78.68^{c}	24.25	0.02
	ADFI (g)	91.40 ± 12.69^{A}	67.51 ± 27.02^{B}	97.77 ± 5.62^{A}	105.59 ± 5.37^{A}	102.57 ± 4.86^{A}	4.53	<0.01
	ADG (g)	57.19 ± 3.38^{a}	48.86 ± 2.95^{b}	53.57 ± 1.89^{ab}	59.19 ± 3.26^{a}	58.00 ± 5.39^{a}	1.25	0.03
	F:G	1.90 ± 0.1^{ab}	2.01 ± 0.28^{a}	1.65 ± 0.06^{bc}	1.57 ± 0.08^{c}	1.86 ± 0.20^{abc}	0.05	0.04

CON, control group; DQ, diquat group; LQG, low-dose quercetagetin group; MQG, medium-dose quercetagetin group; HQG, high-dose quercetagetin group; BW, body weight; ADG, average daily gain; ADFI, average daily feed intake; F:G, feed-to-gain ratio; SEM, standard error of the mean ($n = 6$).
In peer data, no letters or the same letters indicate no significant difference ($P > 0.05$), different lowercase letters indicate a significant difference ($P < 0.05$), and different uppercase letters indicate an extremely significant difference ($P < 0.01$).

TABLE 4 Effects of different concentrations of QG on serum hormonal indicators in broilers.

	Item	CON	DQ	LQG	MQG	HQG	SEM	*P*-value
14 d	ACTH (pg/mL)	17.09 ± 4.85	21.54 ± 9.17	17.07 ± 6.04	12.28 ± 3.70	15.89 ± 8.47	1.38	0.39
	CORT (ng/mL)	2.62 ± 0.41	3.71 ± 1.88	2.96 ± 1.35	2.51 ± 0.89	2.93 ± 0.67	0.21	0.44
	GH (ng/mL)	4.83 ± 0.52	4.43 ± 0.49	4.89 ± 0.37	5.06 ± 0.36	5.02 ± 0.53	0.35	0.16
21 d	ACTH (pg/mL)	17.95 ± 2.94^{b}	27.38 ± 1.95^{a}	18.70 ± 1.16^{ab}	16.98 ± 1.71^{b}	24.14 ± 1.51^{ab}	1.66	0.04
	CORT (ng/mL)	3.09 ± 0.70	3.19 ± 0.24	2.82 ± 0.40	2.72 ± 0.35	3.02 ± 0.27	0.08	0.33
	GH (ng/mL)	5.12 ± 0.48^{a}	4.49 ± 0.39^{b}	5.26 ± 0.51^{a}	5.54 ± 0.49^{a}	4.87 ± 0.40^{ab}	0.91	0.02

CON, control group; DQ, diquat group; LQG, low-dose quercetagetin group; MQG, medium-dose quercetagetin group; HQG, high-dose quercetagetin group; ACTH, adrenocorticotropic hormone; CORT, corticosterone; GH, growth hormone; SEM, standard error of the mean ($n = 6$).
In peer data, no letters or the same letters indicate no significant difference ($P > 0.05$), different lowercase letters indicate a significant difference ($P < 0.05$).

significantly decreased the GH content ($P < 0.05$), while both the LQG and MQG groups were significantly higher than the DQ group ($P < 0.05$), with no significant differences compared to the CON group ($P > 0.05$).

3.3 Serum and tissue sample antioxidant indexes

The effects of different concentrations of QG on the serum antioxidant indices of broiler chickens are presented in Table 5. On day 14 of the experiment, compared to the CON group, the MQG group showed a significant increase in SOD activity ($P < 0.05$); however, there were no significant differences in GSH-Px, CAT, and MDA activity or content among the groups ($P > 0.05$). On day 21 of the experiment, compared to the CON group, the DQ group significantly decreased CAT activity ($P < 0.05$), while the CAT activity in the LQG group was significantly higher than that in the DQ group ($P < 0.05$), with no significant differences compared to the CON group ($P > 0.05$). Moreover, compared to the CON group, the DQ group significantly increased MDA content ($P < 0.05$); however, the MDA content was significantly reduced in the LQG, MQG, and HQG groups compared to the DQ group ($P < 0.05$).

The effect of different concentrations of QG on the intestinal antioxidant indices of broiler chickens is presented in Table 6. At day 21 of the experiment, compared to the CON group, the DQ group significantly decreased the duodenum GSH-Px activity ($P < 0.05$). In contrast, compared to the DQ group, the LQG, MQG, and HQG groups significantly increased the GSH-Px activity ($P < 0.05$). Additionally, compared to the CON group, the DQ group significantly increased the MDA content ($P < 0.05$). However, the MDA content in the LQG group was significantly lower than that in the DQ group ($P < 0.05$), and there was no significant difference compared to the CON group ($P > 0.05$). Furthermore, compared to the DQ group, the MQG and HQG groups significantly increased the jejunum GSH-Px activity ($P < 0.05$). Similarly, compared to the CON group, the DQ group significantly increased the MDA content ($P < 0.05$), while the MDA content in the MQG and HQG groups was significantly lower than that in the DQ group ($P < 0.05$). Finally, compared to the CON group, the DQ group significantly increased the ileum MDA content ($P < 0.05$), while the MDA content in the LQG and MQG groups was significantly lower than that in the DQ group ($P < 0.05$).

3.4 Expression level of the antioxidant-related genes in the intestines

The effects of different concentrations of QG on the expression of antioxidant-related genes in the intestines of broilers are shown

TABLE 5 Effects of different concentrations of QG on serum antioxidant indicators in broilers.

	Item	CON	DQ	LQG	MQG	HQG	SEM	*P*-value
14 d	GSH-Px (U/mL)	3,895.7 ± 29.31	3,895.3 ± 23.45	3,820.4 ± 32.55	3,793.6 ± 31.79	3,217.8 ± 34.79	193.17	0.52
	CAT (U/mL)	4.92 ± 0.68	2.99 ± 0.15	4.41 ± 0.73	3.81 ± 0.48	3.07 ± 0.26	0.46	0.29
	SOD (U/mL)	338.07 ± 25.67^{b}	343.80 ± 31.46^{b}	369.66 ± 22.94^{ab}	442.44 ± 30.51^{a}	379.20 ± 41.22^{ab}	19.37	0.03
	MDA (nmol/mL)	2.70 ± 0.14	2.91 ± 0.22	2.69 ± 0.39	2.10 ± 0.17	2.58 ± 0.30	0.22	0.46
21 d	GSH-Px (U/mL)	2,288.0 ± 247.9	2,215.0 ± 209.5	2,229.2 ± 198.6	2,186.3 ± 233.7	2,331 ± 221.5	269.09	0.88
	CAT (U/mL)	6.10 ± 0.52^{a}	3.49 ± 0.48^{b}	5.47 ± 0.57^{a}	4.51 ± 0.59^{ab}	4.77 ± 0.32^{ab}	0.45	0.03
	SOD (U/mL)	358.49 ± 31.66	353.80 ± 29.53	332.10 ± 30.04	356.23 ± 31.77	346.49 ± 28.19	41.62	0.75
	MDA (nmol/mL)	2.54 ± 0.19^{B}	3.28 ± 0.45^{A}	1.85 ± 0.35^{B}	1.96 ± 0.29^{B}	3.06 ± 0.16^{AB}	0.18	<0.01

CON, control group; DQ, diquat group; LQG, low-dose quercetagetin group; MQG, medium-dose quercetagetin group; HQG, high-dose quercetagetin group; GSH-Px, glutathione peroxidase; CAT, catalase; SOD, superoxide dismutase; MDA, malondialdehyde; SEM, standard error of the mean ($n = 6$).
In peer data, no letters or the same letters indicate no significant difference ($P > 0.05$), different lowercase letters indicate a significant difference ($P < 0.05$), and different uppercase letters indicate an extremely significant difference ($P < 0.01$).

TABLE 6 Effects of different concentrations of QG on small intestine antioxidant indicators in broilers.

	Item	CON	DQ	LQG	MQG	HQG	SEM	*P*-value
Duodenum	GSH-Px (U/mg prot.)	6.69 ± 0.53^{ab}	4.97 ± 0.49^{c}	7.65 ± 0.91^{ab}	9.05 ± 1.43^{a}	8.93 ± 0.69^{a}	0.76	0.02
	CAT (U/mg prot.)	1.22 ± 0.11	1.33 ± 0.25	1.11 ± 0.20	1.49 ± 0.15	1.37 ± 0.26	0.08	0.11
	SOD (U/mg prot.)	358.7 ± 30.17	308.2 ± 28.95	348.4 ± 40.97	373.3 ± 42.11	319.6 ± 45.85	27.1	0.32
	MDA (nmol/mg prot.)	0.74 ± 0.06^{b}	1.18 ± 0.25^{a}	0.66 ± 0.02^{b}	0.84 ± 0.03^{ab}	0.81 ± 0.05^{ab}	0.11	0.03
Jejunum	GSH-Px (U/mg prot.)	6.69 ± 0.53^{ab}	4.97 ± 0.79^{b}	5.65 ± 0.66^{b}	9.05 ± 0.81^{a}	8.15 ± 0.88^{a}	0.76	0.04
	CAT (U/mg prot.)	0.95 ± 0.07	1.20 ± 0.09	0.90 ± 0.05	1.10 ± 0.16	1.09 ± 0.11	0.16	0.11
	SOD (U/mg prot.)	255.43 ± 20.17	259.73 ± 28.67	292.43 ± 32.98	303.03 ± 28.15	285.16 ± 33.69	27.79	0.32
	MDA (nmol/mg prot.)	0.17 ± 0.01^{b}	0.72 ± 0.08^{a}	0.42 ± 0.02^{ab}	0.29 ± 0.01^{b}	0.39 ± 0.01^{b}	0.14	0.02
Ileum	GSH-Px (U/mg prot.)	19.51 ± 2.03	19.79 ± 2.36	20.11 ± 3.58	16.28 ± 1.99	19.28 ± 1.71	3.50	0.53
	CAT (U/mg prot.)	2.07 ± 0.17	2.50 ± 0.33	2.74 ± 0.27	2.32 ± 0.19	1.98 ± 0.27	0.36	0.27
	SOD (U/mg prot.)	442.5 ± 40.18	465.1 ± 55.06	491.9 ± 51.13	472.8 ± 39.88	452.8 ± 44.05	38.62	0.49
	MDA (nmol/mg prot.)	0.60 ± 0.02^{b}	0.93 ± 0.06^{a}	0.70 ± 0.09^{b}	0.63 ± 0.03^{b}	0.87 ± 0.09^{ab}	0.06	0.02

CON, control group; DQ, diquat group; LQG, low-dose quercetagetin group; MQG, medium-dose quercetagetin group; HQG, high-dose quercetagetin group; GSH-Px, glutathione peroxidase; CAT, catalase; SOD, superoxide dismutase; MDA, malondialdehyde; SEM, standard error of the mean ($n = 6$).
In peer data, no letters or the same letters indicate no significant difference ($P > 0.05$), different lowercase letters indicate a significant difference ($P < 0.05$).

in Figure 2. At day 21 of the experiment, compared to the DQ group, both the low and medium QG (LQG and MQG) groups exhibited a significant increase in the expression of *GSH-Px* and *Keap1* mRNAs in the duodenum ($P < 0.05$). In the ileum, compared to the DQ group, the LQG and MQG groups showed a significant increase in the expression of *GSH-Px* and *Nrf2* mRNA ($P < 0.05$), and both the MQG and HQG groups exhibited a significant increase in the expression of *Keap1* mRNA ($P < 0.05$). However, in the jejunum, there were no significant differences in the mRNA expression of *CAT*, *SOD*, *GSH-Px*, *Nrf2*, and *Keap1* among the groups ($P > 0.05$).

3.5 Cecal microbial community diversity

The effects of different concentrations of QG on the species richness and diversity of the cecal microbiota in broilers are shown in Figure 3. As indicated in Figures 3A, B, compared to the CON group, the operational taxonomic units (OTUs) and Chao1 indices were significantly increased in the QG treatment groups (LQG, MQG, and HQG) ($P < 0.05$). However, there were no significant differences in the Shannon and Simpson indices among the groups ($P > 0.05$) (Figures 3C, D). In Figure 3E, the Venn diagram displays the distribution of OTUs in the cecal contents of the experimental groups and the CON group. A total of 396 OTUs were shared across all groups. The CON group contained 61 unique OTUs, while the DQ, LQG, MQC, and HQG groups had 125, 223, 210, and 193 unique OTUs, respectively.

The 16S rRNA sequencing results revealed that, at the phylum level, the main bacterial were Firmicutes, Bacteroidota, Proteobacteria, and Desulfobacterota (Figure 4A). Among them, Firmicutes and Bacteroidota were the predominant phyla, collectively accounting for over 80% of the total microbial community. Compared to the DQ group, the LQG group significantly altered the relative abundance of Firmicutes and Bacteroidota, with a decrease in Firmicutes ($P < 0.05$) and an

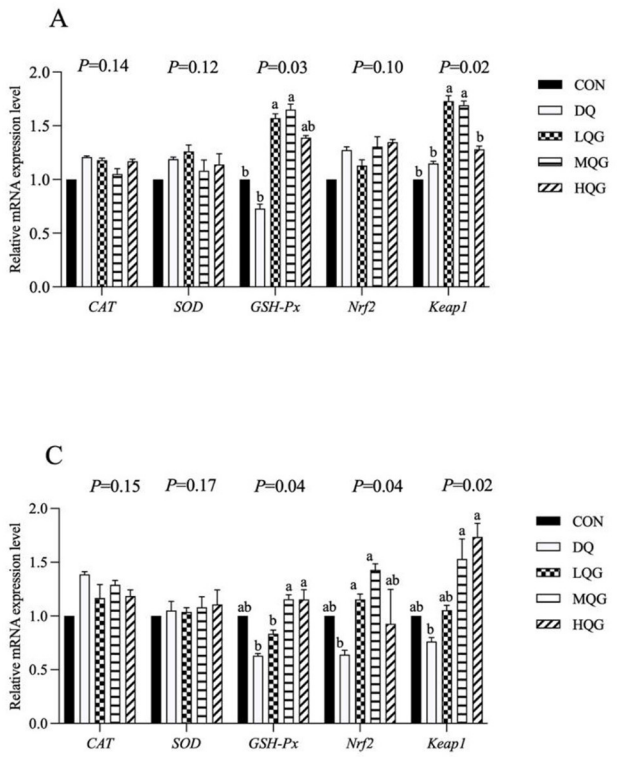

FIGURE 2
Effects of diets with different concentrations QG on antioxidant-related gene expression in the small intestine of broilers challenged with DQ (21 d). CON, control group; DQ, diquat group; LQG, low-dose quercetagetin group; MQG, medium-dose quercetagetin group; HQG, high-dose quercetagetin group. **(A)** Duodenum; **(B)** jejunum; **(C)** ileum. Bars represent the means ± standard deviation (SD) ($n = 6$). [a,b]Different letters in the shoulder markers in the table indicate significant differences between groups ($P < 0.05$).

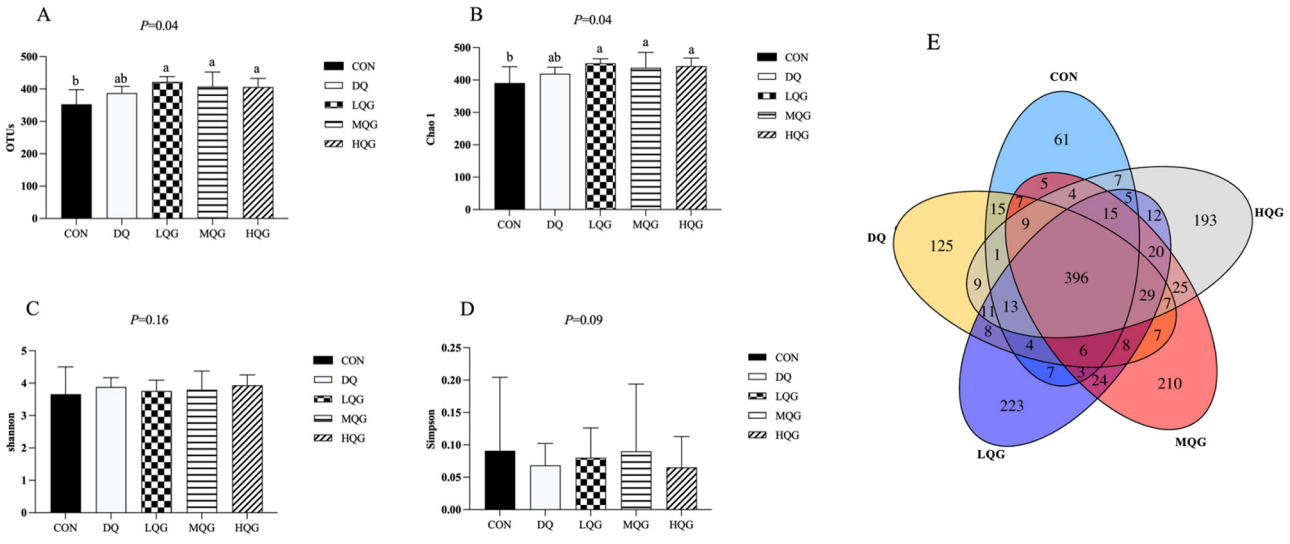

FIGURE 3
Effects of diets with different concentrations of QG on cecal microbial alpha diversity of broilers challenged with DQ. CON, control group; DQ, diquat group; LQG, low-dose quercetagetin group; MQG, medium-dose quercetagetin group; HQG, high-dose quercetagetin group. **(A)** OTUs; **(B)** Chao1 index; **(C)** Shannon index; **(D)** Simpson index; **(E)** Venn diagram of OTU. Bars represent the means ± standard deviation (SD) ($n = 6$). [a,b]Different letters in the shoulder markers in the table indicate significant differences between groups ($P < 0.05$).

increase in Bacteroidota ($P < 0.05$). At the genus level (Figure 4B), compared to the CON group, the DQ group exhibited a significant increase in the relative abundance of *Faecalibacterium* ($P < 0.05$). Compared to the DQ group, the LQG group showed a significant reduction in the relative abundance of *Faecalibacterium* ($P < 0.05$). Additionally, both the LQG and MQG groups significantly reduced

the relative abundance of *Lachnospiraceae_unclassified* ($P < 0.05$). Notably, the relative abundance of *Ligilactobacillus* in the MQG group was significantly higher than in the DQ group ($P < 0.05$) (Table 7).

The linear discriminant analysis (LDA = 4) effect size (LEfSe) algorithm was employed to analyze the taxonomic abundance of the microbiota. The results at the phylum and genus levels are shown in Figure 5. At the phylum level (Figure 5A), the abundance of Proteobacteria was elevated in the CON group, while Firmicutes significantly increased in the DQ group, and Bacteroidota and Desulfobacterota were notably enriched in the LQG group. At the genus level (Figure 5B), the CON group exhibited significant enrichment of *Lactobacillus*, *Romboutsia*, *Escherichia-Shigella*, and *Subdoligranulum*, while the LQG group showed a marked increase in *Bacteroides* and *Bilophila*, and *Erysipelatoclostridium* was significantly elevated in the MQG group. The combined analysis of the sample clustering tree and bar chart (Figure 6) revealed that, at the phylum level (Figure 6A), the microbial composition of the DQ and CON groups exhibited similarities, while the HQG and MQG groups also showed a similar composition. At the genus level (Figure 6B), the HQG and DQ groups demonstrated similarity, whereas the MQG, CON, and LQG groups displayed distinct differences in microbial composition.

3.6 Correlation analysis between the growth performance, oxidative function indicators, and cecal microbiota

The correlation between intestinal microbial proportions at the genus level and growth performance, as well as serum oxidative status among five groups, is illustrated in Figure 7. The results indicate a significant negative correlation between BW and *Escherichia-Shigella*, *Subdoligranulum*, *Romboutsia*, *Butyricicoccus*, and *Lachnospiraceae_unclassified*, while a significant positive correlation was observed with *Alistipes*. ADFI was significantly negatively correlated with *Escherichia-Shigella*, *Romboutsia*, and *Lachnospiraceae_unclassified*, and positively correlated with *Erysipelatoclostridium*, *UCG-005*, *Bilophila*, and *Bacteroides*. ADG exhibited a significant positive correlation with *UCG-005*. Additionally, GSH-Px showed a significant positive correlation with *Subdoligranulum*. SOD demonstrated significant positive correlations with *Romboutsia*, *Lactobacillus*, and *Lachnospiraceae_unclassified*, while showing significant negative correlations with *Bacteroides*, and *Bilophila*.

4 Discussion

Oxidative stress has extremely detrimental effects on the growth performance of poultry, while excessive antibiotics use not only poses significant threats to public health but also limits the sustainable development of animal husbandry (Lee et al., 2019). In this context, the search for green and safe alternatives to antibiotics has become a key focus in animal nutrition research. QG, a major component of extracts from *Tagetes erecta L.*, belongs to the flavanol class and exhibits a range of biological activities, including antioxidant, anti-inflammatory, antibacterial properties, and the regulation of lipid metabolism (Wang et al., 2016). Although its application in poultry farming has been less frequently reported, flavonoid compounds have been shown to effectively enhance the growth performance of livestock and poultry. This study showed that intraperitoneal injection of diquat significantly reduced the BW of the broilers. This observation is consistent with previous studies indicating that diquat induces oxidative stress in broilers, which leads to a pronounced reduction in both ADG and ADFI (Chen et al., 2021). The phenomenon of diquat-induced oxidative stress seems to cause a redistribution of nutrients within the body, reallocating energy and glucose to physiological processes aimed at counteracting stress. This shift in nutrient allocation reduces feed intake, suppresses growth, and ultimately diminishes production efficiency. The mechanism underlying these effects is likely related to oxidative damage at the cellular level, particularly mitochondrial dysfunction, which not only impairs metabolic efficiency but also disrupts nutrient absorption. However, this experiment found that the addition of 20 and 40 mg/kg of QG significantly alleviated the BW decrease caused by diquat, with comparable effects to the basal diet group, and it had no adverse effects on the average daily feed intake or the feed conversion ratio of the broilers. This result suggests that adding quercetin glycoside to feed can improve the production performance of broiler chickens, which may be closely related to the antioxidant capacity and other biological activities of quercetin glycoside.

The levels of CORT and ACTH in serum are common indicators of stress, reflecting the physiological stress status of poultry (Guerreiro et al., 2016). When poultry are under stress, cytokines enter the central nervous system, activating the hypothalamic-pituitary-adrenal (HPA) axis, which leads to a rapid increase in ACTH and glucocorticoids (GC) in the blood. The release of ACTH stimulates the adrenal cortex to synthesize and release steroids, promoting the conversion of cholesterol into CORT, thus raising serum CORT levels (Cheng et al., 2019). Elevated CORT levels enhance the breakdown of nutrients to meet the body's physiological demands, resulting in alterations in nutrient distribution (Liu et al., 2015). Our study found that diquat stimulation significantly increased the concentration of the adrenocorticotropic hormone ACTH in the serum of broilers. This finding is consistent with the results of Li et al. (2015), who demonstrated that LPS stimulation similarly elevated serum ACTH levels while markedly reducing growth hormone (GH) levels in broilers. The observed increase in ACTH combined with the decrease in GH levels indicates that DQ-induced oxidative stress adversely impacts the growth performance of broilers. This impairment is most likely due to disruption of metabolic processes and nutrient absorption, as well as increased energy expenditure required to counteract the physiological stress induced by DQ. The elevation of ACTH suggests activation of theHPA axis, leading to enhanced glucocorticoid release, which in turn affects growth and metabolic efficiency. The concurrent reduction in GH further underscores the detrimental effects of oxidative stress on broiler growth, robust evidence for the role of DQ in inducing a stress response. Moreover, addressing the negative effects of oxidative stress and stress-induced hormonal imbalances, such as those observed with DQ stimulation, is crucial for improving broiler

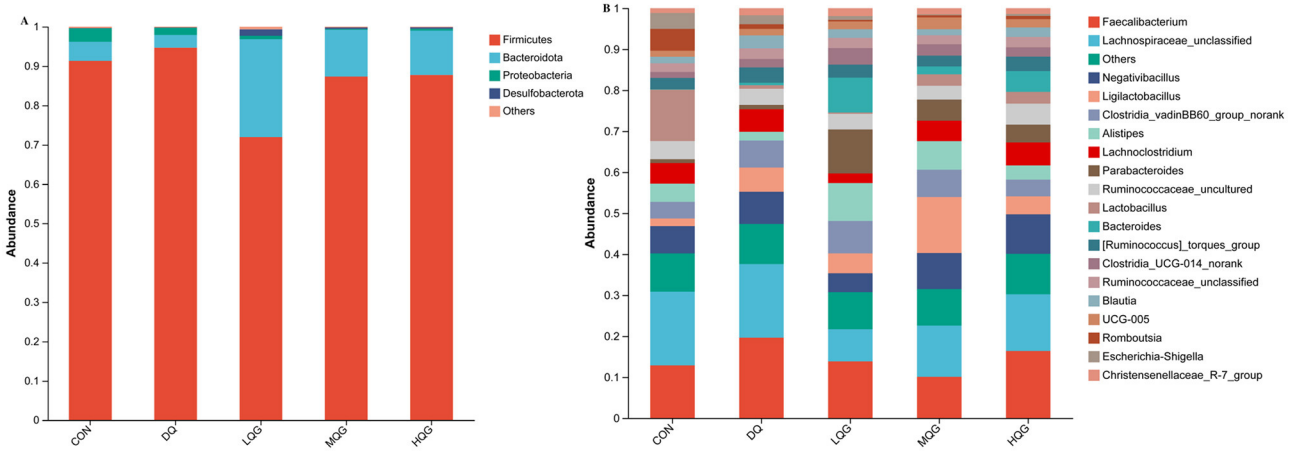

FIGURE 4
Effects of different concentrations of QG in the diet on the relative abundance of cecal microbiota at the phylum **(A)** and genus **(B)** levels in broilers challenged with DQ ($n = 6$). CON, control group; DQ, diquat group; LQG, low-dose quercetagetin group; MQG, medium-dose quercetagetin group; HQG, high-dose quercetagetin group. Cecal microbiota composition at the phylum **(A)** and genus **(B)** levels of broilers.

TABLE 7 Effects of different concentrations of QG in the diet on the relative abundance of cecal microbiota at the phylum and genus levels in broilers challenged with DQ.

	Item	CON	DQ	LQG	MQG	HQG	SEM	*P*-value
Phylum	Firmicutes	0.913 ± 0.04^{A}	0.947 ± 0.02^{A}	0.719 ± 0.02^{B}	0.873 ± 0.02^{A}	0.877 ± 0.02^{A}	0.028	<0.01
	Bacteroidota	0.049 ± 0.00^{B}	0.032 ± 0.00^{B}	0.249 ± 0.02^{A}	0.119 ± 0.01^{B}	0.113 ± 0.01^{B}	0.014	<0.01
Genus	*Faecalibacterium*	0.113 ± 0.00^{ab}	0.190 ± 0.01^{a}	0.121 ± 0.01^{ab}	0.048 ± 0.00^{b}	0.143 ± 0.02^{ab}	0.089	0.03
	Lachnospiraceae_unclassified	0.159 ± 0.00^{a}	0.152 ± 0.01^{a}	0.069 ± 0.00^{b}	0.106 ± 0.01^{ab}	0.121 ± 0.02^{ab}	0.049	0.02
	Negativibacillus	0.059 ± 0.00^{ab}	0.067 ± 0.00^{ab}	0.040 ± 0.00^{b}	0.074 ± 0.01^{ab}	0.084 ± 0.01^{a}	0.031	0.02
	Lactobacillus	0.111 ± 0.01^{a}	0.007 ± 0.01^{c}	0.003 ± 0.00^{c}	0.024 ± 0.00^{b}	0.025 ± 0.00^{b}	0.001	0.03

CON, control group; DQ, diquat group; LQG, low-dose quercetagetin group; MQG, medium-dose quercetagetin group; HQG, high-dose quercetagetin group; SEM, standard error of the mean ($n = 6$).
In peer data, no letters or the same letters indicate no significant difference ($P > 0.05$), different lowercase letters indicate a significant difference ($P < 0.05$), and different uppercase letters indicate an extremely significant difference ($P < 0.01$).

growth performance. Recent studies have highlighted the potential of medicinal plants in mitigating such adverse effects, primarily through their immune-enhancing properties. These plants, rich in secondary metabolites like flavonoids, polysaccharides, and polyphenols, have been shown to modulate the immune system and reduce oxidative stress (Song et al., 2018). By bolstering the immune response and counteracting oxidative damage, these natural compounds may help restore hormonal balance and metabolic efficiency in broilers. Consequently, incorporating medicinal plant extracts into broiler diets may offer a viable strategy to improve growth performance and overall productivity, aligning with efforts to enhance poultry health and mitigate the detrimental impacts of oxidative stress.

The redox state largely reflects the health status of an organism, and livestock and poultry typically possess various antioxidant enzymes to regulate the balance of redox reactions (Pisoschi and Pop, 2015; Doan et al., 2020). Research has demonstrated that flavonoid compounds can enhance the activity of antioxidant enzymes by activating the antioxidant system, thereby alleviating oxidative stress and enhancing the body's antioxidant capacity (Yuan et al., 2017). QG has been extensively studied in mice for its significant antioxidant properties and its positive effects on intestinal barrier function, yet studies in broilers are relatively scarce. Wu F. Y. et al. (2023) observed that dietary QG significantly alleviated the reduction in GSH-Px activity and the increase in MDA content in rabbit serum induced by zearalenone. Our study focused on the effects of dietary QG on the antioxidant performance of broilers, evaluating its impact through measurement of oxidative products in serum and intestines, key antioxidant enzymes, and the expression of genes involved in the antioxidant response. Our experimental results showed that adding 20 mg/kg of QG to the basic diet significantly increased SOD activity in serum. Additionally, feeding QG significantly mitigated the reduction in CAT activity and the increase in MDA content caused by DQ in broiler serum. These results are consistent with the findings of Wu et al. (2022), where QG supplementation also significantly increased GSH-Px activity and reduced MDA content in broiler serum. These observations suggest that adding QG to the feed enhance the activity of antioxidant enzymes and reduces lipid peroxidation products in broiler serum, thereby improving the body's antioxidant capacity and fostering a healthier environment for the growth and development of poultry.

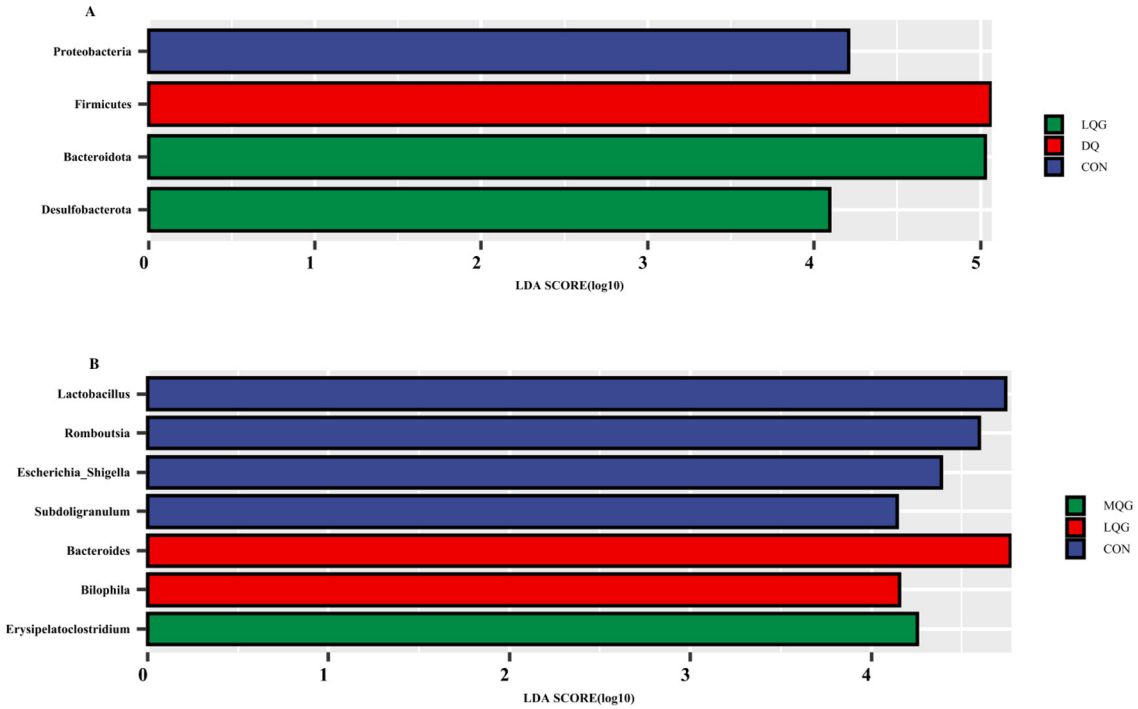

FIGURE 5
Linear discriminant analysis (LDA) effect size (LEfSe) analysis of the cecal microbiota ($n = 6$). CON, control group; DQ, diquat group; LQG, low-dose quercetagetin group; MQG, medium-dose quercetagetin group; HQG, high-dose quercetagetin group. Phylum-level LDA bar chart **(A)** and genus-level LDA bar chart **(B)** display the LDA scores generated for differentially abundant microbiota (LDA > 4, $P < 0.05$).

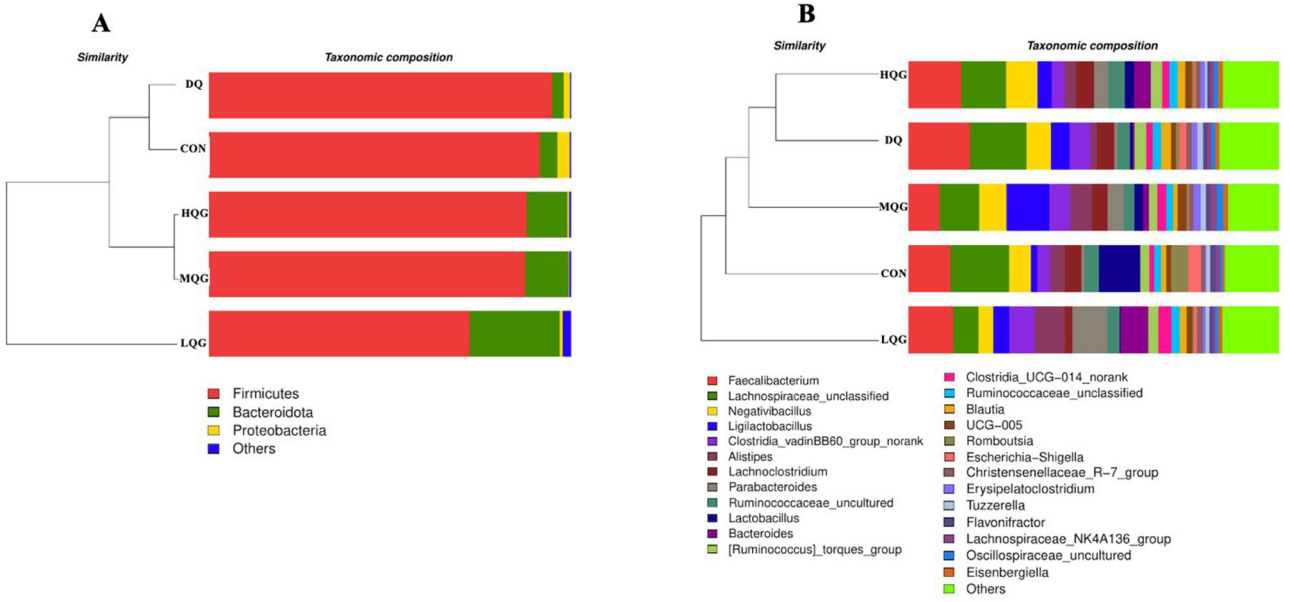

FIGURE 6
Effects of diets with different concentrations of QG on the microbial community barplot with cluster tree of broilers challenged with DQ (n = 6). CON, control group; DQ, diquat group; LQG, low-dose quercetagetin group; MQG, medium-dose quercetagetin group; HQG, high-dose quercetagetin group. Barplot of microbial communities with hierarchical clustering trees at the phylum level **(A)** and genus level **(B)**.

Recent studies have indicated that redox processes begin in the intestine (Salvador et al., 2016). Nutrients absorbed into the small intestine contain numerous antioxidants but also various potential pro-oxidants, the intake of which may cause oxidative damage to the intestinal tract. Thus, maintaining redox balance in the intestines is crucial for overall health, as the intestinal

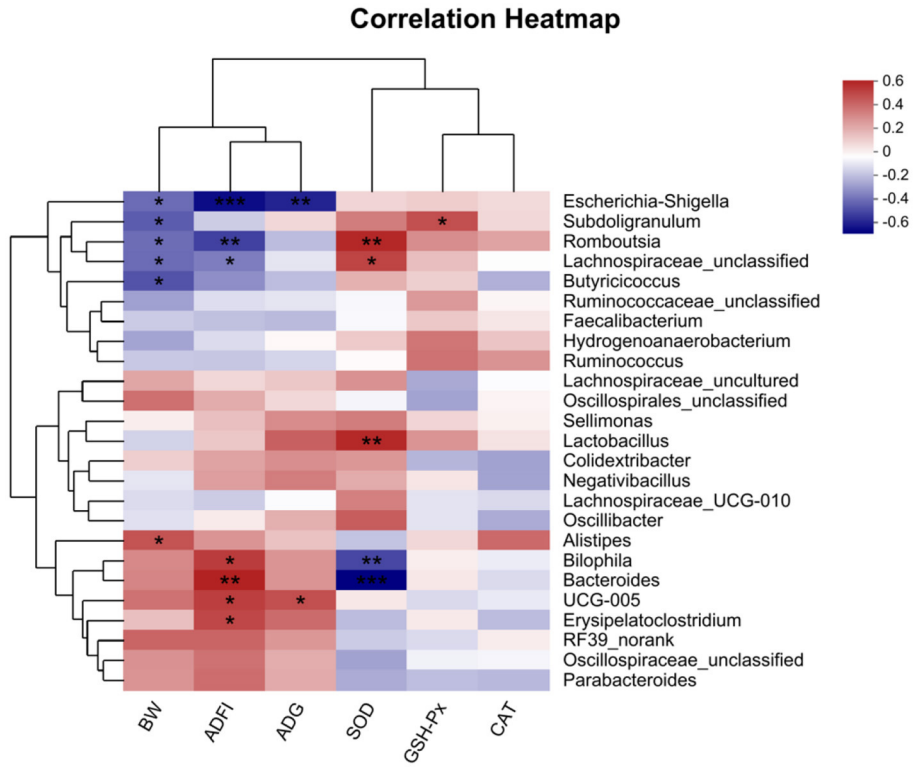

FIGURE 7
Correlation analyses between the Growth performance, oxidative function indicators and top 50 cecal bacterial genera ($n = 6$). The red squares represent the positive correlations while blue ones represent the negative correlations. *$P < 0.05$; **$P < 0.01$; ***$P < 0.001$. BW, body weight; ADFI, average daily feed intake; ADG, average daily gain; GSH-Px, glutathione peroxidase activity; CAT, catalase activity; SOD, superoxide dismutase activity.

mucosa is particularly vulnerable to oxidative damage induced by oxidants. For instance, in poultry and other animals, oxidized fats or lipids in aged grains can trigger severe oxidative stress in the intestines (Tang et al., 2019). Additionally, extensive research has shown that oxidative stress is frequently associated with heat stress or diquat stimulation. Zha et al. (2023) reported that diquat reduced T-AOC, CAT, SOD, and GSH-Px activities in a linear or quadratic manner, while increasing MDAaccumulation in serum, liver, and/or jejunum. Our experimental results demonstrated that the stimulation by diquat significantly reduced GSH-Px activity in the duodenum and significant increased MDA content in the small intestine (duodenum, jejunum, and ileum). Therefore, the judicious selection of dietary additives can help maintain ROS homeostasis and sustain intestinal health, thereby promoting healthy growth in livestock and poultry. Previous studies have demonstrated that plant extracts (Liu et al., 2018), probiotic (Song et al., 2014), and betaine (Saeed et al., 2017) can significantly enhance the antioxidant function of the intestinal tract in broilers. Research by Bakar et al. (2019) found that feeding naringin or hesperidin extracts significantly reduced MDA content in rat small intestine and notably increased SOD and GSH-Px activity in the intestine, alleviating symptoms of colitis. Moreover, our previous experiments found that *Artemisia* flavonoids possess excellent radical-scavenging abilities and antioxidant effects, which can enhance the activity of antioxidant enzymes (CAT, SOD, and GSH-Px) in the small intestine of broiler chickens, thereby improving the intestinal tissue's antioxidant capacity (Zhang P. F. et al., 2020; Yang et al., 2021). This study found that feeding QG significantly mitigated the reduction in GSH-Px activity and the increase in MDA content induced by diquat in broiler chicken small intestine. This indicates that feeding QG can protect the small intestine from lipid peroxidation-induced damage and help maintain redox homeostasis, thus enhancing the antioxidant function of the broiler's intestine. Integrating these results, we hypothesize that QG in the diet can enhance the antioxidant capacity of broiler chickens by increasing enzymatic activity and directly scavenging hydroxyl and superoxide anions in the small intestine, thereby maintaining intestinal redox stability, but the specific mechanisms involved require further investigation.

Antioxidant systems are fundamental to cellular defense against oxidative stress, relying on both enzymatic and non-enzymatic components. The enzymatic antioxidant system includes key enzymes such as SOD, CAT, and GSH-Px, forming the first line of defense against oxidative stress. The expression and activity of these antioxidant enzymes are primarily regulated by nuclear factor erythroid 2-related factor 2 (Nrf2). Under conditions without oxidative stress, Nrf2 forms an inactive complex with Keap1 protein in the cytoplasm. However, when cells encounter oxidative stress, Nrf2 dissociates from Keap1 and translocates to the nucleus, activating the expression of antioxidant response genes (Xing et al., 2021). Studies have shown that certain flavonoid compounds, such as QG, can enhance the activity of antioxidant enzymes by

activating the Nrf2/Keap1 signaling pathway, effectively mitigating oxidative stress. This research further explores the effects of QG on the expression of antioxidant genes in the small intestine of broiler chickens and its potential molecular mechanisms (Sun et al., 2020). The experimental results indicate that the addition of QG to the feed significantly increased the mRNA levels of *GSH-Px* and *Keap1* in the duodenum, as well as *GSH-Px* and *Nrf2* mRNA levels in the ileum of broiler chickens. These findings suggest that QG may enhance the intrinsic antioxidant defense mechanisms of intestinal cells, improving their adaptive response to oxidative stress. Moreover, these results underscore the central role of the Nrf2/Keap1 signaling pathway in regulating the antioxidant defense response of the intestines. By activating this pathway, QG not only enhances the expression of antioxidant enzymes but may also promote the synthesis of other antioxidant-related proteins, providing comprehensive cellular protection. According to research by Sahin et al. (2023), QG enhances the activity of antioxidant enzymes in tissues by upregulating the Keap1/Nrf2/antioxidant response element (ARE) pathway, thereby alleviating oxidative damage in the retinas of mice. Additionally, other studies have found that QG activates the Nrf2/HO-1 signaling pathway in the liver of broiler chickens, increasing the activity of downstream key factors (HO-1) and antioxidant enzymes (SOD), and reducing oxidative damage caused by the herbicide paraquat (Chen et al., 2020). However, the current study found no significant differences in the mRNA expression of *CAT*, *SOD*, *GSH-Px*, *Nrf2*, and *Keap1* in the jejunum across all groups. This finding suggests that while certain parts of the intestine enhance antioxidant defense by upregulating related gene expression in response to specific antioxidants, other parts may respond differently or require different dosages and treatment durations to exhibit effects.

In addition to its well-documented effects on the Nrf2/Keap1 pathway, QG may influence other critical antioxidant defense mechanisms, including the NF-κB and MAPK signaling pathways. These pathways play pivotal roles in regulating cellular responses to oxidative stress and are intricately interconnected with Nrf2. Importantly, they can also exhibit negative feedback mechanisms that modulate Nrf2 activity. The interplay between NF-κB, MAPK, and Nrf2 may provide an additional layer of protection by refining and enhancing cellular adaptive responses to oxidative challenges (Zhou et al., 2018; Wardyn et al., 2015). This synergistic interaction could lead to a more robust cellular defense strategy. For example, activation of NF-κB can upregulate pro-inflammatory cytokines, which may, in turn, influence the expression of Nrf2 target genes. Similarly, the MAPK pathway can modulate Nrf2 activity through phosphorylation, enhancing its transcriptional efficacy under oxidative stress conditions (Hanson and Batchelor, 2022). Furthermore, QG impact may extend beyond enzymatic antioxidants to non-enzymatic systems, notably glutathione (GSH), one of the most abundant intracellular antioxidants. By promoting GSH synthesis or recycling via modulation of related enzymes, QG may enhance the cell's ability to counteract ROS. This is supported by our observation of increased *GSH-Px* mRNA levels, suggesting that QG reinforces the GSH system, a vital component of the antioxidant defense network. These findings underscore the multifaceted role of QG in maintaining cellular redox homeostasis and protecting against oxidative damage across multiple levels. Future research needs to further explore the impact of QG on other antioxidant pathways and how these pathways work synergistically to enhance the overall antioxidant capacity and health status of broiler chickens. This is vital for developing more effective feed additives to improve the production efficiency and animal welfare in the poultry industry.

The cecum is an important site in the body for water regulation, urea recycling, and carbohydrate fermentation, and is crucial for the intestinal nutritional health of broiler chickens. Studies have shown that the diversity and richness of intestinal microbiota are closely related to the likelihood of broiler chicken disease occurrence (Guo et al., 2010). In microbial alpha-diversity analysis, the Chao1 index reflects the abundance of the microbial communities, with a higher Chao1 index indicating greater community abundance. The Shannon and Simpson indices reflect community diversity. Specifically, a higher Shannon index and a lower Simpson index indicate greater species richness. Typically, higher microbial diversity indices indicate a more stable microbial community that is more resistant to disruptions. Our study found that the OTUs and Chao1 indices of the QG treatment groups (LQG, MQG, and HQG) were significantly higher than those of the CON group. It is speculated that the addition of QG to the diet may alter microbial evenness, increase microbial abundance, and enhance diversity. The cecum is the site with the highest microbial content in the poultry intestine. Studies have shown that Firmicutes and Bacteroidetes are the dominant phyla at the phylum level in the cecum of broiler chickens (Zhang Y. et al., 2020), consistent with the results of this experiment. The results of this study indicate that the top four species in terms of total abundance in each group are *Firmicutes*, *Bacteroidota*, *Proteobacteria*, and *Desulfobacterota*, among which *Firmicutes* and *Bacteroidota* are dominant phyla. These findings suggest that *Firmicutes* and *Bacteroidota* are dominant microbial communities in the poultry intestine and are less susceptible to external influences. Research has found that *Bacteroidota* can decompose non-fiber carbohydrates and proteins in feed, thereby promoting the development of the gastrointestinal immune system and playing an important role in providing energy and maintaining normal metabolism in animal bodies (Pandit et al., 2018). The higher abundance of *Bacteroidota* is beneficial for the absorption of nutrients in the intestine. This study found that compared with the DQ group, the addition of QG to the diet significantly reduced the relative abundance of Firmicutes and significantly increased the relative abundance of *Bacteroidota*. This is consistent with the improved growth performance of the experimental chickens in this study. The composition and abundance of microbiota in the intestine have a significant impact on the vital activities, immunity, digestive function, and adaptability of poultry, representing important indicators of their health status and production performance (Lynch and Hsiao, 2019). During the growth process of poultry, many factors can lead to an increase in reactive ROS levels in the body, resulting in oxidative stress. Excessive ROS levels can damage the intestinal structure and disrupt the intestinal microbiota, resulting in poultry diseases and impeding their growth and development (Assimakopoulos et al., 2004). Oxidative stress alters the intestinal environment, favoring the proliferation of pathogenic bacteria and the production of harmful metabolites.

This, in turn, leads to competition with beneficial microbiota and suppresses their proliferation, further exacerbating the damage caused by oxidative stress to the organism. The results of this study indicate that DQ significantly reduces the abundance of *Lactobacillus* and *Alistipes*, whereas the addition of QG significantly alleviated the decrease in abundance of *Lactobacillus* and *Alistipes*. *Alistipes* is a major producer of short-chain fatty acids such as acetic acid and propionic acid. Acetic acid, propionic acid, and butyric acid are the three most abundant short-chain fatty acids in the intestine, accounting for over 90% of total short-chain fatty acids. These short-chain fatty acids play a regulatory role in energy metabolism, intestinal inflammatory response, and immune function (Li et al., 2017). Parker et al. (2020) found that *Alistipes* may have protective effects against certain diseases, including liver fibrosis, colitis, tumor immunotherapy, and cardiovascular diseases. This further validates that the inclusion of QG in the diet can increase the relative abundance of beneficial microbiota, thereby improving intestinal health.

The Spearman correlation analysis underscores the link between broiler growth performance and cecal microbiota, highlighting the influence of oxidative stress and microbial balance on broiler health. Negative correlations between BW and bacteria such as *Escherichia-Shigella*, *Subdoligranulum*, *Romboutsia*, and *Lachnospiraceae_unclassified* suggest their negative impact on growth, potentially through inflammation or nutrient absorption issues. In contrast, the positive correlation between BW and *Alistipes*, a producer of SCFAs, supports its role in enhancing nutrient absorption and energy metabolism. ADFI showed negative correlations with *Escherichia-Shigella*, *Romboutsia*, and *Lachnospiraceae_unclassified*, while positive correlations with *Erysipelatoclostridium*, *UCG-005*, and *Bacteroides* indicate their potential role in promoting feed efficiency and gut health. The positive correlation betweenADG and *UCG-005* highlights its beneficial effects on growth. Regarding antioxidant function, *Subdoligranulum* positively correlated with GSH-Px, while SOD correlated positively with *Romboutsia*, *Lactobacillus*, and *Lachnospiraceae_unclassified*, indicating their role in redox balance. The negative correlations between SOD and *Bacteroides* and *Bilophila* suggests that oxidative stress disrupts beneficial microbes, promoting harmful ones. The addition of QG to the diet mitigated oxidative stress by increasing beneficial bacteria like *Lactobacillus* and *Alistipes*, which produce SCFAs essential for intestinal health and metabolism. QG's ability to restore microbial balance and antioxidant capacity suggests its potential in improving broiler growth and immune response. It is therefore speculated that QG can enhance the antioxidant capacity of broilers by synergistically interacting with intestinal microbiota, reducing oxidative damage caused by oxidative stress, improving the microbial composition related to intestinal health and immune metabolism in the cecum, and ultimately enhancing their growth performance and immune capacity.

5 Conclusion

The results of this experiment indicate that the intraperitoneal injection of DQ successfully established a model of oxidative stress in broiler chickens. Supplementing the basal diet with different levels of QG improved the growth performance of broilers, enhanced serum antioxidant capacity, and mitigated oxidative stress damage in the intestine. The mechanism of action of QG may be related to the regulation of the Nrf2/Keap1 signaling pathway. Furthermore, QG supplementation modulated the cecal microbiota. Comprehensive analysis showed that the optimal effect on broiler chickens was achieved with the addition of 20 mg/kg of QG to the diet. This study provides a theoretical foundation for incorporating QG into broiler diets, aiming to enhance their growth performance and antioxidant capabilities.

Data availability statement

The datasets presented in this study can be found in the NCBI repository, accession number PRJNA1173338.

Ethics statement

The animal study was approved by Animal Care and Use Committee of Hebei University of Engineering (Handan, China). The study was conducted in accordance with the local legislation and institutional requirements.

Author contributions

SY: Writing – original draft, Methodology. MH: Resources, Validation, Writing – original draft. ZS: Data curation, Validation, Writing – review & editing. FW: Writing – review & editing. YZ: Writing – review & editing. CZ: Investigation, Writing – review & editing. YS: Supervision, Validation, Writing – review & editing.

Funding

The author(s) declare financial support was received for the research, authorship, and/or publication of this article. The research described in this paper received financial support from the Natural Science Foundation of Hebei Province under Project Number C2022402040. This funding played a crucial role in facilitating the execution of the study, covering expenses related to experimental materials, equipment, and personnel costs.

Acknowledgments

We express our sincere gratitude for their financial assistance, which enabled the conduct of this study. We also extend our appreciation to our laboratory colleagues for their invaluable assistance, which significantly contributed to this research endeavor.

Conflict of interest

The authors declare that the research was conducted in the absence of any commercial or financial relationships that could be construed as a potential conflict of interest.

Publisher's note

All claims expressed in this article are solely those of the authors and do not necessarily represent those of their affiliated organizations, or those of the publisher, the editors and the reviewers. Any product that may be evaluated in this article, or claim that may be made by its manufacturer, is not guaranteed or endorsed by the publisher.

References

Assimakopoulos, S. F., Vagianos, C. E., Patsoukis, N., Georgiou, C., Nikolopoulou, V., and Scopa, C. D. (2004). Evidence for intestinal oxidative stress in obstructive jaundice-induced gut barrier dysfunction in rats. *Acta Physiol. Scand.* 182, 177–185. doi: 10.1046/j.0001-6772.2003.01229.x

Bakar, E., Ulucam, E., Cerkezkayabekir, A., Sanal, F., and Inan, M. (2019). Investigation of the effects of naringin on intestinal ischemia reperfusion model at the ultrastructural and biochemical level. *Biomed. Pharmacother.* 109, 345–350. doi: 10.1016/j.biopha.2018.10.045

Bhagat, N. R., Chauhan, P., Verma, P., Mishra, A., and Bharti, V. (2023). High-altitude and low-altitude adapted chicken gut-microbes have different functional diversity. *Sci. Rep*. 13:20856. doi: 10.1038/s41598-023-48147-9

Chen, J., Wang, H., Wu, Z., Gu, H., Li, C., Wang, S., et al. (2022). Effects of 5-aminolevulinic acid on the inflammatory responses and antioxidative capacity in broiler chickens challenged with lipopolysaccharide. *Animal* 16:100575. doi: 10.1016/j.animal.2022.100575

Chen, Y. P., Gu, Y. F., Zhao, H. R., and Zhou, Y. M. (2021). Dietary squalene supplementation alleviates diquat-induced oxidative stress and liver damage of broiler chickens. *Poult. Sci.* 100:100919. doi: 10.1016/j.psj.2020.12.017

Chen, Y. Y., Chen, Y. P., Zhang, H., and Wang, T. (2020). Pterostilbene as a protective antioxidant attenuates diquat-induced liver injury and oxidative stress in 21-day-old broiler chickens. *Poult. Sci*. 99, 3158–3167. doi: 10.1016/j.psj.2020.01.021

Cheng, Y. H., Hsieh, Y. C., and Yu, Y. H. (2019). Effect of *Cordyceps militaris* hot water extract on immunomodulation-associated gene expression in broilers, *Gallus gallus*. *J. Poul. Sci.* 56, 128–139. doi: 10.2141/jpsa.0180067

Doan, N., Liu, Y., Xiong, X., Kim, K., Wu, Z., Bravo, D. M., et al. (2020). Organic selenium supplement partially alleviated diquat-induced oxidative insults and hepatic metabolic stress in nursery pigs. *Br. J. Nutr*. 124, 23–33. doi: 10.1017/S0007114520000689

Estévez, M. (2015). Oxidative damage to poultry: from farm to fork. *Poult. Sci*. 94, 1368–1378. doi: 10.3382/ps/pev094

Fuentes, J., Camargo, A. C., Atala, E., Gotteland, M., Olea-Azar, C., and Speisky, H. (2021). Quercetin oxidation metabolite present in onion peel protects Caco2 cells against the oxidative stress, NF-kB activation, and loss of epithelial barrier function induced by NSAIDs. *J. Agric. Food Chem*. 69, 2157–2167. doi: 10.1021/acs.jafc.0c07085

Guerreiro, I., Couto, A., Machado, M., Castro, C., Ferreira, P., Oliva, T. A., et al. (2016). Prebiotics effect on immune and hepatic oxidative status and gut morphology of white sea bream (*Diplodus sargus*). *Fish Shellfish Immunol*. 41, 168–174. doi: 10.1016/j.fsi.2016.01.023

Guo, X., Xia, X., Tang, R., Zhou, J., Zhao, H., and Wang, K. (2010). Development of a real-time PCR method for Firmicutes and Bacteroidetes in faeces and its application to quantify intestinal population of obese and lean pigs. *Lett. Appl. Microbiol*. 47, 367–373. doi: 10.1111/j.1472-765X.2008.02408.x

Hanson, R., and Batchelor, E. (2022). Coordination of MAPK and p53 dynamics in the cellular responses to DNA damage and oxidative stress. *Mol. Syst. Biol*. 18:e11401. doi: 10.15252/msb.202211401

Kong, L., Wang, Z., Xiao, C., Zhu, Q., and Song, Z. (2022). Glycerol monolaurate attenuated immunological stress and intestinal mucosal injury by regulating the gut microbiota and activating AMPK/Nrf2 signaling pathway in lipopolysaccharide-challenged broilers. *Anim. Nutr*. 10, 347–359. doi: 10.1016/j.aninu.2022.06.005

Lee, M. T., Lin, W. C., and Lee, T. T. (2019). Potential crosstalk of oxidative stress and immune response in poultry through phytochemicals-A review. *Asian Aust. J. Anim. Sci*. 32, 309–319. doi: 10.5713/ajas.18.0538

Li, K., Jiang, L., Wang, J., Xia, L., Zhao, R., Cai, C., et al. (2019). Maternal dietary supplementation with different sources of selenium on antioxidant status and mortality of chicken embryo in a model of diquat-induced acute oxidative stress. *Anim. Feed Sci. Technol*. 261:114369. doi: 10.1016/j.anifeedsci.2019.114369

Li, L. Z., Ma, L., and Fu, P. (2017). Gut microbiota–derived short-chain fatty acids and kidney diseases. *Drug. Des. Dev. Ther*. 11, 3531–3542. doi: 10.2147/DDDT.S150825

Li, S. C., Lin, R. Z., Chen, J. X., Hussain, R., Zhang, S. W., Su, Y. L., et al. (2022). Integrated gut microbiota and metabolomic analysis reveals immunomodulatory effects of Echinacea extract and *Astragalus polysaccharides*. *Front. Vet. Sci*. 9:971058. doi: 10.3389/fvets.2022.971058

Li, Y., Zhang, H., Chen, Y. P., Yang, M. X., Zhang, L. L., Lu, Z. X., et al. (2015). *Bacillus amyloliquefaciens* supplementation alleviates immunological stress in lipopolysaccharide-challenged broilers at early age. *Poul. Sci.* 94, 1504–1511. doi: 10.3382/ps/pev124

Li, Z., Zhang, C., Li, B., Zhang, S., Haj, F. G., Zhang, G., et al. (2021). The modulatory effects of alfalfa polysaccharide on intestinal microbiota and systemic health of Salmonella serotype (ser.) Enteritidis-challenged broilers. *Sci. Rep*. 11:10910. doi: 10.1038/s41598-021-90060-6

Liu, H. W., Li, K., Zhao, J. S., and Deng, W. (2018). Effects of chestnut tannins on intestinal morphology, barrier function, pro-inflammatory cytokine expression, microflora and antioxidant capacity in heat-stressed broilers. *J. Anim. Physiol. Anim. Nutr*. 102, 717–726. doi: 10.1111/jpn.12839

Liu, L., Shen, J., Zhao, C., Wang, X., Yao, J., Gong, Y., et al. (2015). Dietary *Astragalus polysaccharide* alleviated immunological stress in broilers exposed to lipopolysaccharide. *Int. J. Biol. Macromol*. 72, 624–632. doi: 10.1016/j.ijbiomac.2014.08.057

Lynch, J. B., and Hsiao, E. Y. (2019). Microbiomes as sources of emergent host phenotypes. *Sci. J*. 365, 1405–1409. doi: 10.1126/science.aay0240

NRC (1994). *Nutrient Requirements of Poultry, 9th Edn*. Washington, DC: The National Academies Press.

Pandit, R. J., Hinsu, A. T., Patel, N. V., Koringa, P. G., Jakhesara, S. J., Thakkar, S. J., et al. (2018). Microbial diversity and community composition of caecal microbiota in commercial and indigenous Indian chickens determined using 16s rDNA amplicon sequencing. *Microbiome* 6:115. doi: 10.1186/s40168-018-0501-9

Parker, B. J., Wearsch, P. A., Veloo, A. C. M., and Palacios, A. R. (2020). The genus *Alistipes*: gut bacteria with emerging implications to inflammation, cancer, and mental health. *Front. Immunol*. 11:906. doi: 10.3389/fimmu.2020.00906

Pisoschi, A. M., and Pop, A. (2015). The role of antioxidants in the chemistry of oxidative stress: a review. *Eur. J. Med. Chem*. 97, 55–74. doi: 10.1016/j.ejmech.2015.04.040

Polansky, O., Sekelova, Z., Faldynova, M., Sebkova, A., Sisak, F., and Rychlik, I. (2015). Important metabolic pathways and biological processes expressed by chicken cecal microbiota. *Appl. Environ. Microb*. 82, 1569–1576. doi: 10.1128/AEM.03473-15

Saeed, M., Babazadeh, D., Naveed, M., Arain, M. A., Hassan, F. U., and Chao, S. (2017). Reconsidering betaine as a natural anti-heat stress agent in poultry industry: a review. *Trop. Anim. Health Prod.* 49, 1329–1338. doi: 10.1007/s11250-017-1355-z

Sahin, E., Orhan, C., Sahin, N., Padigaru, M., Morde, A., Lal, M., et al. (2023). Lutein/zeaxanthin isomers and quercetagetin combination safeguards the retina from photo-oxidative damage by modulating neuroplasticity markers and the Nrf2 pathway. *Pharmaceuticals* 16:1543. doi: 10.3390/ph16111543

Salvador, P., Raquel, T. V., Sergio, R. P., Isabela, F., and Juan, S. (2016). Redox signaling in the gastrointestinal tract. *Free Radic. Biol. Med*. 104, 75–103. doi: 10.1016/j.freeradbiomed.2016.12.048

Shi, L. L., Jin, X., Xu, Y. Q., Xing, Y. Y., Yan, S. M., Guo, Y., et al. (2022). Effects of total flavonoids of *Artemisia ordosica* on growth performance, oxidative stress, and antioxidant status of lipopolysaccharide-challenged broilers. *Antioxidants* 11:1985. doi: 10.3390/antiox11101985

Song, J., Xiao, K., Ke, Y. L., Jiao, L. F., Hu, C. H., Diao, Q. Y., et al. (2014). Effect of a probiotic mixture on intestinal microflora, morphology, and barrier integrity of broilers subjected to heat stress. *Poul. Sci*. 93, 581–588. doi: 10.3382/ps.2013-03455

Song, Z. H., Cheng, K., Zheng, X. C., Ahmad, H., Zhang, L. L., and Wang, T. (2018). Effects of dietary supplementation with enzymatically treated *Artemisia annua* on growth performance, intestinal morphology, digestive enzyme activities, immunity, and antioxidant capacity of heat-stressed broilers. *Poul. Sci*. 97, 430–437. doi: 10.3382/ps/pex312

Sun, L., Xu, G. Q., Dong,Y. Y., Li, M., and Yang, L. Y. (2020). Quercetin protects against lipopolysaccharide-induced intestinal oxidative stress in broiler chickens through activation of Nrf2 pathway. *Molecules* 25:1053. doi: 10.3390/molecules25051053

Tang, D., Wu, J., Jiao, H., Wang, X., Zhao, J., and Lin, H. (2019). The development of antioxidant system in the intestinal tract of broiler chickens. *Poult. Sci*. 98, 664–678. doi: 10.3382/ps/pey415

Waite, D. W., and Taylor, M. W. (2015). Exploring the avian gut microbiota: current trends and future directions. *Front. Microbiol.* 6:673. doi: 10.3389/fmicb.2015.00673

Wan, S. X., Wang, L. Z., Hao, Z. L., Zhu, L., Mao, X. X., Li, H. Q., et al. (2024). Baicalin ameliorates the gut barrier function and intestinal microbiota of broiler chickens. *Acta Biochim. Biophys. Sin.* 56, 634–644. doi: 10.3724/abbs.2024029

Wang, W., Xu, H., Chen, H., Tai, K., Liu, F., and Gao, Y. (2016). *In vitro* antioxidant, antidiabetic and antilipemic potentials of quercetagetin extracted from marigold (*Tagetes erecta* L.) inflorescence residues. *J. Food Sci. Technol.* 53, 2614–2624. doi: 10.1007/s13197-016-2228-6

Wang, Y., Ye, J., Zhang, S., Chen, Z., Fan, Q., and Jiang, S. (2022). Dietary supplementation with anthocyanin attenuates lipopolysaccharide induced intestinal damage through antioxidant effects in yellow-feathered broiler chicks. *Poult. Sci.* 102:102325. doi: 10.1016/j.psj.2022.102325

Wardyn, D. W., Ponsford, A. H., and Sanderson, C. M. (2015). Dissecting molecular cross-talk between Nrf2 andNF-κB response pathways. *Biochem. Soc. Trans.* 43, 621–626. doi: 10.1042/BST20150014

Wu, F., Yang, X., Wang, F., Liu, Y., Han, S., Liu, S., et al. (2023). Dietary curcumin supplementation alleviates diquat-induced oxidative stress in the liver of broilers. *Poult. Sci.* 102:103132. doi: 10.1016/j.psj.2023.103132

Wu, F. Y., Wang, F. X., Tang, Z. H., Yang, X. Y., Liu, Y. H., Zhao, M., et al. (2023). Quercetagetin alleviates zearalenone-induced liver injury in rabbits through Keap1/Nrf2/ ARE signaling pathway. *Front. Pharmacol.* 14:1271384. doi: 10.3389/fphar.2023.1271384

Wu, F. Y., Wang, H. N., Li, S., Wei, Z. H., Han, S. J., and Chen, B. (2022). Effects of dietary supplementation with quercetagetin on nutrient digestibility, intestinal morphology, immunity, and antioxidant capacity of broilers. *Front. Vet. Sci.* 9:1060140. doi: 10.3389/fvets.2022.1060140

Xing, Y. Y., Zheng, Y. K., Yang, S., Zhang, L. H., Guo, S. W., Shi, L. L., et al. (2021). *Artemisia ordosica* polysaccharide alleviated lipopolysaccharide-induced oxidative stress of broilers via Nrf2/Keap1 and TLR4/NF-κB pathway. *Ecotoxicol. Environ. Saf.* 2021:112566. doi: 10.1016/j.ecoenv.2021.112566

Yang, S., Zhang, J., Jiang, Y., Xu, Y. Q., Jin, X., Yan, S. M., et al. (2021). Effects of *Artemisia argyi* flavonoids on growth performance and immune function in broilers challenged with lipopolysaccharide. *Anim. Biosci.* 34, 1–12. doi: 10.5713/ab.20.0656

Yu, G. C., Wang, J. R., Jian, T. Z., Shi, L. K., Zhao, L. W., Li, Y. Q., et al. (2022). Case series: diquat poisoning with acute kidney failure, myocardial damage, and rhabdomyolysis. *Front. Public Health*. 10:991587. doi: 10.3389/fpubh.2022.991587

Yuan, D. X., Hussain, T. Q., Tan, B., Liu, Y. H., Ji, P., and Yin, Y. L. (2017). The evaluation of antioxidant and anti-inflammatory effects of *Eucommia ulmoides* flavones using diquat-challenged piglet models. *Oxid. Med. Cell. Longev.* 2017:8140962. doi: 10.1155/2017/8140962

Zha, P. P., Wei, L. Y., Liu, W. H., Chen, Y. P., and Zhou, Y. M. (2023). Effects of dietary supplementation with chlorogenic acid on growth performance, antioxidant capacity, and hepatic inflammation in broiler chickens subjected to diquat-induced oxidative stress. *Poult. Sci.* 102:102479. doi: 10.1016/j.psj.2023.102479

Zhang, P. F., Chen, H. Y., Shi, B. L., and Yan, S. M. (2020). *In vitro* antioxidant activity of *Artemisia argyi* powder and the effect on hepatic and intestinal antioxidant indices in broiler chickens. *Ann. Anim. Sci.* 20, 156–168. doi: 10.2478/aoas-2020-0029

Zhang, Y., Liu, Y., Li, J., Xing, T., Jiang, Y., Zhang, L., et al. (2020). Dietary corn-resistant starch suppresses broiler abdominal fat deposition associated with the reduced cecal Firmicutes. *Poult. Sci.*, 99, 5827–5837. doi: 10.1016/j.psj.2020.07.042

Zheng, Y. W., Zhang, J. Y., Zhou, H. B., Guo, Y. P., Ma, Q. G., Ji, C., et al. (2020). Effects of dietary pyrroloquinoline quinone disodium supplementation on inflammatory responses, oxidative stress, and intestinal morphology in broiler chickens challenged with lipopolysaccharide. *Poult. Sci.* 99, 5389–5398. doi: 10.1016/j.psj.2020.08.007

Zhou, M., Xu, W., Wang, J., Yan, J., Shi, Y., Zhang, C., et al. (2018). Boosting mTOR-dependent autophagy via upstream TLR4-MyD88-MAPK signalling and downstream NF-κB pathway quenches intestinal inflammation and oxidative stress injury. *EBioMedicine* 35, 345–360. doi: 10.1016/j.ebiom.2018.08.035

frontiers | Frontiers in Microbiology

TYPE Original Research
PUBLISHED 30 October 2024
DOI 10.3389/fmicb.2024.1381423

Check for updates

OPEN ACCESS

EDITED BY
Adrienne Narrowe,
Agricultural Research Service (USDA),
United States

REVIEWED BY
Muhammad Tanweer Khan,
University of Gothenburg, Sweden
Lamya'a M. Dawud,
Colorado State University, United States

*CORRESPONDENCE
Jinqiang Zhang
552450374@qq.com
Zili You
youzili@uestc.edu.cn
Tao Zhou
taozhou88@163.com

RECEIVED 03 February 2024
ACCEPTED 16 October 2024
PUBLISHED 30 October 2024

CITATION
Liu Y-e, Zhao Z, He H, Li L, Xiao C, Zhou T, You Z and Zhang J (2024) Stress-induced obesity in mice causes cognitive decline associated with inhibition of hippocampal neurogenesis and dysfunctional gut microbiota.
Front. Microbiol. 15:1381423.
doi: 10.3389/fmicb.2024.1381423

COPYRIGHT
© 2024 Liu, Zhao, He, Li, Xiao, Zhou, You and Zhang. This is an open-access article distributed under the terms of the Creative Commons Attribution License (CC BY). The use, distribution or reproduction in other forums is permitted, provided the original author(s) and the copyright owner(s) are credited and that the original publication in this journal is cited, in accordance with accepted academic practice. No use, distribution or reproduction is permitted which does not comply with these terms.

Stress-induced obesity in mice causes cognitive decline associated with inhibition of hippocampal neurogenesis and dysfunctional gut microbiota

Yu-e Liu[1], Zhihuang Zhao[1], Haili He[1], Liangyuan Li[1], Chenghong Xiao[1], Tao Zhou[1]*, Zili You[2]* and Jinqiang Zhang[1]*

[1]Guizhou University of Traditional Chinese Medicine, Guiyang, China, [2]The Center of Psychosomatic Medicine, Sichuan Provincial Center for Mental Health, Sichuan Provincial People's Hospital, University of Electronic Science and Technology of China, Chengdu, China

Effects of stress on obesity have been thoroughly studied in high-fat diet fed mice, but not in normal diet fed mice, which is important to clarify because even on a normal diet, some individuals will become obese under stress conditions. Here we compared mice that showed substantial weight gain or loss under chronic mild stress while on a normal diet; we compared the two groups in terms of cognitive function, hypothalamic–pituitary–adrenal signaling, neurogenesis and activation of microglia in hippocampus, gene expression and composition of the gut microbiome. Chronic mild stress induced diet-independent obesity in approximately 20% of animals, and it involved inflammatory responses in peripheral and central nervous system as well as hyperactivation of the hypothalamic–pituitary–adrenal signaling and of microglia in the hippocampus, which were associated with cognitive deficits and impaired hippocampal neurogenesis. It significantly increased in relative abundance at the phylum level (Firmicutes), at the family level (*Prevotellaceae ucg – 001* and *Lachnospiraceae NK4a136*), at the genus level (*Dubosiella* and *Turicibacter*) for some enteric flora, while reducing the relative abundance at the family level (*Lactobacillaceae* and *Erysipelotrichaceae*), at the genus level (*Bacteroidota, Alistipes, Alloprevotella, Bifidobacterium and Desulfovibrio*) for some enteric flora. These results suggest that stress, independently of diet, can induce obesity and cognitive decline that involve dysfunctional gut microbiota. These insights imply that mitigation of hypothalamic–pituitary–adrenal signaling and microglial activation as well as remodeling of gut microbiota may reverse stress-induced obesity and associated cognitive decline.

KEYWORDS

stress, obesity, depression, cognitive function, gut microbiome, adult hippocampus neurogenesis, microglia

Highlights

- Chronic stress can induce diet-independent obesity in mice.
- Stress-induced obesity involves alterations in the gut microbiome and hyperactivation of the hypothalamic–pituitary–adrenal axis.
- Stress-induced obesity in mice causes cognitive decline associated with inhibition of neurogenesis in hippocampus.

1 Introduction

Not only diet but also stress can trigger obesity (Tomiyama, 2019; Zhou et al., 2022), and stress can also increase risk of depression (Jiang et al., 2022), anxiety (De Gregorio et al., 2022) and cognitive impairment (Ma et al., 2023), which obesity can increase further (Fulton et al., 2021). Most of the literature on stress-induced obesity in animal models was obtained using animals on high-fat diets (Jene et al., 2021; Lama et al., 2022; Noronha et al., 2019; Zhu et al., 2020). As a result, many insights about the effects of stress on cognitive function, mood or mental health may be confounded by the influence of diet. In our laboratory, we observed that chronic mild stress can induce obesity in 10–20% mice even when they are maintained on a normal diet (Supplementary Figure S1), suggesting that we could explore the influence of stress on obesity and cognitive function without the complicating influences of diet.

Therefore, the present study compared subsets of mice whose body weight increased or decreased significantly in response to chronic mild stress, even though they were maintained on a normal diet. We wanted to explore whether chronic stress capable of inducing obesity could cause several pathologies observed in the absence of obesity, particularly chronic inflammation, psychotic and mood disorders and cognitive impairment (Baumeister et al., 2016; Holsboer and Ising, 2008; Lasikiewicz et al., 2013), and further explored the underlying mechanisms of stress-induced obesity by focusing on the hypothalamic–pituitary–adrenal (HPA) axis and gut microbiome. In response to stress, the HPA axis is activated in order to trigger adaptive behaviors and re-establish homeostasis (Dalile et al., 2022; Micale and Drago, 2018). Over-activation of the HPA axis causes dysregulation of hormone secretion, which contributes to stress-induced obesity (Schinke et al., 2017; Schinke et al., 2022; Vicennati et al., 2014). Dysregulation in the gut microbiome can lead to obesity by altering the absorption of nutrients in the host, modifying metabolic pathways in the host and secreting bacterial metabolites that target the brain directly via vagal stimulation or indirectly through immune-neuroendocrine mechanisms involving corticotropin-releasing hormone, adrenocorticotropin and corticosterone (Geng et al., 2022; Tseng and Wu, 2019; Wang et al., 2020).

Stress-induced dysregulation of the gut microbiome can permeabilize the gut, activate microglia and induce neuroinflammation (Braniste et al., 2014; Geng et al., 2019; Spadoni et al., 2015), ultimately impairing neurogenesis in the hippocampus and cognitive function (Ma et al., 2023; He et al., 2024; He et al., 2024). Alterations in the gut microbiome can activate the HPA axis (Misiak et al., 2020) and, conversely, activation of the HPA axis can impact the gut microbiota (Rusch et al., 2023; O'Mahony et al., 2020). These observations were made in animals that were not obese or that were made obese through a high-fat diet. Here we examined whether the same was true for animals with stress-induced obesity despite being on a normal diet.

Abbreviations: ACTH, Adrenocorticotropin; CRH, Corticotropin-releasing hormone; CORT, Corticosterone; CMS, Chronic mild stress; FST, Forced swimming test; HDL, High-density lipoprotein cholesterol; HPA, Hypothalamic–pituitary–adrenal; IL-6, Interleukin-6; IL-10, Interleukin-10; LDL, Low-density lipoprotein cholesterol; NLRT, Novel location recognition test; NORT, Novel object recognition test; OFT, Open field test; SPT, Sucrose preference test; TC, Total cholesterol; TG, Triglyceride; TST, Tail suspension test; TNF-α, Tumor necrosis factor α.

2 Materials and methods

2.1 Animals

Male C57BL/6 mice, 7 weeks old and free of specific pathogens, were purchased from Chengdu Dashuo Laboratory Animals (Chengdu, China), housed individually and assigned unique numbers. The mice were acclimated for a week before the experiment. The mice were housed individually under standard condition (23°C ± 2°C, 50% ~ 70% humidity, on a 12–12 h light–dark cycle with lights on at 07,00 and lights off at 19,00, with access to food and water *ad libitum*) and were allowed to habituate to laboratory conditions for 1 week prior to the experiments. Weight-matched animals were randomly divided to control group (Ctrl, $n = 12$ mice) and chronic mild stress group (CMS, $n = 30$ mice). Mice from CMS group were exposed to chronic mild stress as described in 2.3 section. Control mice were not subjected to any stress and housed in their cages similar to the habituation period.

All animal experiments were approved by the Institutional Animal Care and Use Committee at the Guizhou University of Traditional Chinese Medicine (20,231,215,001, Guiyang, China). All experiments were performed in accordance with ARRIVE guidelines 2.0 (2020) (Percie et al., 2020) and with the "Guidelines for the Care and Use of Laboratory Animals" from the United States National Institutes of Health.

2.2 Chronic mild stress

Mice from CMS group were exposed to chronic mild stress for 4 weeks as described (Agudelo et al., 2014). Every day, mice in the stressed group were exposed to 2–3 of the following stressors in random order: tilting of the cage (45°, 24 h), clamping of the tail (10 min), shaking of the cage (30 min), continuous light (24 h), continuous darkness (24 h), restraint (2 h), strobe light (12 h), empty bottle (6 h), wet bedding (12 h), empty cage (24 h), and scent stimuli (mice were placed in a pepper-smelled chamber for 15 min).

During the 4 weeks, all animals were weighed every Wednesday and Sunday at 15:00. Once weekly, they were deprived of food and water for 12 h and assessed in the sucrose preference test (see section 2.3.1 below). Also once weekly, their physical state was assessed in terms of the coat score assay as described (Cao et al., 2013). The fur in the following seven body areas was assigned 0 point if it was unkempt (un-groomed) or 1 point if it was well-groomed: head, neck, forepaws, dorsal coat, ventral coat, hind paws and tail. The seven scores were summed to obtain the total coat score.

After 4 weeks, animals whose body weight was at least one standard deviation smaller or larger than that of unstressed control animals were classified as showing stress-induced weight loss (WL) or gain (WG), respectively. These two groups were confirmed by body mass index and serum lipid level, and compared in several ways such as based on the fecal microbiome, systemic behavior, hormone levels, peripheral and neural cytokines and hippocampal neurogenesis (see below).

2.3 Behavioral testing

2.3.1 Sucrose preference test

This test was performed as described (Zhang et al., 2021). Animals were deprived of water or food for 12 h, then given *ad libitum* access for 12 h to two identical bottles, one containing water and the other 1% sucrose solution. The bottle positions were switched daily to avoid side bias. Both bottles were weighed before and after the 48-h period. Sucrose preference was calculated as follow: sucrose preference (%) = sucrose consumed (g) / [sucrose consumed (g) + water consumed (g)] × 100%.

2.3.2 Open field test

After 4 weeks of chronic mild stress, this test was performed in a box measuring 40 cm × 40 cm × 30 cm as described (Liu et al., 2022). Each mouse was placed in a corner at the start of the test and recorded for 5 min by a camera located above the box. Before each mouse was tested, the feces and urine left by the previous mouse were clean and deodorized with 75% ethanol. Open field lighting is produced by energy-saving lamps with a light intensity of about 200 Lux, and the noise is controlled below 65 db. The OFT100 system for tracking and analysis (Taimeng Tech, Chengdu, China) determined the number of entries into the central zone (covering 50% of the total area), the time spent in the central zone and the total distance traveled.

2.3.3 Tail suspension test

This test was performed as described (Zhang et al., 2021). Mice were elevated 35 cm above the ground by securing their tails with adhesive tape. Mice were recorded for 6 min, and the time spent immobile during the last 5 min was measured using YHTSTM software (LabState ver 2.0, Yihong Tech, Wuhan, China).

2.3.4 Forced swimming test

This test was performed as described (Zhang et al., 2021). Mice were placed for 10 min into a cylinder 25 cm high with a diameter of 10 cm, which was filled up with water at 24°C to two-thirds of the full volume. Then the animals were returned to their cages. After 24 h, the animals were placed again in the cylinder for 6 min, and the duration of immobility during the last 5 min was determined using YHTSTM software (LabState ver 2.0, Yihong Tech).

2.3.5 Tests of novel location recognition and novel object recognition

These tests measure the extent to which animals have retained their innate preferences for new objects and locations and are therefore widely used to assess hippocampus-dependent learning and memory (Ennaceur and Delacour, 1988). The experimental environment was the same as in the open field experiment.

In the training stage of the test of novel location recognition, two identical objects (non-porous/cleaned to make sure there's no scent marking) were placed in different positions in the box, then mice were placed in the central area of the box and allowed to freely explore the two objects for 10 min and thereby develop a memory of the location of the two objects. Before each mouse was tested, the feces and urine left by the previous mouse were clean and deodorized with 75% ethanol. The animals were returned to their cages, 6 min later, the position of one of the objects was randomly changed, and the mice were returned to the box and allowed to explore freely for another 10 min. The number of times that mice sniffed the object in the new location and the total time spent sniffing it (as a proportion of the total exploration time) were recorded. Greater proportion of exploration time that was spent sniffing objects in the new location was taken to indicate stronger location memory.

After animals completed the test of novel location recognition, two objects identical in shape, color, and odor were introduced into the box. Then mice were placed in the central area of the box and allowed to freely explore the two objects for 10 min. The animals were returned to their cages, 30 min later, then one of the original objects and a novel object (differing in the original objects) were placed in the box. The mice were returned to the box and allowed to explore freely for another 10 min. The time spent exploring each object was determined during each session. Greater proportion of exploration time that was spent sniffing the new objects was taken to indicate stronger object memory.

2.4 Analysis of fecal microbiomes

All fecal samples were collected at the same time (19:00) to avoid circadian influences on the microbiome. Fecal samples were examined instead of cecum contents to assess whether differences WL, WG or control. Fecal samples from 7 control animals, 7 WL animals and 6 WG animals were subjected to microbiome analysis. The composition of the fecal microbiome was analyzed using 16S rRNA sequencing, which was performed by Majorbio Bio-Pharm Technology (Shanghai, China). Sequencing experiments involved the following steps: DNA extraction, PCR amplification and product purification, MiSeq library construction, and MiSeq sequencing. PCR amplification was carried out using TransStart FastPfu DNA Polymerase (TransGen Biotech, Beijing, China) and an ABI GeneAmp® 9,700 system (Thermo Fisher Scientific, Wilmington, DE, United States). Bacterial DNA fragments were amplified using forward primer-338 (5′-ACTCCTACGGGAGGAGCAG-3′) and reverse primer-806 (5′-GCACTACHVGGGTWTCTAAT-3′). The DNA was quantified using a Nanodrop spectrophotometer (Thermo Fisher Scientific), and paired end sequencing of the V3-V4 region of 16S rRNA was performed as previously described (Pearson-Leary et al., 2020) using an Illumina MiSeq PE300 platform (Illumina, San Diego, United States). The raw sequencing reads were deposited into the NCBI Sequence Read Archive (BioProject ID PRJNA1047189).

The 300 bp reads were truncated at any site receiving an average quality score of <20 over a 50 bp sliding window, and the truncated reads shorter than 50 bp were discarded, reads containing ambiguous characters were also discarded. Only overlapping sequences longer than 10 bp were assembled according to their overlapped sequence. Barcode accurately matched and separated samples, primers adjusted the sequence direction, and selected sequences with mass greater than 20 (that is, the accuracy of 99%) for downstream analysis. In order to remove the primer cleanly, set the primer mismatch rate to 0.15. Unexcised sequences of primers are discarded directly to prevent false operational taxonomic units (OUTs). Then the optimized sequences were clustered into OTUs using UPARSE 7.1 with 97% sequence similarity level. The most abundant sequence for each OTU was selected as a representative sequence.

Bioinformatic analysis of the gut microbiota was carried out using the Majorbio Cloud platform.[1] Based on the OTUs information, rarefaction curves and alpha diversity indices including observed OTUs, Ace, Chao richness, Simpson and Shannon index were calculated with Mothur v1.30.1. The similarity among the microbial communities in different samples was determined by principal coordinate analysis (PCoA) based on Bray–curtis dissimilarity using Veganv2.5–3 package. The PERMANOVA test was used to assess the percent-age of variation explained by the treatment along with its statistical significance using Vegan v2.5–3 package.

2.5 Analysis of serum lipids, hormones and cytokines

Five mice were randomly selected from each group. These mice were anesthetized (isoflurane 4% induced anesthesia and 2% maintained anesthesia in mice), cardiac puncture was performed to collect the whole blood, and the serum was collected by centrifuging at 4°C 1500 r / min for 15 min. The serum was assayed for low-density lipoprotein cholesterol (LDL), high-density lipoprotein cholesterol (HDL), total cholesterol (TC), triglyceride (TG), corticotropin-releasing hormone (CRH), adrenocorticotropin (ACTH) and corticosterone (CORT), interleukin-6 (IL-6), tumor necrosis factor α (TNF-α) and interleukin-10 (IL-10) (Beyotime. Shanghai, China) in strict accordance with the manufacturer's instructions. These kits obtained from the Guizhou Lvmeng Weiye Biotechnology Co., LTD (Guizhou, China).

After blood collection, all mice were perfused with 0.9% NaCl. Brains were removed and divided into two hemispheres. The intact hippocampus was removed from left hemisphere and used for transcriptome sequencing and cytokine detection while the right hemisphere was used for immunohistochemical staining.

2.6 Analysis of cytokines in the hippocampus

Hippocampi were dissociated and lysed in RIPA lysis buffer (catalog no. R0010, Solarbio, Beijing, United States) containing phenylmethanesulfonyl fluoride (catalog no. IP0280, Solarbio). Lysates were centrifuged for 15 min at 1000 *g* at 4°C, the concentration of total protein in the supernatant was determined using a commercial bicinchoninic acid kit (Boster, Wuhan, China), then samples were diluted to a final total protein concentration of 1 g/mL. The pro-inflammatory factor IL-1β was quantitatively analyzed by the double antibody sandwich method (Piao et al., 2023). The diluted samples were added to 96-well plates coated with anti-mouse IL-1β antibody, labeled with biotin, and incubated with avidin peroxidase complex labeled antibody. OD values were detected at 450 nm and protein expression was calculated. The manufacturer-specified detection limit was 2 pg. / mL.

1 https://cloud.majorbio.com

2.7 Hippocampal gene expression

The hippocampal transcriptome was analyzed as described (Zhang et al., 2021). Total RNA of hippocampus was extracted using TRIzol® (Invitrogen, Carlsbad, CA, United States) according to the manufacturer's instructions. RNA was sequenced by Majorbio Bio-Pharm Technology, and all sequences were uploaded to the NCBI Sequence Read Archive under BioProject ID PRJNA1046681.

2.8 Tissue preparation and immunohistochemistry

The right hemispheres from each group mice were fixed with 4% paraformaldehyde for 48 h, dehydrated, frozen, sliced, thoroughly washed with 0.5% Triton X-100 for 15 min, blocked with 10% donkey serum for 1 h, and incubated at 4°C overnight with monoclonal antibody against Iba1 (1:400; Abcam, Cambridge, United Kingdom) to label microglia or against glial fibrillary acidic protein (1,400; Cell Signaling Technology, Danfoss, MA, United StAtes) to label astrocytes. Sections were washed three times with phosphate-buffered saline (PBS), incubated with secondary antibody in the dark for 2 h, and counterstained with DAPI (1,10,000; Roche, Switzerland).

To measure hippocampal neurogenesis, all mice received intraperitoneal injections of 5-bromo-2-deoxyuridine (5 mg/mL BrdU in 0.9% saline; Sigma, St. Louis, MO, USA) at a dose of 50 mg/kg once every 12 h for 7 days. At 48 h after the last injection, mice were perfused and brains were taken, and one of every six sequential tissue slices containing hippocampus was permeabilized with 0.5% Triton X-100 in PBS for 15 min, incubated in 2 N HCl for 28 min at 37°C, washed twice with 0.1 M borate buffer (pH 8.5) for 10 min each, blocked in 10% donkey serum for 2 h, and incubated with primary antibody against doublecortin (1:300, Cell Signaling Technology) to label immature neurons, BrdU (1:400, Cell Signaling Technology) to label proliferating neural stem/progenitor cells, or nuclear protein NeuN (1:400, Cell Signaling Technology) to label neurons. Then sections were incubated for 2 h at room temperature with Alexa-conjugated secondary antibody (1:300; Invitrogen, Carlsbad, CA, United States), followed by counterstaining with DAPI for 5 min.

In both types of staining, sections were imaged under a fluorescence microscope (Olympus IX 73, Tokyo, Japan), and images were analyzed using Image J 1.45 (United States National Institutes of Health, Bethesda, MD, United States). Percentages of total area that were positively stained or numbers of cells were averaged across five micrographs at 40× magnification per mouse.

2.9 Statistical analysis

Data were analyzed for normal distribution using the Shapiro–Wilk test, and reported as mean ± standard error. Differences among unstressed control mice and those showing stress-induced weight loss or gain were assessed for significance using one-way analysis of variance, followed by Tukey's *post hoc* test for multiple comparisons. All statistical analyses were performed using GraphPad Prism 8.0 (GraphPad, San Diego, CA, United States). Results associated with $p < 0.05$ were considered significant.

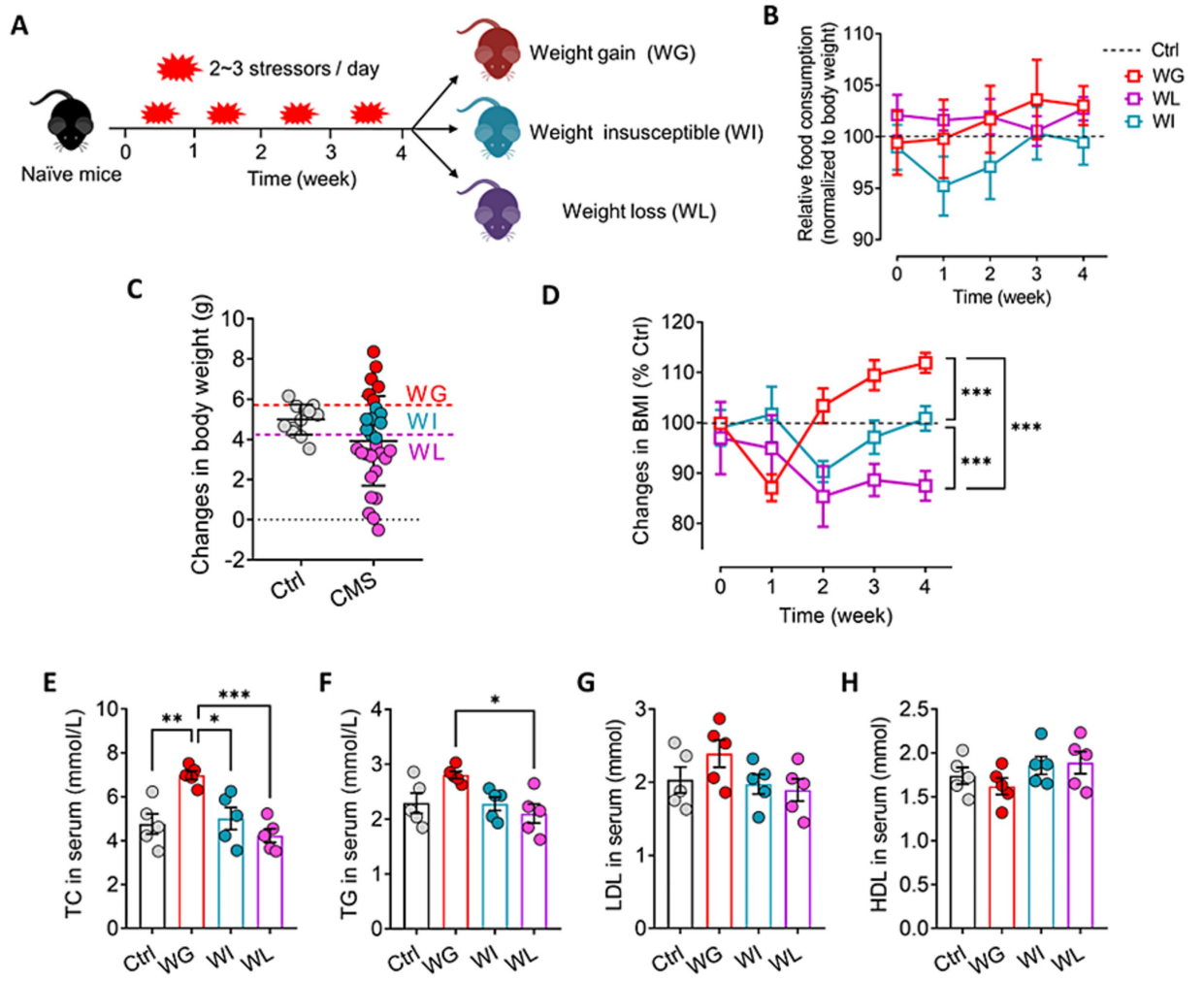

FIGURE 1
Screening of mice that exhibited stress obesity. **(A)** Schematic for identification of mice showing weight gain (WG), weight insusceptible (WI) or weight loss (WL) after stress exposure. **(B)** Changes in food consumption of WG, WI or WL mice during 4 weeks of CMS exposure. Levels were normalized to their body weight. **(C)** Mice were exposed to chronic mild stress (CMS) for 4 weeks, and animals were classified as WG, WI or WL on the basis of their body weight change. Ctrl, control animals never subjected to CMS. **(D)** Changes in body mass index (BMI) of WG, WI or WL mice during 4 weeks of CMS exposure. Levels were normalized to control mice. **(E–H)** Levels of low-density lipoprotein (LDL), high-density lipoprotein (HDL), total cholesterol (TC), and triglyceride (TG) in serum. Results are shown for triplicate samples from five animals per condition. Data are mean ± standard error of the mean (SEM). Quantitative results come from 6 to 15 animals per condition for panel C and D, and from 5 animals per condition for panel E–H. $^{*}p < 0.05$; $^{**}p < 0.01$; $^{***}p < 0.001$, based on one-way ANOVA followed by Tukey's multiple-comparisons test.

3 Results

3.1 Stress-induced obesity in mice involves cognitive impairment

Mice were exposed to CMS for 4 weeks and divided into weight gain (WG), weight loss (WL) and weight insusceptible sub-group based on their body weight changes relative control mice (Figures 1A,B). We traced the changes in body mass index and food consumption of each sub-group of animals during the CMS period, and found that WG mice showed increase and WL mice showed decrease in their body weight from week-2 to week-4 when compared with control mice (Figure 1C). However, there was no significant difference in food consumption among control, WG, WI, and WL mice during 4 weeks of CMS exposure (Figure 1D).

Chronic mild stress led to significant weight gain or loss in subsets of animals starting halfway through the four-week stress paradigm, even though all animals consumed similar amounts of normal diet throughout the paradigm (Figures 1A–D). Animals showing stress-induced weight gain also showed up-regulation of total cholesterol and triglyceride in serum, consistent with obesity (Du et al., 2019; Figures 1E–H). There was no significant difference in the above indexes between weight insusceptible sub-group and the control group.

Chronic mild stress induced depression- and anxiety-like symptoms in mice, regardless of whether they showed significant weight gain or loss (Figure 2; Supplementary Figure S2). However, the

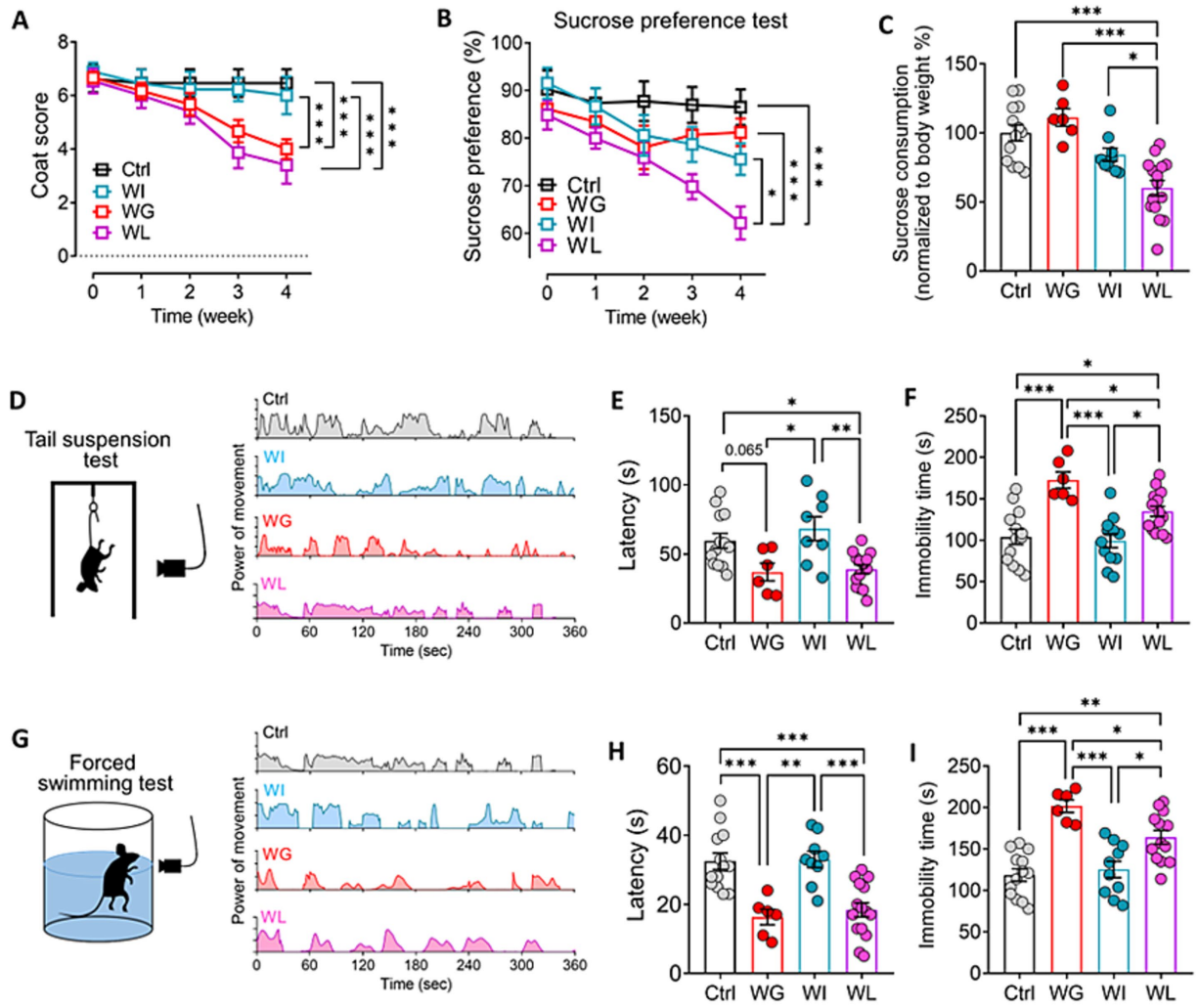

FIGURE 2
Differences between mice showing weight gain, insusceptible or loss after stress exposure in depressive-like behaviors. **(A,B)** Coat score and sucrose preferent of control (Ctrl), weight gain (WG), weight insusceptible (WI) or weight loss (WL) mice. Ctrl, control animals never subjected to CMS. **(C)** Sucrose consumption of mice in sucrose preference test. Levels were normalized to their body weight. **(D)** Power of movement from Ctrl, WG, WI or WL mice in tail suspension test during 6 min. **(E,F)** Quantization of **(E)** latency and **(F)** immobility time of Ctrl, WG, WI or WL mice in tail suspension test. **(G)** Power of movement from Ctrl, WG, WI or WL mice in forced swimming test during 6 min. **(H,I)** Quantization of **(E)** latency and **(F)** immobility time of Ctrl, WG, WI or WL mice in forced swimming test. Data are mean ± standard error of the mean (SEM). Quantitative results come from 6–15 animals per condition. $*p < 0.05$; $**p < 0.01$; $***p < 0.001$, based on one-way ANOVA followed by Tukey's multiple-comparisons test.

detailed nature of the symptoms differed between the two groups: animals that gained weight performed worse in the forced swimming and tail suspension tests than animals that lost weight, indicating greater behavioral despair (Porsolt et al., 2001); conversely, animals that lost weight showed lower sucrose preference, indicating greater anhedonia (Liu et al., 2018).

Chronic mild stress did not alter the animals' natural lack of location preference (Figures 3A–C), but it did significantly reduce the time that animals with weight gain spent exploring objects in novel locations (Figures 3D–F) and exploring novel locations (Figures 3G–I). These results link stress-induced obesity to impaired memory of objects and locations. These behavioral changes were not observed in the weight insusceptible sub-group.

Taken together, these behavioral experiments suggest that chronic mild stress can induce depression- and anxiety-like behaviors in animals regardless of whether it also leads to significant weight gain, whereas such stress impairs cognitive function only when it leads to significant weight gain.

3.2 Stress-induced obesity in mice involves hyperactivation of the HPA axis and alterations in the gut microbiome

Animals showing stress-induced weight gain also showed upregulation of corticotropin-releasing hormone, adrenocorticotropin and corticosterone in serum, consistent with HPA activation (Stout et al., 2002; Figures 4A–C). Animals showing stress-induced weight loss showed upregulation of corticosterone relative to unstressed controls, but the levels were not as high as in mice with stress-induced weight gain. Consistent with the link between HPA activation and upregulation of pro-inflammatory

10.3389/fmicb.2024.1381423

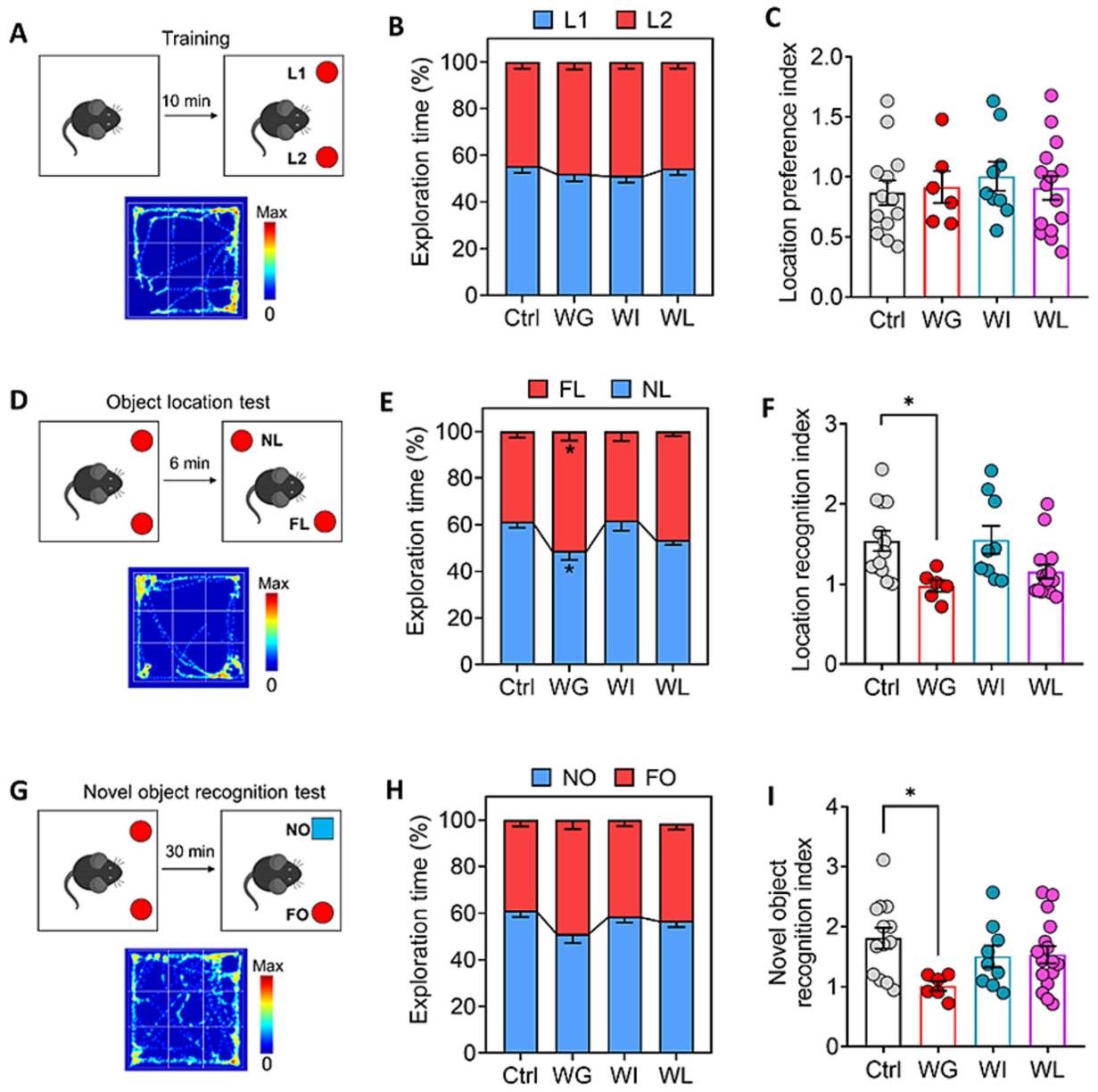

FIGURE 3
Differences between mice showing weight gain, insusceptible or loss after stress exposure in cognitive function. **(A)** Schematic for location preference test. Heatmap shows the exploration track of control mice on the object in location 1 (L1) and location (L2). **(B)** Quantization of time spent exploring objects in L1 and L2 of control (Ctrl), weight gain (WG), weight insusceptible (WI) or weight loss (WL) mice. Ctrl, control animals never subjected to CMS. **(C)** Location preference index was compared between the groups.**(D)** Schematic for object location test. Heatmap shows the exploration track of control mice on the object in novel location (NL) and familiar location (FL). **(E)** Quantization of time spent exploring objects in NL and FL of Ctrl, WG, WI or WL mice. **(F)** Location recognition index was compared between the groups. **(G)** Schematic for object location test. Heatmap shows the exploration track of control mice on the novel object (NO) and familiar object (FO). **(H)** Quantization of time spent exploring objects in NO and FO of Ctrl, WG, WI or WL mice. **(I)** Novel object recognition index was compared between the groups. Data are mean ± standard error of the mean (SEM). Quantitative results come from 6–15 animals per condition. *$p < 0.05$; **$p < 0.01$; ***$p < 0.001$, based on one-way ANOVA followed by Tukey's multiple-comparisons test.

cytokines (Ensminger et al., 2021), we found that animals showing stress-induced weight gain also showed upregulation of tumor necrosis factor-α and interleukin-6 in serum (Figures 4D–F). This upregulation was not observed in animals showing stress-induced weight loss and weight insusceptible. Both WG and WI animals showed downregulation of the anti-inflammatory cytokine interleukin-10. There was no significant difference in the above indexes between weight insusceptible sub-group and the control group.

Since the WI group showed no significant difference from the control group in behavioral test results such as anxiety, depression and cognitive function, and the expression levels of obesity-related indicators and pro-inflammatory factors. Therefore, in the subsequent analysis, we focused on WG and WL groups.

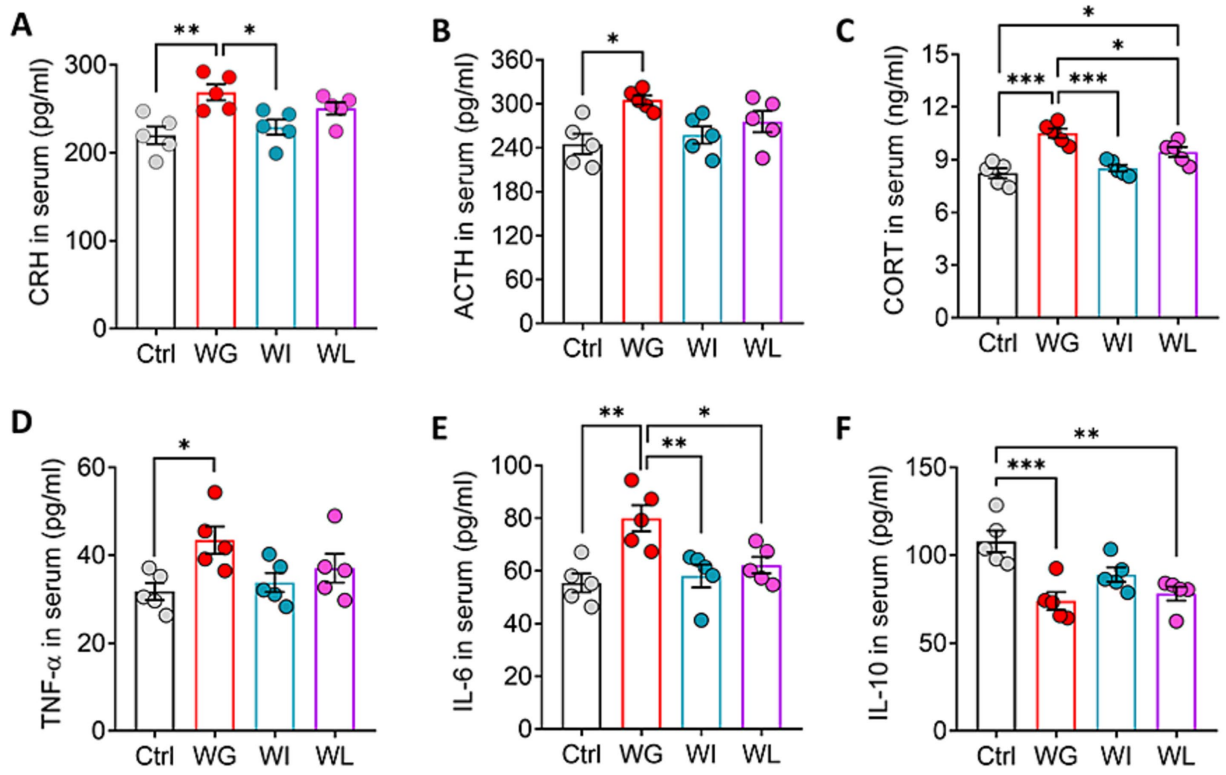

FIGURE 4
Mice that exhibited stress obesity were accompanied by hyperactivation in HPA axis and inflammatory responses. **(A–C)** Levels of corticotropin-releasing hormone (CRH), adrenocorticotropic hormone (ACTH) and corticosterone (CORT) in serum. Results are shown for triplicate samples from five animals per condition. **(D–F)** Levels of tumor necrosis factor-α (TNF-α), interleukin-6 (IL-6) and interleukin-10 (IL-10) in serum. Results are shown for triplicate samples from five animals per condition. Data are mean ± standard error of the mean (SEM). Quantitative results come from 5 animals per condition. *$p < 0.05$; **$p < 0.01$; ***$p < 0.001$, based on one-way ANOVA followed by Tukey's multiple-comparisons test.

Fecal bacteria from animals showing stress-induced weight gain or loss showed significantly higher Ace and Chao indices than those from unstressed controls (Figure 5A), suggesting that stress increased the richness of gut microbiota. In contrast, stress did not significantly affect Shannon or Simpson indices of fecal bacteria, suggesting minimal effects on the alpha diversity of gut microbiota. Principal component analysis of variation in non-phylogenetic Bray–Curtis metrics showed that the structure of the bacterial community differed significantly between animals showing stress-induced weight loss or gain, and between each of those groups and unstressed controls (Figure 5B).

At the phylum level, animals with stress-induced weight gain showed a significant increase in abundance of Firmicutes bacteria but significant decrease in Bacteroidota bacteria, while the opposite was observed in animals with stress-induced weight loss (Figure 5C). At the family level, animals with stress-induced weight gain showed a significant increase in abundance of *Erysipelotrichaceae, Lactobacillaceae* and *Prevotellaceae,* but significant decrease in *Lactobacillaceae* bacteria; the opposite was observed in animals with stress-induced weight loss (Figure 5D).

At the genus level, animals with stress-induced weight gain showed a significant increase in *Dubosiella*, while the opposite was observed in animals with stress-induced weight loss (Figure 5E). Those with weight gain showed a significant increase in abundance of *Turicibacter* bacteria but a significant decrease in abundance of *Lactobacillus* and *Alistipes* bacteria. Animals with weight loss showed a significant increase in abundance of *Enterorhabdus* bacteria. In both groups of mice, stress induced similar changes in abundances of *Alloprevotella*, *bifidobacterium, Desulfovibrio*, *Prevotellaceae UG-001 and Lachnospiraceae NK4A136 bacteria.*

3.3 Stress-induced obesity in mice involves glial hyperactivation and inhibition of neurogenesis in hippocampus

Mice with stress-induced weight gain showed upregulation of 1,431 genes and downregulation of 788 genes in the hippocampus relative to mice with stress-induced weight loss (Figures 6A–C). Most of these differentially expressed genes were involved in processes related to learning or memory, eating behavior, stress response, cytokine production, hormone secretion regulation, oxidative stress response and corticosteroid response; and these processes involved apoptosis, fatty acid biosynthesis, and signaling mediated by PI3K-Akt, NF-κB, PPARs, Toll-like receptor and NOD-like receptor (Figures 6D–F). We found that oxidative stress response in the hippocampus was implicated in stress-induced body weight change (Supplementary Figure S3). Gene set enrichment analysis confirmed that genes involved in responding to oxidative stress were upregulated in the hippocampus of animals showing stress-induced weight gain

10.3389/fmicb.2024.1381423

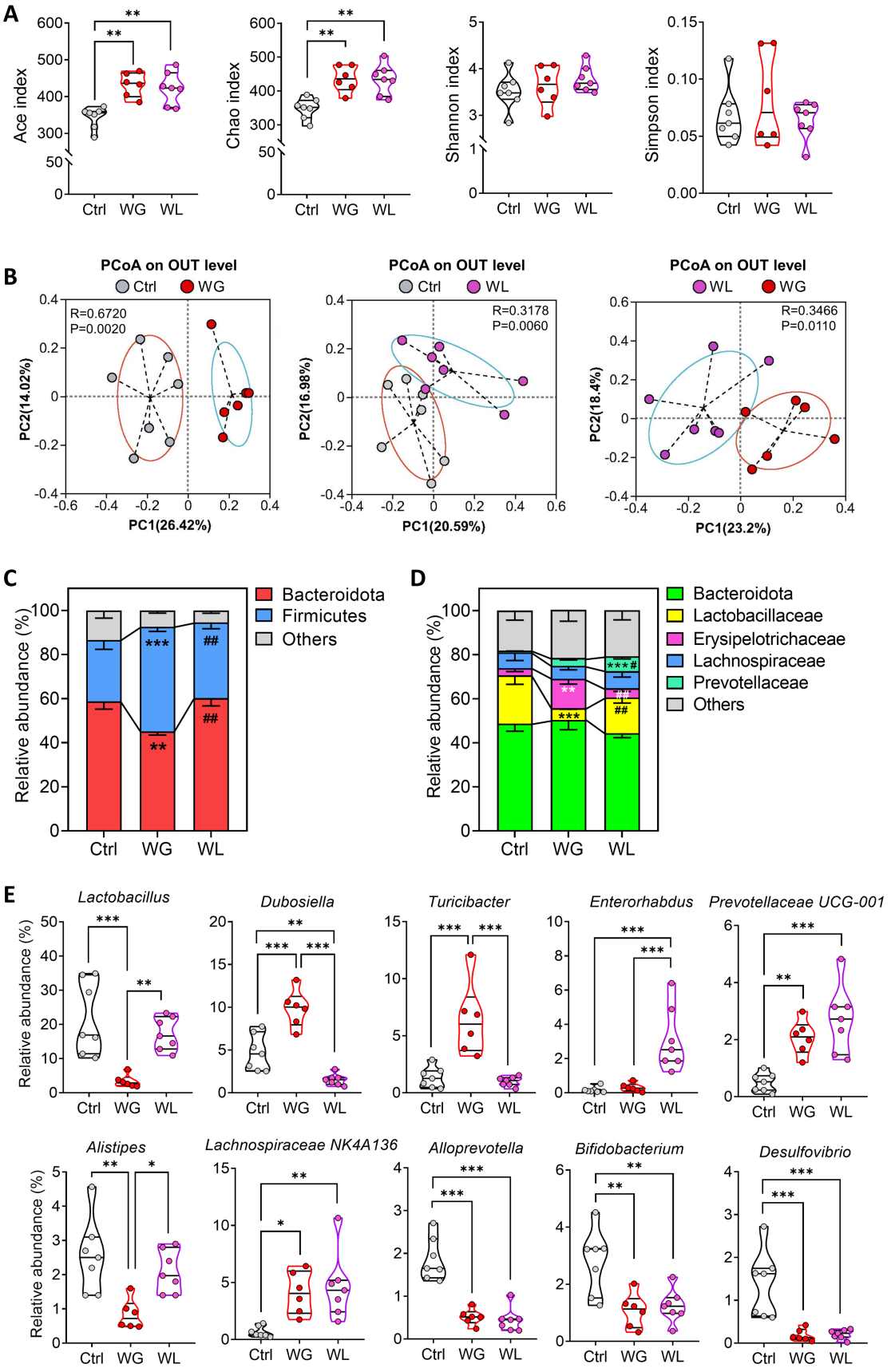

FIGURE 5
Differences in gut microbiome composition between mice showing weight gain or loss after stress exposure. **(A,B)** Alpha diversity and beta diversity of fecal microbiota from control (Ctrl), weight gain (WG), weight insusceptible (WI) or weight loss (WL) mice. Ctrl, control animals never subjected to CMS.

(Continued)

FIGURE 5 (Continued)
OTU, operational taxonomic unit; PCoA, principal component analysis; PC, principal component. **(C,D)** Relative abundances of **(C)** phyla and **(D)** families in fecal microbiota. **(E)** Differences in relative abundance of individual genera. Quantitative results come from 6 to 7 samples per condition. Data in panels **A** and **E** are shown as violin plots. The horizontal line within the violin plots represents the median, upper, and lower quartiles. The width of the plot depicts the density and distribution shape of the data points. $^{*}p < 0.05$, $^{**}p < 0.01$, $^{***}p < 0.001$, based on one-way ANOVA with Tukey's multiple-comparisons test. Data in panel **C** and **D** are mean ± standard error of the mean (SEM), $^{**}p < 0.01$, $^{***}p < 0.001$ vs. Ctrl group, $^{\#}p < 0.05$, $^{\#\#}p < 0.01$ vs. WG group, based on one-way ANOVA with Tukey's multiple-comparisons test.

relative to those showing weight loss (Figures 7A,B; Supplementary Figure S2).

Both groups of mice showed significantly larger numbers of hippocampal microglia (detected based on Iba1 expression) than unstressed controls, and a significantly larger proportion of those microglia had enlarged somata, reduced branching and thicker, shorter processes than in controls (Figures 7C–H). These results indicate stress-induced hyperactivation of hippocampal microglia, which was stronger in animals with weight gain than in animals with weight loss. The greater activation in mice with weight gain was associated with higher levels of the pro-inflammatory cytokine interleukin-1β in hippocampus (Figure 7I). Both groups of mice showed significantly larger numbers of hippocampal astrocytes (detected based on expression of glial fibrillary acid protein; Figures 7J,K).

Consistent with the link between hyperactivation of hippocampal microglia and impaired neurogenesis in the adult hippocampus (He et al., 2022; Su et al., 2023; Zhang et al., 2020), regulating neurogenesis in the hippocampus was implicated in stress-induced body weight change (Supplementary Figure S4). Genes involved in regulating neurogenesis made up a significantly greater proportion of the genes differentially regulated by stress in animals showing weight gain than in those showing weight loss (Figures 8A,B). Immunostaining of thin sections from the subgranular zone of the hippocampus showed that both groups of mice contained significantly fewer immature neurons (detected based on doublecortin expression), proliferating neural stem cells/precursor cells (detected based on BrdU labeling) and newborn neurons (detected based on simultaneous doublecortin staining and BrdU labeling) than unstressed controls (Figures 8C–F). The reductions were significantly more severe in animals showing stress-induced weight gain.

Animals with weight gain, but not those with weight loss, showed significantly less differentiation of neural stem cells/precursor cells into neurons than unstressed controls (Figure 8G). In the subgranular zone, animals showing weight gain contained significantly fewer new mature neurons (detected based on simultaneous NeuN staining and BrdU labeling) than animals showing weight loss (Figures 8H–J).

3.4 Stress-induced obesity in mice causes cognitive decline associated with inhibition of hippocampal neurogenesis and dysfunctional gut microbiota

Given our observation that stress-induced obesity in mice causes hyperactivation of the HPA axis and hippocampal glia, inhibition of hippocampal neurogenesis and cognitive decline, we next wanted to know whether these changes are related to the disturbance of gut microbiome. Our results showed that the abundance of *Firmicutes*, *Dubosiella* and *Turicibacter* correlated positively with stress-induced obesity, activation of HPA axis and hippocampal glia, impairment of hippocampal neurogenesis and cognitive decline. The abundance of Bacteroidota, *Lactobacillus*, *Enterorhabdus*, *Prevotellaceae UCG-001*, *Alistipes*, *Lachnospiraceae NK4A136*, *Alloprevotella*, *Bifidobacterium* and *Desulfovibrio* correlated negatively with stress-induced obesity, activation of HPA axis and hippocampal glia, impairment of hippocampal neurogenesis and cognitive decline (Figure 9A). The stress-induced obesity correlated positively with hyperactivation of the HPA axis and hippocampal glia, impairment of hippocampal neurogenesis and cognitive decline. The hyperactivation of the HPA axis correlated positively with activation of hippocampal glia, and correlated negatively with hippocampal neurogenesis. The hyperactivation of hippocampal glia correlated negatively with hippocampal neurogenesis. The hippocampal neurogenesis correlated negatively with cognitive decline (Figure 9B). These results suggested that stress-induced obesity in mice causes cognitive decline associated with inhibition of hippocampal neurogenesis and dysfunctional gut microbiota.

To further explore the mechanism of overactivation of microglia and neurogenesis impairment in hippocampus of WG mice, gene set enrichment analysis of KEGG pathway based on differentially expressed genes among WG, WL and Ctrl mice were performed. Multichannel gene set enrichment analysis, indicating the differentially expressed genes that positively regulated oxidative phosphorylation, fatty acid biosynthesis, toll-like receptor signaling pathway, adipocytokine signaling pathway, NF-kappa B signaling pathway, NOD-like receptor signaling pathway, TNF signaling pathway and ferroptosis were significantly enriched in hippocampus of WG mice compared to WL or Ctrl animals (Figures 10A–D), suggesting that the hyperactivation of microglia and neuroinflammation in hippocampus induced by stress-mediated obesity are associated with the activation of these signaling pathways. In addition, we found that PPAR signaling pathway, a signaling pathway involved in lipid metabolism and anti-inflammation, was inhibited in hippocampus of WG mice compared to WL animals (Figure 10E). The signaling pathways (PI3K-AKT, cGMP-PKG, ErbB, neurotrophin, Wnt and Notch), which are involved in the proliferation, differentiation and survival of neural stem/precursor cells, were inhibited in hippocampus of WG mice compared to WL animals (Figures 10E,F), suggesting that the impairment in hippocampal neurogenesis of WG mice are associated with the activation of these signaling pathways.

4 Discussion

This study provides the first evidence that several pathologies previously reported in animals suffering stress-induced obesity while

10.3389/fmicb.2024.1381423

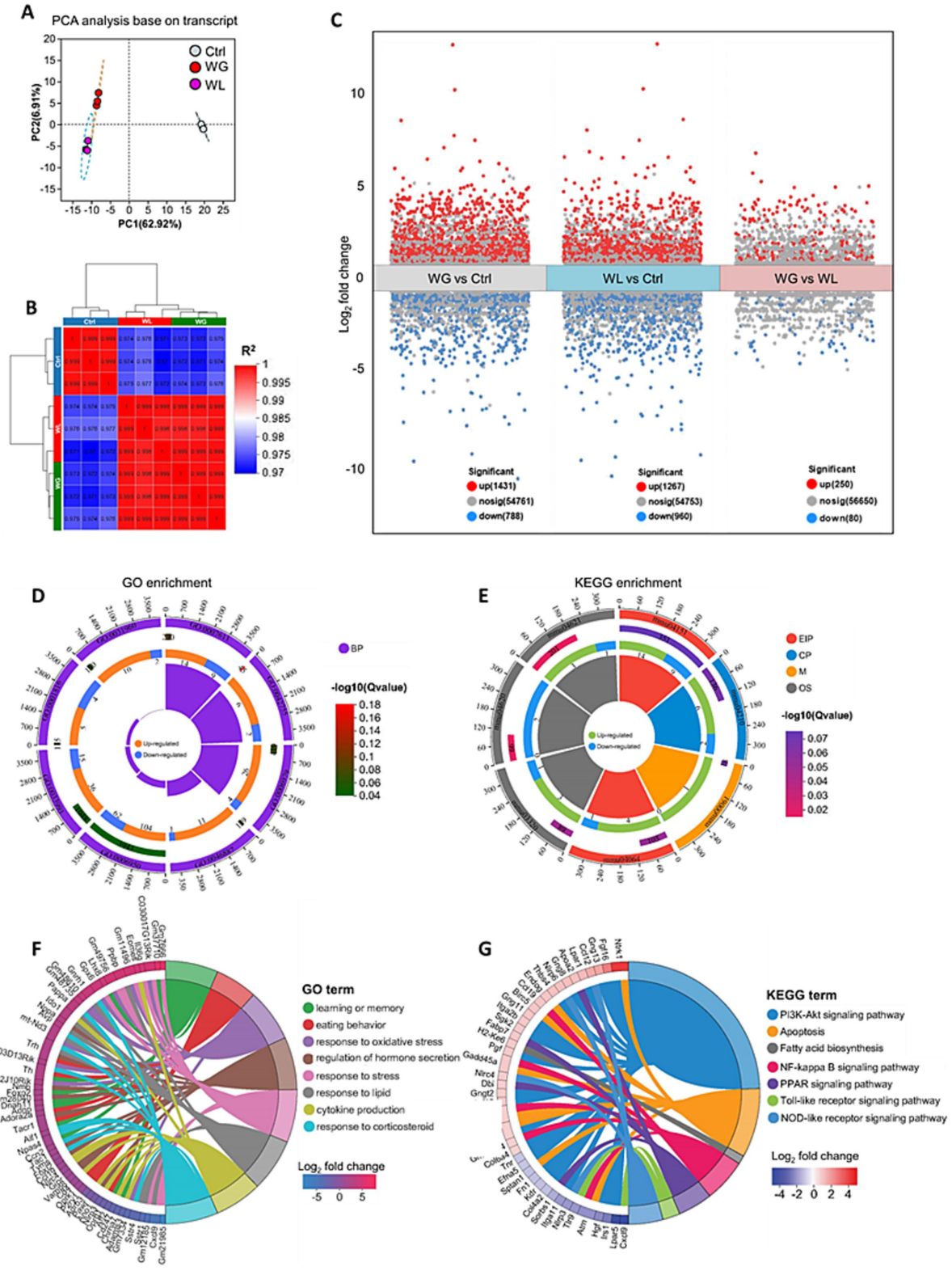

FIGURE 6
Differences between mice showing weight gain, insusceptible or loss after stress exposure in gene expression in the hippocampus. **(A)** Principal component analysis to identify clusters of transcriptomes of hippocampus from control (Ctrl), weight gain (WG) or weight loss (WL) mice. PC, principal component. **(B)** Correlation analysis between samples. **(C)** Volcano plot of differentially expressed genes. Significantly upregulated genes are shown as red dots; significantly downregulated genes, as blue dots. **(D,E)** The loop map of gene enrichment shows GO enrichment (left) and Kyoto Encyclopedia of Genes and Genomes (KEGG) enrichment (right) of up-regulated and down-regulated genes between WG and WL mice. **(F,G)** Circos plot showing the connectivity map derived from the pairwise comparison of transcriptome datasets. The connectivity between DEGs (left) and GO term or KEGG pathway (right) are shown in different color. Each line represents a pairwise dataset overlap, which was determined using Gene Set Enrichment Analysis and filtered by $p < 0.05$ and normalized enrichment score > 1.5. The change in the expression of DEGs was quantified as the log2 fold change.

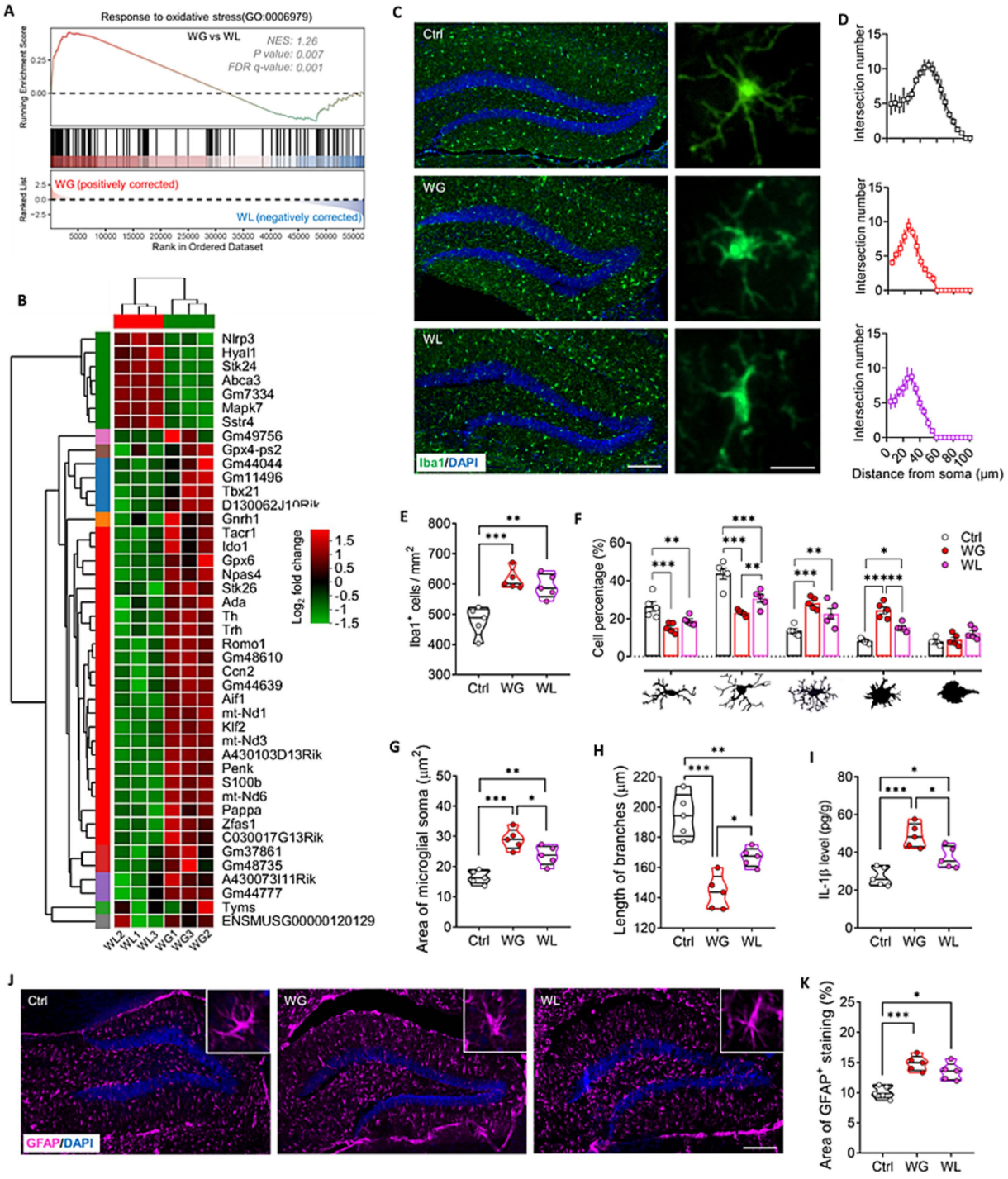

FIGURE 7
Mice that exhibited stress obesity were accompanied by hyperactivation in hippocampal microglia. **(A)** Gene set enrichment analysis, indicating enrichment of processes related to response to oxidative stress (GO:0006979) in the hippocampal transcriptome of weight gain (WG) mice compared to that of weight loss (WL) animals after stress exposure. **(B)** Hierarchical cluster analysis of enriched differentially expressed genes related to response to oxidative stress. **(C)** Representative sections of hippocampal dentate gyrus from mice that were classified as showing WG or WL or from control animals never subjected to stress (Ctrl) were immunostained against "ionized calcium binding adapter molecule 1" (Iba1) as a marker of microglia. Scale bar, 100 μm. The enlarged graphs on the right are the typical morphology of microglia in hippocampus of Ctrl, WG or WL mice. Scale bar, 15 μm. **(D)** The number of intersections of microglial branches were evaluated by Sholl analysis in the hippocampus of Ctrl, WG or WL mice. **(E)** Quantification of the number of microglia hippocampus of Ctrl, WG or WL mice. Results come from five slices of hippocampal dentate gyrus (at 40 × magnification) from each of five mice per condition. Each dot represents the average of all micrographs for one mouse. **(F)** Quantification of the proportions of microglia in the hippocampus that showed, from *left* to *right,* longitudinal branching, radial branching, hyper-branching, or compact and ameboid form. **(G,H)** Quantification of the area of microglial soma and length of microglial branches in hippocampus. **(I)** Assay of levels of interleukin (IL)-1βin hippocampus. Quantitative results come from 5 animals per condition. **(J)** Representative sections of hippocampal dentate gyrus immunostained against glial fibrillary acidic protein (GFAP) as a marker of astrocytes. Nuclei were counterstained with DAPI. Scale bar, 100 μm. **(K)** Quantification of GFAP⁺ area in hippocampus of Ctrl, WG or WL mice. Data are mean ± standard error of the mean (SEM). $*p < 0.05$, $**p < 0.01$, $***p < 0.001$, based on one-way ANOVA with Tukey's multiple-comparisons test.

10.3389/fmicb.2024.1381423

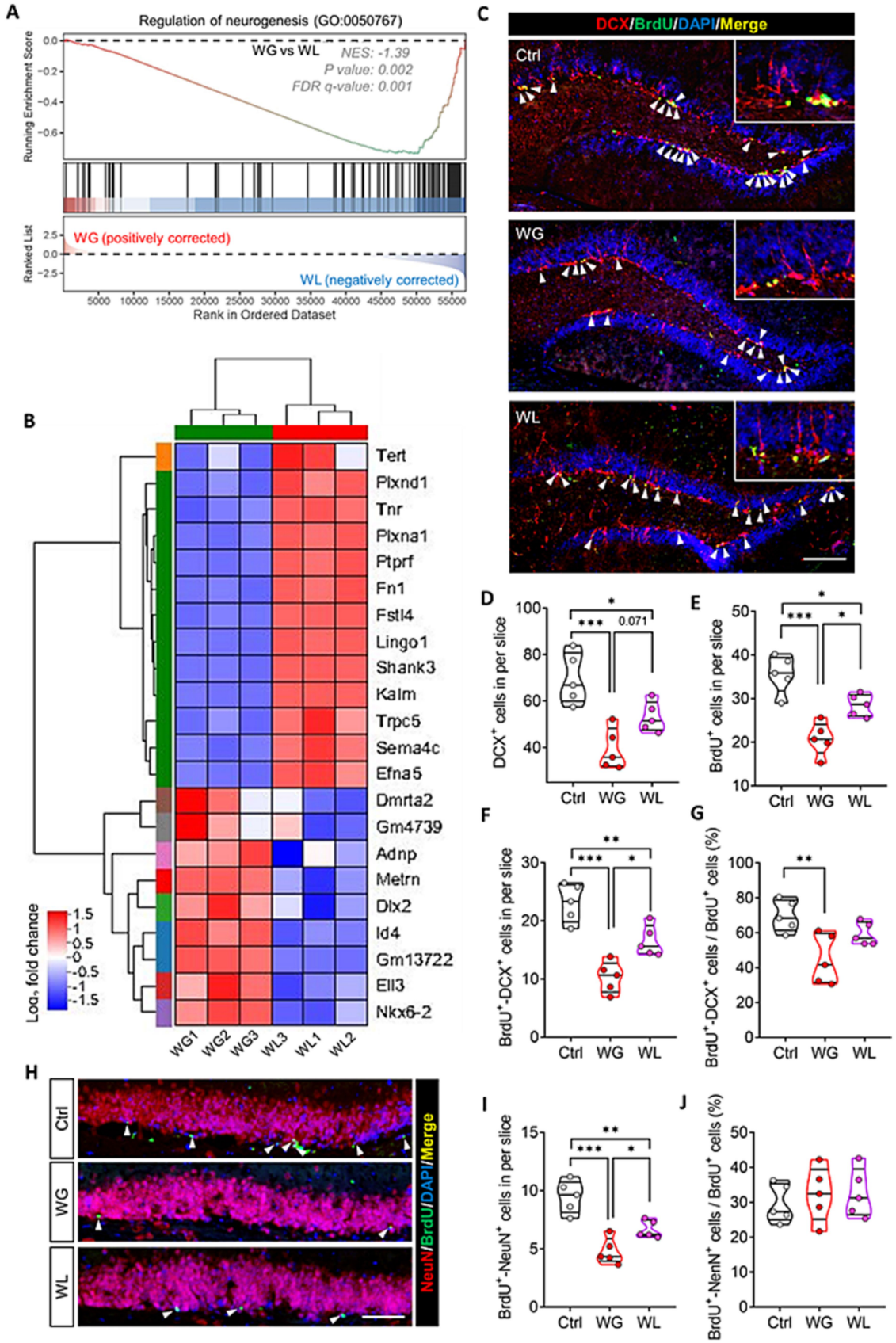

FIGURE 8
Mice that exhibited stress obesity were accompanied by exaggerated impairment in hippocampal neurogenesis. **(A)** Gene set enrichment analysis, indicating enrichment of processes related to regulation of neurogenesis (GO:0050767) in the hippocampal transcriptome of weight gain (WG) mice

(Continued)

FIGURE 8 (Continued)
compared to that of weight loss (WL) animals after stress exposure. **(B)** Hierarchical cluster analysis of enriched differentially expressed genes related to regulation of neurogenesis. **(C)** Representative sections of hippocampal dentate gyrus from mice that were classified as showing WG or WL or from control animals never subjected to stress (Ctrl) were immunostained against doublecortin (DCX) to label immature neurons cells and BrdU to label proliferating neural stem/progenitor cells. Cells staining for both BrdU and DCX were considered to be newborn neurons. Nuclei were counterstained with DAPI. The *top right corner* shows a higher magnification image. White arrowheads indicate newborn neurons. Scale bar, 100 μm. **(D–G)** Quantification of cell subpopulations in the experiments in panel C. Results come from five slices of hippocampal dentate gyrus (at 40 × magnification) from each of five mice per condition. Each dot represents the average of all micrographs for one mouse. Panel E expresses the extent of neural stem/progenitor cell differentiation into neurons. **(H)** Representative sections of hippocampal dentate gyrus were immunostained against NeuN to label mature neurons or BrdU to label proliferating neural stem/progenitor cells. Cells staining for both $BrdU^+$ and $NeuN^+$ were considered to be newly mature neurons (white arrowheads). Nuclei were counterstained with DAPI. Scale bar, 50 μm. **(I,J)** Quantification of the experiments in panel **H**. Panel **I** expresses the extent of newborn neuron maturation into mature neurons. Data are mean ± standard error of the mean (SEM). $*p < 0.05$, $**p < 0.01$, $***p < 0.001$, based on one-way ANOVA with Tukey's multiple-comparisons test.

on a high-fat diet—hyperactivation of HPA axis and microglia, altered gut microbiome, and inhibited neurogenesis—also occur in animals suffering stress-induced obesity on a normal diet. In addition, we link these processes to cognitive deficit in the presence of stress-induced weight gain, but not in the presence of stress-induced weight loss.

Chronic mild stress led to significant weight loss in 50% of our animals, whereas 20% gained significantly in weight. These incidences are consistent with clinical observations that most patients with major depressive disorder lose weight (Kubera et al., 2022; Ma et al., 2019). The remaining 30% of mice did not suffer significant weight loss or gain during the stress paradigm, and these same animals showed no differences from unstressed controls in depression- or anxiety-like symptoms or in memory of objects or locations. In addition, these animals showed a significantly milder increase of corticosterone levels in serum than those that showed stress-induced obesity, even though the levels were still significantly higher than those in unstressed control animals. This group of animals may exhibit stress resistance (Zhang et al., 2021). We also found that WI mice showed a transient decrease in food consumption during the stress response period, while their food consumption returned to normal during the stress resistance period. The molecular basis of stress resistance should be studied further and may involve gene methylation (Dudek et al., 2021; Gonzalez et al., 2021) and life experiences before adulthood (Aydin et al., 2021; Liu et al., 2017; Rab and Admon, 2021).

While the combination of chronic stress and a high-fat diet is known to cause obesity (Liu et al., 2017; Slomp et al., 2019; Zhang et al., 2019), the molecules and pathways linking chronic mild stress to obesity in our mice on a normal diet remain unclear. Our experiments suggest several culprits. One is alterations in the gut microbiome. For example, stress-induced obesity in our animals was associated with a significant increase in the abundance of Firmicutes bacteria and significant decrease in the abundance of Bacteroidota bacteria. Firmicutes bacteria help individuals absorb food calories more effectively than Bacteroidota bacteria, which may increase risk of obesity (Baek et al., 2023; Da et al., 2020; Magne et al., 2020; Zhang et al., 2022).

A second culprit is HPA hyperactivation leading to release of corticotropin-releasing hormone, adrenocorticotropin and corticosterone, the levels of which were significantly elevated in mice showing stress-induced weight gain or loss, with the increases larger in those that gained weight. Stress-induced release of corticosterone from the adrenal cortex in rodents has been linked to obesity on a high-fat diet (Hueston and Deak, 2020; Kinlein et al., 2019; Lowrance et al., 2016; Qiu et al., 2019), at least in part because corticosterone hyperactivates glucocorticoid receptors in adipose tissue, leading to lipid accumulation (Appiakannan et al., 2020; Gado et al., 2023). At the same time, the hyperactivation of glucocorticoid receptors can cause inflammatory response (Bharti et al., 2019; Ferguson et al., 2020; Shimba and Ikuta, 2020; Wu et al., 2021), which may explain why levels of the pro-inflammatory cytokines tumor necrosis factor-α and interleukin-6 were significantly higher in the presence of stress-induced obesity than in its absence. Our results suggest that stress-induced hyperactivation of the HPA axis and peripheral inflammatory responses are more severe in the presence of obesity.

One pathway that explains our results is that stress hyperactivates the HPA axis and induces peripheral inflammation, which together alter the gut microbiome. In support of this idea, stress has been shown to alter the gut microbiota by promoting the secretion of neuroendocrine hormones such as corticotropin-releasing hormone, adrenocorticotropin and corticosterone (Guo et al., 2020; Liu et al., 2020), and changes in the gut microbiome have been associated with stress-induced obesity on a high-fat diet and cognitive changes (Wu et al., 2021; Chen et al., 2017; Rao et al., 2021; Xu et al., 2020). In other words, the gut-brain axis can bi-directionally regulate gut microbiota and brain response to stress (Deng et al., 2021; He et al., 2024; Westfall et al., 2021), which appears to be involved not only in stress-induced obesity but also in depression, anxiety, Alzheimer's disease and irritable bowel syndrome (Liu et al., 2020; Westfall et al., 2021; Ma et al., 2022; Mosaferi et al., 2021). Indeed, our stressed mice showed significant depression and anxiety-like symptoms regardless of whether they gained or lost weight, though different symptoms predominated in the two groups. This may reflect differences in gut microbial composition between them. For example, the significantly lower abundance of *Lactobacillus* in the gut of animals showing stress-induced obesity may help explain their higher level of behavioral despair (Castaneda-Marquez et al., 2020; Wang et al., 2020). Future work should logitudinally analyze HPA activation, inflammatory responses, and the gut microbiome in order to identify the sequence in which they change under stress, which may clarify the mechanisms involved. Future experiments should also examine whether transplantation of fecal microbiota from animals with stress-induced obesity into naïve animals can reproduce the altered gene expression and activation of the HPA axis and hippocampal microglia that we observed here.

We detected microglial activation in the hippocampus of stressed animals regardless of whether they experienced significant weight gain or loss, with the activation more severe in the presence of weight gain. These results are consistent with the susceptibility of hippocampal microglia to corticosterone (Mao et al., 2020; Feng et al., 2019), metabolites of gut microbes (Chang et al., 2014), and inflammatory cytokines (Zhang et al., 2020). They are also consistent with studies implicating activation of hippocampal microglia in stress and depression (Jiang et al., 2022; Bassett et al., 2021; Zhang et al., 2023). Such activation has been linked to obesity on a high-fat diet (Kim

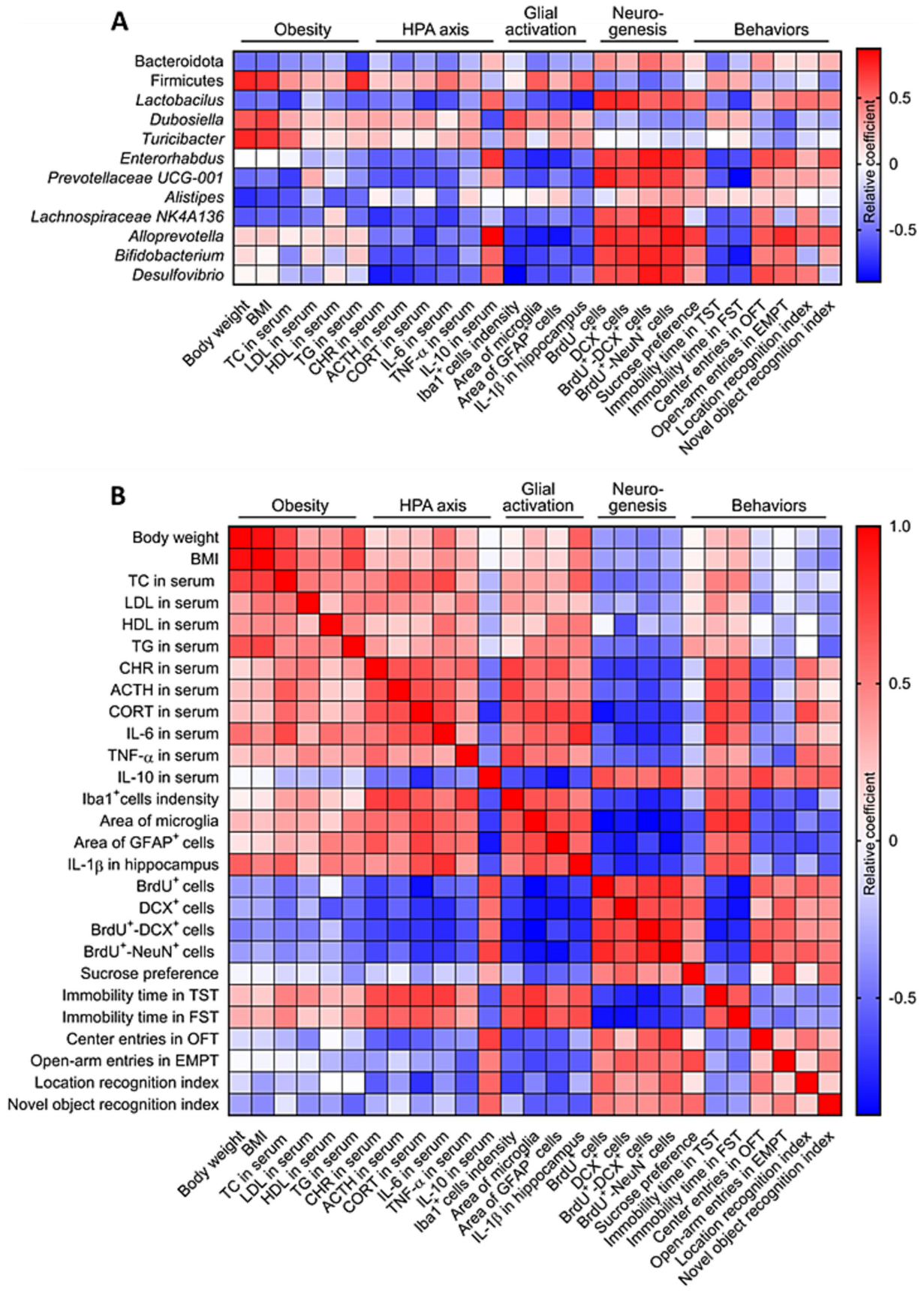

FIGURE 9
Correlation analysis of stress-induced obesity and gut microbiome, HPA axis, glial activation, neurogenesis and behaviors. **(A)** Correlation analysis between gut microbiome, stress-induced obesity, activation of HPA axis and hippocampal glia, impairment of hippocampal neurogenesis and cognitive

(Continued)

FIGURE 9 (Continued)
decline. **(B)** Correlation analysis between obesity, gut microbiome, HPA axis, glial activation, neurogenesis and behaviors. The data used for correlation analysis were all derived from the control (Ctrl), weight gain (WG) and weight loss (WL) mice.

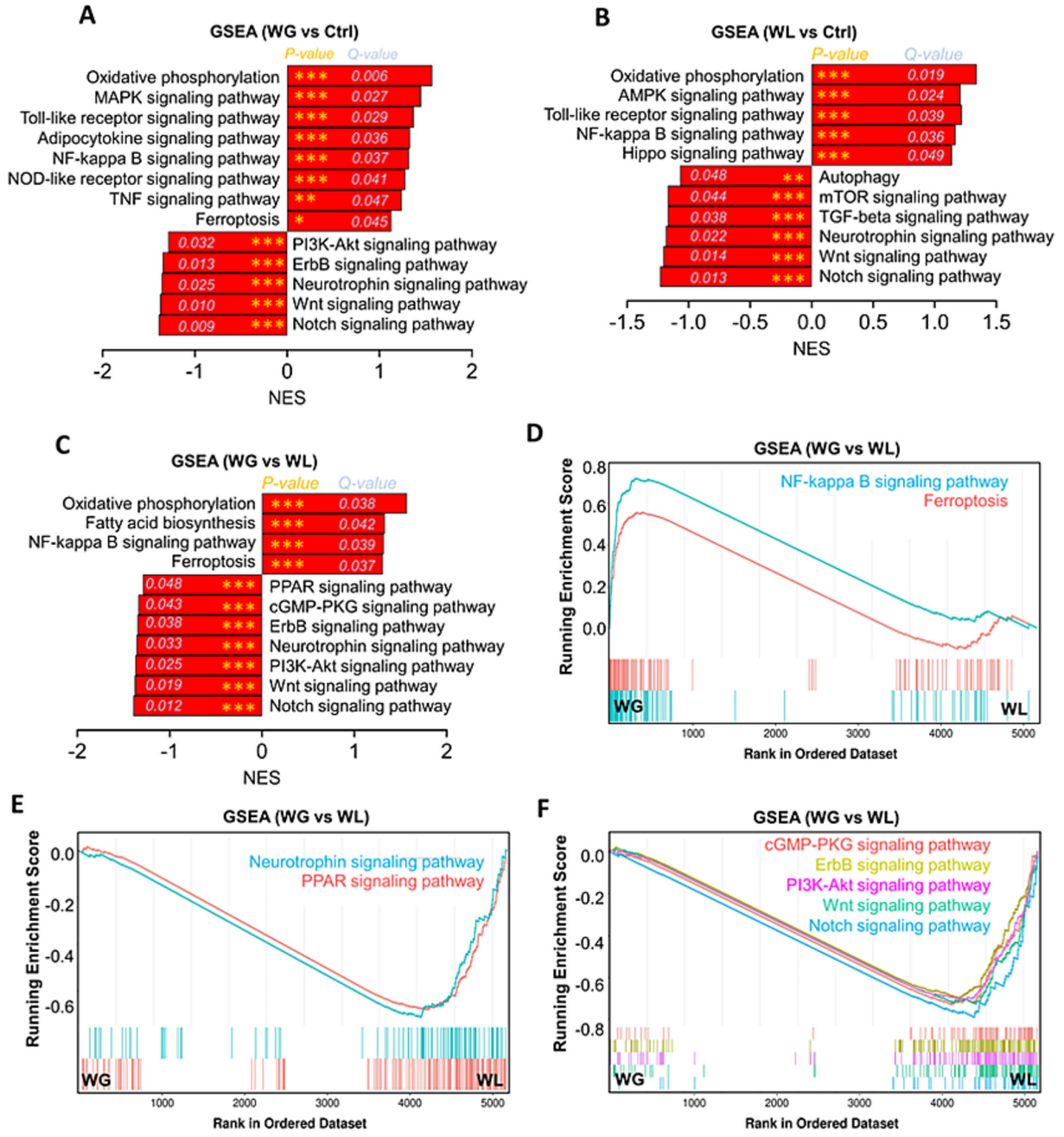

FIGURE 10
Gene set enrichment analysis of KEGG pathway based on differentially expressed genes among WG, WL and Ctrl mice. **(A)** Gene set enrichment analysis (GSEA) of Encyclopedia of Genes and Genomes (KEGG) pathway in the hippocampal transcriptome of weight gain (WG) mice compared to that of control (Ctrl) animals. **(B)** Gene set enrichment analysis of KEGG pathway in the hippocampal transcriptome of weight loss (WL) mice compared to that of Ctrl animals. **(C)** Gene set enrichment analysis of KEGG pathway in the hippocampal transcriptome of WG mice compared to that of WL animals after stress exposure. **(D–F)** Multichannel gene set enrichment analysis, indicating the differentially expressed genes that positively regulated NF-kappa B signaling pathway and ferroptosis, and the differentially expressed genes that negatively regulated PPAR signaling pathway, cGMP-PKG signaling pathway, ErbB signaling pathway, Neurotrophin signaling pathway, PI3K-Akt signaling pathway, Wnt signaling pathway and Notch signaling pathway were significantly enriched in hippocampus of WG mice compared to WL animals. Each line represents overlap between pairwise comparisons, based on gene set enrichment analysis.

et al., 2019). Our transcriptomic analysis suggests that stress-induced obesity on a normal diet causes dysfunction of hippocampal microglia through signaling mediated by NF-κB, Toll-like receptor and NOD-like receptor (Chen et al., 2022; Tang et al., 2019).

Whatever the processes mediating the hyperactivation of hippocampal microglia, this activation seems likely to cause the inhibition of neurogenesis observed in our stressed mice showing significant weight loss or gain, with the inhibition more severe in those showing weight gain. Hyperactivated microglia release tumor necrosis factor-α and interleukin-1β, which inhibit proliferation and differentiation of neural stem/precursor cells (Zhang et al., 2021; Liu et al., 2022). Our assay of interleukin-1β in serum in stressed animals is consistent with this. Inflammation may also contribute to the inhibition of neurogenesis (Zhang et al., 2020; Zhang et al., 2023). Our transcriptomic analysis suggests that microglial hyperactivation inhibits hippocampal neurogenesis by suppressing signaling mediated by PPARs, PI3K-Akt, Wnt and Notch, which normally promote the proliferation and differentiation of neural stem cells in hippocampus (Liu et al., 2022; Zhang et al., 2023). Whatever the pathways inhibiting hippocampal neurogenesis, our results link it to cognitive deficits that we observed in mice with stress-induced obesity, but not in mice with stress-induced weight loss. This is consistent with observations linking inhibition of neurogenesis to depression, anxiety and cognitive dysfunction (Li et al., 2023; Shen et al., 2022; Tunc-Ozcan et al., 2019; Zhang et al., 2023).

Our results should be interpreted with caution in light of several limitations. First, in present study, we screened only 20% of stress-induced obese animals from a small sample size, and this proportion needs to be confirmed in a larger sample size under non-high-fat diet conditions. Second, further work is needed to establish whether the gut microbiota is required for the obesity, and microglial, neurogenic and behavioral changes induced by stress exposure by fecal microbiota transplantation. In addition, the use of only male mice for this study, although narrowing the individual differences, also limits the applicability of the results of this study. Future work should replicate this experimental project in female mice, and explore how gut microbes affect proliferation and differentiation of adipose-derived stem cells. Despite these limitations, our work provides strong evidence that stress-induced obesity causes cognitive decline involving in gut microbiota disturbances and hippocampal neurogenesis impairment. These insights may provide treatment option for stress-induced obesity and cognitive decline by remodeling gut microbiota, inhibiting hyperactivation of hippocampal microglia and HPA axis.

Data availability statement

The datasets presented in this study can be found in online repositories. The names of the repository/repositories and accession number(s) can be found in the article/Supplementary material.

Ethics statement

The animal study was approved by Institutional Animal Care and use Committee at the Guizhou University of Traditional Chinese Medicine. The study was conducted in accordance with the local legislation and institutional requirements.

Author contributions

Y-eL: Data curation, Methodology, Software, Writing – original draft, Writing – review & editing. ZZ: Data curation, Formal analysis, Methodology, Writing – review & editing. HH: Data curation, Investigation, Methodology, Software, Writing – review & editing. LL: Data curation, Formal analysis, Methodology, Writing – review & editing. CX: Data curation, Formal analysis, Methodology, Writing – review & editing. TZ: Funding acquisition, Project administration, Resources, Writing – review & editing. ZY: Funding acquisition, Project administration, Writing – review & editing. JZ: Funding acquisition, Investigation, Methodology, Project administration, Supervision, Writing – original draft, Writing – review & editing.

Funding

The author(s) declare that financial support was received for the research, authorship, and/or publication of this article. This work was supported by the National Natural Science Foundation of China (82201695), the University Science and Technology Innovation Team of the Guizhou Provincial Department of Education [Qian-jiao-ji (2023)071], the Guizhou Provincial Science and Technology Projects [ZK (2022)505], and the National and Provincial Scientific and Technological Innovation Talent Team of the Guizhou University of Traditional Chinese Medicine [Gui-zhong-yi TD he-zi (2022)003] and Sichuan Science and Technology Program (2020YJ0225).

Acknowledgments

We are grateful to Creaducate Consulting GmbH (Munich, Germany) for editorial assistance.

Conflict of interest

The authors declare that the research was conducted in the absence of any commercial or financial relationships that could be construed as a potential conflict of interest.

Publisher's note

All claims expressed in this article are solely those of the authors and do not necessarily represent those of their affiliated organizations, or those of the publisher, the editors and the reviewers. Any product that may be evaluated in this article, or claim that may be made by its manufacturer, is not guaranteed or endorsed by the publisher.

Supplementary material

The Supplementary material for this article can be found online at: https://www.frontiersin.org/articles/10.3389/fmicb.2024.1381423/full#supplementary-material

References

Agudelo, L. Z., Femenia, T., Orhan, F., Porsmyr-Palmertz, M., Goiny, M., Martinez-Redondo, V., et al. (2014). Skeletal muscle pgc-1alpha1 modulates kynurenine metabolism and mediates resilience to stress-induced depression. *Cell* 159, 33–45. doi: 10.1016/j.cell.2014.07.051

Appiakannan, H. S., Rasimowicz, M. L., Harrison, C. B., and Weber, E. T. (2020). Differential effects of high-fat diet on glucose tolerance, food intake, and glucocorticoid regulation in male c57bl/6j and balb/cj mice. *Physiol. Behav.* 215:112773. doi: 10.1016/j.physbeh.2019.112773

Aydin, C., Frohmader, K., Emery, M., Blandino, P. J., and Akil, H. (2021). Chronic stress in adolescence differentially affects cocaine vulnerability in adulthood in a selectively bred rat model of individual differences: role of accumbal dopamine signaling. *Stress* 24, 251–260. doi: 10.1080/10253890.2020.1790520

Baek, G. H., Yoo, K. M., Kim, S. Y., Lee, D. H., Chung, H., Jung, S. C., et al. (2023). Collagen peptide exerts an anti-obesity effect by influencing the firmicutes/bacteroidetes ratio in the gut. *Nutrients* 15:12610. doi: 10.3390/nu15112610

Bassett, B., Subramaniyam, S., Fan, Y., Varney, S., Pan, H., Carneiro, A., et al. (2021). Minocycline alleviates depression-like symptoms by rescuing decrease in neurogenesis in dorsal hippocampus via blocking microglia activation/phagocytosis. *Brain Behav. Immun.* 91, 519–530. doi: 10.1016/j.bbi.2020.11.009

Baumeister, D., Akhtar, R., Ciufolini, S., Pariante, C. M., and Mondelli, V. (2016). Childhood trauma and adulthood inflammation: a meta-analysis of peripheral c-reactive protein, interleukin-6 and tumour necrosis factor-alpha. *Mol. Psychiatry* 21, 642–649. doi: 10.1038/mp.2015.67

Bharti, V., Tan, H., Zhou, H., and Wang, J. F. (2019). Txnip mediates glucocorticoid-activated nlrp3 inflammatory signaling in mouse microglia. *Neurochem. Int.* 131:104564. doi: 10.1016/j.neuint.2019.104564

Braniste, V., Al-Asmakh, M., Kowal, C., Anuar, F., Abbaspour, A., Toth, M., et al. (2014). The gut microbiota influences blood-brain barrier permeability in mice. *Sci. Transl. Med.* 6:263ra158. doi: 10.1126/scitranslmed.3009759

Cao, X., Li, L. P., Wang, Q., Wu, Q., Hu, H. H., Zhang, M., et al. (2013). Astrocyte-derived atp modulates depressive-like behaviors. *Nat. Med.* 19, 773–777. doi: 10.1038/nm.3162

Castaneda-Marquez, A. C., Diaz-Benitez, C. E., Bahena-Roman, M., Campuzano-Benitez, G. E., Galvan-Portillo, M., Campuzano-Rincon, J. C., et al. (2020). *Lactobacillus paracasei* as a protective factor of obesity induced by an unhealthy diet in children. *Obes. Res. Clin. Pract.* 14, 271–278. doi: 10.1016/j.orcp.2020.04.005

Chang, P. V., Hao, L., Offermanns, S., and Medzhitov, R. (2014). The microbial metabolite butyrate regulates intestinal macrophage function via histone deacetylase inhibition. *Proc. Natl. Acad. Sci. U. S. A.* 111, 2247–2252. doi: 10.1073/pnas.1322269111

Chen, Y., Cao, P., Xiao, Z., and Ruan, Z. (2022). M (6)a methyltransferase mettl3 relieves cognitive impairment of hyperuricemia mice via inactivating myd88/nf-kappab pathway mediated nlrp3-asc-caspase1 inflammasome. *Int. Immunopharmacol.* 113:109375. doi: 10.1016/j.intimp.2022.109375

Chen, X., Gianferante, D., Hanlin, L., Fiksdal, A., Breines, J. G., Thoma, M. V., et al. (2017). HPA-axis and inflammatory reactivity to acute stress is related with basal HPA-axis activity. *Psychoneuroendocrinology* 78, 168–176. doi: 10.1016/j.psyneuen.2017.01.035

Da, S. C., Monteil, M. A., and Davis, E. M. (2020). Overweight and obesity in children are associated with an abundance of firmicutes and reduction of bifidobacterium in their gastrointestinal microbiota. *Child. Obes.* 16, 204–210. doi: 10.1089/chi.2019.0280

Dalile, B., La Torre, D., Verbeke, K., Van Oudenhove, L., and Vervliet, B. (2022). When the mind says one thing, but the hpa axis says another: lack of coherence between subjective and neuroendocrine stress response trajectories in healthy men. *Psychoneuroendocrinology* 139:105692. doi: 10.1016/j.psyneuen.2022.105692

De Gregorio, D., Inserra, A., Enns, J. P., Markopoulos, A., Pileggi, M., El, R. Y., et al. (2022). Repeated lysergic acid diethylamide (lsd) reverses stress-induced anxiety-like behavior, cortical synaptogenesis deficits and serotonergic neurotransmission decline. *Neuropsychopharmacology* 47, 1188–1198. doi: 10.1038/s41386-022-01301-9

Deng, Y., Zhou, M., Wang, J., Yao, J., Yu, J., Liu, W., et al. (2021). Involvement of the microbiota-gut-brain axis in chronic restraint stress: disturbances of the kynurenine metabolic pathway in both the gut and brain. *Gut Microbes* 13, 1–21. doi: 10.1080/19490976.2021.1902719

Du, F. M., Kuang, H. Y., Duan, B. H., Liu, D. N., and Yu, X. Y. (2019). Effects of thyroid hormone and depression on common components of central obesity. *J. Int. Med. Res.* 47, 3040–3049. doi: 10.1177/0300060519851624

Dudek, K. A., Kaufmann, F. N., Lavoie, O., and Menard, C. (2021). Central and peripheral stress-induced epigenetic mechanisms of resilience. *Curr. Opin. Psychiatry* 34, 1–09. doi: 10.1097/YCO.0000000000000664

Ennaceur, A., and Delacour, J. (1988). A new one-trial test for neurobiological studies of memory in rats. 1: behavioral data. *Behav. Brain Res.* 31, 47–59. doi: 10.1016/0166-4328(88)90157-X

Ensminger, D. C., Crocker, D. E., Lam, E. K., Allen, K. N., and Vazquez-Medina, J. P. (2021). Repeated stimulation of the hpa axis alters white blood cell count without increasing oxidative stress or inflammatory cytokines in fasting elephant seal pups. *J. Exp. Biol.* 224:198. doi: 10.1242/jeb.243198

Feng, X., Zhao, Y., Yang, T., Song, M., Wang, C., Yao, Y., et al. (2019). Glucocorticoid-driven nlrp3 inflammasome activation in hippocampal microglia mediates chronic stress-induced depressive-like behaviors. *Front. Mol. Neurosci.* 12:210. doi: 10.3389/fnmol.2019.00210

Ferguson, D., Hutson, I., Tycksen, E., Pietka, T. A., Bauerle, K., and Harris, C. A. (2020). Role of mineralocorticoid receptor in adipogenesis and obesity in male mice. *Endocrinology* 161:10. doi: 10.1210/endocr/bqz010

Fulton, S., Decarie-Spain, L., Fioramonti, X., Guiard, B., and Nakajima, S. (2021). The menace of obesity to depression and anxiety prevalence. *Trends Endocrinol. Metab.* 33, 18–35. doi: 10.1016/j.tem.2021.10.005

Gado, M., Heinrich, A., Wiedersich, D., Sameith, K., Dahl, A., Alexaki, V. I., et al. (2023). Activation of beta-adrenergic receptor signaling prevents glucocorticoid-induced obesity and adipose tissue dysfunction in male mice. *Am. J. Physiol. Endocrinol. Metab.* 324, E514–E530. doi: 10.1152/ajpendo.00259.2022

Geng, J., Ni, Q., Sun, W., Li, L., and Feng, X. (2022). The links between gut microbiota and obesity and obesity related diseases. *Biomed. Pharmacother.* 147:112678. doi: 10.1016/j.biopha.2022.112678

Geng, S., Yang, L., Cheng, F., Zhang, Z., Li, J., Liu, W., et al. (2019). Gut microbiota are associated with psychological stress-induced defections in intestinal and blood-brain barriers. *Front. Microbiol.* 10:3067. doi: 10.3389/fmicb.2019.03067

Gonzalez, M. Z., Wroblewski, K. L., Allen, J. P., Coan, J. A., and Connelly, J. J. (2021). Oxtr dna methylation moderates the developmental calibration of neural reward sensitivity. *Dev. Psychobiol.* 63, 114–124. doi: 10.1002/dev.22026

Guo, T. L., Chen, Y., Xu, H. S., McDonough, C. M., and Huang, G. (2020). Gut microbiome in neuroendocrine and neuroimmune interactions: the case of genistein. *Toxicol. Appl. Pharmacol.* 402:115130. doi: 10.1016/j.taap.2020.115130

He, H., He, H., Mo, L., You, Z., and Zhang, J. (2024). Priming of microglia with dysfunctional gut microbiota impairs hippocampal neurogenesis and fosters stress vulnerability of mice. *Brain Behav. Immun.* 115, 280–294. doi: 10.1016/j.bbi.2023.10.031

He, D., Xu, H., Zhang, H., Tang, R., Lan, Y., Xing, R., et al. (2022). Disruption of the il-33-st2-akt signaling axis impairs neurodevelopment by inhibiting microglial metabolic adaptation and phagocytic function. *Immunity* 55, 159–173.e9. doi: 10.1016/j.immuni.2021.12.001

He, H., Zhao, Z., Xiao, C., Li, L., Liu, Y. E., Fu, J., et al. (2024). Gut microbiome promotes mice recovery from stress-induced depression by rescuing hippocampal neurogenesis. *Neurobiol. Dis.* 191:106396. doi: 10.1016/j.nbd.2023.106396

Holsboer, F., and Ising, M. (2008). Central CRH system in depression and anxiety — evidence from clinical studies with CRH1 receptor antagonists. *Eur. J. Pharmacol.* 583, 350–357. doi: 10.1016/j.ejphar.2007.12.032

Hueston, C. M., and Deak, T. (2020). Corticosterone and progesterone differentially regulate hpa axis and neuroimmune responses to stress in male rats. *Stress* 23, 368–385. doi: 10.1080/10253890.2019.1678025

Jene, T., Ruiz, D. A. I., Hasch, A., Klupfel, J., Deuster, J., Maas, M., et al. (2021). Chronic social stress lessens the metabolic effects induced by a high-fat diet. *J. Endocrinol.* 249, 19–30. doi: 10.1530/JOE-20-0633

Jiang, X., Yi, S., Liu, Q., Su, D., Li, L., Xiao, C., et al. (2022). Asperosaponin vi ameliorates the cms-induced depressive-like behaviors by inducing a neuroprotective microglial phenotype in hippocampus via ppar-gamma pathway. *J. Neuroinflammation* 19:115. doi: 10.1186/s12974-022-02478-y

Kim, J. D., Yoon, N. A., Jin, S., and Diano, S. (2019). Microglial ucp2 mediates inflammation and obesity induced by high-fat feeding. *Cell Metab.* 30, 952–962.e5. doi: 10.1016/j.cmet.2019.08.010

Kinlein, S. A., Phillips, D. J., Keller, C. R., and Karatsoreos, I. N. (2019). Role of corticosterone in altered neurobehavioral responses to acute stress in a model of compromised hypothalamic-pituitary-adrenal axis function. *Psychoneuroendocrinology* 102, 248–255. doi: 10.1016/j.psyneuen.2018.12.010

Kubera, B., Kohlmann, T., and Peters, A. (2022). Psychological stress, body shape and cardiovascular events: results from the Whitehall ii study. *Compr. Psychoneuroendocrinol.* 9:104. doi: 10.1016/j.cpnec.2021.100104

Lama, A., Pirozzi, C., Severi, I., Morgese, M. G., Senzacqua, M., Annunziata, C., et al. (2022). Palmitoylethanolamide dampens neuroinflammation and anxiety-like behavior in obese mice. *Brain Behav. Immun.* 102, 110–123. doi: 10.1016/j.bbi.2022.02.008

Lasikiewicz, N., Hendrickx, H., Talbot, D., and Dye, L. (2013). Exploring stress-induced cognitive impairment in middle aged, centrally obese adults. *Stress* 16, 44–53. doi: 10.3109/10253890.2012.682109

Li, Y. D., Luo, Y. J., Xie, L., Tart, D. S., Sheehy, R. N., Zhang, L., et al. (2023). Activation of hypothalamic-enhanced adult-born neurons restores cognitive and affective function in alzheimer's disease. *Cell Stem Cell* 30, 415–432.e6. doi: 10.1016/j.stem.2023.02.006

Liu, S., Guo, R., Liu, F., Yuan, Q., Yu, Y., and Ren, F. (2020). Gut microbiota regulates depression-like behavior in rats through the neuroendocrine-immune-mitochondrial pathway. *Neuropsychiatr. Dis. Treat.* 16, 859–869. doi: 10.2147/NDT.S243551

Liu, H., Huang, X., Li, Y., Xi, K., Han, Y., Mao, H., et al. (2022). Tnf signaling pathway-mediated microglial activation in the pfc underlies acute paradoxical sleep deprivation-

induced anxiety-like behaviors in mice. *Brain Behav. Immun.* 100, 254–266. doi: 10.1016/j.bbi.2021.12.006

Liu, L., Yang, J., Qian, F., and Lu, C. (2017). Hypothalamic-pituitary-adrenal axis hypersensitivity in female rats on a post-weaning high-fat diet after chronic mild stress. *Exp. Ther. Med.* 14, 439–446. doi: 10.3892/etm.2017.4498

Liu, M. Y., Yin, C. Y., Zhu, L. J., Zhu, X. H., Xu, C., Luo, C. X., et al. (2018). Sucrose preference test for measurement of stress-induced anhedonia in mice. *Nat. Protoc.* 13, 1686–1698. doi: 10.1038/s41596-018-0011-z

Liu, Q., Zhang, J., Xiao, C., Su, D., Li, L., Yang, C., et al. (2022). Akebia saponin d protects hippocampal neurogenesis from microglia-mediated inflammation and ameliorates depressive-like behaviors and cognitive impairment in mice through the pi3k-akt pathway. *Front. Pharmacol.* 13:927419. doi: 10.3389/fphar.2022.927419

Lowrance, S. A., Ionadi, A., McKay, E., Douglas, X., and Johnson, J. D. (2016). Sympathetic nervous system contributes to enhanced corticosterone levels following chronic stress. *Psychoneuroendocrinology* 68, 163–170. doi: 10.1016/j.psyneuen.2016.02.027

Ma, Y., Liu, T., Li, X., Kong, A., Xiao, R., Xie, R., et al. (2022). Estrogen receptor beta deficiency impairs gut microbiota: a possible mechanism of ibd-induced anxiety-like behavior. *Microbiome* 10:160. doi: 10.1186/s40168-022-01356-2

Ma, J., Rosas, L. G., Lv, N., Xiao, L., Snowden, M. B., Venditti, E. M., et al. (2019). Effect of integrated behavioral weight loss treatment and problem-solving therapy on body mass index and depressive symptoms among patients with obesity and depression: the rainbow randomized clinical trial. *JAMA* 321, 869–879. doi: 10.1001/jama.2019.0557

Ma, J., Wang, R., Chen, Y., Wang, Z., and Dong, Y. (2023). 5-ht attenuates chronic stress-induced cognitive impairment in mice through intestinal flora disruption. *J. Neuroinflammation* 20:23. doi: 10.1186/s12974-023-02693-1

Magne, F., Gotteland, M., Gauthier, L., Zazueta, A., Pesoa, S., Navarrete, P., et al. (2020). The firmicutes/bacteroidetes ratio: a relevant marker of gut dysbiosis in obese patients? *Nutrients* 12:474. doi: 10.3390/nu12051474

Mao, Z. F., Ouyang, S. H., Zhang, Q. Y., Wu, Y. P., Wang, G. E., Tu, L. F., et al. (2020). New insights into the effects of caffeine on adult hippocampal neurogenesis in stressed mice: inhibition of cort-induced microglia activation. *FASEB J.* 34, 10998–11014. doi: 10.1096/fj.202000146RR

Micale, V., and Drago, F. (2018). Endocannabinoid system, stress and hpa axis. *Eur. J. Pharmacol.* 834, 230–239. doi: 10.1016/j.ejphar.2018.07.039

Misiak, B., Loniewski, I., Marlicz, W., Frydecka, D., Szulc, A., Rudzki, L., et al. (2020). The hpa axis dysregulation in severe mental illness: can we shift the blame to gut microbiota? *Prog. Neuro-Psychopharmacol. Biol. Psychiatry* 102:109951. doi: 10.1016/j.pnpbp.2020.109951

Mosaferi, B., Jand, Y., and Salari, A. A. (2021). Gut microbiota depletion from early adolescence alters anxiety and depression-related behaviours in male mice with Alzheimer-like disease. *Sci. Rep.* 11:22941. doi: 10.1038/s41598-021-02231-0

Noronha, S., Lima, P. M., Campos, G., Chirico, M., Abreu, A. R., Figueiredo, A. B., et al. (2019). Association of high-fat diet with neuroinflammation, anxiety-like defensive behavioral responses, and altered thermoregulatory responses in male rats. *Brain Behav. Immun.* 80, 500–511. doi: 10.1016/j.bbi.2019.04.030

O'Mahony, S. M., McVey, N. K., Waworuntu, R. V., Pusceddu, M. M., Manurung, S., Murphy, K., et al. (2020). The enduring effects of early-life stress on the microbiota-gut-brain axis are buffered by dietary supplementation with milk fat globule membrane and a prebiotic blend. *Eur. J. Neurosci.* 51, 1042–1058. doi: 10.1111/ejn.14514

Pearson-Leary, J., Zhao, C., Bittinger, K., Eacret, D., Luz, S., and Vigderman, A. S. (2020). The gut microbiome regulates the increases in depressive-type behaviors and in inflammatory processes in the ventral hippocampus of stress vulnerable rats. *Mol. Psychiatry* 25, 1068–1079. doi: 10.1038/s41380-019-0380-x

Percie, D. S. N., Hurst, V., Ahluwalia, A., Alam, S., Avey, M. T., Baker, M., et al. (2020). The arrive guidelines 2.0: updated guidelines for reporting animal research. *Br. J. Pharmacol.* 177, 3617–3624. doi: 10.1111/bph.15193

Piao, J., Li, N., Zhang, L., Meng, H., Sun, Q., and He, Z. (2023). Quantitatively detecting *Candida albicans* enolase1 with a one-step double monoclonal antibody sandwich elisa assay. *Front. Microbiol.* 14:1078709. doi: 10.3389/fmicb.2023.1078709

Porsolt, R. D., Brossard, G., Hautbois, C., and Roux, S. (2001). Rodent models of depression: forced swimming and tail suspension behavioral despair tests in rats and mice. *Curr. Protoc. Neurosci.* 8, 8–10. doi: 10.1002/0471142301.ns0810as55

Qiu, D., Xia, Z., Deng, J., Jiao, X., Liu, L., and Li, J. (2019). Glucorticoid-induced obesity individuals have distinct signatures of the gut microbiome. *Biofactors* 45, 892–901. doi: 10.1002/biof.1565

Rab, S. L., and Admon, R. (2021). Parsing inter- and intra-individual variability in key nervous system mechanisms of stress responsivity and across functional domains. *Neurosci. Biobehav. Rev.* 120, 550–564. doi: 10.1016/j.neubiorev.2020.09.007

Rao, X., Liu, L., Wang, H., Yu, Y., Li, W., Chai, T., et al. (2021). Regulation of gut microbiota disrupts the glucocorticoid receptor pathway and inflammation-related pathways in the mouse hippocampus. *Exp. Neurobiol.* 30, 59–72. doi: 10.5607/en20055

Rusch, J. A., Layden, B. T., and Dugas, L. R. (2023). Signalling cognition: the gut microbiota and hypothalamic-pituitary-adrenal axis. *Front Endocrinol (Lausanne).* 14:1130689. doi: 10.3389/fendo.2023.1130689

Schinke, C., Hesse, S., Stoppe, M., Meyer, K., Schmidt, E., Orthgiess, J., et al. (2017). Post-dexamethasone serum copeptin corresponds to hpa axis responsiveness in human obesity. *Psychoneuroendocrinology* 78, 39–47. doi: 10.1016/j.psyneuen.2017.01.004

Schinke, C., Rullmann, M., Luthardt, J., Drabe, M., Preller, E., Becker, G. A., et al. (2022). Hpa axis responsiveness associates with central serotonin transporter availability in human obesity and non-obesity controls. *Brain Sci.* 12:1430. doi: 10.3390/brainsci12111430

Shen, S. Y., Yu, R., Li, W., Liang, L. F., Han, Q. Q., Huang, H. J., et al. (2022). The neuroprotective effects of gpr55 against hippocampal neuroinflammation and impaired adult neurogenesis in csds mice. *Neurobiol. Dis.* 169:105743. doi: 10.1016/j.nbd.2022.105743

Shimba, A., and Ikuta, K. (2020). Control of immunity by glucocorticoids in health and disease. *Semin. Immunopathol.* 42, 669–680. doi: 10.1007/s00281-020-00827-8

Slomp, M., Belegri, E., Blancas-Velazquez, A. S., Diepenbroek, C., Eggels, L., Gumbs, M., et al. (2019). Stressing the importance of choice: validity of a preclinical free-choice high-caloric diet paradigm to model behavioural, physiological and molecular adaptations during human diet-induced obesity and metabolic dysfunction. *J. Neuroendocrinol.* 31:e12718. doi: 10.1111/jne.12718

Spadoni, I., Zagato, E., Bertocchi, A., Paolinelli, R., Hot, E., Di Sabatino, A., et al. (2015). A gut-vascular barrier controls the systemic dissemination of bacteria. *Science* 350, 830–834. doi: 10.1126/science.aad0135

Stout, S. C., Owens, M. J., and Nemeroff, C. B. (2002). Regulation of corticotropin-releasing factor neuronal systems and hypothalamic-pituitary-adrenal axis activity by stress and chronic antidepressant treatment. *J. Pharmacol. Exp. Ther.* 300, 1085–1092. doi: 10.1124/jpet.300.3.1085

Su, D., Jiang, W., Yuan, Q., Guo, L., Liu, Q., Zhang, M., et al. (2023). Chronic exposure to aflatoxin b1 increases hippocampal microglial pyroptosis and vulnerability to stress in mice. *Ecotoxicol. Environ. Saf.* 258:114991. doi: 10.1016/j.ecoenv.2023.114991

Tang, C. Z., Zhang, D. F., Yang, J. T., Liu, Q. H., Wang, Y. R., and Wang, W. S. (2019). Overexpression of microrna-301b accelerates hippocampal microglia activation and cognitive impairment in mice with depressive-like behavior through the nf-kappab signaling pathway. *Cell Death Dis.* 10:316. doi: 10.1038/s41419-019-1522-4

Tomiyama, A. J. (2019). Stress and obesity. *Annu. Rev. Psychol.* 70, 703–718. doi: 10.1146/annurev-psych-010418-102936

Tseng, C. H., and Wu, C. Y. (2019). The gut microbiome in obesity. *J. Formos. Med. Assoc.* 118, S3–S9. doi: 10.1016/j.jfma.2018.07.009

Tunc-Ozcan, E., Peng, C. Y., Zhu, Y., Dunlop, S. R., Contractor, A., and Kessler, J. A. (2019). Activating newborn neurons suppresses depression and anxiety-like behaviors. *Nat. Commun.* 10:3768. doi: 10.1038/s41467-019-11641-8

Vicennati, V., Garelli, S., Rinaldi, E., Di Dalmazi, G., Pagotto, U., and Pasquali, R. (2014). Cross-talk between adipose tissue and the hpa axis in obesity and overt hypercortisolemic states. *Horm Mol Biol Clin Investig.* 17, 63–77. doi: 10.1515/hmbci-2013-0068

Wang, P., Gao, J., Ke, W., Wang, J., Li, D., Liu, R., et al. (2020). Resveratrol reduces obesity in high-fat diet-fed mice via modulating the composition and metabolic function of the gut microbiota. *Free Radic. Biol. Med.* 156, 83–98. doi: 10.1016/j.freeradbiomed.2020.04.013

Wang, T., Yan, H., Lu, Y., Li, X., Wang, X., Shan, Y., et al. (2020). Anti-obesity effect of *Lactobacillus rhamnosus* ls-8 and *Lactobacillus crustorum* mn047 on high-fat and high-fructose diet mice base on inflammatory response alleviation and gut microbiota regulation. *Eur. J. Nutr.* 59, 2709–2728. doi: 10.1007/s00394-019-02117-y

Westfall, S., Caracci, F., Estill, M., Frolinger, T., Shen, L., and Pasinetti, G. M. (2021). Chronic stress-induced depression and anxiety priming modulated by gut-brain-axis immunity. *Front. Immunol.* 12:670500. doi: 10.3389/fimmu.2021.670500

Wu, W. L., Adame, M. D., Liou, C. W., Barlow, J. T., Lai, T. T., Sharon, G., et al. (2021). Microbiota regulate social behaviour via stress response neurons in the brain. *Nature* 595, 409–414. doi: 10.1038/s41586-021-03669-y

Xu, C., Lee, S. K., Zhang, D., and Frenette, P. S. (2020). The gut microbiome regulates psychological-stress-induced inflammation. *Immunity* 53, 417–428.e4. doi: 10.1016/j.immuni.2020.06.025

Zhang, Y., Fan, Q., Hou, Y., Zhang, X., Yin, Z., Cai, X., et al. (2022). Bacteroides species differentially modulate depression-like behavior via gut-brain metabolic signaling. *Brain Behav. Immun.* 102, 11–22. doi: 10.1016/j.bbi.2022.02.007

Zhang, J., He, H., Qiao, Y., Zhou, T., He, H., Yi, S., et al. (2020). Priming of microglia with ifn-gamma impairs adult hippocampal neurogenesis and leads to depression-like behaviors and cognitive defects. *Glia* 68, 2674–2692. doi: 10.1002/glia.23878

Zhang, J., Li, L., Liu, Q., Zhao, Z., Su, D., Xiao, C., et al. (2023). Gastrodin programs an arg-1(+) microglial phenotype in hippocampus to ameliorate depression- and anxiety-like behaviors via the nrf2 pathway in mice. *Phytomedicine* 113:154725. doi: 10.1016/j.phymed.2023.154725

Zhang, J., Liu, Q., Su, D., Li, L., Xiao, C., He, H., et al. (2023). Akebia saponin d acts via the ppar-gamma pathway to reprogramme a pro-neurogenic microglia that can restore hippocampal neurogenesis in mice exposed to chronic mild stress. *CNS Neurosci. Ther.* 29, 2555–2571. doi: 10.1111/cns.14196

Zhang, J., Rong, P., Zhang, L., He, H., Zhou, T., Fan, Y., et al. (2021). Il4-driven microglia modulate stress resilience through bdnf-dependent neurogenesis. *Sci. Adv.* 7:abb9888. doi: 10.1126/sciadv.abb9888

Zhang, K., Wang, F., Zhai, M., He, M., Hu, Y., Feng, L., et al. (2023). Hyperactive neuronal autophagy depletes bdnf and impairs adult hippocampal neurogenesis in a

corticosterone-induced mouse model of depression. *Theranostics* 13, 1059–1075. doi: 10.7150/thno.81067

Zhang, S., Zhang, Y., Zhang, W., Chen, S., and Liu, C. (2019). Chronic exposure to green light aggravates high-fat diet-induced obesity and metabolic disorders in male mice. *Ecotoxicol. Environ. Saf.* 178, 94–104. doi: 10.1016/j.ecoenv.2019.04.013

Zhou, N., Qi, H., Liu, J., Zhang, G., Liu, J., Liu, N., et al. (2022). Deubiquitinase otud3 regulates metabolism homeostasis in response to nutritional stresses. *Cell Metab.* 34, 1023–1041.e8. doi: 10.1016/j.cmet.2022.05.005

Zhu, C., Xu, Y., Jiang, Z., Tian, J. B., Cassidy, R. M., Cai, Z. L., et al. (2020). Disrupted hypothalamic crh neuron responsiveness contributes to diet-induced obesity. *EMBO Rep.* 21:e49210. doi: 10.15252/embr.201949210

frontiers | Frontiers in Microbiology

TYPE Opinion
PUBLISHED 08 January 2025
DOI 10.3389/fmicb.2024.1497083

Check for updates

OPEN ACCESS

EDITED BY
Rasha Hammamieh,
Walter Reed Army Institute of Research, United States

REVIEWED BY
Babak Momeni,
Boston College, United States

*CORRESPONDENCE
Daniel Rios Garza
✉ danielriosgarza@gmail.com

RECEIVED 16 September 2024
ACCEPTED 23 December 2024
PUBLISHED 08 January 2025

CITATION
Bouchez T, Liu B and Garza DR (2025) Healthy gut microbiomes are host-controllable microbiomes. *Front. Microbiol.* 15:1497083. doi: 10.3389/fmicb.2024.1497083

COPYRIGHT
© 2025 Bouchez, Liu and Garza. This is an open-access article distributed under the terms of the Creative Commons Attribution License (CC BY). The use, distribution or reproduction in other forums is permitted, provided the original author(s) and the copyright owner(s) are credited and that the original publication in this journal is cited, in accordance with accepted academic practice. No use, distribution or reproduction is permitted which does not comply with these terms.

Healthy gut microbiomes are host-controllable microbiomes

Théodore Bouchez[1], Bin Liu[2] and Daniel Rios Garza[1]*

[1]Université Paris-Saclay, Institut national de recherche pour l'agriculture, l'alimentation et l'environnement (INRAE), PRocédés biOtechnologiques au Service de l'Environnement, Antony, France, [2]Key Laboratory of Environmental Biotechnology, Research Center for Eco-Environmental Sciences, Chinese Academy of Sciences, Beijing, China

KEYWORDS

microbiome, control theory, microbiome ecology and evolution, dysbiosis, gut microbiome

Introduction

"The instinct of each species is good for itself but has never, as far as we can judge, been produced for the exclusive good of others" (Darwin, 1859). Why, then, do humans and other mammals benefit from their microbes?

Evolutionary theory predicts that natural selection can act at organizational levels higher than the gene or individual—such as on groups or even species—provided that the selective advantages for the group outweigh evolutionary conflicts. Darwin suggested that natural selection can act "on the family, and not the individual," "for the sake of gaining a serviceable end" (Darwin, 1859). This idea was later formalized as kin selection (Hamilton, 1964). Even distantly related organisms can align their evolutionary goals, as demonstrated by the longstanding partnership between eukaryotic cells and mitochondria (Margulis, 1970).

Microbes are an integral part of animal and plant hosts, fulfilling essential physiological roles, such as enabling access to otherwise unavailable nutrients, training the immune system, supporting mucosal development, and providing protection. Some microbes are even vertically transmitted from parents to offspring. The numerous examples of microbes performing vital functions for their macrobial hosts makes it tempting to assume that humans and the microbes residing on and within our bodies—particularly in our guts—evolved to share common selective interests that outweigh potential evolutionary conflicts (Rosenberg and Zilber-Rosenberg, 2013; Zilber-Rosenberg and Rosenberg, 2008; Gilbert et al., 2012; Malard et al., 2021). Supporting this assumption, several reports suggest that humans and other mammals are selected for harboring "good" microbes and that these "good" microbes thrive by helping their hosts, for example, by contributing over 95% of our organism's genetic repertoire (Malard et al., 2021; Grice and Segre, 2012; Martino et al., 2022). But is group-level selection a necessary and sufficient mechanism to explain why microbiomes benefit their hosts?

Microbes certainly influence a host's chances of survival and reproductive success (Yuval, 2017; Gould et al., 2018) but the reasons why microbes would reduce their own fitness to form an evolutionarily aligned group with their hosts and other microbial populations—an essential condition for group-level selection—are not easily explained (Douglas and Werren, 2016; van Vliet and Doebeli, 2019). For example, during a 25-year human generation, gut microbes undergo more than 50,000 generations (assuming a conservative 4-h generation time), competing with thousands of microbial species. Roughly half of the bacterial biomass in the colon is lost daily and replaced by new bacterial growth (Arnoldini et al., 2018; Stephen and Cummings, 1980). Before a human reproduces, any trait unfavorable to a microbe's growth or survival would likely be eliminated. Moreover, the human gut is a relatively open system, regularly exposed to

diverse environmental microbes. Vertical transmission accounts for only a small fraction of the microbiome. About 20 species are consistently shared among most adults (Qin et al., 2010). How, then, has evolution shaped such a diverse, rapidly evolving microbial ecosystem to consistently benefit individual health?

One might argue that by providing advantages to "good" microbes, the host mitigates evolutionary conflicts, encouraging microbes to sacrifice some fitness for the host's benefit. However, as microbes rapidly evolve, new genotypes with similar needs can emerge to exploit these host-provided advantages without incurring costs—an example of the tragedy of the commons (Hardin, 1968). These benefits are shared among all compatible microbes, whether or not they contribute to the host's wellbeing, creating an imbalance between contributors and free riders. A free rider, for example, could be a bacterium that feeds on mucin glycans provided by the host while invading tissue and potentially causing severe illness.

Why, then, do humans and other mammals benefit from their microbes? A recent model by Sharp and Foster (2022) suggests that one way to overcome this evolutionary conundrum is for hosts to evolve mechanisms to actively control their microbes and limit the opportunities for microbes to evade control. This would require mechanisms of enforcement or policing to maintain cooperation (Ågren et al., 2019). In this view, hosts are selected not for harboring "beneficial" microbes but for their ability to maintain their microbiomes in a healthy state. In other words, evolution might favor hosts as microbiome control engineers—or, more accurately, control tinkerers (Jacob, 1977)—who make use of various control methods within reach of the evolutionary landscape to sustain their microbiomes in a healthy state. These include responses ranging from rudimentary mechanisms such as inflammation or diarrhea to the sophisticated responses driven by the adaptive immune system. From this perspective, control theory—the study of how systems regulate themselves to achieve desired outcomes—parallels host-microbial interactions, suggesting that healthy microbiomes might be, by definition, host-controllable microbiomes.

Will a large complex microbiome be stable?

In the 1970s, writing in *Nature*, Robert May proposed a limit to the stability of ecosystems as complexity increases, particularly as the number and strength of species interactions grow (May, 1972). May analyzed a simplified Generalized Lotka-Volterra (GLV) model to explore this concept. The model simulates random communities where population sizes are constrained by resource availability (represented as negative self-interactions) and by mutual positive or negative influences on one another's growth. According to the GLV model, assembled communities are predicted to remain stable only when interactions are sufficiently weak or when strong interactions are confined to a few species (Figure 1).

GLV-like models are commonly applied to the study of microbiomes, where similar stability/complexity trade-offs are assumed to hold (Coyte et al., 2015; Yonatan et al., 2022). However, even in May's simplified model, introducing a controller—an agent that directs the system toward a predetermined objective, such as through energy expenditure—is one way to continuously stabilize an otherwise unstable system and reshape the stability-complexity landscape (Figure 1).

Increased microbiome diversity is generally associated with a healthy gut. For example, patients suffering from pathogen invasions, gut inflammation, colitis, inflammatory bowel disease, or colorectal cancer show reduced alpha diversity compared to healthy controls. Similarly, factors such as aging, obesity, the Western diet, and urbanization are also linked to a decline in microbiome diversity (Le Chatelier et al., 2013). Diversity is not necessarily the cause of a healthy microbiome, but it could rather be a consequence of and indirect evidence for host control. In other words, host control effectively drives the microbiome toward a healthy state, which, in the gut microbiome, is also a more diverse state than would occur in the absence of control (due, for example, to stability constraints). In this case, when control is impaired, diversity also declines.

In other biological systems, active control mechanisms can instead reduce microbial diversity. Some examples are laboratory techniques like selective media and dilution-to-extinction procedures, which isolate single strains, or environmental factors such as antibiotics, physical barriers, extreme pH, or heat conditions that similarly reduce microbial diversity. In nature, we see examples of active control reducing diversity, such as the Hawaiian bobtail squid, which isolates a single species of Vibrio fischeri from the ocean in its light organ (Wollenberg and Ruby, 2009). However, it is less often appreciated that active control can also promote greater diversity than would be stable in the absence of control.

An intriguing and underexplored perspective is that the host actively controls the microbiome's natural diversity and that declining diversity may signal a loss of controllability, as suggested by this simplified model (Figure 1). For instance, microbiomes established in reactors that simulate the gastrointestinal tract are significantly less diverse than their original stool inocula (Chassaing et al., 2017). Although these reactors replicate the physicochemical conditions and flow rates of the gut, they lack host-control mechanisms, such as the immune system and dynamically regulated environmental factors. Overall, viewing the gut microbiome as an interconnected, island-like ecosystem—where each individual serves as a microbial patch colonized by dispersal, local diversification, environmental selection, and drift (Costello et al., 2012)—becomes clearer when we consider environmental selection processes as active, energy-expending efforts by the host to target desired diversity, composition, and functions.

Beyond diversity, the host's control also extends to the microbiome's "state-space," which includes microbial populations and their biochemical activities. In an ideal scenario of tight, full-state control, the host would control both the abundance and function of each microbial population, including their chemical outputs and inputs. However, a more realistic scenario involves limited, partial-state control, where the host exerts varying degrees of influence over distinct aspects of the state-space. For example, a recent theoretical framework proposed that the composition of the gut microbiome can be controlled by targeting specific sets of microbes, referred to as "minimal control elements" (Angulo

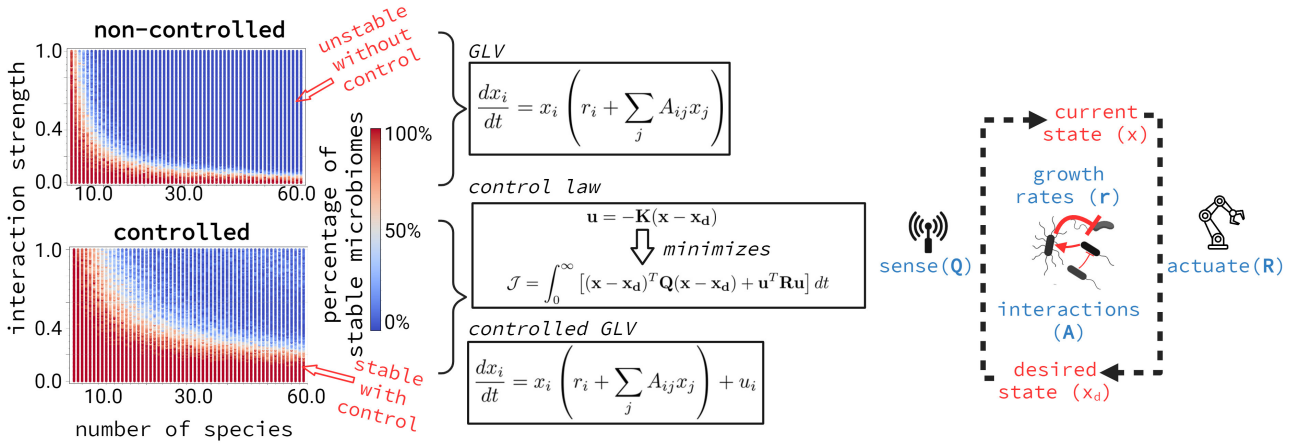

FIGURE 1
Fraction of stable microbiomes with and without a controller in 10,000 GLV simulations. Random microbiomes were simulated with increasing interaction strengths and numbers of species. Each dot represents 100 simulations and is colored according to the fraction that resulted in a stable microbiome. Dark blue dots indicate cases where all 100 simulations were unstable, while dark red dots indicate cases where all were stable. The white transition zone represents intermediate stability. The results show that adding a controller—here idealized as a device that senses the microbiome's current composition and adjusts species growth rates to guide the system toward a desired composition—significantly increases the range of stable microbiomes. Stability, as defined here following May's original model, refers to whether the system returns to equilibrium after a small perturbation based on the signs of the eigenvalues of the Jacobian matrix at the equilibrium point.

et al., 2019). This control can be achieved by leveraging species-species interactions, which form control chains connecting external controllers to the intrinsic dynamics of community interactions (Angulo et al., 2019). Although this framework still lacks empirical validation, it highlights the potential for identifying specific control elements to restore a dysbiotic microbiome.

How control theory helps explain microbiomes

The mammalian gut contains various active control mechanisms (Wilde et al., 2024; Foster et al., 2017), which can be categorized into microbiome-independent and microbiome-dependent processes. For example, transit time ranges from 2 to 5 h in the small intestine and 10 to 59 h in the large intestine (Lee et al., 2014). These parameters directly influence the microbiome—favoring host absorption over microbial growth in the small intestine and microbial growth and fermentation in the large intestine—but are generally independent of sensing microbiome features. From the microbiome control perspective, these processes are open-loop controllers (Brunton and Kutz, 2022)—that is, they operate without feedback from the microbiome itself. By contrast, the immune system's targeting of specific microbiome features exemplifies a closed-loop controller, which adjusts its actions based on feedback from microbial dynamics.

Evolving closed-loop microbiome controllers likely allowed humans and other mammals to fine-tune their responses and maximize their benefits from large, diverse, and densely populated microbiomes. For example, a meta-study comparing cultures of fresh stool samples in reactors that, to varying degrees, model the gut environment (e.g., SHIME, TIM-2) found that interindividual variation in the inoculum is the primary driver of community composition (Garcia Mendez et al., 2024)—i.e., interindividual variation outweighs the selective pressure exerted by the reactor's operational design (biotope). The evolution of closed-loop control likely ensures that these widely different, personalized microbial communities, assembled by each individual over their lifetime, continue to perform essential functions despite their variability.

Controllability and observability are fundamental limit conditions for microbiome control

If microbiome control is necessary for the host to maintain a healthy state, then we need models and experimental systems to elucidate two essential limit conditions for microbiome control: observability (which aspects of the state-space can the host observe?) and controllability (which states can the host influence through control inputs, ideally within a finite time?). Numerous studies associate high consumption of simple sugars and low dietary fiber intake with dysbiotic microbiomes. However, the underlying mechanisms remain widely debated. One possible explanation is the loss of both controllability and observability.

Experiments with synthetic microbiomes suggest that complex substrates result in history dependence, where microbiomes diverge in taxonomic composition and function (Bittleston et al., 2020; Leventhal et al., 2018; Silverstein et al., 2024). In contrast, simple substrates lead to more deterministic compositions, particularly at higher taxonomic levels (Goldford et al., 2018). Put simply, multiple states are possible for microbiomes grown on complex substrates, even when isolated from the same source and maintained under identical conditions (Leventhal et al., 2018). A subset of these states in the gut may correspond to healthy microbial communities. The host's control mechanisms could guide the microbiome toward these healthy states.

In contrast, synthetic communities grown on simple substrates tend to converge to similar taxonomic compositions and metabolic profiles, regardless of their sources (Goldford et al., 2018; Estrela et al., 2022). In this scenario, the host's control may be limited, as healthy microbiome states could be outside its reach. For example, patients with low microbiome richness often respond poorly to therapeutic interventions, including dietary restriction and cancer immunotherapy (Routy et al., 2018).

Controllability is inherently dependent on observability. Specifically, controlled colonization events educate the immune system to recognize pathogens and enhance the host's ability to monitor microbial states. For instance, *Bacteroides fragilis* produces an immunomodulatory polysaccharide that, in germ-free mice, trains a population of immune cells to protect against *Helicobacter hepaticus*, a pathogen responsible for colitis in immunocompromised animals (Mazmanian et al., 2005, 2008). Another example is segmented filamentous bacteria (SFB) (*Candidatus Arthromitus*), a species-specific filamentous bacteria found in the guts of several vertebrates. SFB forms millimeter-long filaments that attach directly to the ileal epithelium via a specialized cell called a holdfast, without triggering inflammation (Schnupf et al., 2015). In several species, SFB colonization peaks during early life (Hedblom et al., 2018), training the immune system against future invasive pathogens.

Interestingly, SFB occupies a spatial gradient similar to environmental cable bacteria, connecting the oxygen-rich epithelium to the anoxic lumen. Although they share similar morphology—long, single-layered filaments—it remains to be tested whether SFB plays a similar ecological role in conducting electrons between these zones (Nielsen et al., 2010) and sharing them with other species (Bjerg et al., 2023). Ericsson and colleagues observed that only the stool of mice harboring SFB produced a strong exoelectrogenic current in microbial fuel cells, even though the SFB itself was not found on the electrodes (Ericsson et al., 2015). Their study also showed that differences in the electrical current production by exoelectrogens were predictive of lymphocyte trafficking to the gut. In other words, the mammalian gut may monitor and respond to the unique electrical signatures of its microbiome, targeting microbes at locations with unusual signatures. By adapting its immune response to specific electrical signatures or redox gradients, the host may enhance its ability to observe and react to changes in the microbiome's state-space.

Host-microbiome dynamics: Pinocchio and Geppetto

Overall, control incurs fitness costs for the host, both for gathering information and for acting on that information. From an evolutionary perspective, hosts minimize these costs to invest on growth and reproduction. Over different timescales, an evolutionary arms race develops between hosts and microbial populations: hosts benefit from efficient, cost-effective control strategies, while microbes evolve ways to evade such control—especially when it restricts their survival and growth (Wilde et al., 2024).

For example, inflammation is a systemic response by the host to counter microbial invasion. When triggered, reactive oxygen species are released. Some opportunistic pathogens exploit this response by tolerating the released hydrogen peroxide and expressing molecular machinery that allows them to absorb it into their cytoplasm. There, they quickly convert it into oxygen for use in their respiratory chain, giving them an advantage over fermentative organisms (Crowley and Vallance, 2020). *Salmonella enterica serotype* Typhimurium goes a step further. Under normal conditions, the gut detoxifies hydrogen sulfide, produced in large quantities by the microbiota, by converting it into thiosulfate. During inflammation, reactive species convert thiosulfate into tetrathionate, which *S. Typhimurium* respires (Winter et al., 2010), effectively feeding on the host's defense mechanisms.

A healthy, symbiotic microbiome remains under host control, maintained by the host's regulatory mechanisms to ensure beneficial function. In contrast, a dysbiotic microbiome arises when this control is impaired—whether because a healthy composition becomes unreachable, necessary cues become unobservable, or the mechanisms of control (effectors) become ineffective. In other words, microbes are not our Geppetto (Stilling et al., 2016); instead, we attempt to control them. Like Pinocchio, they strive—and often succeed—to evade our control.

Author contributions

TB: Conceptualization, Writing – review & editing. BL: Conceptualization, Writing – review & editing. DG: Conceptualization, Formal analysis, Funding acquisition, Supervision, Writing – original draft.

Funding

The author(s) declare financial support was received for the research, authorship, and/or publication of this article. This work benefited from State aid managed by the National Research Agency under France 2030 (ANR-24-RRII-0003), EXPLOR'AE program supported by INRAE.

Conflict of interest

The authors declare that the research was conducted in the absence of any commercial or financial relationships that could be construed as a potential conflict of interest.

Publisher's note

All claims expressed in this article are solely those of the authors and do not necessarily represent those of their affiliated organizations, or those of the publisher, the editors and the reviewers. Any product that may be evaluated in this article, or claim that may be made by its manufacturer, is not guaranteed or endorsed by the publisher.

References

Ågren, J. A., Davies, N. G., and Foster, K. R. (2019). Enforcement is central to the evolution of cooperation. *Nat. Ecol. Evol.* 3, 1018–1029. doi: 10.1038/s41559-019-0907-1

Angulo, M. T., Moog, C. H., and Liu, Y. Y. (2019). A theoretical framework for controlling complex microbial communities. *Nat. Commun.* 10:1045. doi: 10.1038/s41467-019-08890-y

Arnoldini, M., Cremer, J., and Hwa, T. (2018). Bacterial growth, flow, and mixing shape human gut microbiota density and composition. *Gut Microbes*. 9, 559–566. doi: 10.1080/19490976.2018.1448741

Bittleston, L. S., Gralka, M., Leventhal, G. E., Mizrahi, I., and Cordero, O. X. (2020). Context-dependent dynamics lead to the assembly of functionally distinct microbial communities. *Nat. Commun.* 11:1440. doi: 10.1038/s41467-020-15169-0

Bjerg, J. J., Lustermans, J. J. M., Marshall, I. P. G., Mueller, A. J., Brokjær, S., Thorup, C. A., et al. (2023). Cable bacteria with electric connection to oxygen attract flocks of diverse bacteria. *Nat. Commun.* 14:1614. doi: 10.1038/s41467-023-37272-8

Brunton, S. L., and Kutz, J. N. (2022). *Data-Driven Science and Engineering: Machine Learning, Dynamical Systems, and Control*. 2nd edition. Cambridge, United Kingdom, New York, NY: Cambridge University Press, 614. doi: 10.1017/9781009089517

Chassaing, B., de Wiele, T. V., Bodt, J. D., Marzorati, M., and Gewirtz, A. T. (2017). Dietary emulsifiers directly alter human microbiota composition and gene expression ex vivo potentiating intestinal inflammation. *Gut* 66, 1414–1427. doi: 10.1136/gutjnl-2016-313099

Costello, E. K., Stagaman, K., Dethlefsen, L., Bohannan, B. J. M., and Relman, D. A. (2012). The application of ecological theory toward an understanding of the human microbiome. *Science* 336, 1255–1262. doi: 10.1126/science.1224203

Coyte, K. Z., Schluter, J., and Foster, K. R. (2015). The ecology of the microbiome: networks, competition, and stability. *Science* 350, 663–666. doi: 10.1126/science.aad2602

Crowley, S. M., and Vallance, B. A. (2020). Microbial respiration in the colon: using H2O2 to catch your breath. *Cell Host Microbe*. 28, 771–773. doi: 10.1016/j.chom.2020.11.006

Darwin, C. (1859). *On the Origin of Species by Means of Natural Selection, or, The Preservation of Favoured Races in the Struggle for Life*. London: John Murray, Albemarle Street. doi: 10.5962/bhl.title.68064

Douglas, A. E., and Werren, J. H. (2016). Holes in the hologenome: why host-microbe symbioses are not holobionts. *MBio* 7:15. doi: 10.1128/mBio.02099-15

Ericsson, A. C., Davis, D. J., Franklin, C. L., and Hagan, C. E. (2015). Exoelectrogenic capacity of host microbiota predicts lymphocyte recruitment to the gut. *Gut Microb. Health Dis.* 47, 243–252. doi: 10.1152/physiolgenomics.00010.2015

Estrela, S., Vila, J. C. C., Lu, N., Bajić, D., Rebolleda-Gómez, M., Chang, C. Y., et al. (2022). Functional attractors in microbial community assembly. *Cell Syst.* 13, 29–42.e7. doi: 10.1016/j.cels.2021.09.011

Foster, K. R., Schluter, J., Coyte, K. Z., and Rakoff-Nahoum, S. (2017). The evolution of the host microbiome as an ecosystem on a leash. *Nature* 548, 43–51. doi: 10.1038/nature23292

Garcia Mendez, D. F., Egan, S., Wist, J., Holmes, E., and Sanabria, J. (2024). Meta-analysis of the microbial diversity cultured in bioreactors simulating the gut microbiome. *Microb. Ecol.* 87:57. doi: 10.1007/s00248-024-02369-0

Gilbert, S. F., Sapp, J., and Tauber, A. I. (2012). A symbiotic view of life: we have never been individuals. *Q. Rev. Biol.* 87, 325–341. doi: 10.1086/668166

Goldford, J. E., Lu, N., Baji,ć, D., Estrela, S., Tikhonov, M., Sanchez-Gorostiaga, A., et al. (2018). Emergent simplicity in microbial community assembly. *Science* 361, 469–474. doi: 10.1126/science.aat1168

Gould, A. L., Zhang, V., Lamberti, L., Jones, E. W., Obadia, B., Korasidis, N., et al. (2018). Microbiome interactions shape host fitness. *Proc. Nat. Acad. Sci.* 115, E11951–E11960. doi: 10.1073/pnas.1809349115

Grice, E. A., and Segre, J. A. (2012). The human microbiome: our second genome*. *Annu. Rev. Genomics Hum. Genet.* 13, 151–170. doi: 10.1146/annurev-genom-090711-163814

Hamilton, W. D. (1964). The genetical evolution of social behaviour. I. *J. Theor. Biol.* 7, 1–16. doi: 10.1016/0022-5193(64)90038-4

Hardin, G. (1968). The tragedy of the commons. *Science* 162, 1243–1248. doi: 10.1126/science.162.3859.1243

Hedblom, G. A., Reiland, H. A., Sylte, M. J., Johnson, T. J., and Baumler, D. J. (2018). Segmented filamentous bacteria – metabolism meets immunity. *Front. Microbiol.* 9:01991. doi: 10.3389/fmicb.2018.01991

Jacob, F. (1977). Evolution and tinkering. *Science* 196, 1161–1166. doi: 10.1126/science.860134

Le Chatelier, E., Nielsen, T., Qin, J., Prifti, E., Hildebrand, F., Falony, G., et al. (2013). Richness of human gut microbiome correlates with metabolic markers. *Nature* 500, 541–546. doi: 10.1038/nature12506

Lee, Y. Y., Erdogan, A., and Rao, S. S. C. (2014). How to assess regional and whole gut transit time with wireless motility capsule. *J. Neurogastroenterol. Motil.* 20, 265–270. doi: 10.5056/jnm.2014.20.2.265

Leventhal, G. E., Boix, C., Kuechler, U., Enke, T. N., Sliwerska, E., Holliger, C., et al. (2018). Strain-level diversity drives alternative community types in millimetre-scale granular biofilms. *Nat. Microbiol.* 3, 1295–1303. doi: 10.1038/s41564-018-0242-3

Malard, F., Dore, J., Gaugler, B., and Mohty, M. (2021). Introduction to host microbiome symbiosis in health and disease. *Mucosal Immunol.* 14, 547–554. doi: 10.1038/s41385-020-00365-4

Margulis, L. (1970). *Origin of eukaryotic cells : evidence and research implications for a theory of the origin and evolution of microbial, plant, and animal cells on the Precambrian earth*. New Haven: Yale University Press, 388. Available at: http://archive.org/details/originofeukaryot0000marg (accessed June 27, 2024).

Martino, C., Dilmore, A. H., Burcham, Z. M., Metcalf, J. L., Jeste, D., Knight, R., et al. (2022). Microbiota succession throughout life from the cradle to the grave. *Nat. Rev. Microbiol.* 20, 707–720. doi: 10.1038/s41579-022-00768-z

May, R. M. (1972). Will a large complex system be stable? *Nature* 238, 413–414. doi: 10.1038/238413a0

Mazmanian, S. K., Liu, C. H., Tzianabos, A. O., and Kasper, D. L. (2005). An immunomodulatory molecule of symbiotic bacteria directs maturation of the host immune system. *Cell* 122, 107–118. doi: 10.1016/j.cell.2005.05.007

Mazmanian, S. K., Round, J. L., and Kasper, D. L. (2008). A microbial symbiosis factor prevents intestinal inflammatory disease. *Nature* 453, 620–625. doi: 10.1038/nature07008

Nielsen, L. P., Risgaard-Petersen, N., Fossing, H., Christensen, P. B., and Sayama, M. (2010). Electric currents couple spatially separated biogeochemical processes in marine sediment. *Nature* 463, 1071–1074. doi: 10.1038/nature08790

Qin, J., Li, R., Raes, J., Arumugam, M., Burgdorf, K. S., Manichanh, C., et al. (2010). A human gut microbial gene catalogue established by metagenomic sequencing. *Nature* 464, 59–65. doi: 10.1038/nature08821

Rosenberg, E., and Zilber-Rosenberg, I. (2013). *The Hologenome Concept: Human, Animal and Plant Microbiota*. Cham: Springer International Publishing. doi: 10.1007/978-3-319-13904-3

Routy, B., Le Chatelier, E., Derosa, L., Duong, C. P. M., Alou, M. T., Daillère, R., et al. (2018). Gut microbiome influences efficacy of PD-1–based immunotherapy against epithelial tumors. *Science* 359, 91–97. doi: 10.1126/science.aan3706

Schnupf, P., Gaboriau-Routhiau, V., Gros, M., Friedman, R., Moya-Nilges, M., Nigro, G., et al. (2015). Growth and host interaction of mouse segmented filamentous bacteria in vitro. *Nature* 520, 99–103. doi: 10.1038/nature14027

Sharp, C., and Foster, K. R. (2022). Host control and the evolution of cooperation in host microbiomes. *Nat. Commun.* 13:3567. doi: 10.1038/s41467-022-30971-8

Silverstein, M. R., Bhatnagar, J. M., and Segrè, D. (2024). Metabolic complexity drives divergence in microbial communities. *Nat. Ecol. Evol.* 8, 1493–1504. doi: 10.1038/s41559-024-02440-6

Stephen, A. M., and Cummings, J. H. (1980). The microbial contribution to human faecal mass. *J. Med. Microbiol.* 13, 45–56. doi: 10.1099/00222615-13-1-45

Stilling, R. M., Dinan, T. G., and Cryan, J. F. (2016). The brain's Geppetto—microbes as puppeteers of neural function and behaviour? *J. Neurovirol.* 22, 14–21. doi: 10.1007/s13365-015-0355-x

van Vliet, S., and Doebeli, M. (2019). The role of multilevel selection in host microbiome evolution. *Proc. Nat. Acad. Sci.* 116, 20591–20597. doi: 10.1073/pnas.1909790116

Wilde, J., Slack, E., and Foster, K. R. (2024). Host control of the microbiome: mechanisms, evolution, and disease. *Science* 385:eadi3338. doi: 10.1126/science.adi3338

Winter, S. E., Thiennimitr, P., Winter, M. G., Butler, B. P., Huseby, D. L., Crawford, R. W., et al. (2010). Gut inflammation provides a respiratory electron acceptor for Salmonella. *Nature* 467, 426–429. doi: 10.1038/nature09415

Wollenberg, M. S., and Ruby, E. G. (2009). Population structure of vibrio fischeri within the light organs of euprymna scolopes squid from two oahu (Hawaii) populations. *Appl. Environ. Microbiol.* 75, 193–202. doi: 10.1128/AEM.01792-08

Yonatan, Y., Amit, G., Friedman, J., and Bashan, A. (2022). Complexity–stability trade-off in empirical microbial ecosystems. *Nat. Ecol. Evol.* 6, 693–700. doi: 10.1038/s41559-022-01745-8

Yuval, B. (2017). Symbiosis: gut bacteria manipulate host behaviour. *Curr. Biol.* 27, R746–R747. doi: 10.1016/j.cub.2017.06.050

Zilber-Rosenberg, I., and Rosenberg, E. (2008). Role of microorganisms in the evolution of animals and plants: the hologenome theory of evolution. *FEMS Microbiol. Rev.* 32, 723–735. doi: 10.1111/j.1574-6976.2008.00123.x

frontiers | Frontiers in Microbiomes

TYPE Original Research
PUBLISHED 04 February 2025
DOI 10.3389/frmbi.2025.1473292

Check for updates

OPEN ACCESS

EDITED BY
Adrienne Narrowe,
Agricultural Research Service (USDA), United States

REVIEWED BY
Apollo Stacy,
Cleveland Clinic, United States
John Common,
Agency for Science, Technology and Research (A*STAR), Singapore

*CORRESPONDENCE
Vidhya Vijayakumar
vvijayakumar@draper.com

†These authors have contributed equally to this work

RECEIVED 30 July 2024
ACCEPTED 03 January 2025
PUBLISHED 04 February 2025

CITATION
Maloney AL, Crawford T, Hurlbut J, Martinez M, Mulhern TJ, Wiellette EL, Vedula EM and Vijayakumar V (2025) A multi-strain human skin microbiome model provides a testbed for disease modeling. *Front. Microbiomes* 4:1473292. doi: 10.3389/frmbi.2025.1473292

COPYRIGHT
© 2025 Maloney, Crawford, Hurlbut, Martinez, Mulhern, Wiellette, Vedula and Vijayakumar. This is an open-access article distributed under the terms of the Creative Commons Attribution License (CC BY). The use, distribution or reproduction in other forums is permitted, provided the original author(s) and the copyright owner(s) are credited and that the original publication in this journal is cited, in accordance with accepted academic practice. No use, distribution or reproduction is permitted which does not comply with these terms.

A multi-strain human skin microbiome model provides a testbed for disease modeling

Angela L. Maloney†, Tyler Crawford†, Jordan Hurlbut†, Monica Martinez, Thomas J. Mulhern, Elizabeth L. Wiellette, Else M. Vedula and Vidhya Vijayakumar*

Bioengineering Division, Draper, Cambridge, MA, United States

The skin microbiome plays a critical role at the interface between the human epidermis and the environment, providing colonization resistance against pathogenic strains, training host immunity, and supporting epithelial turnover. Inversely, dysbiotic skin microbiome states are associated with skin disease, particularly inflammatory conditions such as atopic dermatitis and psoriasis. Current evaluation of human host and microbiome interactions relies on *post hoc* studies after disease onset. This limits the ability to evaluate the causal roles of host and microbe during disease progression. One approach to characterizing microbial and host biology in a controlled and reproducible context is to derive *in vitro* models of sufficient complexity and stability to support perturbation and response. Current tools for studying these processes are focused on testing antagonistic or synergistic relations between two or more strains for short (hours to days) culture durations, thereby precluding studies of relevant complexity and chronic disease states. Here, we present an *in vitro* model of the human skin microbiome comprising a six strain consortium colonizing primary human keratinocyte-derived tissue in Air-Liquid Interface for up to 7 days. We evaluated readouts of tissue health including histology, gene expression, and transepithelial electrical resistance (TEER), as well as relative strain abundance to characterize microbiome stability over time. Skin cells formed a complex tissue structure over two weeks and maintained stable or increasing TEER after 7 days of co-culture with the microbial consortium. Up to five of the six strains were viable on the skin tissue surface on day 7 as validated by custom qPCR assays, demonstrating a robust and stable testbed for microbiome studies. A remarkable feature of this model is the persistence of *Cutibacterium acnes* in an aerobic tissue culture environment, since *C. acnes* growth is typically demonstrated under anaerobic conditions, suggesting that the skin tissue model is conducive to more natural growth states of native skin strains. The addition of cytokines representative of atopic dermatitis elicited a marked decrease in tissue barrier by day 7 compared to healthy controls, irrespective of the microbiome presence. Furthermore, an alteration in relative strain abundance was observed in diseased model tissues, demonstrating capability to study the impact of disease states on

the microbiome and vice versa. We envision this model system as a test bed to evaluate the influence of commensals on host biology, the influence of external environment on microbiome stability, and chronic diseases impacted by dysbiosis.

KEYWORDS

skin, microbiome, consortium, atopic dermatitis, organ-on-chip, *in vitro* model

1 Introduction

Human skin health relies in part on a partnership between the host epidermis and the resident microbiota, a diverse community of microbes composed of bacteria, fungi, and viruses. Together, the host and microbes maintain a homeostatic tissue barrier that protects the body from the external environment (Flowers and Grice, 2020; Swaney and Kalan, 2021; Harris-Tryon and Grice, 2022). The outer layer of the skin, the epidermis, provides a supportive environment for commensal microbes, which in turn delivers a defense against pathogen colonization, trains the immune system, supports wound healing, and promotes dermatological health (Matsui and Amagai, 2015; Naik et al., 2015; Rosso et al., 2016; Belkaid and Harrison, 2017; Linehan et al., 2018; Uberoi et al., 2024). Despite the harsh, acidic environment of the skin surface, colonizing microbes thrive in a commensal community, which includes ubiquitous bacteria like S*taphylococcus epidermidis* and highly prevalent *Cutibacterium acnes*, an anaerobic bacteria of the skin microbiome (Conwill et al., 2022; Severn and Horswill, 2023) (Conwill et al., 2022). Recent advances in sequencing technology and longitudinal sampling studies have provided a general recognition that skin health and resilience are predominantly indicated by microbial complexity and longitudinal stability (Oh et al., 2016; Byrd et al., 2018).

While they typically support healthy skin biology, the microbiota can become dysbiotic, or imbalanced, either by introduction of a pathogenic strain or by a change in metabolism or composition of the microbiome. It has been well documented that a dysbiotic skin microbiome is often correlated with inflammatory skin diseases such as atopic dermatitis (AD), psoriasis, and acne, further emphasizing the synergistic relationship between mammalian and microbial cells of the human skin (Lee and Kim, 2022; Severn and Horswill, 2023). For instance, in the case of AD, the relative abundances of *Staphylococcus aureus* and *S. epidermidis* are elevated compared to healthy or non-flared skin (Byrd, 2017; Kong et al., 2012; Fyhrquist et al., 2019). Due to the interdependency between host inflammatory status and microbial metabolism, it is challenging to disentangle causal and response effects after disease onset (Harris-Tryon and Grice, 2022). Typically, evaluation of the causative role of a particular bacterial strain is carried out through correlation of a strain or metabolite with disease state, isolation of the candidate strain, and evaluation on an animal model for disease induction (Li et al., 2006; McIntyre et al., 2016). However, animals are particularly distinct from humans in immune profile and microbiome composition and do not always provide a relevant background microbiome or host immune response (Ross et al., 2018; Bjornson-Hooper et al., 2022). Alternatively, microbial cells or extracts can be evaluated directly on human cells *in vitro* for reactivity. This strategy can be successful to characterize host cell activation, but current microbiome models lack the complexity to test the converse causality of host factors on a balanced microbiome (Kang et al., 2015; Nakatsuji et al., 2017)

There is a need to develop and improve representative, *in vitro* models of human skin tissue and its resident, complex microbiota (Smythe and Wilkinson, 2023). Such model systems should readily enable investigation of host-microbiome interactions in healthy states, the induction of pathogenicity, and the causes and treatments of skin diseases. Complex human skin reconstructions are available, including commercial versions (Labskin, EpiDerm) as well as cultured biopsies collected directly from human skin, which are typically sterilized (De Wever, 2015; Hardwick et al., 2020; Hofmann et al., 2023). A model that incorporates a commensal consortium of microbes in a stable co-culture with host tissue, with demonstrated feedback signaling between host and the resident microbes would fill existing gaps in microbiome toolkit to study host-microbiome interactions. Ideal representations of the human skin and its microbiota require both microbial diversity and stable longevity, features which will together provide a reliable and predictive context for evaluating host-microbe symbiosis and its disruption.

As a step towards a complex *in vitro* host-microbiome model, we present here a human skin microbiome testbed, SURFACE (Skin microbiome (μbiome) Reconstruction For Assessment of Cutaneous Effects), which supports a multi-strain bacterial culture on a human skin equivalent model. Combinatorial screening of candidate human skin commensal bacterial strains identified six strains and inoculation concentrations; resulting consortia were applied to mature skin tissues cultured at air-liquid interface (ALI). Direct quantification of the microbes periodically during the co-culture demonstrated that the strains could colonize and persist for 7 days, including the anaerobic strain, *Cutibacterium acnes*, and the pathobiont species *Staphylococcus*

epidermidis. We also demonstrate that the SURFACE platform can be used as an appropriate model of host-microbiome response to a disease state. When exposed to Atopic Dermatitis (AD)-associated cytokines, the host tissue loses barrier function and secretes inflammation-relevant cytokines. Strikingly, the host response is paired with consistent modulation of the six-strain microbial consortium, which loses diversity similar to changes in AD patient microbiomes (Kong et al., 2012; Kim and Kim, 2019). These results present an important advance in models of host-microbiome interactions and can support the future evaluation of microbiome responses to pathogens, toxins, environmental changes, and introduction of engineered microbes.

2 Materials and methods

2.1 Skin tissue culture

Primary human keratinocytes (Normal Human Epidermal Keratinocytes; NHEK) were purchased from Lifeline Cell Technology (Frederick, MD). NHEKs were expanded in CnT-PR (CellNTec) and cryopreserved for seeding. On the day of seeding, noted as Day -7, PET Transwell inserts with 0.4 micron pores and a 0.33 cm^2 growth area (Corning) were coated in 50 μg/mL (5 μg/insert) of human plasma fibronectin (Millipore) for 1 hour at 37°C. Cryopreserved NHEKs were thawed quickly, added to 10x volume of fresh media, and centrifuged at 150 X g for 4 minutes to remove cryopreservation agents. Media was aspirated from the cell pellet and resuspended to 250,000 cells/mL in CnT-PR-FTAL5 (CellNTec). Cells were seeded into inserts at 50,000 cells/insert and maintained in submerged culture for 3 days. Media was changed every other day.

On the fourth day of submerged culture, Day -3, TEER was measured using the EVOM-3 (World Precision Instruments) and STX-III electrodes (World Precision Instruments). Media was aspirated from apical and basal chambers and replaced with only 300 μL of media in the basal chamber to begin ALI culture. NHEKs were allowed to differentiate at Air Liquid Interface (ALI) conditions for 3 days before bacterial inoculum was introduced on Day 0, with basal media being refreshed every other day. For AD disease model, basal media was supplemented with 10ng/ml of rhIL-22, rhTNF-α, rhIL-4 and rhIL-3 (R&D Systems) on Day 0 of bacterial inoculation and refreshed every other day until takedown.

At takedown, on either Day 4 or Day 7, media was added to apical and basal chambers to collect TEER. TEER measurements were normalized by subtracting the blank TEER value of Transwell and multiplied by the surface area of the Transwell insert. TEER is represented as mean and standard deviation of multiple Transwells (n≥3 per condition) within a timepoint for a single experiment.

2.2 Bacterial strains and inoculation

Bacterial strains were purchased from ATCC and grown in indicated agar conditions atmosphere prior to inoculation (Table 1). All strains were lifted from agar plates and resuspended in TSB (BD Biosciences). The Optical Density (OD_{600}) was measured using a NanoDrop (Thermo Scientific NanoDrop 2000c Spectrophotometer) and diluted until an OD_{600} of 0.1 was achieved. The bacterial solution was pelleted and then resuspended in twice the original volume of FTAL media for the six inoculated strains: *S. epidermidis*, *C. acnes*, *S. thermophilus*, *S. hominis*, *R. dentocariosa*, and *C. striatum*. All strains except *S. epidermidis* were diluted further to 1:500 and *S. epidermidis* was diluted 1:50,000. Single strain suspensions were plated, and Colony Forming Units (CFU) counted to determine the initial composition of the consortia that had been applied to the tissue.

TABLE 1 Strains used in this study, along with culture conditions and identification numbers.

Strain	Agar	Atmospheric Conditions	ATCC ID
S. epidermidis FDA strain PCI 1200	Tryptic Soy Agar	Aerobic	12228
C. acnes 417/52 [VPI 0391]	Tryptic Soy Agar +5% Sheep Blood	Anaerobic	11828
S. thermophilus (LMD-9)	S. thermophilus Agar Hi Media	5% CO2	BAA-491
S. hominis (NCTC 11320)	Tryptic Soy Agar	Aerobic	27844
R. dentocariosa CDC X599 [XDIA]	Tryptic Soy Agar +5% Sheep Blood	Aerobic	17931
C. striatum NCTC 764 [IFO 15291]	Tryptic Soy Agar +5% Sheep Blood + 0.1% Tween80	5% CO2	6940

To prepare the final mixed inoculum, each individual bacterial dilution was combined in equal volume. 100 μL of the mixed strain inoculum was then applied to the apical side of the SURFACE model. The tissue was incubated for two hours at 37°C, 5% CO_2 to allow the bacteria to engraft to the tissue. The excess inoculum was removed, and tissues were washed twice with 200 μL of Full Thickness media, restored to ALI, and returned to 37°C, 5% CO_2. Microbiome replete skin tissue was maintained in ALI for up to 7 days, with the media in the basal chamber being changed every other day. Transwell replicates were taken down for evaluation at either day 4 or day 7 and compared to uninoculated Transwell tissue replicates. Each figure represent data from a single experiment.

2.3 Quantitative PCR for strain specific assay validation

To produce single strain gDNA template for qPCR standard curve generation, a modified protocol of New England Biolab's Genomic DNA Purification Kit (NEB #T3010) was utilized on each strain used in the study. The standard protocol for Gram-positive bacteria was used with two modifications – During lysozyme treatment, additional enzymes were added for improved cell lysis (10 μL lysostaphin at 10 mg/mL and 10 μL mutanolysin at 5 mg/mL). Two freeze thaw cycles in liquid nitrogen were incorporated prior to spin column extractions. The extracted gDNA was then normalized to a concentration of 1 ng/μL. Standards were tested against every

assay used in the qPCR quantification process. For *S. epidermidis*, *C. acnes*, and *C. striatum*, TaqMan Microbe Detection Assays from ThermoFisher were used, while in-house primer-probes were developed for *S. thermophilus*, *S. hominis*, and *R. dentocariosa* (Table 2). The reaction mix and cycling conditions were followed for all assays as per the guidelines provided with the TaqMan™ Fast Advanced Master Mix for qPCR (CAT#: 4444557) with the exception of *S. hominis* assay, which was run at an annealing temperature of 64° C. Cutoffs for CT values were determined as per Hays et al. (Hays et al., 2022) (Supplementary Figure 1).

2.4 Bacterial quantification and relative abundance from microbiome replete tissues

On the day of take down, the SURFACE tissue was removed from the Transwell by gentle scraping to detach the circular disc of skin tissue. It was then processed using Qiagen's QIAamp DNA Microbiome Kit (Cat #51704) to extract bacterial genomic DNA (henceforth called microbiome gDNA). Briefly, the kit first selectively lyses host cells via a detergent-based method while microbial cells are kept intact. The released host DNA is degraded enzymatically while maintaining the bacterial cells. The bacterial cell lysis is then performed by a mechanical and chemical method for a final isolation of bacterial DNA through a spin-column. Multiple Transwell samples (n≥3) were harvested per condition tested in a single timepoint. Samples were never pooled, a single Transwell tissue's derived microbial DNA is represented as a single data point.

The abundance of each individual bacterial strain in the microbiome gDNA samples was quantified via qPCR using strain specific assays as listed in Table 2 and standard curves as shown in Supplementary Figure S1. The reaction was run in duplicates for each microbiome gDNA sample and the mean of the duplicates was used to calculate copies for one Transwell tissue.

The Ct value for each strain specific amplification curve was extrapolated to gDNA concentration from the standard curve. The genome size as reported by ATCC was used to calculate the genome copies per picogram of gDNA (Table 3). These two values were used to calculate the number of genome copies using the following formula:

$$\begin{aligned} &Number\ of\ genome\ copies\ per\ \mu l \\ &= gDNA\ concentration\ of\ strain\ from\ microbiome\ sample\left(\frac{pg}{\mu l}\right) \times genome\ copies\ per\ pg\ of\ DNA\left(\frac{copies}{pg}\right) \end{aligned}$$

Relative abundance was calculated by summing the genome copies of all strains per microbiome gDNA extract. Biodiversity within groups of samples was measured using Shannon's diversity index (Shannon, 1948).

$$H = -\sum[(pi)x\log(pi)]$$

Where H= Shannon diversity index; pi = proportion of individuals of the -ith species in a whole community or individuals of a given species over total number of individuals in a community.

Ct values from qPCR were analyzed using QuantStudio Real-Time PCR Software v1.7.2 (Thermo Fisher Scientific). Data analysis and plotting was performed using GraphPad Prism software v10.

2.5 Histology

On the day of takedown, SURFACE tissues designated for histology were fixed in 4% Paraformaldehyde (Sigma) in Phosphate Buffered Saline (PBS) for at least 15 minutes at room temperature. Tissues were removed from Transwell inserts and stored in 70% ethanol at 4°C for further sectioning and staining steps. All samples were processed at NoVo Vita Histopathology Laboratory (Natick, MA). The staining protocol used was a modified gram stain that was optimized for the detection of Gram-positive and Gram-negative bacteria within tissue as describe in Becerra et al. (Becerra et al., 2016).

2.6 RNA isolation and qRT-PCR analysis

Harvested NHEKs from the tissue model were stored at 4°C in RNAlater Stabilization Solution (Thermo Fisher Scientific) until day of RNA extraction. RNA from NHEKs was then isolated using RNeasy Plus Mini Kit (Qiagen) as per vendor instructions.

TaqMan Gene Expression Assays (Thermo Fisher Scientific) were acquired, and target gene expression was normalized using the housekeeping (HK) gene glyceraldehyde-3-phosphate dehydrogenase (GAPDH) (Assay ID: Hs02786624_g1). Gene

TABLE 2 Commercial (Thermo Fisher) and in-house assays used to amplify unique target sequences for each strain of the consortium.

Strain	Assay ID	Forward Primer	Reverse Primer	Probe
S. epidermidis	Ba04646141_s1	—	—	—
C. acnes	Ba07922019_s1	—	—	—
S. thermophilus	—	CAAGTTTGCACGTGAAGTGCC	CGAACTCACTCGTGAGTTTAAC	GAGTCGTTTGGACGGT GAAGTGTAACTTCG
S. hominis	—	GAAGTAACAGTTGAAGATGTTAACAAA	TTCATACCAACAACATCTGATGAT	CTGCTGACGAATCAT
R. dentocariosa	—	GTGGTATTCCCCCTCATACAC	CCTTCATAAAGTGCTTATCCATACC	CGTCACGCCGCATCCTACA
C. striatum	Ba07921944_s1	—	—	—

10.3389/frmbi.2025.1473292

TABLE 3 Calculation of approximate genome copies per picogram of extracted DNA.

Strain	Genome Size (bp)	Copies/pg DNA
C. acnes	2,497,484	3.653×10^2
S. thermophilus	1,861,212	4.902×10^2
S. hominis	2,261,062	4.035×10^2
S. epidermidis	2,575,951	3.542×10^2
R. dentocariosa	2,506,228	3.641×10^2
C. striatum	2,945,796	3.097×10^2

Genome sizes were taken from ATCC product information.

expression assays for SERPINB4 (Assay ID: Hs00741313_g1) and S100A9 (Assay ID: Hs00610058_m1) were pooled with the HK gene while assays for KRT1 (Assay ID: Hs01549615_g1), FLG (Assay ID: Hs00856927_g1), and DEFB4B (Assay ID: Hs00175474_m1) were run in separate reactions due to large differences in relative transcript levels interfering with parallel amplification.

RNA was isolated from multiple Transwell tissues per condition (n≥3) and reaction was run in duplicates for each RNA sample isolated. Samples were never pooled, single Transwell tissue derived RNA is represented as a single data point. Mean Ct values were used to calculate fold change by delta Ct method over HK gene.

Relative expression of genes of interest were analyzed using QuantStudio Real-Time PCR Software v1.7.2 (Thermo Fisher Scientific). Delta Ct values were plotted, and data analysis, including statistics, was performed using GraphPad Prism software v10.

2.7 Luminex

On the day of takedown, media was collected from the basal compartment of each Transwell tissue (n≥3 Transwell tissues per condition). Collected media was filtered through Nanosep centrifugal filters (Cytiva) and frozen at -80°C until day of use. On the day of assay, samples were placed on ice until defrosted. Using a custom Luminex Discovery Assay (R&D Systems), samples were tested for fifteen analytes (TNF-α, IFN-γ, IL-6, IL-8/CXCL-8, IL-1α/IL-1F2, IL-1β/IL-1F2, IL-1ra/IL-1F3, IL-36β/IL-1F8, CCL5/RANTES, CCL20/MIP-3α, CCL27/CTACK, S100A9, TSLP, IL-12p70, CXCL1/GROalpha/KC/CINC-1). Luminex assay was performed following the manufacturer's instruction and results were read using the FlexMap 3D program (FlexMAP). Data was analyzed and exported using FlexMAP 3D Xponent software. Standard curve results were verified and fit to five- or four-point log weighted scales ensuring all R^2 >.99. Exported data was normalized to account for 1:2 dilution during assay. Final values were graphed and analyzed for statistical significance using GraphPad Prism software v10.

3 Results

3.1 Skin-commensal co-culture method development

Three main parameters were identified as critical to the establishment of the SURFACE model: barrier formation by NHEKs prior to bacterial introduction, microbial composition of inoculum, and inoculum titration. An epidermal-equivalent tissue with relevant barrier function was grown from NHEKs over the two weeks of total culture time and is described in Figure 1. Total culture time included initial NHEK seeding at Day -7, introduction of ALI at Day -3, inoculation at Day 0, and 7 days of co-culture with the 6-strain consortium, at which point samples were collected for various assays (Figure 1A). Prior to multi-strain microbial inoculation, NHEKs established TEER (Trans-epithelial electrical resistance) of at least 300 Ohms*cm^2, providing an impermeable surface on which to seed the commensal microbes.

Strains of human skin commensal bacteria were selected based on three main criteria: prevalence in previous literature and the Human Microbiome Project (Turnbaugh et al., 2007), availability of the strain from commercial vendors so that the strain source and genome are well documented, and diversity of strains at the genus level to allow for microbial quantification using a strain-specific assay. The final consortium comprises *S. epidermidis*, *C. acnes*, *S. thermophilus*, *S. hominis*, *R. dentocariosa*, and *C. striatum*. We adopted an optical density-based method to produce a consistent inoculum at the strain level. This approach works around two challenges encountered in direct enumeration of the applied consortium. First, individual species of the consortium require specific growth supplements and atmospheric conditions disallowing enumeration after mixing. Natural resistance to antibiotics was determined with standard e-test (data not shown), however no single strain was uniquely resistant to a specific antibiotic precluding enumeration in antibiotic selective agar plates. Second, CFU counts are not available at the time of consortium inoculation due to multi-day growth conditions. We therefore titrated each strain to a measured OD and diluted from this to generate components of the consortium. After screening multiple dilutions of specific strains, we identified an optimal dilution factor for each strain in the consortium that allowed for prolonged tissue culture but avoided bacterial overgrowth. Prior to mixing the consortium strains for inoculation, the diluted strains were plated in appropriate agar plates (Table 1) for CFU enumeration. This served as a benchmark of applied strains across experiments. The composition of the applied inoculum varied between experiments despite similar preparation (Figurea 2A; Supplementary Figure S2A), however this variability was tolerated by our model across experiments where microbiome replete tissue continued to show rise in TEER (Figure 1C; Supplementary Figures S2C, S3C).

10.3389/frmbi.2025.1473292

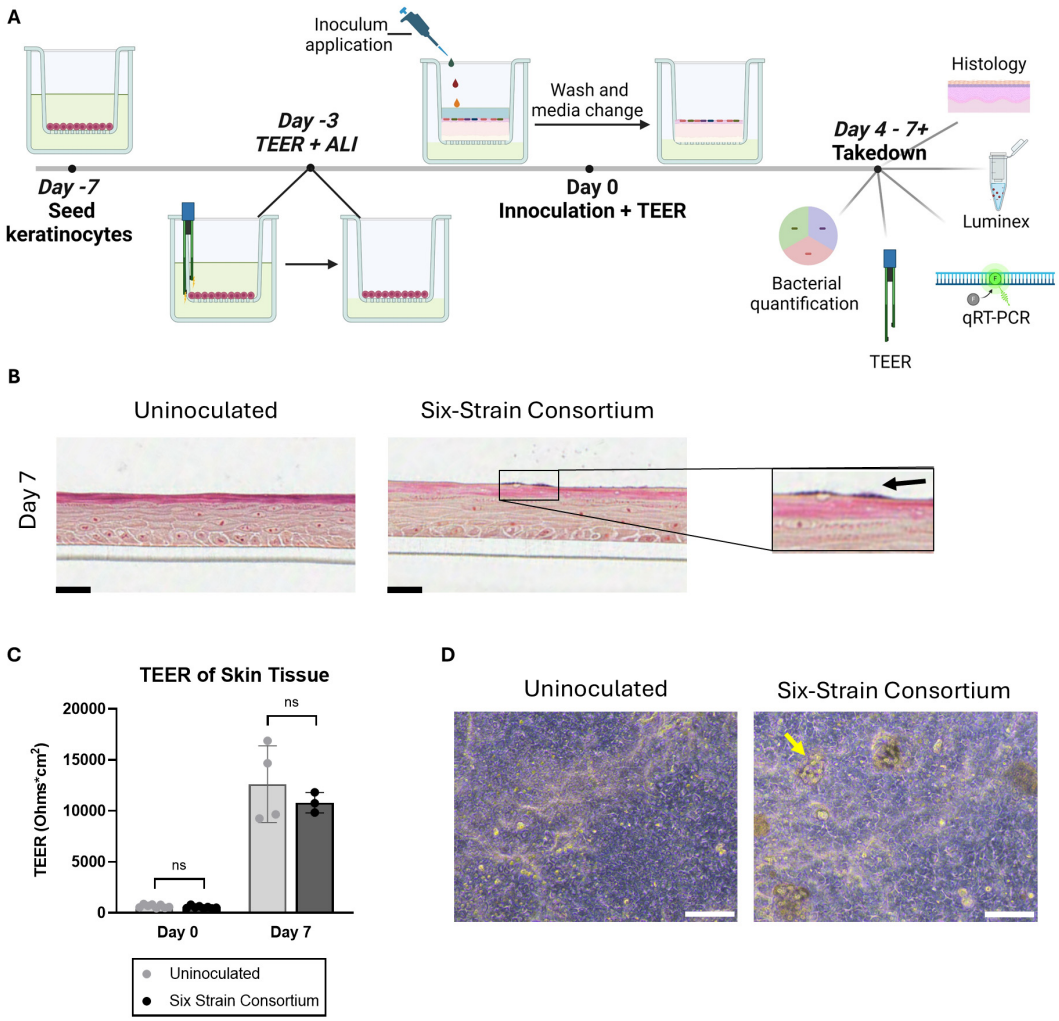

FIGURE 1
Overview of the *in vitro* model of a human skin microbiome, SURFACE. **(A)** Experimental timeline of SURFACE establishment, including cell seeding, air-liquid interface (ALI) introduction, inoculation of 6-strain consortium, and model readouts. Illustration was drawn with Biorender software. **(B)** Histological sections of tissue with and without a 6-strain microbiome at days 4- and 7- post-inoculation. Tissue was stained with modified hematoxylin and eosin Gram stain with a safranin counterstain. Scale bars represent 25μm. **(C)** Tissue barrier function measured by TEER at day 0 (before inoculation) and 7 days post-inoculation as compared to uninoculated tissue. Each dot represents TEER measured on a single Transwell tissue which was uninoculated (grey dots) or inoculated with the six-strain consortium (black dots). TEER was not measured on one instance of bacterial overgrowth and subsequent barrier breach observed on Day 7 in an inoculated tissue sample. Significance was determined by Multiple unpaired t-test with Welch correction, $p<.05$. **(D)** Phase contrast images of the differentiated SURFACE tissue in uninoculated conditions (left) and with resident six-strain consortium (right) on Days 4 post-inoculation. Yellow arrows point to an example bacterial colony on the surface of the tissue. Scale bar represents 100 μm. Ns, not significant.

3.1.1 Six strain consortium co-culture on skin tissue

Following introduction of bacteria, NHEKs maintained characteristic tissue structure on days 4 and 7 post-inoculation, with spatially distinct apical and basal layers (Figure 1B). The skin barrier, as measured by TEER, increased ~10 fold from time of inoculation to time of take-down 7 days later. On the first day of inoculation, Day 0, the TEER average was ~600 Ohms*cm^2, while on Day 7 average TEER reached over 12,000 Ohms*cm^2 (Figure 1C). A similar trend in barrier function was seen independent of microbes presence, indicating that the tissue continued to improve barrier function after the bacteria were co-cultured on the skin surface.

Initial trial studies tested up to 4 days of microbiome integration, at which point bacterial relative abundance (Supplementary Figure S2B) and TEER (Supplementary Figure S2C) were measured. Subsequent studies were extended out to 7 days after microbiome addition. Each figure corresponds to a single experiment in which at least 2 Transwells replicates were allocated per condition.

Occasionally, tissues were damaged during handling, resulting in microbial access to the lower chamber, overgrowth in the rich media and ultimately tissue breakdown; in these cases, it was appropriate to identify and exclude the individual samples from the data set. Indeed, barrier breach instances decreased when tissue handling procedures were modified to minimize touch time on the Transwell.

Histological sectioning of the tissue demonstrated the complex tissue architecture including layers similar to *in vivo* basal, spinous, granulosum and stratum corneum layers (Figure 1B) (Yousef et al., 2024). Evidence of early cornification is seen in tissues as a pink apical layer. A modified Gram stain (Becerra et al., 2016) highlights in dark purple the presence of bacterial colonies on the surface of the skin, which appear in isolated groups and are mirrored by phase contrast images of the tissue (Figures 1B, D). In summary, the SURFACE model shows stable skin tissue characteristics such as high TEER and stratified morphology, providing a relevant testbed for human skin microbiome studies.

3.1.2 Microbial consortium characterization

To characterize the stability of the six-strain microbial consortium on our tissue model, we determined the relative genetic abundance of the applied strains over the course of 7 days. On day 0, inoculum containing all six strains in the ratios established (as above) was applied to the surface of each skin tissue sample. The applied inoculum was enumerated by CFU plating the individual strains used for creating the mixed inoculum (Figure 2A) indicating viability of the strains. Once the strains were combined and cultured together on the tissue model, it was not possible to measure CFU of individual strains, given differential culture conditions for each strain. Therefore, on Day 4 and Day 7 following inoculation of the six-strain consortium, the resulting microbial composition on the tissue was evaluated using qPCR analysis of strain-specific target sequences to enumerate genome copies. Specificity of each strain-specific PCR assay was evaluated for cross-reactivity with the other strains (Supplementary Figure S1A). To calculate absolute copies of each strain present we used a two-step method to extrapolate genomic DNA to genome copies. First, standard curves were generated from known concentrations of genomic DNA of each strain to support the conversion of Ct value to absolute genomic DNA (Supplementary Figure S1B). Then we determined the absolute weight of a single genome to extrapolate the number of genomic copies present in strain specific genomic DNA yielded from the microbiome sample (Table 3).

Using these tools, absolute genome copies were measured from total extracted microbial genomic DNA on days 4 and 7 post-inoculation of the skin tissue as shown in Table 4 and plotted as relative abundance (Figure 2B). On day 4, genome copies of *C. acnes* and *C. striatum* were dominant on the tissue. *S. epidermidis*, *S. hominis*, and *R. dentocariosa* were present at low but detectable levels (Figure 2B; Table 4). *S. thermophilus* genome was undetectable. By day 7 of culture with the six-strain consortium, the skin surface was still supporting five of the six bacterial strains and remained relatively stable based on calculated relative genetic abundance. Furthermore, the alpha diversity of the strains - using Shannon diversity index - illustrates no significant shift in alpha diversity between days 4 and 7 of co-culture (Figure 2C). The shift to a stable state with high representation of *C. acnes* and *C. striatum* was reproduced over two independent experiments (Supplementary Figure S2B). Although *S. thermophilus* was no longer detected by day 4, its exclusion from the inoculum in prior studies led to decreased barrier function and increased barrier breach incidence. When *S. thermophilus* was excluded from the consortium, 30% (3/10) tissue replicates experienced barrier breach by 7 days post-inoculation, while no tissues that included *S. thermophilus* lost barrier function (0/14) (data not shown).

Several strains in our six-strain consortium require specific media supplements or atmospheric conditions for growth in defined media (Table 1). These constraints precluded co-culture of strains under standard growth conditions to study species-level interactions. This is demonstrated when the six-strain inoculum was plated in typical growth conditions, Tryptic Soy Agar, under aerobic conditions for 24 hours- the resulting colonies were entirely

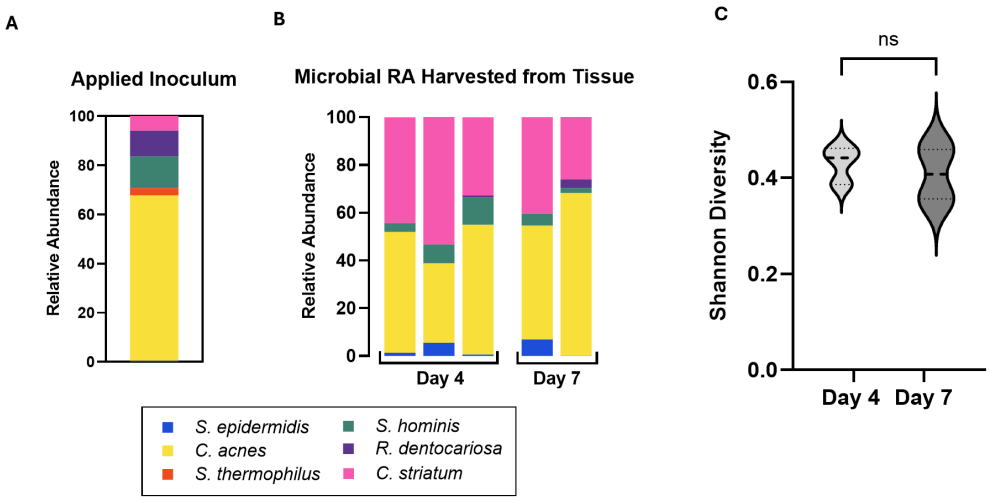

FIGURE 2
(A) Relative abundance of the six applied consortia species in applied inoculum on Day 0 as measured by CFU. **(B)** Relative Abundance of the six strains harvested from skin tissue on Day 4 and Day 7 as measured by qPCR of microbiome genomic DNA. Absolute abundance values are reported in Table 4. Each bar represents a single Transwell tissue within an experiment. **(C)** Alpha diversity was interpreted using Shannon Diversity. Significance was determined by unpaired t-test with Welch correction. Ns, not significant.

TABLE 4 Calculated total genome copies per Transwell (0.33cm^2) represented in Figure 2B.

	S. epidermidis	*C. acnes*	*S. thermophilus*	*S. hominis*	*R. dentocariosa*	*C. striatum*	Total Genome Copies
Day 4	6.72E+04	2.43E+06	0.00E+00	1.82E+05	0.00E+00	2.13E+06	*4.80E+06*
	2.91E+05	1.73E+06	0.00E+00	4.12E+05	0.00E+00	2.77E+06	*5.21E+06*
	2.09E+04	1.82E+06	0.00E+00	3.87E+05	2.67E+04	1.10E+06	*3.35E+06*
Day 7	7.57E+05	5.20E+06	0.00E+00	5.46E+05	5.30E+03	4.41E+06	*1.09E+07*
	9.79E+03	5.05E+06	0.00E+00	1.60E+05	2.57E+05	1.94E+06	*7.41E+06*

Total tissue was collected on the indicated days post-inoculation. Values in each row represents genome copies from a single Transwell tissue. Genome copies were calculated using the formula in Section 2.4.

S. hominis (Supplementary Figure S4). The same initial inoculum of our core consortia strains when applied on the *in vitro* skin model was able to support an assortment of strains in one test bed (Figure 2B; Supplementary Figure S4B), including the anaerobic strain, *Cutibacterium acnes*. These findings indicate that the skin surface provides a more supportive growth environment for commensals compared to agar, enabling the simultaneous existence of at least 5 strains in one microenvironment.

3.2 Effect of commensal microbes on a model of atopic dermatitis

We wished to expand the capability of the SURFACE model by studying the effect of a relevant skin disease on the tissue testbed. At the time of bacterial inoculation, a pro-inflammatory cytokine mixture of IL-22, TNF-α, IL-4, and IL-13 was added to the basal media to simulate atopic dermatitis (AD+) while healthy control conditions were maintained in standard growth media (AD-). Through the seven days of co-culture, the AD- tissue continued to rise in TEER regardless of the presence of the microbiome. In AD + tissues, TEER increased from Day 0 to Day 4 in the absence of the microbiome and plateaued by day 7. However, in the presence of the microbiome, TEER declined, suggesting an additive effect on loss of barrier function, but without observable spread of bacteria into the basal media (Figure 3A; Supplementary Figure S3C).

To better understand the mechanism of tissue breakdown, we evaluated host tissue gene expression of 5 literature-derived AD-associated markers at day 4 and day 7 using q-RT PCR (Sivaprasad et al., 2015; Totsuka et al., 2017; Nedoszytko et al., 2020; Lang et al., 2021). S100A9, SERPINB4, DEFB4B, KRT1, and FLG were found to be differentially expressed in tissues exposed to AD+ conditions (Figure 3B). At day 4 post-inoculation, there was significant upregulation of the genes S100A9, SERPINB4, and DEFB4B in inoculated AD+ tissue when compared to inoculated AD- tissue (Figure 3B). No significant increase in these genes was measured as a result of introduction of only bacteria or from AD cytokines alone, indicating a synergistic response to the combination of bacteria and cytokines. At day 7 post-inoculation, all three genes for secreted proteins trended to higher expression with cytokine exposure irrespective of inoculation, although only reached significance in the case of SERPINB4 without bacteria. Structural genes KRT1 and FLG were down regulated in the AD+ condition, and this effect was not observed until day 7 post-inoculation (Figure 3B). The KRT1 downregulation was observed when disease cytokines or microbes were introduced independent of each other. This was further exacerbated by introduction of both perturbations. FLG downregulation was significantly impacted by disease but the addition of microbes had no significant changes in gene expression although a downward trend was observed.

In parallel, we collected media and evaluated secreted factors with a focus on cytokines and secreted factors predominantly expressed by keratinocytes: IL-8, IL-1β, IL-1ra, CCL20, S100A9, TSLP, IL-36β, CCL27, CXCL1, TNFα, IL-6, IFNγ, CCL5, and IL-12 p70. Luminex assays were performed on the basal media collected at days 4 and 7. Out of the 15 selected analytes (Supplementary Table S1), four showed notable trends in diseased condition with or without microbiome presence (Figure 3C). On day 4, IL-8 was significantly upregulated in the diseased conditions irrespective of bacteria addition. The levels of IL-8 declined by day 7, at which point levels were significantly higher in only in the disease plus microbe context compared to either perturbation alone. S100A9, IL-36β and IL-1 Receptor Antagonist (IL-1RA) were also significantly changed across the experiment; in these cases, no significant change was measured on day 4, but on day 7 the combination of disease-driving cytokines plus microbes uniquely induced significant secretion of the factors (Figure 3C). Overall, a synergistic effect of the AD+ cytokines with commensal bacteria can drive secretion of cytokines from NHEKs after seven days of co-culture. Overall, the SURFACE model responds to AD-associated cytokines with relevant tissue responses, and the integration of commensal bacteria sensitizes the tissue to disease induction.

3.3 Induction of dysbiosis in the disease model

In addition to the changes to the host epithelium, the introduction of AD+ cytokines impacted the consortium of microbes present on the skin model. Notably, the modulation of the consortium was not observed until 7 days after inoculation. Two groups of skin tissue samples were treated with inoculum of identical composition (Figure 4A) and grown in identical conditions

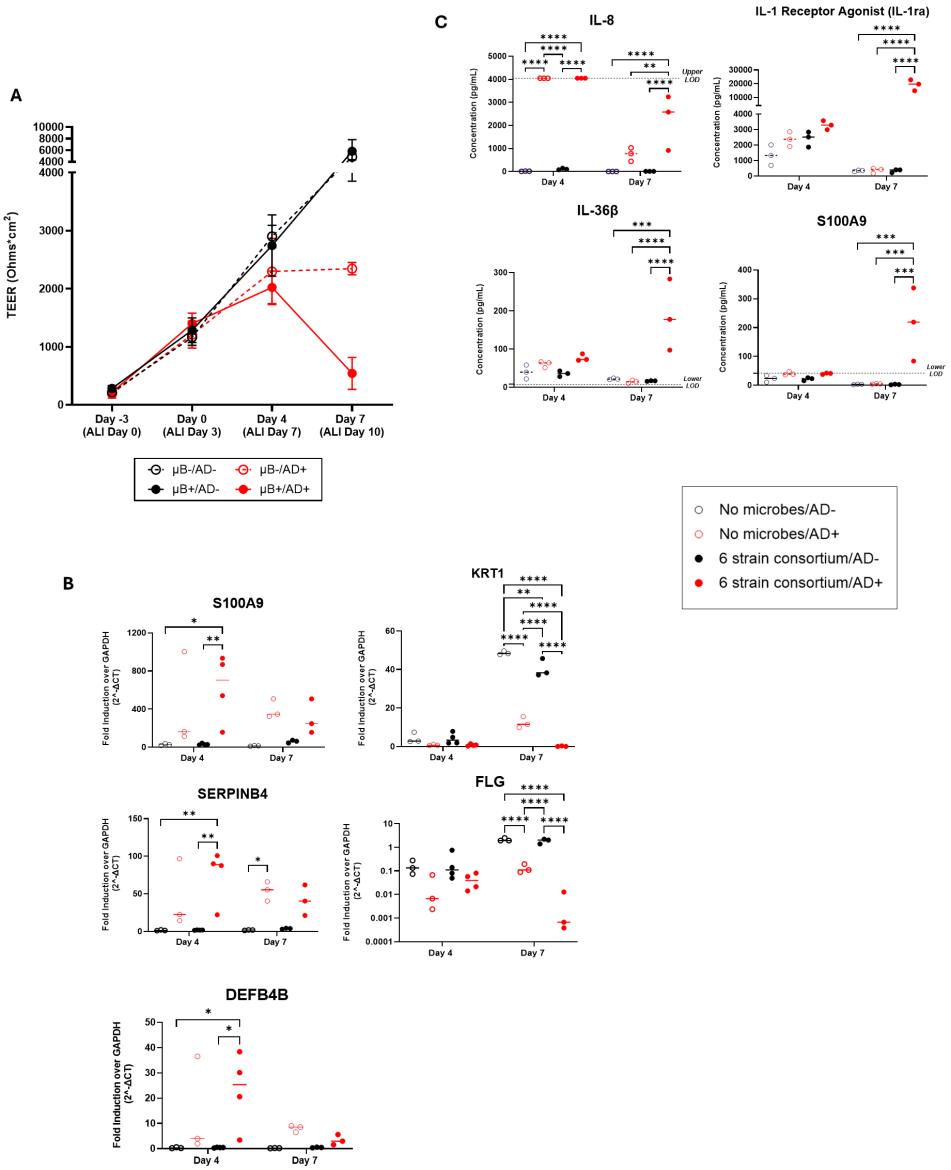

FIGURE 3
(A) Measured TEER of tissue with (filled circle) or without (open circle) bacterial consortium inoculation and with (red circle) or without (black circle) simulated AD-cytokine mix added to basal media. **(B)** S100A9, SERPINB4, DEFB4B, KRT1, and FLG gene expression in tissues with cytokine mix added to the basal media (AD+) compared to tissues without the mixture (AD-) on the skin model with or without bacterial consortium. **(C)** Levels (pg/mL) of IL-8/CXCL8, S100A9, IL-1ra/IL-1F3, and IL-36β secretion in the basal media as determined by Luminex. Dotted horizontal line represents upper limit of detection (IL-8) or blank media control (S100A9, IL-36β). Each dot represents data collected from a single Transwell tissue within an experiment. Statistical significance was determined using Two-way ANOVA with Tukey's multiple comparisons. Any comparisons not shown are non-significant. *p<0.05, **p<0.01, ***p<0.001 and ****p<0.0001. Ns, not significant.

aside from the introduction of the disease state by concurrent addition of the AD+ cytokines. At day 4 post-inoculation and introduction of AD+ conditions, there was not a statistically significant difference in consortia composition detected between the two groups (Figure 4C). However, there was a slight increase in absolute bacterial abundance in the AD+ group compared to the untreated group (p= 0.0385, Student's t-test) (Figure 4D; Table 5). By day 7, however, there was a marked change in the composition between the AD+ and AD- groups. While the untreated tissues maintained a similar consortia composition to the previous timepoint, the experimental AD+ group showed decreased abundance of *C. acnes* and increased *C. striatum* and *S. hominis*, with an overall significant decrease in Shannon diversity (Figure 4B, C). In addition, there was an increase in overall microbial abundance under AD+ conditions (p=0.0252, Student's t-test) (Figure 4D; Table 5). The dysbiosis was observed across a total of 2 experiments with Shannon Diversity trending downward (Supplementary Figures S3A, S3B). Our findings indicate that SURFACE provides sufficient complexity in the microbiome to support evaluation of changes to composition and abundance.

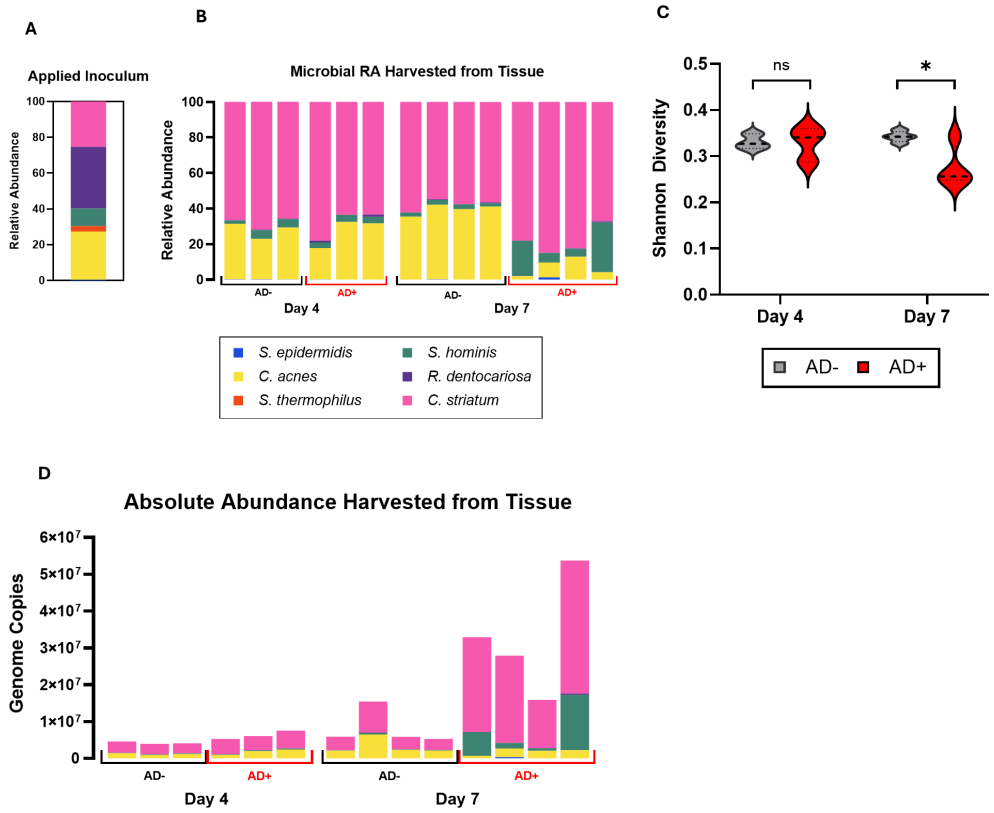

FIGURE 4
(A) Relative abundance of applied inoculum on Day 0 as measured by CFU. **(B)** Relative abundance of the six strains on Day 4 and Day 7 as measured by strain specific qPCR assays of microbiome genomic DNA extracted from tissues with (AD+) or without (AD-) the addition of an AD cytokine mix. **(C)** Alpha Diversity of relative abundance as interpreted by a Shannon Diversity calculation. **(D)** Absolute abundance of strains harvested from tissue as measured by qPCR. Each bar represents microbiome harvested from single Transwell tissue within an experiment. Numerical values of absolute abundance are reported in Table 5. Significance was determined by Multiple unpaired t-test with Welch correction, *p<.05. Ns, not significant.

4 Discussion

4.1 A novel model of host-microbe interaction

The human skin microbiome model reported here represents a major advance in the complexity and longevity of *in vitro* models containing both host tissue and a microbial consortium. There have been several studies reporting 3D-Skin tissue models as ideal substrates to study strain-strain interactions or the establishment of stable microbiome for durations ranging from hours to a few days (Larson et al., 2021; Holland et al., 2008; Holland et al., 2008; Kirker et al., 2009; de Breij et al., 2012; Haisma et al., 2013; Popov et al., 2014; Cadau et al., 2017; Lemoine et al., 2020; Kohda et al., 2021; Lemoine et al., 2021; Loomis et al., 2021). In our current work, we have demonstrated the feasibility of establishing a stable microbiome on a skin tissue model with six important skin microbiome strains for a period of 7 days. Furthermore, we showed the potential to study chronic skin diseases to understand the interaction between host and microbe during pathogenesis. This body of work is the first of its kind to demonstrate consistent modulation of the microbiome in response to a disease state in a physiologically relevant *in vitro* model of human skin microbiome.

A review from Smyth and Wilkinson comprehensively summarizes the challenges associated with skin microbiome research (Smythe and Wilkinson, 2023). Microbiome research relies largely on sample collection from healthy or diseased volunteers and longitudinal analysis of collected samples by 16s, shotgun or whole genome sequencing (Chng et al., 2016). For instance, Kang et al. were able to uncover the molecular mechanism driving Acne in humans supplemented with vitamin B12 via meta transcriptomic profile of microbes in Acne patients vs normal individuals (Kang et al., 2015). Zhang et al. performed elegant studies to demonstrate via mouse models and extracts from skin of healthy vs Dengue and Zika virus-infected patients that flavivirus promoted the growth of acetophenone producing bacteria in the microbiome (Zhang et al., 2022). While these methods are helpful in hypothesis-generating research to understand correlative factors in microbiome and disease states, they often cannot uncover cause vs. effect of dysbiosis or inflammation. Such characterization will be well served by *in vitro* models that capture microbial metabolism in the context of a diverse microbial population colonizing the skin. To provide a relevant, skin-like microenvironment for microbial culture, we cultured NHEKs for 7 days including at ALI, generating a complex, differentiated skin tissue including a layer of cornified epithelium on the surface providing a potentially

TABLE 5 Calculated total genome copies per Transwell (0.33 cm^2) represented in Figures 4B, D.

		S. epidermidis	*C. acnes*	*S. thermophilus*	*S. hominis*	*R. dentocariosa*	*C. striatum*	Total Genome Copies
Day 4	**AD-**	9.30E+03	1.44E+06	0.00E+00	8.64E+04	5.33E+03	3.07E+06	*4.61E+06*
		9.29E+03	9.01E+05	0.00E+00	1.96E+05	1.03E+04	2.84E+06	*3.96E+06*
		5.39E+03	1.20E+06	0.00E+00	1.92E+05	1.06E+04	2.70E+06	*4.11E+06*
	AD+	7.57E+03	9.43E+05	0.00E+00	1.69E+05	5.04E+04	4.16E+06	*5.33E+06*
		0.00E+00	1.97E+06	0.00E+00	2.45E+05	0.00E+00	3.84E+06	*6.06E+06*
		0.00E+00	2.40E+06	0.00E+00	2.74E+05	9.50E+04	4.80E+06	*7.58E+06*
Day 7	**AD-**	4.87E+03	2.10E+06	0.00E+00	1.37E+05	0.00E+00	3.69E+06	*5.93E+06*
		2.62E+04	6.51E+06	0.00E+00	4.13E+05	5.55E+04	8.49E+06	*1.55E+07*
		4.06E+03	2.33E+06	0.00E+00	1.63E+05	0.00E+00	3.38E+06	*5.87E+06*
		0.00E+00	2.18E+06	0.00E+00	1.03E+05	2.14E+04	3.00E+06	*5.31E+06*
	AD+	0.00E+00	6.86E+05	0.00E+00	6.53E+06	9.56E+03	2.57E+07	*3.29E+07*
		3.72E+05	2.35E+06	0.00E+00	1.50E+06	2.25E+04	2.37E+07	*2.80E+07*
		3.83E+03	2.06E+06	0.00E+00	7.02E+05	4.75E+04	1.31E+07	*1.59E+07*
		0.00E+00	2.26E+06	0.00E+00	1.50E+07	3.53E+05	3.61E+07	*5.37E+07*

Total tissue was collected on the indicated days post-inoculation and in the presence (+) or absence (–) of added cytokines (AD). Values in each row represent genome copies from a single Transwell tissue. Genome copies were calculated using the formula in section 2.4.

relevant microenvironment for skin microbiome culture. At this point, the bacterial consortium was added and co-cultured for an additional 7 days. At day 7 the tissues remained stable with six-strain consortium suggesting we could extend duration to >7 days. Further prolonged culture periods may define a steady state of microbial growth such that the total number of bacteria are in equilibrium with the tissue culture.

The establishment of a multi-strain, multi-day skin microbiome model depends on the initial concentration of single strains as well as the ratios between consortium strains. However, there is an innate variability of starting inoculum that is due to titrating small volumes and numbers of total bacteria, which can be seen across up to 3 experiments in the day 0 CFU enumeration. Despite the Day 0 inoculum variability, a multi-strain consortium of human skin microbes is still supported on skin tissue for 4-7 days, indicating a degree of robustness to the protocol, and emphasizing aspects that are likely critical to model establishment: strain type, relative strain amounts and inoculation methodology.

Characterization of consortium composition was critical to our understanding of the model over time. However, characterization of a mixed population of bacteria is not straightforward given the range of genera involved and their variety of selective culture conditions. Therefore, we chose to work with strains for which unique PCR-based assays were commercially available or could be designed. This allowed for the calculation of relative microbial abundance across multiple Transwell replicates, although assumptions were made. First, we assumed a single genome copy per bacterial cell, which may not be the case in actively dividing bacterial cells. Confidence in this assumption was provided from our characterization that the rate of bacterial division was slow based on the total microbial genomic DNA yield on day 7 which was less than twice the yield from day 4. Literature also supports that commensal microbes on the skin are slow to replicate compared to the denser gut microbiome (Lu et al., 2014; Byrd et al., 2018; Cundell, 2018). Second, we are aware that any persistent plasmid DNA in a bacterial strain would add to the total DNA weight extracted; this genetic material is not accounted for in genome size-based calculations. For these calculations, we assumed that this DNA did not contribute significantly to our overall composition calculations.

Estimates of bacterial density in the human skin vary depending on the method of collection (tape lift, punch biopsy) and subsequent culture methods making it challenging to interrogate the full range of microbes present. When approximated, the total concentration of bacterial genomes normalized to the surface area in our model ranges from 1E+7/cm^2 to 3E+7/cm^2 (Table 4). This density of bacterial cells is >10-fold higher than 1E+3 to 1E+5 in most skin areas as measured by a more stringent CFU method for aerobic bacteria (Reichel et al., 2011). The genetic method used here, which captures any residual genomic sequence from dead bacterial cells, would be expected to overestimate the number of viable cells/area.

Of the six strains introduced to the skin tissue on day 0, five species are present in the final stable population across both timepoints investigated. *S. thermophilus* fails to appear in detectable quantities through qPCR analysis across multiple

timepoints, Transwell replicates, and experimental trials. Despite this, the addition of *S. thermophilus* appears to impact the overall health and composition of the model and therefore was maintained as a member of the consortia used in these studies. This finding indicates the potential role that *S. thermophilus* may play in the early establishment of a commensal relationship within the microbiota and the host tissue. *S. thermophilus* is widely used as a prebiotic agent and has been shown to increase ceramide levels in stratum corneum (Di Marzio et al., 2003; Lombardi et al., 2022). We speculate that its presence early in coculture may provide a metabolic niche that supports establishing the surviving strains as a balanced consortium.

4.2 Disease modeling

A key facet of an *in vitro* skin tissue culture-based model is to mimic skin conditions such as atopic dermatitis, psoriasis, pathogen response, and wound healing. Integration of the microbiome on healthy or diseased skin enables us to probe underlying mechanisms and therapeutic interventions. The host immune system is a key modulator of microbiome balance as well as a primary host response to pathogens and dysbiosis (Belkaid and Harrison, 2017). To capture inflammatory responses associated with chronic skin diseases we adopted a previously established acellular model of atopic dermatitis in which NHEK are exposed to a cytokine milieu that is characteristic of AD (Bernard et al., 2012). Previous work showed upregulation of AD associated biomarkers but the effect of the microbiome was not explored. In this work, we significantly expanded the characterization of the host tissue response to these cytokines and evaluated changes to our bacterial consortium as the result of epithelial damage induction. Simulated AD disease states were apparent, although not until Day 7, based on tissue gene expression of key AD associated markers and shifts in microbial composition, indicating the critical need for long term culture systems. Our model provides necessary longitudinal growth to support characterization of disease states and microbial response that happens over extended timelines.

Currently, AD pathology is primarily determined by epithelial barrier function and immune cell response (Bin and Leung, 2016). In our study involving disease induction, we were particularly interested to characterize the NHEK response as proof of relevant disease induction, and to expand characterization of secreted factors that could affect microbiome balance. S100A9 and S100A8 belong to the Damage Associated Molecular Pattern (DAMP) family of secreted factors and are elevated in AD patient serum (Saito-Sasaki and Sawada, 2023; Guttman-Yassky et al., 2024). SERPINB4 and SERPINB3 are serine protease inhibitors which are elevated in chronic inflammatory diseases and serve an important role in the cross-linking of structural proteins, moderating immune responses, and maintaining of epidermal homeostasis (Sun et al., 2017). In clinical atopic dermatitis, expression of SERPINB3/B4 is thought to be induced by Th2 inflammatory cytokines, IL-4 and IL-13 (Sun et al., 2017). DEFB4b is a beta-defensin produced by activated epithelial cells and exhibits high levels of antimicrobial activity towards Gram-negative bacteria (García et al., 2001; Sharma and Nagaraj, 2015; Meade and O'Farrelly, 2019). It is significantly overexpressed in AD tissue and other inflammatory skin conditions (Cieślik et al., 2021). At the gene expression level, S100A9, SERPINB4 and DEFB4B were all upregulated in the NHEK tissue at 4 days following introduction of cytokines, but only significantly increased in the presence of bacteria. By 7 days following disease induction, upregulated gene expression subsided to non-significance over healthy tissue. In a similar but delayed pattern, key secreted proteins were upregulated by day 7 following cytokine introduction, but only in the presence of consortia. IL-8, IL-36β and IL-1ra factors are produced by keratinocytes in response to inflammatory factors, although they play distinct pro- and anti-inflammatory roles (Iznardo and Puig, 2022). Blockade of IL-1 family factors is being researched as a therapeutic strategy for treating AD (Dinarello et al., 2012). IL-8 was strongly secreted by day 4 in response to disease induction, but by day 7 modulated with significantly higher detection only in the presence of consortium. It is possible that bacteria sensitize cells to upregulate these genes or change the secretion of the proteins. In the singular case of S100A9 where we were able to evaluate both gene expression and protein secretion, gene expression parallels protein secretion. The synergistic induction of relevant AD genes and proteins suggests that bacteria can sensitize the tissue response to inflammatory cues and demonstrates the critical importance of including relevant microbial species in tissue models when studying human disease mechanisms.

Filaggrin (FLG) is an important epidermal structural protein required for corneocyte formation, production of water retention molecules, and maintenance of pH stability within the stratum corneum (Totsuka et al., 2017). FLG deficiency is correlated with keratinocyte cellular abnormalities and FLG gene mutations are a high-risk indicator of AD pathogenesis (Osawa et al., 2011; Gupta and Margolis, 2020). Keratin 1 (KRT1) is a marker gene for early differentiation of tissue, and an integral component of the intermediate filament cytoskeleton, providing structural integrity to keratinocytes (Roth et al., 2012). One study demonstrated that KRT and other structural proteins and adhesion molecules were downregulated in the context of AD lesional skin, impairing tissue barrier function (Totsuka et al., 2017). Upon exposure to the AD cytokine cocktail, we measured a significant decrease in KRT1 and FLG transcripts, a decrease that was present with and without bacteria. However, the decrease in both genes was significantly enhanced in the presence of bacteria. This result accurately matches the observed effects on TEER, where bacteria alone did not change tissue integrity, while the effect of AD cytokines was significantly and synergistically enhanced by addition of bacteria. Taken together, the data indicate that the inclusion of commensal bacterial enhances the sensitivity of human skin tissue to inflammatory factors, recommending the inclusion of microbes in mechanistic studies of human skin disease.

4.3 Microbiome shifts in disease context

Chronic disease phenotypes like atopic dermatitis and psoriasis are characterized by periods of flare up and punctuated by changes in microbial diversity (Grice et al., 2009; Chng et al., 2016; Fyhrquist et al., 2019; Edslev et al., 2020). AD patients are characterized by distinct microbial signatures and general decline in microbial diversity with dominance of some species such as *S. aureus* and depletion of *Dermacoccus* spp (Tay et al., 2021; Koh et al., 2022). Reduction in *C. acnes* abundance in AD diseased tissue has been previously reported in human sample collection studies (Fyhrquist et al., 2019; Rozas et al., 2021; Green et al., 2023). Furthermore, reinvestigation of metagenomic data sets from pediatric AD cohorts revealed increases in *Corynebacterium kefirresidentii* during and after AD flares (Salamzade et al., 2022). All of these studies rely on human sampling-based approaches, which do not allow prospective studies of cause and effect during pathogenesis. Our model provides a test bed to study host-microbiome mechanisms that drive disease states characterized by dysbiosis and inflammation. This work demonstrates a reproducible change in microbial balance in response to a disease state, where the combination of bacteria outgrowth and loss of diversity mirrors the human disease. The ability to mimic aspects of microbiome response highlights a strength of this system. By integrating a defined but complex consortium of bacteria, we are able to measure variations in the composition. More complex readouts across a range of multi-omic approaches will provide a clearer understanding of the factors that drive the dysbiosis, while alterations in timing of addition of disease and microbes will enhance cause and effect understanding. In addition, there is an opportunity to evaluate the role of pathobionts such as *S. aureus*, a species strongly indicated as a driving factor in AD (Seite et al., 2014). Preliminary work with *S. aureus* in this model resulted in the strain rapidly taking over the culture and immediate termination of the studies (data not shown). Modified strategies for introduction of the species will allow us to study its causative role in disease initiation. Further, this model provides a basis to evaluate the role of the commensal microbiome in suppression or enhancement of pathogenesis from exogenous bacteria and viruses. The demonstration that the microbial consortium provides a consistent and relevant response to introduction of a disease state presents the most robust platform that we are aware of for controlled study of the symbiotic connection between microbial community and host biology.

Taken together, the data presented here demonstrate a first of its kind platform that provides an *in vitro*, human-specific skin model system of the host tissue and defined microbiome. We have highlighted the importance of including relevant microbes when studying inflammatory disease by showing enhanced sensitivity of the tissue to cytokines in the presence of commensal bacterial species, particularly after 7 days of co-culture. In addition, we have shown the utility of the platform for characterizing the responsiveness of the microbiome to host biology and indicated the potential to use these methods to better understand symbiotic relationships among bacterial strains. We recognize significant potential to leverage this type of model system to provide new understanding of host-microbe symbiosis, to characterize safety of skin applications, and to unlock potential therapeutic opportunities present in the skin microbiome.

Data availability statement

The original contributions presented in the study are included in the article/Supplementary Material. Further inquiries can be directed to the corresponding author.

Ethics statement

Ethical approval was not required for the studies on humans in accordance with the local legislation and institutional requirements because only commercially available established cell lines were used.

Author contributions

AM: Data curation, Formal analysis, Investigation, Methodology, Validation, Writing – original draft, Writing – review & editing. TC: Data curation, Formal analysis, Investigation, Methodology, Validation, Writing – original draft. JH: Data curation, Formal analysis, Investigation, Methodology, Validation, Writing – original draft. MM: Methodology, Visualization, Writing – review & editing. TM: Methodology, Writing – review & editing. EW: Conceptualization, Data curation, Formal analysis, Funding acquisition, Investigation, Methodology, Project administration, Resources, Software, Supervision, Validation, Visualization, Writing – original draft, Writing – review & editing. EV: Conceptualization, Data curation, Formal analysis, Funding acquisition, Investigation, Methodology, Project administration, Resources, Software, Supervision, Validation, Visualization, Writing – original draft, Writing – review & editing. VV: Conceptualization, Data curation, Formal analysis, Funding acquisition, Investigation, Methodology, Project administration, Resources, Software, Supervision, Validation, Visualization, Writing – original draft, Writing – review & editing.

Funding

The author(s) declare financial support was received for the research, authorship, and/or publication of this article. The work presented here was funded solely by Draper.

Acknowledgments

The authors would like to thank Rob Gaibler and Michaela Welch for their excellent work supporting development of the skin tissue culture methods. In addition, we thank Richard Winegar for his patient coaching on bioinformatics methods.

Conflict of interest

The authors declare that the research was conducted in the absence of any commercial or financial relationships that could be construed as a potential conflict of interest.

Publisher's note

All claims expressed in this article are solely those of the authors and do not necessarily represent those of their affiliated organizations, or those of the publisher, the editors and the reviewers. Any product that may be evaluated in this article, or claim that may be made by its manufacturer, is not guaranteed or endorsed by the publisher.

Supplementary material

The Supplementary Material for this article can be found online at: https://www.frontiersin.org/articles/10.3389/frmbi.2025.1473292/full#supplementary-material

References

Becerra, S. C., Roy, D. C., Sanchez, C. J., Christy, R. J., and Burmeister, D. M. (2016). An optimized staining technique for the detection of Gram positive and Gram negative bacteria within tissue. *BMC Res. Notes* 9, 216. doi: 10.1186/s13104-016-1902-0

Belkaid, Y., and Harrison, O. J. (2017). Homeostatic immunity and the microbiota. *Immunity* 46, 562–576. doi: 10.1016/j.immuni.2017.04.008

Bernard, F.-X., Morel, F., Camus, M., Pedretti, N., Barrault, C., Garnier, J., et al. (2012). Keratinocytes under fire of proinflammatory cytokines: bona fide innate immune cells involved in the physiopathology of chronic atopic dermatitis and psoriasis. *J. Allergy (Cairo)* 2012, 718725. doi: 10.1155/2012/718725

Bin, L., and Leung, D. Y. M. (2016). Genetic and epigenetic studies of atopic dermatitis. *Allergy Asthma Clin. Immunol.* 12, 52. doi: 10.1186/s13223-016-0158-5

Bjornson-Hooper, Z. B., Fragiadakis, G. K., Spitzer, M. H., Chen, H., Madhireddy, D., Hu, K., et al. (2022). A comprehensive atlas of immunological differences between humans, mice, and non-human primates. *Front. Immunol.* 13, 867015. doi: 10.3389/fimmu.2022.867015

Byrd, A. L. (2017). Staphylococcus aureus and Staphylococcus epidermidis strain diversity underlying pediatric atopic dermatitis. *Sci. Trans. Med.* 9, eaal4651. doi: 10.1126/scitranslmed.aal4651

Byrd, A. L., Belkaid, Y., and Segre, J. A. (2018). The human skin microbiome. *Nat. Rev. Microbiol.* 16, 143–155. doi: 10.1038/nrmicro.2017.157

Cadau, S., Rival, D., Andre-Frei, V., Chavan M, M., Fayol, D., Salducci, M., et al. (2017). New bioprinted skin, cosmetic *in vitro* model. *J. Cosmet Sci.* 68, 85–90.

Chng, K. R., Tay, A. S. L., Li, C., Ng, A. H. Q., Wang, J., Suri, B. K., et al. (2016). Whole metagenome profiling reveals skin microbiome-dependent susceptibility to atopic dermatitis flare. *Nat. Microbiol.* 1, 1–10. doi: 10.1038/nmicrobiol.2016.106

Cieślik, M., Bagińska, N., Górski, A., and Jończyk-Matysiak, E. (2021). Human β-defensin 2 and its postulated role in modulation of the immune response. *Cells* 10 (11), 2991. doi: 10.3390/cells10112991

Conwill, A., Kuan, A. C., Damerla, R., Poret, A. J., Baker, J. S., Tripp, A. D., et al. (2022). Anatomy promotes neutral coexistence of strains in the human skin microbiome. *Cell Host Microbe* 30, 171–182.e7. doi: 10.1016/j.chom.2021.12.007

Cundell, A. M. (2018). Microbial ecology of the human skin. *Microbial Ecol.* 76, 113–120. doi: 10.1007/s00248-016-0789-6

de Breij, A., Haisma, E. M., Rietveld, M., El Ghalbzouri, A., van den Broek, P. J., Dijkshoorn, L., et al. (2012). Three-dimensional human skin equivalent as a tool to study Acinetobacter baumannii colonization. *Antimicrob. Agents Chemother.* 56, 2459–2464. doi: 10.1128/AAC.05975-11

De Wever, B., Kurdykowski, S., and Descargues, P. (2015). Human skin models for research applications in pharmacology and toxicology: introducing nativeSkin ®, the "Missing Link" bridging cell culture and/or reconstructed skin models and human clinical testing. *App In Vitro Toxicol.* 1 (1), 26. doi: 10.1089/aivt.2014.0010

Di Marzio, L., Centi, C., Cinque, B., Masci, S., Giuliani, M., Arcieri, A., et al. (2003). Effect of the lactic acid bacterium Streptococcus thermophilus on stratum corneum ceramide levels and signs and symptoms of atopic dermatitis patients. *Exp. Dermatol.* 12, 615–620. doi: 10.1034/j.1600-0625.2003.00051.x

Dinarello, C. A., Simon, A., and van der Meer, J. W. M. (2012). Treating inflammation by blocking interleukin-1 in a broad spectrum of diseases. *Nat. Rev. Drug Discovery* 11, 633–652. doi: 10.1038/nrd3800

Edslev, S. M., Agner, T., and Andersen, P. S. (2020). Skin microbiome in atopic dermatitis. *Acta Derm Venereol* 100, 5769. doi: 10.2340/00015555-3514

Flowers, L., and Grice, E. A. (2020). The skin microbiota: balancing risk and reward. *Cell Host Microbe* 28, 190–200. doi: 10.1016/j.chom.2020.06.017

Fyhrquist, N., Muirhead, G., Prast-Nielsen, S., Jeanmougin, M., Olah, P., Skoog, T., et al. (2019). Microbe-host interplay in atopic dermatitis and psoriasis. *Nat. Commun.* 10, 4703. doi: 10.1038/s41467-019-12253-y

García, J. R., Krause, A., Schulz, S., Rodríguez-Jiménez, F. J., Klüver, E., Adermann, K., et al. (2001). Human beta-defensin 4: a novel inducible peptide with a specific salt-sensitive spectrum of antimicrobial activity. *FASEB J.* 15 (10), 1819–1821.

Green, M., Kashetsky, N., Feschuk, A., and Maibach, H. (2023). Beyond acne vulgaris: role of cutibacterium acnes in atopic dermatitis and psoriasis. *SKIN J. Cutaneous Med.* 7, 1208–1210. doi: 10.25251/skin.7.6.24

Grice, E. A., Kong, H. H., Conlan, S., Deming, C. B., Davis, J., Young, A. C., et al. (2009). Topographical and temporal diversity of the human skin microbiome. *Science* 324, 1190–1192. doi: 10.1126/science.1171700

Gupta, J., and Margolis, D. J. (2020). Filaggrin gene mutations with special reference to atopic dermatitis. *Curr. Treat Options Allergy* 7, 403–413. doi: 10.1007/s40521-020-00271-x

Guttman-Yassky, E., Facheris, P., Gomez-Arias, P. J., Del Duca, E., Da Rosa, J. C., Weidinger, S., et al. (2024). Effect of abrocitinib on skin biomarkers in patients with moderate-to-severe atopic dermatitis. *Allergy* 79 (5), 1258–1270. doi: 10.1111/all.15969

Haisma, E., Rietveld, M., Breij, A., Dissel, J., Ghalbzouri, A., and Nibbering, P. (2013). Inflammatory and antimicrobial responses to methicillin-resistant Staphylococcus aureus in an *in vitro* ound infection model. *PloS One* 8, e82800. doi: 10.1371/journal.pone.0082800

Hardwick, R. N., Betts, C. J., Whritenour, J., Sura, R., Thamsen, M., Kaufman, E. H., et al. (2020). Drug-induced skin toxicity: gaps in preclinical testing cascade as opportunities for complex *in vitro* models and assays. *Lab. Chip* 20, 199–214. doi: 10.1039/C9LC00519F

Harris-Tryon, T. A., and Grice, E. A. (2022). Microbiota and maintenance of skin barrier function. *Science* 376, 940–945. doi: 10.1126/science.abo0693

Hays, A., Islam, R., Matys, K., and Williams, D. (2022). Best Practices in qPCR and dPCR Validation in Regulated Bioanalytical Laboratories. *AAPS J.* 24, 36. doi: 10.1208/s12248-022-00686-1

Hofmann, E., Schwarz, A., Fink, J., Kamolz, L.-P., and Kotzbeck, P. (2023). Modelling the complexity of human skin *in vitro*. *Biomedicines* 11, 794. doi: 10.3390/biomedicines11030794

Holland, D. B., Bojar, R. A., Jeremy, A. H. T., Ingham, E., and Holland, K. T. (2008). Microbial colonization of an *in vitro* model of a tissue engineered human skin equivalent–a novel approach. *FEMS Microbiol. Lett.* 279, 110–115. doi: 10.1111/j.1574-6968.2007.01021.x

Iznardo, H., and Puig, L. (2022). IL-1 family cytokines in inflammatory dermatoses: pathogenetic role and potential therapeutic implications. *Int. J. Mol. Sci.* 23, 9479. doi: 10.3390/ijms23169479

Kang, D., Shi, B., Erfe, M. C., Craft, N., and Li, H. (2015).Vitamin B12 modulates the transcriptome of the skin microbiota in acne pathogenesis. *Sci. Transl. Med.* 7, 293ra103. doi: 10.1126/scitranslmed.aab2009

Kim, J. E., and Kim, H. S. (2019). Microbiome of the skin and gut in atopic dermatitis (AD): understanding the pathophysiology and finding novel management strategies. *J. Clin. Med.* 8, 444. doi: 10.3390/jcm8040444

Kirker, K. R., Secor, P. R., James, G. A., Fleckman, P., Olerud, J. E., and Stewart, P. S. (2009). Loss of viability and induction of apoptosis in human keratinocytes exposed to Staphylococcus aureus biofilms *in vitro*. *Wound Repair Regener.* 17, 690–699. doi: 10.1111/j.1524-475X.2009.00523.x

Koh, L. F., Ong, R. Y., and Common, J. E. (2022). Skin microbiome of atopic dermatitis. *Allergol Int.* 71, 31–39. doi: 10.1016/j.alit.2021.11.001

Kohda, K., Li, X., Soga, N., Nagura, R., Duerna, T., Nakajima, S., et al. (2021). An *in vitro* mixed infection model with commensal and pathogenic staphylococci for the exploration of interspecific interactions and their impacts on skin physiology. *Front. Cell Infect. Microbiol.* 11, 712360. doi: 10.3389/fcimb.2021.712360

Kong, H. H., Oh, J., Deming, C., Conlan, S., Grice, E. A., Beatson, M. A., et al. (2012). Temporal shifts in the skin microbiome associated with disease flares and treatment in children with atopic dermatitis. *Genome Res.* 22, 850. doi: 10.1101/gr.131029.111

Lang, C. C. V., Renert-Yuval, Y., Del Duca, E., Pavel, A. B., Wu, J., Zhang, N., et al. (2021). Immune and barrier characterization of atopic dermatitis skin phenotype in Tanzanian patients. *Ann. Allergy Asthma Immunol.* 127, 334–341. doi: 10.1016/j.anai.2021.04.023

Larson, P., Chong, D., Fleming, E., and Oh, J. (2021). Challenges in developing a human model system for skin microbiome research. *J Invest Dermatol.* 141 (1), 228–231.e4. doi: 10.1016/j.jid.2020.05.096

Lee, H.-J., and Kim, M. (2022). Skin barrier function and the microbiome. *Int. J. Mol. Sci.* 23, 13071. doi: 10.3390/ijms232113071

Lemoine, L., Bayrambey, D., Roloff, A., Hutzler, C., Luch, A., and Tralau, T. (2021). Commensal-related changes in the epidermal barrier function lead to alterations in the benzo[a]Pyrene metabolite profile and its distribution in 3D skin. *mBio* 12, e0122321. doi: 10.1128/mBio.01223-21

Lemoine, L., Dieckmann, R., Al Dahouk, S., Vincze, S., Luch, A., and Tralau, T. (2020). Microbially competent 3D skin: a test system that reveals insight into host-microbe interactions and their potential toxicological impact. *Arch. Toxicol.* 94, 3487–3502. doi: 10.1007/s00204-020-02841-z

Li, M., Hener, P., Zhang, Z., Kato, S., Metzger, D., and Chambon, P. (2006). Topical vitamin D3 and low-calcemic analogs induce thymic stromal lymphopoietin in mouse keratinocytes and trigger an atopic dermatitis. *Proc. Natl. Acad. Sci. U.S.A.* 103, 11736–11741. doi: 10.1073/pnas.0604575103

Linehan, J. L., Harrison, O. J., Han, S.-J., Byrd, A. L., Vujkovic-Cvijin, I., Villarino, A. V., et al. (2018). Non-classical immunity controls microbiota impact on skin immunity and tissue repair. *Cell* 172, 784–796.e18. doi: 10.1016/j.cell.2017.12.033

Lombardi, F., Augello, F. R., Artone, S., Bahiti, B., Sheldon, J. M., Giuliani, M., et al. (2022). Efficacy of probiotic Streptococcus thermophilus in counteracting TGF-β1-induced fibrotic response in normal human dermal fibroblasts. *J. Inflammation (Lond)* 19, 27. doi: 10.1186/s12950-022-00324-9

Loomis, K. H., Wu, S. K., Ernlund, A., Zudock, K., Reno, A., Blount, K., et al. (2021). A mixed community of skin microbiome representatives influences cutaneous processes more than individual members. *Microbiome* 9, 22. doi: 10.1186/s40168-020-00963-1

Lu, H.-P., Lai, Y.-C., Huang, S.-W., Chen, H.-C., Hsieh, C., and Yu, H.-T. (2014). Spatial heterogeneity of gut microbiota reveals multiple bacterial communities with distinct characteristics. *Sci. Rep.* 4, 6185. doi: 10.1038/srep06185

Matsui, T., and Amagai, M. (2015). Dissecting the formation, structure and barrier function of the stratum corneum. *Int. Immunol.* 27, 269–280. doi: 10.1093/intimm/dxv013

McIntyre, M. K., Peacock, T. J., Akers, K. S., and Burmeister, D. M. (2016). Initial characterization of the pig skin bacteriome and its effect on *in vitro* models of wound healing. *PloS One* 11, e0166176. doi: 10.1371/journal.pone.0166176

Meade, K. G., and O'Farrelly, C. (2019). β-defensins: farming the microbiome for homeostasis and health. *Front. Immunol.* 9, 3072. doi: 10.3389/fimmu.2018.03072

Naik, S., Bouladoux, N., Linehan, J. L., Han, S.-J., Harrison, O. J., Wilhelm, C., et al. (2015). Commensal–dendritic-cell interaction specifies a unique protective skin immune signature. *Nature* 520, 104–108. doi: 10.1038/nature14052

Nakatsuji, T., Chen, T. H., Narala, S., Chun, K. A., Two, A. M., Yun, T., et al. (2017). Antimicrobials from human skin commensal bacteria protect against Staphylococcus aureus and are deficient in atopic dermatitis. *Sci. Transl. Med.* 9, eaah4680. doi: 10.1126/scitranslmed.aah4680

Nedoszytko, B., Reszka, E., Gutowska-Owsiak, D., Trzeciak, M., Lange, M., Jarczak, J., et al. (2020). Genetic and Epigenetic aspects of atopic dermatitis. *Int. J. Mol. Sci.* 21, 6484. doi: 10.3390/ijms21186484

Oh, J., Byrd, A. L., Park, M., NISC Comparative Sequencing Program, Kong, H. H., and Segre, J. A. (2016). Temporal stability of the human skin microbiome. *Cell* 165, 854–866. doi: 10.1016/j.cell.2016.04.008

Osawa, R., Akiyama, M., and Shimizu, H. (2011). Filaggrin gene defects and the risk of developing allergic disorders. *Allergology Int.* 60, 1–9. doi: 10.2332/allergolint.10-RAI-0270

Popov, L., Kovalski, J., Grandi, G., Bagnoli, F., and Amieva, M. R. (2014). Three-dimensional human skin models to understand staphylococcus aureus skin colonization and infection. *Front. Immunol.* 5, 41. doi: 10.3389/fimmu.2014.00041

Reichel, M., Heisig, P., and Kampf, G. (2011). Identification of variables for aerobic bacterial density at clinically relevant skin sites. *J. Hosp Infect.* 78, 5–10. doi: 10.1016/j.jhin.2011.01.017

Ross, A. A., Müller, K. M., Weese, J. S., and Neufeld, J. D. (2018). Comprehensive skin microbiome analysis reveals the uniqueness of human skin and evidence for phylosymbiosis within the class Mammalia. *Proc. Natl. Acad. Sci.* 115, E5786–E5795. doi: 10.18653/v1/K18-2

Rosso, J. D., Zeichner, J., Alexis, A., Cohen, D., and Berson, D. (2016). Understanding the epidermal barrier in healthy and compromised skin: clinically relevant information for the dermatology practitioner. *J. Clin. Aesthet Dermatol.* 9 (4 Suppl 1), S2–S8.

Roth, W., Kumar, V., Beer, H.-D., Richter, M., Wohlenberg, C., Reuter, U., et al. (2012). Keratin 1 maintains skin integrity and participates in an inflammatory network in skin through interleukin-18. *J. Cell Sci.* 125 (Pt 22), 5269–5279. doi: 10.1242/jcs.116574

Rozas, M., Hart de Ruijter, A., Fabrega, M. J., Zorgani, A., Guell, M., Paetzold, B., et al. (2021). From dysbiosis to healthy skin: major contributions of cutibacterium acnes to skin homeostasis. *Microorganisms* 9, 628. doi: 10.3390/microorganisms9030628

Saito-Sasaki, N., and Sawada, Y. (2023). S100 proteins in the pathogenesis of psoriasis and atopic dermatitis. *Diagnostics* 13, 3167. doi: 10.3390/diagnostics13203167

Salamzade, R., Swaney, M. H., and Kalan, L. R. (2022). Comparative genomic and metagenomic investigations of the corynebacterium tuberculostearicum species complex reveals potential mechanisms underlying associations to skin health and disease. *Microbiol. Spectr.* 11, e03578–e03522. doi: 10.1101/2022.08.31.506047

Seite, S., Flores, G. E., Henley, J. B., Martin, R., Zelenkova, H., Aguilar, L., et al. (2014). Microbiome of affected and unaffected skin of patients with atopic dermatitis before and after emollient treatment. *J. Drugs Dermatol.* 13 (11), 1365–1372.

Severn, M. M., and Horswill, A. R. (2023). Staphylococcus epidermidis and its dual lifestyle in skin health and infection. *Nat. Rev. Microbiol.* 21, 97–111. doi: 10.1038/s41579-022-00780-3

Shannon, C. E. (1948). A mathematical theory of communication. *The Bell System Technical J.* 27 (3), 379–423. doi: 10.1002/j.1538-7305.1948.tb01338.x

Sharma, H., and Nagaraj, R. (2015). Human β-defensin 4 with non-native disulfide bridges exhibit antimicrobial activity. *PloS One* 10, e0119525. doi: 10.1371/journal.pone.0119525

Sivaprasad, U., Kinker, K. G., Ericksen, M. B., Lindsey, M., Gibson, A. M., Bass, S. A., et al. (2015). SERPINB3/B4 contributes to early inflammation and barrier dysfunction in an experimental murine model of atopic dermatitis. *J. Invest. Dermatol.* 135, 160–169. doi: 10.1038/jid.2014.353

Smythe, P., and Wilkinson, H. N. (2023). The skin microbiome: current landscape and future opportunities. *Int. J. Mol. Sci.* 24, 3950. doi: 10.3390/ijms24043950

Swaney, M. H., and Kalan, L. R. (2021). Living in your skin: microbes, molecules, and mechanisms. *Infect. Immun.* 89, e00695–e00620. doi: 10.1128/IAI.00695-20

Sun, Y., Sheshadri, N., and Zong, W.-X. (2017). SERPINB3 and B4: from biochemistry to biology. *Semin Cell Dev Biol.* 62, 170–177. doi: 10.1016/j.semcdb.2016.09.005

Tay, A. S. L., Li, C., Nandi, T., Chng, K. R., Andiappan, A. K., Mettu, V. S., et al. (2021). Atopic dermatitis microbiomes stratify into ecologic dermotypes enabling microbial virulence and disease severity. *J. Allergy Clin. Immunol.* 147, 1329–1340. doi: 10.1016/j.jaci.2020.09.031

Totsuka, A., Omori-Miyake, M., Kawashima, M., Yagi, J., and Tsunemi, Y. (2017). Expression of keratin 1, keratin 10, desmoglein 1 and desmocollin 1 in the epidermis: possible downregulation by interleukin-4 and interleukin-13 in atopic dermatitis. *Eur. J. Dermatol.* 27, 247–253. doi: 10.1684/ejd.2017.2985

Turnbaugh, P. J., Ley, R. E., Hamady, M., Fraser-Liggett, C. M., Knight, R., and Gordon, J. I. (2007). The human microbiome project. *Nature* 449, 804–810. doi: 10.1038/nature06244

Uberoi, A., McCready-Vangi, A., and Grice, E. A. (2024). The wound microbiota: microbial mechanisms of impaired wound healing and infection. *Nat. Rev. Microbiol.* 22 (8), 507–521. doi: 10.1038/s41579-024-01035-z

Yousef, H., Alhajj, M., and Sharma, S. (2024). "Anatomy, Skin (Integument), Epidermis," in *StatPearls* (StatPearls Publishing, Treasure Island (FL).

Zhang, H., Zhu, Y., Liu, Z., Peng, Y., Peng, W., Tong, L., et al. (2022). A volatile from the skin microbiota of flavivirus-infected hosts promotes mosquito attractiveness. *Cell* 185, 2510–2522.e16. doi: 10.1016/j.cell.2022.05.016

frontiers | Frontiers in Microbiology

TYPE Systematic Review
PUBLISHED 27 February 2025
DOI 10.3389/fmicb.2025.1483794

Check for updates

OPEN ACCESS

EDITED BY
Rasha Hammamieh,
Walter Reed Army Institute of Research, United States

REVIEWED BY
Oleksandr Kamyshnyi,
Ternopil State Medical University, Ukraine
Pavlo Petakh,
Uzhhorod National University, Ukraine

*CORRESPONDENCE
Lin Sun
✉ sunlin_9999@163.com

RECEIVED 20 August 2024
ACCEPTED 22 January 2025
PUBLISHED 27 February 2025

CITATION
Zhong Z, Fan F, Lv J, Wang Z, Wang B, Deng C and Sun L (2025) Changes of potential shorty-chain fatty acids producing bacteria in the gut of patients with spinal cord injury: a systematic review and meta-analysis. *Front. Microbiol.* 16:1483794. doi: 10.3389/fmicb.2025.1483794

COPYRIGHT
© 2025 Zhong, Fan, Lv, Wang, Wang, Deng and Sun. This is an open-access article distributed under the terms of the Creative Commons Attribution License (CC BY). The use, distribution or reproduction in other forums is permitted, provided the original author(s) and the copyright owner(s) are credited and that the original publication in this journal is cited, in accordance with accepted academic practice. No use, distribution or reproduction is permitted which does not comply with these terms.

Changes of potential shorty-chain fatty acids producing bacteria in the gut of patients with spinal cord injury: a systematic review and meta-analysis

Zaowei Zhong[1], Fei Fan[2], Junqiao Lv[1], Zhiqiang Wang[1], Beiyang Wang[1], Chen Deng[1] and Lin Sun[1]*

[1]Third Hospital of Shanxi Medical University, Shanxi Bethune Hospital, Shanxi Academy of Medical Sciences, Tongji Shanxi Hospital, Taiyuan, China, [2]Department of Orthopedics, The Third People's Hospital of Datong, Datong, China

Gut bacteria that potential produce short-chain fatty acids (SCFAs) influences the recovery of motor function in the host in patients with spinal cord injury (SCI). We aimed to conduct a review and meta-analysis of the literature on gut microbiota in SCI patients. Following the Preferred Reporting Project for Systematic Review and Meta-Analysis (PRISMA), we searched Embase, PubMed, Cochrane Library, Web of Science (WOS) and ClinicalTrials.gov. The search period was from inception to March 31, 2024. We reported standardized mean differences (d) with 95% confidence intervals (CI) and used funnel plots and Egger tests to assess publication bias. The subacute of SCI data set revealed the microflora changes in the subacute phase, and meta-analysis summarized the changes in the chronic phase. Eleven studies (720 participants) were included, 2 phyla, 1 order, and 14 genus meta-analyses performed. No substantial heterogeneity was observed, and significant publication bias was not found among the studies included. In the subacute phase of spinal cord injury, the relative abundance of Bacteroidetes, Clostridiales, Faecalbacterium, Ruminococcus, Coprococcus, Lachnospira, Dorea, Prevotella, Roseburia, Atopobium, Bifidobacterium, Bacteroides, and Blautia increased. Firmicutes and Lactobacillus decreased. In the chronic phase, Firmicutes decreased in the SCI group. Bifidobacterium, Bacteroides, Blautia, and Eubacterium were found to have a higher average proportion of abundance in patients with SCI compared to non-SCI persons, and Clostridiales, Ruminococcus, Faecalbacterium, Coprococcus, and Lachnospira showed a lower relative abundance in SCI. The genus of potential SCFAs-producing bacteria is lower in the chronic phase of spinal cord injury than in the subacute phase, and gut dysbiosis is present in both the subacute and chronic phases.

KEYWORDS

spinal cord injury, trauma spinal cord injury, gut microbiota, meta-analysis, short-chain fatty acids

1 Introduction

Spinal cord injury (SCI) is a severe trauma to the central nervous system, often accompanied by complications such as immune dysfunction, intestinal dysfunction, and autonomic dysfunction. Both SCI and its associated complications impose a significant burden on patients' lives and contribute to a high social cost (Ahuja et al., 2017; Ding et al., 2022; GBD 2016 Traumatic Brain Injury and Spinal Cord Injury Collaborators, 2019). The gut microbiota is believed to play an important role in host digestion, production and absorption of nutrients, immune system, and other important physiological functions (Jandhyala et al., 2015). Due to the enormous potential of the gut microbiota, more and more experts and scholars are paying attention to the gut microbiota of patients. Targeting the gut microbiota of SCI patients may have therapeutic value (Jogia and Ruitenberg, 2020; Turroni et al., 2018).

In recent years, there has been evidence of gut dysbiosis in humans and mice after SCI (Bazzocchi et al., 2021; Kigerl et al., 2016; Yu et al., 2021). Some animal studies have shown that dysbiosis of the gut microbiota can exacerbate inflammation of the spinal cord and colon, impairing the recovery of motor function (Kigerl et al., 2016; Rong et al., 2021; Schmidt et al., 2021). After specific types of fecal transplantation or probiotic supplementation treatment, it was observed that SCI mice had better motor function recovery than the control group (He et al., 2022; Jing et al., 2021; Kigerl et al., 2016). These animal studies also found that intervention in the gut micro-biota of SCI mice resulted in an increase in the detection level of SCFA in feces. Animal experiments have been conducted to investigate the effects of SCFAs on SCI mice. Feeding SCFAs resulted in better motor function recovery, higher neuronal survival rate, and better axon formation than the control group (Jing et al., 2023; Jing et al., 2021). Intestinal symbiotic bacteria produce SCFAs in the colon through anaerobic fermentation. Short-chain fatty acids have many beneficial properties and can improve neurological function in various central nervous system diseases through immune, vagus, endocrine, or other humoral pathways (Dalile et al., 2019; Dicks, 2022; Khan et al., 2021; Li et al., 2021). SCFAs might significantly impact the recovery of motor function and other physiological functions in patients with SCI. We propose that potential SCFA-producing bacteria may serve as critical targets for enhancing motor function recovery through modulation of the gut microbiota in patients with spinal cord injury.

Therefore, the changes of potential SCFAs-producing bacteria after human spinal cord injury deserve our special attention. Differences in the relative abundance of bacteria at the genus level have been observed across studies following spinal cord injury, which may be attributed to variations in the study populations' genetics, diet, geography, and analytical procedures. We analyzed the data of the subacute stage of spinal cord injury to obtain the changes in the abundance of SCFAs-producing bacteria in the subacute stage. We included the studies of the chronic stage of spinal cord injury for meta-analysis so as to objectively compare the changes in the relative abundance of intestinal SCFA bacteria in the subacute stage and the chronic stage of spinal cord injury. Our research is expected to provide theoretical support for future researchers to intervene in the development of spinal cord injury by targeting the gut microbiota of SCI, enriching the theory of the brain-gut axis.

2 Materials and methods

2.1 Design and registration

The study was reported according to the Preferred Reporting Items for Systematic Review and Meta-Analysis (PRISMA) (Page et al., 2021). The protocol was informed by the Cochrane Handbook for Systematic Review of Interventions and registered via the International Prospective Register of Systematic Reviews (PROSPERO) (CRD42023417200).[1]

2.2 Search strategy

We selected relevant studies published before March 31, 2024, by searching Embase, PubMed, Cochrane Library, Web of Science (WOS), and ClinicalTrials.gov. We applied no language restrictions. A combination of Mesh with free text search was applied using the keywords gut microbiota, spinal cord injury, and their associated subject words. The specific retrieval strategies are detailed in Supplementary Table S1.

2.3 Inclusion and exclusion criteria for the initial search

The same two investigators (Zaowei Zhong and Junqiao Lv) implemented study selection on an independent basis by firstly screening the titles and abstracts, followed by reviewing the full texts of eligible articles. Disagreements, if any, were resolved by consulting a third investigator (Lin Sun). Specifically, the inclusion criteria were: (1) applied an observational design (e.g., case–control study, cross-sectional study, and cohort study); (2) performed gut microbiota analysis with available data on diversity or abundance measures; and (3) included participants with spinal cord injury.

2.4 Potential short-chain fatty acids produced bacteria chosen

We used the retrieval method in PubMed to search for literature. We conducted a meta-analysis of identified bacteria that potential produce short-chain fatty acids by reviewing literature from establishing the database to April 7, 2024. Retrieval strategy: ((((“produced”)) AND (“bacteria”)) OR (“bacterial fermentation”)) AND (“short-chain fatty acids”)) AND (Review).

2.5 Eligible criteria and quality assessment

The eligible studies are as follows: (1) the samples are from patients with SCI, and 16S rRNA gene sequencing technology to elucidate the relative abundance changes of gut microbiota. (2) original research to compare the composition of gut microbiota between patients with SCI and non-SCI controls. The exclusion

1 https://www.crd.york.ac.uk/prospero/

criteria were as follows: (1) the comparative study of microbial relative abundance between patients with SCI and non-SCI controls could not be provided; (2) There were no data on gut microbiota relative abundance. The Newcastle Ottawa scale (NOS) was used to assess the quality of case–control studies (Wells et al., 2018).

2.6 Outcome measures and data extraction

The primary outcomes were as follows: the relative abundance of bacteria. Two reviewers independently extracted details from the studies included in the meta-analysis. It included the first author, year of publication, location, sample size, sex, days or months from injury, injury level, injury degree, sequencing platform, and relative abundance of bacteria. However, most of the results were presented as a graph rather than an exact report of the raw data they obtained, which meant that the actual numbers had to be estimated from the data extracted from the graph. Some study results' mean and standard deviation could not be obtained, so we used the sample's quartile, median, maximum, minimum, and *p*-value to estimate the mean and standard deviation (Luo et al., 2018; Shi et al., 2023; Shi et al., 2020; Wan et al., 2014). Some study results included two subgroups, which we combined as one and estimated their mean and standard deviation for follow-up analyses (Altman et al., 2000). Numerical values from the graphs were estimated by GetData Graph Digitizer 2.22 software,[2] and the study will be excluded if data were not presented or obtainable. Any controversies lead to a third reviewer settling the problem by discussion.

2.7 16S rRNA gene sequencing processing

Demultiplexed raw DNA sequences from the stools of SCI and non-SCI subjects from different studies were downloaded from the NCBI. The data set of subacute(PRJNA 724686) was only the SCI, and the data set of people from the same region was used as the control(PRJNA 247489, PRJNA792991). The dataset has been analyzed to obtain the mean relative abundance and SD. The raw sequencing data were imported into QIIME2/2024.01 for data processing (Bolyen et al., 2019). Due to the technical variation in the data sets included in these studies (DNA extraction kits, primers, sequencing, and platform), each data set was separately denoised and processed into amplicon sequence variants using DADA2 (Bolyen et al., 2019). The reads were trimmed that the Quartile quality score was <30. we also trimmed 21 nucleotides from the 5′ end of each read. Taxonomic classification of the operational taxonomic units (OTUs) was conducted using the classify-sklearn classification methods based on the SILVA database[3] and the q2- feature-classifier plugin.

2.8 Statistical analysis

The standardized mean difference (SMD) was used as the effect indicator because the outcome indicators were all continuous variables, and point estimates and 95% confidence intervals (CI) were given for each effect measure. Statistical results were presented with a forest map. We ran I^2 testing to assess the magnitude of the heterogeneity among the studies included. Suppose the heterogeneity test result was $I^2 \leq 50\%$, meta-analysis was performed using a fixed effects model; if the heterogeneity test result was $I^2 > 50\%$, me-ta-analysis was performed using a random effects model, and the sources of heterogeneity needed to be further analyzed. After excluding obvious clinical and methodological heterogeneity, a random effects model was used for the meta-analysis (Higgins et al., 2003). Sensitivity analyses were conducted by omitting each study in turn and then rerunning the meta-analysis and assessing the differences between the results and the actual combined results.

We assessed the possibility of publication bias with a funnel plot. Egger's tests were used to assess funnel plot asymmetry, and no significant publication bias was defined as a *p*-value >0.1. The effect of publication bias on the results of the meta-analysis was assessed using the trim-fill method (Duval and Tweedie, 2000). Egger's tests and trim-fill method were performed with R language version 4.2.2,[4] All graphical presentations in this study were performed with GraphPad Prism version 9,[5] and Review Manager version 5.3 (Cochrane Collaboration).[6]

3 Results

3.1 Search flow and overview of studies

Three hundred seventy-eight studies were retrieved from PubMed, Embase, WOS, CNKI, and Cochrane Library; 164 studies marked as ineligible by automation tools were excluded, and the remaining 174 articles were evaluated. After carefully reading the titles and abstracts, 196 articles were excluded because they needed to meet the inclusion criteria. Three articles were excluded as they did not set a health control group. After reading the full texts carefully and comparing the selection criteria, 11 studies were finally included. All studies included were published between 2016 and 2024, yielding 720 individual fecal samples for microbiome analysis. Seven studies were conducted in China, one in Turkey, one in United States, one from Israel, and one in Italy. Seven studies included male and female participants, while two studies included male only (Figure 1).

All studies included in the meta-analyses were compared between patients with SCI and non-SCI controls, who were adjusted with age, and all participants without any chronic conditions. Additionally, body mass index (BMI) was matched in two studies, dietary habits were matched in four studies by all patients, and non-SCI individuals were provided standard hospital food before sample collection. Seven studies excluded the participants treated with antibiotics within 1 to 3 months before stool collection; two studies used antibiotics for inflammation in the acute stage. Five studies excluded the participants who used probiotics before enrollment. The ASIA neurological function scale of patients with SCI ranged from A to D in four studies and A, C, and D in one study: three included patients with only an A score. The rest of the studies did not specify the ASIA scores.

2 http://www.getdata-graph-digitizer.com/

3 https://data.qiime2.org/2024.01/common/silva-138-99-nb-classifier.qza

4 meta packages https://www.r-project.org/

5 https://www.graphpad-prism.cn

6 https://training.cochrane.org/online-learning/core-software/revman

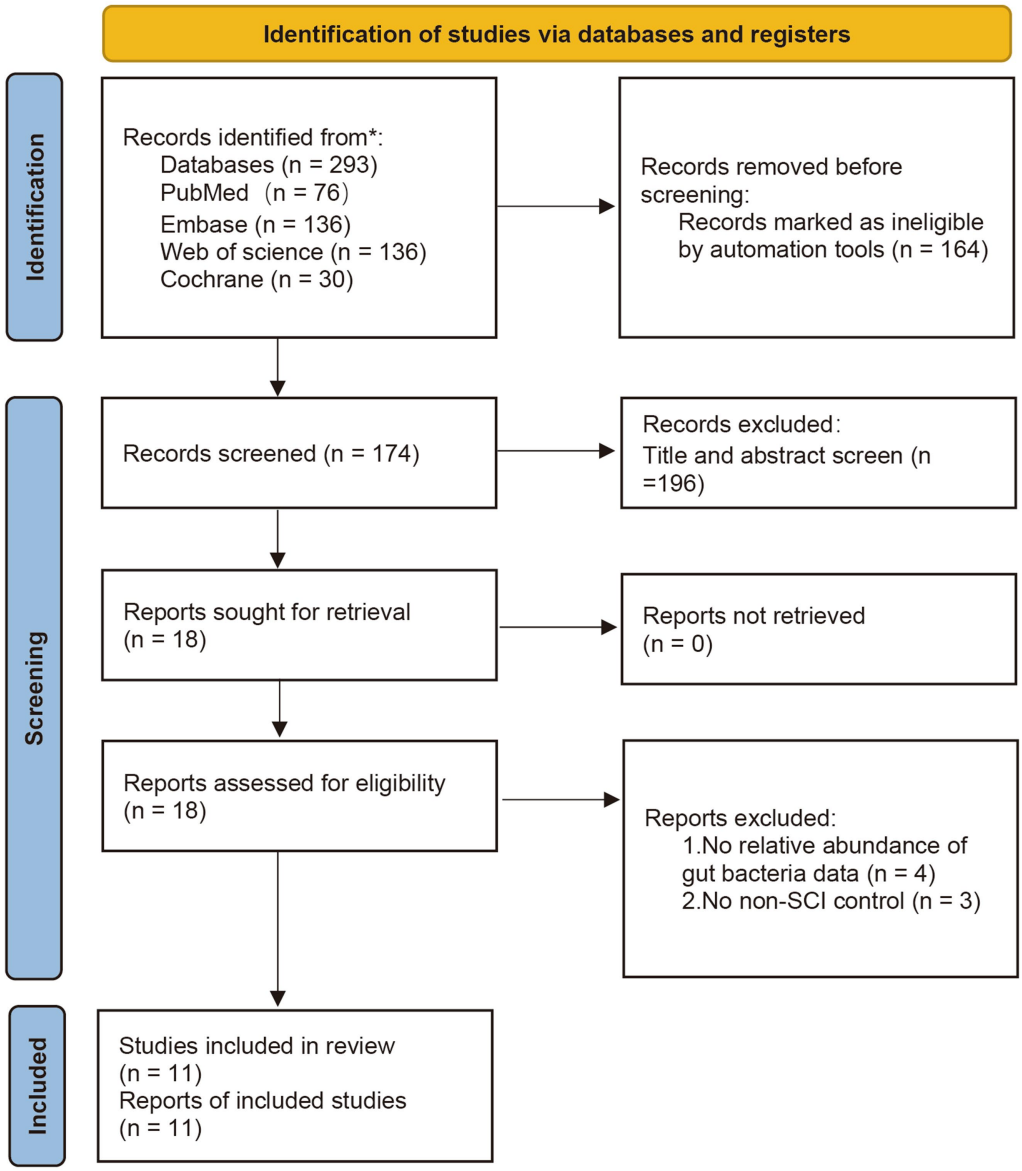

FIGURE 1
PRISMA flow diagram of study identification.

All studies used 16S rRNA sequencing to evaluate gut microbiota samples. Seven studies measured the V3-V4 regions, and four measured the V4 region. As for Sequencing platforms used, Illumina was used in 10 studies and microbial ecology in one study. Bacterial and archaeal rRNA databases for taxonomic assignments of sequence data in studies included are SILVA or GreenGenes. More details are shown in Table 1. The quality of case–control studies is shown in Table 2.

3.2 Bacteria selected for meta-analyses

We searched for literature and summarized the bacterial genera that potential produce SCFAs (Dalile et al., 2019; Dicks, 2022; Vacca et al., 2020). Summarized in Table 3.

3.3 Gut bacteria changed of SCI subacute and chronic stage

We analyzed the PRJNA724686 dataset, a sample collected from 21 to 36 days after SCI. We identify the data as subacute. The injury time and sampling time of the study population included in the meta-analyses range from 2 months to 10 years, and we consider it the chronic phase.

In patients with SCI during the subacute phase, the relative abundance of Firmicutes and Lactobacillus decreases. In contrast, the relative abundance of Bacteroidetes, Bacteroides, Blautia, Clostridales, Faecalbacterium, Ruminococcus, Coprococcus, Lachnospira, Dorea, Prevotella, Roseburia, Atopobium, and Bifidobacterium increases. There is no significant difference in Eubacteria (Figure 2).

TABLE 1 Studies characteristics and assessments of included studies.

Study	Level of injury	SCI duration	Antibiotic use	Country	Sequencing platform, database used
Gungor et al. (2016)	Cervical, Thoracic, Lumbar	13–105 months	No	Turkey	Illumina TruSeq DNA library, GreenGenes
Zhang et al. (2018)	Cervical, Thoracic, Lumbar	6 or more months	No	China	Illumina MiSeq, SILVA, Greengenes
Zhang et al. (2019)	Cervical	6 or more months	No	China	Illumina MiSeq, SILVA, Greengenes
Lin et al. (2020)	Cervical, Thoracic, Lumbar	11 ± 2.68 months	No	China	Illumina Miseq, SILVA
Yu et al. (2021)	Thoracic	2–12 months	Yes	China	Microbial ecology platform, Greengenes
Bazzocchi et al. (2021)	Cervical, Thoracic, Lumbar	within 60 days	Yes	Italy	Illumina MiSeq, Greengenes
Pang et al. (2022)	Cervical, Thoracic, Lumbar	1–300 months	No	China	Illumina MiSeq, nucleic acid database
Li et al. (2021)	Cervical, Thoracic, Lumbar	4 days-53 years	Yes	America	Illumina Miseq, SILVA
Kong et al. (2023)	Cervical, Thoracic	22.81 ± 1.15 months	Yes	China	Illumina MiSeq/HiSeq
Jing et al. (2023)	Cervical, Thoracic, Lumbar	2-70 month	no	China	Illumina Miseq, SILVA
Gur Arie et al. (2024)	Cervical, Thoracic, Lumbar	60-259 days	Yes	Israel	Illumina MiSeq, Greengenes

In the meta-analyses of patients with chronic SCI, the number of Firmicutes decreased in the SCI group, while there was no significant difference in the number of Bacteroidetes. The average abundance proportion of Bifidobacterium, Bacteroides, Blautia, and Eubacterium in SCI patients is higher, with statistical differences. In contrast, the abundance of Clostridiales, Ruminococcus, Feacalbacterium, Coprococcus, and Lachnospira in SCI patients is lower, achieving statistical differences. There was no significant difference in Dorea, Prevotella, Roseburia, Atopobium, and *Lactobacillus* (Figures 3–6).

3.4 Publication bias and heterogeneity

We use funnel plots and Egger's test to evaluate publication bias (Figures 7, 8; Table 4). We observed a phenomenon in the meta-analyses of the genera Bacteroidetes, Bluatia, and Bifidobacterium, where there was one study in their funnel plots, and the effectiveness of the study was outside the dashed range of the funnel plots. We consider that the results of these studies beyond the dashed range may have significant biases or anomalies, which may be due to methodological issues, data quality considerations, or other potential factors (Supplementary Figures S1, S2). We paid special attention to this study and tested its impact on the overall results in subsequent sensitivity analysis. Considering their significant bias in the meta-analyses of bacterial abundance, we have decided to exclude them. Then, a meta-analysis was conducted again, and it was found that heterogeneity was significantly reduced (Figures 3, 4) After Egger's test, there are public biases in Bacteroides and Prevotella. The trim-fill shows that bias does not affect the meta-analyses result. The rest of the bacteria were not found in public bias. After applying the trim-fill method, the meta of Bacteroides changed direction and showed no significant difference. The meta-analysis of Prevotella did not show significant differences after using the trim-fill method, and there is no evidence of publication bias (Table 4; Supplementary Figure S3).

We performed sensitivity analyses by omitting each study, and the results were stable, except Bacteroides and Eubacterium were unstable. At the same time, we also summarized the studies that significantly impacted heterogeneity in the meta-analyses of the relative abundance of various bacteria (Table 5). The study by Zhang et al. (2018) significantly impacts the *p*-value results of Bacteroides, which may be due to the higher relative abundance of genus Bacteroides in the population with ASIA grade A SCI in the chronic phase compared to other grades. ASIA grade may be a source of heterogeneity (Zhang et al., 2018).

The meta-analysis of Eubacterium showed no significant difference after excluding studies by Yu et al. (2021) which may be related to their study only including the causes of thoracic spinal cord injury. In Blautia meta-analysis, the study by Kong et al. showed the opposite direction compared to others (Kong et al., 2023). After exclusion, it was found that there was a significant difference in the meta-analysis results and a significant reduction in heterogeneity. After comparing it with other studies, it was found that the study of Kong et al. population used antibiotics. Antibiotics may be a source of heterogeneity and bias, and antibiotics may significantly influence the relative abundance of Blautia. After conducting a sensitivity analysis in Ruminococcus, significant heterogeneity was observed in the study by Kong et al., but it did not alter the results of the meta-analysis. After incorporating study of Lin et al. into the meta-analysis of Bifidobacterium, it was found that there was a significant increase in heterogeneity and a change in the results of the meta-analysis, with a significant increase in p-value. We found bias in the funnel plot and compared it with the results of other studies. We found that research of Lin et al. direction was the opposite, and the different lengths of injury time may be the reason (Lin et al., 2020). Research of Yu et al. contributed to all heterogeneity in the meta-analysis of Faecalbacterium, and we speculate that the source of heterogeneity is the damaged segment. For the meta-analysis of Prevotella, studies from Yu et al.

TABLE 2 The Newcastle Ottawa scale scores of studies included.

Studies	Adequate definition of cases	Representativeness of the cases	Selection of controls	Definition of controls	Comparability control for important factor	Ascertainment of exposure	Same method of ascertainment for cases and controls	Nonresponse rate	Scores
Zhang et al. (2018)	★	★	☆	★	★★	★	★	★	8
Li et al. (2022)	★	★	★	★	★	★	★	★	8
Lin et al. (2020)	★	★	★	★	★	★	★	★	8
Gungor et al. (2016)	★	★	☆	★	★	★	★	★	7
Pang et al. (2022)	★	★	☆	★	★	★	★	★	7
Kong et al. (2023)	★	★	☆	★	★	★	★	★	7
Yu et al. (2021)	★	★	★	★	★★	★	★	★	9
Zhang et al. (2019)	★	★	☆	★	★	★	★	★	7
Bazzocchi et al. (2021)	★	★	☆	★	★	★	★	★	7
Gur Arie et al. (2024)	★	★	☆	★	★	★	★	★	7
Jing et al. (2023)	★	★	☆	★	★	★	★	★	7

10.3389/fmicb.2025.1483794

10.3389/fmicb.2025.1483794

TABLE 3 Bacteria selected for meta-analysis.

Bacteria	Reason to meta
Fimicutes	Produce high amounts of butyrate; butyrate can reduce neuroinflammatory responses.
Bacteroidetes	Produce high levels of acetate and propionate; both have anti-inflammatory properties.
Clostridiales	Correlates with locomotor recovery in SCI mice.
Atopobium	The relative abundance of Atopobium in the gut increases in patients with colitis who take rifaximin, and rifaximin has been observed to have neuroprotective effects in mice with craniocerebral injury.
Bacteroides	Produces neurotransmitters such as GABA. Converts tryptophan in food to 5-HT.
Bifidobacterium	Correlates with butyric acid and valeric acid in SCI patients and converts tryptophan in food to 5-HT.
Blautia	It can convert polymethoxyflavones with various biological functions, such as anti-inflammatory and neuroprotective activities.
Coprococcus	Positively correlated with tryptophan metabolites, affecting the host's intestinal barrier function and antioxidant activity.
Dorea	A positive correlation between protein 1 receptor and cytotoxic T lymphocyte-associated protein 4 blockade, along with increased levels of Dorea, has been reported.
Eubacterium	Butyrate is the main SCFA produced by the Roseburia/*Eubacterium rectale* group, especially at a mildly acidic pH, along with the consumption of acetate.
Faecalibacterium	Correlates with acetic acid, propionic acid, isobutyric acid, butyric acid, and isovaleric acid in SCI patients.
Lachnospira	Pectin-utilizing Firmicutes species.
Lactobacillus	Produces neurotransmitters such as GABA and converts tryptophan in food to 5-HT.
Prevotella	Converts tryptophan in food to 5-HT.
Roseburia	Butyrate is the main SCFA produced by the Roseburia/*Eubacterium rectale* group, especially at a mildly acidic pH, along with the consumption of acetate. Converts tryptophan in food to 5-HT.
Ruminococcus	Correlates with acetic acid, butyric acid, and valeric acid in SCI patients.

2 phyla, 1 order, and 14 genus.

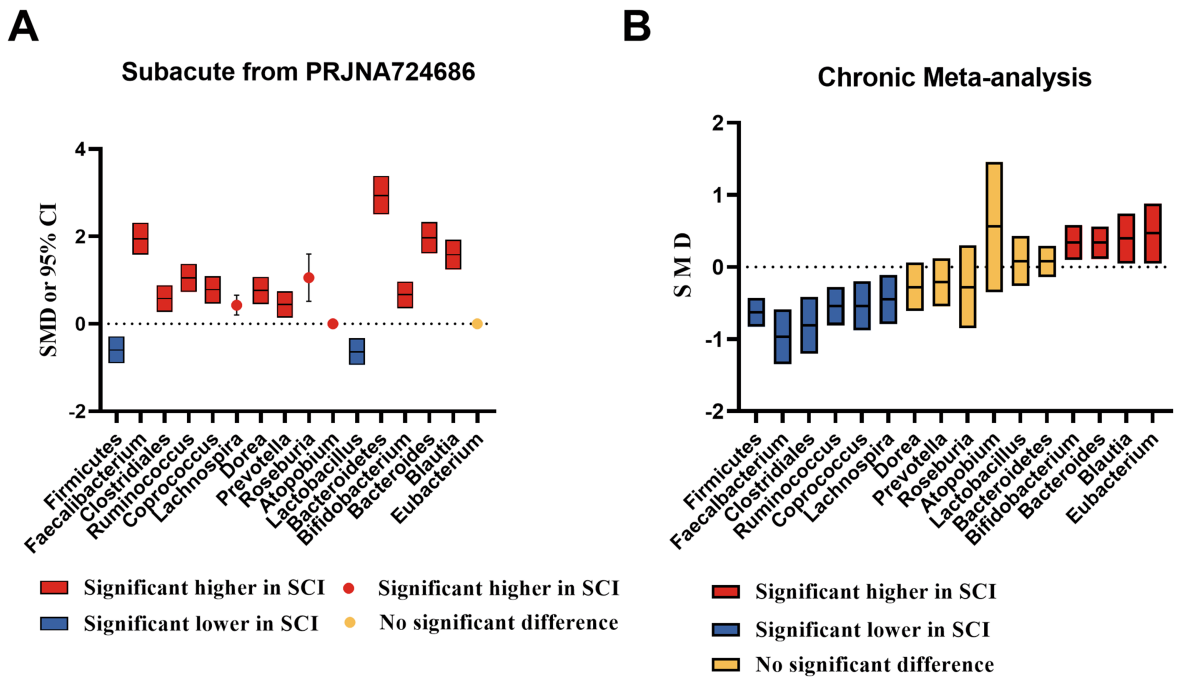

FIGURE 2
SCFAs-producing bacteria changed of SCI subacute and chronic stage **(A)** Subacute phase. **(B)** Chronic phase. SMD, standard mean differences; CI, confidence interval.

and Lin et al. significantly influenced heterogeneity, and the use of antibiotics or damaged segments may affect the relative abundance of Prevotella. Clostridiales did not observe significant heterogeneity (Table 4; Figures 3–6).

4 Discussion

This study assessed gut microbiota alterations across a spectrum of SCI through meta-analyses. The main findings were: (1) In subacute

A

Study or Subgroup	SCI Mean	SCI SD	SCI Total	Control Mean	Control SD	Control Total	Weight	Std. Mean Difference IV, Fixed, 95% CI
Ayelet Gur Arie 2024	15.67	20.03	30	34.14	15.73	18	10.7%	-0.98 [-1.60, -0.36]
Binbin Yu 2021	67.29	22.92	45	80.58	15.82	24	16.0%	-0.63 [-1.14, -0.13]
Chao Zhang 2018	58	16.64	43	66	16.64	23	15.6%	-0.48 [-0.99, 0.04]
Chao Zhang 2019	52.05	16.74	20	65.38	16.74	23	10.6%	-0.78 [-1.41, -0.16]
Ganggang Kong 2023	56.22	19.52	11	75.14	19.52	10	4.9%	-0.93 [-1.84, -0.02]
Rizhao Pang 2022	43.62	23.1	23	50.48	22.12	21	11.6%	-0.30 [-0.89, 0.30]
Ruizhu Lin 2020	49.89	13.82	23	59.45	10.34	23	11.4%	-0.77 [-1.37, -0.17]
Yingli Jing 2023	72	20.06	59	82.4	20.06	27	19.2%	-0.51 [-0.98, -0.05]
Total (95% CI)			**254**			**169**	**100.0%**	**-0.63 [-0.83, -0.43]**

Heterogeneity: Chi² = 3.86, df = 7 (P = 0.80); I² = 0%
Test for overall effect: Z = 6.09 (P < 0.00001)

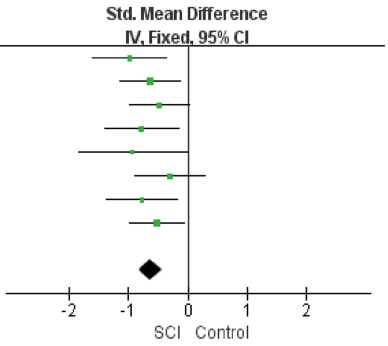

B

Study or Subgroup	SCI Mean	SCI SD	SCI Total	Control Mean	Control SD	Control Total	Weight	Std. Mean Difference IV, Fixed, 95% CI
Binbin Yu 2021	2.81	6.62	45	2.36	4.81	24	19.2%	0.07 [-0.42, 0.57]
Chao Zhang 2018	28.67	8.87	40	27.33	8.87	23	17.9%	0.15 [-0.36, 0.66]
Chao Zhang 2019	31.28	10.63	20	29.49	10.64	23	13.1%	0.17 [-0.44, 0.77]
Rizhao Pang 2022	41.57	16.31	23	43.62	23.1	21	13.4%	-0.10 [-0.69, 0.49]
Ruizhu Lin 2020	33.34	14.5	23	27.17	15.54	23	13.8%	0.40 [-0.18, 0.99]
Yingli Jing 2023	4.4	6.32	59	5.2	6.32	27	22.7%	-0.13 [-0.58, 0.33]
Total (95% CI)			**210**			**141**	**100.0%**	**0.08 [-0.14, 0.29]**

Heterogeneity: Chi² = 2.47, df = 5 (P = 0.78); I² = 0%
Test for overall effect: Z = 0.69 (P = 0.49)

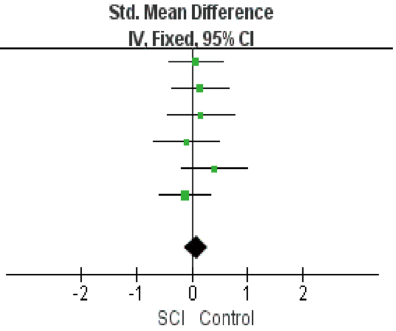

C

Study or Subgroup	SCI Mean	SCI SD	SCI Total	Control Mean	Control SD	Control Total	Weight	Std. Mean Difference IV, Fixed, 95% CI
Binbin Yu 2021	0.28	0.422	45	0.64	0.26	24	56.4%	-0.95 [-1.47, -0.43]
Ruizhu Lin 2020	43.09	13.17	23	50.89	11.3	23	43.6%	-0.62 [-1.22, -0.03]
Total (95% CI)			**68**			**47**	**100.0%**	**-0.81 [-1.20, -0.42]**

Heterogeneity: Chi² = 0.65, df = 1 (P = 0.42); I² = 0%
Test for overall effect: Z = 4.05 (P < 0.0001)

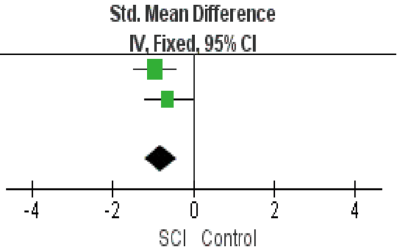

D

Study or Subgroup	SCI Mean	SCI SD	SCI Total	Control Mean	Control SD	Control Total	Weight	Std. Mean Difference IV, Random, 95% CI
Bilgi Gungor 2016	0.0081	0.0245	30	0.0067	0.0076	10	46.4%	0.06 [-0.65, 0.78]
Binbin Yu 2021	0.01	0.01	45	0	0.01	24	53.6%	0.99 [0.47, 1.51]
Total (95% CI)			**75**			**34**	**100.0%**	**0.56 [-0.35, 1.46]**

Heterogeneity: Tau² = 0.33; Chi² = 4.18, df = 1 (P = 0.04); I² = 76%
Test for overall effect: Z = 1.21 (P = 0.23)

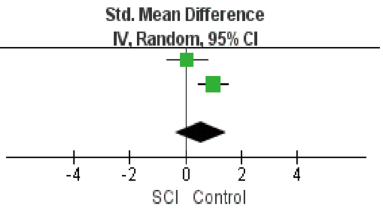

E

Study or Subgroup	SCI Mean	SCI SD	SCI Total	Control Mean	Control SD	Control Total	Weight	Std. Mean Difference IV, Fixed, 95% CI
Bilgi Gungor 2016	1.64	1.3572	30	1.49	1.26	10	9.8%	0.11 [-0.61, 0.83]
Binbin Yu 2021	3.15	7.38	45	2.34	4.76	24	20.4%	0.12 [-0.37, 0.62]
Chao Zhang 2018	21.78	12.03	43	12.22	12.03	23	18.2%	0.79 [0.26, 1.31]
Chao Zhang 2019	25.79	12.9	20	12.63	12.9	23	12.3%	1.00 [0.36, 1.64]
Ruizhu Lin 2020	20.46	11.34	23	18.96	13.66	23	15.0%	0.12 [-0.46, 0.70]
Yingli Jing 2023	3.63	14.35	59	2.63	14.35	27	24.2%	0.07 [-0.39, 0.52]
Total (95% CI)			**220**			**130**	**100.0%**	**0.34 [0.11, 0.56]**

Heterogeneity: Chi² = 9.95, df = 5 (P = 0.08); I² = 50%
Test for overall effect: Z = 2.94 (P = 0.003)

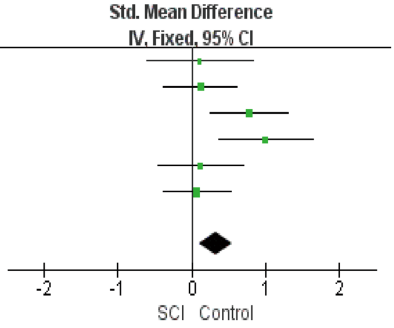

FIGURE 3
Forest map of Relative abundance of bacteria in gut between SCI and non-SCI control. **(A)** Firmicutes, **(B)** Bacteroidetes, **(C)** Clostridiales, **(D)** Atopobium, and **(E)** Bacteroides. SMD, standard mean differences; CI, confidence interval.

F

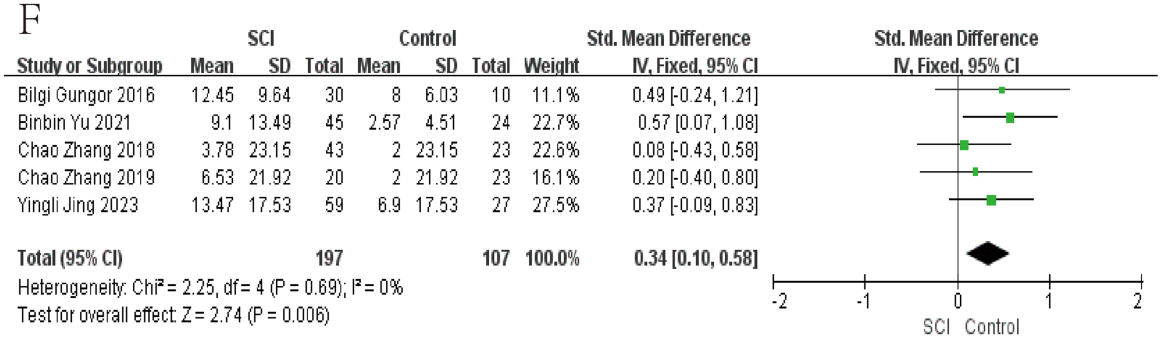

G

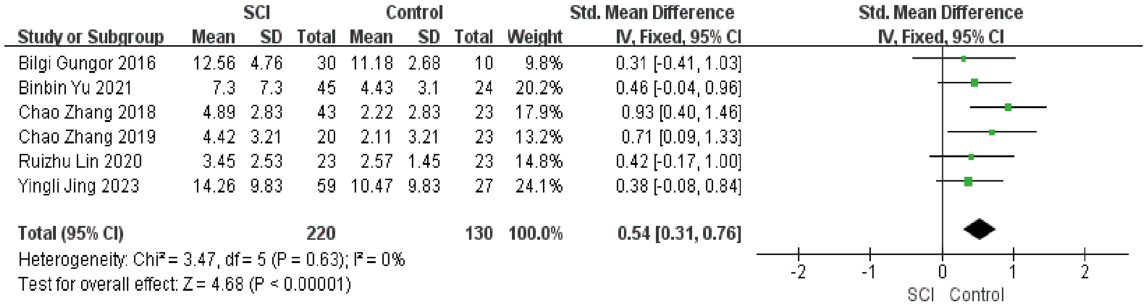

H

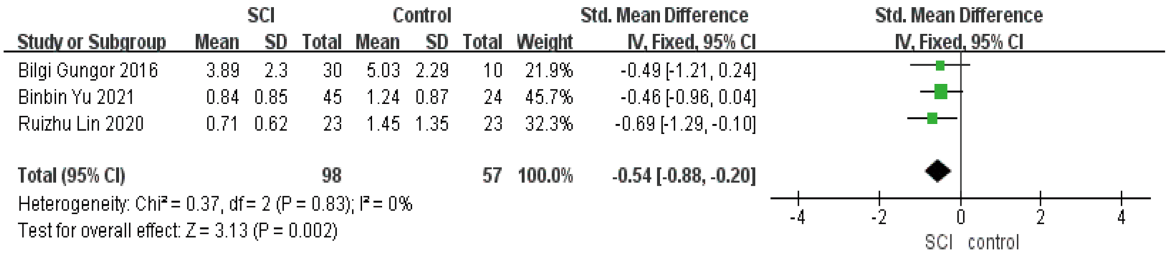

I

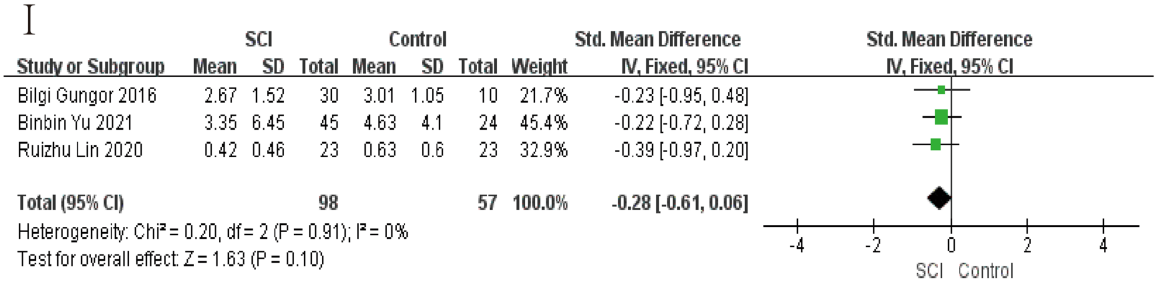

J

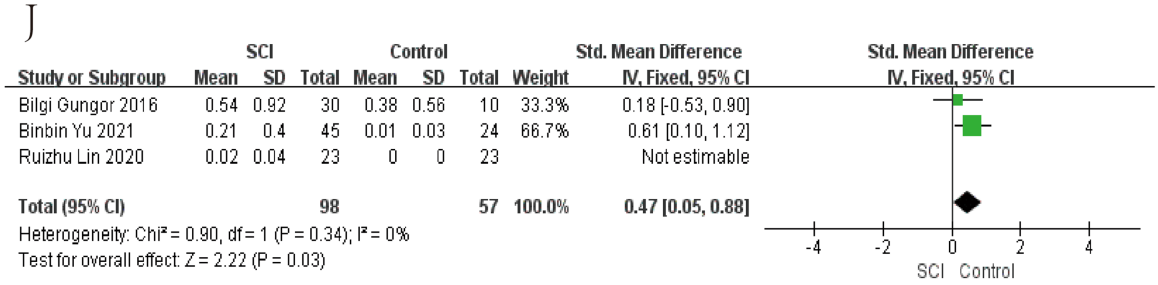

FIGURE 4
Forest map of Relative abundance of bacteria in gut between SCI and non-SCI control. **(F)** Bifidobacterium, **(G)** Blautia, **(H)** Coprococcus, **(I)** Dorea, and **(J)** Eubacterium. SMD, standard mean differences; CI, confidence interval.

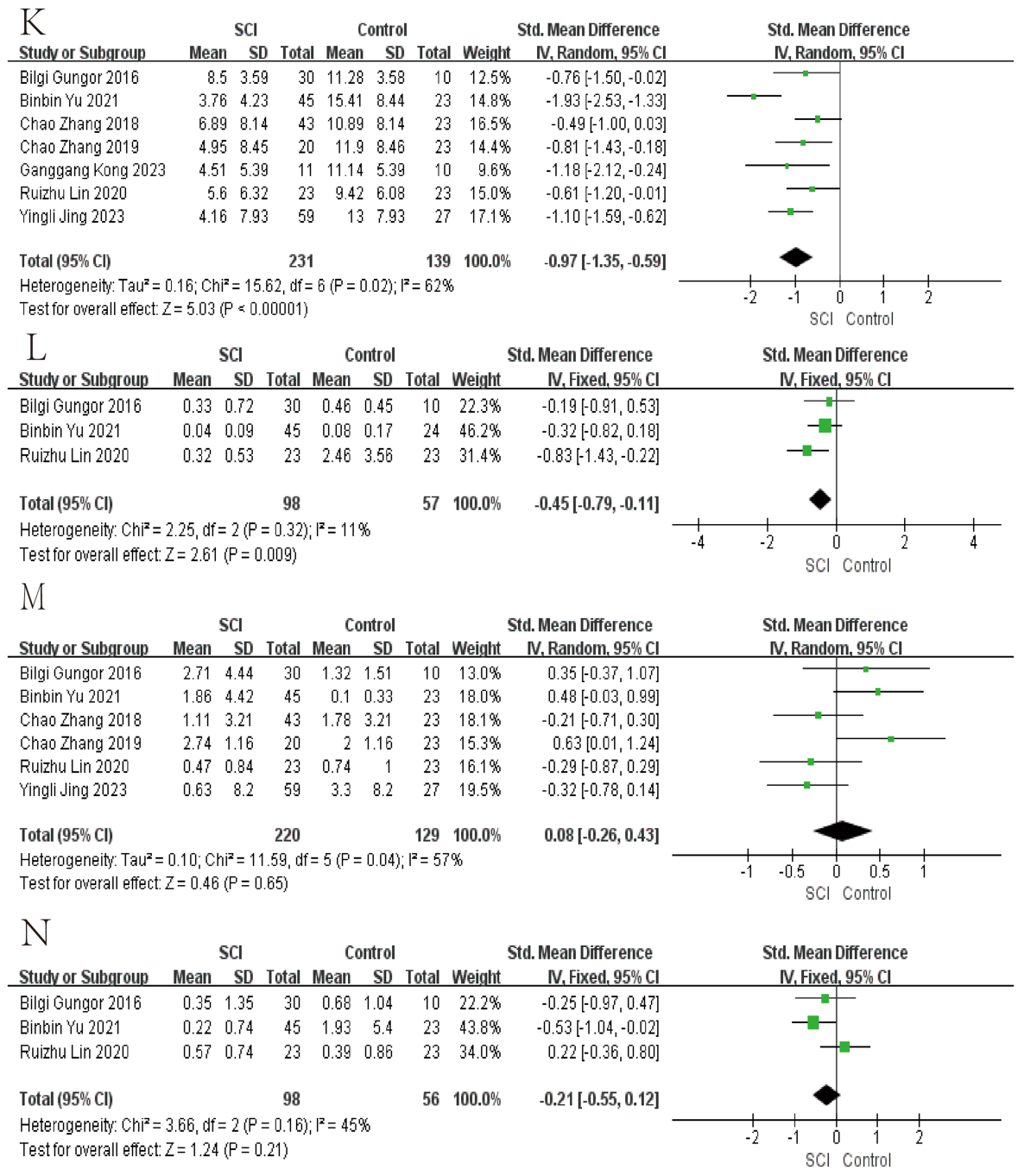

FIGURE 5
Forest map of Relative abundance of bacteria in gut between SCI and non-SCI control. **(K)** Faecalibacterium, **(L)** Lachnospira, **(M)** Lactobacillus, and **(N)** Prevotella. SMD, standard mean differences; CI, confidence interval.

phase of spinal cord injury, the relative abundance of Bacteroidetes, Clostridiales, Faecalbacterium, Ruminococcus, Coprococcus, Lachnospira, Dorea, Prevotella, Roseburia, Atopobium, Bifidobacterium, Bacteroides, and Blautia increased. Firmicutes and Lactobacillus decreased. (2) In chronic phase. Firmicutes decreased in the SCI group, and Bacteroidetes showed no significant difference. Bifidobacterium, Bacteroides, Blautia, and Eubacterium were found to have a higher average proportion of abundance in patients with SCI compared to non-SCI persons, and Clostridiales, Ruminococcus, Faecalbacterium, Coprococcus, and Lachnospira showed a lower abundance in SCI; statistical differences were reached. Dorea, Prevotella, Roseburia, Atopobium, and Lactobacillus found no significant difference.

Substantial heterogeneity was not observed in this study. The composition of gut microbiota among individuals was influenced by age, gender, diet, genes, and environment. We evaluated all included studies and found that some of these studies differ in several ways, including sex, SCI duration, level of injury, ASIA scores, country design, and database used, which contribute to heterogeneity in meta-analyses of some bacteria. But overall, heterogeneity is acceptable. Egger's test indicated the presence of publication bias. The trim-and-fill method was used to

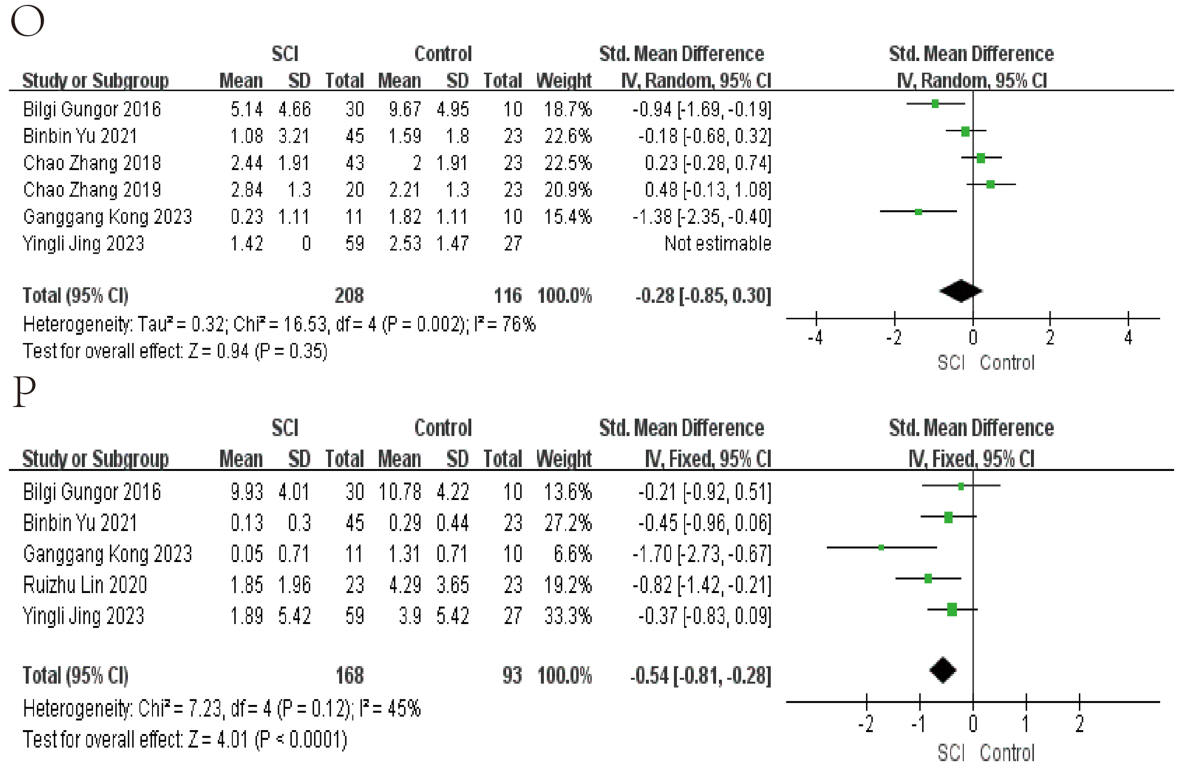

FIGURE 6
Forest map of Relative abundance of bacteria in gut between SCI and non-SCI control. **(O)** Roseburia and **(P)** Ruminococcus. SMD, standard mean differences; CI, confidence interval.

assess the impact of this bias on Bacteroides and Prevotella. The results showed that the bias had no significant effect on Bacteroides, but it did affect Prevotella. Therefore, no meta-analysis was conducted on Prevotella. The source of publication bias for Prevotella may be related to population-specific gut microbiota profiles, where studies may have been unpublished due to the lack of significant differences observed after spinal cord injury (Arumugam et al., 2011).

Multiple studies on SCI in mice have found a negative correlation between Clostridiales and BMS, so we have paid extra attention to this (He et al., 2022; Jing et al., 2019; Kigerl et al., 2016). Zhang et al. (2023) examined the diversity and relative abundance of gut microbiota in mice with SCI. They found that the Clostridiales significantly increased in the mice gut after SCI. However, currently published studies on the gut microbiota of SCI mice are acute or subacute-phase samples, unlike human samples, which are mainly chronic-phase samples (Gungor et al., 2016; Jing et al., 2023; Yu et al., 2021; Zhang et al., 2018). In this study, the Clostridiales increased in the subacute phase and decreased in the chronic phase. Further research is needed to determine whether the increase in Clostridiales during the acute phase and decrease during the chronic phase after SCI affects the recovery of motor function in mice or humans after SCI. In the meta-analysis by Zhang et al., there was no significant difference in the relative abundance of Firmicutes, Bacteroidetes, Bacteroides, and Lactobacillus compared to the sham surgery group, which may be due to the high heterogeneity (greater than 70) in the included studies. Because in multiple studies on spinal cord injury in humans and mice, it has been observed that the content of SCFAs in feces is lower than that in the control group, the SCFAs-producing bacteria in the gut was likely reduced (Jing et al., 2023; Kigerl et al., 2016).

Firmicutes and Bacteroidetes are dominant bacteria in the human gut, and their relative abundance rapidly changes, leading to gut dysbiosis (Arumugam et al., 2011). In subacute phase of spinal cord injury, data showed a decrease in the relative abundance of Firmicutes compared to the non-spinal cord injury control group, an increase in the relative abundance of Bacteroidetes. In chronic phase, the relative abundance of Firmicutes decreased, and there was no significant difference in the relative abundance of Bacteroidetes compared to the control group without spinal cord injury. Gut dysbiosis has been observed in the population's subacute and chronic phases.

For the overall gut microbiota, the genus of potential SCFAs-producing bacteria is lower in the chronic phase of spinal cord injury than in the subacute phase, and gut dysbiosis is present in both the subacute and chronic phases. The gut microbiota has coexisted with the host for a long time; recently, some have regarded the gut microbiota as an endocrine organ of the host (Jogia and Ruitenberg, 2020; Turroni et al., 2018). We speculate that the general increase in the relative abundance of SCFAs-producing bacterial genera during the subacute phase of spinal cord injury is a compensatory response of the gut microbiota to the injury, while in the chronic phase, there is a certain degree of decompensation. The decrease in regenerative potential from the intestine may result in partial loss of motor function recovery. For Lactobacillus, a study using melatonin to treat mice with spinal cord injury found that after administration, the relative abundance of Lactobacillus was positively correlated with BMS and negatively correlated with FITC-dextran permeability, and an increase in the molecules Occludin and ZO-1 associated with intestinal permeability was also observed (Jing et al., 2019). An earlier animal study found that after spinal cord injury, the intestinal permeability of

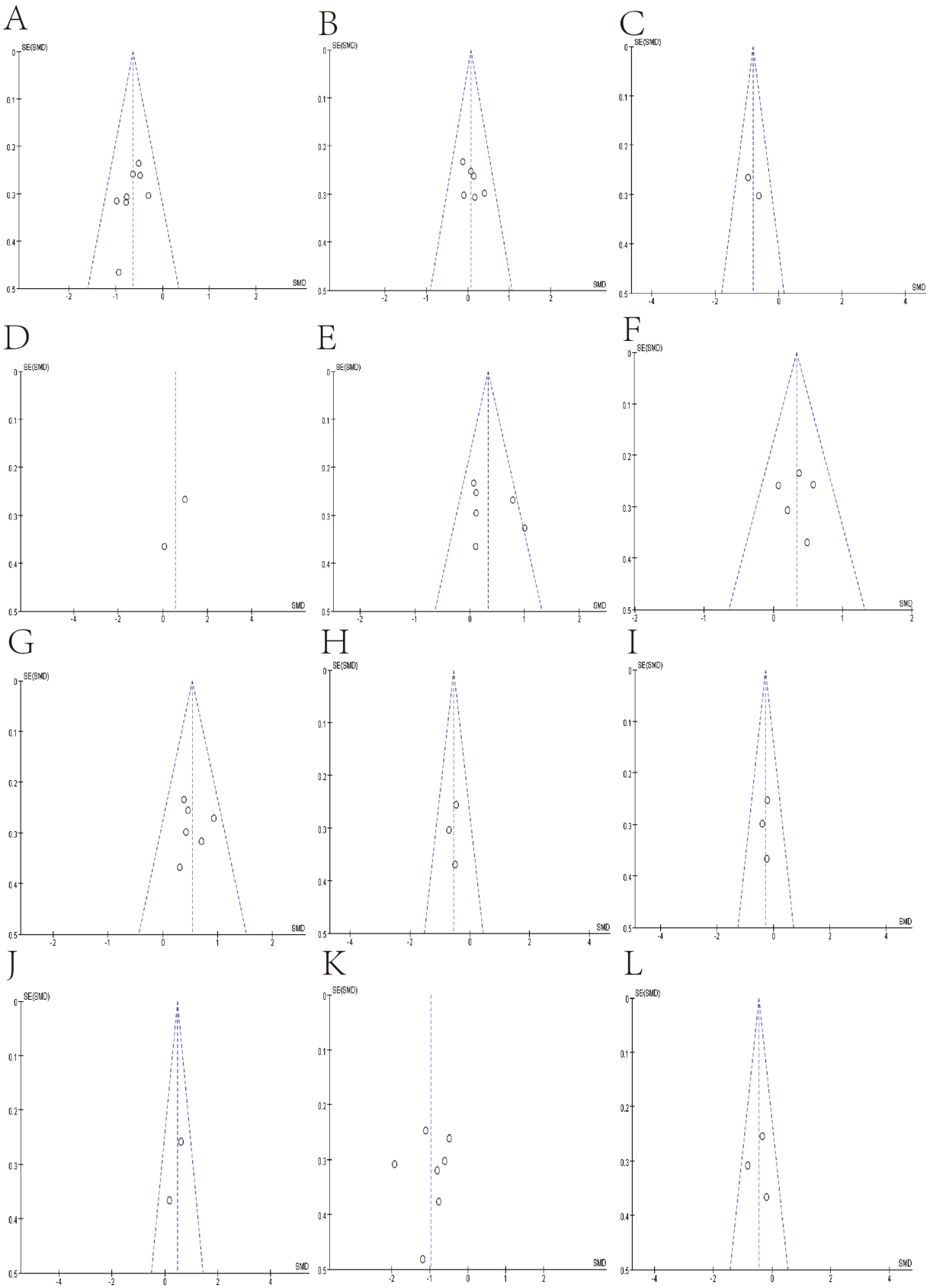

FIGURE 7
Funnel plot of Relative abundance of bacteria in gut between SCI and non-SCI control. **(A)** Firmicutes, **(B)** Bacteroidetes, **(C)** Clostridiales, **(D)** Atopobium, **(E)** Bacteroides. **(F)** Bifidobacterium, **(G)** Blautia, **(H)** Coprococcus, **(I)** Dorea, **(J)** Eubacterium, **(K)** Faecalibacterium, and **(L)** Lachnospira,

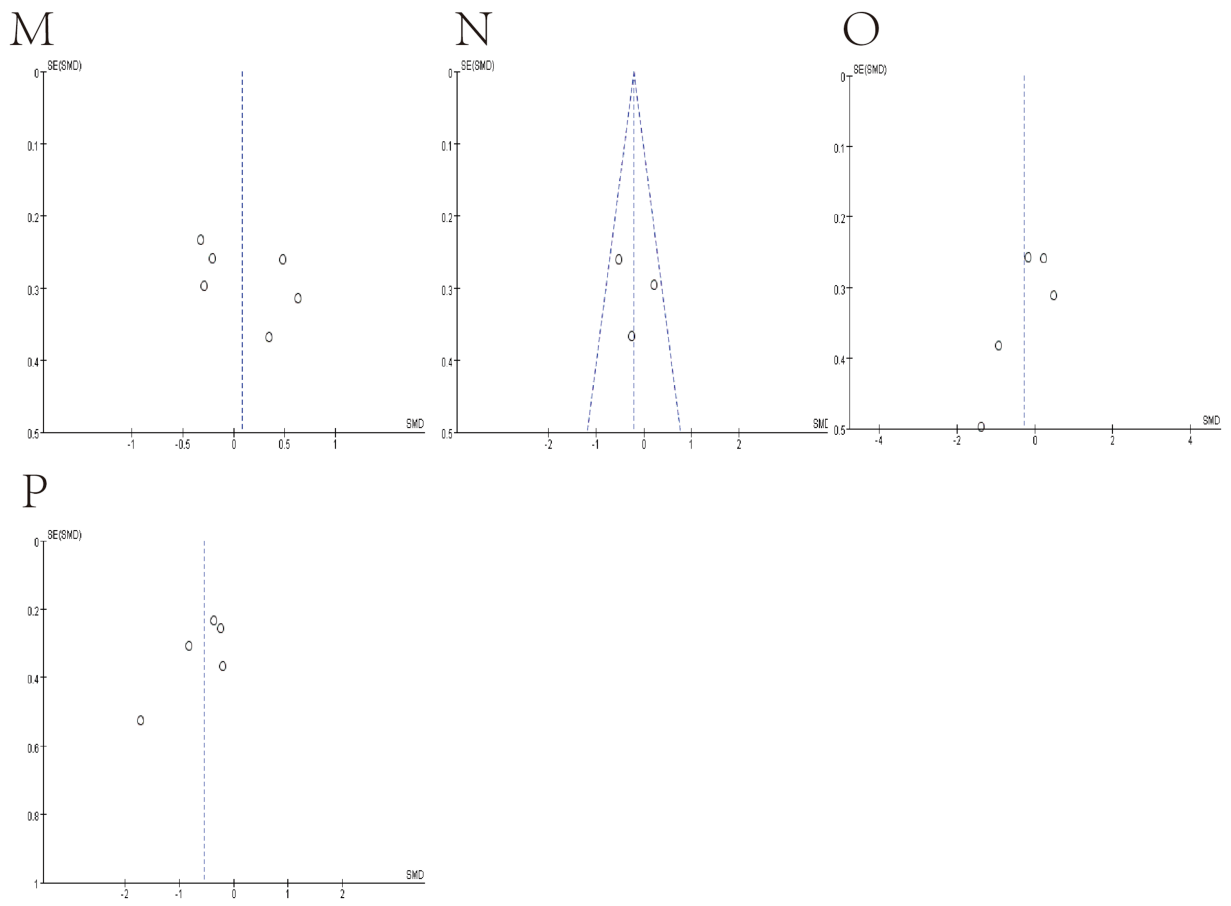

FIGURE 8
Funnel plot of Relative abundance of bacteria in gut between SCI and non-SCI control. (M) Lactobacillus, (N) Prevotella, (O) Roseburia and (P) Ruminococcus.

TABLE 4 Egg's test results of bacteria.

Bacteria	*p* value of Egg's test
Firmicutes	0.7672
Bacteroidetes	0.3081
Atopobium	–
Bacteriodes	0.0943
Bifidobacterium	0.3694
Blautia	0.6368
Clostridiales	–
Coprococcus	0.3488
Dorea	0.181
Faecalbacterium	0.3241
Lachnospira	0.3425
Lactobacillus	0.8412
Prevotella	0.0959
Roseburia	0.235
Ruminococcus	0.11

mice increased, and bacteria in the gut entered and spread with the bloodstream, activating pathological immune responses in the gut-associated lymphoid tissues, while these bacteria translocated throughout the body caused systemic inflammation. Supplementation of probiotics rich in Lactobacillus in mice with spinal cord injury was observed to reduce pathological immune responses in intestinal mucosal lymph nodes, mainly through activation of regulatory T lymphocytes. Lactobacillus may benefit mice with spinal cord injury by reducing the translocation of intestinal bacteria and regulating the immune response in the intestinal mucosal lymph nodes (Kigerl et al., 2016). During the subacute phase, the abundance of Lactobacillus decreases, possibly because it is more prone to leakage from the intestine, thereby affecting the recovery of host motor function. The impact of Lactobacillus on spinal cord injury deserves further research.

The role of SCFAs in the nervous system is increasingly being revealed through research. After supplementation with SCFA in mice with spinal cord injury, it was observed that astrocyte proliferation decreased, microglial activation was inhibited, NF- κ B signal transduction was downregulated, and lower levels of neuroinflammation and better motor recovery compared to the sham surgery group (Jing et al., 2023). In a mouse model of chronic cerebral hypoperfusion, SCFAs inhibit the NF-κB pathway and activate the Erk1/2 cascade, subsequently reducing neuroinflammation and neuronal apoptosis in the hippocampus after injury (Xiao et al., 2022). After atorvastatin treatment, Firmicutes and Lactobacillus increased, Bacteroidetes decreased, and neuroinflammation of ischemic stroke mice was attenuated (Zhang et al., 2021). 10-strain isolated from the infant's gut as a probiotic cocktail to treat mice modulated the gut microbiome,

TABLE 5 Studies that significantly impacted heterogeneity or *p*- value in the meta-analysis.

Bacteria	Heterogeneity (over 30%)	*p*- value (changed over 0.05)
Bacteroides	–	Zhang et al. (2018)
Bifidobacterium	Lin et al. (2020)	Lin et al. (2020)
Blautia	Kong et al. (2023)	Kong et al. (2023)
Eubacterium	–	Yu et al. (2021)
Faecalbacterium	Yu et al. (2021)	–
Ruminococcus	Kong et al. (2023)	–

increased SCFA production, and ameliorated gut microbiome dysbiosis (Nagpal et al., 2018). SCFAs can reach the whole body through the blood, cross the blood–brain barrier, and exert neuroprotective effects, which is an important part of understanding the brain-gut axis (Mitchell et al., 2011).

Our study verified the overall change trend of SCFAs-producing bacteria in human samples during chronic spinal cord injury through meta-analysis. SCFAs-producing bacteria play an essential role in the brain-gut axis and have been shown in multiple animal studies to promote neuromotor function recovery, so increasing the abundance of these bacteria in the gut or avoiding their decline as much as possible (more cautious use of antibiotics) may benefit motor function recovery after spinal cord injury. We hope that our results will provide reference and theoretical support for targeting gut microbiota in patients with spinal cord injury.

5 Conclusion

The genus of potential SCFAs-producing bacteria is lower in the chronic phase of spinal cord injury than in the subacute phase, and gut dysbiosis is present in both the subacute and chronic phases.

Data availability statement

The original contributions presented in the study are included in the article/Supplementary material, further inquiries can be directed to the corresponding author/s.

Author contributions

ZZ: Data curation, Investigation, Methodology, Project administration, Visualization, Writing – original draft. FF: Data curation, Writing – review & editing. JL: Investigation, Supervision, Validation, Writing – review & editing. ZW: Investigation, Supervision, Validation, Writing – review & editing. BW: Investigation, Supervision, Validation, Writing – review & editing. CD: Investigation, Supervision, Validation, Writing – review & editing. LS: Methodology, Project administration, Supervision, Validation, Writing – review & editing.

Funding

The author(s) declare that financial support was received for the research, authorship, and/or publication of this article. This study was supported by a grant from the National Natural Science Foundation of China (no. 81870976), "136" Hospital Open Fund of Shanxi Bethune Hospital by the Shanxi Provincial Health Commission (no. 2021YZ04).

Conflict of interest

The authors declare that the research was conducted in the absence of any commercial or financial relationships that could be construed as a potential conflict of interest.

Publisher's note

All claims expressed in this article are solely those of the authors and do not necessarily represent those of their affiliated organizations, or those of the publisher, the editors and the reviewers. Any product that may be evaluated in this article, or claim that may be made by its manufacturer, is not guaranteed or endorsed by the publisher.

Supplementary material

The Supplementary material for this article can be found online at: https://www.frontiersin.org/articles/10.3389/fmicb.2025.1483794/full#supplementary-material

SUPPLEMENTARY FIGURE S1
Funnel plot of no studies excluded. **(A)** Bacteroidetes, **(B)** Blautia, and **(C)** Bifidobacterium.

SUPPLEMENTARY FIGURE S2
Forest map of no studies excluded. **(A)** Bacteroidetes, **(B)** Blautia, and **(C)** Bifidobacterium.

SUPPLEMENTARY FIGURE S3
Trim-fill method result of **(A)** Bacteroides and **(B)** Prevotella.

SUPPLEMENTARY TABLE S1
Retrieval strategies of this study.

References

Ahuja, C. S., Wilson, J. R., Nori, S., Kotter, M. R. N., Druschel, C., Curt, A., et al. (2017). Traumatic spinal cord injury. *Nat. Rev. Dis. Primers* 3:17018. doi: 10.1038/nrdp.2017.18

Altman, D. G., Bryant, T. N., and Gardner, M. J. (2000). *Statistics with confidence second edition*. BMJ.

Arumugam, M., Raes, J., Pelletier, E., Le Paslier, D., Yamada, T., Mende, D. R., et al. (2011). Enterotypes of the human gut microbiome. *Nature* 473, 174–180. doi: 10.1038/nature09944

Bazzocchi, G., Turroni, S., Bulzamini, M. C., D'Amico, F., Bava, A., Castiglioni, M., et al. (2021). Changes in gut microbiota in the acute phase after spinal cord injury correlate with severity of the lesion. *Sci. Rep.* 11:12743. doi: 10.1038/s41598-021-92027-z

Bolyen, E., Rideout, J. R., Dillon, M. R., Bokulich, N. A., Abnet, C. C., Al-Ghalith, G. A., et al. (2019). Reproducible, interactive, scalable and extensible microbiome data science using QIIME 2. *Nat. Biotechnol.* 37, 852–857. doi: 10.1038/s41587-019-0209-9

Dalile, B., Van Oudenhove, L., Vervliet, B., and Verbeke, K. (2019). The role of short-chain fatty acids in microbiota-gut-brain communication. *Nat. Rev. Gastroenterol. Hepatol.* 16, 461–478. doi: 10.1038/s41575-019-0157-3

Dicks, L. M. T. (2022). Gut Bacteria and neurotransmitters. *Microorganisms* 10:838. doi: 10.3390/microorganisms10091838

Ding, W., Hu, S., Wang, P., Kang, H., Peng, R., Dong, Y., et al. (2022). Spinal cord Injury: the global incidence, prevalence, and disability from the global burden of disease study 2019. *Spine (Phila Pa 1976)* 47, 1532–1540. doi: 10.1097/brs.0000000000004417

Duval, S., and Tweedie, R. (2000). Trim and fill: a simple funnel-plot-based method of testing and adjusting for publication bias in meta-analysis. *Biometrics* 56, 455–463. doi: 10.1111/j.0006-341x.2000.00455.x

GBD 2016 Traumatic Brain Injury and Spinal Cord Injury Collaborators (2019). Global, regional, and national burden of traumatic brain injury and spinal cord injury, 1990-2016: a systematic analysis for the global burden of disease study 2016. *Lancet Neurol.* 18, 56–87. doi: 10.1016/S1474-4422(18)30415-0

Gungor, B., Adiguzel, E., Gursel, I., Yilmaz, B., and Gursel, M. (2016). Intestinal microbiota in patients with spinal cord Injury. *PLoS One* 11:e0145878. doi: 10.1371/journal.pone.0145878

Gur Arie, A., Toren, I., Hadar, R., Braun, T., Efroni, G., Glick Saar, E., et al. (2024). Lack of gut microbiome recovery with spinal cord injury rehabilitation. *Gut Microbes*. 16:2309682. doi: 10.1080/19490976.2024.2309682

He, N., Shen, G., Jin, X., Li, H., Wang, J., Xu, L., et al. (2022). Resveratrol suppresses microglial activation and promotes functional recovery of traumatic spinal cord via improving intestinal microbiota. *Pharmacol. Res.* 183:106377. doi: 10.1016/j.phrs.2022.106377

Higgins, J. P., Thompson, S. G., Deeks, J. J., and Altman, D. G. (2003). Measuring inconsistency in meta-analyses. *BMJ* 327, 557–560. doi: 10.1136/bmj.327.7414.557

Jandhyala, S. M., Talukdar, R., Subramanyam, C., Vuyyuru, H., Sasikala, M., and Nageshwar Reddy, D. (2015). Role of the normal gut microbiota. *World J. Gastroenterol.* 21, 8787–8803. doi: 10.3748/wjg.v21.i29.8787

Jing, Y., Yang, D., Bai, F., Wang, Q., Zhang, C., Yan, Y., et al. (2023). Spinal cord injury-induced gut dysbiosis influences neurological recovery partly through short-chain fatty acids. *NPJ Biofilms Microbiomes* 9:99. doi: 10.1038/s41522-023-00466-5

Jing, Y., Yang, D., Bai, F., Zhang, C., Qin, C., Li, D., et al. (2019). Melatonin treatment alleviates spinal cord Injury-induced gut Dysbiosis in mice. *J. Neurotrauma* 36, 2646–2664. doi: 10.1089/neu.2018.6012

Jing, Y., Yu, Y., Bai, F., Wang, L., Yang, D., Zhang, C., et al. (2021). Effect of fecal microbiota transplantation on neurological restoration in a spinal cord injury mouse model: involvement of brain-gut axis. *Microbiome* 9:59. doi: 10.1186/s40168-021-01007-y

Jogia, T., and Ruitenberg, M. J. (2020). Traumatic spinal cord Injury and the gut microbiota: current insights and future challenges. *Front. Immunol.* 11:704. doi: 10.3389/fimmu.2020.00704

Khan, A., Park, T. J., Ikram, M., Ahmad, S., Ahmad, R., Jo, M. G., et al. (2021). Antioxidative and anti-inflammatory effects of Kojic acid in Aβ-induced mouse model of Alzheimer's disease. *Mol. Neurobiol.* 58, 5127–5140. doi: 10.1007/s12035-021-02460-4

Kigerl, K. A., Hall, J. C., Wang, L., Mo, X., Yu, Z., and Popovich, P. G. (2016). Gut dysbiosis impairs recovery after spinal cord injury. *J. Exp. Med.* 213, 2603–2620. doi: 10.1084/jem.20151345

Kong, G., Zhang, W., Zhang, S., Chen, J., He, K., Zhang, C., et al. (2023). The gut microbiota and metabolite profiles are altered in patients with spinal cord injury. *Mol. Brain* 16:26. doi: 10.1186/s13041-023-01014-0

Li, H., Xiang, Y., Zhu, Z., Wang, W., Jiang, Z., Zhao, M., et al. (2021). Rifaximin-mediated gut microbiota regulation modulates the function of microglia and protects against CUMS-induced depression-like behaviors in adolescent rat. *J. Neuroinflammation* 18:254. doi: 10.1186/s12974-021-02303-y

Li, J., Van Der Pol, W., Eraslan, M., McLain, A., Cetin, H., Cetin, B., et al. (2022). Comparison of the gut microbiome composition among individuals with acute or long-standing spinal cord injury vs. able-bodied controls. *J Spinal Cord Med.* 45, 91–99. doi: 10.1080/10790268.2020.1769949

Lin, R., Xu, J., Ma, Q., Chen, M., Wang, L., Wen, S., et al. (2020). Alterations in the fecal microbiota of patients with spinal cord injury. *PLoS One* 15:e0236470. doi: 10.1371/journal.pone.0236470

Luo, D., Wan, X., Liu, J., and Tong, T. (2018). Optimally estimating the sample mean from the sample size, median, mid-range, and/or mid-quartile range. *Stat. Methods Med. Res.* 27, 1785–1805. doi: 10.1177/0962280216669183

Mitchell, R. W., On, N. H., Del Bigio, M. R., Miller, D. W., and Hatch, G. M. (2011). Fatty acid transport protein expression in human brain and potential role in fatty acid transport across human brain microvessel endothelial cells. *J. Neurochem.* 117, 735–746. doi: 10.1111/j.1471-4159.2011.07245.x

Nagpal, R., Wang, S., Ahmadi, S., Hayes, J., Gagliano, J., Subashchandrabose, S., et al. (2018). Human-origin probiotic cocktail increases short-chain fatty acid production via modulation of mice and human gut microbiome. *Sci. Rep.* 8:12649. doi: 10.1038/s41598-018-30114-4

Page, M. J., McKenzie, J. E., Bossuyt, P. M., Boutron, I., Hoffmann, T. C., Mulrow, C. D., et al. (2021). The PRISMA 2020 statement: an updated guideline for reporting systematic reviews. *BMJ* 372:n71. doi: 10.1136/bmj.n71

Pang, R., Wang, J., Xiong, Y., Liu, J., Ma, X., Gou, X., et al. (2022). Relationship between gut microbiota and lymphocyte subsets in Chinese Han patients with spinal cord injury. *Front Microbiol.* 13:986480. doi: 10.3389/fmicb.2022.986480

Rong, Z., Huang, Y., Cai, H., Chen, M., Wang, H., Liu, G., et al. (2021). Gut microbiota disorders promote inflammation and aggravate spinal cord Injury through the TLR4/MyD88 signaling pathway. *Front. Nutr.* 8:702659. doi: 10.3389/fnut.2021.702659

Schmidt, E. K. A., Raposo, P. J. F., Torres-Espin, A., Fenrich, K. K., and Fouad, K. (2021). Beyond the lesion site: minocycline augments inflammation and anxiety-like behavior following SCI in rats through action on the gut microbiota. *J. Neuroinflammation* 18:144. doi: 10.1186/s12974-021-02123-0

Shi, J., Luo, D., Wan, X., Liu, Y., Liu, J., Bian, Z., et al. (2023). Detecting the skewness of data from the five-number summary and its application in meta-analysis. *Stat. Methods Med. Res.* 32, 1338–1360. doi: 10.1177/09622802231172043

Shi, J., Luo, D., Weng, H., Zeng, X. T., Lin, L., Chu, H., et al. (2020). Optimally estimating the sample standard deviation from the five-number summary. *Res. Synth. Methods* 11, 641–654. doi: 10.1002/jrsm.1429

Turroni, S., Brigidi, P., Cavalli, A., and Candela, M. (2018). Microbiota-host Transgenomic metabolism, bioactive molecules from the inside. *J. Med. Chem.* 61, 47–61. doi: 10.1021/acs.jmedchem.7b00244

Vacca, M., Celano, G., Calabrese, F. M., Portincasa, P., Gobbetti, M., and De Angelis, M. (2020). The controversial role of human gut Lachnospiraceae. *Microorganisms* 8:573. doi: 10.3390/microorganisms8040573

Wan, X., Wang, W., Liu, J., and Tong, T. (2014). Estimating the sample mean and standard deviation from the sample size, median, range and/or interquartile range. *BMC Med. Res. Methodol.* 14:135. doi: 10.1186/1471-2288-14-135

Wells, G. A., O'Connell, D., Peterson, J., Welch, V., Losos, M., et al. (2018). *The Newcastle-Ottawa scale (NOS) for assessing the quality of nonrandomised studies in Meta-analyses*. Available at: https://www.ohri.ca/programs/clinical_epidemiology/oxford.asp.

Xiao, W., Su, J., Gao, X., Yang, H., Weng, R., Ni, W., et al. (2022). The microbiota-gut-brain axis participates in chronic cerebral hypoperfusion by disrupting the metabolism of short-chain fatty acids. *Microbiome* 10:62. doi: 10.1186/s40168-022-01255-6

Yu, B., Qiu, H., Cheng, S., Ye, F., Li, J., Chen, S., et al. (2021). Profile of gut microbiota in patients with traumatic thoracic spinal cord injury and its clinical implications: a case-control study in a rehabilitation setting. *Bioengineered* 12, 4489–4499. doi: 10.1080/21655979.2021.1955543

Zhang, Z., Cheng, N., Liang, J., Deng, Y., Xiang, P., Hei, Z., et al. (2023). Gut microbiota changes in animal models of spinal cord injury: a preclinical systematic review and meta-analysis. *Ann. Med.* 55:2269379. doi: 10.1080/07853890.2023.2269379

Zhang, P., Zhang, X., Huang, Y., Chen, J., Shang, W., Shi, G., et al. (2021). Atorvastatin alleviates microglia-mediated neuroinflammation via modulating the microbial composition and the intestinal barrier function in ischemic stroke mice. *Free Radic. Biol. Med.* 162, 104–117. doi: 10.1016/j.freeradbiomed.2020.11.032

Zhang, C., Zhang, W., Zhang, J., Jing, Y., Yang, M., Du, L., et al. (2018). Gut microbiota dysbiosis in male patients with chronic traumatic complete spinal cord injury. *J. Transl. Med.* 16:353. doi: 10.1186/s12967-018-1735-9

Zhang, C., Jing, Y., Zhang, W., Zhang, J., Yang, M., Du, L., et al. (2019). Dysbiosis of gut microbiota is associated with serum lipid profiles in male patients with chronic traumatic cervical spinal cord injury. *Am J Transl Res.* 11, 4817–4834.

frontiers | Frontiers in Microbiomes

TYPE Brief Research Report
PUBLISHED 05 March 2025
DOI 10.3389/frmbi.2025.1454909

Check for updates

OPEN ACCESS

EDITED BY
Camilla Mauzy,
Wright-Patterson Air Force Base,
United States

REVIEWED BY
Jean Debédat,
University of California, Davis, United States
Muhammad Tanweer Khan (mtk),
University of Gothenburg, Sweden

*CORRESPONDENCE
Cassandra M. Flynn
cmf050@mun.ca
Qi Yuan
qyuan@mun.ca

RECEIVED 25 June 2024
ACCEPTED 11 February 2025
PUBLISHED 05 March 2025

CITATION
Flynn CM, Blackburn LM and Yuan Q (2025) Probiotic supplementation prevents stress-impaired spatial learning and enhances the effects of environmental enrichment. *Front. Microbiomes* 4:1454909. doi: 10.3389/frmbi.2025.1454909

COPYRIGHT
© 2025 Flynn, Blackburn and Yuan. This is an open-access article distributed under the terms of the Creative Commons Attribution License (CC BY). The use, distribution or reproduction in other forums is permitted, provided the original author(s) and the copyright owner(s) are credited and that the original publication in this journal is cited, in accordance with accepted academic practice. No use, distribution or reproduction is permitted which does not comply with these terms.

Probiotic supplementation prevents stress-impaired spatial learning and enhances the effects of environmental enrichment

Cassandra M. Flynn*, Lara M. Blackburn and Qi Yuan*

Biomedical Sciences, Faculty of Medicine, Memorial University of Newfoundland, St. John's, NL, Canada

Probiotics are live microorganisms that offer health benefits, influencing the microbiota-gut-brain axis. Probiotics can improve cognitive functions, including learning and memory, by modulating the gut microbiota, reducing inflammation, and producing neuroactive substances. This study examined the effects of probiotic supplementation prior to chronic stress or enrichment (EE) treatment on cognitive function and brain physiology. Rats received probiotics or control diet starting at 6 months of age for 3 months. They were then randomly assigned to unpredictable stress, or EE for 6 weeks, with a home cage control group on a control diet included. Results showed that probiotic supplementation prevented spatial memory impairments induced by chronic stress and enhanced learning when combined with EE. These behavioral improvements were linked to increased gut microbiome diversity. Higher levels of the microglia marker Iba-1 were found in the stressed group compared to the EE group in the locus coeruleus, which probiotic reversed. Differences in blood-brain-barrier integrity were observed between the stress and EE groups, as indicated by albumin levels. Higher levels of tyrosine hydroxylase were observed in the hippocampus of the EE groups. The interaction of probiotic supplementation, chronic stress, and environmental EE offers a promising area for enhancing cognitive function and brain health.

KEYWORDS

gut-brain axis, inflammation, probiotic, spatial learning, stress

1 Introduction

Chronic stress negatively impacts learning and behavior, and increases susceptibility to age-related diseases, including Alzheimer's disease (AD), by disrupting cognitive processes, healing mechanisms, coping abilities, and overall quality of life (Polsky et al., 2022; Sotiropoulos et al., 2011; Torraville et al., 2023). Activation of neurobiological stress responses, such as the sympathetic nervous system and the hypothalamic-pituitary-adrenal (HPA) axis, contributes to higher morbidity and mortality rates, highlighting the profound impact of chronic stress on health and aging (Schneiderman et al., 2005; Shields and Slavich, 2017).

The locus coeruleus (LC)-noradrenergic system is critically involved in stress-related disorders, with its dysregulation negatively impacting health and cognition (Suárez-Pereira et al., 2022). Noradrenergic neurons project to the hypothalamus and key structures involved in learning and memory, therefore, stress-induced alterations in LC health and norepinephrine release can significantly impair brain function (Wang et al., 2017). Additionally, stress hormones impair hippocampal function via glucocorticoid receptors, affecting various types of memories (Lupien et al., 2018). Chronic stress also disrupts microglial function, potentially compromising brain homeostasis and contributing to anxiety phenotypes (Chen et al., 2024).

In contrast, environmental enrichment (EE) promotes cognitive health and resilience by providing cognitive, sensory, and motor stimulation that enhances brain plasticity and cognitive reserve (Mandolesi et al., 2017; Torraville et al., 2023). EE fosters neurobiological adaptations, such as improved learning and memory, increased neurotrophic factors, enhanced hippocampal neurogenesis, and improved synaptic connections (Mora et al., 2007; Van Praag et al., 2000; Segovia et al., 2009; Leggio et al., 2005), which collectively fortify brain health against age-related cognitive decline and neurodegenerative diseases (Rolland et al., 2008; Marx, 2005).

Emerging research highlights the interaction between gut microbiota and stress. The gut microbiota, comprising trillions of microorganisms in the gastrointestinal tract, plays a critical role in nutrient metabolism, immune modulation, and overall health (Thursby and Juge, 2017). Maintaining a balanced gut microbiome is essential for health, as disruptions, known as microbial dysbiosis, can lead to inflammation and accelerated aging (Thevaranjan et al., 2017). Stress alters gut microbiota composition and function by affecting gastrointestinal motility, increasing gut permeability, and influencing microbial growth (Ulrich-Lai and Herman, 2009; Van Wijck et al., 2012; Galley and Bailey, 2014).

Probiotics, live microorganisms conferring health benefits, have gained attention for their potential to modulate gut microbiota composition, enhance gut health, and improve immunity (Liu et al., 2021). Lactobacillus and Bifidobacterium species, extensively studied for their stress-alleviating, gastrointestinal barrier-enhancing, and anti-inflammatory effects, may also impact neurobiological pathways involved in stress resilience and cognitive function (Arseneault-Bréard et al., 2012; Moya-Pérez et al., 2017; Liu et al., 2020), though the exact mechanisms remain unclear.

Our study investigates whether probiotic supplementation can alter the brain's response to chronic stress and amplify the positive effects of EE on cognition, and brain health. By exploring these interactions, we aim to uncover mechanisms through which probiotics may mitigate stress-induced effects and cognitive resilience and overall brain health.

2 Materials and methods

2.1 Subjects and ethics statement

Sprague-Dawley rats of both sexes were used. Rats were kept in a standard 12-hour light–dark cycle, with food and water *ad libitum* except during the probiotic feeding stage. The regular water was filtered three times (0.2 microns) and the diet (Catalog number: Teklad 2018) was irradiated. Experimental procedures were approved by the Institutional Animal Care Committee at Memorial University of Newfoundland and followed the Canadian Council's Guidelines on Animal Care.

2.2 Experimental design

Figure 1A shows the flow of the experiment. Rats underwent diet supplementation at 6 months of age, for 3 months. Following that, animals underwent randomly assigned stress and EE, or cage control paradigms daily for 6 weeks, from 9–10 months of age. Animals then underwent a battery of behavioral tasks to assess general behavior and cognitive function before being sacrificed for Immunohistochemistry and Western Blot assays. A separate cohort of animals had fecal collection following probiotic supplementation, for 16S rRNA sequencing and gut microbiome analysis. Surfaces were sterilized with 70% ethanol, cages and toys were autoclaved.

Rats were randomly assigned to five conditions, (1) Cage (control without stress or EE manipulation + control diet), (2) Stress (STR) (stress paradigm + control diet), (3) STR + P/P (stress paradigm + probiotic/prebiotic diet), (4) EE (EE paradigm + control diet), or (5) EE + P/P (EE paradigm + probiotic/prebiotic diet). Groups were sex balanced.

2.3 Probiotic diet supplementation

ProBiotic-4, comprised of *Bifidobacterium Lactis* (50%), *Lactobacillus casei* (25%), *Bifidobacterium bifidum* (12.5%), and *Lactobacillus acidophilus* (12.5%), were purchased from Swanson (Fargo, ND, USA). Rats received ProBiotic-4 (3 × 109 CFU) once daily for three months at 6–9 months of age, dissolved in 30 ml water (Yang et al., 2020), for a final concentration of 10.9 CFU/ml daily. The prebiotics were mixed with prebiotic oligofructose/FOS Orafti® P95 powder (200 mg/kg; Quadra Chemicals) (Li et al., 2023), to improve the effectiveness of probiotics (Roy and Dhaneshwar, 2023). Regular water was provided only after the probiotic mixture was fully consumed, ensuring that the rats received the entire dose of the probiotics. Control rats received regular water only. Body weight was measured bi-weekly.

2.4 Stress paradigms

Stress paradigms were implemented using a chronic unpredictable stress paradigm for six weeks from 9–10 months of age following a protocol similar to those previously described (Yalcin et al., 2005; Zhou et al., 2019; Strekalova et al., 2022). Stressors were applied for the same 2 hours per day for the duration, including restraint, wetted bedding, tilted cage, and an irregular light cycle.

2.5 EE paradigms

EE paradigms were implemented by placing 4–5 animals together in a 60 × 60 × 50 cm Plexiglas play arena for 2 hours per day for six weeks, at 9–10 months of age (Leggio et al., 2005).

10.3389/frmbi.2025.1454909

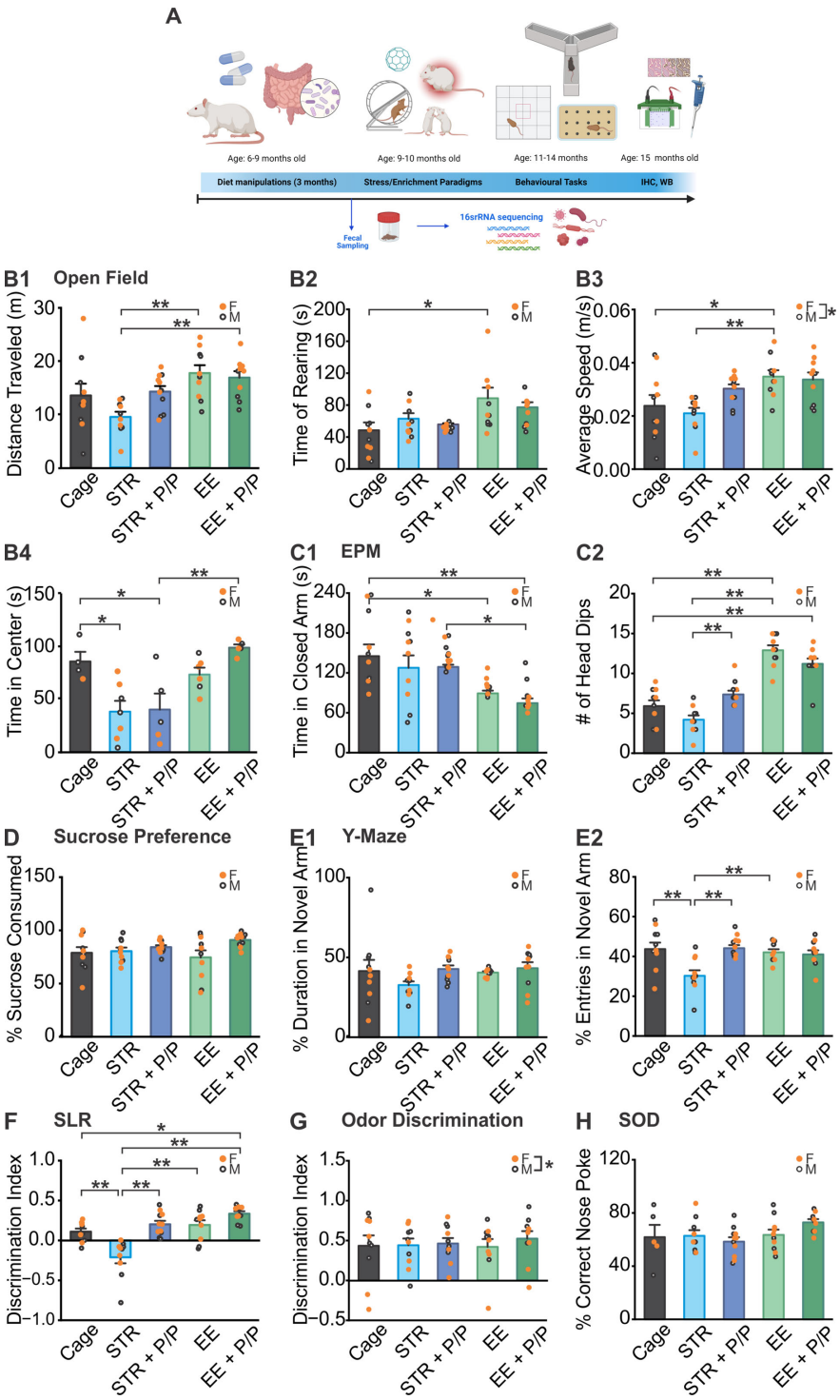

FIGURE 1
The effects of probiotics in combination with stress and EE on behavioral tasks. **(A)** Schematic of experimental design timeline. A separate cohort with probiotic or control diet was used for fecal sampling. **(B1–B4)** Distance traveled **(B1)**, time spent rearing **(B2)**, average speed **(B3)** and time spent in center **(B4)** measurements in an open field maze test. **(C1, C2)**. Time spent in the closed arm **(C1)** and number of head dips over the edge **(C2)** in an elevated plus maze (EPM) test. **(D)** Percentage of sucrose solution consumption over a 24 hr period. **(E1, E2)**. Percentage of time **(E1)** and number of entries **(E2)** in the novel arm in a Y-maze test. **(F)** Discrimination index in a spontaneous location recognition (SLR) task. **(G)** Discrimination index in an odor discrimination task. **(H)** Percentage of correct nose poke in standard object discrimination (SOD) task. STR, stress; EE, environmental enrichment; P/P, probiotic + prebiotic; N (except B4): Cage: 5F/5M; STR: 5F/5M; STR + P/P Diet: 6F/5M; EE: 5F/5M; EE + P/P Diet: 6F/4M. N **(B4)**: Cage: 1F/3M; STR: 4F/3M; STR + P/P Diet: 2F/3M; EE: 4F/2M; EE + P/P Diet: 3F/2M *$p < 0.05$, **$p < 0.01$. Source: **(A)** Created with BioRender.com.

The play arena contained toys, exercise equipment, and treats. Males and female animals were separated into different arenas.

2.6 Fecal collection

Fecal samples were collected from a separate set of female rats following probiotic or control diet feeding. Animals were placed in clean autoclaved cages, where freshly voided fecal material was collected in sterile centrifuge tubes before being stored at −80°C until DNA extraction.

2.7 DNA extraction from feces

Isolation of microbial genomic DNA from each animal's stool sample was performed using the QIAamp PowerFecal Pro DNA Kit (Qiagen, Hilden, Germany) as per the manufacturer's instruction.

Prior to storage, quality control measures were implemented to evaluate DNA purity via the Thermo ScientificTM NanoDropTM One Spectrophotometer (Thermo ScientificTM 840274100). The DNA concentration from 1µl of each sample was determined by absorbance at 260nm (A260), and the purity was estimated by determining the A260/A280 ratio with the Nanodrop spectrophotometer, then samples were stored in -20°C until shipment.

2.8 Microbiome analysis

16S rRNA sequencing was performed at the Integrated Microbiome Resource (Dalhousie University, Halifax, Canada). Only samples from female rats were included. The V6–V8 bacterial region of 16S rRNA genes was analyzed as previously described (Comeau et al., 2011). The library was sequenced on an Illumina MiSeq platform.

2.9 Behavioral testing

2.9.1 Exploratory, anxiety and depressive behavior

Rats were given one 10-minute trial to explore an open field (60 × 60 × 40.5 cm^3) and recorded with ANY-Maze software (Stoelting). Distance traveled, time spent rearing (including free and supported rearing), average speed, and time spent in center (indicating the level of anxiety) were recorded and analyzed offline as previously described (Omoluabi et al., 2021).

Anxiety was measured by the open field behavior, a 5 minute Elevated Plus Maze trial (50 × 10 cm^2/arm with an 11 × 11 cm^2 central platform, 38 cm walls on the closed arms), where time spent inside closed arms vs. open arms as well as head dips over the open arms were analyzed. Depressive behavior was measured by 24 hours sucrose (0.75%) percentage consumption.

2.9.2 Spatial memory assessments

To assess short-term spatial memory, the Y-maze was used and to assess long-term spatial memory, animals underwent the spontaneous location recognition (SLR) task.

In the Y-maze, animals explored a black opaque Plexiglas Y-shaped maze with three arms 120 apart (50 cm × 16 cm × 32 cm^3). For the training phase, animals had a 15-minute trial in which they were allowed to freely explore two of three arms. Which of the arms was closed for this training phase was counterbalanced between groups and animals. For the testing phase, animals were re-placed into the same "start" arm for another 15-minute trial and allowed to explore the full maze with all three arms open, with the previously closed arm considered to be the "novel" arm. Number of entries into the arms and duration in each arm was recorded for analysis (Dellu et al., 1992).

For the SLR task, rats were given 10 minutes in an open arena (60 × 60 × 40.5 cm^3) with three identical objects (1, 2, and 3) placed at specific positions. During testing (24 hours later), rats were placed in the same arena with two identical objects, one in the same position as Object 1 (a familiar location, F), the other midway between previous Objects 2 and 3 (a novel location, N). The discrimination ratio was the difference between time spent at the novel and familiar objects over the total time spent on both objects (Bekinschtein et al., 2013).

2.9.3 Odor discrimination task

Discrimination of similar odors was tested with an odor detection and discrimination task (ODAD), using perforated micro-centrifuge tube containing filter paper with 60 µl of odorant or mineral oil. The first three trials used odorless mineral oil, the next three trials used odor 1 (O1, 1-heptanol, 0.001%), and the last trial used an odor mixture that had a similar smell to O1 (O2, 1-heptanol and 1-octanol in a 1:1 ratio, 0.001%). The discrimination index was the ratio of the sniffing time difference between the O2 and the third presentation of O1 to the total sniffing time (tO2-tO1-3)/(tO2+tO1-3).

2.9.4 Odor associative learning

Rats were food deprived for 3–6 days before the onset of the experiments and food deprivation continued during the experiment. Rats were placed in an open arena (60 × 60 × 40.5 cm^3) with 2 scented sponges, and Reese's puff cereal was used as a food reward. This procedure consisted of a habituation phase, followed by an associative training phase. In the habituation phase, rats were exposed to an unscented sponge placed in random locations, baited with food.

In the associative training phase, rats were placed in a designated home corner and presented with 2 scented sponges (locations varied each trial randomly) and given a maximum of 300 s to retrieve the cereal pellet from a retrievable center hole in one scented sponge. Percentage of correct responses was counted as the number of correct responses over the number of total nose pokes.

2.10 Immunohistochemistry and imaging

LC tissue was extracted after decapitation and stored in 4% paraformaldehyde before being transferred to 20% sucrose in 0.1 M phosphate-buffered saline (PBS). Fifty µm sections at 150 µm intervals were collected in PVP cryoprotectant for free-floating IHC.

All histology and IHC followed established procedures (Ghosh et al., 2019; Omoluabi et al., 2021). Primary antibodies used included: Ionized calcium-binding adaptor molecule 1 (Iba1) (019-19741, Wako, 1:2000), and Albumin (16475-l-AP, ProteinTech, 1:1000). Alexa Fluor secondary antibodies (Invitrogen, 1:1000) were used.

Bright-field and fluorescence microscopy used an Olympus BX53 (Olympus) and EVOS M5000 imaging system (Thermo Fisher Scientific), respectively. Image analysis was conducted with ImageJ. The light intensity and exposure parameters were standardized across all captured images. In the LC, the numbers of positive stained cells for Iba-1 were counted and normalized to the region of interest (/mm^2). Albumin expression was measured as the mean density of the fluorescence in the LC, normalized to the background level in the lateral vestibular nucleus (Kelly et al., 2019). Three sections of each marker within the same rostral to caudal range were used from all animals and counts from the two hemispheres were averaged. Analysis was conducted by experimenters that were blind to the experimental conditions.

2.11 Western blotting

Hippocampal tissue was extracted after decapitation and stored frozen. Brain tissue processing followed established protocols (Morrison et al., 2013). Total protein concentration was quantified by standard Pierce BCA protein assay kit (Thermo Scientific, 23225). Equal amounts of protein (20 µg) were separated by SDS-PAGE on 10% gels and were then transferred to Immobilon-P Transfer PVDF membranes (Merck Millipore, IPVH00010). Following transfer, the membranes were briefly rinsed with 1× low salt TBS-T (containing 1.5M NaCl, 1M Tris Base and 0.1% Tween 20) and blocked for 1 hr with 5% nonfat skim milk at room temperature. They were then incubated for 2 hrs at room temperature with the following antibodies: Glucocorticoid receptor (GR; AB92627, Abcam, 1:2000), Tumour Necrosis Factor alpha (TNFa; AB6671, Abcam, 1:2000), tyrosine hydroxylase (TH; MAB318, Millipore Sigma, 1:2000). The membranes were rinsed in TBS-T (containing 5M NaCl, 1M Tris Base and 0.1% Tween 20) and incubated for 1.5 hrs at room temperature, with either horseradish peroxidase-labeled anti-rabbit immunoglobulin G (IgG; 31460, 1:4000) or anti-mouse IgG (31430, Thermo Fisher Scientific, 1:4000). The protein bands were visualized using chemiluminescent substrate (ThermoFisher Supersignal West PICO, 34577) on a digital image scanner (ImageQuant LAS 4000) and quantified with the ImageJ software.

2.12 Statistical analysis

All data are shown as mean ± standard error of the mean. Statistical analysis was conducted with OriginPro 2022b software. The 16S rRNA data were analyzed using statistical tools provided by MicrobiomeAnalyst.ca. For the analysis of the sequencing data, QIIME used was for initial quality filtering, operational taxonomic unit (OTU) picking, and taxonomic assignment. Following this, in MicrobiomeAnalyst, we applied several data processing steps to ensure the integrity and accuracy of our results. Features with identical values across all samples were excluded to enhance differential analysis, and those appearing in only one sample were removed as artifacts. We employed a low count filter, setting a minimum count threshold of 4, with a 20% prevalence filter to exclude features likely resulting from sequencing errors or low-level contamination. Additionally, we applied a low variance filter, excluding features with minimal variance across conditions, as measured by the inter-quantile range (IQR). Data were scaled using the default Total Sum Scaling (TSS) method to normalize sample sizes. Importantly, the data were not rarefied or transformed prior to analysis.

Alpha diversity was assessed using the Chao1 index, and differences between the two groups were evaluated with a t-test. Beta diversity was quantified using the Bray-Curtis index, and statistical significance was determined via PERMANOVA. Additionally, heat tree analysis, which leverages the hierarchical structure of taxonomic classifications, was used to visualize and compare taxonomic differences between microbial communities. The differences were quantitatively represented using median abundance and statistically evaluated using the non-parametric Wilcoxon Rank Sum test, with FDR (false discovery rate)-adjusted P-value cutoff set at 0.1, and log LDA (linear discriminant analysis) score set at 2.0. Behavioral results were analyzed by two-way ANOVA (group × sex). IHC and Western blotting results were analyzed by three-way ANOVA (treatment × diet × sex). *Post-hoc* Tukey tests were used for group comparisons. Homogeneity of variance was assessed with Levene's test. Normality of the data was assessed with Shapiro-Wilk test, and met before t-tests or ANOVAs. One outlier in the TH measurement with Western blotting (> mean ± 2SD) was removed from the final analysis.

3 Results

3.1 EE increased exploratory behavior while stress induced anxiety

The open field task revealed significant differences between groups in distance traveled ($F_{4,41}$ = 4.732; p = 0.0031; Figure 1B1), rearing ($F_{4,41}$ = 3.781; p = 0.01; Figure 1B2), speed ($F_{4,41}$ = 5.119; p = 0.0019; Figure 1B3), and time spent in center ($F_{4,17}$ = 8.439; p = 6.09E-4; Figure 1B4). Both EE groups regardless of diet type traveled significantly longer distance than the STR group (p < 0.01). In terms of exploration, EE animals spent significantly more time rearing compared to cage control animals (p < 0.05). Similarly, the EE groups had higher travel speed compare to cage (p < 0.05), and STR (p < 0.01) groups. A sex difference was observed ($F_{1,41}$ = 4.395; p = 0.042), with females moving at a higher speed than males. STR animals showed a significantly lower time spent in the center compared to cage groups (p < 0.05), regardless of diet

type. There was no significant diet × sex × time interaction on body weight (Supplementary Figure 1).

Anxiety levels were then measured using the elevated plus maze, with a significant difference observed between groups for time spent in the closed arm ($F_{4,41}$ = 5.394; p = 0.0014; Figure 1C1), no significance was observed between sexes. EE animals spent significantly less time in the closed arm than caged animals regardless of diet type (control diet, $p < 0.05$; probiotic diet, $p < 0.01$). When measuring head dips, another indicator for anxiety level, a significant difference was found between groups ($F_{4,41}$ = 35.7789; $p = 7.18E^{-13}$; Figure 1C2). Similarly, EE and EE + probiotic groups showed significantly higher levels of this behavior over cage ($p < 0.01$). Interestingly, probiotic supplementation significantly increased this exploratory behavior in STR animals compared to control diet-fed ones ($p < 0.01$). No sex differences were observed.

The sucrose preference test assessed the level of anhedonia, as animals with anhedonia are less interested in palatable food. Our result revealed no significant differences in the consumption of sucrose water between groups, or sexes (Figure 1D).

3.2 Probiotic supplementation rescued the spatial learning deficiency in STR rats, and enhanced memory of EE rats

In the Y-maze task, a group × sex interaction was observed in duration of time spent in the novel arm ($F_{4,41}$ = 2.908, p = 0.033; Figure 1E1), although no significant difference was found in the *post-hoc* Tukey test. However, there was a significant difference between groups for the number of entries in the novel arm ($F_{4,41}$ = 6.441, $p = 4.06E^{-4}$; Figure 1E2). Following stress, animals displayed a deficit compared to cage control groups ($p < 0.01$) and EE groups ($p < 0.05$ or $p < 0.01$), and this was prevented by probiotic feeding ($p < 0.01$).

In the SLR task, there was a significant difference between groups ($F_{4,41}$ = 14.508, $p = 1.83E^{-7}$; Figure 1F). A memory deficit was observed for STR animals compared to cage control animals ($p < 0.01$). Like the Y-maze task, this deficit was restored, with a significant increase in discrimination observed in STR + probiotic group ($p < 0.01$). Probiotic feeding in EE animals led to a significantly better discrimination ability than cage ($p < 0.05$) and STR ($p < 0.01$) animals.

Olfactory impairments were tested using a similar odor discrimination task. No differences were observed between groups. Interestingly, in general, male rats performed better than female rats ($F_{1,41}$ = 4.2, p = 0.046; Figure 1G). Additionally, an olfactory dependent rewards association task revealed no differences between groups or sexes (Figure 1H).

3.3 Probiotic supplementation enriches microbiome diversity in the gut

Levels of alpha diversity and beta diversity were obtained from 16S rRNA sequencing. Using the Chao1 index, alpha diversity level, a metric measuring the richness (number of taxa), or evenness (relative abundance of those taxa) was analyzed. A significant increase in microbiome alpha diversity was observed in the probiotic diet groups compared to control diet groups (t = −2.405, p = 0.027; Figure 2A). Levels of beta diversity, representing the diversity and variability of community composition, showed a non-significant increase in beta diversity was observed in the probiotic diet groups, compared to control diet groups (F_{17} = 1.566, p =0.066; Figure 2B).

Changes in the taxa species induced by Probiotic-4 mixture feeding were further assessed (Supplementary Table 1). At the genus level, bacterial taxa were analyzed for abundance levels between groups to observe any effect from the introduction of probiotics (Figure 2C). The heat map in Figure 3C shows average levels of each taxon and significance levels of the probiotic diet groups compared to the control diet using the Wilcoxon test. A labeled taxa is indicative of a significant difference between groups. Overall, 5 taxa genera were increased in abundance in the probiotic diet groups, and one was decreased, compared to control, demonstrating a significant difference in gut microbiome makeup from specific bacterial taxonomic groups. This includes the increase of Actinobacteria (including Bifidobacterium and Rothia species), Ruminococcaceae, Monoglobales, Streptococcaceae, and Barneseillaceae, as well as a decrease of Lachnoclostridium abundance.

3.4 Stress increased levels of microglia in the locus coeruleus compared to EE, which was reversed by probiotic supplementation

LC is critically involved in stress response and novelty-associated EE (Prokopiou et al., 2022; Suárez-Pereira et al., 2022). We therefore tested LC inflammation levels using Iba-1 microglial marker. We also measured blood-brain barrier (BBB) integration with albumin staining. Stress has been shown to impair BBB and probiotic supplementation has been associated with improved BBB (Torraville et al., 2023).

For Iba-1 levels, there was a significant treatment × diet interaction ($F_{1,29}$ = 4.866, p = 0.035; Figures 3A1, 3A2), with STR animals showing a significant increase compared to animals in EE groups ($p < 0.05$ or $p < 0.01$) which was reserved by probiotic supplementation ($p < 0.05$). Albumin levels showed a significant difference between treatment groups ($F_{1,29}$ = 4.811, p = 0.036; Figures 3B1, 3B2), with significantly higher levels in STR animals compared to EE animals ($p < 0.05$). A sex difference was also observed in albumin levels ($F_{1,29}$ = 4.788, p = 0.037), with females showing higher levels of albumin than males.

Furthermore, measurements of GR (Figure 4A), inflammation marker TNFa (Figure 4B), and norepinephrine marker TH (Figure 4C) were conducted in the hippocampus. There were no significant differences among groups in the levels of GR and TNFa. TH levels were higher in the EE treated rats than the STR rats ($F_{1,30}$ = 8.941, p = 0.006; Figure 4C).

4 Discussion

Current research underscores the intricate relationship between stress and the gut microbiota, with probiotic interventions emerging as

10.3389/frmbi.2025.1454909

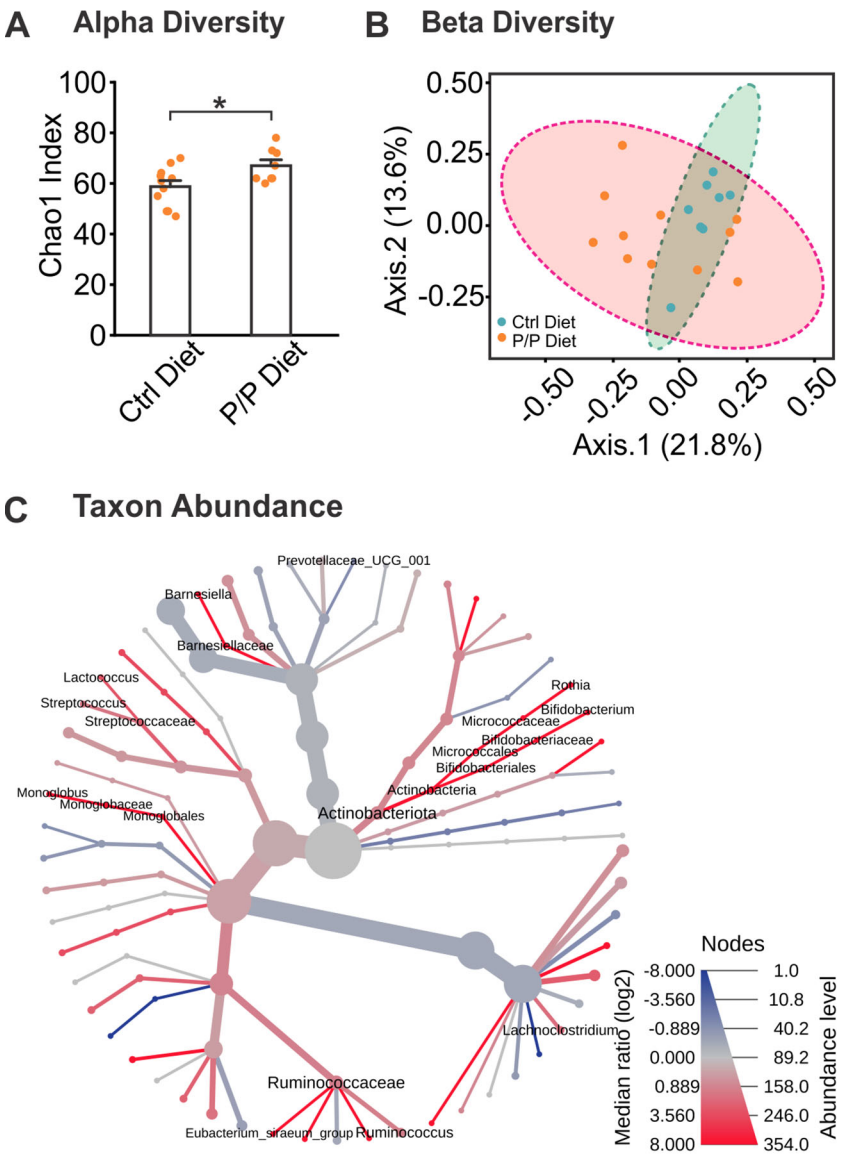

FIGURE 2
Alterations of microbiota in diversity and abundance following probiotic supplementation. **(A)** Chao1 analysis of Alpha Diversity levels between control diet and probiotic-fed groups. **(B)** Ordination plot of Beta Diversity index between diet groups, using Bray-Curtis index distance method. **(C)** A heat tree demonstrating bacterial abundance differences between diet groups. Labeled branches represent a significant abundance level between groups. N: Control diet: 11F; Probiotic diet: 8F. *$p < 0.05$, **$p < 0.01$.

a promising strategy to modulate these interactions. Our study explored the effects of administrating probiotics prior to stress or EE on cognition and inflammation. We observed increased anxiety in animals exposed to chronic stress, while the EE paradigm promoted exploration and reduced anxiety. Probiotic supplementation enhanced gut microbiome diversity, alleviated anxiety, prevented spatial learning impairment in stressed rats, and boosted learning in the EE group. Additionally, chronic stress increased microglial activity (Iba-1) in the LC, a change that probiotics prevented. BBB integrity was lower in stressed animals compared to those in the EE group. Higher tyrosine hydroxylase levels in the hippocampus of enriched groups may correlate with better LC function and axonal release. These findings suggest a mechanistic link between reduced stress, improved gut health, and decreased brain inflammation. Chronic stress can significantly impact the immune system through the microbiota-gut-brain axis, as evidenced by systemic inflammatory increases coinciding with stress and changes in microbiota composition and barrier function (Pasiakos et al., 2016; De Palma et al., 2015; Moya-Pérez et al., 2017). In addition, this response triggers a dysregulated HPA axis, as shown by elevated corticosterone and adrenocorticotropic hormone in germ-free mouse studies (Ackerman et al., 1978). Stress-induced inflammation can exacerbate psychiatric disorders like depression and anxiety, further disrupting gut microbiota composition and creating a vicious cycle of stress and dysbiosis (Li et al., 2019). This cycle is associated with increased intestinal permeability, often referred to as "leaky gut," and increased BBB permeability, which we observed in our study. This

10.3389/frmbi.2025.1454909

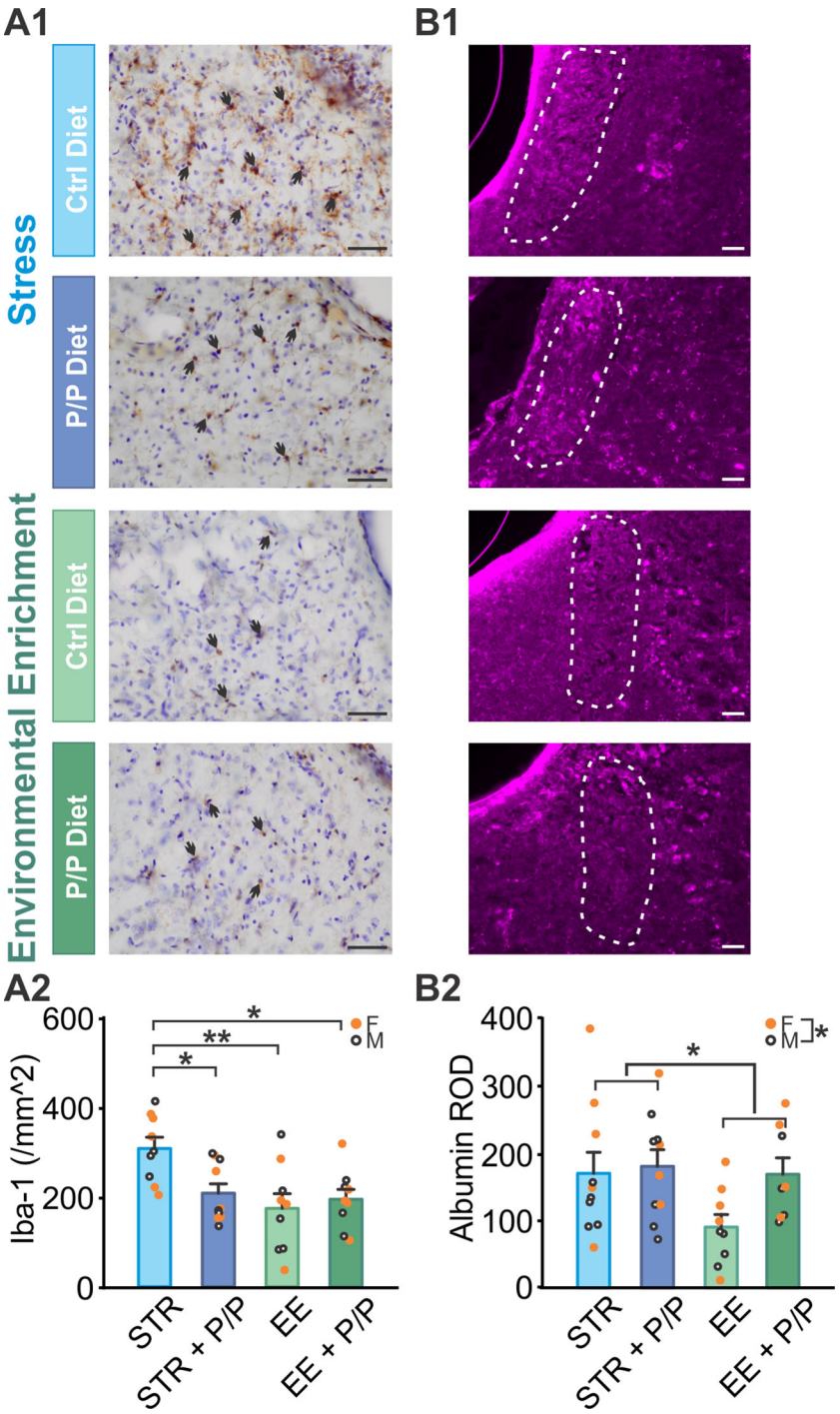

FIGURE 3
The effects of stress, EE and diet manipulation on microglia and albumin levels in the locus coeruleus (LC). **(A1)** Example images of Iba-1 staining in the LC. Arrows indicate positively stained cells. **(A2)** Number of Iba1 cells per mm^2 in the LC. N: STR: 5F/4M; STR + P/P Diet: 5F/5M; EE: 4F/5M; EE + P/P Diet: 5F/4M. **(B1)** Example images of albumin staining in the LC. White circles indicated the LC region. **(B2)** Mean intensity of albumin staining in the LC. N: STR: 5F/5M; STR + P/P Diet: 4F/5M; EE: 5F/4M; ER + P/P Diet: 5F/4M. STR, stress; EE, environmental enrichment; P/P, probiotic + prebiotic. Scale bars: 50 µm. *$p < 0.05$, **$p < 0.01$.

barrier weakening can lead to systemic inflammation and contribute to various health issues (Chatzaki et al., 2003; Dodiya et al., 2020; Welcome and Mastorakis, 2020).

Probiotics, beneficial live microorganisms, can positively influence the gut microbiota and, by extension, the gut-brain axis (Arseneault-Bréard et al., 2012; Moya-Pérez et al., 2017). They help restore the balance of gut microbiota disrupted by stress by outcompeting pathogenic bacteria and promoting the growth of beneficial microbes, thereby improving overall microbiota composition (Dimidi et al., 2017). This restoration can reduce inflammation and enhance both gut and mental health (Arseneault-Bréard et al., 2012; O'Sullivan et al., 2011; Bravo et al., 2011). Notably, our study demonstrates that

10.3389/frmbi.2025.1454909

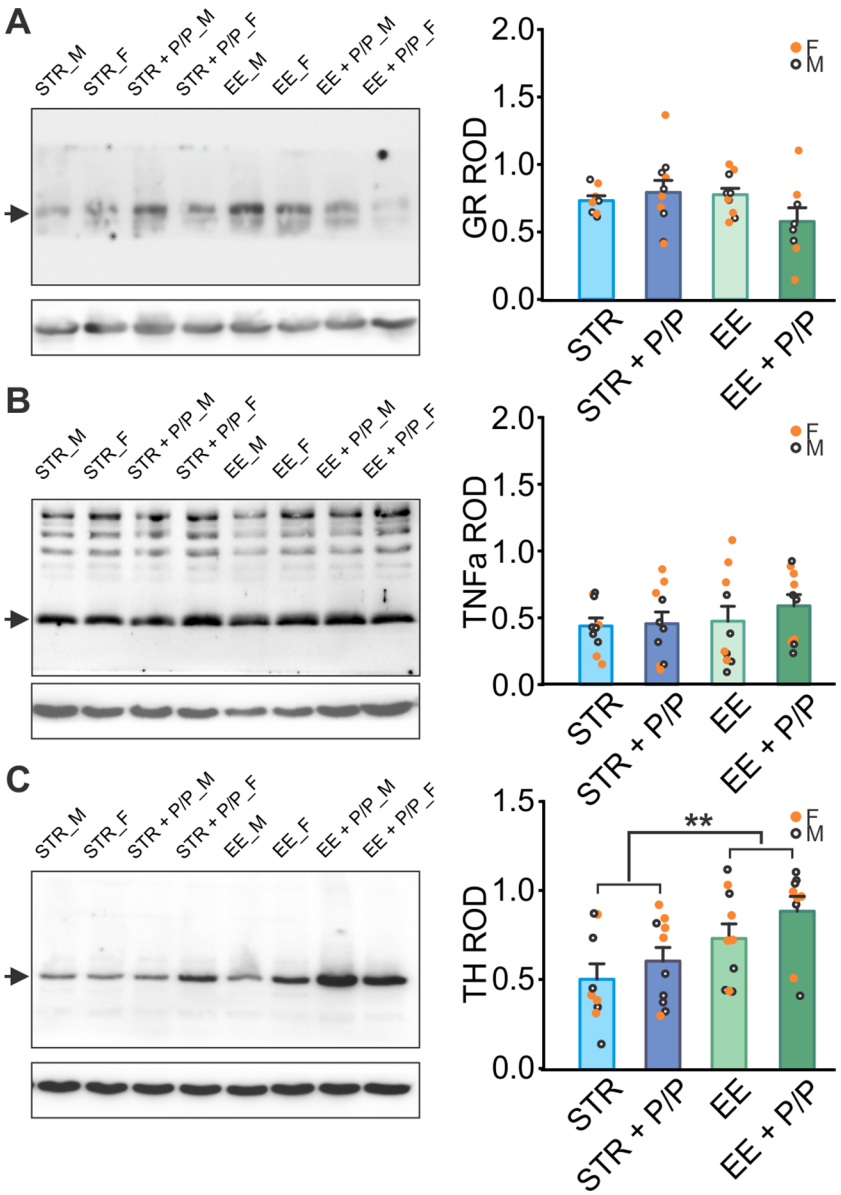

FIGURE 4
The effects of stress, EE and diet manipulation on hippocampal markers. **(A)** Representative blot and quantity of glucocorticoid receptor (GR) normalized to beta-actin levels in the hippocampus. N: STR: 4F/4M; STR + P/P Diet: 5F/5M; EE: 5F/5M; ER + P/P Diet: 4F/4M. **(B)** Representative blot and quantity of Tumour Necrosis Factor aloha (TNFa) normalized to beta-actin levels in the hippocampus. N: STR: 5F/5M; STR + P/P Diet: 5F/5M; EE: 5F/5M; ER + P/P Diet: 5F/5M. **(C)** Representative blot and quantity of tyrosine hydroxylase (TH) normalized to beta-actin levels in the hippocampus. N: STR: 5F/4M; STR + P/P Diet: 5F/5M; EE: 5F/5M; ER + P/P Diet: 5F/4M. STR, stress; EE, environmental enrichment; P/P, probiotic + prebiotic. $^{**}p < 0.01$.

prior probiotic supplementation can increase animals' resistance to chronic stress. Probiotics have also been shown to boost the production of anti-inflammatory cytokines while reducing pro-inflammatory cytokines, thereby modulating immune responses and reducing chronic inflammation (Virk et al., 2024). Additionally, probiotics can increase the expression of tight junction proteins, reducing intestinal permeability and preventing systemic inflammation (Gou et al., 2022). Certain probiotic strains produce neurotransmitters like serotonin and GABA, which can improve mood and reduce anxiety (Duranti et al., 2020; Akram et al., 2024). Importantly, probiotic feeding has been associated with increased levels of short-chain fatty acid (SCFA)-producing bacteria, which can further promote anti-inflammatory cytokine release and enhance tight junction integrity (Markowiak-Kopeć and Śliżewska, 2020). In our study, levels of beneficial Bifidobacterium species were found to be increased through probiotic feeding. Levels of SCFA-producing genera, such as Ruminococcaceae (Grabinger et al., 2019), were found to be increased following feeding, while levels of Lachnoclostridium could influence immune system responses (Yu et al., 2024).

Dietary interventions involving probiotics have shown promise in clinical settings, particularly as adjunctive treatments for managing chronic stress, improving mental health, and enhancing overall immune function (Den et al., 2020; Mazziotta et al., 2023). This approach is especially beneficial for conditions characterized by both

psychological and gastrointestinal symptoms. In our study, animals were fed probiotics prior to significant environmental manipulation. Prolonged probiotic supplementation prevented stress-induced learning deficiencies and neuroinflammation, suggesting that probiotic supplementation could serve as a preventive strategy against stress-induced physiological and psychological disorders.

In summary, the relationship between the gut microbiome and stress can be modulated through immune responses and reduced inflammation via probiotic supplementation. Incorporating probiotics into the diet is a viable strategy to mitigate the adverse effects of chronic stress on the immune system, thereby supporting better mental and physical health. One limitation of our study is the small sample size for sex-dependent analysis. Additionally, further research is needed to characterize the gut microbiome in male animals. Another limitation of our study is the lack of separate control groups for probiotics or prebiotics alone. We opted to include a single group receiving both probiotics and prebiotics, as previous research has shown that the combination, referred to as 'synbiotics,' provides optimal effects (Chunchai et al., 2018; Morshedi et al., 2020). In contrast, prebiotics alone have yielded mixed results, with some studies showing no effect (Kazemi et al., 2019; Alli et al., 2022) while others reported some benefits (Alli et al., 2022). Despite these limitations, our study underscores the importance of the gut-brain-immune axis in developing therapeutic interventions, offering a holistic approach to health management.

Data availability statement

The original contributions presented in the study are publicly available. This data can be found here: 10.6084/m9.figshare.28501892.

Ethics statement

The animal study was approved by Institutional Animal Care Committee at Memorial University of Newfoundland. The study was conducted in accordance with the local legislation and institutional.

Author contributions

CF: Conceptualization, Data curation, Formal Analysis, Investigation, Methodology, Writing – original draft, Writing – review & editing. LB: Data curation, Writing – review & editing. QY: Conceptualization, Funding Acquisition, Methodology, Resources, Supervision, Writing – original draft, Writing – review & editing.

Funding

The author(s) declare that financial support was received for the research, authorship, and/or publication of this article. This work was supported by the Canadian Institutes of Health Research Project grant under grant number (PJT-169197) to QY.

Acknowledgments

The authors wish to thank Dr. Shyamchand Mayengbam, Dr. Susan Walling, Sarah Torraville, Brenda Negandhi, Jessie Piche, Emma Rodgers and Tamunotonye Omoluabi for technical assistance and helpful discussions.

Conflict of interest

The authors declare that the research was conducted in the absence of any commercial or financial relationships that could be construed as a potential conflict of interest.

The author(s) declared that they were an editorial board member of Frontiers, at the time of submission. This had no impact on the peer review process and the final decision.

Publisher's note

All claims expressed in this article are solely those of the authors and do not necessarily represent those of their affiliated organizations, or those of the publisher, the editors and the reviewers. Any product that may be evaluated in this article, or claim that may be made by its manufacturer, is not guaranteed or endorsed by the publisher.

Supplementary material

The Supplementary Material for this article can be found online at: https://www.frontiersin.org/articles/10.3389/frmbi.2025.1454909/full#supplementary-material

References

Ackerman, S. H., Hofer, M. A., and Weiner, H. (1978). Early maternal separation increases gastric ulcer risk in rats by producing a latent thermoregulatory disturbance. *Science* 201, 373–376. doi: 10.1126/science.566471

Akram, N., Faisal, Z., Irfan, R., Shah, Y. A., Batool, S. A., Zahid, T., et al. (2024). Exploring the serotonin-probiotics-gut health axis: A review of current evidence and potential mechanisms. *Food Sci. Nutr.* 12, 694–706. doi: 10.1002/fsn3.v12.2

Alli, S. R., Gorbovskaya, I., Liu, J. C.W., Kolla, N. J., Brown, L., and Müller, D. J. (2022). The gut microbiome in depression and potential benefit of prebiotics, probiotics and synbiotics: A systematic review of clinical trials and observational studies. *Int. J. Mol. Sci.* 23, 44945. doi: 10.3390/ijms23094494

Arseneault-Bréard, J., Rondeau, I., Gilbert, K., Girard, Stéphanie-Anne, Tompkins, T. A., Godbout, R., et al. (2012). Combination of lactobacillus helveticus R0052 and

bifidobacterium longum R0175 reduces post-myocardial infarction depression symptoms and restores intestinal permeability in a rat model. *Br. J. Nutr.* 107, 1793–1995. doi: 10.1017/S0007114511005137

Bekinschtein, P., Kent, B. A., Oomen, C. A., Clemenson, G. D., Gage, F. H., Saksida, L. M., et al. (2013). BDNF in the dentate gyrus is required for consolidation of 'Pattern-separated' Memories. *Cell Rep.* 5, 759–685. doi: 10.1016/j.celrep.2013.09.027

Bravo, J. A., Forsythe, P., Chew, M. V., Escaravage, E., Savignac, HélèneM., Dinan, T. G., et al. (2011). Ingestion of lactobacillus strain regulates emotional behavior and central GABA receptor expression in a mouse via the vagus nerve. *Proc. Natl. Acad. Sci. United States America* 108, 16050–16555. doi: 10.1073/pnas.1102999108

Chatzaki, E., Charalampopoulos, I., Leontidis, C., Mouzas, I. A., Tzardi, M., Tsatsanis, C., et al. (2003). Urocortin in human gastric mucosa: relationship to inflammatory activity. *J. Clin. Endocrinol. Metab.* 88, 478–483. doi: 10.1210/jc.2002-020853

Chen, D., Lou, Q., Song, X.-J., Kang, F., Liu, An, Zheng, C., et al. (2024). Microglia govern the extinction of acute stress-induced anxiety-like behaviors in male mice. *Nat. Commun.* 15, 449. doi: 10.1038/s41467-024-44704-6

Chunchai, T., Thunapong, W., Yasom, S., Wanchai, K., Eaimworawuthikul, S., Metzler, G., et al. (2018). Decreased microglial activation through gut-brain axis by prebiotics, probiotics, or synbiotics effectively restored cognitive function in obese-insulin resistant rats. *J. Neuroinflamm.* 15, 11. doi: 10.1186/s12974-018-1055-2

Comeau, AndréM., Li, W. K.W., Tremblay, Jean-Éric, Carmack, E. C., and Lovejoy, C. (2011). Arctic Ocean Microbial Community Structure before and after the 2007 Record Sea Ice Minimum. *PloS One* 6, e274925. doi: 10.1371/journal.pone.0027492

Dellu, F., Mayo, W., Cherkaoui, J., Le Moal, M., and Simon, H. (1992). A two-trial memory task with automated recording: study in young and aged rats. *Brain Res.* 588, 132–139. doi: 10.1016/0006-8993(92)91352-F

Den, H., Dong, X., Chen, M., and Zou, Z. (2020). Efficacy of probiotics on cognition, and biomarkers of inflammation and oxidative stress in adults with alzheimer's disease or mild cognitive impairment - a meta-analysis of randomized controlled trials. *Aging* 12, 4010–4395. doi: 10.18632/aging.102810

De Palma, G., Blennerhassett, P., Lu, J., Deng, Y., Park, A. J., Green, W., et al. (2015). Microbiota and host determinants of behavioural phenotype in maternally separated mice. *Nat. Commun.* 6, 7735. doi: 10.1038/ncomms8735

Dimidi, E., Christodoulides, S., Mark Scott, S., and Whelan, K. (2017). Mechanisms of action of probiotics and the gastrointestinal microbiota on gut motility and constipation. *Adv. Nutr.* 8, 484–945. doi: 10.3945/an.116.014407

Dodiya, H. B., Forsyth, C. B., Voigt, R. M., Engen, P. A., Patel, J., Shaikh, M., et al. (2020). Chronic stress-induced gut dysfunction exacerbates parkinson's disease phenotype and pathology in a rotenone-induced mouse model of parkinson's disease. *Neurobiol. Dis.* 135, 104352. doi: 10.1016/j.nbd.2018.12.012

Duranti, S., Ruiz, L., Lugli, G. A., Tames, Héctor, Milani, C., Mancabelli, L., et al. (2020). Bifidobacterium adolescentis as a key member of the human gut microbiota in the production of GABA. *Sci. Rep.* 10, 14112. doi: 10.1038/s41598-020-70986-z

Galley, J. D., and Bailey, M. T. (2014). Impact of stressor exposure on the interplay between commensal microbiota and host inflammation. *Gut Microbes* 5, 390–965. doi: 10.4161/gmic.28683

Ghosh, A., Torraville, S. E., Mukherjee, B., Walling, S. G., Martin, G. M., Harley, C. W., et al. (2019). An experimental model of braak's pretangle proposal for the origin of alzheimer's disease: the role of locus coeruleus in early symptom development. *Alzheimer's Res. Ther.* 11, 595. doi: 10.1186/s13195-019-0511-2

Gou, H.-Z., Zhang, Y.-L., Ren, L.-F., Li, Z.-J., and Zhang, L. (2022). How do intestinal probiotics restore the intestinal barrier? *Front. Microbiol.* 13, 929346. doi: 10.3389/fmicb.2022.929346

Grabinger, T., Garzon, J. F. G., Hausmann, M., Geirnaert, A., Lacroix, C., and Hennet, T. (2019). Alleviation of intestinal inflammation by oral supplementation with 2-fucosyllactose in mice. *Front. Microbiol.* 10, 1385. doi: 10.3389/fmicb.2019.01385

Kazemi, A., Noorbala, A. A., Azam, K., Eskandari, M. H., and Djafarian, K. (2019). Effect of probiotic and prebiotic vs placebo on psychological outcomes in patients with major depressive disorder: A randomized clinical trial. *Clin. Nutr. (Edinburgh Scotland)* 38, 522–285. doi: 10.1016/j.clnu.2018.04.010

Kelly, S. C., McKay, E. C., Beck, J. S., Collier, T. J., Dorrance, A. M., and Counts, S. E. (2019). Locus coeruleus degeneration induces forebrain vascular pathology in a transgenic rat model of alzheimer's disease. *Journal of Alzheimer's disease : JAD* 70 (2), 371–388. doi: 10.3233/JAD-190090

Leggio, M. G., Mandolesi, L., Federico, F., Spirito, F., Ricci, B., Gelfo, F., et al. (2005). Environmental enrichment promotes improved spatial abilities and enhanced dendritic growth in the rat. *Behav. Brain Res.* 163, 78–905. doi: 10.1016/j.bbr.2005.04.009

Li, G.-Q., Wang, X.-Z., Liu, Yi, Yang, Y.-Z., Wang, C., Gong, S.-M., et al. (2023). The effect of Bacillus subtilis and fructooligosaccharide as antibiotic substituent on goose performance parameters, serum biochemical indicators and intestinal morphology. *Kafkas Univ Vet. Fak Derg* 29, 247–2545. doi: 10.9775/kvfd.2023.29134

Li, N., Wang, Qi, Wang, Y., Sun, A., Lin, Y., Jin, Ye, et al. (2019). Fecal microbiota transplantation from chronic unpredictable mild stress mice donors affects anxiety-like and depression-like behavior in recipient mice via the gut microbiota-inflammation-brain axis. *Stress* 22, 592–6025. doi: 10.1080/10253890.2019.1617267

Liu, Y., Wang, J., and Wu, C. (2021). Modulation of gut microbiota and immune system by probiotics, pre-biotics, and post-biotics. *Front. Nutr.* 8, 634897. doi: 10.3389/fnut.2021.634897

Liu, Q., Yu, Z., Tian, F., Zhao, J., Zhang, H., Zhai, Q., et al. (2020). Surface components and metabolites of probiotics for regulation of intestinal epithelial barrier. *Microbial Cell Factories* 19, 235. doi: 10.1186/s12934-020-1289-4

Lupien, S. J., Juster, R.-P., Raymond, C., and Marin, M.-F. (2018). The effects of chronic stress on the human brain: from neurotoxicity, to vulnerability, to opportunity. *Front. Neuroendocrinol.* 49, 91–105. doi: 10.1016/j.yfrne.2018.02.001

Mandolesi, L., Gelfo, F., Serra, L., Montuori, S., Polverino, A., Curcio, G., et al. (2017). Environmental factors promoting neural plasticity: insights from animal and human studies. *Neural Plasticity* 2017, 7219461. doi: 10.1155/2017/7219461

Markowiak-Kopeć, P., and Śliżewska, K. (2020). The effect of probiotics on the production of short-chain fatty acids by human intestinal microbiome. *Nutrients* 12 (4), 1107. doi: 10.3390/nu12041107

Marx, J. (2005). Alzheimer's disease. Play and exercise protect mouse brain from amyloid buildup. *Science* 307, 1547. doi: 10.1126/science.307.5715.1547

Mazziotta, C., Tognon, M., Martini, F., Torreggiani, E., and Rotondo, J. C. (2023). Probiotics mechanism of action on immune cells and beneficial effects on human health. *Cells* 12 (1), 184. doi: 10.3390/cells12010184

Mora, F., Segovia, G., and Arco, A. d. (2007). Aging, plasticity and environmental enrichment: structural changes and neurotransmitter dynamics in several areas of the brain. *Brain Res. Rev.* 55, 78–885. doi: 10.1016/j.brainresrev.2007.03.011

Morrison, G. L., Fontaine, C. J., Harley, C. W., and Yuan, Qi (2013). A role for the anterior piriform cortex in early odor preference learning: evidence for multiple olfactory learning structures in the rat pup. *J. Neurophysiol.* 110, 141–525. doi: 10.1152/jn.00072.2013

Morshedi, M., Saghafi-Asl, M., and Hosseinifard, E.-S. (2020). The potential therapeutic effects of the gut microbiome manipulation by synbiotic containing-lactobacillus plantarum on neuropsychological performance of diabetic rats. *J. Trans. Med.* 18, 185. doi: 10.1186/s12967-019-02169-y

Moya-Pérez, A., Perez-Villalba, A., Benítez-Páez, A., Campillo, I., and Sanz, Y. (2017). Bifidobacterium CECT 7765 modulates early stress-induced immune, neuroendocrine and behavioral alterations in mice. *Brain Behavior Immun.* 65, 43–56. doi: 10.1016/j.bbi.2017.05.011

O'Sullivan, E., Barrett, E., Grenham, S., Fitzgerald, P., Stanton, C., Ross, R. P., et al. (2011). BDNF expression in the hippocampus of maternally separated rats: does bifidobacterium breve 6330 alter BDNF levels? *Beneficial Microbes* 2, 199–207. doi: 10.3920/BM2011.0015

Omoluabi, T., Torraville, S. E., Maziar, A., Ghosh, A., Power, K. D., Reinhardt, C., et al. (2021). Novelty-like activation of locus coeruleus protects against deleterious human pretangle tau effects while stress-inducing activation worsens its effects. *Alzheimer's Dementia: J. Alzheimer's Assoc.* 7, e122315. doi: 10.1002/trc2.12231

Pasiakos, S. M., Margolis, L. M., Murphy, N. E., McClung, H. L., Martini, S., Gundersen, Y., et al. (2016). Effects of exercise mode, energy, and macronutrient interventions on inflammation during military training. *Physiol. Rep.* 4 (11), e12820. doi: 10.14814/phy2.12820

Polsky, L. R., Rentscher, K. E., and Carroll, J. E. (2022). Stress-induced biological aging: A review and guide for research priorities. *Brain Behavior Immun.* 104, 97–109. doi: 10.1016/j.bbi.2022.05.016

Prokopiou, P. C., Engels-Domínguez, N., Papp, K. V., Scott, M. R., Schultz, A. P., Schneider, C., et al. (2022). Lower novelty-related locus coeruleus function is associated with Aβ-related cognitive decline in clinically healthy individuals. *Nat. Commun.* 13, 1571. doi: 10.1038/s41467-022-28986-2

Rolland, Y., van Kan, G. A., and Vellas, B. (2008). Physical activity and alzheimer's disease: from prevention to therapeutic perspectives. *J. Am. Med. Directors Assoc.* 9, 390–4055. doi: 10.1016/j.jamda.2008.02.007

Roy, S., and Dhaneshwar, S. (2023). Role of prebiotics, probiotics, and synbiotics in management of inflammatory bowel disease: Current perspectives. *World J. Gastroenterol.* 29, 2078–2100. doi: 10.3748/wjg.v29.i14.2078

Schneiderman, N., Ironson, G., and Siegel, S. D. (2005). Stress and health: psychological, behavioral, and biological determinants. *Annu. Rev. Clin. Psychol.* 1, 607–628. doi: 10.1146/annurev.clinpsy.1.102803.144141

Segovia, G., Arco, A. d., and Mora, F. (2009). Environmental enrichment, prefrontal cortex, stress, and aging of the brain. *J. Neural Transm.* 116, 1007–1165. doi: 10.1007/s00702-009-0214-0

Shields, G. S., and Slavich, G. M. (2017). Lifetime stress exposure and health: A review of contemporary assessment methods and biological mechanisms. *Soc. Pers. Psychol. Compass* 11 (8), e12335. doi: 10.1111/spc3.12335

Sotiropoulos, I., Catania, C., Pinto, L. G., Silva, R., Pollerberg, G.E., Takashima, A., et al. (2011). Stress acts cumulatively to precipitate alzheimer's disease-like tau pathology and cognitive deficits. *J. Neuroscience: Off. J. Soc. Neurosci.* 31, 7840–7475. doi: 10.1523/JNEUROSCI.0730-11.2011

Strekalova, T., Liu, Y., Kiselev, D., Khairuddin, S., Chiu, J. L. Yu, Lam, J., et al. (2022). Chronic mild stress paradigm as a rat model of depression: facts, artifacts, and future perspectives. *Psychopharmacology* 239, 663–693. doi: 10.1007/s00213-021-05982-w

Suárez-Pereira, I., Llorca-Torralba, M., Bravo, L., Camarena-Delgado, C., Soriano-Mas, C., and Berrocoso, E. (2022). The role of the locus coeruleus in pain and associated stress-related disorders. *Biol. Psychiatry* 91, 786–975. doi: 10.1016/j.biopsych.2021.11.023

Thevaranjan, N., Puchta, A., Schulz, C., Naidoo, A., Szamosi, J. C., Verschoor, C. P., et al. (2017). Age-associated microbial dysbiosis promotes intestinal permeability, systemic inflammation, and macrophage dysfunction. *Cell Host Microbe*. 21 (4), 455–466.e4. doi: 10.1016/j.chom.2017.03.002

Thursby, E., and Juge, N. (2017). Introduction to the human gut microbiota. *Biochem. J.* 474, 1823–1365. doi: 10.1042/BCJ20160510

Torraville, S. E., Flynn, C. M., Kendall, T. L., and Yuan, Qi (2023). Life experience matters: enrichment and stress can influence the likelihood of developing alzheimer's disease via gut microbiome. *Biomedicines* 11 (7), 1884. doi: 10.3390/biomedicines11071884

Ulrich-Lai, Y. M., and Herman, J. P. (2009). Neural regulation of endocrine and autonomic stress responses. *Nat. Rev. Neurosci.* 10, 397–4095. doi: 10.1038/nrn2647

Van Praag, H., Kempermann, G., and Gage, F. H. (2000). Neural consequences of environmental enrichment. *Nat. Rev. Neurosci.* 1, 191–985. doi: 10.1038/35044558

Van Wijck, K., Lenaerts, K., Van Bijnen, A. A., Boonen, B., Van Loon, L. J.C., Dejong, C. H.C., et al. (2012). Aggravation of exercise-induced intestinal injury by ibuprofen in athletes. *Med. Sci. Sports Exercise* 44, 2257–2625. doi: 10.1249/MSS.0b013e318265dd3d

Virk, M. S., Virk, M. A., He, Y., Tufail, T., Gul, M., Qayum, A., et al. (2024). The anti-inflammatory and curative exponent of probiotics: A comprehensive and authentic ingredient for the sustained functioning of major human organs. *Nutrients* 16 (4), 546. doi: 10.3390/nu16040546

Wang, B., Wang, Y., Wu, Q., Huang, H. P., and Li, S. (2017). Effects of α2A adrenoceptors on norepinephrine secretion from the locus coeruleus during chronic stress-induced depression. *Front. Neurosci.* 11, 243. doi: 10.3389/fnins.2017.00243

Welcome, M. O., and Mastorakis, N. E. (2020). Stress-induced blood brain barrier disruption: molecular mechanisms and signaling pathways. *Pharmacol. Research: Off. J. Ital. Pharmacol. Soc.* 157, 104769. doi: 10.1016/j.phrs.2020.104769

Yalcin, I., Aksu, F., and Belzung, C. (2005). Effects of desipramine and tramadol in a chronic mild stress model in mice are altered by yohimbine but not by pindolol. *Eur. J. Pharmacol.* 514, 165–174. doi: 10.1016/j.ejphar.2005.03.029

Yang, X., Yu, D., Xue, Li, Li, H., and Du, J. (2020). Probiotics modulate the microbiota-gut-brain axis and improve memory deficits in aged SAMP8 mice. *Acta Pharm. Sinica B* 10, 475–875. doi: 10.1016/j.apsb.2019.07.001

Yu, Z., Wang, Q., Wang, Z., Liu, S., Xia, T., Duan, C., et al. (2024). Lachnoclostridium intestinal flora is associated with immunotherapy efficacy in nasopharyngeal carcinoma. *Head Neck August.* 47 (1), 269–281. doi: 10.1002/hed.27917

Zhou, X.-D., Shi, D.-D., and Zhang, Z.-J. (2019). Antidepressant and anxiolytic effects of the proprietary chinese medicine shexiang baoxin pill in mice with chronic unpredictable mild stress. *J. Food Drug Anal.* 27, 221–305. doi: 10.1016/j.jfda.2018.08.001

frontiers | Frontiers in Microbiology

TYPE Original Research
PUBLISHED 19 March 2025
DOI 10.3389/fmicb.2025.1507336

Check for updates

OPEN ACCESS

EDITED BY
Jessica Galloway-Pena,
Texas A&M University, United States

REVIEWED BY
Florentin Constancias,
ETH Zürich, Switzerland
Mridul Sharma,
University of California, Los Angeles,
United States

*CORRESPONDENCE
Duozhuang Tang
ndefy11234@ncu.edu.cn

RECEIVED 21 October 2024
ACCEPTED 18 February 2025
PUBLISHED 19 March 2025

CITATION
Huang Y, Liao L, Jiang Y, Tao S and Tang D (2025) Role of gut microbiota in predicting chemotherapy-induced neutropenia duration in leukemia patients. *Front. Microbiol.* 16:1507336. doi: 10.3389/fmicb.2025.1507336

COPYRIGHT
© 2025 Huang, Liao, Jiang, Tao and Tang. This is an open-access article distributed under the terms of the Creative Commons Attribution License (CC BY). The use, distribution or reproduction in other forums is permitted, provided the original author(s) and the copyright owner(s) are credited and that the original publication in this journal is cited, in accordance with accepted academic practice. No use, distribution or reproduction is permitted which does not comply with these terms.

Role of gut microbiota in predicting chemotherapy-induced neutropenia duration in leukemia patients

Yezi Huang[1,2], Lihong Liao[1,2], Yanjun Jiang[1,2], Si Tao[3] and Duozhuang Tang[1,2]*

[1]Department of Hematology, The Second Affiliated Hospital of Nanchang University, Nanchang, China, [2]Jiangxi Provincial Key Laboratory of Hematological Diseases, Nanchang, China, [3]Department of Oncology, The Second Affiliated Hospital of Nanchang University, Nanchang, China

Background: Acute leukemia is an aggressive malignancy with high morbidity and mortality, and chemotherapy is the primary treatment modality. However, chemotherapy often induces neutropenia (chemotherapy-induced neutropenia, CIN), increasing the risk of infectious complications and mortality. Current research suggests that gut microbiota may play a significant role in chemotherapy's efficacy and side effects.

Objective: This study aimed to investigate whether gut microbiota can predict the duration of chemotherapy-induced neutropenia in leukemia patients.

Methods: We included 56 leukemia patients from the Hematology Department of the Second Affiliated Hospital of Nanchang University, collecting fecal samples 1 day before and 1 day after chemotherapy. The diversity and community structure of gut microbiota were analyzed using 16S rRNA gene sequencing. Patients were divided into two groups based on the duration of neutropenia post-chemotherapy: Neutropenia ≤7 Days Group (NLE7 Group) and Neutropenia > 7 Days Group (NGT7 Group). Comparative analysis identified characteristic microbiota.

Results: After chemotherapy, gut microbiota diversity significantly decreased ($p < 0.05$). In the NGT7 Group, the relative abundance of *Enterococcus* before chemotherapy was significantly higher than in the NLE7 Group ($p < 0.05$). ROC curve analysis showed that the relative abundance of *Enterococcus* had high predictive accuracy for the duration of neutropenia (AUC = 0.800, 95% CI: 0.651–0.949).

Conclusion: The abundance of *Enterococcus* before chemotherapy can predict the duration of chemotherapy-induced neutropenia. These findings provide new evidence for gut microbiota as a predictive biomarker for chemotherapy side effects and may guide personalized treatment for leukemia patients.

KEYWORDS

leukemia, gut microbiota, 16S rRNA, chemotherapy, neutropenia

1 Introduction

Acute leukemia is a highly aggressive malignancy with both high incidence and mortality rates, characterized by the clonal proliferation of bone marrow progenitor cells with a blockade in differentiation. The standard treatment for leukemia typically involves intensive chemotherapy with cytarabine and anthracycline (the 7 + 3 regimen) and hypomethylating agents (Liu, 2021). However, this type of chemotherapy significantly affects multiple normal, rapidly dividing cells. In particular, when chemotherapy leads to the depletion of hematopoietic progenitor cells, acute bone marrow suppression may occur. At this point, hematopoietic stem cells initiate self-renewal and proliferate to form progenitor cells in order to maintain the homeostasis of the hematopoietic system (China Anti-Cancer Association Tumor Clinical Chemotherapy Professional Committee and China Anti-Cancer Association Tumor Support Therapy Professional Committee, 2023). Several studies have demonstrated that the degree and duration of chemotherapy-induced neutropenia (CIN) are strongly correlated with the risk of infectious complications and mortality. Notably, the occurrence of febrile neutropenia (FN) further exacerbates the risks, leading to potential reductions in chemotherapy dosage and/or delays in treatment, and in severe cases, even death (Bodey et al., 1966; Lalami and Klastersky, 2017). Factors such as poor physical condition, suboptimal nutritional status, low baseline, nadir blood cell counts during the first chemotherapy cycle, and high-dose chemotherapy have been identified as key predictors of CIN (Lyman et al., 2005). Additionally, patient comorbidities, age, individual pharmacokinetics and pharmacodynamics also influence the occurrence of CIN (Kloft et al., 2006; Stabell et al., 2008). Nonetheless, these factors only partially explain the variation among patients. Despite receiving the same chemotherapy, there are significant differences in the frequency, severity, and duration of neutropenia among patients (Stabell et al., 2008). Therefore, identifying the underlying causes and risk factors of chemotherapy-induced neutropenia is crucial.

The gut microbiota, comprising bacteria, archaea, and eukaryotes organisms residing in the gastrointestinal tract, is a critical component of the human body's complex micro-ecosystem, interacting with the host to influence various physiological processes and pathological conditions (O'Toole and Paoli, 2023; Caballero-Flores et al., 2023). The connection between microbiota and tumours has garnered significant attention in recent years. Studies have shown that conventional treatments, including radiotherapy, chemotherapy, and immunotherapy, can alter the gut microbiota composition. Furthermore, the composition of the microbiota and specific bacterial species can influence these treatments' efficacy and side effects by modulating the inflammatory response and immune system (Andreeva et al., 2020; Cheng et al., 2020). For example, the chemotherapy drug irinotecan, while effective in killing cancer cells, also damages normal intestinal epithelial cells and symbiotic microorganisms, leading to gastrointestinal toxicity and microbiota dysbiosis. Additionally, β-glucuronidase secreted by gut bacteria prolongs irinotecan's clearance time in the body, exacerbating its gastrointestinal toxicity (Yue et al., 2021). Recent studies by Yoon et al. reported that in a cohort of newly diagnosed diffuse large B-cell lymphoma patients, the abundance of Enterobacteriaceae was associated with febrile neutropenia and poor survival following R-CHOP chemotherapy (Yoon et al., 2023). Similarly, Galloway-Peña et al. demonstrated that baseline microbiome diversity is a strong independent predictor of infection during induction chemotherapy in acute myeloid leukemia patients, with higher levels of Porphyromonadaceae seeming to protect against infections (Galloway-Peña et al., 2020). Moreover, the gut microbiota plays a key role in normal hematopoiesis and may affect the white blood cell counts through hematopoietic function (Staffas et al., 2018). For instance, long-term antibiotic use, which alters the gut microbiota, has been linked to hematological side effects, including anemia and neutropenia. Mouse studies have shown that antibiotic-induced microbiota depletion and bone marrow suppression are due to a lack of stable microbial products, which circulate in the blood and promote hematopoiesis through basal inflammatory signalling. These mechanisms are particularly relevant for patients undergoing long-term antibiotic treatment or recovering from hematopoietic stem cell transplants (Galloway-Peña et al., 2020). These studies highlight the close relationship between the gut microbiota, the hematopoietic system, and chemotherapy-related complications.

Existing studies primarily focus on the relationship between the gut microbiota and the incidence, severity, and frequency of bone marrow suppression, as well as its association with FN after chemotherapy. The innovation of this study lies in exploring the predictive role of the pre-chemotherapy gut microbiota in determining the duration of bone marrow suppression. Based on the risk stratification of patients with febrile neutropenia, those with neutropenia lasting longer than 7 days are classified as high-risk (Galloway-Peña et al., 2020). Therefore, this study stratifies patients into two groups based on the duration of neutropenia (7 days) and utilizes microbiome sequencing technology to compare the diversity and community structure of gut microbiota before and after chemotherapy in leukemia patients. Characteristic bacterial taxa are identified in both groups. Predicting the duration of neutropenia can help optimize patient management, prevent infectious complications, and facilitate the rational use of antibiotics and granulocyte colony-stimulating factor (G-CSF). Furthermore, the results of this study may provide new insights for subsequent research into microbiome-based therapies aimed at reducing chemotherapy-induced bone marrow suppression.

2 Materials and methods

2.1 Study patients and fecal sample collection

This study is a retrospective analysis involving 56 newly diagnosed leukemia patients treated in the Hematology Department of the Second Affiliated Hospital of Nanchang University between 2023 and 2024. To be eligible, patients had to meet the following inclusion criteria: (i) age > 18 years, (ii) newly diagnosed with leukemia according to the WHO classification of myeloid neoplasms, and (iii) no gastrointestinal surgery or antitumor treatment within 6 months before enrollment. The exclusion criteria were: (i) patients with acute promyelocytic leukemia, (ii) those with other gastrointestinal diseases, (iii) those who had previously received antitumor treatment, (iv) those with other tumours, and (v) patients who had used antibiotics and/or probiotics within 90 days or had received nasal tube feeding or parenteral nutrition during the study period. After obtaining informed

consent, fecal samples (5-10 g) were collected from patients 1 day before the first chemotherapy and on the first day after chemotherapy. A total of 47 pre-chemotherapy and 34 post-chemotherapy fecal samples were collected. All samples were immediately frozen and transported to the laboratory within 24 h using cold-chain logistics. Basic information and baseline clinical data at admission were obtained from the hospital's case management system.

2.2 DNA extraction and library construction

DNA was extracted from fecal samples using the Advanced Stool DNA Kit. PCR amplification of the 16S rRNA V3-V4 region of standard bacteria was performed using primers (human: 341F-806R, 341F 5′-CCTAYGGGRBGCASCAG-3′ and 806R 5′-GGACTAC NNGGGTWTCTAAT-3′).

PCR reactions were carried out on a BioRad S1000 thermal cycler (Bio-Rad Laboratory, CA, USA) with the following cycling conditions: 94°C for 5 min (initial denaturation), followed by 30 cycles of 94°C for 30 s, 57°C for 30 s, and 72°C for 30 s, with a final extension at 72°C for 10 min and storage at 4°C. PCR products from the same sample were pooled. The fragment size and length of PCR products were verified using 1% agarose gel electrophoresis. Concentrations were compared using GeneTools Analysis Software (Version 4.03.05.0, SynGene), and PCR products were mixed in appropriate ratios according to sequencing volume requirements.

PCR products were purified using the E.Z.N.A.® Gel Extraction Kit (Omega, USA) and eluted with TE buffer. Libraries were constructed following the standard protocol of the NEBNext® Ultra™ II DNA Library Prep Kit for Illumina® (New England Biolabs, USA). The constructed amplicon libraries were sequenced on an Illumina Nova 6,000 platform for PE250 sequencing (Guangdong Magigene Biotechnology Co., Ltd., Guangzhou, China).

2.3 Sequencing data bioinformatics analysis

2.3.1 Analysis of raw date

The raw sequencing data were assembled and subjected to quality control to ensure accuracy and optimization. The samples were then distinguished, followed by operational taxonomic unit (OTU) clustering and species classification analysis. Based on the OTUs, various diversity indices were further analyzed. Additionally, multivariate analyses, significance testing, and a series of statistical and visual analyses were conducted to examine the community composition and phylogenetic information of multiple species.

2.3.2 Community composition analysis

OTU table sequences were categorized at five taxonomic levels: phylum, class, order, family, and genus. Relative abundance was calculated for each taxon and represented by community bar charts. Venn diagrams were used to analyze shared and unique OTUs in the gut microbiota.

2.3.3 Alfa diversity and beta diversity analysis

To assess the ecological diversity and structure of the fecal microbiota, alfa diversity was calculated using the Chao richness index, Ace index, Shannon index, and Simpson index. Beta diversity was evaluated by performing principal coordinates analysis (PCoA) based on the weighted UniFrac distance algorithm, allowing for comparison of microbial diversity across all samples.

2.3.4 Species difference analysis

Based on the community abundance data, differences in microbial community abundance were detected. Linear discriminant analysis (LDA) was used to estimate the impact of species abundance differences, followed by the Mann–Whitney U test to identify significantly different taxa.

2.4 Statistical analysis

Continuous data were presented as mean ± standard deviation (SD) and compared between groups using an independent sample t-test. Categorical data were expressed as n (%) and compared using the chi-square test or Fisher's exact test. A p-value <0.05 was considered statistically significant. ACE, Chao1, Shannon, and Simpson indices represented the Alpha diversity of gut microbiota. Beta diversity was compared using principal coordinate analysis (PCoA) and analysis of similarities (ANOSIM). Linear discriminant analysis (LDA) and effect size (LEfSe) were used to analyze the relative abundance of different taxa. Discriminatory features with a log LDA score > 2 and Kruskal-Wallis $p < 0.05$ were identified. The Spearman correlation was used to analyze the relationship between gut microbiota and clinical indicators. ROC curves were plotted to evaluate the predictive value of gut microbiota features for neutropenia duration greater than 7 days, and the area under the curve (AUC) was calculated. All significant tests were two-sided, with $p < 0.05$ or adjusted $p < 0.05$ considered statistically significant.

3 Results

3.1 Baseline characteristics

This study included 56 leukemia patients diagnosed at the Hematology Department of the Second Affiliated Hospital of Nanchang University. A total of 81 fecal samples were collected, with 47 samples before and 34 samples after chemotherapy. Due to some patients being discharged early, only 37 patients had complete clinical data for assessing the duration of grade 4 myelosuppression after chemotherapy. Based on this, patients were divided into the Neutropenia ≤7 Days Group (NLE7 Group) and the Neutropenia >7 Days Group (NGT7 Group). The clinical characteristics of the 56 patients are summarized in Table 1.

3.2 Changes in gut microbiota diversity and composition before and after chemotherapy

The 81 fecal samples were diided into the Pre-Chemotherapy Group (Pre-C Group) and the Post-Chemotherapy Group (Post-C Group) based on collection time. Based on 16S rRNA gene sequencing analysis, the microbial diversity and composition of the two groups

TABLE 1 Clinical characteristics of the 56 leukemia patients.

Patient characteristic	Total (n = 56)	NLE7 Group (n = 15)	NGT7 Group (n = 22)
Age, median years, mean (±SD)	62.34 ± 13.64	63 ± 15.4	59.5 ± 12.4
Sex, man, n (%)	32 (57.1%)	9 (60%)	11 (50%)
Weight, mean (±SD)	60.2 ± 8.3	60.0 ± 9.2	61.0 ± 8.3
AML phenotype, n (%)			
M0	3 (5.4%)	1 (6.7%)	0 (0%)
M1	10 (17.9%)	0 (0%)	7 (31.8%)
M2	18 (32.1%)	4 (26.7%)	5 (22.7%)
M4	17 (30.4%)	7 (46.7%)	6 (27.3%)
M5	8 (14.3%)	3 (20%)	4 (18.2%)
Risk categorization, n (%)			
Favourable	26 (57.1%)	8 (53.3%)	13 (59.1%)
Intermediate	16 (28.6%)	3 (20%)	5 (22.7%)
Adverse	12 (21.4%)	4 (26.7%)	4 (18.2%)
Chemotherapy regimens, n (%)			
7&3	32 (57.1%)	5 (33.3%)	14 (63.6%)
Ven + HMA	20 (35.7%)	9 (60%)	5 (22.7%)
Others	4 (7.1%)	1 (6.7%)	3 (13.6%)
Baseline leukocyte count mean (±SD)	57.74 ± 63.67	48.41 ± 53.90	60.30 ± 61.80
Baseline platelet count mean (±SD)	52.75 ± 65.48	50.6 ± 57.52	67.78 ± 76.33
Baseline Hemoglobin count mean (±SD)	75.51 ± 22.90	86 ± 28.42	77.45 ± 28.42
Duration of neutropenia (days)		3 ± 2.5	20.4 ± 11.0

NLE7, Neutropenia ≤7 Days; NGT7, Neutropenia >7 Days;M0, Acute Myeloblastic Leukemia (without maturation); M1, Acute Myeloblastic Leukemia (with minimal maturation); M2, Acute Myeloblastic Leukemia (with maturation); M3, Acute Promyelocytic Leukemia; M4, Acute Myelomonocytic Leukemia; M5, Acute Monocytic Leukemia; 7&3, Cytarabine + Daunorubicin; Others, Decitabine+Cytarabine, Azacitidine+Cytarabine; SD, standard deviation.

were further statistically analyzed. OTU abundance represented richness, while alpha diversity was represented by Chao1, ACE, Shannon, and Simpson indices. At the OTU level, both alpha and beta diversity indices are shown in Figures 1A–D. According to the Wilcoxon rank-sum test, alpha diversity significantly decreased post-chemotherapy compared to pre-chemotherapy ($p = 0.011$ [Chao1], 0.013 [ACE], 0.019 [PD_whole_tree], 0.033 [Shannon]). Although principal coordinate analysis (PCoA) based on the weighted UniFrac distance algorithm showed statistically significant differences between pre-chemotherapy and post-chemotherapy samples (ANOSIM $R = 0.035$, $p = 0.041$), the overall gut microbiota structure was not significantly separated (Figure 2A). The Venn diagram showed 1750 shared OTUs between the two groups, with 1,542 unique OTUs in the Pre-C group and 849 in the Post-C group (Figure 3). These results indicate a significant reduction in gut microbiota diversity after chemotherapy, with no significant change in community structure composition.

In the taxonomic comparison of gut microbiota composition at the class level, it was found that the baseline abundance of *Clostridia* (P: 0.012) and *Saccharimonadia* (P: 0.004) in the Post-C group was significantly lower than in the Pre-C group. At the order level, the abundance of *Clostridiales* and *Saccharimonadales* was significantly reduced post-chemotherapy (P: 0.023). At the family level, *Lachnospiraceae* decreased (P: 0.0433). Outside the top 20 in abundance, *Atopobiaceae* and *Saccharimonadaceae* also decreased. At the genus level, the top five bacteria in both groups were *Enterococcus*, *Bacteroides*, *Escherichia-Shigella*, *Bifidobacterium*, and *Streptococcus*, with no significant species differences observed (Figure 4).

3.3 Gut microbiota differences in NLE7 group and NGT7 group before chemotherapy

This study collected pre-chemotherapy fecal samples from 37 leukemia patients and assessed the duration of grade 4 myelosuppression. Patients were divided into two groups based on a seven-day threshold. The gut microbiota in pre-chemotherapy samples of both groups was compared using 16S rRNA gene sequencing analysis. The NLE7 Group had lower Chao1 and ACE indices, and higher Shannon and Simpson indices compared to the NGT7 Group, but the differences were not statistically significant (Figures 1A–D). Beta diversity comparison using the Bray-Curtis algorithm and distance matrix analysis with ANOSIM indicated that inter-group differences were greater than intra-group differences but not significant ($R = 0.056$, $p = 9.5e\text{-}02$) (Figure 2B), suggesting no significant differences in the species number, diversity, and community structure of microbiota between the two groups.

To further identify significantly different abundant microbiota between the groups, LEfSe analysis with an LDA score (Log10) = 2

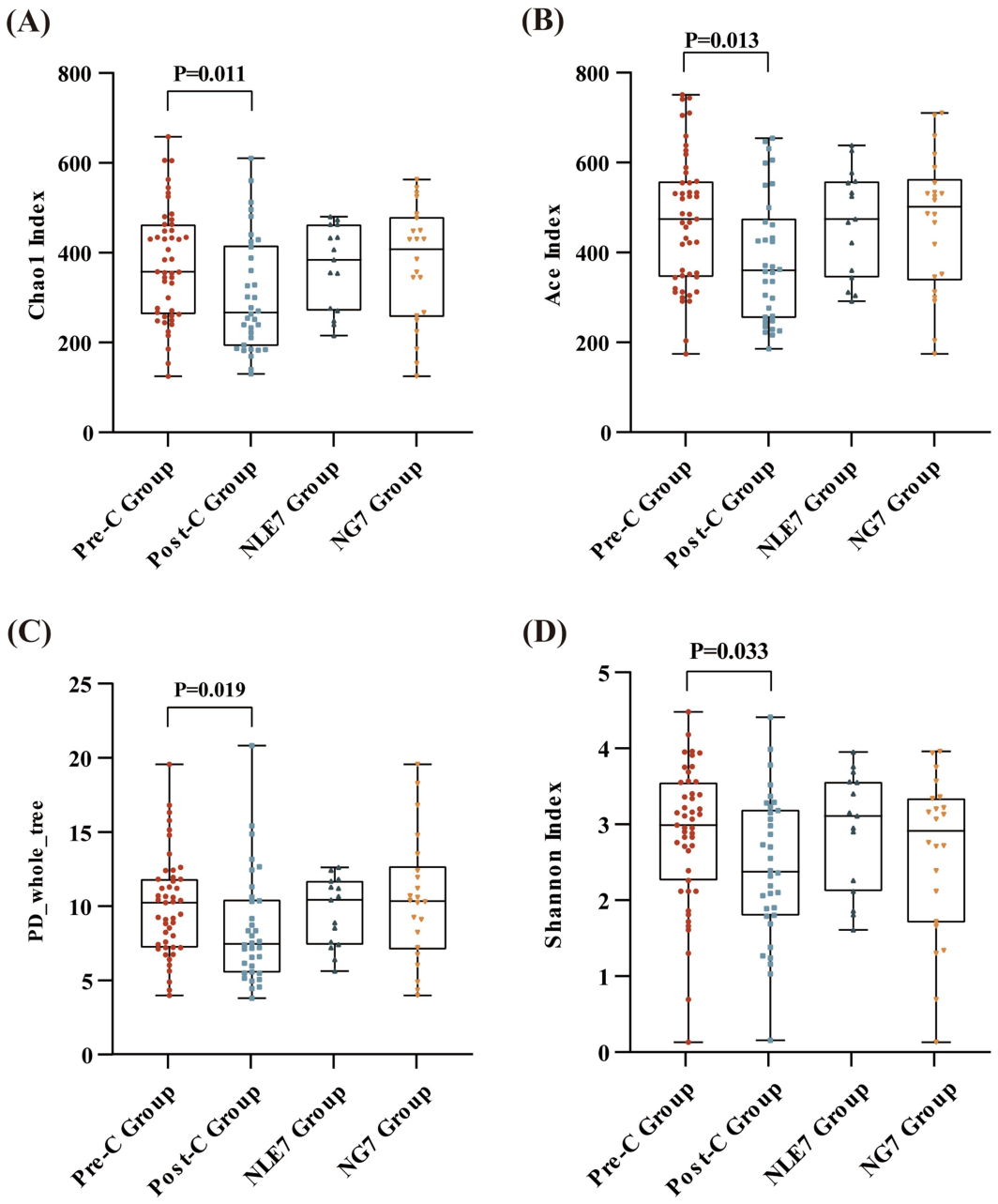

FIGURE 1
Alpha diversity at the OTU level (measured in terms of the **(A)** Chao1 Index, **(B)** Ace Index, **(C)** PD_whole_tree Index, **(D)** and Shannon index) between the Pre-C Group (n = 47) and Post-C Group (n = 36), and the NLE7 Group (n = 47) and NG7 Group (n = 36). Differences across groups were compared using the Wilcoxon rank-sum test. $p < 0.05$ was considered statistically significant.

was used to screen important microbial biomarkers. The NLE7 Group had characteristic species, mainly at the class level (*Campylobacteria*), order level (*Cytophagales*, *Campylobacterales*), family level (*Cyclobacteriaceae*, *Leuconostocaceae*), and genus level (*Stomatobaculum*). The NGT7 Group had significantly different species mainly at the phylum level (*Epsilonbacteraeota*), family level (*Enterococcaceae*, *Mycobacteriaceae*), and genus level (*Enterococcus*) (Figure 5).

Based on the LEfSe results, further analysis of the community distribution and verification of relative abundance differences between the two groups was conducted using the Mann–Whitney U test. Analysis at the phylum level showed that the main phyla in both groups were *Firmicutes*, *Bacteroidetes*, *Proteobacteria*, *Actinobacteria*, and *Verrucomicrobia*. Among these, differences in *Firmicutes* and *Bacteroidetes* were not significant. However, *Proteobacteria* had a lower mean relative abundance in the NLE7 Group (5.78%) compared to the NGT7 Group (13.04%). *Actinobacteria* had a higher mean relative abundance in the NLE7 Group (8.17%) compared to the NGT7 Group (4.36%), but the differences were not statistically significant. At the family level, the top three families were *Lachnospiraceae*, *Enterococcaceae*, and *Ruminococcaceae*. *Enterococcaceae* had a significantly lower mean relative abundance in

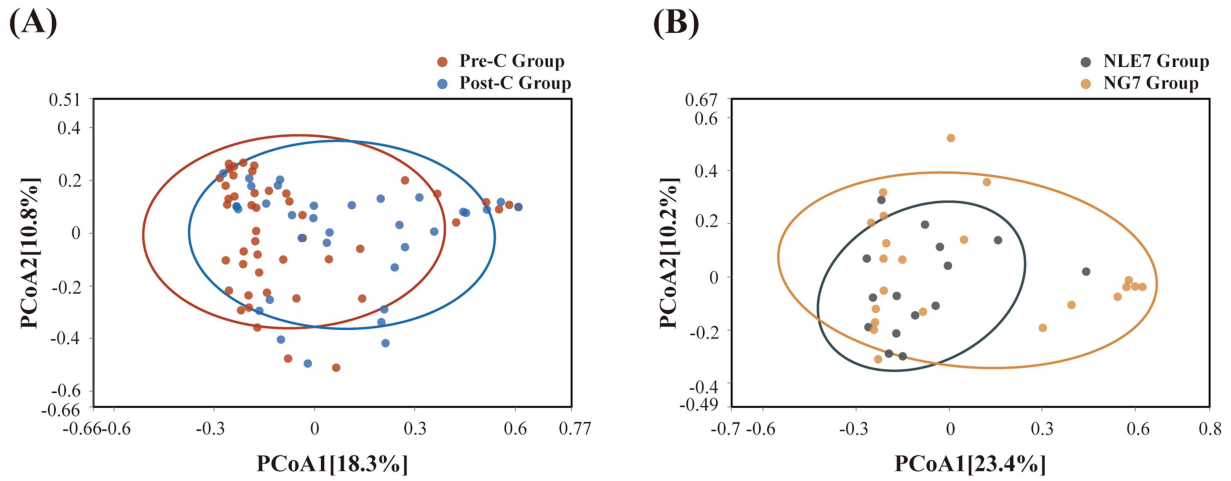

FIGURE 2
(A) Beta diversity was evaluated by Principal coordinate analysis of Bray-Curtis between the Pre-C Group and Post-C Group, and **(B)** the NLE7 Group and NG7 Group.

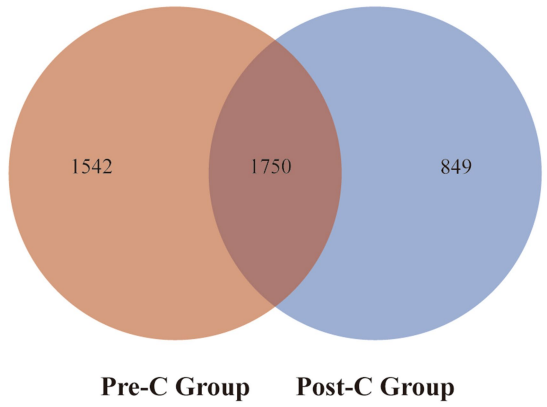

FIGURE 3
The Venn diagram of the total gut bacteria at the OTUs level for the Pre-C Group and the Post-C Group. Red represents the Pre-C Group, blue refers to the Post-C Group, and the overlapping part stands for the number of common bacteria at the OTUs level in the two groups.

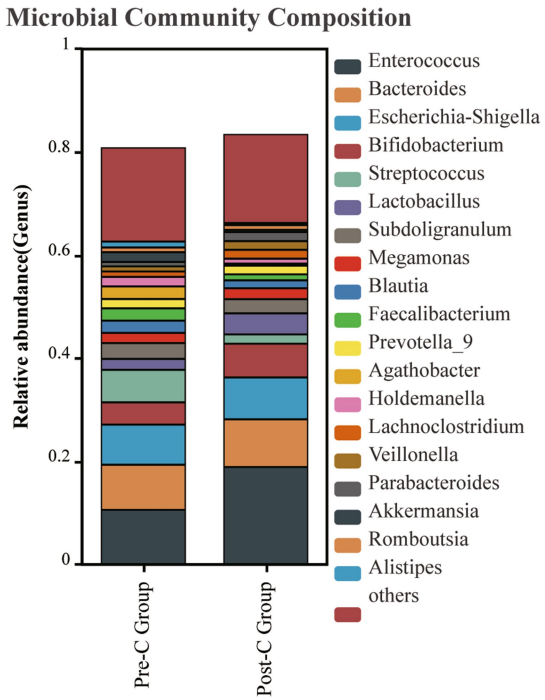

FIGURE 4
The gut bacteria composition at the genus level between the Pre-C Group and the Post-C Group was plotted. The abscissa is the group name, and the ordinate represents the relative abundance of bacteria in the sample. Different colors represent different bacterial genus, and the length of the column represents the proportion of bacterial groups.

the NLE7 Group (3.38%) compared to the NGT7 Group (21.25%) ($p = 0.002$). At the genus level, *Enterococcus* showed a significant difference in relative abundance between the two groups ($p = 0.02$).

3.4 Correlation between gut microbiota, clinical characteristics, and neutropenia duration

To determine the correlation between gut microbiota, clinical characteristics, and neutropenia duration, we collected data on age at diagnosis, weight, Chemotherapy regimens, baseline white blood cell count, baseline hemoglobin, and baseline platelet count from 37 AML patients. These clinical characteristics did not show significant correlations with neutropenia duration post-chemotherapy. Among the top 20 most abundant bacterial families, post-chemotherapy neutropenia duration was positively correlated with *Enterococcaceae* (r = 0.370, $p = 0.024$). Patient weight was positively correlated with *Holdemanella* (r = 0.479, $p = 0.003$); baseline white blood cell count was negatively correlated with *Lactobacillaceae* (r = −0.337, $p = 0.42$);

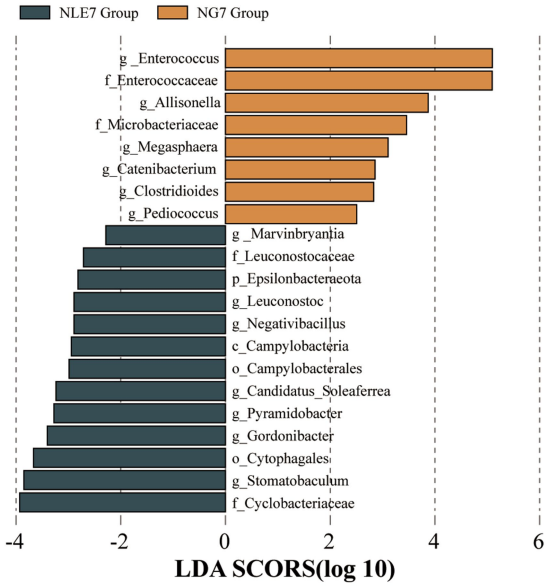

FIGURE 5
(1)The bar chart of Linear Discriminant Analysis (LDA) scores shows the taxa with the most significant differences between the NLE7 Group and NGT7 Group. Only taxa with an LDA score > 2 are shown.

platelet count was negatively correlated with *Alistipes* (r = −0.343, $p = 0.036$) *Bacteroides* (r = −0.363, $p = 0.027$) and *Ruminococcus_gnavus_group* (r = −0.349, $p = 0.034$), hemoglobin was negatively correlated with *Alistipes* (r = −0.347, $p = 0.035$) (Figure 6).

3.5 Predictive role of *Enterococcus*

We evaluated the potential of gut microbiota as a biomarker to predict whether neutropenia lasts more than 7 days. ROC curve analysis showed that the relative abundance of *Enterococcaceae* at baseline had strong predictive power for whether leukemia patients would experience neutropenia lasting more than 7 days post-chemotherapy (AUC = 0.800; 95% CI: 0.651–0.949; $p = 0.002$). The abundance threshold for *Enterococcaceae* was 22%, with a sensitivity of 53% and a specificity of 100% (Figure 7). Based on this abundance threshold, patients were divided into two groups. Binary logistic regression analysis showed significant differences between the two groups [$p = 0.024$, EEP(B) = 1.246]. Overall, a relative abundance of *Enterococcaceae* > 22% can predict grade 4 myelosuppression >7 days post-chemotherapy, validating *Enterococcus* as a predictive role.

4 Discussion

Increasing research has focused on the relationship between gut microbiota and chemotherapy-induced toxicity and related complications in cancer treatment. However, determining the specific connection between these factors remains challenging. Few studies have directly explored the relationship between gut microbiota characteristics in leukemia patients and the duration of neutropenia following chemotherapy. In our study, leukemia patients were divided into two groups based on a seven-day threshold for the duration of post-chemotherapy neutropenia. Comparing the diversity and community structure of gut microbiota before chemotherapy, there were no significant differences between the two groups. However, the differential species analysis revealed that the species primarily characterizing the <7 days group included *Campylobacteria*, *Cytophagales*, *Campylobacterales*, *Cyclobacteriaceae*, *Leuconostocaceae*, and *Stomatobaculum*. In contrast, the ≥7 days group was characterized by *Epsilonbacteraeota*, *Enterococcaceae*, and *Mycrobacteriaceae*. Correlation analysis showed that *Enterococcaceae* was associated with the duration of neutropenia, suggesting its predictive value. Additionally, our study confirmed that both the alpha diversity and beta diversity of gut microbiota in AML patients decreased after chemotherapy, consistent with previous extensive research (Montassier et al., 2015).

The correlation between gut microbiota and chemotherapy has been extensively studied. Gut microbiota can regulate chemotherapeutic drugs through various mechanisms, including direct cytotoxicity, bacterial translocation, immune response, drug metabolism, drug efficacy, and the elimination and impairment of anti-cancer effects (Yip and Chan, 2015). On the other hand, chemotherapy significantly reduces gut microbial diversity, even without antibiotic use, and our findings corroborate this (Lee et al., 2019). In addition, studies have demonstrated the association between gut microbiota and hematopoiesis. For example, Staffas et al. utilized a germ-free mouse model of HSCT. They found that providing additional enteral nutrition to the germ-free mice improved gut microbiota depletion, thereby promoting hematopoietic recovery (Staffas et al., 2018). Hao Guo et al. discovered that the increased abundance of *Muribaculaceae* and *Enterococcaceae* was associated with hematopoietic recovery and gastrointestinal repair after radiotherapy (Guo et al., 2020).

Enterococcus is a genus of Gram-positive, facultative anaerobic cocci commonly found in the gastrointestinal tracts of humans and animals. In healthy individuals, *Enterococcus* acts as a commensal organism, maintaining gut microbial balance and regulating the immune system. However, it is also considered an opportunistic pathogen, especially in immunocompromised individuals, where it is more likely to cause infections. Multiple studies have linked *Enterococcus* to adverse events. For instance, in children with ALL, the dominance of *Enterococcus* in the gut predicts FN or diarrheal diseases post-chemotherapy (Hakim et al., 2018). Sørum et al. recently explored the connection between gut microbiota composition and the duration of neutropenia, finding that prolonged neutropenia in children with acute lymphoblastic leukemia post-chemotherapy was associated with reduced abundances of *Ruminococcaceae* and *Lachnospiraceae*, as well as a decrease in *Veillonella* and an overgrowth of *Enterococcus* (Sørum et al., 2024), which is consistent with our conclusion. The *Enterococcus* can trigger a systemic inflammatory response (Yuen and Ausubel, 2014), releasing pro-inflammatory cytokines (Park et al., 2013), which attract neutrophils to migrate to extravascular tissues. Combined with decreased bone marrow function, this can reduce peripheral blood ANC, thereby prolonging the duration of neutropenia post-chemotherapy. Additionally, studies have shown that a high abundance of *Enterococcus* prior to chemotherapy predicts an increased risk of infection during the neutropenic phase post-chemotherapy (Hakim et al., 2018), leading to an increased use of antibiotics. Antibiotic use alters the microbiome composition

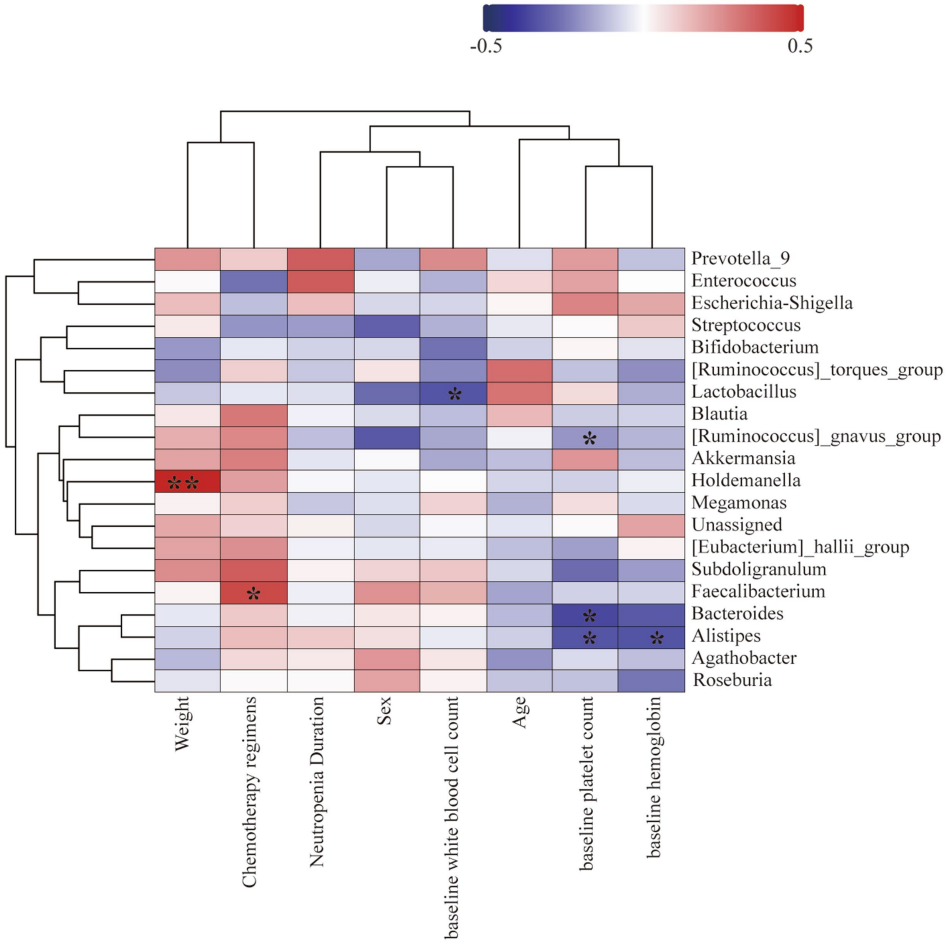

FIGURE 6
The heatmap illustrates the correlation between different bacteria and patient age, gender, weight, baseline white blood cell count, baseline hemoglobin, baseline platelet count, and the duration of neutropenia. Blue squares represent negative Spearman rank correlation coefficients, while red squares represent positive Spearman rank correlation coefficients. Darker shades of blue or red indicate higher correlation values. Pearson's correlation coefficients are shown in the figure (* $p < 0.05$, ** $p < 0.01$).

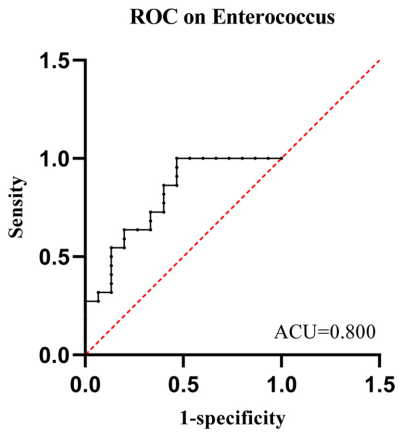

FIGURE 7
The ROC curve demonstrates the predictive value of Enterococcaceae for outcomes in the NLE7 Group and NGT7 Group.

and metabolites, which in turn impacts hematopoietic homeostasis and increases the likelihood of neutropenia (Fernandez-Sanchez et al., 2024). Chen et al. explored the relationship between granulopoiesis and gut microbiota in a chemotherapy-induced neutropenic mouse model and found that gut decontamination with oral antibiotics suppressed T-cell production of IL-17A and impaired neutrophil recovery (Chen et al., 2022). Josefsdottir et al. demonstrated that broad-spectrum antibiotic treatment-induced microbiota depletion disrupted baseline Stat1 signalling and altered T cell homeostasis, leading to impaired granulocyte maturation (Josefsdottir et al., 2017). Based on these findings, we hypothesize that a high abundance of *Enterococcus* prior to chemotherapy may indirectly prolong the time required for granulopoiesis. The relationship and underlying mechanisms between *Enterococcus* and prolonged neutropenia post-chemotherapy warrant further investigation.

An important contribution of our study is the identification of *Enterococcus* as a potential biomarker for predicting the duration of chemotherapy-induced neutropenia in leukemia

patients. ROC curve analysis showed that the relative abundance of *Enterococcus* had a high accuracy in predicting the duration of neutropenia, suggesting new possibilities for utilizing gut microbiota in personalized treatment in future clinical practice. Additionally, given the increasing preclinical evidence that modulation of gut microbiota can mitigate chemotherapy-related complications, translating our findings into clinical practice could represent a significant breakthrough in preventing such complications. For example, supplementing specific probiotics may help maintain or restore the healthy balance of gut microbiota, thereby reducing chemotherapy-induced neutropenia and other complications (Chrysostomou et al., 2023). However, it is important to note that with the increasing use of probiotics, there have been more reports on the incidence of bacteremia associated with probiotic use in both immunocompetent and immunocompromised patients (Sada et al., 2024). Therefore, probiotics must be used cautiously, and more clinical evidence is needed to guide their safe application.

This study has some limitations. Firstly, the sample size is relatively small, and not all patients provided stool samples after chemotherapy, which may limit the statistical power and generalizability of the findings. Additionally, it did not account for other factors that could contribute to differences in the gut microbiota, such as diet, age, and body mass index. Future studies with larger sample sizes may improve our ability to detect inter-group differences and minimize the impact of these factors through subgroup analyses. Additionally, although we found an association between the abundance of *Enterococcus* and the duration of neutropenia, the specific mechanisms remain unclear and require further experimental investigation.

Overall, our study reveals the potential role of gut microbiota, particularly *Enterococcus*, in predicting the duration of chemotherapy-induced neutropenia in leukemia patients. This finding provides new evidence for gut microbiota as predictive biomarkers for chemotherapy side effects and may offer important guidance for the personalized treatment of leukemia patients. Future research should further explore the regulatory mechanisms of gut microbiota and validate our results in larger-scale clinical trials to facilitate the clinical translation and application of these findings.

5 Conclusion

Our study confirmed the association between gut microbiota and the duration of neutropenia following chemotherapy in leukemia patients. Given the increasing preclinical evidence that modulating gut microbiota can mitigate chemotherapy-related complications, translating these findings into clinical practice could represent a significant breakthrough in preventing such complications.

Data availability statement

The data presented in this study are deposited in the NCBI SRA repository, accession number PRJNA1233767.

Ethics statement

The studies involving humans were approved by Ethics Committee of the Second Affiliated Hospital of Nanchang University. The studies were conducted in accordance with the local legislation and institutional requirements. The participants provided their written informed consent to participate in this study.

Author contributions

YH: Data curation, Software, Writing – original draft, Writing – review & editing. LL: Conceptualization, Data curation, Writing – original draft. YJ: Data curation, Writing – review & editing DT: Conceptualization, Funding acquisition, Supervision, Writing – review & editing. ST: Conceptualization, Writing – review & editing.

Funding

The author(s) declare that financial support was received for the research and/or publication of this article. This research was supported by the National Natural Science Fund of China (NSFC-82160029 and NSFC-8236050479) and Jiangxi Provincial Nature Science Foundation (20232ACB206014).

Acknowledgments

The authors thank all the patients participating in the study and all the caregivers and physicians in the Second Affiliated Hospital of Nanchang University.

Conflict of interest

The authors declare that the research was conducted in the absence of any commercial or financial relationships that could be construed as a potential conflict of interest.

Generative AI statement

The author(s) declare that no Gen AI was used in the creation of this manuscript.

Publisher's note

All claims expressed in this article are solely those of the authors and do not necessarily represent those of their affiliated organizations, or those of the publisher, the editors and the reviewers. Any product that may be evaluated in this article, or claim that may be made by its manufacturer, is not guaranteed or endorsed by the publisher.

References

Andreeva, N. V., Gabbasova, R. R., and Grivennikov, S. I. (2020). Microbiome in cancer progression and therapy. *Curr. Opin. Microbiol.* 56, 118–126. doi: 10.1016/j.mib.2020.09.001

Bodey, G. P., Buckley, M., Sathe, Y. S., and Freireich, E. J. (1966). Quantitative relationships between circulating leukocytes and infection in patients with acute leukemia. *Ann. Intern. Med.* 64, 328–340. doi: 10.7326/0003-4819-64-2-328

Caballero-Flores, G., Pickard, J. M., and Núñez, G. (2023). Microbiota-mediated colonization resistance: mechanisms and regulation. *Nat. Rev. Microbiol.* 21, 347–360. doi: 10.1038/s41579-022-00833-7

Chen, X., Hashimoto, D., Ebata, K., Takahashi, S., Shimizu, Y., Shinozaki, R., et al. (2022). Reactive granulopoiesis depends on T-cell production of IL-17A and neutropenia-associated alteration of gut microbiota. *Proc. Natl. Acad. Sci. USA* 119:e2211230119. doi: 10.1073/pnas.2211230119

Cheng, W. Y., Wu, C. Y., and Yu, J. (2020). The role of gut microbiota in cancer treatment: friend or foe? *Gut* 69, 1867–1876. doi: 10.1136/gutjnl-2020-321153

China Anti-Cancer Association Tumor Clinical Chemotherapy Professional Committee and China Anti-Cancer Association Tumor Support Therapy Professional Committee (2023). Consensus on clinical diagnosis, treatment, and prevention of chemotherapy-induced neutropenia in China (2023 edition). *Zhonghua Zhong Liu Za Zhi* 45, 575–583. doi: 10.3760/cma.j.cn112152-20230224-00076

Chrysostomou, D., Roberts, L. A., Marchesi, J. R., and Kinross, J. M. (2023). Gut microbiota modulation of efficacy and toxicity of cancer chemotherapy and immunotherapy. *Gastroenterology* 164, 198–213. doi: 10.1053/j.gastro.2022.10.018

Fernandez-Sanchez, J., Rodgers, R., Maknojia, A. A., Shaikh, N., Yan, H., Mejia, M. E., et al. (2024). Antibiotic-associated neutropenia is marked by the depletion of intestinal Lachnospiraceae and associated metabolites in pediatric patients. *Hemasphere* 8:e70038. doi: 10.1002/hem3.70038

Galloway-Peña, J. R., Shi, Y., Peterson, C. B., Sahasrabhojane, P., Gopalakrishnan, V., Brumlow, C. E., et al. (2020). Gut microbiome signatures are predictive of infectious risk following induction therapy for acute myeloid Leukemia. *Clin. Infect. Dis.* 71, 63–71. doi: 10.1093/cid/ciz777

Guo, H., Chou, W. C., Lai, Y., Liang, K., Tam, J. W., Brickey, W. J., et al. (2020). Multi-omics analyses of radiation survivors identify radioprotective microbes and metabolites. *Science* 370:aay9097. doi: 10.1126/science.aay9097

Hakim, H., Dallas, R., Wolf, J., Tang, L., Schultz-Cherry, S., Darling, V., et al. (2018). Gut microbiome composition predicts infection risk during chemotherapy in children with acute lymphoblastic Leukemia. *Clin. Infect. Dis.* 67, 541–548. doi: 10.1093/cid/ciy153

Josefsdottir, K. S., Baldridge, M. T., Kadmon, C. S., and King, K. Y. (2017). Antibiotics impair murine hematopoiesis by depleting the intestinal microbiota. *Blood* 129, 729–739. doi: 10.1182/blood-2016-03-708594

Kloft, C., Wallin, J., Henningsson, A., Chatelut, E., and Karlsson, M. O. (2006). Population pharmacokinetic-pharmacodynamic model for neutropenia with patient subgroup identification: comparison across anticancer drugs. *Clin. Cancer Res.* 12, 5481–5490. doi: 10.1158/1078-0432.CCR-06-0815

Lalami, Y., and Klastersky, J. (2017). Impact of chemotherapy-induced neutropenia (CIN) and febrile neutropenia (FN) on cancer treatment outcomes: an overview about well-established and recently emerging clinical data. *Crit. Rev. Oncol. Hematol.* 120, 163–179. doi: 10.1016/j.critrevonc.2017.11.005

Lee, S., Ritchie, E. K., Miah, S., Andy, C., Curcio, T., Goudy, F., et al. (2019). Changes in gut microbial diversity and correlations with clinical outcomes in patients with newly diagnosed acute myeloid Leukemia (AML) receiving intensive chemotherapy. *Blood* 134:1336. doi: 10.1182/blood-2019-125441

Liu, H. (2021). Emerging agents and regimens for AML. *J. Hematol. Oncol.* 14:49. doi: 10.1186/s13045-021-01062-w

Lyman, G. H., Lyman, C. H., and Agboola, O. (2005). Risk models for predicting chemotherapy-induced neutropenia. *Oncologist* 10, 427–437. doi: 10.1634/theoncologist.10-6-427

Montassier, E., Gastinne, T., Vangay, P., Al-Ghalith, G. A., Bruley Des Varannes, S., Massart, S., et al. (2015). Chemotherapy-driven dysbiosis in the intestinal microbiome. *Aliment. Pharmacol. Ther.* 42, 515–528. doi: 10.1111/apt.13302

O'Toole, P. W., and Paoli, M. (2023). The human microbiome, global health and the sustainable development goals: opportunities and challenges. *Nat. Rev. Microbiol.* 21, 624–625. doi: 10.1038/s41579-023-00924-z

Park, O. J., Han, J. Y., Baik, J. E., Jeon, J. H., Kang, S. S., Yun, C. H., et al. (2013). Lipoteichoic acid of *Enterococcus faecalis* induces the expression of chemokines via TLR2 and PAFR signaling pathways. *J. Leukoc. Biol.* 94, 1275–1284. doi: 10.1189/jlb.1012522

Sada, R. M., Matsuo, H., Motooka, D., Kutsuna, S., Hamaguchi, S., Yamamoto, G., et al. (2024). *Clostridium butyricum* Bacteremia associated with probiotic use, Japan. *Emerg. Infect. Dis.* 30, 665–671. doi: 10.3201/eid3004.231633

Sørum, ME, Boulund, U, De Pietri, S, Weischendorff, S, Enevold, C, Rathe, M, et al. Changes in gut microbiota predict neutropenia after induction treatment in childhood acute lymphoblastic leukemia. Blood Adv. (2024), doi: 10.1182/bloodadvances.2024013986. [Epub ahead of print].

Stabell, N., Nordal, E., Stensvold, E., Gammelsrud, K. W., Lund, B., Taxt, A., et al. (2008). Febrile neutropenia in children with cancer: a retrospective Norwegian multicentre study of clinical and microbiological outcome. *Scand. J. Infect. Dis.* 40, 301–307. doi: 10.1080/00365540701670436

Staffas, A., Burgos da Silva, M., Slingerland, A. E., Lazrak, A., Bare, C. J., Holman, C. D., et al. (2018). Nutritional support from the intestinal microbiota improves hematopoietic reconstitution after bone marrow transplantation in mice. *Cell Host Microbe* 23, 447–57.e4. doi: 10.1016/j.chom.2018.03.002

Yip, L. Y., and Chan, E. C. (2015). Investigation of host-gut microbiota modulation of therapeutic outcome. *Drug Metab. Dispos.* 43, 1619–1631. doi: 10.1124/dmd.115.063750

Yoon, S. E., Kang, W., Choi, S., Park, Y., Chalita, M., Kim, H., et al. (2023). The influence of microbial dysbiosis on immunochemotherapy-related efficacy and safety in diffuse large B-cell lymphoma. *Blood* 141, 2224–2238. doi: 10.1182/blood.2022018831

Yue, B., Gao, R., Wang, Z., and Dou, W. (2021). Microbiota-host-Irinotecan Axis: a new insight toward Irinotecan chemotherapy. *Front. Cell. Infect. Microbiol.* 11:710945. doi: 10.3389/fcimb.2021.710945

Yuen, G. J., and Ausubel, F. M. (2014). *Enterococcus* infection biology: lessons from invertebrate host models. *J. Microbiol.* 52, 200–210. doi: 10.1007/s12275-014-4011-6

frontiers | Frontiers in Microbiology

TYPE Original Research
PUBLISHED 25 March 2025
DOI 10.3389/fmicb.2025.1504264

Check for updates

OPEN ACCESS

EDITED BY
Jason W. Soares,
Combat Capabilities Development Command United States Army, United States

REVIEWED BY
Yafei Duan,
South China Sea Fisheries Research Institute, China
Yuanyang Dong,
Shanxi Agricultural University, China

*CORRESPONDENCE
Minhong Zhang
zhangminhong@caas.cn

RECEIVED 30 September 2024
ACCEPTED 10 March 2025
PUBLISHED 25 March 2025

CITATION
Yu M, Xu M, Wang G, Feng J and Zhang M (2025) Effects of different photoperiods on melatonin level, cecal microbiota and breast muscle morphology of broiler chickens.
Front. Microbiol. 16:1504264.
doi: 10.3389/fmicb.2025.1504264

COPYRIGHT
© 2025 Yu, Xu, Wang, Feng and Zhang. This is an open-access article distributed under the terms of the Creative Commons Attribution License (CC BY). The use, distribution or reproduction in other forums is permitted, provided the original author(s) and the copyright owner(s) are credited and that the original publication in this journal is cited, in accordance with accepted academic practice. No use, distribution or reproduction is permitted which does not comply with these terms.

Effects of different photoperiods on melatonin level, cecal microbiota and breast muscle morphology of broiler chickens

Miao Yu[1], Mengjie Xu[1], Guangju Wang[1,2], Jinghai Feng[1] and Minhong Zhang[1]*

[1]State Key Laboratory of Animal Nutrition and Feeding, Institute of Animal Sciences, Chinese Academy of Agricultural Sciences, Beijing, China, [2]Adaptation Physiology Group, Wageningen University and Research, Wageningen, Netherlands

Long photoperiods are often characterized by enhanced oxidative stress-induced damage to skeletal muscle, reduced melatonin (MT) levels and intestinal microbiota dysfunction in broilers. In this study, we aimed to investigate the association of breast muscle morphology with melatonin levels and the cecal microbiota of broilers under different photoperiods. A total of 216 healthy 5-day-old Arbor Acres (AA) male broilers were randomly assigned to 12 L:12D, 18 L:6D and 24 L:0D photoperiods for 4 weeks (L = hours of light, D = hours of darkness). The concentration of inflammatory factors and MT concentrations was measured using ELISA kits, whereas breast muscle morphology was examined through the hematoxylin (H) and eosin (E) staining, and microbiota composition was identified through 16 s rRNA analysis. Extended light exposure significantly improved the growth rate of broilers, but significantly decreased feed efficiency (FE). Furthermore, it upregulated the concentration of IL-1β, IL-6 and TNF-α and induced an abnormal breast muscle morphology. Extended light exposure significantly decreased MT levels in the hypothalamus, cecum and breast muscle, while triggering the cecal microbiota composition disorder. Specifically, there was significant alteration to the dominant bacterial phylum, following exposure to long photoperiods, with the abundance of Firmicutes decreasing and the abundance of Bacteroidota increasing. Notably, the relative abundance of *Lactobacillus* showed a positive correlation with MT levels and a negative correlation with inflammatory cytokines. In conclusion, the present findings indicated that extended light exposure reduced the MT levels, which were related to disturbed cecal microbiota, damaging breast muscle morphology and inducing breast muscle inflammation in broilers.

KEYWORDS

photoperiod, melatonin, cecal microbiota, breast muscle morphology, inflammation

1 Introduction

Long photoperiods, which are commonly applied in the modern and intensive broiler industry, aim to maximize the production efficiency through enhanced feed intake (Lewis and Gous, 2007). The photoperiods have also been reported to be critical factors in creating a suitable breeding environment to meet the increasing demand in the broiler chicken market. However, long photoperiods have been shown to induce detrimental effects on the quality of chicken products have been reported. For instance, it was reported that long photoperiods increased oxidative stress levels in the breast muscle of broilers (Li et al., 2010; Tuell et al., 2020), which may potentially damage the skeletal muscle morphology and induce atrophy

(Zhang et al., 2023). Long photoperiods effectively increased the white striping occurrence of broilers, a muscle myopathy associated with oxidative stress (Gratta et al., 2023). Furthermore, photobiomodulation was found to enhance breast muscle atrophy in mice (Scalon et al., 2022). However, the influence of photoperiod treatments on breast muscle morphology is not completely understood.

Nighttime light exposure was demonstrated to decrease melatonin (MT) synthesis and secretion in broilers (Yang et al., 2022; Zhao et al., 2019; Saito et al., 2005). Notably, MT is a photoperiod-regulated hormone, involved in the transmission of photoperiodic signals to the peripheral organs (Tiwari et al., 2023). Understanding how the MT pathway regulates peripheral organ function in response to diverse photoperiods is a critical frontier in biological research. Some studies postulated that MT may alter skeletal muscle growth in birds and mammals: improving the myofiber formation of chick embryos (Bai et al., 2019), enhancing lipid mobilizing action in the skeletal muscle of the pigeon (John and George, 1976) and increasing the RNA content in the breast muscle of Japanese quail *Coturnix coturnix japonica* (Zeman et al., 1993). In mice, MT plays a role in the repair of skeletal muscle morphology injury (Su et al., 2023; Salagre et al., 2023), and, in rats, it accelerates the repair of muscle injury to promote skeletal muscle development and growth (Duan et al., 2022; Salucci et al., 2021). MT maintains the homeostasis of gut microbiota has been shown by influencing the intestinal bacterial community in broilers (Wang et al., 2020). Specifically, MT altered microbiota diversity, composition and function in geese (Li et al., 2020) and improved ileal morphology, barrier function, short-chain fatty acid (SCFA) profile, and microbial flora in laying ducks (Cui et al., 2022). Exogenous melatonin supplementation attenuated the intestinal microbiota disruption and restored normal intestinal microbiota function in mice (Li et al., 2023; Li et al., 2023).

Studies have uncovered that gut microbiota imbalance is often positively correlated with stress (Clavijo and Flórez, 2018). Exposure to different photoperiods induced alterations of the gut microbiota composition in broilers and mice (Oyola et al., 2021; Wang et al., 2018). Elsewhere, it was found that endogenous gut microbes studies have found that endogenous gut microbes regulated skeletal muscle growth in broilers (Jiang et al., 2023). In broiler, intestinal microbiota plays an important role in skeletal muscle development by modulating body metabolism and immunity (Zhang et al., 2022; Yin et al., 2024; Zhang et al., 2022). There is evidence that gut microbiota may regulate wooden breast myopathy by fine-tuning the dynamic changes in digestive metabolites in broilers (Kang et al., 2022). Moreover, breast muscle metabolites were strongly associated with various aspects of cecal microbes in broilers (Feng et al., 2022; Wen et al., 2023). However, research on the association of melatonin and cecal microbiota with the morphology of breast muscle under different photoperiods is limited. In this study, we speculated that melatonin and gut microbiota might be potential regulatory pathways mediating the effects of photoperiods. The aim of this study was to investigate the association between MT and cecal microbiota under extended light exposure and explore the potential regulatory pathways by which different photoperiods affect breast muscle morphology of broilers.

2 Materials and methods

The study was approved by the Institutional Ethics Committee of Experiment Animal Welfare and Ethics at the Institute of Animal Science of Chinese Academy of Agricultural Sciences (CAAS) (permit number: IAS 2022–117), and all the methods were carried out in accordance with relevant Institutional guidelines and regulations. And this study was confirmed that all methods were carried out in accordance with the guidelines and regulations of The ARRIVE guidelines 2.0.

2.1 Birds and experimental design

A total of 216 Arbor Acres (AA) male broilers (5-day old) with similar body weight (75 g ± 10) were randomly assigned to 3 photoperiod treatments (SD, LD and FD) with 6 replicates per treatment, with 12 broilers per replicate. The 3 groups (SD, LD and FD) received different photoperiods with 12 L:12D (SD, 12 h light), 18 L:6D (LD, 18 h light) and 24 L:0D (FD, 24 h light) for 4 weeks, respectively. The bird houses illuminated with LED lighting with 20 lux light intensity. All groups (SD, LD, and FD) received a standard corn and soybean meal basal diet in three feeding programs (5–7 days-old, 8–20 days-old and 21–32 days-old) (Table 2), formulated according to AA broiler recommendations (SCRIBD, 2019). The formal experimental period lasted 4 weeks (from 5 to 32 day of age). Broilers were housed in stainless steel cages without roofs (0.82 m width×0.70 m length×0.60 m height). The temperature and humidity shall be carried out according to the standard of the AA Broiler Feeding Management Manual. All broilers were farmed in different artificial climate chambers with the same size (4.08 m × 2.88 m × 2.38 m) of State Key Laboratory of Animal Nutrition and Feeding, Chinese Academy of Agricultural Sciences. Except for the photoperiods in the artificial climate chambers, other environmental parameters remained the same. Broilers were allowed free access to experimental diets and water (Table 1).

2.2 Sample collection

On 14 d and 28 d, one broiler from each replicate was selected with body weights close to the average after 12 h of feed deprivation. Then, the broilers from each group were killed by carbon dioxide (CO_2). Tissue samples of the hypothalamus and breast muscle rinsed with sterile normal saline (NaCl 9 g/L) were immediately collected and snap-frozen in liquid nitrogen, then kept in a − 80°C freezer for measurements of gene expression and biochemical analysis. Another part of the breast muscle was immobilized by 4% paraformaldehyde to hematoxylin–eosin (HE) staining for histomorphological analysis. Cecal contents were immediately collected at d 28, and snap-frozen in liquid nitrogen, then kept in a − 80°C freezer for high-throughput sequencing and further analysis.

2.3 Performance

On 14 d and 28 d, the provided and residual feed amount, and broiler body weight of each replicate were recorded. The average body weight, average daily gain (ADG), average daily feed intake (ADFI), and feed efficiency (FE, FE = ADG/ADFI) were calculated. The right breast muscle of 1 broiler chicken from each replicate was randomly selected to determine the right breast muscle weight and right breast muscle mass-body mass ratio.

TABLE 1 Composition and nutrient levels of basic diets.

Items	5–7 days-old	8–20 days-old	21–32 days-old
Ingredient	Content (%)		
Corn	51.44	54.08	56.85
Soybean meal	40.21	36.82	33.86
Soybean oil	3.94	5.00	5.50
Limestone	1.00	0.85	0.90
$CaHPO_4$	1.89	1.80	1.50
NaCl	0.30	0.30	0.30
DL-Methionine	0.21	0. 19	0. 19
L-Lysine	0.36	0.32	0.30
L-Threonine	0. 15	0. 14	0. 10
Premix[1]	0.50	0.50	0.50
Total	100	100	100
Nutrient levels[2]			
ME/(MJ/Kg)	2,961	3,038	3,095
CP (%)	22. 55	21.18	19.97
CF (%)	10.54	10.38	11.35
Ca (%)	0.94	0.85	0.79
AP (%)	0.43	0.41	0.35
Lysine (%)	1.46	1.34	1.25
Methionine (%)	0.54	0.51	0.49
Methionine+ cysteine (%)	0.92	0.87	0.84

ME, metabolizable energy; CP, crude protein; CF, crude fat; AP, available phosphorus.
[1]Premix provided the following per kg of the diet: 5–7 days-old: vitamin A 12000 IU, vitamin D_3 5,000 IU, vitamin E 80 mg, vitamin K_3 3.2 mg, vitamin B_1 3.2 mg, vitamin B_2 8.6 mg, vitamin B_6 4.3 mg, vitamin B_{12} 17 μg, pantothenic acid calcium 20 mg, nicotinic acid 65 mg, folic acid 2.2 mg, biotin 0.22 mg, choline 1,020 mg, Cu ($CuSO_4{\cdot}5H_2O$) 16 mg, Fe ($FeSO_4{\cdot}7H_2O$) 20 mg, Zn ($ZnSO_4{\cdot}7H_2O$) 110 mg, Mn ($MnSO^4{\cdot}H_2O$) 120 mg, Se (Na_2SeO_3) 0.3 mg, I (KI) 1.25 mg; 8–20 days-old: vitamin A 10000 IU, vitamin D_3 4,500 IU, vitamin E 65 mg, vitamin K_3 3.0 mg, vitamin B_1 2.5 mg, vitamin B_2 6.5 mg, vitamin B_6 3.2 mg, vitamin B_{12} 17 μg, pantothenic acid calcium 18 mg, nicotinic acid 60 mg, folic acid 1.9 mg, biotin 0.18 mg, choline 1,020 mg, Cu ($CuSO_4{\cdot}5H_2O$) 16 mg, Fe ($FeSO_4{\cdot}7H_2O$) 20 mg, Zn ($ZnSO_4{\cdot}7H_2O$) 110 mg, Mn ($MnSO_4{\cdot}H_2O$) 120 mg, Se (Na_2SeO_3) 0.3 mg, I (KI) 1.25 mg; 21–32 days-old: vitamin A 9000 IU, vitamin D_3 4,000 IU, vitamin E 55 mg, vitamin K_3 2.2 mg, vitamin B_1 2.2 mg, vitamin B_2 5.4 mg, vitamin B_6 2.2 mg, vitamin B_{12} 11 μg, pantothenic acid calcium 15 mg, nicotinic acid 45 mg, folic acid 1.6 mg, biotin 0.15 mg, choline 950 mg, Cu ($CuSO_4{\cdot}5H_2O$) 16 mg, Fe ($FeSO_4{\cdot}7H_2O$) 20 mg, Zn ($ZnSO_4{\cdot}7H_2O$) 110 mg, Mn ($MnSO_4{\cdot}H_2O$) 120 mg, Se (Na_2SeO_3) 0.3 mg, I (KI) 1.25 mg.
[2]ME determination was performed in the State Key Laboratory of Animal Nutrition and Feeding according to the bionic digestive Operation manual SDS3, CP content determination was conducted by using a Kjeldahl nitrogen analyzer and CF content determination was conducted by using a Soxhlet extractor. Other Nutrient levels were calculated value according to the Tables of Feed Composition and Nutritive Values in China (2022).

2.4 Inflammatory cytokines analysis of the breast muscle

The interleukin (IL)-1β (ZB00001DU, Zhongshang Boao Biotechnology Co., Ltd., Beijing, China), IL-6 (ZB00006DU, Zhongshang Boao Biotechnology Co., Ltd., Beijing, China) and tumor necrosis factor (TNF)-α (KJEIA0018D, Kangjia Hongyuan Biotechnology Co., Ltd., Beijing, China) concentrations in breast muscle were measured using ELISA kits by the Multiskan MK3 microplate reader (Thermo Fisher Scientific, Massachusetts, United States) according to the manufacturer's instructions. Transfer the breast muscle into a glass homogenizer and add 5–10 mL of pre-cooled PBS buffer (1: 5 mass/volume ratio of tissue to PBS buffer is recommended) for thorough grinding, centrifuge the prepared homogenate at 3500 r/min for 15 min, and then retain the supernatant for assay (Yu et al., 2024). All the kits are chicken-specific. The intra-assay coefficient and the inter-assay coefficient of variation were 5 and 10%, respectively.

2.5 Breast muscle histology analysis

4% Paraformaldehyde-fixed breast muscle were embedded in paraffin (KD-BMIV biological tissue embedding machine, KEDEE, Jinhua, China) after being trimmed, dehydrated, transparentized, and waxed. After the wax block was made, the samples were sectioned (KD-2268 paraffin microtome, KEDEE, Jinhua, China) and then stained with hematoxylin (H) and eosin (E). The sections of each tissue were observed using a panoramic scanner (PANORAMIC® 250 Flash III DX, 3DHISTECH Ltd., Budapest, Hungary) and photographed.

2.6 MT concentrations analysis of hypothalamus and cecum

The concentrations of MT in the hypothalamus and cecum were measured using ELISA kits (CEA908Ge, Kangjia Hongyuan Biotechnology Co., Ltd., Beijing, China) by the Multiskan MK3 microplate reader (Thermo Fisher Scientific, Massachusetts, United States) according to the manufacturer's instructions. The sample handling procedure was the same as described in 2.4. This kit was specifically used to detect MT and showed no obvious cross-reactivity with other similar substances. This kit was suitable for the pan-species (general) in all tissues. The intra-assay coefficient and the inter-assay coefficient of variation were 5 and 10%, respectively.

2.7 DNA extraction and 16 s rRNA analysis

Total microbial genomic DNA was extracted from cecal content samples using the E.Z.N.A.® soil DNA Kit (Omega Bio-tek, Norcross, GA, U.S.) according to the manufacturer's instructions. The quality and concentration of DNA were determined by 1.0% agarose gel electrophoresis and a NanoDrop2000 spectrophotometer (Thermo Scientific, United States) and kept at −80°C before further use. The hypervariable region V3-V4 of the bacterial 16S rRNA gene was amplified with primer pairs 338F (5'-ACTCCTACGGGAGG CAGCAG-3′) and 806R (5'-GGACTACHVGGGTWTCTAAT-3′) (Liu et al., 2016) byT100 Thermal Cycler PCR thermocycler (BIO-RAD, United States). The PCR product was extracted from 2% agarose gel and purified using the PCR Clean-Up Kit (YuHua, Shanghai, China) according to manufacturer's instructions and quantified using Qubit 4.0 (Thermo Fisher Scientific, USA). Purified amplicons were pooled in equimolar amounts and paired-end sequenced on an Illumina PE300/PE250 platform (Illumina, San Diego, USA) according to the standard protocols by Majorbio Bio-Pharm

10.3389/fmicb.2025.1504264

TABLE 2 Effects of different photoperiods on the performance of broilers.

Item	SD	LD	FD	SEM	*p* value
1-14d					
Average body weight/g	679.56^{b}	781.89^{a}	794.21^{a}	12.89	<0.001
ADG/g	42.74^{b}	50.10^{a}	50.90^{a}	0.93	<0.001
ADFI/g	45.07^{c}	53.21^{b}	65.10^{a}	2.02	<0.001
FE	0.95^{a}	0.94^{a}	0.78^{b}	0.02	<0.001
Right breast muscle mass/g	50.35^{b}	62.81^{a}	66.43^{a}	1.89	<0.001
Right breast muscle mass-body mass ratio/%	7.31^{c}	7.89^{b}	8.51^{a}	0.15	0.001
15-28d					
ADG/g	91.17^{b}	101.01^{a}	101.53^{a}	1.32	<0.001
ADFI/g	113.55^{c}	137.27^{b}	152.10^{a}	3.94	<0.001
FE	0.80^{a}	0.74^{b}	0.67^{c}	0.01	<0.001
Right breast muscle growth/g	153.85^{b}	173.83^{a}	182.60^{a}	3.99	0.003
Right breast muscle growth-body growth ratio/%	12.13	12.43	12.72	0.93	0.576
1-28d					
Average body weight/g	1956.00^{b}	2195.99^{a}	2215.60^{a}	29.71	<0.001
ADG/g	68.21^{b}	76.76^{a}	77.47^{a}	1.06	<0.001
ADFI/g	78.15^{c}	93.69^{b}	101.50^{a}	2.40	<0.001
FE	0.87^{a}	0.82^{b}	0.76^{c}	1.18	<0.001
Right breast muscle mass/g	204.20^{b}	236.65^{a}	249.03^{a}	5.32	<0.01
Right breast muscle mass-body mass ratio/%	10.44^{b}	10.78^{ab}	11.24^{a}	0.16	0.109

ADG, average daily gain; ADFI, average daily feed intake; FE, feed efficiency. ^{a,b}Within a row, values with different superscripts indicate the significant difference ($p < 0.05$).

Technology Co. Ltd. (Shanghai, China). Raw FASTQ files were de-multiplexed using an in-house perl script, and then quality-filtered by fastp version 0.19.6 and merged by FLASH version 1.2.7. To minimize the effects of sequencing depth on alpha and beta diversity measure, the number of 16S rRNA gene sequences from each sample were rarefied to 20,000, which still yielded an average Good's coverage of 99.09%, respectively.

2.8 Statistical analysis

All the results from the experiment were analyzed by using the 1-way ANOVA, performed using SPSS 23.0 (SPSS Inc., Chicago, IL). GraphPad Prism 8.0 (GraphPad Inc., San Diego, CA) was used for drawing. Replicate ($n = 6$) served as the experimental unit. The results in the tables are shown with the mean ± standard error of the mean (SEM). The $p > 0.05$, and $p < 0.05$ were deemed the statistical non-significance and significance, respectively. Bioinformatic analysis of the cecal content microbiota was carried out using the Majorbio Cloud platform.[1] The taxonomy of each OTU representative sequence was analyzed by RDP Classifier version 2.2 against the 16S rRNA gene database (eg. Silva v138) using confidence threshold of 0.7. Based on the OTUs information, rarefaction curves and alpha diversity indices were calculated with Mothur v1.30.1 (Schloss et al., 2009). The similarity among the microbial communities in different samples was determined by principal coordinate analysis (PCoA) based on Bray–curtis dissimilarity using Vegan v2.5–3 package. The PERMANOVA test was used to assess the percentage of variation explained by the treatment along with its statistical significance using Vegan v2.5–3 package. A correlation between two nodes was considered to be statistically robust if the spearman's correlation coefficient over 0.6 or less than −0.6, and the *p* value less than 0.01.

3 Results

3.1 Effects of different photoperiods on growth performance

As shown in Table 2, long photoperiods had significant effects on the ADG and ADFI ($p < 0.05$). Furthermore, in the FD group, FE was significantly reduced ($p < 0.05$). In the 1–14 days of the experiment, the LD group and the FD group broilers had a significant increase in the ADG and ADFI compared to those in the SD group, with increases of 17.33 and 19.33%, and 18.07 and 22.37%, respectively. Additionally, compared with the SD group, the right breast muscle mass ($p < 0.05$) and right breast muscle mass-body mass ratio ($p < 0.05$) were significantly increased due to long photoperiods. However, there was a significant decrease in FE in the LD group and the FD group by 17.38 and 16.81% compared to the SD group, respectively ($p < 0.05$). During weeks 3 to 4 of the experiment, the LD group and the FD group had significantly higher ADG and ADFI than the SD group ($p < 0.05$), while the FE of the LD group and the FD group significantly decreased by 8.26 and 16.77% compared to that of the SD group,

1 https://cloud.majorbio.com

respectively. The increasing light time had a significant effect on right breast muscle growth, with a 14.90 and 20.75% increase in the LD group and the FD group, respectively ($p < 0.05$), while there was no significant effect on the right breast muscle growth-body growth ratio ($p = 0.576$). Additionally, compared with the SD group, both the LD group and the FD group significantly increased the ADG and ADFI over the 4 weeks ($p < 0.05$), but the LD group and the FD group had a significant decrease in the FE ($p < 0.05$). On day 28 of the trial, both the LD group and the FD group significantly increased the right breast muscle mass compared to the SD group ($p < 0.05$). However, only the right breast muscle mass-body mass ratio of the FD group significantly increased, whereas that of the LD group had no significant effect compared to the SD group ($p = 0.109$). These data suggest that the long photoperiods led to a substantial improvement in growth rate, with a significant decrease in the FE.

3.2 Effects of different photoperiods on MT levels of hypothalamus and cecum

To investigate the impact of different photoperiods on melatonin, we measured the MT concentrations in the hypothalamus, cecum and breast muscle (Figure 1). As depicted in Figure 1, following treatment with extending light exposure, the concentrations of MT significantly decreased in the hypothalamus, cecum and breast muscle ($p < 0.05$).

3.3 Effects of different photoperiods on breast muscle tissue morphology by HE staining

As depicted in Figures 2A–C, we observed abnormal organizational structure in both the LD group and the FD group during 14 days. The overall structure of the breast muscle appeared normal in the 14d SD group, with no signs of muscle fiber atrophy or necrosis (black arrow indicates muscle fiber) (Figure 2A). However, the 14d LD group exhibited mild histopathological abnormalities in the breast muscle, including necrosis (black arrow indicates muscular bundle morphology lysis and disappearance) and minor myogenic injury in the muscular bundle (red arrow indicates intranuclear migration) (Figure 2B). Additionally, the 14d FD group showed injuries to the overall structure of the breast muscle, such as extensive muscular bundle injury and atrophy (black arrow indicates increasing gap, red arrows indicate intranuclear migration), muscular bundle interstitium fibrosis (yellow arrow indicates fibroblast hyperplasia), and inflammatory cell infiltration (green arrow) (Figure 2C).

As also shown in Figures 2D–F, the abnormal organizational structure was observed to increase in the LD group and the FD group at 28 days. The overall structure of the breast muscle in the 28d SD group was normal, similar to that of the 14d SD group (Figure 2D). The 28-day LD group exhibited both myogenic injury and atrophy, as indicated by the increasing gap (black arrows) and intranuclear migration (red arrows) (Figure 2E). Similarly, the breast muscle in the 28-day FD group showed abnormalities throughout the day, with myogenic injury and atrophy observed in the muscular bundle, along with increasing gaps (black arrows), intranuclear migration (red arrows), and fibroblast hyperplasia in the muscular bundle interstitium (yellow arrows) (Figure 2F). The above results suggested that extended light exposure could injure the breast muscle morphology with inflammatory cell infiltration.

To further verify the inflammation levels of the breast muscles, we examined the levels of IL-1 β, IL-6 and TNF α in the breast muscle. The inflammatory factor concentrations on the breast muscle of broilers significantly increased under extending light exposure. On 14d and 28d, compared with the SD group, the concentrations of IL-1 β, IL-6 and TNF α in breast muscle significantly increased in the LD group and the FD group ($p < 0.05$; Figure 3).

3.4 Effects of different photoperiods on cecal microbiota of broilers

Finally, we analyzed the composition of cecal microbiota. The ACE index (A), Chao index (B), Shannon index (C), and Simpson index (D) are shown in Figure 4. The results indicated that the indices reflecting species richness (ACE index and Chao index) had no significant effect under different photoperiods ($p > 0.05$). However, the indices of community diversity (Shannon index and Simpson index) were significantly affected ($p < 0.05$) under different photoperiods. These findings suggested that the community diversity

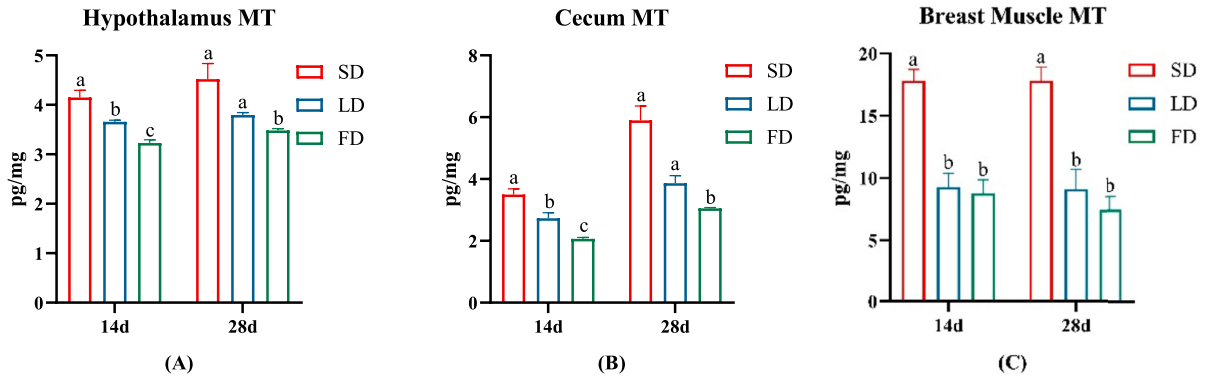

FIGURE 1
Effects of different photoperiods on MT concentrations of broilers. **(A)** Hypothalamus. **(B)** Cecum. **(C)** Breast muscle. Data are presented as Mean ± SEMs. Different superscripts (a, b, c) in each parameter indicate significance ($p < 0.05$).

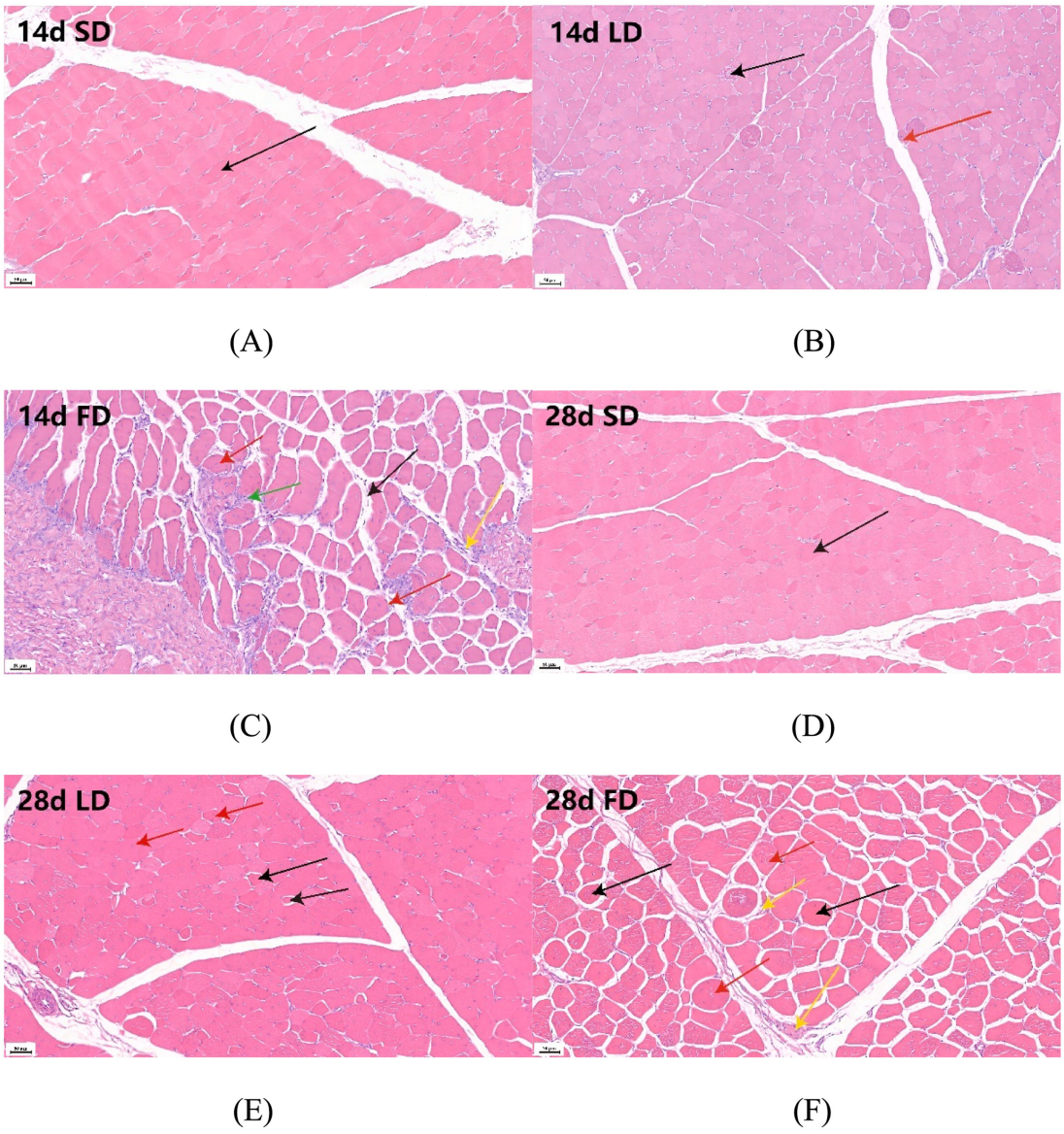

FIGURE 2
Effects of different photoperiods on the breast muscle morphology of broilers. **(A)** 14d SD group. **(B)** 14d LD group. **(C)** 14d FD group. **(D)** 28d SD group. **(E)** 28d LD group. **(F)** 28d FD group. Figures were 20× magnification. **(A)** The black arrow indicates muscle fiber. **(B)** The black arrow indicates muscular bundle morphology lysis and disappearance; the red arrow indicates intranuclear migration. **(C)** The black arrow indicates an increasing gap; the red arrows indicate intranuclear migration; the yellow arrow indicates fibroblast hyperplasia; the green arrow indicates inflammatory cell infiltration. **(D)** The black arrow indicates muscle fiber. **(E)** The black arrow indicates an increasing gap; the red arrow indicates intranuclear migration. **(F)** The black arrow indicates an increasing gap; the red arrows indicate intranuclear migration; the yellow arrow indicates fibroblast hyperplasia.

exhibited an increase followed by a decrease with the increase of photoperiods. At the OTU level, Venn diagram showed microorganisms found in the cecal content were identified with 664, 698, and 813 OTUs, respectively. (Figure 5). Moreover, the overall structure of the cecal microbiota on the OTU level in the three groups significantly differed ($R^2 = 0.4282$, $p = 0.001$), as analyzed by principal coordinate analysis (PCoA) (Figure 6).

Taxon-based analysis showed the cecal microbial composition markedly changed on account of different light treatments (Figures 7A,B). Relative abundance analysis of the top 10 phyla in the cecal microbiota was shown in Figure 7A, it was found that *Firmicutes* and *Bacteroidota* were the dominant microbiota, with the relative abundance in the three groups 95.91, 90.75, 41.28, and 2.99%, 8.22, 52.22%, respectively. The relative abundance of *Firmicutes* and *Bacteroidota* was significantly decreased and increased in the FD group, respectively, compared with the SD group and LD group ($p < 0.05$). The FD group significantly increased the relative abundance of *Proteobacteria* in comparison with the SD group ($p < 0.05$). Compared with the LD group, the relative abundance of *Cyanobacteria* had markedly increased in the FD group ($p < 0.05$). Relative abundance analysis of bacteria in the cecal microbiota was shown in Figure 7B, it was found that *Lactobacillus*, *Bacteroides*, *Faecalibacterium*, *norank_f__norank_o__Clostridia_UCG-014*, *norank_f__norank_o__Clostridia_vadinBB60_group*, *Alistipes*, *Barnesiella*, *unclassified_f__Lachnospiraceae*, *UCG-005* and *norank_f__Ruminococcaceae* was the top 10 bacteria with higher

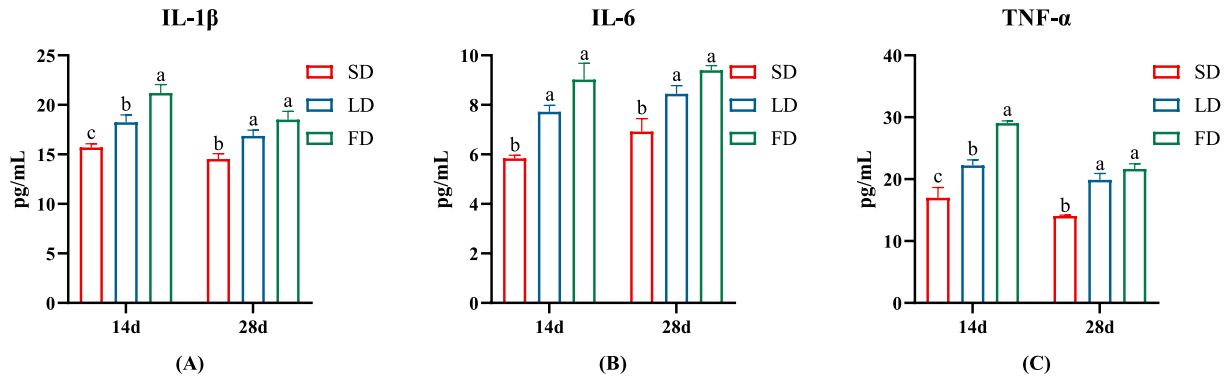

FIGURE 3
Effects of different photoperiods on inflammatory cytokines concentrations of broilers. **(A)** IL-1β. **(B)** IL-6. **(C)** TNF-α. Data are presented as Mean ± SEMs. Different superscripts (a, b, c) in each parameter indicate significance ($p < 0.05$).

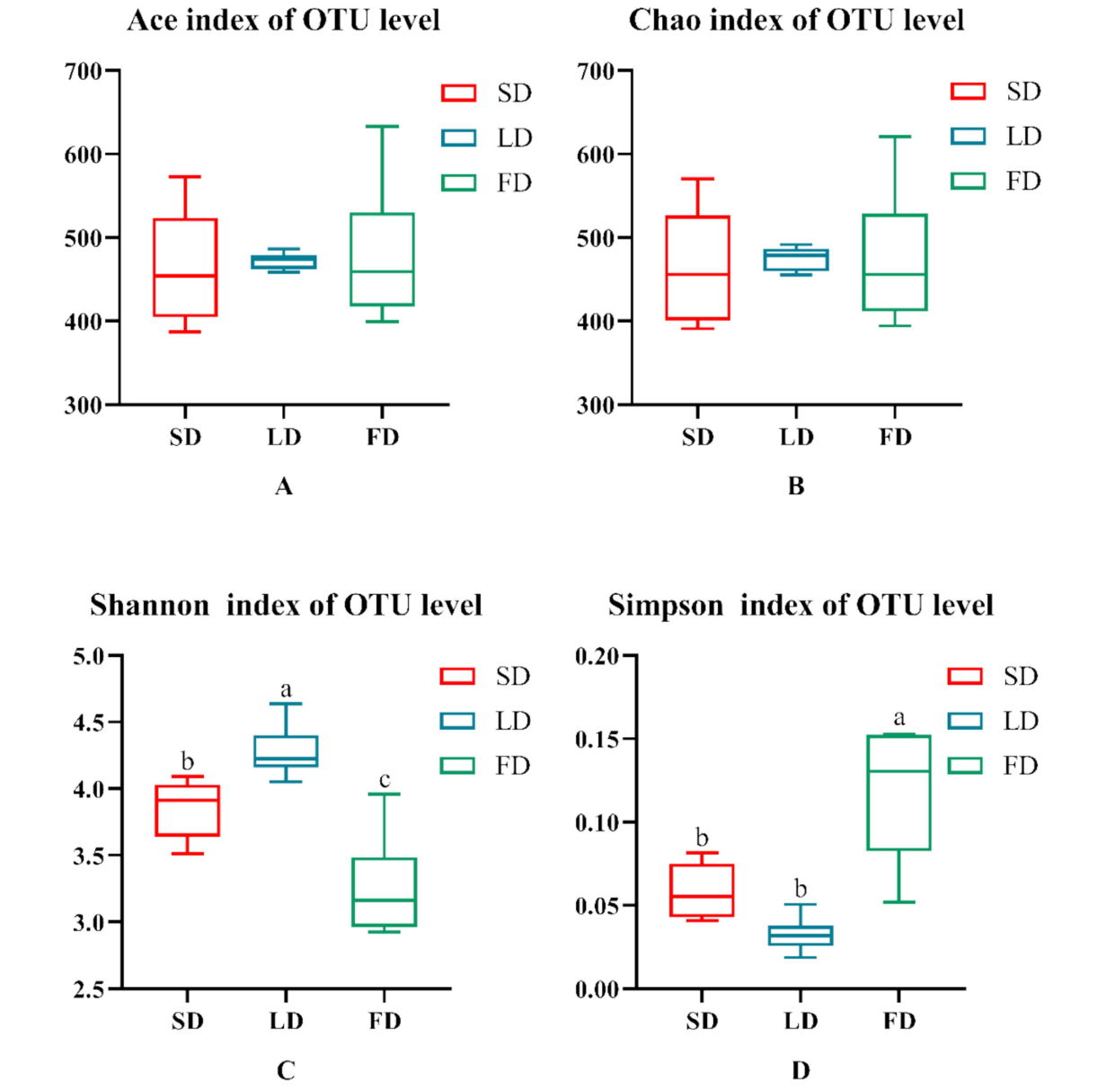

FIGURE 4
Indexes of alpha diversity of the microbiota. **(A)** Ace. **(B)** Chao. **(C)** Shannon. **(D)** Simpson. Data are presented as Mean ± SEMs. Different superscripts (a, b, c) in each parameter indicate significance ($p < 0.05$).

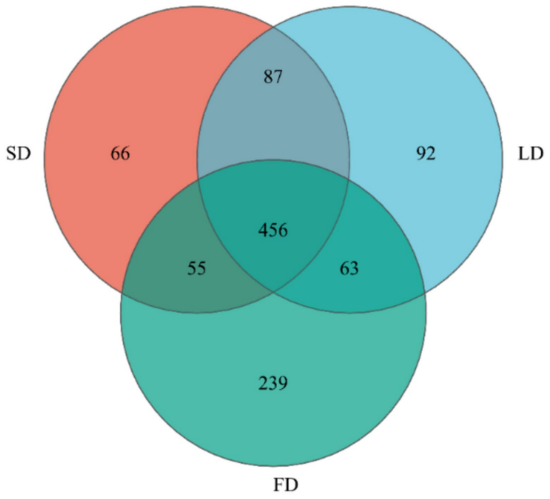

FIGURE 5
Venn diagram on OTU level.

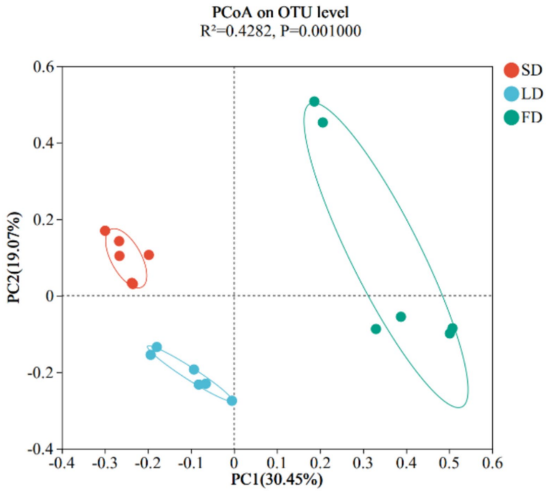

FIGURE 6
Beta diversity was calculated using Principle Coordinates Analysis plots based on unweighted UniFrac distance.

relative abundance. To evaluate the impact of different photoperiods on the taxonomic composition of microorganisms in the cecal contents, Kruskal-Wallis H test was employed to determine the genera with significant effects on the three groups. As shown in Figure 8, the results were mainly evaluated for the top 20 bacteria under three different photoperiods. The results indicated that there were 8 bacteria (*Lactobacillus*, *norank_f__norank_o__Clostridia_UCG-014*, *unclassified_f__Lachnospiraceae*, *norank_f__Ruminococcaceae*, *Ruminococcus_torques_group*, *norank_f__Eubacterium_coprostanoligenes_group*, *norank_f__norank_o__RF39*, *unclassified_f__Oscillospiraceae*) was significantly changed under different photoperiods. The relative abundance of *Lactobacillus*, *norank_f__norank_o__Clostridia_UCG-014*, *norank_f__Eubacterium_coprostanoligenes_group* was markedly reduced with longer photoperiods ($p < 0.05$; Figures 8A,B,F). As the photoperiods increased, the relative abundance of *unclassified_f__Lachnospiraceae*, *norank_f__Ruminococcaceae*, *Ruminococcus_torques_group*, *norank_f__norank_o__RF39* and *unclassified_f__Oscillospiraceae* first enriched and then reduced ($p < 0.05$; Figures 8C–E,G,H).

To investigate the correlation between microbiota abundance with MT, IL-1β, IL-6 and TNF-α, we analyzed that by environmental factor correlation analysis based on Spearman correlation analysis (Figure 9). At the genus level, the relative abundance of *Lactobacillus*, *norank_f__norank_o__Clostridia_UCG-014*, *norank_f__Eubacterium_coprostanoligenes_group* and *norank_f__norank_o__RF39* was a positive correlation with MT and negative correlation with IL-1β, IL-6 and TNF-α, *Bacteroides* and *Barnesiella* was negative correlation with MT and positive correlation with IL-1β, IL-6 and TNF-α. Furthermore, *Prevotellaceae_NK3B31_group* had a negative correlation with MT, and norank_f__norank_o__Clostridia_vadinBB60_group had a negative correlation with IL-1β.

4 Discussion

The main aim of this study was to explore the association between MT and cecal microbiota under extended light exposure as well as the potential regulatory pathways mediating the effects of different photoperiods on the breast muscle morphology of broilers. Recent studies have shown that continuous long photoperiods may negatively affect broiler health and welfare (Tuell et al., 2020). The results indicated that exposure to long photoperiods increased growth rate but decreased FE, impaired breast muscle morphology and significantly increased the concentrations of IL-1β, IL-6 and TNFα in breast muscle. Furthermore, MT was found to be related to cecal microbiota under different photoperiods, which also affected breast muscle morphology and inflammation of broilers.

Previous research has shown that long photoperiods enhance the growth rate and overall chicken production performance (Zhang et al., 2022; Ingram et al., 2000). Similarly, this study found LD and FD photoperiods increased the growth rate of broilers. During the 4-week trial period, the FE was significantly decreased following FD treatment. This finding was consistent with results from previous studies, which uncovered faster growth rates and higher FCR (Olanrewaju et al., 2006; Shynkaruk et al., 2022).

Notably, broilers are highly sensitive to changes in light, with studies showing that light stimulation enhances the inhibition of MT secretion from the pineal gland via the superior cervical ganglion by the suprachiasmatic nucleus of the hypothalamus under light stimulation, whereas in the absence of light stimulation at night, the pineal gland secretes MT (Shichida and Matsuyama, 2009). Nighttime light exposure decreases MT secretion (Yang et al., 2024), and in this study, we found that MT concentrations in the hypothalamus, cecum and breast muscle of broilers decreased significantly under extended light exposure. This is consistent with previous studies (Yang et al., 2024), demonstrating that extended light exposure may decrease MT levels.

Modern broilers are often genetically selected for higher breast muscle yield and faster growth rates. However, they are particularly vulnerable to oxidative stress (Xing et al., 2022; Pontes et al., 2023). Guob et al. reported that a longer photoperiod may increase oxidative stress levels (Guo et al., 2010). In this study, the concentrations of

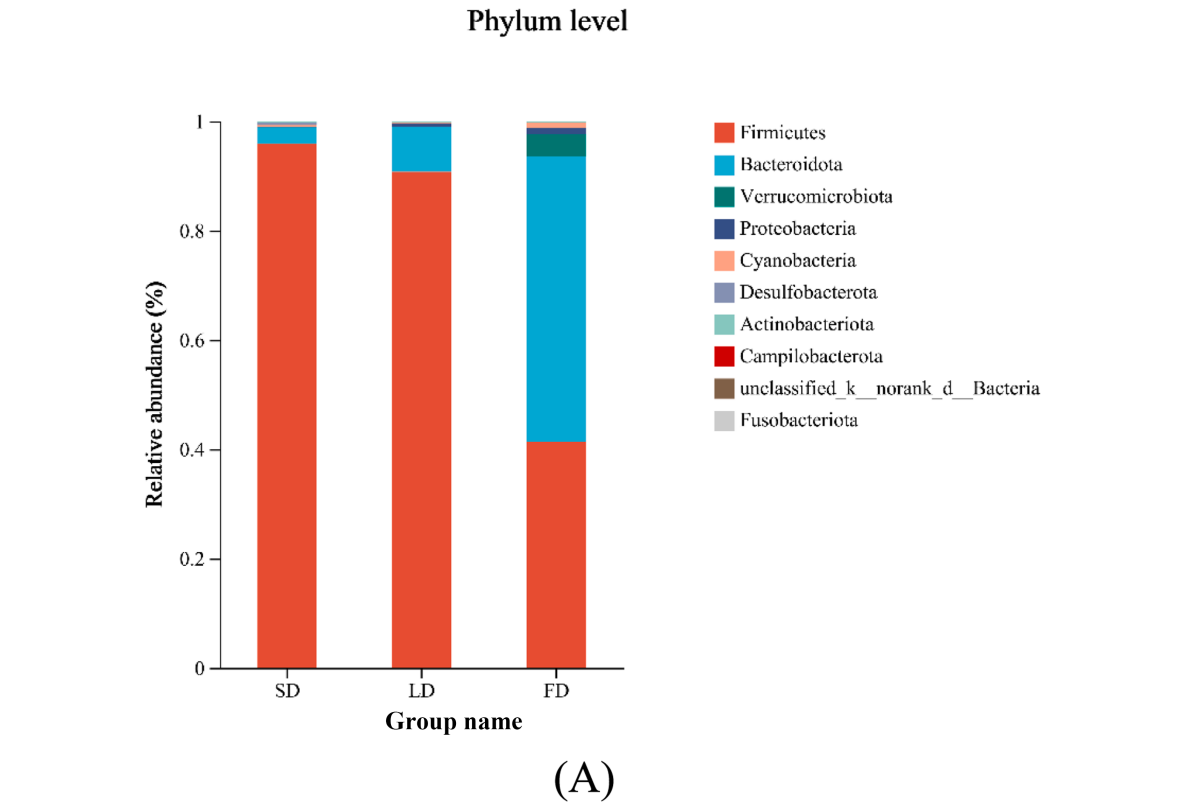

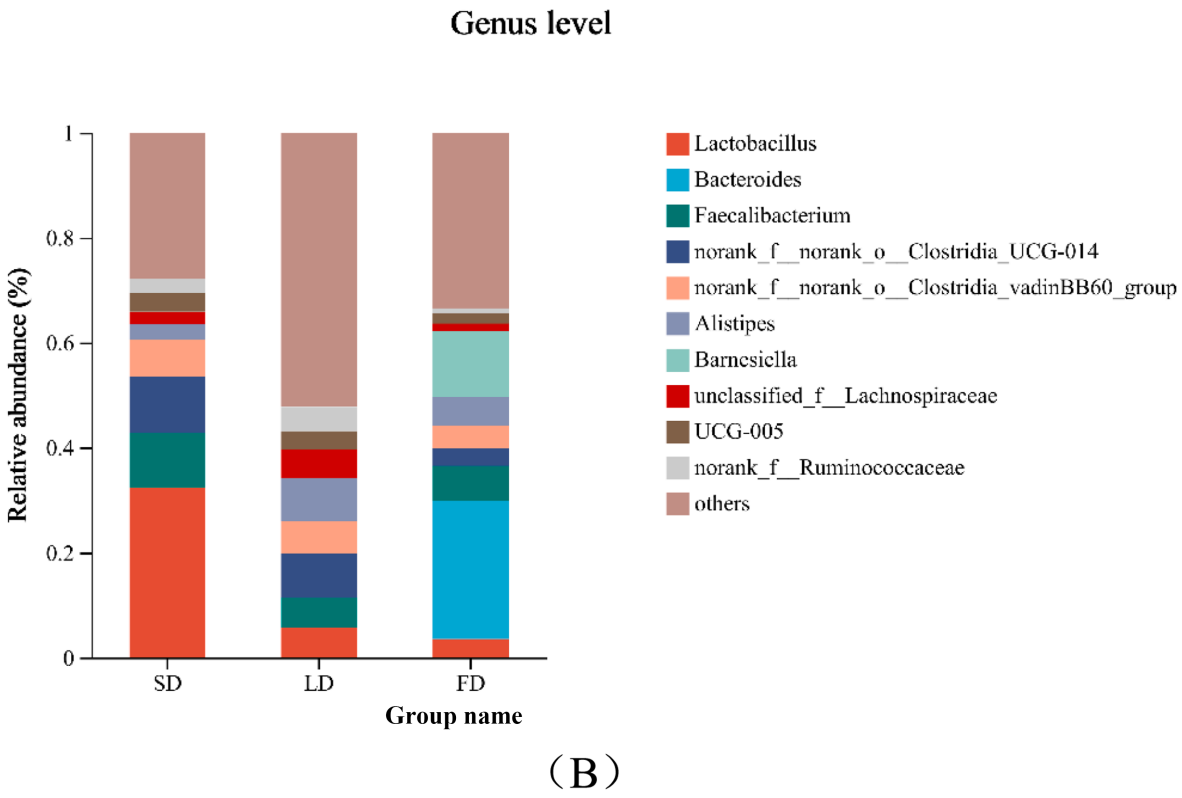

FIGURE 7
Relative abundance of cecal microbiology composition at the phylum and genus and species in the different photoperiods group. **(A)** Relative abundance of cecal microbiology at the phylum; **(B)** relative abundance of cecal microbiology at the genus.

10.3389/fmicb.2025.1504264

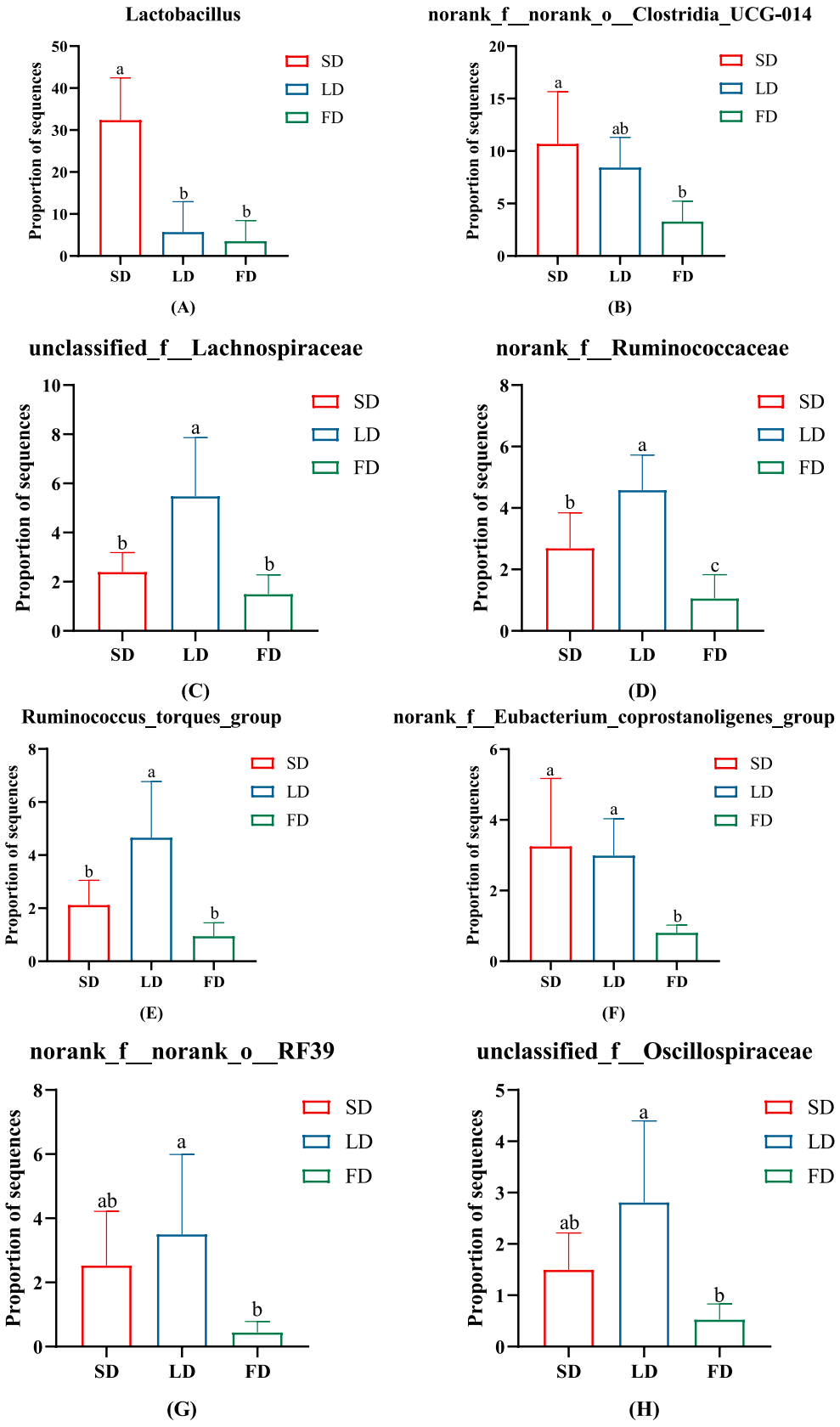

FIGURE 8
The significant change in the relative abundance of cecal microbiota on genus levels. **(A)** *Lactobacillus*. **(B)** *norank_f__norank_o__Clostridia_UCG-014*. **(C)** *unclassified_f__Lachnospiraceae*. **(D)** *norank_f__Ruminococcaceae*. **(E)** *Ruminococcus_torques_group*. **(F)** *norank_f__Eubacterium_coprostanoligenes_group*. **(G)** *norank_f__norank_o__RF39*. **(H)** *unclassified_f__Oscillospiraceae*. Data are presented as Mean ± SDs. Different superscripts (a, b, c) in each parameter indicate significance ($p < 0.05$).

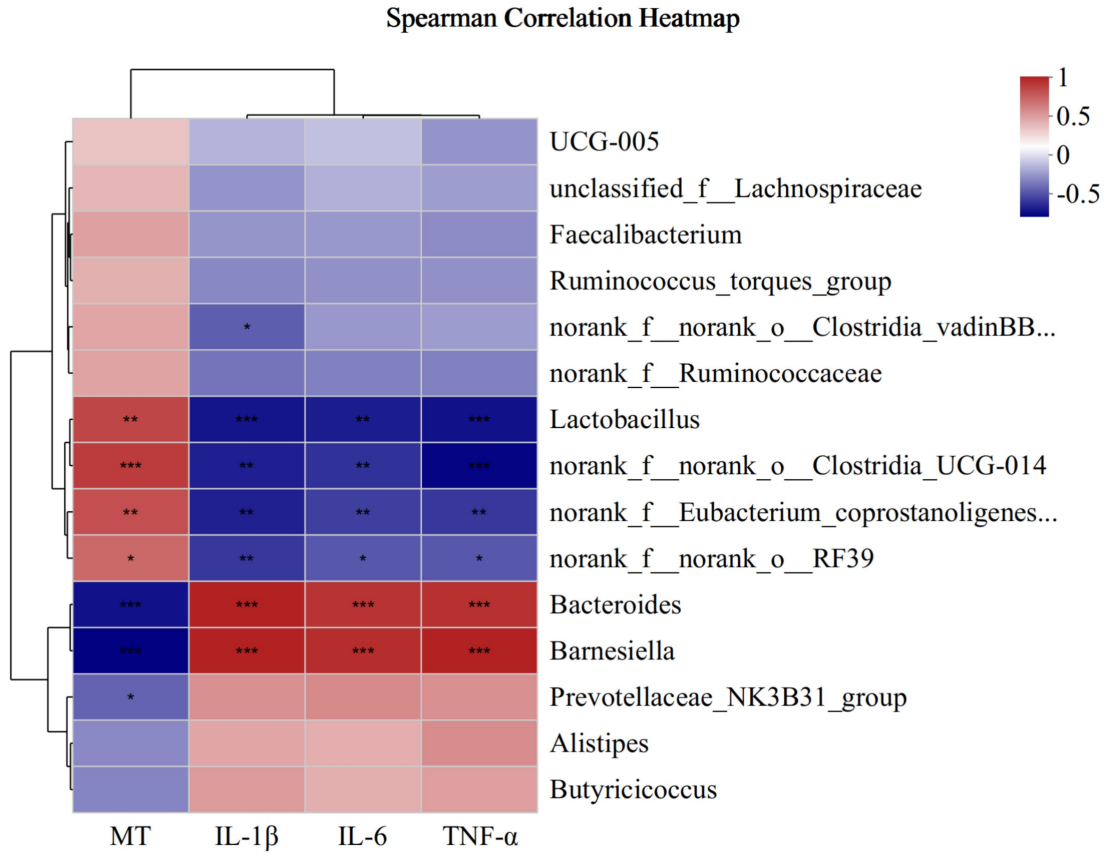

FIGURE 9
Correlation between microbiota abundance with cecum MT, IL-1β, IL-6 and TNF-α at the genus. * means $p \leq 0.05$, ** means $p \leq 0.01$, *** means $p \leq 0.001$.

IL-1β, IL-6 and TNFα increased in the breast muscle accompanied by inflammatory cell infiltration in the breast muscle of broilers under FD treatment. Moreover, the injury to the breast muscle was positively correlated with the IL-1β, IL-6 and TNFα levels. Therefore, we speculated that the injury was induced by an inflammatory response following long photoperiod which might be related to oxidative stress. In summary, the results of this study showed that prolonged exposure to light exposure caused morphological injury and inflammation in the breast muscles of broiler chickens, especially under the FD treatment.

Cecal microbiota are important modulators of various pathological processes. The cecum harbors a wide range of symbiotic bacteria, which participate in microbial fermentation and prevent pathogen colonization (Huang et al., 2018; Guarner and Malagelada, 2003). Therefore, the diversity and composition of cecal microflora mature and stabilize as the broilers age, reaching a stable state in 21 days (Zhou et al., 2021). In this study, we characterized the cecal microbiota composition of 33-day-old broilers following exposure to different photoperiods. The alpha richness index (diversity within a community) of cecal microbiota first increased and then reduced with longer photoperiods. This was consistent with findings from previous studies exploring the effects of 12.5 L:11.5D and 16 L: 8D photoperiods, suggesting that the obtained observations were induced by the effects of long photoperiods on broiler metabolism (Wang et al., 2018). At the phylum level, Firmicutes was the dominant bacterial phylum across the three photoperiods. The dominant bacterial phylum in the FD group changed to *Bacteroidota* instead of *Firmicutes*, and *Bacteroidota*, *Proteobacteria*, and *Cyanobacteria* were significantly elevated in the FD group. Researchers have shown that *Firmicutes* are beneficial bacteria, and a decrease in their relative abundance increases the risk of systemic inflammation and development of certain diseases (Samaddar et al., 2022; Qu et al., 2022). Numerous pathogens belonging to the *Proteobacteria*, may cause diseases to broilers (He et al., 2022). Therefore, the observed difference in the FD group may be explained by the increased effect of the treatment on cecal microbiota, which enhanced cecal microbial disorders and increased the relative abundance of harmful bacteria. At the genus level, *Lactobacillus* was enriched in the SD group. The genus *Lactobacillus* contains probiotics which has been reported to be decreased under long photoperiods (Song et al., 2020; Zhang et al., 2022). A study found that the relative abundance of *Lactobacillus* influenced the development of inflammation in broilers (Yang et al., 2020; Khalique et al., 2019), suggesting that exposure to long photoperiods may suppress the abundance of probiotics and trigger cecal microbiota disorder, possibly by increasing inflammation levels. Interestingly, we found that the relative abundance of *Ruminococcus_torques_group* initially increased and then reduced with the prolongation of light exposure. The *Ruminococcus_torques_group* has been associated with inflammation and the occurrence of various health issues, including neurological diseases and abdominal fat deposition (Zheng et al., 2020; Blacher et al., 2019; Chen et al., 2022; Xiang et al., 2024; Lyu et al., 2021). However, the function of *Ruminococcus_torques_group* on broilers and its

changes under different photoperiods has not been clarified. The decrease in *Ruminococcus_torques_group* in the FD treatment may be attributed to the severe disruption of cecal microbial composition. Notably, the *Ruminococcus_torques_group* belongs to *Firmicutes*, which was reduced by 46.63% in the FD treatment, accompanied by a decrease in the relative abundance of *Ruminococcus_torques_group*. The ratio of *Ruminococcus_torques_group* to *Firmicutes* increased, suggesting enhanced relative abundance. Altogether, our results indicated that prolonged exposure to light significantly altered the cecal microbial composition in broiler chickens by reducing beneficial bacteria and enriching the relative abundance of harmful bacteria, causing the cecal microbiota disorder.

The brain-gut axis involves the bidirectional communication between the nervous, endocrine and immune systems (Liu et al., 2018). Numerous studies have shown that MT regulates gut microbiota composition (Iesanu et al., 2022; Ma et al., 2020). Studies have reported that alterations in the intestinal microbial composition could affect inflammation (Niu et al., 2022). To further explore the correlations among MT, cecal microbiota and inflammation in breast muscle under different photoperiods, we analyzed the association of cecal microbiota with changes in MT, IL-1β, IL-6 and TNF-α levels. It was observed that the composition of cecal microbiota was significantly influenced by changes in MT, IL-1β, IL-6 and TNF-α concentrations. *Lactobacillus*, which is the most important probiotic in the cecum of broilers, was positively correlated with MT levels and negatively correlated with IL-1β, IL-6 and TNF-α levels. On the other hand, *Bacteroides* was found to enhance inflammation in mice (Li et al., 2020), and negatively correlated with MT levels and positively with IL-1β, IL-6 and TNF-α levels in this study. In comparison, *Barnesiella* has been reported to play dual roles in enteric infections: exerting colonization resistance against pathogenic invaders, while also inducing detrimental effects on the host (Bornet and Westermann, 2022). In this study, the relative abundance of Barnesiella increased as the concentrations of inflammatory markers increased and the MT levels decreased. This suggested that the decreased MT levels resulted in the down-regulation of the beneficial bacteria and an increased in harmful bacteria, inducing inflammation in the breast muscle of broilers.

Notably, the brain-gut axis is increasingly being recognized and studied. Here, we found that prolonged exposure of mice to light weakened the MT levels thereby reducing the number of beneficial bacteria and enriching the number of harmful bacteria, which caused morphological injury and inflammation in the breast muscle of broilers. Therefore, we speculated that the MT-gut axis may mediate the morphological injury and inflammation induced by prolonged exposure to light in the breast muscle of broilers. Furthermore, *Lactobacillus* was significantly reduced under extended light exposure, and closely related to MT, IL-1β, IL-6 and TNF-α levels, indicating that this bacterial genus may have an important regulator function on MT and inflammation; however, this requires further research.

In summary, this study demonstrated that prolonged exposure to light enhanced the growth rate of broilers. However, it reduced the FE, induced morphological injury and inflammation in the breast muscle of broilers, suppressed the MT levels and disrupted the cecal microbial structure. Moreover, the regulatory pathways mediating the effects of extended light exposure included inflammatory signaling in breast muscle driven by the MT-gut axis. These findings have important implications for future research into the role of MT and cecal microbiota in breast muscle morphology injury and inflammation under different photoperiods. To improve the meat quality of broilers, we recommend that the 18 L:6D photoperiod may be optimal compared with the 12 L:12D and 24 L:0D photoperiod.

Data availability statement

The data presented in the study are deposited in NCBI/SRA repository, accession number PRJNA1190345.

Ethics statement

The animal study was approved by the Institutional Ethics Committee of Experiment Animal Welfare and Ethics at the Institute of Animal Science of Chinese Academy of Agricultural Sciences (CAAS). The study was conducted in accordance with the local legislation and institutional requirements.

Author contributions

MY: Conceptualization, Data curation, Formal analysis, Investigation, Writing – original draft, Methodology, Project administration, Resources, Supervision, Visualization, Writing – review & editing. MX: Writing – review & editing, Investigation, Resources. GW: Writing – review & editing. JF: Writing – review & editing. MZ: Conceptualization, Methodology, Writing – review & editing, Supervision.

Funding

The author(s) declare that financial support was received for the research and/or publication of this article. This work was financially supported by grants from the Science and Technology Innovation Project of the Chinese Academy of Agricultural Sciences (Grant No. CAAS-ASTIP-IAS-08).

Acknowledgments

We would kindly to thank all workers in the State Key Laboratory of Animal Nutrition and Feeding for their help in completed the experiment.

Conflict of interest

The authors declare that the research was conducted in the absence of any commercial or financial relationships that could be construed as a potential conflict of interest.

Generative AI statement

The authors declare that no Gen AI was used in the creation of this manuscript.

Publisher's note

All claims expressed in this article are solely those of the authors and do not necessarily represent those of their affiliated organizations, or those of the publisher, the editors and the reviewers. Any product that may be evaluated in this article, or claim that may be made by its manufacturer, is not guaranteed or endorsed by the publisher.

References

Bai, X., Cao, J., Dong, Y., Wang, Z., and Chen, Y. (2019). Melatonin mediates monochromatic green light-induced satellite cell proliferation and muscle growth in chick embryo. *PLoS One* 14:e0216392. doi: 10.1371/journal.pone.0216392

Blacher, E., Bashiardes, S., Shapiro, H., Rothschild, D., Mor, U., Dori-Bachash, M., et al. (2019). Potential roles of gut microbiome and metabolites in modulating ALS in mice. *Nature* 572, 474–480. doi: 10.1038/s41586-019-1443-5

Bornet, E., and Westermann, A. J. (2022). The ambivalent role of Bacteroides in enteric infections. *Trends Microbiol.* 30, 104–108. doi: 10.1016/j.tim.2021.11.009

Chen, Z., Wang, Z., Li, D., Zhu, B., Xia, Y., Wang, G., et al. (2022). The gut microbiota as a target to improve health conditions in a confined environment. *Front. Microbiol.* 13:1067756. doi: 10.3389/fmicb.2022.1067756

Clavijo, V., and Flórez, M. J. V. (2018). The gastrointestinal microbiome and its association with the control of pathogens in broiler chicken production: a review. *Poult. Sci.* 97, 1006–1021. doi: 10.3382/ps/pex359

Cui, Y. M., Wang, J., Zhang, H. J., Qi, G. H., Qiao, H. Z., Gan, L. P., et al. (2022). Effect of changes in photoperiods on melatonin expression and gut health parameters in laying ducks. *Front. Microbiol.* 13:819427. doi: 10.3389/fmicb.2022.819427

Duan, J., Cheng, M., Xu, Y., Chen, Y., Gao, T., Gu, Q., et al. (2022). Exogenous melatonin alleviates skeletal muscle wasting by regulating hypothalamic neuropeptides expression in Endotoxemia rats. *Neurochem. Res.* 47, 885–896. doi: 10.1007/s11064-021-03489-6

Feng, Y., Liu, D., Liu, Y., Yang, X., Zhang, M., Wei, F., et al. (2022). Host-genotype-dependent cecal microbes are linked to breast muscle metabolites in Chinese chickens. *iScience* 25:104469. doi: 10.1016/j.isci.2022.104469

Gratta, F., Bošković Cabrol, M., Xiccato, G., Birolo, M., Bordignon, F., and Trocino, A. (2023). Effect of light restriction on productive results and behavior of broiler chickens. *Poult. Sci.* 102:103084. doi: 10.1016/j.psj.2023.103084

Guarner, F., and Malagelada, J. R. (2003). Gut flora in health and disease. *Lancet (London, England)* 361, 512–519. doi: 10.1016/S0140-6736(03)12489-0

Guo, Y. L., Li, W. B., and Chen, J. L. (2010). Influence of nutrient density and lighting regime in broiler chickens: effect on antioxidant status and immune function. *Br. Poult. Sci.* 51, 222–228. doi: 10.1080/00071661003746503

He, S., Cui, S., Song, W., Jiang, Y., Chen, H., Liao, D., et al. (2022). Interleukin-17 weakens the NAFLD/NASH process by facilitating intestinal barrier restoration depending on the gut microbiota. *MBio* 13:e0368821. doi: 10.1128/mbio.03688-21

Huang, P., Zhang, Y., Xiao, K., Jiang, F., Wang, H., Tang, D., et al. (2018). The chicken gut metagenome and the modulatory effects of plant-derived benzylisoquinoline alkaloids. *Microbiome* 6:211. doi: 10.1186/s40168-018-0590-5

Iesanu, M. I., Zahiu, C. D. M., Dogaru, I. A., Chitimus, D. M., Pircalabioru, G. G., Voiculescu, S. E., et al. (2022). Melatonin-microbiome two-sided interaction in Dysbiosis-associated conditions. *Antioxidants* 11:2244. doi: 10.3390/antiox11112244

Ingram, D. R., Hattens, L. F., and McPherson, B. N. (2000). Effects of light restriction on broiler performance and specific body structure measurements. *J. Appl. Poult. Res.* 9, 501–504. doi: 10.1093/japr/9.4.501

Jiang, X., Zhang, B., Lan, F., Zhong, C., Jin, J., Li, X., et al. (2023). Host genetics and gut microbiota jointly regulate blood biochemical indicators in chickens. *Appl. Microbiol. Biotechnol.* 107, 7601–7620. doi: 10.1007/s00253-023-12814-8

John, T. M., and George, J. C. (1976). Diurnal variation in the effect of melatonin on plasma and muscle free fatty acid levels in the pigeon. *Endocrinol. Exp.* 10, 131–137

Kang, K., Zhou, N., Peng, W., Peng, F., Ma, M., Li, L., et al. (2022). Multi-omics analysis of the microbiome and metabolome reveals the relationship between the gut microbiota and wooden breast myopathy in broilers. *Front. Vet. Sci.* 9:922516. doi: 10.3389/fvets.2022.922516

Khalique, A., Zeng, D., Wang, H., Qing, X., Zhou, Y., Xin, J., et al. (2019). Transcriptome analysis revealed ameliorative effect of probiotic *Lactobacillus johnsonii* BS15 against subclinical necrotic enteritis induced hepatic inflammation in broilers. *Microb. Pathog.* 132, 201–207. doi: 10.1016/j.micpath.2019.05.011

Lewis, P. D., and Gous, R. M. (2007). Broilers perform better on short or step-up photoperiods. *S. Afr. J. Anim. Sci.* 37, 90–96. doi: 10.4314/SAJAS.V37I2.4032

Li, W.-B., Guo, Y.-L., Chen, J.-L., Wang, R., He, Y. D., and Su, D.-G. (2010). Influence of lighting schedule and nutrient density in broiler chickens: effect on growth performance, carcass traits and meat quality. *Asian Australas. J. Anim. Sci.* 23, 1510–1518. doi: 10.5713/ajas.2010.10087

Li, W., Lu, L., Liu, B., and Qin, S. (2020). Effects of phycocyanin on pulmonary and gut microbiota in a radiation-induced pulmonary fibrosis model. *Biomed. Pharmacother.* 132:110826. doi: 10.1016/j.biopha.2020.110826

Li, W., Wang, Z., Cao, J., Dong, Y., and Chen, Y. (2023). Melatonin improves the homeostasis of mice gut microbiota rhythm caused by sleep restriction. *Microbes Infect.* 25:105121. doi: 10.1016/j.micinf.2023.105121

Li, X., Wang, F., Gao, Z., Huang, W., Zhang, X., Liu, F., et al. (2023). Melatonin attenuates chronic intermittent hypoxia-induced intestinal barrier dysfunction in mice. *Microbiol. Res.* 276:127480. doi: 10.1016/j.micres.2023.127480

Li, X., Zheng, Z., Pan, J., Jiang, D., Tian, Y., and Huang, Y. (2020). Influences of melatonin and endotoxin lipopolysaccharide on goose productive performance and gut microbiota. *Br. Poult. Sci.* 61, 217–224. doi: 10.1080/00071668.2019.1687851

Liu, F., Horton-Sparks, K., Hull, V., Li, R. W., and Martínez-Cerdeño, V. (2018). The valproic acid rat model of autism presents with gut bacterial dysbiosis similar to that in human autism. *Mol. Autism.* 9:61. doi: 10.1186/s13229-018-0251-3

Liu, C., Zhao, D., Ma, W., Guo, Y., Wang, A., Wang, Q., et al. (2016). Denitrifying sulfide removal process on high-salinity wastewaters in the presence of Halomonas sp. *Appl. Microbiol. Biotechnol.* 100, 1421–1426. doi: 10.1007/s00253-015-7039-6

Lyu, W., Liu, X., Lu, L., Dai, B., Wang, W., Yang, H., et al. (2021). Cecal microbiota modulates fat deposition in Muscovy ducks. *Front. Vet. Sci.* 8:609348. doi: 10.3389/fvets.2021.609348

Ma, N., Zhang, J., Reiter, R. J., and Ma, X. (2020). Melatonin mediates mucosal immune cells, microbial metabolism, and rhythm crosstalk: a therapeutic target to reduce intestinal inflammation. *Med. Res. Rev.* 40, 606–632. doi: 10.1002/med.21628

Niu, W., Yang, F., Fu, Z., Dong, Y., Zhang, Z., and Ju, J. (2022). The role of enteric dysbacteriosis and modulation of gut microbiota in the treatment of inflammatory bowel disease. *Microb. Pathog.* 165:105381. doi: 10.1016/j.micpath.2021.105381

Olanrewaju, H. A., Thaxton, J. P., Dozier Iii, W. A., Purswell, J. L., Roush, W. B., and Branton, S. L. (2006). A review of lighting programs for broiler production. *Int. J. Poult. Sci.* 5, 301–308. doi: 10.3923/ijps.2006.301.308

Oyola, M. G., Johnson, R. C., Bauman, B. M., Frey, K. G., Russell, A. L., Cho-Clark, M., et al. (2021). Gut microbiota and metabolic marker alteration following dietary isoflavone-photoperiod interaction. *Endocrinol. Diabetes Metab.* 4:e00190. doi: 10.1002/edm2.190

Pontes, M. P., Khatlab, A. S., Del Vesco, A. P., Granzoto, G. H., Soares, M. A. M., Sousa, F. C. B., et al. (2023). The effect of light regime and time of slaughter in broiler on broiler performance, liver antioxidant status, and expression of genes related to peptide absorption in the jejunum and melatonin synthesis in the brain. *J. Anim. Physiol. Anim. Nutr.* 107, 607–620. doi: 10.1111/jpn.13712

Qu, C., Li, Q. P., Su, Z. R., Ip, S. P., Yuan, Q. J., Xie, Y. L., et al. (2022). Nano-Honokiol ameliorates the cognitive deficits in TgCRND8 mice of Alzheimer's disease via inhibiting neuropathology and modulating gut microbiota. *J. Adv. Res.* 35, 231–243. doi: 10.1016/j.jare.2021.03.012

Saito, S., Tachibana, T., Choi, Y. H., Denbow, D. M., and Furuse, M. (2005). ICV melatonin reduces acute stress responses in neonatal chicks. *Behav. Brain Res.* 165, 197–203. doi: 10.1016/j.bbr.2005.06.045

Salagre, D., Raya Álvarez, E., Cendan, C. M., Aouichat, S., and Agil, A. (2023). Melatonin improves skeletal muscle structure and oxidative phenotype by regulating mitochondrial dynamics and autophagy in Zücker diabetic fatty rat. *Antioxidants* 12:1499. doi: 10.3390/antiox12081499

Salucci, S., Taurone, S., Burattini, S., Gobbi, P., Clausi, J., and Battistelli, M. (2021). Melatonin role in skeletal muscle disorders. *Eur. Rev. Med. Pharmacol. Sci.* 25, 1024–1033. doi: 10.26355/eurrev_202101_24672

Samaddar, A., van Nispen, J., Armstrong, A., Song, E., Voigt, M., Murali, V., et al. (2022). Lower systemic inflammation is associated with gut firmicutes dominance and reduced liver injury in a novel ambulatory model of parenteral nutrition. *Ann. Med.* 54, 1701–1713. doi: 10.1080/07853890.2022.2081871

Scalon, D., Picada, J. N., de Sousa, J. T., da Silva, A. T., Colares, J. R., and Marroni, N. A. P. (2022). Photobiomodulation intervention improves oxidative, inflammatory, and morphological parameters of skeletal muscle in cirrhotic Wistar rats. *Lasers Med. Sci.* 37, 1973–1982. doi: 10.1007/s10103-021-03458-z

Schloss, P. D., Westcott, S. L., Ryabin, T., Hall, J. R., Hartmann, M., Hollister, E. B., et al. (2009). Introducing mothur: open-source, platform-independent, community-supported software for describing and comparing microbial communities. *Appl. Environ. Microbiol.* 75, 7537–7541. doi: 10.1128/AEM.01541-09

SCRIBD. (2019). *Aviagen, Arbor Acres Broiler Nutrition Specifications 2019*.

Shichida, Y., and Matsuyama, T. (2009). Evolution of opsins and phototransduction. *Philos. Trans. R. Soc. Lond. Ser. B Biol. Sci.* 364, 2881–2895. doi: 10.1098/rstb.2009.0051

Shynkaruk, T., Buchynski, K., and Schwean-Lardner, K. (2022). Lighting programme as a management tool for broilers raised without antibiotics - impact on productivity and welfare. *Br. Poult. Sci.* 63, 761–767. doi: 10.1080/00071668.2022.2083943

Song, E. J., Han, K., Lim, T. J., Lim, S., Chung, M. J., Nam, M. H., et al. (2020). Effect of probiotics on obesity-related markers per enterotype: a double-blind, placebo-controlled, randomized clinical trial. *EPMA J.* 11, 31–51. doi: 10.1007/s13167-020-00198-y

Su, C. M., Tsai, C. H., Chen, H. T., Wu, Y. S., Chang, J. W., Yang, S. F., et al. (2023). Melatonin improves muscle injury and differentiation by increasing Pax7 expression. *Int. J. Biol. Sci.* 19, 1049–1062. doi: 10.7150/ijbs.79169

Tiwari, J., Sur, S., Naseem, A., Rani, S., and Malik, S. (2023). Photoperiodic modulation of melatonin receptor and immune genes in migratory redheaded bunting. *Comp. Biochem. Physiol. A Mol. Integr. Physiol.* 279:111381. doi: 10.1016/j.cbpa.2023.111381

Tuell, J. R., Park, J. Y., Wang, W., Cooper, B., Sobreira, T., Cheng, H. W., et al. (2020). Effects of photoperiod regime on meat quality. Oxidative stability, and metabolites of postmortem broiler fillet (M. pectoralis major) muscles. *Foods* 9:215. doi: 10.3390/foods9020215

Wang, J., Nesengani, L. T., Gong, Y., Yang, Y., and Lu, W. (2018). 16S rRNA gene sequencing reveals effects of photoperiod on cecal microbiota of broiler roosters. *PeerJ* 6:e4390. doi: 10.7717/peerj.4390

Wang, Y., Zhang, Z., Yang, P., Zhang, M., Xi, L., Liu, Q., et al. (2020). Molecular mechanism underlying the effect of illumination time on the growth performance of broilers via changes in the intestinal bacterial community. *PeerJ* 8:e9638. doi: 10.7717/peerj.9638

Wen, C., Gou, Q., Gu, S., Huang, Q., Sun, C., Zheng, J., et al. (2023). The cecal ecosystem is a great contributor to intramuscular fat deposition in broilers. *Poult. Sci.* 102:102568. doi: 10.1016/j.psj.2023.102568

Xiang, S., Chen, J., Deng, M., Wang, Z., Li, X., Lin, D., et al. (2024). Celastrol ameliorates experimental autoimmune uveitis through STAT3 targeting and gut microenvironment reprofiling. *Int. Immunopharmacol.* 127:111339. doi: 10.1016/j.intimp.2023.111339

Xing, T., Xu, X., Zhang, L., and Gao, F. (2022). Overexpression of heat shock protein 70 ameliorates meat quality of broilers subjected to pre-slaughter transport at high ambient temperatures by improving energy status of pectoralis major muscle and antioxidant capacity. *Antioxidants* 11:1468. doi: 10.3390/antiox11081468

Yang, Y., Cong, W., Liu, J., Zhao, M., Xu, P., Han, W., et al. (2022). Constant light in early life induces fear-related behavior in chickens with suppressed melatonin secretion and disrupted hippocampal expression of clock-and BDNF-associated genes. *J. Anim. Sci. Biotechnol.* 13:67. doi: 10.1186/s40104-022-00720-4

Yang, X., Liang, S., Guo, F., Ren, Z., Yang, X., and Long, F. (2020). Gut microbiota mediates the protective role of *Lactobacillus plantarum* in ameliorating deoxynivalenol-induced apoptosis and intestinal inflammation of broiler chickens. *Poult. Sci.* 99, 2395–2406. doi: 10.1016/j.psj.2019.10.034

Yang, Y., Liu, Q., Pan, C., Chen, J., Xu, B., Liu, K., et al. (2024). Species sensitivities to artificial light at night: a phylogenetically controlled multilevel meta-analysis on melatonin suppression. *Ecol. Lett.* 27:e14387. doi: 10.1111/ele.14387

Yin, H. C., Yao, W. Q., Zhang, H., Liu, S., Ma, T. Y., and Xia, C. Y. (2024). Multiomics analysis reveals that microbiota regulate fat and muscle synthesis in chickens. *Poult. Sci.* 103:103417. doi: 10.1016/j.psj.2023.103417

Yu, M., Xu, M., Wang, G., Feng, J., and Zhang, M. (2024). Effects of different photoperiods on peripheral 5-Hydroxytryptamine metabolism, breast muscle glucose metabolism, and myopathies in broilers. *Meta* 14:567. doi: 10.3390/metabo14100567

Zeman, M., Výboh, P., Juráni, M., Lamosová, D., Kostal, L., Bilcík, B., et al. (1993). Effects of exogenous melatonin on some endocrine, behavioural and metabolic parameters in Japanese quail *Coturnix coturnix* japonica. *Comp. Biochem. Physiol. Comp. Physiol.* 105, 323–328. doi: 10.1016/0300-9629(93)90215-P

Zhang, X., Akhtar, M., Chen, Y., Ma, Z., Liang, Y., Shi, D., et al. (2022). Chicken jejunal microbiota improves growth performance by mitigating intestinal inflammation. *Microbiome* 10:107. doi: 10.1186/s40168-022-01299-8

Zhang, X., Hu, Y., Ansari, A. R., Akhtar, M., Chen, Y., Cheng, R., et al. (2022). Caecal microbiota could effectively increase chicken growth performance by regulating fat metabolism. *Microb. Biotechnol.* 15, 844–861. doi: 10.1111/1751-7915.13841

Zhang, H., Qi, G., Wang, K., Yang, J., Shen, Y., Yang, X., et al. (2023). Oxidative stress: roles in skeletal muscle atrophy. *Biochem. Pharmacol.* 214:115664. doi: 10.1016/j.bcp.2023.115664

Zhang, Y., Wang, Z., Dong, Y., Cao, J., and Chen, Y. (2022). Effects of different monochromatic light combinations on Cecal microbiota composition and Cecal tonsil T lymphocyte proliferation. *Front. Immunol.* 13:849780. doi: 10.3389/fimmu.2022.849780

Zhang, J., Wang, W., Guo, D., Bai, B., Bo, T., and Fan, S. (2022). Antidiabetic effect of millet bran polysaccharides partially mediated via changes in gut microbiome. *Foods* 11:3406. doi: 10.3390/foods11213406

Zhao, R. X., Cai, C. H., Wang, P., Zheng, L., Wang, J. S., Li, K. X., et al. (2019). Effect of night light regimen on growth performance, antioxidant status and health of broiler chickens from 1 to 21 days of age. *Asian Australas. J. Anim. Sci.* 32, 904–911. doi: 10.5713/ajas.18.0525

Zheng, J., Hoffman, K. L., Chen, J. S., Shivappa, N., Sood, A., Browman, G. J., et al. (2020). Dietary inflammatory potential in relation to the gut microbiome: results from a cross-sectional study. *Br. J. Nutr.* 124, 931–942. doi: 10.1017/S0007114520001853

Zhou, Q., Lan, F., Li, X., Yan, W., Sun, C., Li, J., et al. (2021). The spatial and temporal characterization of gut microbiota in broilers. *Front. Vet. Sci.* 8:712226. doi: 10.3389/fvets.2021.712226

frontiers | Frontiers in Microbiology

TYPE Original Research
PUBLISHED 10 April 2025
DOI 10.3389/fmicb.2025.1470731

Check for updates

OPEN ACCESS

EDITED BY
Zhoujin Tan,
Hunan University of Chinese Medicine, China

REVIEWED BY
Chen Shunmei,
Kunming Medical University, China
Zipeng Jiang,
Zhejiang University, China
Lei Zhao,
Heilongjiang Bayi Agricultural University, China

*CORRESPONDENCE
Hualin Fu
✉ fuhl2005@sohu.com

†These authors have contributed equally to this work

RECEIVED 26 July 2024
ACCEPTED 17 March 2025
PUBLISHED 10 April 2025

CITATION
Li D, Li C, Liu N, Liu H, Yu Z, Liu Q, Shu G, Lin J, Zhang W, Peng G, Zhao L, Tang H, Li H, Xu F and Fu H (2025) Integrated metabolomics and intestinal microbiota analysis to reveal anti-post-weaning diarrhea mechanisms of Modified Yupingfeng Granule in Rex rabbits.
Front. Microbiol. 16:1470731.
doi: 10.3389/fmicb.2025.1470731

COPYRIGHT
© 2025 Li, Li, Liu, Liu, Yu, Liu, Shu, Lin, Zhang, Peng, Zhao, Tang, Li, Xu and Fu. This is an open-access article distributed under the terms of the Creative Commons Attribution License (CC BY). The use, distribution or reproduction in other forums is permitted, provided the original author(s) and the copyright owner(s) are credited and that the original publication in this journal is cited, in accordance with accepted academic practice. No use, distribution or reproduction is permitted which does not comply with these terms.

Integrated metabolomics and intestinal microbiota analysis to reveal anti-post-weaning diarrhea mechanisms of Modified Yupingfeng Granule in Rex rabbits

Dongbo Li[1†], Chao Li[1†], Ning Liu[2†], Hanzhong Liu[2], Zhiju Yu[2], Quanjin Liu[1], Gang Shu[1], Juchun Lin[1], Wei Zhang[1], Guangneng Peng[1], Ling Zhao[1], Huaqiao Tang[1], Haohuan Li[1], Funeng Xu[1] and Hualin Fu[1]*

[1]Department of Pharmacy, College of Veterinary Medicine, Sichuan Agricultural University, Chengdu, Sichuan, China, [2]Sichuan Academy of Grassland Sciences, Chengdu, Sichuan, China

Introduction: Post-weaning Diarrhea (PWD) is a kind of physiological stress diarrhea in Rex rabbits after weaning, which can lead to death in severe cases. Traditional Chinese medicine (TCM) has been widely used in animal due to its advantages of natural origin, diverse functions, safety, reliability, economy and environmental protection. Modified Yupingfeng Granule (MYPFG) is an improved Yupingfeng prescription based on the famous traditional Chinese prescription Yupingfeng (YPF), which is combined with other TCM and has obvious synergistic and additive activity in order to obtain an excellent natural medicine for PWD.

Methods: In this study, 120 weaned Rex rabbits were randomly allocated to 4 treatment groups, including control (CON), low dose (LD), medium dose (MD), high dose (HD). Rabbits were fed a control diet or a different MYPFG proportions of diet for 30 days. The study combined 16S rRNA analysis of intestinal microbiota and cecal contents metabolomics to explore the MYPFG effect on weaned Rex rabbits.

Results: MYPFG increased average daily gain, villus length to crypt depth ratio and decreased the feed to meat ratio, diarrhea frequency, mortality rate, depth of crypt ($p < 0.05$). The intestinal microbiota test found that MYPFG could change the abundances of Patescibacteria, *Sphingobium*, *Ruminococcus,* and *Oxalobacter*. Metabolomics analysis found that effect may be related to its regulation of Glycine, serine and threonine metabolism, Arginine and proline metabolism. Nicotinate and nicotinamide metabolism.

Discussion: MYPFG could regulate intestinal microbiota and change the metabolic pathway of some amino acids to alleviate the PWD in Rex rabbits.

KEYWORDS

Modified Yupingfeng Granule, post-weaning diarrhea, intestinal microbiota, metabolomics, Rex rabbits

1 Introduction

Rex rabbits (*Oryctolagus Cuniculus*), known for their excellent fur, rapid growth, and delicious and nutritious meat, are valuable animals with high economic potential (Gao-yun, 2017). However, they are prone to diarrhea and even death after weaning, which can significantly reduce their breeding success and affect economic benefits (Zhi-ping, 2017).

Changes in the intestinal microbiota may play an important role in the development of diarrhea (Zhao L. et al., 2025). Studies have shown that the intestinal microbiota of rabbits undergoes significant changes at different developmental stages, especially after weaning and the cessation of breast milk (Fu et al., 2024). It has been reported that regulating the intestinal microbiota can improve the function of the intestinal mucosa and that altering the intestinal microbiota can enhance intestinal barrier function and have a positive effect on intestinal tight junction proteins (Soufi et al., 2024; Zhao L. et al., 2025). Intestinal barrier damage in rabbits also affects the regulation of the intestinal microbiota (Fan et al., 2024). When Rex rabbits are weaned, the type of food is changed while the intestinal villi are not yet fully developed, leading to the destruction and invasion of the intestinal mucosa by undigested products and toxins (Hongli et al., 2017). Meanwhile, changes in endogenous metabolites and the intestinal microbiota further exacerbate the symptoms of diarrhea and can lead to death. The intestinal microbiota of newborn rabbits has a higher abundance of lipid-metabolizing bacteria, which helps the host extract more energy from breast milk lipids. It was reported that the abundance of *Clostridium* and *Ruminococcus* significantly increased after weaning (Zhao M. et al., 2024), assisting the rabbit in digesting solid feed. The introduction of solid feed is an important driving factor affecting the composition of the rabbit intestinal microbiota. Solid feed can disturb the intestinal microbiome, potentially leading to heat stress, reduced antioxidant defense, and increased inflammation risk, thereby triggering diarrhea (Lei et al., 2019).

Traditional Chinese medicine (TCM) contains a large number of beneficial substances, such as polysaccharides, flavonoids, and saponins (JiaHua et al., 2022; Zhe et al., 2022; Yu and Li, 2025). The water extracts of TCM have been used for disease control for thousands of years (Zhe et al., 2022). TCM offers unique advantages in the treatment of diarrhea. Shenling Baizhu powder (SLBZP), a TCM prescription renowned for its efficacy, is specifically recognized for its therapeutic effects in managing diarrhea associated with spleen qi deficiency. It has recently been reported to treat diarrhea induced by a lard diet in mice (Qiao et al., 2024). Another TCM, Sishen pill, has been shown to alleviate diarrhea associated with kidney-yang deficiency syndrome (Xie S. et al., 2024). Similar studies have also shown that Sishen pills effectively treat diarrhea associated with kidney-yang deficiency syndrome by regulating the kidney-intestinal bacteria-metabolic pathway (Li X. et al., 2024). Bohe pill is also a TCM that can treat diarrhea induced by a high-fat and high-protein diet by regulating intestinal mucosal bacteria (Huang et al., 2022). It has been reported that Qiweibaizhu powder is an effective TCM prescription for treating diarrhea (Shao et al., 2020). Meanwhile, TCM and the intestinal microbiota share a common characteristic of adopting a holistic view as their theoretical foundation. TCM, as a medical system based on holistic principles, focuses on the overall balance and regulation of the body (Geng et al., 2025). The intestinal microbiota is a part of the mutual relationship between the intestinal environment and living organisms (Wlazło et al., 2025). The intestinal microbiota participates in the metabolism process, and metabolites further interact with the immune and antioxidant systems (JiaHua et al., 2022). The application of these traditional Chinese medicines can promote the growth of beneficial bacteria, improve animal meat quality, inhibit the reproduction of harmful bacteria, and thus regulate the balance of the intestinal microbiota (Yu and Li, 2025). TCM can influence the immune regulation of the body through the intestinal microbiota. It emphasizes tonifying yin and yang, regulating qi and blood, and restoring the balance of yin and yang in the body through the use of medicinal herbs. TCM can affect the body's metabolic function by regulating the intestinal microbiota. The intestinal microbiota plays an important metabolic role in the body by breaking down substances in food that are difficult to digest and producing beneficial metabolites. Given the fact that most TCMs are administered orally the intestinal microbiota significantly impacts their metabolism.

In recent years, TCM has shown significant advantages in regulating metabolomics and the intestinal microbiota. Based on the metabolomics and intestinal microbiota analysis, the mechanisms through which traditional Chinese medicine impacts certain diseases have become a popular research hotspot. For example, a study explored the mechanism of Suanzaoren decoction in improving insomnia in rats by integrating metabolomics and intestinal microbiota analysis (He et al., 2022). Research on the mechanism of quercetin in the treatment of hyperlipidemia was based on metabolomics and intestinal microbiota analysis (Tongtong et al., 2023). Some studies have examined the spleen-strengthening effect of TCM through metabolomics and intestinal microbiota analysis (Yanling et al., 2022).

Yupingfeng (YPF), a Chinese herbal formula consisting of *Astragalus*, *Atractylodes*, and Radix Sileris, is a traditional Chinese medicine immunomodulator with a history of use spanning over 800 years (Sun et al., 2017). A recent study, which integrated metabolome, lipidome, and intestinal microbiome analysis, revealed the immunomodulation effects of Astragali Radix in healthy human patients (Gui et al., 2024). Another study also confirmed that it possesses a variety of biological activities, including antioxidant, anti-inflammatory, antibacterial, and anti-stress properties (Zhao W. et al., 2025). *Atractylodes* is a perennial herbaceous plant in the family Asteraceae, and its rhizome is often used in the production of medicines. Polysaccharides, the main active components extracted and isolated from *Atractylodes*, show significant pharmacological activities both *in vivo* and *in vitro*, such as immunomodulatory, antioxidant, antidiabetic, and intestinal protective effects (Lin F. et al., 2024). *Atractylodes* polysaccharides ameliorated colitis by regulating the intestinal microbiota and tryptophan metabolism (Zhang et al., 2024). Radix Sileris could inhibit inflammation and control apoptosis by regulating the PI3K/Akt, p53, and NF-κB signaling pathways to treat enteritis (Wang et al., 2023). Prim-O-glucosylcimifugin, the active componetn in Radix Sileris, has effects such as dispelling wind, relieving exterior symptoms, and providing anti-inflammatory and pain-relieving benefits. Previous research indicates that prim-O-glucosylcimifugin can improve intestinal permeability and visceral sensitivity, inhibit inflammatory reactions, and alleviate various symptoms of diarrhea (Li and Hu, 2024). Furthermore, the clinical effectiveness of YPF in treated diarrhea has been well established (Cheng et al., 2014). YPF has been also used in combination with other herbs to treat diarrhea (Jingxue and Jianguo, 2017). It could improve animal growth performance and immune function (Chu et al., 2023). Additionally, researchers have revealed that YPF

Abbreviations: PWD, Post-weaning Diarrhea; TCM, Traditional Chinese medicine; YPFP, Yupingfeng Powder; MYPFG, Modified Yupingfeng Granule; HPLC, High-performance liquid chromatography; LC-MS, liquid chromatography-mass spectrometry; ASVs, Amplicon Sequence Variables.

promotes intestinal microbiota immunity in mice (Dong-qi et al., 2018). Recent research has found that YPF can promote the growth of chickens by regulating the intestinal microbiota (Guan et al., 2024). Zheng et al. (2023) also found that YPF can improve the immune function and intestinal microbiota of chickens.

Chinese herbal formulas primarily embody the therapeutic principles of treatment based on syndrome differentiation and the combination of complementary herbs in TCM. Considering the poor digestion and decreased immunity in weaned Rex rabbits, Modified Yupingfeng Granule (MYPFG) was developed by incorporating *Bupleurum chinense*, hawthorn, and Shenqu into YPF, based on the principles of liver soothing, Qi replenishment, and digestive support. *Bupleurum chinense* is known to relieve exterior conditions and fever, soothe the liver, alleviate depression, and treat stress-induced diarrhea (Yan-hong and Yan-fang, 2017). Saikoside A, an active ingredient in Bupleurum chinense, has significant anti-inflammatory activities (Lin Y. et al., 2024). It can promote intestinal repair and stabilize the function of the intestinal microbiota by regulating the levels of inflammatory cytokines, functional proteins, and enzyme activities (Jia et al., 2023). Recent research has shown that hawthorn can improve growth, feed conversion, digestive enzymes, and the intestinal microbiota (Wang et al., 2024). Shenqu (medicated leaven) has been reported to aid digestion and is also useful in the treatment of gastric diseases (Beihua et al., 2015). In the early stage of this experiment, we used the method described by researchers (Shao et al., 2017). *Bupleurum chinense*, hawthorn, and Shenqu were used to modify MYPFG. According to the efficacy of each traditional Chinese medicine in the prescription, an orthogonal design was used to optimize the prescription of MYPFG, and the optimal prescription of MYPFG was screened out. The clinical effects (diarrhea rate and mortality) of MYPFG were better than those of the original YPF granule.

There is a close relationship between the intestinal microbiota and TCM (Runzhi et al., 2020). YPF has become a research hotspot for regulating the intestinal microbiota, enhancing immunity, improving animal growth performance, and maintaining intestinal health. For example, YPF could promote the growth of chickens by regulating the intestinal microbiota (Guan et al., 2024). It has been reported that YPF can improve the immune function of chicks and regulate the intestinal microbiota (Zheng et al., 2023). YPF also improved intestinal barrier integrity and suppressed intestinal inflammation (Yao et al., 2023). YPF granules could ameliorate cyclophosphamide-induced immune injury by protecting the intestinal barrier (Huang et al., 2025). YPF can improve the growth performance, intestinal tissue development, and immune system of broiler chicks (Xue et al., 2025). Furthermore, YPF can also improve intestinal health by affecting the intestinal barrier, immune system, and microbiota of *Macrobrachium rosenbergii* (Liu M. et al., 2024). In summary, YPF can promote the growth of beneficial bacteria and inhibit the reproduction of harmful bacteria, thereby regulating the balance of the intestinal microbiota. The application of YPF in animals can improve the intestinal environment, enhance the function of the intestinal immune system, and improve the resistance to diseases. YPF can also improve the intestinal environment, regulate the composition and function of the intestinal microbiota, and affect metabolic processes in the body. Using MYPFG, we can optimize the treatment plan for diarrhea and provide personalized adjustments based on the specific conditions of the intestinal microbiota.

In this study, MYPFG demonstrated a protective effect on the intestines of weaned Rex rabbits, and the main mechanisms included promoting intestinal development, repairing the mucosal barrier, and regulating the intestinal microbiota and endogenous metabolites. These effects may be attributed to MYPFG's regulation of the structure of the intestinal microbiota and its influence on metabolite changes. The research showed the protective effect of MYPFG on weaned Rex rabbits. The study ultimately integrated 16S rRNA and metabolomics analyses to examine the intestinal function, microbial composition, and metabolites in Rex rabbits with post-weaning diarrhea (PWD) that were treated with MYPFG.

2 Materials and methods

2.1 Chemicals and reagents

Saikosaponin A and prim-O-glucosylcimifugin were purchased from the Shanghai Yuanye Bio-Technology Co., Ltd. (Shanghai, China). p-Dimethylaminobenzaldehyde and vanillin were purchased from Shanghai Macklin Biochemical Co., Ltd. (Shanghai, China). Hematoxylin and eosin Y were obtained from Sigma-Aldric. Alcian Blue 8GX was purchased from Beijing Solarbio Technology Co., Ltd. (Beijing, China). Other reagents were provided by Chengdu Chron Chemicals Co., Ltd.

2.2 Animals

Rex rabbits, approximately 40 days old and weighing approximately 1,000 g, were provided by the Rex Rabbit Research Institute of Sichuan Academy of Grassland Sciences. The animals were given a basal diet and tap water at liberty and were maintained in cages under controlled conditions (23 ± 2°C, 12-h light/dark cycle). All experiments and procedures were carried out in accordance with the Regulations of Experimental Animal Administration issued by the State Committee of Science and Technology of China. The composition and nutrient levels of the basal diet are listed in Table 1.

TABLE 1 The composition and nutrient levels of basal diet (air-dry basis) %.

Items	Content	Nutrient levels	Content
Ingredients		Digestible Energy (DE, MJ/kg)	10.21
Corn	20.0	Crude Protein (CP)	16.00
Bran	22.8	Crude Fiber (CF)	14.29
Peanut vine	40.1	EE	3.02
Soybean meal	14.6	Met+Cys	0.46
NaCl	0.5	Lys	0.56
$CaHPO_4$	1.0	Ca	0.58
Premix	1.0	P	0.62
Total	100	I (mg/kg)	0.22

The premix provided the following per kilogram of the diet: Lys, 1.5 g; VA, 8000 IU; VD, 31000 IU; VE, 50 mg; Fe, 100 mg; Cu, 50 mg; Mg, 150 mg; Zn, 50 mg; Mn, 30 mg; and Se, 0.1 mg.
Nutrition levels were calculated values.

All animal procedures were conducted in accordance with the national standard, Laboratory Animal-Requirements of Environment and Housing Facilities (GB14925-2001), and approved by the Sichuan Agricultural University Institutional Animal Care and Use Committee under permit number CSQ-2020303006.

2.3 Preparation of MYPFG

MYPFG was formulated into granules by adding inactive ingredients to the hot water extract of a mixture of six crude herbs. *Bupleurum chinense*, *Astragalus*, *Atractylodes*, hawthorn, Shenqu, and Radix Sileris were mixed in a dosage ratio of 5:4:4:3:3:4 and wetted with distilled water (1:8, w/v) for 2 h. Then, the herbs were boiled at 100°C for 3 h and filtered through a multi-layer gauze, and the filtrate was collected. After the herbs were repeatedly boiled and filtered three times, all filtrates were mixed. To facilitate the preparation of the granules, the filtrate was concentrated to half the weight of the original Chinese herbal medicine. The extracts were granulated by adding inactive ingredients and wetting agents. The concentration of MYPFG was determined such that each gram of the granules contained 1 g of raw plant material. All the above herbs were purchased from Sichuan Qianyuan Traditional Chinese Medicine Slices Co., Ltd.

2.4 Determination of the major components using high-performance liquid chromatography (HPLC)

The quality control of traditional Chinese medicine preparations aims to ensure the stability and clinical efficacy of the preparations by detecting the content of active ingredients in the prescription (Zhuang et al., 2024). In this study, Radix Sileris was the traditional Chinese medicine in the original prescription of YPF, while *Bupleurum chinense* was the representative of the modified medicine. We chose the active ingredient prim-O-glucosylcimifugin in Radix Sileris and the active ingredient Saikoside A in *Bupleurum chinense* as the quality control standards for MYPFG.

MYPFG was analyzed using high-performance liquid chromatography (HPLC) with the Corona ultra Charged Aerosol Detector (CAD) on an Agilent HPLC system. Approximately 0.1 g of the MYPFG was weighed and dissolved in 1 mL of a 5% concentrated ammonia methanol solution. The solution was dissolved using ultrasound, filtered through a 0.45-μM filter, washed twice with methanol, evaporated to dryness, and then diluted with methanol. Saikoside A and prim-O-glucosylcimifugin were dissolved in methanol. The complete sample solution was filtered through a 0.22-μM filter. Subsequently, 20 μL supernatant was injected into the HPLC system for analysis. The chromatographic conditions were as follows: a reverse-phase column (Intersil ODS-3.5 μm, 4.6 mm × 250 mm I.D.) connected to a guard column (C18, 5 μm, 4.6 mm × 10 mm I.D.). The elution flow rate was 1.0 mL/min with a mobile phase gradient of A-B (A: H_2O; B: acetonitrile), which was varied as follows: 0 ~ 25 min, 97 ~ 5% A and 3 ~ 95% B. The injection volume was 20 μL, and the UV detection wavelengths were set at 210 nm for Saikoside A and 250 nm for prim-O-glucosylcimifugin. The quantitative test results showed that the concentrations of Saikoside A and prim-O-glucosylcimifugin were 49.703 and 18.797 μg/g in the MYPFG, respectively.

2.5 Experimental design

A total of 120 Rex rabbits, after 7 days of adaptive feeding, were randomly divided into four groups, with 30 rabbits in each group: control (CON), low dose (LD), medium dose (MD), and high dose (HD). The CON group was fed the basic diet, as shown in Table 1. The MYPFG formulations (0.5, 1, and 2%) were administrated to the LD, MD, and HD groups, respectively, as a dietary supplement for 30 consecutive days. All rabbits were included in the analysis of the growth performance, diarrhea frequency, and mortality rate. In consideration of animal ethics and welfare, only six animals from each group were sacrificed to collect additional data, despite there being 30 animals in each group. The ileal and cecal samples were collected and preserved in liquid nitrogen.

2.6 Growth performance

All Rex rabbits were weighed on Day 1 and Day 30 of the experiment, and the feed intake per cage was recorded daily. The average daily feed intake (ADFI) and average daily gain (ADG) were calculated. The feed conversion ratio (FCR) was expressed as ADFI/ADG.

$$\mathrm{ADFI} = \frac{\textit{Total consumption of feed}}{\text{Feeding days} \times \text{rabbit } \textit{number}}$$

$$\mathrm{ADG} = \frac{\text{Final weight} - \text{initial weight}}{\text{Feeding days}}$$

$$\mathrm{FCR} = \frac{\mathrm{ADFI}}{\mathrm{ADG}}$$

2.7 Diarrhea and mortality percentage

The total number of diarrhea frequency of each Rex rabbit in all groups was recorded every day during the test. The number of dead Rex rabbits were recorded in each group every day during the trial period. Meanwhile the total number of dead Rex rabbits were counted. $P_{\text{diarrhea percentage}}$ was calculated as Equation 1, while $P_{\text{mortality percentage}}$ was calculated as Equation 2.

$$p_{\text{diarrhea percentage}} = \frac{\sum A}{\sum B} \times 100\% \quad (1)$$

Where A represents the total times of diarrhea; B represents the sum of survival days of each rabbit in the group.

$$p_{\text{mortality percentage}} = \frac{\sum A}{\sum B} \times 100\% \quad (2)$$

Where A represents the total number of dead Rex rabbits; B represents total number of Rex rabbits.

2.8 Histomorphology

The small intestine tissues from the CON and HD groups were fixed with 4% paraformaldehyde for 7 days. Then, they were washed under running water for 30 min, placed into a pathological embedding plastic basket for dehydration to transparency with a gradient of alcohol, and finally embedded in paraffin (Zhao L. et al., 2025). The tissues were sliced into 5 μm thick sections using a slicer (Ultra-Thin Semiautomatic Microtome, RM2235, from Leica, Germany), flattened in warm water, mounted on slides, and baked at 60°C for 2 h. Then, the sections were placed in xylene to remove the paraffin and stained with hematoxylin, eosin, or Alcian blue. The tissues were dehydrated with 85% alcohol for 5 min, 95% alcohol for 5 min, and 100% alcohol for 10 min. Finally, the tissues were placed in xylene to make them transparent and sealed with resin glue.

The slides were observed under the CX22 microscope (Leica, Germany), and the entire tissue slice was examined using the DM 1000 Leica microscopic imaging system. Image-Pro Plus 6.0 (Media Cybernetics, America) was used to count goblet cells in the Alcian blue-stained tissues and measure the length of the villi and the depth of the crypts. At least ten intact villi and corresponding crypts in the intestinal tissue were measured. Their ratio was calculated as follows:

$$R_{(V/C)} = \frac{L_{villi}}{D_{crypt}}$$

Where L_{villi} and D_{crypts} represent the length of the villi and the depth of the crypts, respectively.

2.9 DNA extraction, PCR, and sequencing of the intestinal microbiota

Total genomic DNA was extracted from the ileal and cecal content samples of the CON and HD groups using ZymoBIOMICS DNA isolation kits (ZymoBIOMICS, California, USA) according to the manufacturer's instructions. The 16S rRNA genes in distinct regions were amplified using specific primers and barcodes. The V3-V4 hypervariable region of the 16 s rRNA gene was amplified using a PCR instrument (Applied Bio- systems® Gene Amp® PCR System 9700) with primers 515F (5′-GTGCCAGCMGCCGCGGTAA-3′) and 806R (5′-GGAC TACNNGGGTATCTAAT-3′). All PCR mixtures contained 15 μL of the Phusion® High-Fidelity PCR Master Mix (New England Biolabs), 0.2 μM of each primer, and 10 ng of target DNA. The cycling conditions consisted of an initial denaturation step at 98°C for 1 min, followed by 30 cycles at 98°C (10 s), 50°C (30 s), and 72°C (30 s), with a final 5-min extension at 72°C. An equal volume of a loading buffer (containing SYB green) was mixed with the PCR products, and electrophoresis was performed on a 2% agarose gel for DNA detection. The PCR products were then mixed in equal proportions, and the Qiagen Gel Extraction Kit (Qiagen, Germany) was used to purify the mixed PCR products. Furthermore, the DNA library was established using the TruSeq DNA PCR-Free Sample Prep Kit (Illumina, FC-121-3001/3003) according to standard protocols.

2.10 16S rRNA gene high-throughput sequencing

Species notes: The raw reads obtained from sequencing were filtered using the Trimmomatic software; primer sequences were identified and removed using the Cutadapt software to obtain clean reads without primer sequences. The DADA2 method in QIIME2 was used for denoising, merging paired-end sequences, and removing chimera sequences to obtain amplicon sequence variants (ASVs). The ASV feature sequences were compared with the reference sequences in the SILVA database to obtain classification information for each ASV. Using the QIIME2 software, the sequence number of each sample in the ASV abundance matrix was randomly extracted at different depths, and the sequence number extracted at each depth and the corresponding ASV number were used to draw rarefaction curves.

Alpha diversity analysis: The Dominance index, the Chao1 index, Observed_asvs, the Shannon index, the Simpson index, and Pielou_e of each group were calculated to compare the richness and evenness of the ASVs between the different samples.

Beta diversity analysis: Principal coordinate analysis (PCoA) and non-metric multidimensional scaling (NMDS) were used for visualization.

Characteristic microbiota analysis: The QIIME2 software was used to obtain composition and abundance tables for each sample at different taxonomic levels, which were presented as bar charts. To further validate the regulatory effects of MYPFG on the intestinal microbiota of Rex rabbits, we performed an LEfSe analysis to further characterize distinguishing phylotypes in the intestinal microbiota of the different groups, using a linear discriminant analysis (LDA) score of 4 as the screening criterion. Microorganisms with LDA scores greater than the set value were considered biomarkers with statistically significant differences. Multiple comparisons were made among the groups to identify characteristic genera with significant differences between them.

2.11 Sample preparation and UHPLC–MS of the untargeted metabolomics

The cecal content samples were individually ground with liquid nitrogen, and the homogenate was resuspended in prechilled 80% methanol using thorough vortexing. The samples were incubated on ice for 5 min and then were centrifuged at 15,000 *g*, 4°C for 20 min. Some of the supernatant was diluted to a final concentration of 53% methanol using LC–MS grade water. The samples were subsequently transferred to a fresh Eppendorf tube and were centrifuged at 15,000 *g*, 4°C for 20 min. Finally, the supernatant was injected into the LC–MS/MS system for analysis. UHPLC–MS/MS analyses were performed using a Vanquish UHPLC system (Thermo Fisher, Germany) coupled with an Orbitrap Q Exactive™ HF-X mass spectrometer (Thermo Fisher, Germany) at Novogene Co., Ltd. (Beijing, China). The samples

were injected into a Hypesil Gold column (100 × 2.1 mm, 1.9 μm) using a 17-min linear gradient at a flow rate of 0.2 mL/min. The eluents for the positive polarity mode were eluent A (0.1% FA in Water) and eluent B (Methanol). The eluents for the negative polarity mode were eluent A (5 mM ammonium acetate, pH = 9.0) and eluent B (Methanol). The solvent gradient was set as follows: 2% B, 1.5 min; 2–85% B, 3 min; 100% B, 10 min; 100–2% B, 10.1 min; and 2% B, 12 min. The Q Exactive™ HF-X mass spectrometer was operated in positive/negative polarity mode with a spray voltage of 3.5 kV, a capillary temperature of 320°C, a sheath gas flow rate of 35 psi, an aux gas flow rate of 10 L/min, an S-lens RF level of 60, and an aux gas heater temperature of 350°C. The QC samples were injected into the UPLC–MS system at the beginning and end of the entire analysis process, as well as after every three test samples.

2.12 Metabolomics analysis

Principal component analysis (PCA) and partial least squares discriminant analysis (PLS-DA): The peaks extracted from all experimental and QC samples were analyzed using PCA. In the PCA of the QC samples in both positive and negative ion modes, the QC samples (purple) were tightly clustered and clearly separated from the experimental samples, indicating that the data were of good quality and that the instrument was stable. To obtain the biomarkers of MYPFG regulating the contents of the cecum, we used PLS-DA to analyze the differences in the metabolites between the model group and the blank group.

Volcanic map: The volcanic map screening of differential metabolites mainly involves three parameters: VIP, FC, and *p*-value. VIP refers to the Variable Importance in the Projection of the first principal component of the PLS-DA model, with the VIP value representing the contribution of metabolites to the grouping. FC refers to fold change, which is the ratio of the mean value of all biological replicate quantitative values for each metabolite in the comparison group. The threshold values were set as VIP > 1.0, FC > 1.2 or FC < 0.833, and a *p*-value of <0.05.

KEGG: KEGG was used for metabolic analysis and metabolic network research in the organisms. Pathway enrichment analysis can identify the main biochemical metabolic pathways and signal transduction pathways involved with differential metabolites. Using the hypergeometric test method, *p*-values for pathway enrichment were obtained, with a P_{value} of ≤0.05 set as the threshold. KEGG pathways that met this condition were defined as significantly enriched in the differential metabolites. Based on the enrichment results, we drew the bubble diagram of the enriched KEGG pathways.

2.13 Correlation analysis between the intestinal microbiota and metabolites

Based on the Pearson correlation coefficient, correlation analysis was conducted between the intestinal microbiota with significant differences at the genus level obtained from the 16S rDNA analysis and the metabolites with significant differences obtained from the metabolomics analysis. A heatmap was drawn to measure the degree of association between the species diversity and metabolites in the environmental samples. Another heatmap was drawn to measure the degree of association between the species diversity and metabolites in the intestinal samples. The range of values for the correlation coefficient was between −1 and 1. When the correlation coefficient was less than 0, it indicated a negative correlation. When it was greater than 0, it indicated a positive correlation.

2.14 Statistical analysis

A one-way analysis of variance (ANOVA) was used to analyze the experimental data with SPSS 25.0. All values were presented as mean ± SD, and a *p*-value of <0.05 was considered statistically significant.

3 Results

3.1 Growth

As shown in Table 2, the average daily gain (ADG) of the weaned Rex rabbits in the HD and MD groups significantly increased compared to the CON groups ($p < 0.05$). MYPFG significantly reduced the feed-to-meat ratio (FCR) in the weaned Rex rabbits ($p < 0.05$), indicating that MYPFG could promote growth.

3.2 Diarrhea frequency and mortality rate

As shown in Table 3, MYPFG significantly reduced the frequency of diarrhea in the weaned Rex rabbits compared to the CON group ($p < 0.05$). The HD group exhibited the most obvious effect. Compared to the CON group, the mortality rate in the three test groups was also significantly reduced ($p < 0.05$). The HD group exhibited the most significant effect in reducing both diarrhea frequency and mortality in the weaned Rex rabbits, indicating that MYPFG can alleviate the effects of diarrhea on the growth of weaned Rex rabbits and help maintain intestinal health.

Based on the clinical effects observed in the different dose groups, the diarrhea and mortality rates in the HD group were significantly lower than those in the other groups. The growth performance of the HD group was also significantly better than that of the other groups. Subsequent experiments used the HD group as the YPF group to explore the inhibitory mechanism of MYPFG on post-weaning diarrhea in Rex rabbits.

TABLE 2 Effects of MYPFG on the growth performance of Rex rabbits.

Index	CON	LD	MD	HD
ADFI/(g/d)	48.08 ± 0.82	48.07 ± 1.93	48.09 ± 1.45	47.77 ± 2.60
ADG/(g/d)	5.17 ± 0.24c	7.00 ± 1.00bc	9.33 ± 0.33b	15.33 ± 2.31a
FCR	9.31 ± 0.27a	6.91 ± 0.45b	5.26 ± 0.24c	3.15 ± 0.33d

Data are expressed as mean ± SD ($n = 6$). In the same row, values with no letters or the same letter superscripts indicate no significant difference ($p > 0.05$), while values with different small letters indicate a significant difference ($p < 0.05$).

TABLE 3 Effects of MYPFG on diarrhea frequency and mortality percentage in Rex rabbits.

Index	CON	LD	MD	HD
Diarrhea percentage (%)	7.67 ± 0.25a	6.22 ± 0.25b	4.33 ± 0.25c	2.33 ± 0.25d
Mortality percentage (%)	86.67 ± 7.46a	36.67 ± 7.46b	23.33 ± 9.13c	13.34 ± 7.46c

Data are expressed as mean ± SD ($n = 6$). In the same row, values with no letters or the same letter superscripts indicate no significant difference ($p > 0.05$), while values with different small letters indicate a significant difference ($p < 0.05$).
According to the clinical effects observed in the different dose groups, the diarrhea and mortality rates of the HD group were significantly lower than those of the other groups. The growth performance of the HD group was also significantly better than the other groups. Subsequent experiments used the HD group as the YPF group to explore the inhibitory mechanism of MYPFG on post-weaning diarrhea in Rex rabbits.

3.3 Effects of MYPFG on the intestinal mucosal structure

Histopathological examination was used to evaluate the integrity of the intestinal tissue. At the end of the experiment, tissue samples from the duodenum, jejunum, and ileum were collected and sectioned for HE staining. The results of the HE staining assay demonstrated that, in the CON group, part of the intestinal villi was shed, the intestinal villi were shortened, the lamina propria was wide, and the connective tissue in the lamina propria was loosened. However, the results of the YPF group showed that the intestinal structure was intact, the stage was clear, and the intestinal villi were neatly arranged in all groups. The tissue structure of the samples in all groups was normal, with no obvious histopathological damage found. Occasionally, the mucosal epithelium showed cell abscission and necrosis.

As shown in Table 4, MYFPG increased the length of the villi, the depth of the crypt, and their ratio R(V/C). Moreover, the depth of the crypt and R(V/C) were significantly increased in the jejunum in the YPF group, suggesting that the maturity of the jejunum in the YPF group was better. Overall, MYPFG provided better protection for the intestinal mucosa, especially in the jejunum.

3.4 Effects of MYPFG on the morphology of the goblet cells in the intestines

The main function of goblet cells is to synthesize and secrete mucin, forming a mucosal barrier to protect epithelial cells. The number of goblet cells indicates the protective effect of the intestinal mucus barrier. The number of goblet cells in the duodenum, jejunum, and ileum of the YPF group increased (Table 5). In general, the number of goblet cells increased insignificantly, possibly because MYPFG had a minimal effect on the intestinal mucus barrier.

3.5 Effect of MYPFG on the intestinal microbiota

In the ileal microbiota, the CON group had 3,565 ASVs, with 2,766 unique ASVs, while the YPF group had 2,866 ASVs, with 2,067 unique ASVs. The two ileum groups shared a total of 5,632 ASVs. In the cecal microbiota, the CON group had 3,405 ASVs, with 1,616 unique ASVs, while the YPF group had 3,190 ASVs, with 1,401 unique ASVs. The two cecum groups shared a total of 4,806 ASVs. The results showed that MYPFG had a powerful effect on changing the intestinal microbiota, especially the ileal microbiota. This finding indicated that the MYPFG treatment significantly altered the species composition and diversity of the intestinal microbiota in Rex rabbits. As shown in Figure 1, alpha diversity analysis of the microbial communities was performed to compare species richness (Dominance index, Chao1 index, and Observed_asvs) and diversity (Shannon index, Simpson index, and Pielou_e) among the two ileum groups and the two cecum groups. MYPFG effectively altered the species richness and diversity of the microbiota in Rex rabbits. In PCoA and NMDS analyses (Figure 2), the closer the distance between two points on the coordinate axis, the more similar their community composition is in the respective dimensions. Based on the weighted UniFrac distance, the PCoA analysis showed that the contribution rate of the horizontal axis (PCoA1) was 48.76% and the contribution rate of the vertical axis (PCoA2) was 25.64%. Based on the unweighted UniFrac distance, the PCoA analysis showed that the contribution rate of the horizontal axis (PCoA1) was 29.94% and the contribution rate of the vertical axis (PCoA2) was 12.22%. The ileum samples were completely separated from the cecum samples. The CON samples partially overlapped with the MYPFG samples between the ileum groups. Similar results were also observed between the cecum groups. The differences in the composition of the intestinal microbiota could be identified in the PCoA analysis and NMDS analysis. The results of the NMDS analysis were consistent with those of the PCoA analysis, indicating that MYPFG influenced the body functions by altering the intestinal microbiota.

To investigate the effect of MYPFG on the intestinal microbiota of Rex rabbits, we selected the top 10 dominant phyla and genera with a relative abundance of more than 1% and used bar charts to represent their abundance. Comparing the structural changes of the intestinal microbiota in each group based on the

TABLE 4 Effects of MYPFG on $R_{(V/C)}$ in the intestines of the weaned Rex rabbits.

Group	Item	Duodenum	Jejunum	Ileum
CON	L_{villi} (μm)	828.71 ± 156.19	565.98 ± 80.64	432.68 ± 111.49
YPF		832.75 ± 120.16	590.90 ± 86.89	486.33 ± 145.57
CON	D_{crypt} (μm)	109.36 ± 35.39	112.27 ± 20.48	99.31 ± 20.60
YPF		110.44 ± 24.86	100.91 ± 14.58*	100.87 ± 24.26
CON	$R_{(V/C)}$	7.98 ± 1.90	4.85 ± 1.32	4.64 ± 1.78
YPF		7.85 ± 1.78	5.98 ± 1.21*	4.87 ± 1.30

Data are expressed as mean ± SD ($n = 6$).
The asterisk (*) indicates that there is a significant difference between the YPF group and the CON group ($p < 0.05$).

TABLE 5 The number of goblet cells in the duodenum, jejunum, and ileum in the same visual field.

Group	Duodenum	Jejunum	Ileum
CON	30.17 ± 3.90	36.50 ± 6.50	66.58 ± 18.83
YPF	36.00 ± 6.94	42.08 ± 4.08	71.92 ± 16.94

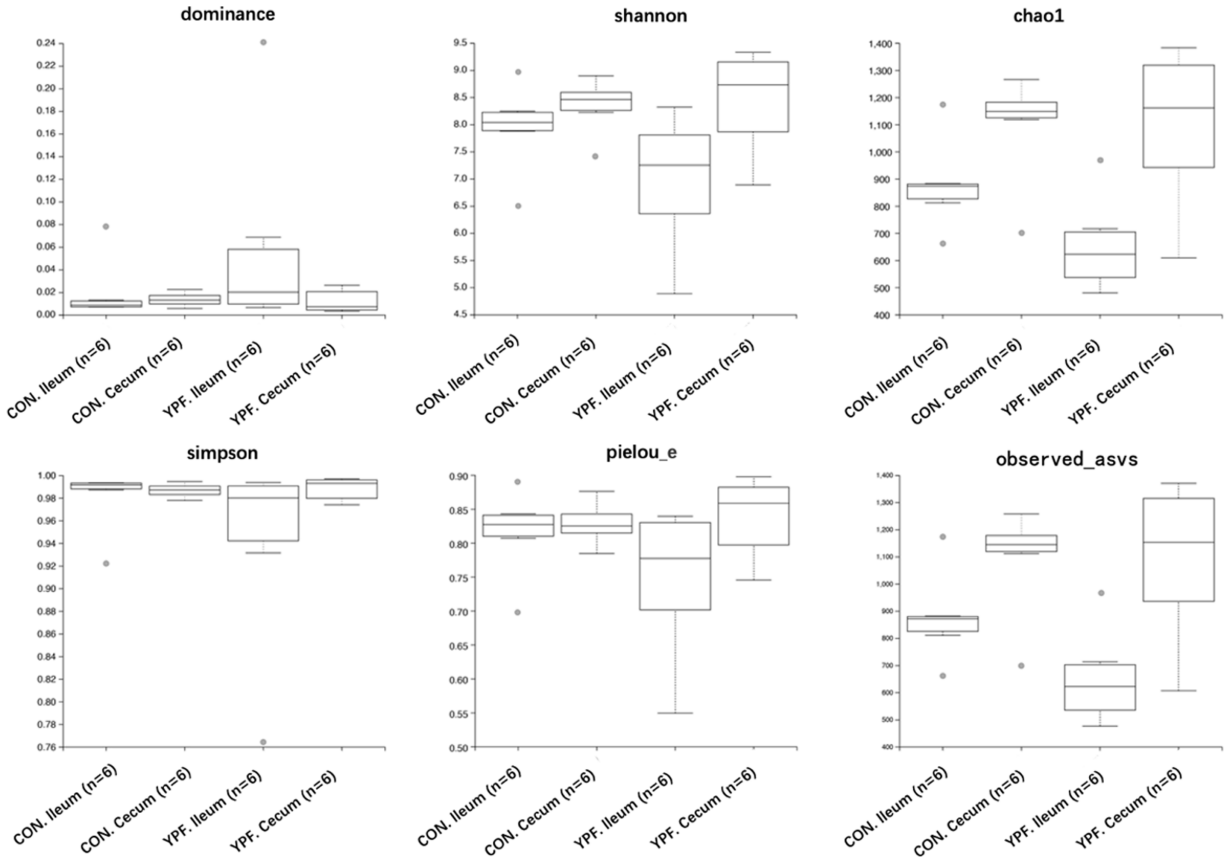

FIGURE 1
Dominance, shannon, chaol, simpson, pielou e, observed asvs.

ASVs, Myxococcota, Nitrospirota, Chloroflexi, Actinobacteriota, Acidobariota, Bacteroidota, Verrucomicrobiota, Proteobacteria, Euryarchaeota, and Firmicutes exhibited higher abundance at the phylum level (Figure 3A). The top 10 classes with the highest abundance at the class level were Anaerolineae, Coriobacterriia, Acidobacteriae, Bacilli, Grammaproteobacteria, Bacteroidia, Verrucomicrobiae, Alphaproteobactaria, Methanobacteria, and Clostridia (Figure 3B). The orders with relatively high abundance at the order level were Ersipelotrichales, Christensenellales, Laphnospirales, Rhizobiales, Sphingomonadales, Bacteroidales, Verrucomicrobiales, Oscillospirales, Methanobacteriales, and Eubacteriales (Figure 3C). Similarly, we conducted an analysis at the family level. The 10 families with relatively high abundance were Christensenellaceae, Ruminococcaceae, Lachnospiraceae, Beijerinkiaceae, Muribaculaceae, Sphingomonadaceae, Akkermansiaceae, Oscillospiraceae, Methanobacteriaceae, and Eubacteriaceae (Figure 3D). At the genus level, the higher abundance of *Clostridia-UGG-014*, *Christensenellaceae-R-7-group*, *Methanosphaera*, *Methylobacterium-Methylorubrum*, *V9D2013-group*, *NK4A214-group*, *Muribaculaceae*, *Sprhingomonas*, *Akkermansia*, and *Methanobrevibacter* indicated that these genera played an important role in each group (Figure 3E).

Figure 4 shows the microbiota with significant differences in abundance. The length of the histogram represents the impact of the significantly different species. Bacteroidales, Bacteroidia, Bacteroidota, Lachnospirales, Lachnospirales, Akkermansiaceae, Akkermansia, Verrucomicrobiales, Verrucomicrobiae, Clostridia, Christensenellaceae, Christensenellales, Clostridia, and Christensenellaceae exhibited higher expression in the YPF cecum group, while Oscillosprirales, Oscillosprirales, NK4A214, and V9D2013 exhibited higher expression in the CON cecum group. Acidobacteriota exhibited higher expression in the CON ileum group, while Eubacteriaceae, Eubaceriales, and Actinobacteriota exhibited higher expression in the YPF ileum group. The results of the study showed that the structure of the cecal microbiota underwent significant changes after the MYFPG treatment. The results also showed that the intestinal microbiota plays an important role in the prevention and treatment of post-weaning diarrhea. The results of the species with significant differences in abundance between the YPF group and the CON group are shown in Figure 5. The abundance of Patencibacteria in the YPF ileum group was significantly lower than that in the CON ileum group. The abundance of *Sphingobium* in the YPF ileum group was also significantly lower than that in the CON ileum group. The abundance of *Oxalobacter* and *Ruminococcus* in the YPF cecum group was significantly higher than that in the CON cecum group.

3.6 Effect of MYPFG on the metabolomics of the cecal contents

In the PCA (Figures 6A,B), the horizontal axis PC1 and vertical axis PC2 in the figure represent the scores of the first- and

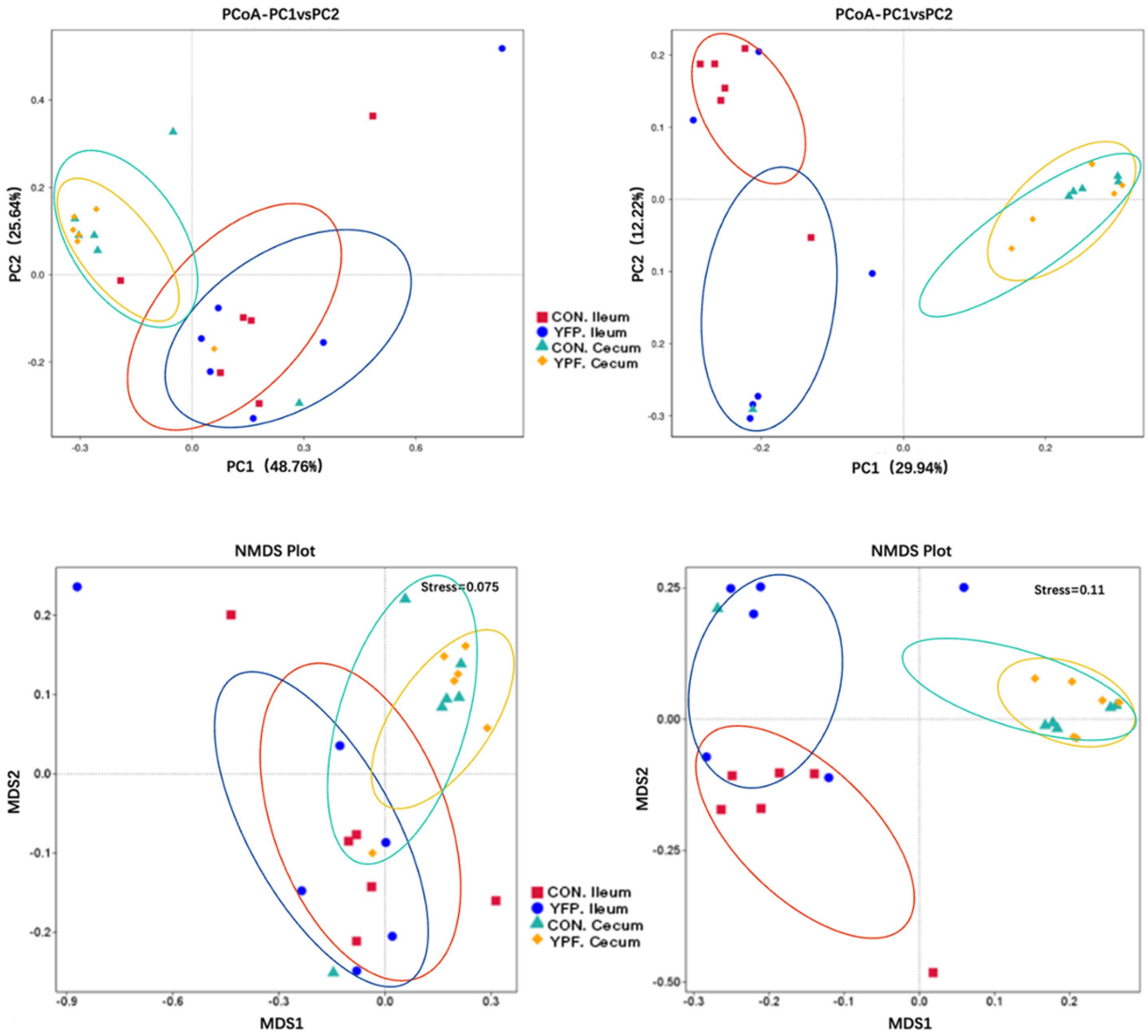

FIGURE 2
PCoA and NMDS analysis of each group. Left: Based on Weighted Unifrac distance. Right: Based on Unweighted Unifrac distance. Weighted Unifrac distance is more sensitive to species with higher abundance, while Uweighted Unifrac distance is more sensitive to rare species.

second-ranked principal components, respectively. Different colored scatter points represent samples from different experimental groups, and the ellipse indicates the 95% confidence interval. In the positive ion mode, the PCA analysis showed that the contribution rate of the horizontal axis PC1 was 60.34% and the contribution rate of the vertical axis PC2 was 9.42%. In the negative ion mode, the PCA analysis showed that the contribution rate of the horizontal axis PC1 was 56.41% and the contribution rate of the vertical axis PC2 was 9.28%. In the positive ion PLS-DA ($R^2 = 0.80$, $Q^2 = 0.15$), most of the samples were separated, indicating differences in the metabolite levels between the two groups (Figure 6C). In the negative ion PLS-DA ($R^2 = 0.84$, $Q^2 = 0.15$), most of the samples were also separated (Figure 6D). The volcanic map directly displays the overall distribution of differential metabolites (Figures 7A,B). In the positive ion mode, nine differential metabolites were upregulated and three were downregulated. The screened differential metabolites are shown in Table 6. In the negative ion mode, 16 differential metabolites were upregulated and two were downregulated. The screened differential metabolites are shown in Table 7. In the KEGG pathway enrichment (Figures 7C,D), the horizontal axis in the figure represents the number of differential metabolites in the corresponding metabolic pathway and the vertical axis represents the total number of metabolites identified in the pathway. The results showed that nicotinate and nicotinamide metabolism, glycine, serine, and threonine metabolism, and arginine and proline metabolism were enriched in the positive ion mode. Pyrimidine metabolism and bile metabolism were enriched in the negative ion mode.

3.7 Correlation between the intestinal microbiota and metabolites

The correlation analysis of the metabolites and intestinal microbiota showed that there was a significant correlation between *Oxalobacter* and N-(9-oxodecyl) acetamide, 1-3-ethylurea, and hematoxylin. *Ruminococcus_torques_group* was significantly

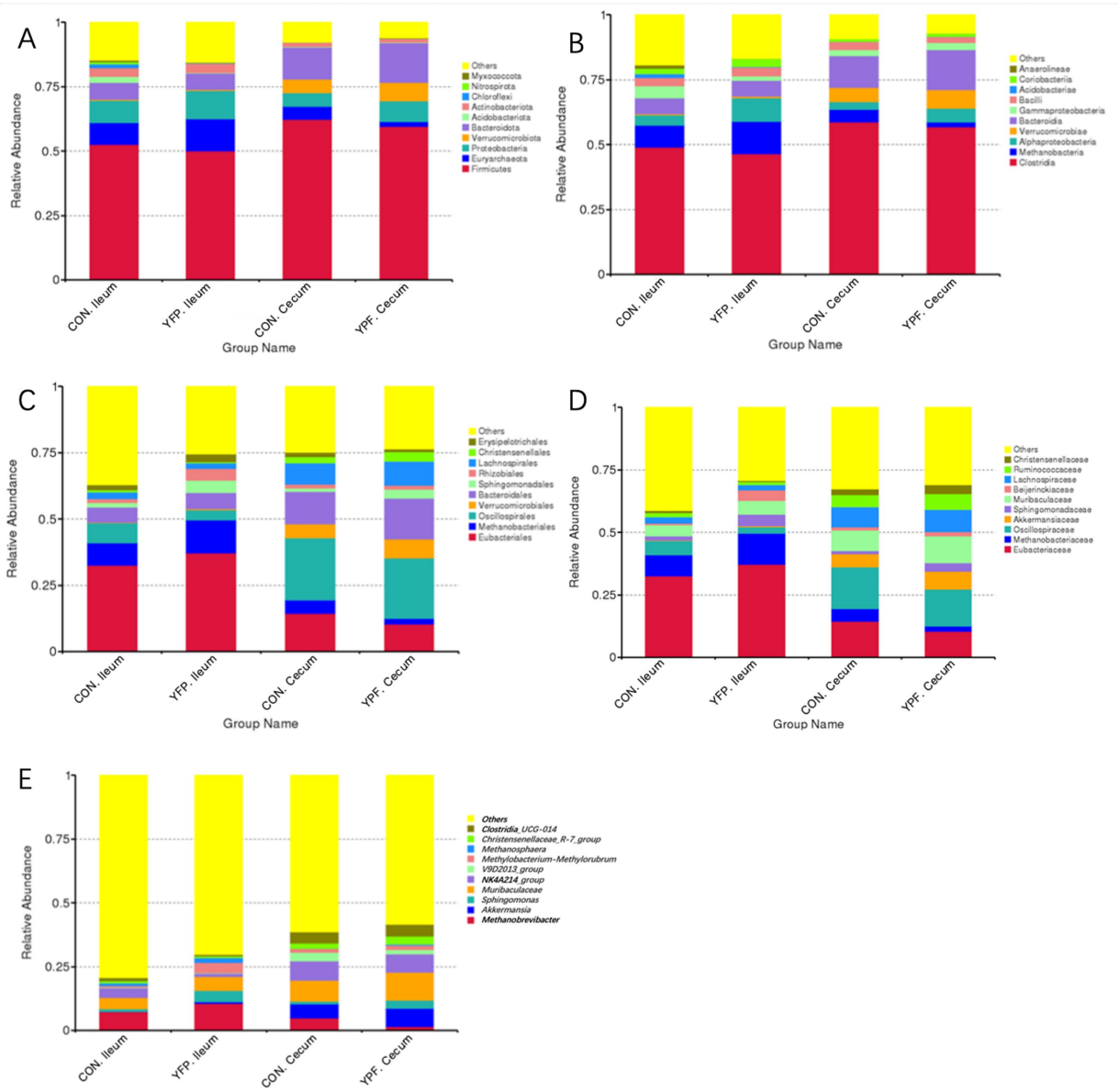

FIGURE 3
Effect ofYPF on intestinal microbiota abundance and specific taxa. Differences in the abundance of bacteria in each group at the **(A)** phylum, **(B)** class, **(C)** order, **(D)** family, **(E)** genus level.

correlated with creatine, linolelaidic acid, N-(9-oxodecyl) acetamide, ferulic acid, N1-(4-chlorophenyl)-2-cyano-4, 4-dimethyl-3-oxopentanamide, and thymidine 5′-monophosphate (Figure 8).

4 Discussion

4.1 MYPFG could protect the intestinal barrier

Traditional Chinese medicine (TCM) plays a crucial role in animal growth performance and intestinal barrier protection. Growth performance is the gold standard for evaluating the effectiveness of TCM additives (Li et al., 2025). Meanwhile, growth performance is also an important indicator of intestinal health and is inversely proportional to the diarrhea rate. The small intestine is an important site for nutrient absorption (Lei et al., 2022). Meanwhile, the small intestine is rich in various digestive enzymes. The longer the epithelial villi, the more epithelial cells there are. The shallower the crypt depth, the higher the rate of epithelial cell maturation (Muyang et al., 2022). The villi and crypt represent the absorptive function of the small intestine. The main effect of MYFPG on the development of the small intestine is to increase villus length, reduce crypt depth, and improve the villus-to-crypt ratio. The intestinal mucosal barrier function refers to the combined structure and function that prevent harmful substances from crossing the intestinal mucosa and entering other tissues, organs, and the bloodstream (Zhao L. et al., 2025). Barrier proteins can organize harmful substances to damage the intestines, brain, and reproductive glands (Li M. Y. et al., 2024; Zhao L. et al., 2024). The protective effect of the intestinal mucosa is closely related

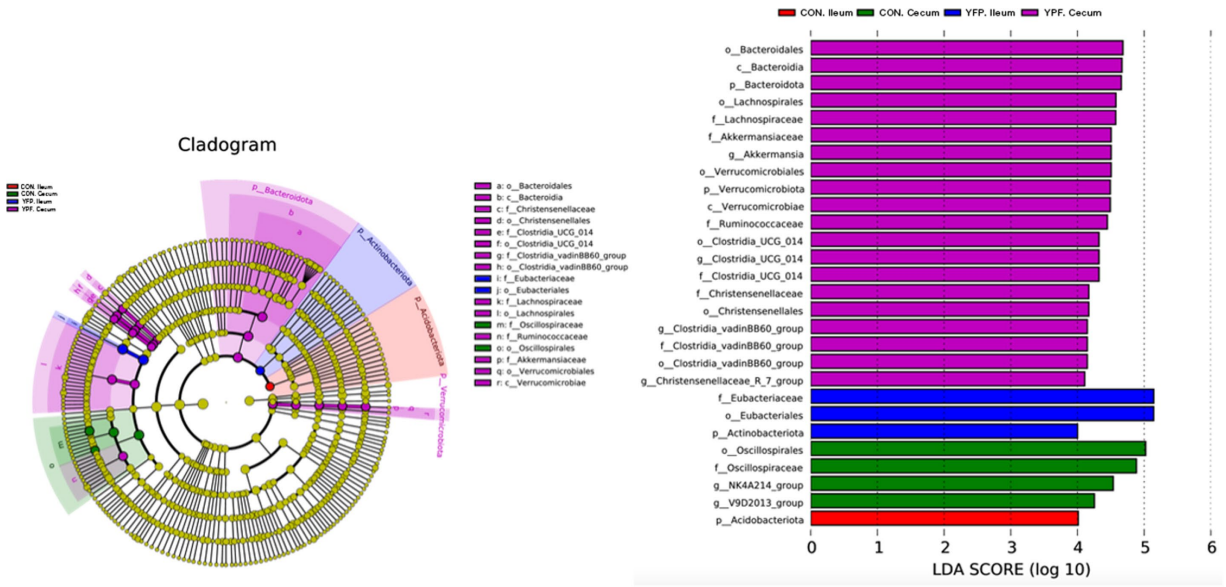

FIGURE 4
Expression of important microbiota in each group.

to goblet cells. Goblet cells can synthesize and secrete mucin needed for the intestinal mucosal barrier (Ma et al., 2020). Sijunzi decoction has been shown to be effective in improving the immunity of the small intestine and ensuring the integrity of the mucosal barrier in weaned Rex rabbits (Li et al., 2022). Another report showed that TCM could improve the growth performance of weaned Rex rabbits (Ning et al., 2018). Berberine can alleviate diarrhea and improve intestinal mucosal barrier function in piglets (Du et al., 2025). It has been shown that long-term administration of total glucosides of *Paeonia lactiflora* improves intestinal epithelial barrier damage in rats (Rui et al., 2023). Our research showed that MYFPG can increase the number of goblet cells, increasing the protective effect of the intestinal mucosal barrier.

4.2 MYPFG could alleviate diarrhea by regulating the intestinal microbiota

TCM is advantageous for treating diarrhea and regulating the intestinal microbiota. Our study showed that MYPFG could regulate the intestinal microbiota in Rex rabbits to decrease post-weaning diarrhea. Similarly, Lingguizhugan decoction could regulate the intestinal microbiota to treat diarrhea by promoting the growth of Muribaculaceae and *Dubosiella*, while inhibiting the growth of Christensenellaceae, Christensenellaceae_R_7_group, and UCG_005 (Huang et al., 2024). Christensenellaceae and Christensenellaceae_R_7_group also played an important role in our study, as they were key intestinal microbiota associated with diarrhea. It was reported that the Yangyin-ningshen formula could also decrease the abundance of Actinobiota while increasing the abundance of Bacteriodia to treat diarrhea (Lei et al., 2024). However, Actinobiota and Bacteriodia did not appear in the MYPFG regulation intestinal microbiota. Another report showed that the TCM Shenling Baizhu decoction could regulate *Monoglobus*, *Dubosiella*, and *Akkermansia* to treat diarrhea (Shao et al., 2024). The abundance of *Akkermansia* was also changed by MYPFG in our intestinal microbiota results. Rice water-fried Atractylodis Rhizoma could treat diarrhea by significantly enriching beneficial bacteria, such as *Lactobacillus*, and decreasing the abundance of potentially pathogenic fungi, such as *Aspergillus* (Chunping et al., 2023). However, neither *Lactobacillus* nor *Aspergillus* appeared in our research, which may be related to the use of different experimental animals. We found that, after being given MYPFG, the abundance of *Ruminococcus* significantly increased, leading to an increase in the secretion of carbohydrate-degrading enzymes and an increase in their ability to absorb carbohydrates from solid feed. The result is consistent with those of a study conducted by Zhao M. et al. (2024) which showed a significant increase in *Ruminococcus* in the intestinal microbiota of weaned rabbits. It was reported that adding carbohydrate-degrading enzymes to the diet can improve the intestinal health of weaned piglets (Ribeiro et al., 2024), which is consistent with our study. At the same time, the abundance of *Oxalobacter* significantly improved under the influence of MYPFG, which greatly enhanced the ability of otter rabbits to absorb oxalic acid from feed in their intestines, eliminating the phenomenon of oxalic acid accumulation in the intestines due to poor absorption (Pegah and John, 2022). The abundance of *Ruminococcus_torques_group* and *Oxalobacter* was significantly higher in the YPF cecum groups than in the CON cecum group at the genus level. *Ruminococcus* is associated with intestinal diseases (inflammatory bowel disease, irritable bowel syndrome, Crohn, etc.) (He C. et al., 2019; Buffet-Bataillon et al., 2024), immune diseases (allergy, eczema, asthma, etc.) (Ji et al., 2022), and nervous system diseases (autism, depression, etc.) (Morioka et al., 2022; Yan et al., 2022). It has been confirmed that *Ruminococcus* can repair intestinal mucosal barrier damage (Xia et al., 2022) and that *Oxalobacter* can degrade oxalic acid and prevent the formation of oxalate (Li et al., 2015). The colonization of *Oxalobacter* can normalize oxalic acid excretion (Canales and Hatch, 2017). Other studies have shown that *Oxalobacter* could help intestinal epithelial cells transfer oxalic acid (Donna et al., 2023). Oxalic acid can reduce the

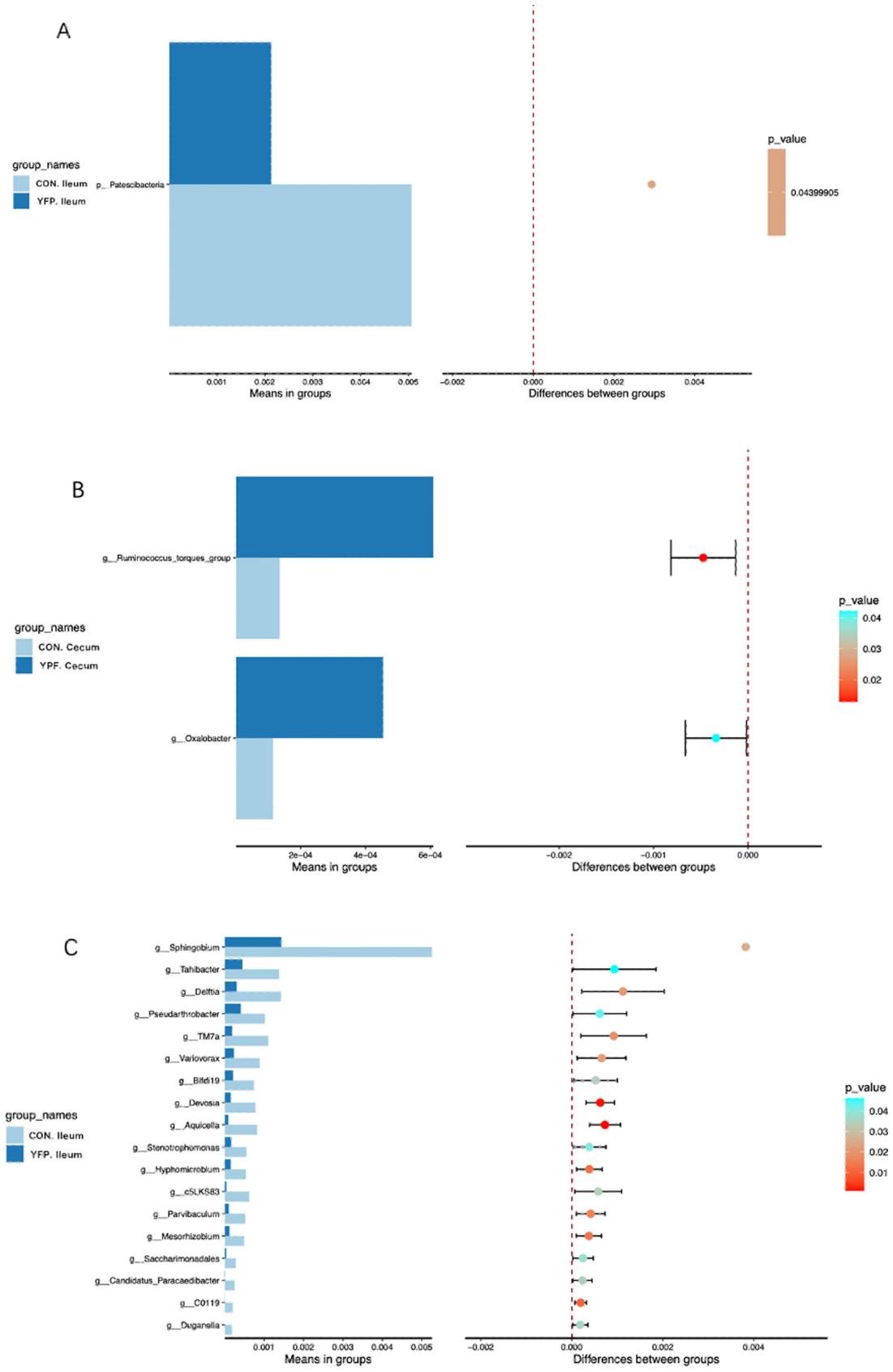

FIGURE 5
The abundances of species with significant differences between groups. **(A)**: phylum level; **(B,C)**: genus level.

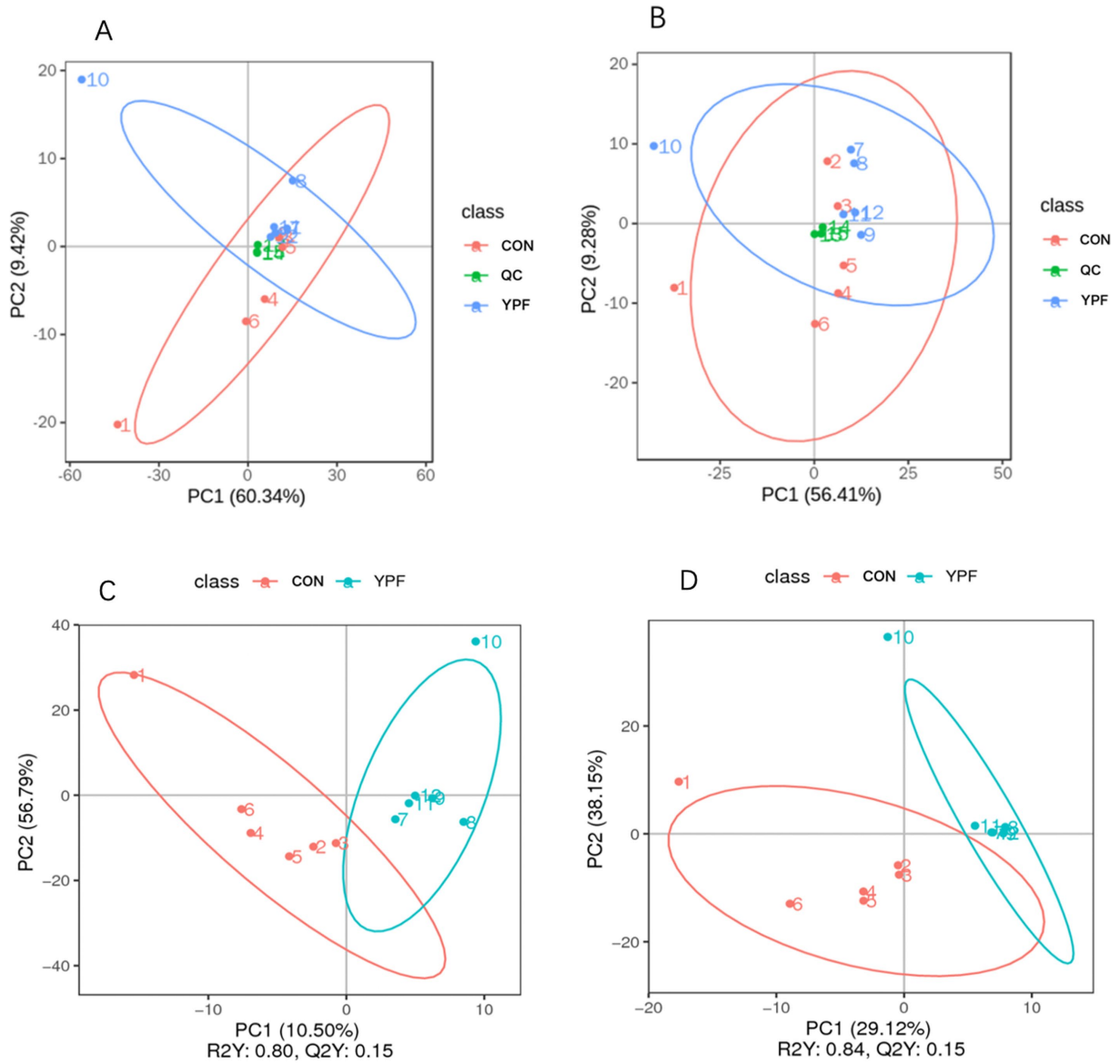

FIGURE 6
Effect of MYPFG on metabolites. **(A)** PCA in positive ion mode. **(B)** PCA in negative ion mode. **(C)** PLS-DA in positive ion mode. **(D)** PIS-DA in negative ion mode.

bioavailability of mineral elements, and it is easy to form calcium oxalate with calcium ions in animals, leading to kidney stones. These findings indicate that *Ruminococcus* and *Oxalobacter* play important roles in intestinal microorganisms. MYPFG can alleviate diarrhea symptoms in several ways by regulating *Ruminococcus* and *Oxalobacter*. There have been many reports on changes in the intestinal microbiota of other weaned animals after treatment with TCM. Scholars have shown that dietary *Astragalus* can regulate the intestinal immunity and intestinal microbiota of weaned piglets, and it can improve the growth performance and intestinal health of weaned piglets (Che et al., 2024). Recent studies have shown a correlation between piglet diarrhea and the intestinal microbiota, with Bacteroidaceae and Caudoviricetes being the main differential organisms strongly correlated with host status (Xie F. et al., 2024). Licorice extract could improve growth performance, enhance antioxidant capacity, and alter the abundance of the intestinal microbiota *Rikenellaceae* in weaned piglets (Zhu et al., 2024). Dietary Qi-Weng-Huangbo powder reduced diarrhea rates, improved growth performance, and enhanced immune function in weaned piglets. These improvements were potentially supported by changes in the ileum and colonic morphology and the modulation of the colonic microbial profiles (Chuanpi et al., 2023). Dietary berberine and ellagic acid supplementation could improve growth performance and reduce intestinal damage by regulating the structural function of the intestinal microbiota in weaned piglets. This regulation altered the composition of the microbiota, including Firmicutes, *Bacteroidetes*, *Lactobacillus*, *Phascolarctobacterium*, and *Parabacteroides* (Wenxia et al., 2023). Dietary berberine supplementation improves growth performance and alleviates intestinal injury in weaned piglets by modulating the ileal microbiota and metabolites (Cui et al., 2023).

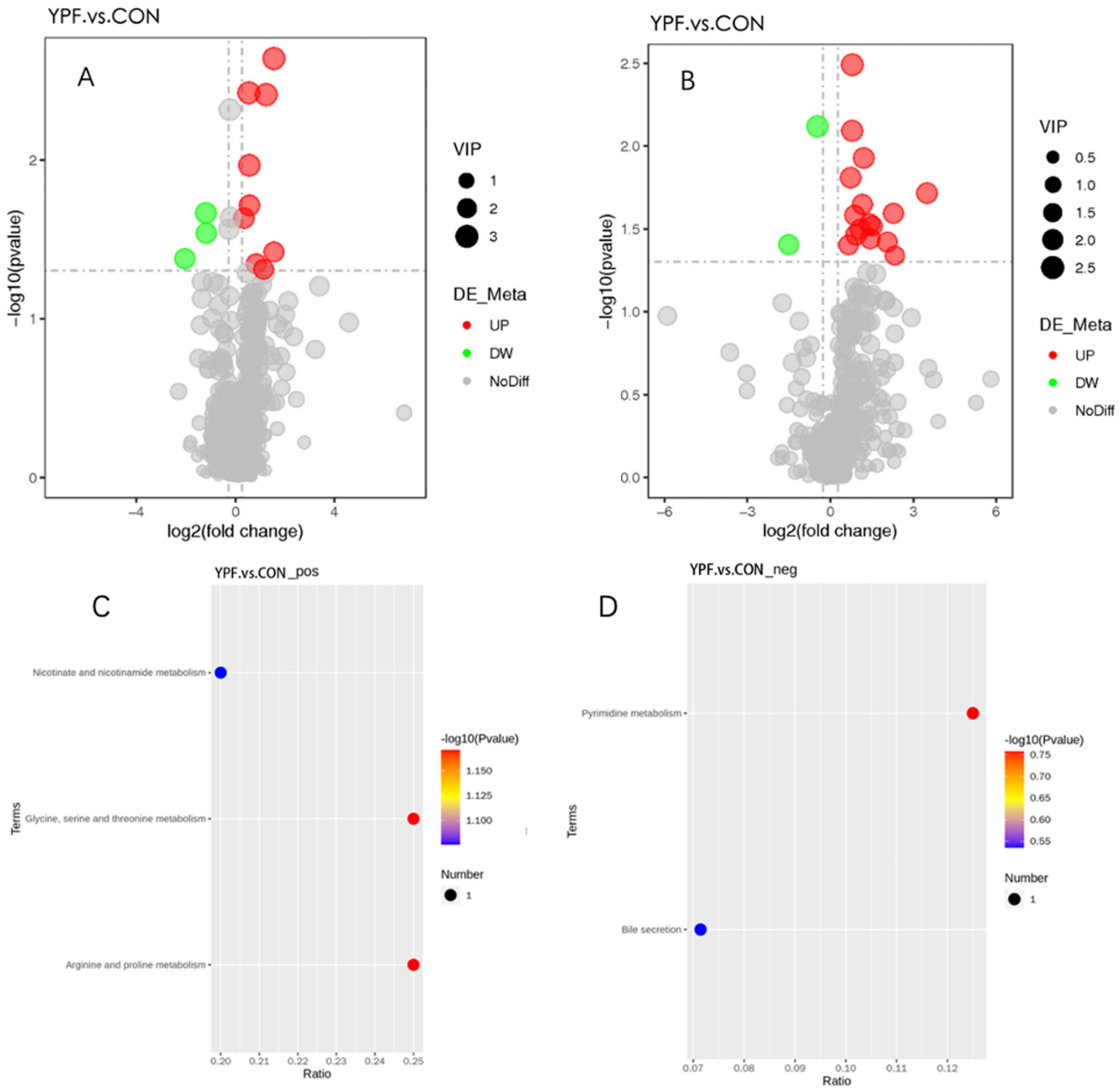

FIGURE 7
Volcano plot of the differential metabolites between the YPF group and the CON group under positive **(A)** and negative **(B)** ion mode. Enrichment analysis of differential metabolite pathways between the YFP group and the CON group under positive **(C)** and negative **(D)** ion mode.

4.3 MYPFG could alleviate diarrhea by altering the metabolites of cecal contents

Analyzing the mechanism of action of TCM through metabolomics has become a hot research topic in recent years. Some scholars have found that *Coptis chinensis* could significantly downregulate 76 metabolites and upregulate 31 metabolites to treat diarrhea (Ting et al., 2022). Another TCM, Alfalfa polysaccharides, has been shown to alleviate diarrhea by altering metabolites in calves (Zhao J. et al., 2025). It was reported that metabolomics revealed the therapeutic effect of Pueraria polysaccharides on calf diarrhea (Liuhong et al., 2023). In our study, we found 30 metabolites that were significantly different between the CON group and the YPF group based on the screening conditions. The enrichment analysis of the metabolites revealed that glycine, serine, and threonine metabolism; arginine and proline metabolism; and nicotinate and nicotinamide metabolism differed between the groups. Some studies have shown that adding glycine, serine, and threonine to diets can increase the growth performance of animals, which may be due to changes in the metabolic pathways of glycine, serine, and threonine (Ospina-Rojas et al., 2018; Hilliar et al., 2019). These metabolic pathways are closely related to diarrhea and intestinal injury in Rex rabbits. Meanwhile, it has also been shown that glycine, serine, and threonine metabolism enhances the elimination of pathogenic bacteria in the body (Chen et al., 2019). MYPFG can increase the resistance and growth performance of weaned Rex rabbits through glycine, serine, and threonine metabolism. Arginine and proline metabolism can serve as markers for functional gastrointestinal diseases, such as functional dyspepsia and irritable bowel syndrome (Karpe et al., 2022). It was also found that arginine and proline metabolism were changed in the

TABLE 6 Identified potential biomarkers in the cecal contents in the positive ion mode.

No.	Metabolite	FC	VIP	Up/Down
1	4-oxo-4-[(1-phenylethyl)amino] but-2-enoic acid	2.93	3.16	Up
2	N-Tetradecanamide	1.45	3.11	Up
3	Linolelaidic acid (C18:2N6T)	2.36	3.14	Up
4	(2E,4E)-N-(2-methylpropyl) dodeca-2,4-dienamide	1.48	2.97	Up
5	(2E,4E)-N-(2-methylpropyl) deca-2,4-dienamide	1.48	2.69	Up
6	Creatine	0.44	2.67	Down
7	N-(9-oxodecyl)acetamide	1.27	2.62	Up
8	5α-Pregnan-3,20-dione	0.44	2.56	Down
9	6-(3-hydroxybutan-2-yl)-5-(hydroxymethyl)-4-methoxy-2H-pyran-2-one	2.94	2.45	Up
10	Guanidineacetic acid	0.24	2.51	Down
11	Nicotinic acid	1.79	2.40	Up
12	Linoleoyl ethanolamide	2.21	2.34	Up

TABLE 7 Identified potential biomarkers in the cecal contents in the negative ion mode.

No.	Metabolite	FC	VIP	Up/Down
1	(±)18-HEPE	1.73	2.51	Up
2	Deoxycholic acid	0.72	2.36	Down
3	Hematoxylin	1.73	2.31	Up
4	1-[(1R,2S,3R,5R)-5-Cyclohexyl-2,3-dihydroxycyclopentyl]-3-ethylurea	2.31	2.21	Up
5	Ferulic acid	1.66	2.17	Up
6	4-(morpholinosulfonyl)aniline	11.28	2.19	Up
7	Indoxylsulfuric acid	2.23	2.04	Up
8	Thymidine 5′-monophosphate	4.85	2.04	Up
9	N-{[2-(2-thienyl)-1,3-thiazol-4-yl] methyl}benzamide	1.84	2.03	Up
10	8-iso-15-keto Prostaglandin F2α	2.68	2.06	Up
11	4-Hydroxy-2-Oxoglutaric acid	2.87	1.96	Up
12	Uridine monophosphate (UMP)	2.11	1.98	Up
13	(+/−)12(13)-DiHOME	1.90	2.20	Up
14	1-acetyl-N-(6-chloro-1,3-benzothiazol-2-yl)-4-piperidinecarboxamide	2.71	2.00	Up
15	Uridine	4.16	2.03	Up
16	N′1-(3,4-dichlorobenzoyl)-2-(hydroxymethyl)benzene-1-carbohydrazide	0.35	2.01	Down
17	Hydroxyglutaric acid	1.58	1.89	Up
18	N1-(4-chlorophenyl)-2-cyano-4,4-dimethyl-3-oxopentanamide	5.03	1.84	Up

liver injury model (Guo Chang et al., 2022). The scholars also found that animals with defects in arginine and proline metabolism would suffer from malnutrition (Abdullah et al., 2017). These findings also confirm that arginine and proline metabolism is closely related to diarrhea. Anti-inflammatory-related potential biomarkers are associated with nicotinic acid and nicotinamide metabolism (Ma et al., 2016). Another study suggested that amino acid metabolism is also related to animal stress (He J. et al., 2019). Studies on nicotinic acid and nicotinamide metabolism have shown that diarrhea is not only related to weaning but also to animal stress and inflammation. Our research showed that these amino acid metabolic pathways can be used as markers for diarrhea and that MYPFG can also treat diarrhea through multiple targets.

4.4 Correlation analysis between the intestinal microbiota and metabolites

Integrated metabolomics and intestinal microbiota analysis can provide us with a deeper understanding of the mechanism of MYPFG in treating diarrhea. Recently, some scholars have reported exploring the mechanism of TCM by integrating metabolomics and intestinal microbiota analysis. It was reported that integrating metabolomics and intestinal microbiota analysis revealed the prevention mechanism of TCM (Gushudan) in rats with kidney-yang deficiency syndrome (Xin et al., 2024). Another report showed that a new strategy for studying the mechanism of TCM, by integrating metabolomics and intestinal microbiota analysis together, was developed and proposed, with platycodin D as an example (Yuanhan et al., 2023). Scholars have explored the effects of Astragali Radix against cisplatin-induced liver injury using 16S rRNA gene sequencing and LC/MS-based metabolomics (Ling et al., 2022). Our study combined the cecal microbiota and the metabolomics of the cecal contents. In the correlation analysis between the cecal microbiota and cecal contents metabolites, the correlations between *Oxalobacter* and N-(9-oxodecyl) acetamide, 1-3-ethylurea, and hematoxylin, as well as the correlations between *Ruminococcus* and creatine, linolelaidic acid, N-(9-oxodecyl) acetamide, ferulic acid, N1-(4-chlorophenyl)-2-cyano-4, 4-dimethyl-3-oxopentanamide, and thymidine 5′-monophosphate, indicated their important roles in the treatment of diarrhea. MYPFG exerts an anti-diarrhea effect by regulating the relative abundance of *Ruminococcus* and *Oxalobacter* and by participating in the metabolism of glycine, serine, and threonine; arginine and proline; and nicotinate and nicotinamide. Scholars have confirmed that *Ruminococcus* can repair intestinal damage (Jiang et al., 2025). It has been reported that the abundance of *Oxalobacter* affects the absorption of oxalic acid (Lama et al., 2021). Glycine plays an important role in regulating the morphology, barrier function, and intestinal microbiota of ducks (Yaqi et al., 2023). Serine alleviates colitis by regulating intestinal α 1,2-fucosylation (Yao et al., 2024). Threonine could help mice excrete harmful metal ions from their intestines (Yongbin et al., 2022). Supplementing arginine in the diet could improve the growth performance of piglets through the intestinal microbiota (Liu C. et al., 2024). Proline promotes the activation of lymphoid tissue inducer cells to maintain intestinal homeostasis (Di et al., 2023).

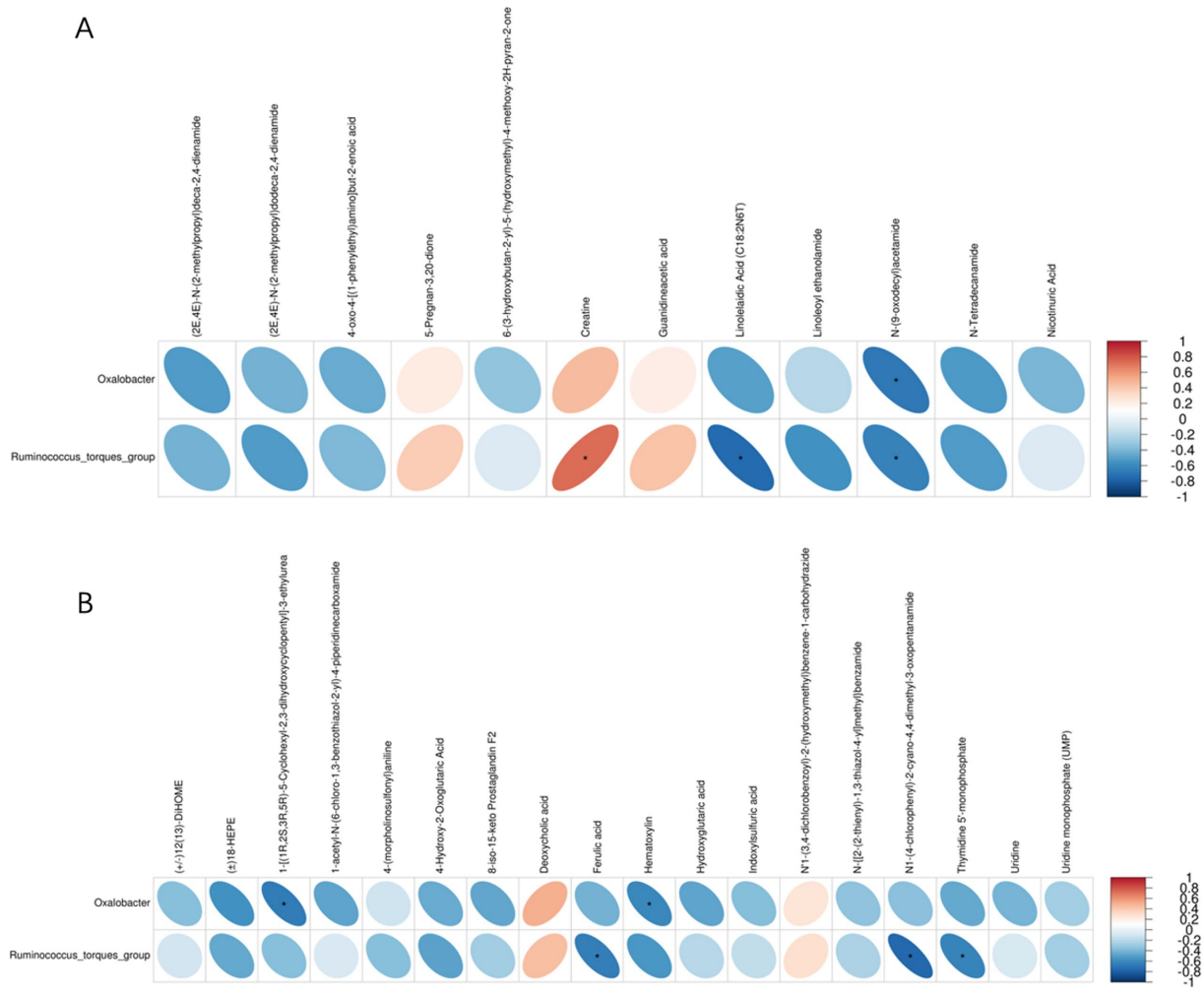

FIGURE 8
Correlations between the relative abundance of intestinal microbiota and metabolites. **(A)** Positive ion mode. **(B)** Negative ion mode. Blue indicates a negative correlation, and red indicates a positive correlation. The blank area in the figure indicates a $p > 0.05$, and the area marked by an asterisk (*) indicates $p < 0.05$.

Nicotinate and nicotinamide could regulate the intestinal microbiota of rats, reduce intestinal barrier permeability, and avoid inflammatory reactions (Sai et al., 2025). All of the above-discussed similar studies indicate that MYPFG affects intestinal health from different directions, such as the abundance of intestinal microbiota and amino acid metabolism pathways.

This study investigated the protective effect of MYPFG on the intestinal tract of weaned rabbits using intestinal microbiota and metabolomics methods and explored the specific pathways through which the intestinal microbiota and metabolomics protect the intestinal tract of rabbits. In the future, we will further investigate the mechanism of action of the key active ingredients in MYPFG and conduct large-scale clinical trials to verify its effects. We will also explore the potential application of MYPFG in treating diarrhea in other animals or humans. With an increasing number of TCM treatments being able to elucidate the mechanism of treating diarrhea using modern medical methods, we believe this study has enormous value and potential for the clinical translation of TCM.

5 Conclusion

MYPFG could decrease post-weaning diarrhea by regulating the intestinal microbiota and metabolites. We identified 30 differentially expressed metabolites as potential biomarkers of PWD, including nicotinic acid and creatine. MYPFG regulated the abundance of Patescibacteria, *Sphingobium*, *Oxalobacter,* and *Ruminococcus* and participated in the activities of three metabolic pathways, thereby alleviating the symptoms of PWD through multiple targets and mechanisms. The results further characterized the pharmacological mechanism of MYPFG against PWD.

Data availability statement

The datasets presented in this study can be found in online repositories. The names of the repository/repositories and accession number(s) can be found at: https://www.ncbi.nlm.nih.gov/, PRJNA1084245.

Ethics statement

The animal study was approved by the National Standard, Laboratory Animal-Requirements of Environment and Housing Facilities (GB14925-2001), the Sichuan Agricultural University Institutional Animal Care and Use Committee under permit number CSQ-2020303006. The study was conducted in accordance with the local legislation and institutional requirements.

Author contributions

DL: Data curation, Methodology, Writing – original draft, Writing – review & editing. CL: Formal analysis, Validation, Writing – review & editing. NL: Funding acquisition, Investigation, Writing – review & editing. HZL: Visualization, Writing – review & editing. ZY: Supervision, Writing – review & editing. QL: Visualization, Writing – review & editing. GS: Supervision, Writing – review & editing. JL: Supervision, Writing – review & editing. WZ: Software, Writing – review & editing. GP: Software, Writing – review & editing. LZ: Writing – review & editing. HT: Software, Writing – review & editing. HHL: Visualization, Writing – review & editing. FX: Writing – review & editing. HF: Project administration, Writing – review & editing.

Funding

The author(s) declare that financial support was received for the research and/or publication of this article. This work was financially supported by the Earmarked Fund for the China Agriculture Research System (CARS-43-A-3), the Science and Technology Department of Sichuan Province (2016NYZ0046), and the basic scientific research operating expenses of the Sichuan Science and Technology Department.

Conflict of interest

The authors declare that the research was conducted in the absence of any commercial or financial relationships that could be construed as a potential conflict of interest.

Publisher's note

All claims expressed in this article are solely those of the authors and do not necessarily represent those of their affiliated organizations, or those of the publisher, the editors and the reviewers. Any product that may be evaluated in this article, or claim that may be made by its manufacturer, is not guaranteed or endorsed by the publisher.

References

Abdullah, M., Kornegay, J. N., Honcoop, A., Parry, T. L., Balog-Alvarez, C. J., O'Neal, S. K., et al. (2017). Non-targeted metabolomics analysis of golden retriever muscular dystrophy-affected muscles reveals alterations in arginine and proline metabolism, and elevations in glutamic and oleic acid in vivo. *Meta* 7:38. doi: 10.3390/metabo7030038

Beihua, Z., Rui, G., Zhenhua, L., Baoshuang, L., Fengyun, W., and Xudong, T. (2015). Data mining analysis of Chinese medicine experts' experiences in treating chronic gastritis. *J. Tradit. Chin. Med.* 56, 79–83. doi: 10.13288/j.11-2166/r.2015.08.019

Buffet-Bataillon, S., Bouguen, G., Fleury, F., Cattoir, V., and Cunff, Y. L. (2024). Gut microbiota analysis for prediction of clinical relapse in Crohn's disease. *Sci. Rep.* 12:19609. doi: 10.1038/s41598-022-23757-x

Canales, B. K., and Hatch, M. (2017). *Oxalobacter formigenes* colonization normalizes oxalate excretion in a gastric bypass model of hyperoxaluria. *Surgery Obesity Related Dis.* 13, 1152–1157. doi: 10.1016/j.soard.2017.03.014

Che, Y., Li, L., Kong, M., Geng, Y., Wang, D., Li, B., et al. (2024). Dietary supplementation of Astragalus flavonoids regulates intestinal immunology and the gut microbiota to improve growth performance and intestinal health in weaned piglets. *Front. Immunol.* 15, –1459342. doi: 10.3389/fimmu.2024.1459342

Chen, Z., Guo, C., Chen, Z., Yang, T., Zhang, J., Wang, J., et al. (2019). Glycine, serine and threonine metabolism confounds efficacy of complement-mediated killing. *Nat. Commun.* 10, 3325–3317. doi: 10.1038/s41467-019-11129-5

Cheng, R. D., Lan, W. U., Zhang, R., and Wang, Z. X. (2014). Yupingfeng powder immunomodulatory effects on children with persistent diarrhea. *Chinese J. Immunol.* 30, 61–63. doi: 10.3969/j.issn.1000-484X.2014.01.011

Chu, H., Zong, Y., Yang, H., Chen, S., Ma, Z., and Li, H. (2023). Effects of Yu-Ping-Feng polysaccharides on animal growth performance and immune function: a review. *Front. Vet. Sci.* 10:1260208. doi: 10.3389/fvets.2023.1260208

Chuanpi, X., Kai, L., Chunran, T., Zeou, W., Jiaheng, L., Shunfeng, Z., et al. (2023). Dietary Qi-Weng-Huangbo powder enhances growth performance, diarrhoea and immune function of weaned piglets by modulating gut health and microbial profiles. 13. *Front. Immunol.* 14:1342852. doi: 10.3389/FIMMU.2023.1342852

Chunping, X., Meiyi, W., Xueqing, Y., Jin, S., Lili, W., and Zhidong, Q. (2023). Rice water-fried Atractylodis Rhizoma relieves spleen deficiency diarrhea by regulating the intestinal microbiome. *Oxidative Med. Cell. Longev.* 2023:1983616. doi: 10.1155/2023/1983616

Cui, Z., Meifang, L., Zhentao, H., Yinshan, B., Jun, Y., Jinling, Y., et al. (2023). Dietary berberine supplementation improves growth performance and alleviates gut injury in weaned piglets by modulating ileal microbiota and metabolites. *Food Funct.* 14, 4143–4162. doi: 10.1039/D3FO01044A

Di, W., Zongxian, L., Yime, Z., Yinlian, Z., Guanqun, R., Yanyu, Z., et al. (2023). Proline uptake promotes activation of lymphoid tissue inducer cells to maintain gut homeostasis. *Nat. Metab.* 5, 1953–1968. doi: 10.1038/S42255-023-00908-6

Dong-qi, L., Shu-wen, T., Min-ru, W., Peng-fei, M., Wen-hao, Y., and Hui, Y. (2018). Effect of Yupingfeng polysaccharide on immune function in mice with intestinal Flora. *Chinese J. Vet. Med.* 54, 97–99.

Donna, A., Changsoo, C., Altayeb, A., Christine, T., Gyorgy, B., Don, W., et al. (2023). Sel1-like proteins and peptides are the major *Oxalobacter formigenes*-derived factors stimulating oxalate transport by human intestinal epithelial cells. *Am. J. Physiol. Cell Physiol.* 325, C344–C361. doi: 10.1152/AJPCELL.00466.2021

Du, M., Liu, X., Ji, X., Wang, Y., Liu, X., Zhao, C., et al. (2025). Berberine alleviates enterotoxigenic *Escherichia coli*-induced intestinal mucosal barrier function damage in a piglet model by modulation of the intestinal microbiome. *Front. Nutr.* 11:1494348. doi: 10.3389/FNUT.2024.1494348

Fan, J., Li, C., Han, W., Wu, F., Fan, H., Fan, D., et al. (2024). Yeast peptides alleviate lipopolysaccharide-induced intestinal barrier damage in rabbits involving toll-like receptor signaling pathway modulation and gut microbiota regulation. *Front. Vet. Sci.* 11:1393434. doi: 10.3389/FVETS.2024.1393434

Fu, C., Ma, Y., Xia, S., Shao, J., Tang, T., Sun, W., et al. (2024). Study on changes in gut microbiota and microbiability in rabbits at different developmental stages. *Animals* 14:1741. doi: 10.3390/ANI14121741

Gao-yun, K. (2017). Current situation, problems and development direction of rex rabbit industry in China. *J. Anim. Sci. Vet. Med.* 36, 48–49.

Geng, W., Liu, S., Dong, H., Arachchige, B. N. P., Qi, D., and Wang, X. (2025). Exploration of active substances and its potential mechanism of Gancao Fuzi decoction on inflammatory based on metabolomics and network pharmacology. *Rapid Commun. Mass Spectr.* 39:e10007. doi: 10.1002/RCM.10007

Guan, Y., Zheng, W., Bai, Y., and Wu, B. (2024). Yupingfeng polysaccharide promote the growth of chickens via regulating gut microbiota. *Front. Vet. Sci.* 11:1337698. doi: 10.3389/FVETS.2024.1337698

Gui, W. Y., Yin, J. G., Liao, J. C., Luo, H. Z., You, Q., Gong, J. H., et al. (2024). Integrated analysis of metabolome, lipidome, and gut microbiome reveals the immunomodulation of Astragali radix in healthy human subjects. *Chin. Med.* 19:174. doi: 10.1186/S13020-024-01045-2

Guo Chang, Z. L., Shuyu, C., Xuxian, L., Xue, S., Yue, W., Baoyu, H., et al. (2022). Thymol ameliorates ethanol-induced hepatotoxicity via regulating metabolism and autophagy. *Chem. Biol. Interact.* 370:110308. doi: 10.1016/j.cbi.2022.110308

He, J., Guo, H., Zheng, W., Xue, Y., Zhao, R., and Yao, W. (2019). Heat stress affects fecal microbial and metabolic alterations of primiparous sows during late gestation. *J. Anim. Sci. Biotechnol.* 10:84. doi: 10.1186/s40104-019-0391-0

He, D., JiaXing, L., Yan, Y., and ChenHui, D. (2022). Mechanism of Suanzaoren decoction in improving insomnia rats by integrating metabolomics and intestinal flora analysis. *China J. Chinese Materia Med.* 47, 6741–6752. doi: 10.19540/J.CNKI.CJCMM.20220902.701

He, C., Wang, H., Liao, W.-D., Peng, C., Shu, X., Zhu, X., et al. (2019). Characteristics of mucosa-associated gut microbiota during treatment in Crohn's disease. *Gut Pathogens* 25, 2204–2216. doi: 10.3748/wjg.v25.i18.2204

Hilliar, M., Huyen, N., Girish, C. K., Barekatain, R., Wu, S., and Swick, R. A. (2019). Supplementing glycine, serine, and threonine in low protein diets for meat type chickens. *Poult. Sci.* 98, 6857–6865. doi: 10.3382/ps/pez435

Hongli, L., Chaohui, F., Lei, L., and Fuchang, L. (2017). Effects of dietary glutamine supplemental level on Fur quality and intestinal barrier of rex rabbits during weaner to 3 months of age. *Chinese J. Anim. Nutr.* 29, 356–362. doi: 10.3969/j.issn.1006?267x.2017.05.041

Huang, L., Liu, M., Shen, L., Chen, D., Wu, T., and Gao, Y. (2025). Polysaccharides from Yupingfeng granules ameliorated cyclophosphamide-induced immune injury by protecting intestinal barrier. *Int. Immunopharmacol.* 146:113866. doi: 10.1016/J.INTIMP.2024.113866

Huang, W., Wang, J., Xiao, Z., Lin, J., Tan, Z., and Sun, G. (2024). Lingguizhugan decoction alleviates obesity in rats on a high-fat diet through the regulation of lipid metabolism and intestinal microbiota. *Front. Microbiol.* 15:1462173. doi: 10.3389/FMICB.2024.1462173

Huang, L., Zheng, T., Liu, Y., Guo, T., and Tan, Z. (2022). Diarrheal mice induced by a high-fat and high-protein diet could be cured by Bohe pill regulating intestinal mucosal Bacteria. *J. Food Nutr. Res.* 10, 459–466. doi: 10.12691/JFNR-10-7-3

Ji, X., Su, L., Zhang, P., Yue, Q., Zhao, C., Sun, X., et al. (2022). Lentinan improves intestinal inflammation and gut dysbiosis in antibiotics-induced mice. *Sci. Rep.* 12:19609. doi: 10.1038/s41598-022-23469-2

Jia, F., Hui, M., Yanrui, Y., Lijun, W., Keyang, H., Yanan, Z., et al. (2023). Saikosaponin a ameliorates diet-induced fatty liver via regulating intestinal microbiota and bile acid profile in laying hens. *Poult. Sci.* 102:103155. doi: 10.1016/J.PSJ.2023.103155

JiaHua, D., MengYue, X., Yi, W., Zhao, L., Zhe, Y., and MuYang, L. (2022). Evaluation of *Taraxacum mongolicum* flavonoids in diets for *Channa argus* based on growth performance, immune responses, apoptosis and antioxidant defense system under lipopolysaccharide stress. *Fish Shellfish Immunol.* 131, 1224–1233. doi: 10.1016/J.FSI.2022.11.034

Jiang, Y. H., Li, Y. Y., Xin, W. G., Zhao, Y. T., Chen, X. Y., Song, J. J., et al. (2025). *Lactiplantibacillus plantarum* DACNJS22 alleviates benzo(a)pyrene-induced neurobehavioral injury in mice: insights from gut microbiota and short-chain fatty acids. *Food Biosci.* 64:105865. doi: 10.1016/J.FBIO.2025.105865

Jingxue, H., and Jianguo, S. (2017). Moxa with YuPingFeng san in treating 38 cases of infantile diarrhea of weakness of the spleen and stomach. *Western J. Traditi. Chinese Med.* 30, 89–91. doi: 10.3969/j.issn.1004-6852.2017.02.030

Karpe, A. V., Liu, J.-W., Shah, A., Koloski, N., Holtmann, G., and Beale, D. J. (2022). Utilising lipid and, arginine and proline metabolism in blood plasma to differentiate the biochemical expression in functional dyspepsia (FD) and irritable bowel syndrome (IBS). *Metabolomics* 18, 38–11. doi: 10.1007/s11306-022-01900-z

Lama, N., Fritz, F., Nora, H., Menghan, L., Huilin, L., Hyunwook, K., et al. (2021). Effect of antibiotic treatment on *Oxalobacter formigenes* colonization of the gut microbiome and urinary oxalate excretion. *Sci. Rep.* 11, –16428. doi: 10.1038/S41598-021-95992-7

Lei, L., Dong, Z., Mingyue, Y., Bin, W., Jing, L., Yi, Z., et al. (2019). Probiotic *Clostridium butyricum* improves the growth performance, immune function, and gut microbiota of weaning rex rabbits. *Probiot. Antimicrob. Proteins* 11, 1278–1292. doi: 10.1007/s12602-018-9476-x

Lei, Z., JunLiang, Z., Zhihui, B., Jiahua, D., Yanchao, S., Yi, W., et al. (2022). Polysaccharide from dandelion enriched nutritional composition, antioxidant capacity, and inhibited bioaccumulation and inflammation in *Channa asiatica* under hexavalent chromium exposure. *Int. J. Biol. Macromol.* 201, 557–568. doi: 10.1016/J.IJBIOMAC.2021.12.117

Lei, H., Liu, J., Deng, J., Zou, P., Zou, Z., Li, Z., et al. (2024). Behavior, hormone, and gut microbiota change by YYNS intervention in an OVX mouse model. *Front. Cell. Infect. Microbiol.* 14:1445741. doi: 10.3389/FCIMB.2024.1445741

Li, X., Ellis, M. L., and Knight, J. (2015). *Oxalobacter formigenes* colonization and oxalate dynamics in a mouse model. *Appl. Environ. Microbiol.* 81, 5048–5054. doi: 10.1128/AEM.01313-15

Li, H., and Hu, Y. (2024). Research progress on the treatment of diarrhea type irritable bowel syndrome with Tongxie Yaofang. *Asia Pacific Traditi. Med.* 20, 240–244. doi: 10.11954/ytctyy.202409050

Li, M. Y., Liu, Y. Z., Chen, X. M., Niu, X. T., Chen, L., Zhao, L., et al. (2025). Astaxanthin ameliorates high-carbohydrate diet-induced ER stress, immunosuppression and hepatic glucose metabolism through AMPK/autophagy pathway in *Channa argus*. *Aquaculture* 598:742010. doi: 10.1016/J.AQUACULTURE.2024.742010

Li, X., Qiao, B., Wu, Y., Deng, N., Yuan, J., and Tan, Z. (2024). Sishen pill inhibits intestinal inflammation in diarrhea mice via regulating kidney-intestinal bacteria-metabolic pathway. *Front. Pharmacol.* 15:1360589. doi: 10.3389/FPHAR.2024.1360589

Li, M. Y., Shi, Y. C., Xu, W. X., Zhao, L., and Zhang, A. Z. (2024). Exploring Cr(VI)-induced blood-brain barrier injury and neurotoxicity in zebrafish and snakehead fish, and inhibiting toxic effects of astaxanthin. *Environ. Pollut.* 355:124280. doi: 10.1016/J.ENVPOL.2024.124280

Li, D., Wang, Y., Li, N., Chen, S., Liu, H., Wang, P., et al. (2022). Modified Sijunzi granule decreases post-weaning diarrhea in rex rabbits via promoting intestinal development. *Front. Vet. Sci.* 9:972326. doi: 10.3389/fvets.2022.972326

Lin, Y., Wanli, L., Wei, J., Haoyu, W., and Jinhua, Z. (2024). Research progress in biological functions of saikosaponins. *Chinese J. Vet. Sci.* 44, 1307–1315. doi: 10.16303/j.cnki.1005-4545.2024.06.27

Lin, F., Xu, Y., Liu, B., Li, H., and Chen, L. (2024). Research progress on extraction, separation, structure, and biological activities of polysaccharides from the genus Atractylodes: a review. *Int. J. Biol. Macromol.* 283:137550. doi: 10.1016/J.IJBIOMAC.2024.137550

Ling, W., Xian-long, D., Xue-mei, Q., and Zhen-yu, L. (2022). Investigating the inter-individual variability of Astragali Radix against cisplatin-induced liver injury via 16S rRNA gene sequencing and LC/MS-based metabolomics. *Phytomedicine* 101:154107. doi: 10.1016/J.PHYMED.2022.154107

Liu, M., Sun, C., Zhou, Q., Xu, P., Wang, A., Zheng, X., et al. (2024). Supplementation of Yupingfeng polysaccharides in low fishmeal diets enhances intestinal health through influencing the intestinal barrier, immunity, and microflora in *Macrobrachium rosenbergii*. *Front. Immunol.* 15:1480897. doi: 10.3389/FIMMU.2024.1480897

Liu, C., Yang, Y., Wang, M., Jiang, W., Du, Y., Hao, Z., et al. (2024). Effects of L-arginine on gut microbiota and muscle metabolism in fattening pigs based on omics analysis. *Front. Microbiol.* 15:1490064. doi: 10.3389/FMICB.2024.1490064

Liuhong, S., Yu, S., Liuchao, Y., Yue, Z., Zhetong, S., Guangneng, P., et al. (2023). Blood metabolomics reveals the therapeutic effect of Pueraria polysaccharide on calf diarrhea. *BMC Vet. Res.* 19:98. doi: 10.1186/S12917-023-03662-9

Ma, Y., Bao, Y., Wang, S., Li, T., Chang, X., Yang, G., et al. (2016). Anti-inflammation effects and potential mechanism of Saikosaponins by regulating nicotinate and nicotinamide metabolism and arachidonic acid metabolism. *Inflammation* 39, 1453–1461. doi: 10.1007/s10753-016-0377-4

Ma, J., Shah, A. M., Wang, Z. R., Hu, H. Z., Wang, X., Cao, G., et al. (2020). Comparing the gastrointestinal barrier function between growth-retarded and normal yaks on the Qinghai-Tibetan Plateau. *PeerJ* 8:e9851. doi: 10.7717/PEERJ.9851

Morioka, D., Kobayashi, R., Hayashi, H., Kawakatsu, S., and Suzuki, A. (2022). Clonazepam-induced misidentification in prodromal dementia with Lewy bodies. *Psychogeriatrics* 22, 767–769. doi: 10.1111/psyg.12873

Muyang, L., Lu, C., Yiran, Z., Hui, S., and Lei, Z. (2022). Research on the mechanism of HRP relieving IPEC-J2 cells immunological stress based on transcriptome sequencing analysis 13. *Front. Nutr.* 9:944390. doi: 10.3389/FNUT.2022.944390

Ning, L., Hualin, F., Hanzhong, L., Rui, L., Kai, Z., Zhiju, Y., et al. (2018). Effects of different Chinese herbal compound on growth performance and serum biochemical indexes of weaned rex rabbits. *China Anim. Husbandry Vet. Med.* 45, 151–157. doi: 10.16431/j.cnki.1671-7236.2018.02.017

Ospina-Rojas, I., Murakami, A., Pozza, P., Aguihe, P., and Sakamoto, M. (2018). PSIII-35 dietary glycine+serine and threonine effects on performance, creatine muscle content and meat lipid oxidation of broiler chickens from 21 to 42 days of age. *J. Anim. Sci.* 96:313. doi: 10.1093/jas/sky404.689

Pegah, D., and John, L. C. (2022). New therapeutics for primary hyperoxaluria type 1. *Curr. Opin. Nephrol. Hypertension* 31, 344–350. doi: 10.1097/MNH.0000000000000790

Qiao, B., Xiao, N., Deng, N., and Tan, Z. (2024). Shenling Baizhu powder attenuates lard diet in a fatigued state-induced diarrhea via targeting microbial metabolites short chain fatty acids-mediated lipid metabolism. *Biotech* 14:203. doi: 10.1007/S13205-024-04045-Z

Ribeiro, D. M., Luise, D., Costa, M., Carvalho, D. F. P., Martins, C. F., Correa, F., et al. (2024). Impact of dietary *Laminaria digitata* with alginate lyase or carbohydrase mixture on nutrient digestibility and gut health of weaned piglets. *Animal* 18:101189. doi: 10.1016/J.ANIMAL.2024.101189

Rui, X., Jine, P., Zhe, M., Kaili, X., Meijing, L., Qi, W., et al. (2023). Prolonged administration of total glucosides of paeony improves intestinal immune imbalance and epithelial barrier damage in collagen-induced arthritis rats based on metabolomics-network pharmacology integrated analysis. *Front. Pharmacol.* 14:1187797. doi: 10.3389/FPHAR.2023.1187797

Runzhi, Z., Xi, G., Hong, B., and Kang, N. (2020). Traditional Chinese medicine and gut microbiome: their respective and concert effects on healthcare. *Front. Pharmacol.* 11:538. doi: 10.3389/fphar.2020.00538

Sai, Y., Ge, W., Zhong, L., Zhang, Q., Xiao, J., Shan, Y., et al. (2025). The role of the gut microbiota and the nicotinate/nicotinamide pathway in rotenone-induced neurotoxicity. *Curr. Res. Toxicol.* 8, –100212. doi: 10.1016/j.crtox.2024.100212

Shao, J., Liu, Z., Wang, L., Song, Z., Chang, H., Han, N., et al. (2017). Screening of the optimized prescription from Suqingwan in terms of its therapeutic effect on DSS-

induced ulcerative colitis by its regulation of inflammatory and oxidative mediators. *J. Ethnopharmacol.* 202, 54–62. doi: 10.1016/j.jep.2017.03.006

Shao, H., Wang, L., and Zhang, H. (2024). Chinese herbal medicine, Tongxieyaofang, alleviates diarrhea via gut microbiota remodeling: evidence from network pharmacology and full-length 16S rRNA gene sequencing. *Front. Cell. Infect. Microbiol.* 14, –1502373. doi: 10.1186/S12866-024-03592-Y

Shao, H., Zhang, C., Wang, C., and Tan, Z. (2020). Intestinal mucosal bacterial diversity of antibiotic-associated diarrhea (AAD) mice treated with Debaryomyces hansenii and Qiweibaizhu powder. *3 Biotech* 10:392. doi: 10.1007/s13205-020-02383-2

Soufi, S. A., Losada, A. P., Alonso, M. L., Cobas, A. C., Mora, A., Lamas, A., et al. (2024). Effects of dietary inclusion of *Saccharina latissima* and *Ulva lactuca* on growth performance and gut health in growing rabbits. *Agriculture* 14:1605. doi: 10.3390/AGRICULTURE14091605

Sun, H., Ni, X., Zeng, D., Zou, F., Yang, M., Peng, Z., et al. (2017). Bidirectional immunomodulating activity of fermented polysaccharides from Yupingfeng. *Res. Vet. Sci.* 110, 22–28. doi: 10.1016/j.rvsc.2016.10.015

Ting, W., Chongyang, Z., Hui, L., Rui, Z., Xiaoli, Y., Yong, Y., et al. (2022). The underlying rationality of Chinese medicine herb pair *Coptis chinensis* and *Dolomiaea souliei*: from the perspective of metabolomics and intestinal function. *J. Ethnopharmacol.* 289:115065. doi: 10.1016/J.JEP.2022.115065

Tongtong, W., Ling, L., Jun, D., Yu, J., Xiao, Y., and Wen, L. (2023). Analysis of the mechanism of action of quercetin in the treatment of hyperlipidemia based on metabolomics and intestinal flora. *Food Funct.* 14, 2112–2127. doi: 10.1039/D2FO03509J

Wang, F., Lai, G., Zhou, F., Nie, D., Wang, Y., Bai, Q., et al. (2023). Mechanism of Fangfeng Shaoyao decoction in the treatment of radiation enteritis based on network pharmacology and molecular docking. *Inner Mongolia J. Traditi. Chinese Med.* 42, 147–153. doi: 10.16040/j.cnki.cn15-1101.2023.11.003

Wang, H., Zhao, H., Tai, B., Wang, S., Ihsan, A., Hao, H., et al. (2024). Development and evaluation of non-antibiotic growth promoters for food animals. *Vet. Sci.* 11:672. doi: 10.3390/VETSCI11120672

Wenxia, Q., Zhendong, Y., Zhechang, L., Hengfeng, L., Wei, L., Jianan, Z., et al. (2023). Dietary Berberine and Ellagic acid supplementation improve growth performance and intestinal damage by regulating the structural function of gut microbiota and SCFAs in weaned piglets. *Microorganisms* 11:1254. doi: 10.3390/microorganisms11051254

Wlazło, Ł., Kowalska, D., Bielański, P., Ossowski, M., Czech, A., Łukaszewicz, M., et al. (2025). Study of the possibility of modulating the composition of the gastrointestinal microbiome of rabbits fed fermented rapeseed meal. *Ann. Anim. Sci.* 25, 271–279. doi: 10.2478/AOAS-2024-0068

Xia, X., Lin, H., Luo, F., Wu, X., Zhu, L., Chen, S., et al. (2022). Oryzanol ameliorates DSS-stimulated gut barrier damage via targeting the gut microbiota accompanied by the TLR4/NF-κB/NLRP3 Cascade response in vivo. *J. Agric. Food Chem.* 70, 15747–15762. doi: 10.1021/acs.jafc.2c04354

Xie, S., Fang, L., Deng, N., Shen, J., Tan, Z., and Peng, X. (2024). Targeting the gut-kidney axis in diarrhea with kidney-Yang deficiency syndrome: the role of Sishen pills in regulating TMAO-mediated inflammatory response. *Med. Sci. Monitor* 30, –e944185. doi: 10.12659/MSM.944185

Xie, F., Zhou, M., Li, X., Li, S., Ren, M., and Wang, C. (2024). Macrogenomic and Metabolomic analyses reveal mechanisms of gut microbiota and microbial metabolites in diarrhea of weaned piglets. *Animals* 14:2327. doi: 10.3390/ANI14162327

Xin, L., Ren, M., Lou, Y., Yin, H., Qin, F., and Xiong, Z. (2024). Integrated UHPLC-MS untargeted metabolomics and gut microbe metabolism pathway-targeted metabolomics to reveal the prevention mechanism of Gushudan on kidney-yang-deficiency-syndrome rats. *J. Pharm. Biomed. Anal.* 242:116062. doi: 10.1016/J.JPBA.2024.116062

Xue, L. G., Guo, T. K., Wang, J., Shan, Y. Q., Guo, L., Zhang, D. X., et al. (2025). Effects of in-ovo injection of Yu ping feng polysaccharides on growth performance, intestinal development, and immunity in broiler chickens. *Poult. Sci.* 104:104574. doi: 10.1016/J.PSJ.2024.104574

Yan, F., Xia, L., Xu, L., Deng, L., and Jin, G. (2022). A comparative study to determine the association of gut microbiome with schizophrenia in Zhejiang, China. *BMC Psychiatry* 22, 731–710. doi: 10.1186/s12888-022-04328-w

Yan-hong, M., and Yan-fang, W. (2017). Thirty cases of diarrhea due to diabetes with concurrence of cold and heat syndromes treated with Bupleurum and cinnamon twig and dried ginger decoction. *Henan Traditi. Chinese Med.* 37, 45–47. doi: 10.16367/j.issn.1003-5028.2017.06.0341

Yanling, Y., Yao, L., Sheng, G., and Hui, Y. (2022). Elucidation of the reinforcing spleen effect of jujube fruits based on metabolomics and intestinal Flora analysis. *Front. Cell. Infect. Microbiol.* 12:847828. doi: 10.3389/FCIMB.2022.847828

Yao, Y., Pan, X., Dai, Y., Chen, Y., Chang, Z., Pei, Z., et al. (2024). D-serine alleviates colitis by regulating intestinal α1,2-fucosylation. *Food Biosci.* 62:105057. doi: 10.1016/J.FBIO.2024.105057

Yao, W., Yanchun, W., Jun, M., Yanan, L., Lu, C., Tianxiang, Z., et al. (2023). YuPingFengSan ameliorates LPS-induced acute lung injury and gut barrier dysfunction in mice. *J. Ethnopharmacol.* 312:116452. doi: 10.1016/J.JEP.2023.116452

Yaqi, C., Ke, W., Min, W., Bing, W., Guangmang, L., Hua, Z., et al. (2023). Organic zinc Glycine chelate is better than inorganic zinc in improving growth performance of Cherry Valley ducks by regulating intestinal morphology, barrier function, and the gut microbiome. *J. Anim. Sci.* 101:skad279. doi: 10.1093/JAS/SKAD279

Yongbin, L., Zhijia, F., Xuewei, Z., Jian, G., Jingwen, W., Linru, H., et al. (2022). Threonine facilitates cd excretion by increasing the abundance of gut *Escherichia coli* in cd-exposed mice. *Molecules* 28:177. doi: 10.3390/MOLECULES28010177

Yu, Z., and Li, M. (2025). Application of nutrition interventions strategy to enhance fish flesh quality. *J. Food Compos. Anal.* 138:107010. doi: 10.1016/J.JFCA.2024.107010

Yuan-han, Z., Jian, L., Qian, Q., Yu-jie, W., Yi-ming, P., Ting, Z., et al. (2023). The activities and mechanisms of intestinal microbiota metabolites of TCM herbal ingredients could be illustrated by a strategy integrating spectrum-effects, network pharmacology, metabolomics and molecular docking analysis: Platycodin D as an example. *Phytomedicine* 115:154831. doi: 10.1016/J.PHYMED.2023.154831

Zhang, Q. W., Yang, M. J., Liao, C. Y., Taha, R., Li, Q. Y., Abdelmotalab, M. I., et al. (2024). Atractylodes macrocephala Koidz polysaccharide ameliorates DSS-induced colitis in mice by regulating the gut microbiota and tryptophan metabolism. *Br. J. Pharmacol.* 182, 1508–1527. doi: 10.1111/BPH.17409

Zhao, L., Duan, H., Liu, Y., Wang, Y., Li, M., and Li, M. (2024). Long-term exposure of zebrafish (*Danio rerio*) to Cr(VI): reproductive toxicity and neurotoxicity. *Reg. Stud. Mar. Sci.* 74:103559. doi: 10.1016/J.RSMA.2024.103559

Zhao, W., Li, C., Wu, X., Zhang, J., Wang, L., Chen, X., et al. (2025). Synergistic effects of dietary *Forsythia suspensa* extract and *Astragalus membranaceus* polysaccharides on growth enhancement, antioxidant boost, and inflammation alleviation in juvenile *Larimichthys crocea*. *Aquaculture* 598:742029. doi: 10.1016/J.AQUACULTURE.2024.742029

Zhao, M., Liu, H., Liu, M., Yue, Z., Li, C., Liu, L., et al. (2024). Metagenomics and metabolomics reveal that gut microbiome adapts to the diet transition in Hyla rabbits. *Microbiol. Res.* 283:127705. doi: 10.1016/J.MICRES.2024.127705

Zhao, J., Tian, H., Kong, X., Dang, D., Liu, K., Su, C., et al. (2025). Microbiomic and Metabolomic insights into the mechanisms of alfalfa polysaccharides and seaweed polysaccharides in alleviating diarrhea in pre-weaning Holstein calves. *Animals* 15:485. doi: 10.3390/ANI15040485

Zhao, L., Yu, J., Liu, Y., Liu, Y., Zhao, Y., and Li, M. Y. (2025). The major roles of intestinal microbiota and TRAF6/NF-κB signaling pathway in acute intestinal inflammation in mice, and the improvement effect by *Hippophae rhamnoides* polysaccharide. *Int. J. Biol. Macromol.* 296:139710. doi: 10.1016/J.IJBIOMAC.2025.139710

Zhe, Y., Lei, Z., Jun-Liang, Z., Wanxin, X., Zehao, G., Ai-Zhong, Z., et al. (2022). Dietary Taraxacum mongolicum polysaccharide ameliorates the growth, immune response, and antioxidant status in association with NF-κB, Nrf2 and TOR in Jian carp (*Cyprinus carpio* var. Jian). *Aquaculture* 547:737522. doi: 10.1016/J.AQUACULTURE.2021.737522

Zheng, W., Guan, Y., and Wu, B. (2023). Effects of Yupingfeng polysaccharides as feed supplement on immune function and intestinal microbiome in chickens. *Microorganisms* 11:2774. doi: 10.3390/microorganisms11112774

Zhi-ping, H. (2017). Economic benefit analysis of rex rabbit breeding. *J. Anim. Sci. Vet. Med.* 36, 110–111.

Zhu, J., Lian, J., Deng, H., Luo, J., Chen, T., Sun, J., et al. (2024). Effects of spinach extract and licorice extract on growth performance, antioxidant capacity, and gut microbiota in weaned piglets. *Animals* 14:321. doi: 10.3390/ANI14020321

Zhuang, Z., Hou, W., Liu, W., Li, W., and Liu, Y. (2024). Research progress on quantitative value transfer of traditional Chinese medicine preparations. *Chin. Tradit. Herb. Drug* 55, 6448–6454. doi: 10.7501/j.issn.0253-2670.2024.18.034

frontiers | Frontiers in Microbiomes

TYPE Original Research
PUBLISHED 09 September 2025
DOI 10.3389/frmbi.2025.1531991

Check for updates

OPEN ACCESS

EDITED BY
Jason W Soares,
Combat Capabilities Development Command United States Army, United States

REVIEWED BY
Paola Roncada,
Magna Græcia University, Italy
Santiago Cadena,
Autonomous University of the State of Morelos, Mexico

*CORRESPONDENCE
Yuxiang Zhang
15810550308@163.com
Jiaxing Wang
wangjiaxing012@163.com
Guifeng Zhao
zgfcardio@126.com

RECEIVED 21 November 2024
ACCEPTED 19 August 2025
PUBLISHED 09 September 2025

CITATION
Xuan L, Sun X, Wang B, Chen F, Yi Y, Mao H, Wang Y, Zhao G, Wang J and Zhang Y (2025) Cold-water immersion alleviates intestinal damage induced by exertional heat stroke via modulation of gut microbiota in rats.
Front. Microbiomes 4:1531991.
doi: 10.3389/frmbi.2025.1531991

COPYRIGHT
© 2025 Xuan, Sun, Wang, Chen, Yi, Mao, Wang, Zhao, Wang and Zhang. This is an open-access article distributed under the terms of the Creative Commons Attribution License (CC BY). The use, distribution or reproduction in other forums is permitted, provided the original author(s) and the copyright owner(s) are credited and that the original publication in this journal is cited, in accordance with accepted academic practice. No use, distribution or reproduction is permitted which does not comply with these terms.

Cold-water immersion alleviates intestinal damage induced by exertional heat stroke via modulation of gut microbiota in rats

Lyu Xuan[1,2], Xiaojun Sun[2], Baozhong Wang[2], Feng Chen[3], Yuhao Yi[3], Handing Mao[4], Yuxi Wang[1], Guifeng Zhao[3]*, Jiaxing Wang[1]* and Yuxiang Zhang[1]*

[1]Department of Critical Care Medicine, The Eighth Medical Center of Chinese People's Liberation Army (PLA) General Hospital, Beijing, China, [2]Department of Emergency and Internal Medicine, Heilongjiang Armed Police Corps Hospital, Harbin, Heilongjiang, China, [3]Department of Critical Care Medicine, Chinese People's Liberation Army Rocket Force Characteristic Medical Center, Beijing, China, [4]Department of Emergency, The Sixth Medical Center of Chinese People's Liberation Army General Hospital, Beijing, China

Objective: The pathogenesis of exertional heatstroke (EHS) involves substantial contributions from gut microbiota and their metabolites. In this study, we assessed whether cold water immersion (CWI) mitigates EHS-induced intestinal damage via alterations in the microbiome.

Methods: An EHS model was created with 18 Wistar rats divided into three groups, that is, the EHS group comprising rats with exertional heat stroke, the CWI group with rats with heatstroke treated with cold water immersion, and the control (CTRL) group (rats with normothermia control). Pathological changes, core temperature (Tcore), and lactic acid (Lac) and endotoxin lipopolysaccharide (LPS) levels were evaluated. Fecal samples were subjected to metagenomic shotgun sequencing and liquid chromatography–mass spectrometry for microbiota and metabolomic profiling.

Results: Hematoxylin and eosin staining showed that CWI treatment significantly reduced EHS-induced intestinal congestion, edema, and necrosis compared to the EHS group. The EHS group had the highest Tcore, while the CWI group had significantly lower Tcore than the EHS group. The CWI group had significantly reduced LPS and Lac levels, similar to those observed in the CTRL group. Microbiome analysis indicated that EHS disrupted gut bacteria, with an increase in the proportion of pathogens such as *Desulfovibrio fairfieldensis, Desulfamplus magnetovallimortis*, and *Desulfococcus oleovorans* ($P<0.05$). CWI treatment resolved these disturbances and restored the gut microbiota to a level similar to that of the CTRL group. Metagenomic analysis showed that CWI restored gut microbiota diversity (Shannon index, $P<0.05$), significantly reducing the proportion of pathogenic *Desulfovibrio*. Metabolomic profiling identified key metabolites, such as inosine, hypoxanthine, guanosine, and taurine (Variable importance in projection>1, $P<0.05$ with P-values adjusted for multiple comparisons using the Benjamini-Hochberg method, $FDR<0.05$), differentiating between the CWI and EHS groups.

Conclusion: The metabolites inosine, taurine, hypoxanthine, and guanosine correlated with restored gut microbiota, reduced proportion of *Desulfovibrio*,

and attenuated inflammation (lower LPS/Lac), suggesting that their dual role in mitigating intestinal damage. These findings underscore the therapeutic potential of CWI by modulating microbial-derived metabolites, highlighting its impact on the intestinal health of patients with EHS.

KEYWORDS

exertional heat stroke, gut microbiota, metabolic disorder, cold-water immersion, lipopolysaccharide

1 Introduction

Exertional heatstroke (EHS) is a life-threatening metabolic disorder characterized by thermoregulatory failure (Leyk et al., 2019). EHS leads to the breakdown of sweat glands, dysregulation of body temperature and electrolyte balances, causing severe neurological and circulatory damage. This includes delirium, seizures, convulsions, rhabdomyolysis, acute lung injury, and in extreme cases, disseminated intravascular coagulation, multiple organ dysfunction syndrome, and death (Li Z. et al., 2021). The underlying mechanisms of EHS are complex and not entirely understood, however, it is often linked with inflammatory imbalances, oxidative stress, coagulation anomalies, rhabdomyolysis, and intestinal dysfunction.

The gastrointestinal (GI) tract, a selectively permeable barrier between the GI lumen and circulating blood, is the most extensive mucosal interface in the human body, covering approximately 250–400 m^2 (Qiang et al., 2021). Studies indicate that EHS causes significant intestinal damage, primarily through circulatory disturbances that lead to ischemia in the GI tract. This affects the viability of intestinal cells and the permeability of the cell walls during EHS episodes (Tang et al., 2021). Moreover, mounting evidence suggests that dysbiosis in the gut microbiota plays a crucial role in the pathophysiology of intestinal injuries (Liu et al., 2022). Recent research has shown that such dysbiosis compromises the integrity of the intestinal barrier, leading to gut-derived endotoxemia, systemic inflammatory responses, and injuries across multiple organs (Jing et al., 2021). Thus, intestinal damage due to altered gut microbiota is a critical pathological feature of EHS progression. Preserving intestinal homeostasis is vital for preventing the onset and advancement of EHS.

Cold-water immersion (CWI) is often used as a recovery technique after intense physical activity (Babak et al., 2021). It is recognized as the primary treatment for EHS, with a critical emphasis on the rapid initiation of CWI once Tcore exceeds 40°C (Demartini et al., 2015). As such, CWI is regarded as the leading therapeutic approach for EHS management. The method offers several benefits, including a cold-induced analgesic effect, reduction of hyperthermia and its impacts on the central nervous system, and decreased cardiovascular strain (Ihsan et al., 2016). However, it also presents risks such as the 'afterdrop' phenomenon, where body temperature continues to drop post-immersion, potential mortality, overcooling, hypothermia, and organ dysfunction (Douma et al., 2020). While various mechanisms have been proposed, the exact factors that contribute to EHS improvements via CWI are still not fully understood. CWI is thought to improve cardiac blood flow and reduce the hypermetabolic state of the heart, thereby yielding therapeutic outcomes (Knapik and Epstein, 2019). The gut microbiota also plays a vital role in energy metabolism, dependent on appropriate temperature and environmental conditions for growth (Li et al., 2023). Research indicates that gut commensal bacteria can interact with pathogens, regulate virulence expression, and reduce toxin production, influencing susceptibility to EHS (Armstrong et al., 2018). (Li L. et al., 2021) found that administering *Bacillus licheniformis* for a week prior to heat exposure reduced high body temperatures, improved survival rates, and reduced immune responses and organ damage, likely by maintaining gut barrier integrity and regulating the gut microbiota to promote beneficial bacteria and reduce harmful ones. Despite these findings, the effect of CWI on EHS-induced intestinal injury remains underexplored. It is therefore essential to further investigate the role of CWI in managing EHS-induced intestinal injuries. This study aims to establish an EHS rat model and explore the mechanisms by which CWI improves EHS-induced intestinal injuries through modifications in the gut microbiome.

Microbial metabolites serve as vital mediators between bacteria and their hosts (Krautkramer et al., 2021). Specific metabolites from the intestinal flora can influence the balance between pro- and anti-inflammatory mechanisms in the gut by regulating intestinal barrier function and the oxidative stress response (Ghosh et al., 2021). Metabolomics, a sophisticated technique, allows for the identification of unique molecular 'fingerprints' that characterize different physiological and pathological conditions. This method is used to study the pathogenesis of metabolic diseases and the action mechanisms of therapeutic drugs (Johnson et al., 2016). Alterations in intestinal metabolic profiles are key to understanding the molecular biology of intestinal injuries resulting from EHS.

We hypothesized that CWI alleviates EHS-induced intestinal damage by modulating sulfur-metabolizing bacteria and restoring

Abbreviations: CWI, cold-water immersion; EHS, exertional heat stroke; MODS, multiple organ dysfunction syndrome; DIC, Disseminated Intravascular Coagulation; GI, gastrointestinal; SPF, specific pathogen-free.

anti-inflammatory metabolites. This study aimed to test this through integrated microbiome-metabolome analysis. To test this hypothesis, the purpose of this study is to evaluate the protective effects of CWI on EHS-induced intestinal injuries and to explore the potential mechanisms involving the gut microbiome. An EHS model was established, and metabolomics analysis was performed to assess changes in the metabolic profiles of gut microbiota. Additionally, a correlation analysis was conducted to explore the interactions between gut microbiota and metabolites.

2 Materials and methods

2.1 Ethical approval

All procedures involving animals were carried out in strict accordance with the regulations and laws of China. The Institutional Ethics Committee at the Eighth Medical Center of the PLA General Hospital granted approval for these animal studies, as indicated by Acceptance Number: 3092024105301321.

2.2 Animals

Eighteen specific pathogen-free (SPF) Wistar rats (male, aged 8–12 weeks) from Charles River were used to minimize confounding microbial exposures. Before EHS and CWI modeling, the experimental rats were placed in a thermal environmental chamber and acclimatized at a room temperature of 25±1°C and a relative humidity of 25%, using the step training method for a period of 1-week. Animal procedures followed the NIH Guide for the Care and Use of Laboratory Animals and were approved by the Institutional Ethics Committee at the Eighth Medical Center of the PLA General Hospital.

2.3 EHS model establishment and CWI treatment

All wistar rats were divided into 3 groups according to the random number table method, each group comprised 6 rats: the normothermia control group (CTRL), the exertional heat stroke group (EHS), and the cold-water immersion groups (CWI). All rats were fed standard chow (LabDiet 5053) ad libitum, housed individually under identical conditions at 25±1°C with 12-hour light/dark cycles to minimize confounding variables, and confirmed to be healthy through a veterinary inspection before the experiment. The CTRL group underwent a training regimen in a room set at a temperature of 25±1°C and RH of 50±10%, following the same protocol as the experimental groups. Continuous monitoring was employed to observe any changes in the rat's consciousness or mental status. Rats that met the diagnostic criteria for EHS were promptly removed from the chamber, and heat exposure was ceased immediately. Diagnostic criteria for EHS included neurological dysfunction (e.g., unresponsiveness to stimuli >5s). We attempt to distinguish consciousness by monitoring it every 5 minutes using reflex tests (pinna and corneal reflexes), as validated in prior studies (Wang et al., 2024). The EHS groups were successfully induced under conditions maintained at 39.5±0.3°C and 55±5% relative humidity. Rats in the CWI group underwent identical EHS induction as the EHS group (39.5±0.3°C, 55±5% humidity) until neurological dysfunction (unresponsiveness to stimuli >5s) was confirmed. After EHS induction, rats were immersed in 10.0±0.5°C water for 30 min until Tcore reached <35°C, as per the US National Athletic Trainers'Association guidelines (Proulx et al., 2003; Casa et al., 2015). The rats underwent CWI for approximately 30 min until their temperatures dropped to sub-cold levels, after which they were allowed to recover at room temperature. At 120 minutes from the start of the experiment, rats under 1.2% isoflurane anesthesia (350 mg/kg) were euthanized, and samples of plasma, colon, and feces were collected.

2.4 Blood, fecal and organ collection

Blood samples were collected under isoflurane anesthesia by puncturing the abdominal aorta, immediately placed into 600μL microcentrifuge tubes pre-coated with Ethylene diamine tetraacetic acid (EDTA) and lithium heparin, and then cooled on ice. Lac levels were measured using a GEM Premier 3000 analyzer (Instrumentation Laboratory, USA). For histological examination, colon tissues were excised, rinsed with a balanced salt solution, embedded in OCT, and sectioned into serial frozen slices. Sections with a thickness of 5 μm underwent staining using HE, and subsequent examination was performed with an OLYMPUS CKX41 light microscope from Japan. Additionally, plasma samples from each rat group underwent LPS analysis by Majorbio Bio-Pharm Technology Co., Ltd. in Shanghai, China.

2.5 Metagenomic analysis

Before DNA analysis, rat fecal samples were stored at -80°C. DNA extraction was performed using the DNA Library Prep Kit for Illumina (DP712, Tiangen Biochemical Technology (Beijing) Co. Ltd.), and microbial DNA was separated in a fume hood. The purity and concentration of the DNA were assessed using a NanoDrop 2000 spectrophotometer (Thermo Fisher Scientific, USA). DNA integrity was verified through 1.8% agarose gel electrophoresis. Fragmentation of DNA to approximately 350 bp was achieved with a Covaris M220 (Gene Company Ltd., China) for the preparation of paired-end libraries. These libraries were constructed with the TruSeq DNA Sample Preparation Kit (Illumina, San Diego, CA, USA) and sequenced on an Illumina NovaSeq platform at Majorbio Bio-Pharm Technology Co. Ltd. (Shanghai, China) using NovaSeq reagent kits according to the guidelines provided by the manufacturer.

Following sequencing, the paired-end reads from Illumina were refined by trimming and discarding low-quality sequences to eliminate host-derived contaminants. This refinement was

executed using the Burrows-Wheeler Aligner toolkit (version 0.7.17). Contigs were then constructed using MEGAHIT (version 1.13). MetaGene (version 1.1.3; http://metagene.nig.ac.jp/metagene/metagene.html) was utilized for gene prediction and annotation, retrieving and translating open reading frames longer than 100 base pairs (bp). Genes with 95% sequence similarity were grouped using CD-HIT (version 4.8.1). To assess gene abundance, reads were aligned to representative sequences with a 95% similarity threshold using SOAPaligner (version 2.21) (Gu et al., 2013). For further quantification, feature counts and differential expression analysis were performed using DESeq2 (Varet et al., 2016). KEGG annotations were performed using diamond to search the KEGG database with an E-value cutoff of $1e^{-5}$ (Nguyen Thanh et al., 2014). Similarly, taxonomic annotations were done using diamond, targeting the nonredundant (N) DB with identical settings. Taxonomic classification was further refined using Kraken2 (version 2.0) and Bracken to improve the accuracy of species-level classification (Wishart et al., 2018).

2.6 Metabolomics analysis

Samples were thawed at 4°C before analysis. To each fecal sample weighing 25 mg, a cold methanol solution composed of methanol, acetonitrile, and water in a 2:2:1 ratio (v/v) was added, including an isotopically-labeled internal standard mixture (500 µl). This mixture was homogenized at low temperatures using a high-throughput tissue homogenizer to ensure uniform mixing. The solution underwent an extraction process on ice, repeated 3 times for 10 min each, to achieve full extraction. Subsequently, the mixture was purified by heating at 220°C for 30 min. The samples were then centrifuged at 12,000 rpm at 4°C for 15 min to isolate the desired components. The clear supernatant was carefully decanted into a vial for further analysis by liquid chromatography-mass(LC-MS), which integrates liquid chromatography with mass spectrometry to detect and measure molecules within the samples.

The analysis was conducted using a UPLC-Triple-TOF MS/MS system equipped with a BEH C18 column (100 mm × 2.1 mm, ID 1.7 µm) serving as the stationary phase. The mobile phase included water with 0.1% formic acid (component A), and a 1:1 mixture of acetonitrile and isopropanol with 0.1% formic acid (component B), with a flow rate of 0.40 ml/min and an injection volume of 20 µl. The temperature of the column was controlled at 40°C. The settings for the electrospray lonization (ESI) cap voltage were at 1.0 kv, injection voltage at 40 v, and collision voltage at 6 ev. Temperatures for the ion source and desolvation were set at 120°C and 500°C, respectively, while the carrier gas was flowed at 900 l/h. The system scanned a mass-to-charge ratio (m/z) from 50 to 1,250 with a resolution of 30,000. Progenesis QI software (version 2.5, Waters Corporation, Milford, MA, USA) processed the data, with metabolites identified and quantified through databases such as HMDB (version 5) (Smith et al., 2005) and METLIN (version 1.0) (Chong et al., 2018). For further metabolite identification and pathway enrichment analysis, the MetaboAnalyst platform was utilized. This included performing principal component analysis (PCA), orthogonal partial least squares discriminant analysis (OPLS-DA), and pathway analysis to visualize the differences between groups and identify key metabolic pathways (Tang et al., 2023). Raw LC-MS data were log-transformed and normalized using total ion count (TIC) normalization to correct for batch effects. The sequencing data were uploaded to the public National Center for Biotechnology Information (NCBI) (version 2023, http://www.ncbi.nlm.nih.gov/) database under BioProject accession no. PRJNA1116604.

2.7 Statistics and data analysis

The experiments were conducted with meticulous precision, repeating each sample thrice. To assess differences among groups, a variety of statistical techniques were employed. For binary group analyses, both the T-test and the nonparametric Wilcoxon Mann-Whitney test were administered. For evaluations involving 3 groups, methods such as nonparametric ANOVA and the Kruskal-Wallis H test were adopted. Following these assessments, the Tukey HSD method was applied for multiple comparisons. All statistical analyses involving multiple comparisons (e.g., metagenomic species, metabolites) utilized the Benjamini-Hochberg method to control the false discovery rate (FDR <0.05). Alpha and Beta diversity measures were determined using the Vegan package were assessed with permutation-based multivariate analysis of variance and Bray-Curtis distances, respectively. Low-abundance taxa (<0.001% relative abundance) were filtered to minimize noise. Metabolite data were log-transformed. Statistical analyses used R v4.3 with packages DESeq2, MetaboAnalystR and FDR adjustment was applied. The statistical evaluations utilized software tools like GraphPad Prism 9 for conducting T-tests, Wilcoxon Mann-Whitney tests, and ANOVAs, while other statistical computations were carried out using Perl. A significance threshold of $P<0.05$ was set for determining statistical significance. Correlations between metabolites, gut microflora, and various parameters were analyzed using Pearson and Spearman methods.

3 Results

3.1 Flowchart of the rat model

During the EHS experiment, 6 rats showed signs of lethargy, including diminished activity, dull eyesight, slow corneal reflexes, weakened limb strength, and paleness of the mouth upon successful establishment of the model. In contrast, rats in the CWI group demonstrated a stable mental state and voluntary movements, reacted to external stimuli, maintained stable respiratory rates, although their limb grip strength was slightly reduced, and exhibited redness in the mouth and lips (Figure 1).

To evaluate the effects of CWI on the physical parameters of rats subjected to EHS, Tcore was monitored continuously during the study period (Figure 2A). Initial Tcore measurements were consistent across the

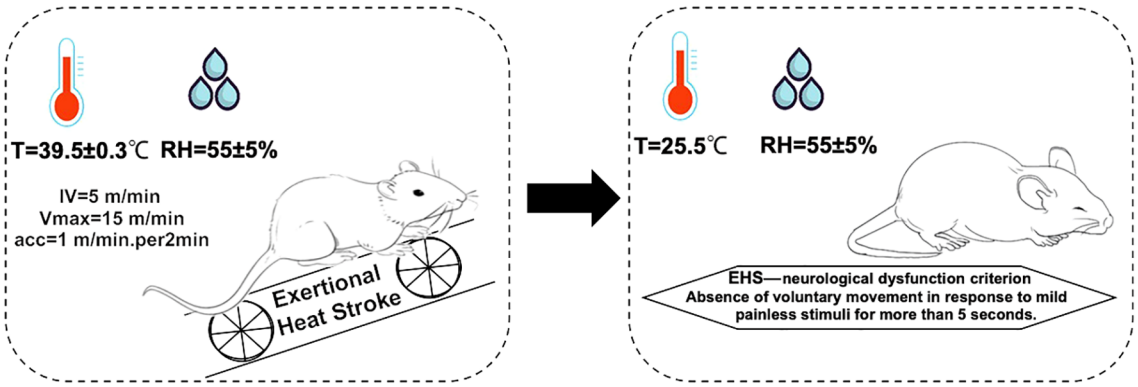

FIGURE 1
Molding regimen. The environmental conditions for the EHS model formation are as follows: the hot chamber temperature is 39.5±0.3°C, with humidity 55±5%. For fatigue training, the initial velocity is 5 m/min, increasing by 1 m/min every 2 min until reaching the maximum velocity of 15 m/min. Diagnostic criteria for EHS: failure to elicit crawling or a change in position in response to mild, painless stimuli for more than 5 s. Exertional heat stroke (EHS), Cold-water immersion (CWI), Normothermia control (CTRL).

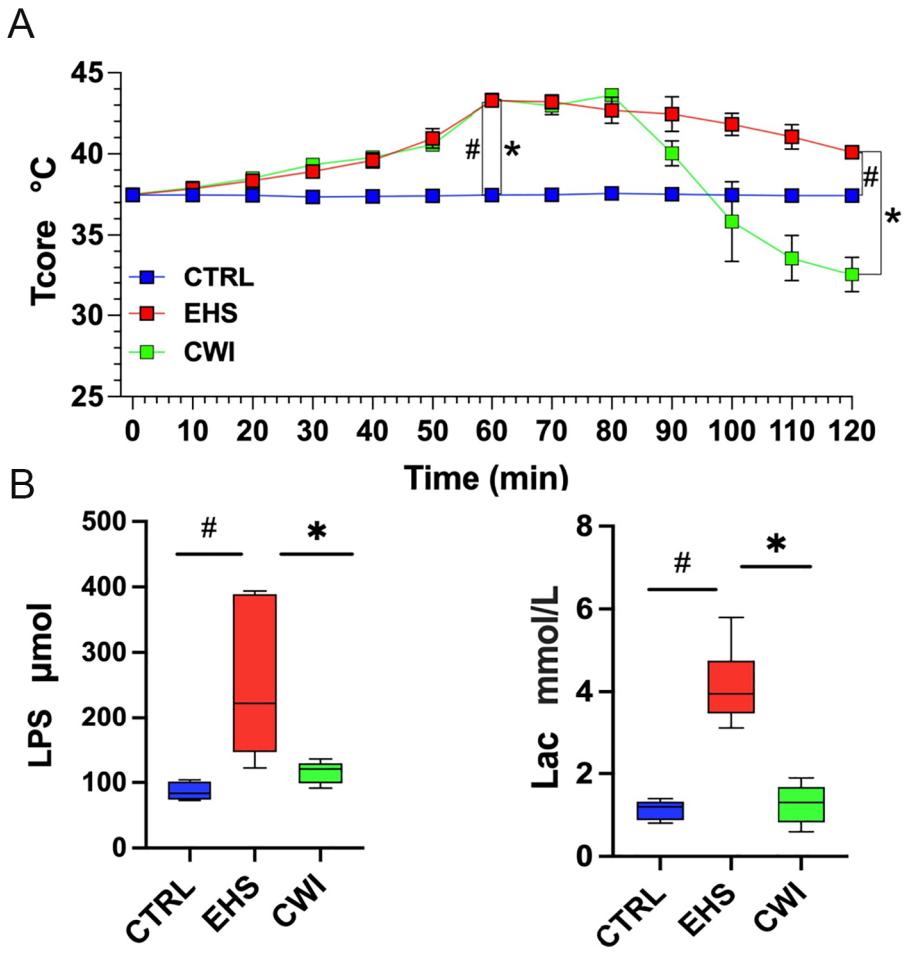

FIGURE 2
The levels of Tcore, LPS, Lac among CTRL, EHS, and CWI groups. **(A)** The Tcore of rats in each group. Blue lines denote CTRL group, red lines denote EHS group and green lines denote CWI group. **(B)** Circulatory changes of (Lipopolysaccharide, LPS), (Blood lactic acid, Lac) in each group of rats (n=6/group). #P<0.05 vs. CTRL group, *P<0.05 vs. EHS group; Wilcoxon Mann-Whitney ANOVA. Exertional heat stroke (EHS), Cold-water immersion (CWI), Normothermia control (CTRL).

three groups before the experiments commenced (CTRL=37.5±0.12°C, EHS=37.5±0.09°C, CWI=37.5±0.16°C). 60-min post-exposure in the hot chamber, significant elevations in Tcore were observed in both the EHS and CWI groups compared to the CTRL group (EHS=43.3±0.30°C, CWI=43.4±0.22°C, P<0.05). At the 120 min time point, following the cooling procedure, Tcore in the EHS group remained significantly higher than in the CTRL group (EHS=40.1±0.26°C, CTRL=37.4±0.09°C, P<0.05), whereas the CWI group exhibited a considerable reduction in Tcore compared to the EHS group (CWI=32.6±0.10°C, P<0.05). This 'afterdrop' in Tcore was statistically significant. Additionally, notable decreases were recorded in LPS (EHS=250.4±105.85, CWI=116.3±15.55, P<0.05) and Lac (EHS=4.1±0.84, CWI=1.3±0.44, P<0.05) concentrations within the CWI group compared to the EHS group, aligning closely with the levels seen in the CTRL group (Figure 2B), raw data are in Supplementary Tables S1 and S2.

3.2 CWI mitigates EHS-induced intestinal damage

The EHS group suffered from severe intestinal edema and bleeding compared to the CTRL group. These conditions were significantly ameliorated following CWI treatment (Figure 3A). Furthermore, pathological damage to the colon triggered by EHS was pronounced, but the disruption of mucosal congestion and integrity caused by EHS was effectively reduced by CWI (Figure 3B).

3.3 Intestinal microbial structure analysis

To examine the influence of CWI on the prevalent species within the gut microbiota, the analysis focused on the dominant phyla and genera. As depicted in Figures 4A, B, the primary phyla in all study groups were Bacteroidetes, Firmicutes, and Proteobacteria, which collectively comprised over 70% of the microbiota. Although no statistical difference in the EHS group, a notable increase in the presence of Firmicutes (58.29%) and Proteobacteria (5.89%) compared to the CTRL group, which had Firmicutes (57.34%) and Proteobacteria (3.32%). Conversely, the CWI group, with Bacteroidetes (14.80%), showed a similar composition to the CTRL group (7.62%) but exhibited an increased presence of Bacteroidetes relative to the EHS group (10.73%). The research further pinpointed *Lactobacillus* (EHS 4.79% vs. CWI 2.56%), *Clostridium* (EHS 4.55% vs. CWI 4.54%) and *Eubacterium* (EHS

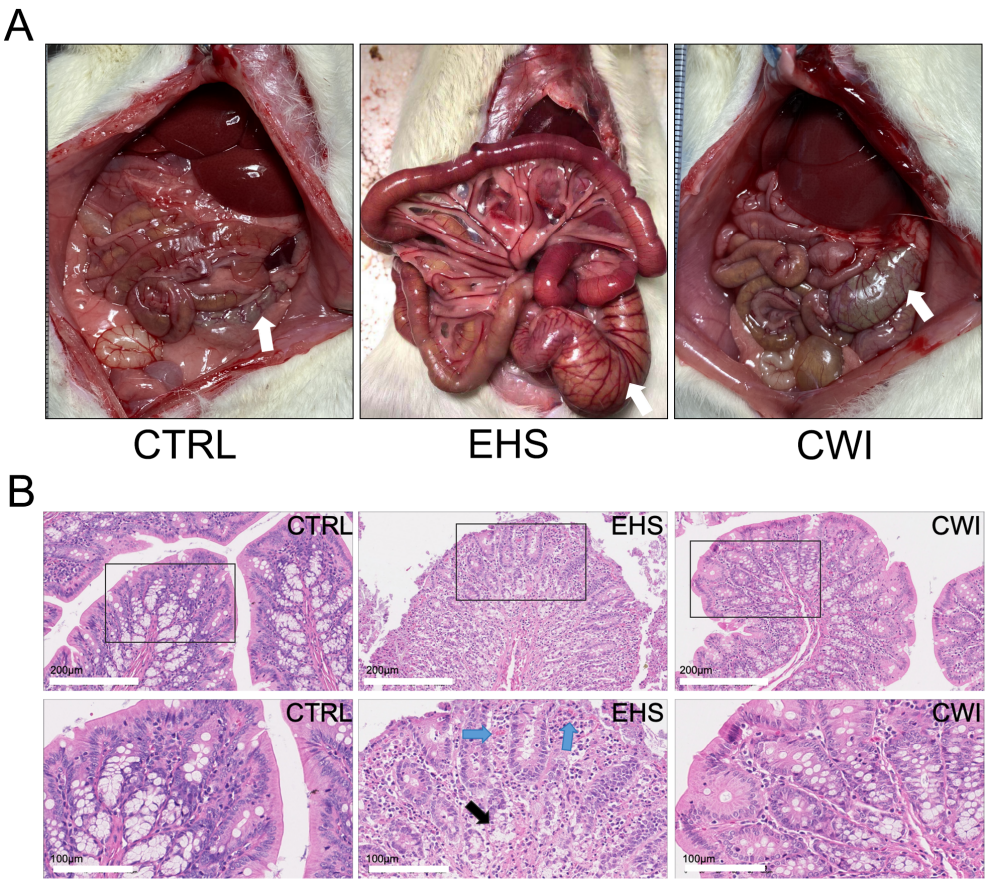

FIGURE 3
Rat anatomy and histological in each group. **(A)** The observed anatomical changes in the intestinal tract (colon tissue, white arrow) using the naked eye. **(B)** CWI mitigated EHS-induced mucosal congestion and epithelial integrity. Hematoxylin-eosin staining of the colon (200×). Black boxes represent the enlarged images below (100×). The blue arrow indicates mucosal congestion. Black arrows indicate damage to the colon lamina propria. Exertional heat stroke (EHS), Cold-water immersion (CWI), Normothermia control (CTRL).

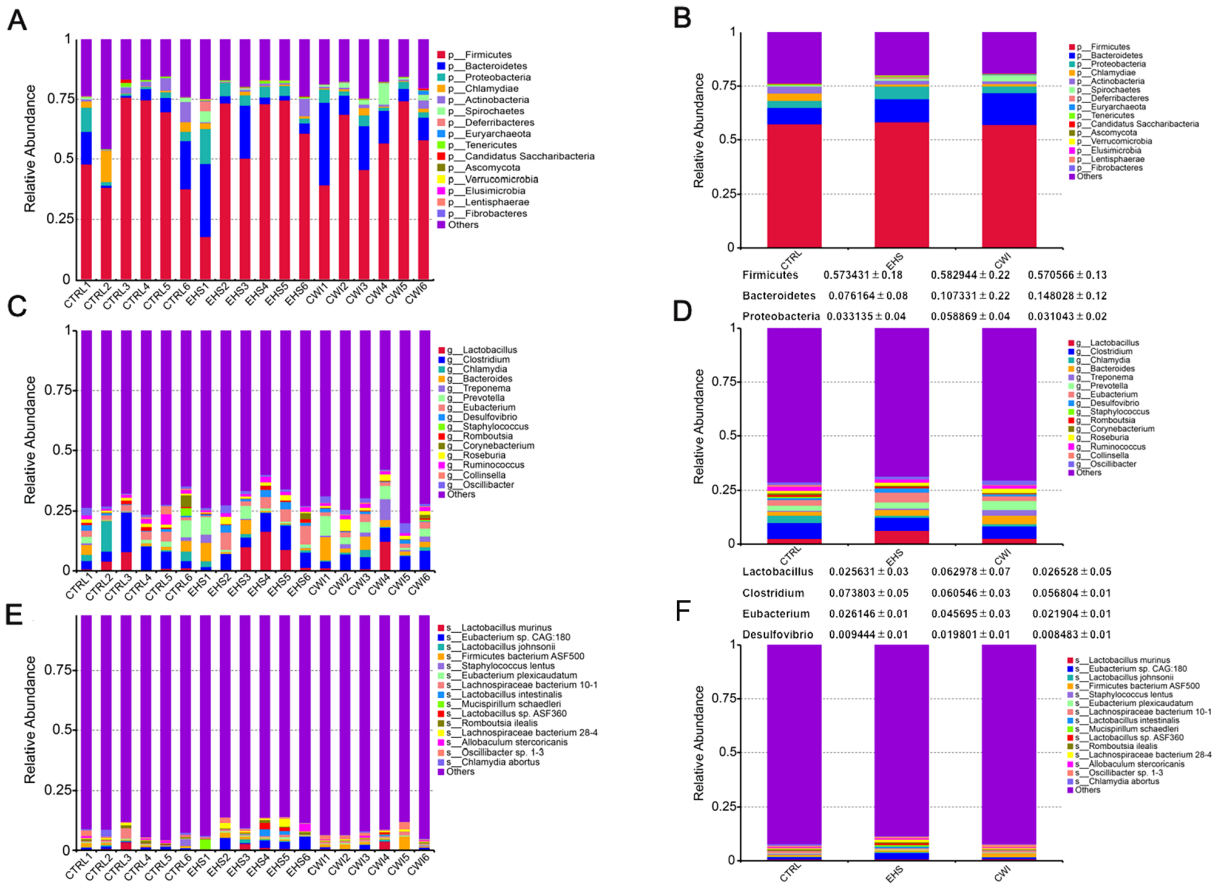

FIGURE 4
Effect of CWI on intestinal microbial diversity and structure. **(A, B)** Relative bacterial distribution at the phylum level (top 15). **(C, D)** Relative bacterial distribution at the genus level (top 15). **(E, F)** Relative bacterial distribution at the species level (top 15). Exertional heat stroke (EHS), Cold-water immersion (CWI), Normothermia control (CTRL).

4.57% vs. CWI 2.19%) as the most prevalent genera within the Firmicutes, and *Desulfovibrio* as the dominant genus within Proteobacteria, as shown in Figures 4C, D. The proportions of *Lactobacillus murinus* and *Eubacterium* sp*14–2* were higher in the EHS group than in the CTRL group, with the average percentage of *Lactobacillus murinus* being 0.82% in the EHS group, compared to 0.79% in the CTRL group and 0.89% in the CWI group. Similarly, the average percentage of *Eubacterium plexicaudatum* was 0.41% in the EHS group, compared to 0.25% in the CTRL group and 0.30% in the CWI group, but both diminished following the CWI treatment (Figures 4E, F). These findings suggest that CWI may normalize the altered gut microbial composition in EHS rats by reducing the relative abundance of Proteobacteria, *Lactobacillus*, and *Eubacterium*, CWI group's microbial profiles aligned more closely with CTRL.

3.4 Intestinal microbial structure analysis

Gene sequencing of fecal samples was first carried out to evaluate the impact of CWI on the intestinal microbial population in rats subjected to EHS, relative to the CTRL group. The adequacy of sample sizes was verified by analyzing the core-pan gene number dilution curves (Figure 5A). Variations in gut microbiota were assessed using data from macrogenetic shotgun sequencing. Species-level alpha diversity was evaluated through indices such as chao1, simpson, shannon, and coverage. Following exposure to heat stroke and subsequent cold-water immersion, significant variations in fecal microbiota alpha diversity were noted. In comparison with the CTRL group, the richness indices (shannon and simpson) were significantly reduced in the EHS group, but showed marked improvements in the CWI group ($P<0.05$, Table 1). This suggests that CWI helps restore the disrupted bacterial community diversity caused by EHS. Additionally, UPGMA clustering showed that CWI restored microbial composition closer to CTRL, reversing EHS-induced dysbiosis (Figure 5B).

A correlation network was established based on the relative abundance profiles of genera that were commonly abundant in both the CWI and CTRL groups (Supplementary Figure S1A). Further analysis revealed that within EHS group, 18 genera increased significantly (e.g., *Desulfovibrio*), while CWI reduced their abundance ($P<0.05$, Wilcoxon test) (Figure.S1B). The analysis also included differentially abundant species across the groups,

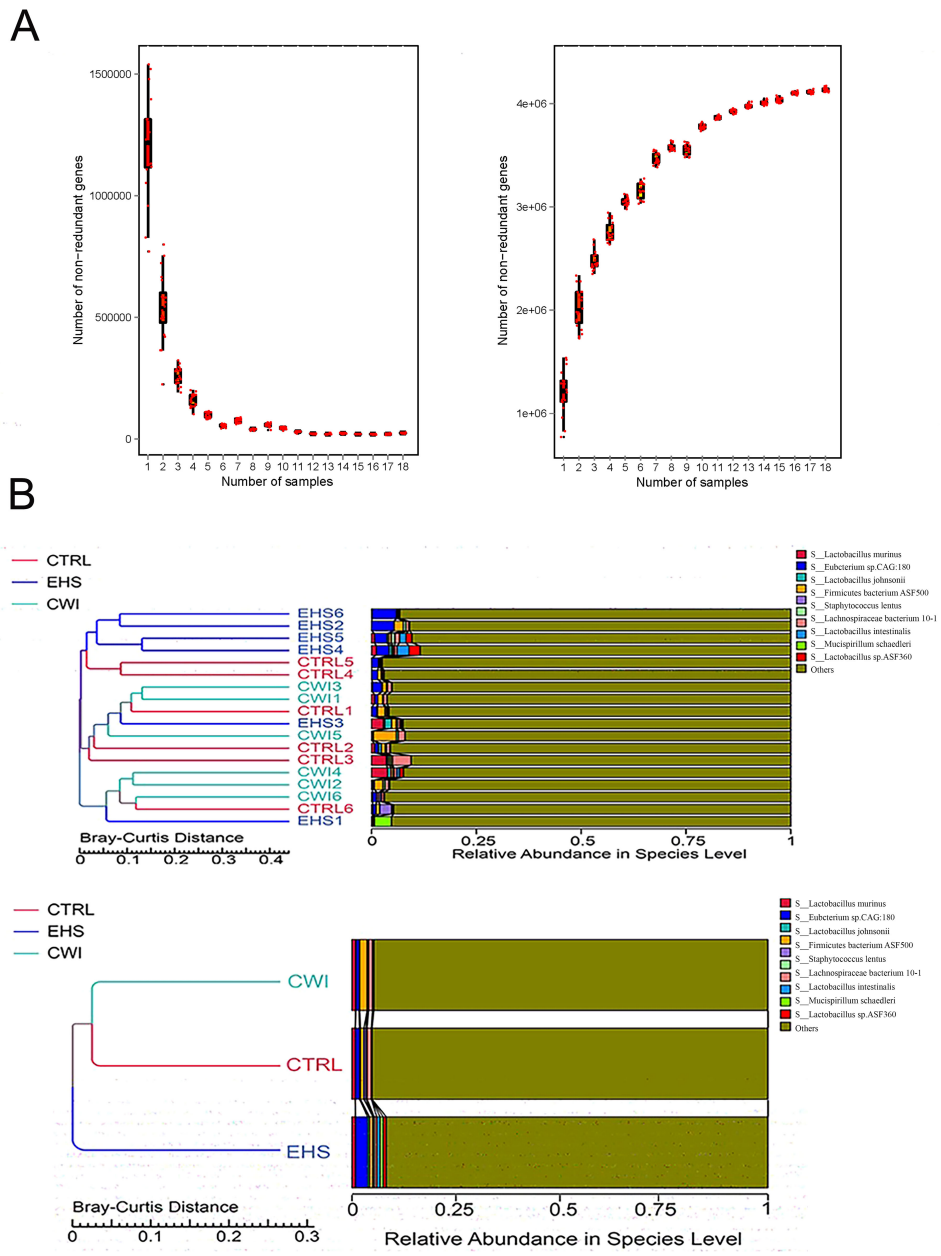

FIGURE 5
Gene counts in CTRL, CWI, and EHS groups **(A)** Sparse curves of the Core-Pan gene showing that the sample capacity is adequate. **(B)** Bray-Curtis distance-based (UPGMA) cluster tree analysis at the species level among the three groups (P<0.05 indicates significance). Exertional heat stroke (EHS), Cold-water immersion (CWI), Normothermia control (CTRL).

TABLE 1 Alpha diversity index of the gut microbial community at the species level for each groups.

Group	Observed_species	Shannon	Simpson	Chao1	Goods_coverage
CTRL	6713.8±821.6	8.27±0.35	0.99±0.01	6978.3±838.2	>99%
EHS	6946.8±299.5	8.1±0.24	0.98±0.01	7269±302.5	>99%
CWI	7421.2±283.6	8.6±0.36	0.99±0.01	7746.8±246.2	>99%
P value	0.061	0.0148	0.0218	0.061	0.0568

The Chao index represents the bacterial community richness. The shannon and simpson indices represent bacterial community diversity. The coverage index describes the sample sequencing coverage, community richness, evenness, and variety. Alpha diversity indices are presented as mean±S, P<0.05 indicates significance. Exertional heat stroke (EHS), Cold-water immersion (CWI), Normothermia control (CTRL).

identifying 203 species that showed differential abundance (ANOVA P<0.05), with 38 species uniquely enriched in EHS such as *Eubacterium* sp. 14-2, *Lactobacillus plantarum*, *Desulfovibrio fairfieldensis*, *Desulfamplus magnetovallimortis*, and *Desulfococcus oleovorans* (P<0.05). Notably, this elevated abundance was mitigated in the CWI group (Figures 6A, B). Additionally, the CWI group showed increases in the abundance of genera such as *Allisonella*, *Megamonas*, and *Succinispira* compared to the EHS group. These results highlight the positive effects of CWI in modulating the gut microbiome by reinstating microbial equilibrium in rats affected by EHS.

3.5 KEGG pathway analysis

Significant disparities in KEGG pathways between the EHS and CWI groups were analyzed to elucidate the functional consequences of microbial community changes following EHS and CWI interventions (Figure 6C). A pathway related to stress response was significantly elevated in the EHS group compared to the CWI group, while 12 pathways, predominantly associated with metabolic processes, were enhanced in both the CWI and CTRL groups (P<0.05). Among these, pathways involved in amino acid metabolism were most prevalent, particularly those related to the biosynthesis of valine, leucine, isoleucine, lysine, and the metabolism of D-glutamine and D-glutamate. In contrast, the EHS group showed enhancement in pathways linked to apoptosis, pyrimidine metabolism, and an increase in DNA repair mechanisms associated with resistance to platinum-based drugs (ko01524). These results indicate that CWI treatment can modulate microbial function, thereby providing a protective effect on the gastrointestinal tract.

3.6 Regulation of EHS-induced metabolic profile alterations by CWI

To explore the distribution of metabolites across the three experimental groups and pinpoint metabolites with significant variations, PCA and OPLS-DA were utilized. The analyses highlighted clear distinctions between the EHS and CTRL groups, while the CWI group differentiated from the EHS group and aligned more closely with the CTRL group. Furthermore, an evaluation of the robustness of the OPLS-DA model was conducted, confirming the model's effectiveness, particularly in the positive ion mode, in consistently distinguishing between the groups (Figures 7A–H).

3.7 Differential metabolite and pathway identification

Variable Importance in Projection (VIP) values from the first principal component of the OPLS-DA model were calculated to identify metabolites that significantly differ, considering VIP>1 and

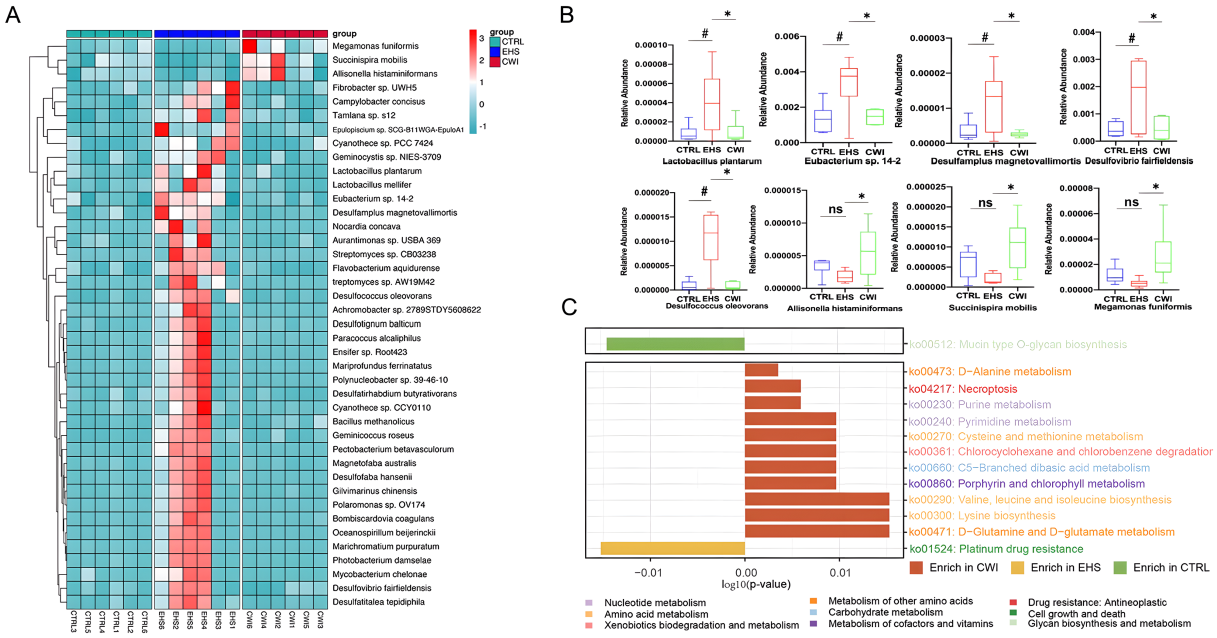

FIGURE 6
CWI regulates EHS-induced changes in microbial community and function. **(A)** Differences in enriched strains among experimental groups. **(B)** Representative differentially abundant strains in the each group. Benjamini-Hochberg method (FDR< 0.05) for balancing Type I error and statistical power in multi-omics data. **(C)** Bar graph demonstrates the difference in KEGG rectangle (KO) pathway among the three groups. The color of the KO pathway denotes the KEGG pathway class. Mann-Whitney ANOVA. #P<0.05 vs. CTRL group, *P<0.05 vs. EHS group, ns, No significance; CTRL, Normothermia control; EHS, Exertional heat stroke; CWI, Cold-water immersion. Exertional heat stroke (EHS), Cold-water immersion (CWI), Normothermia control (CTRL).

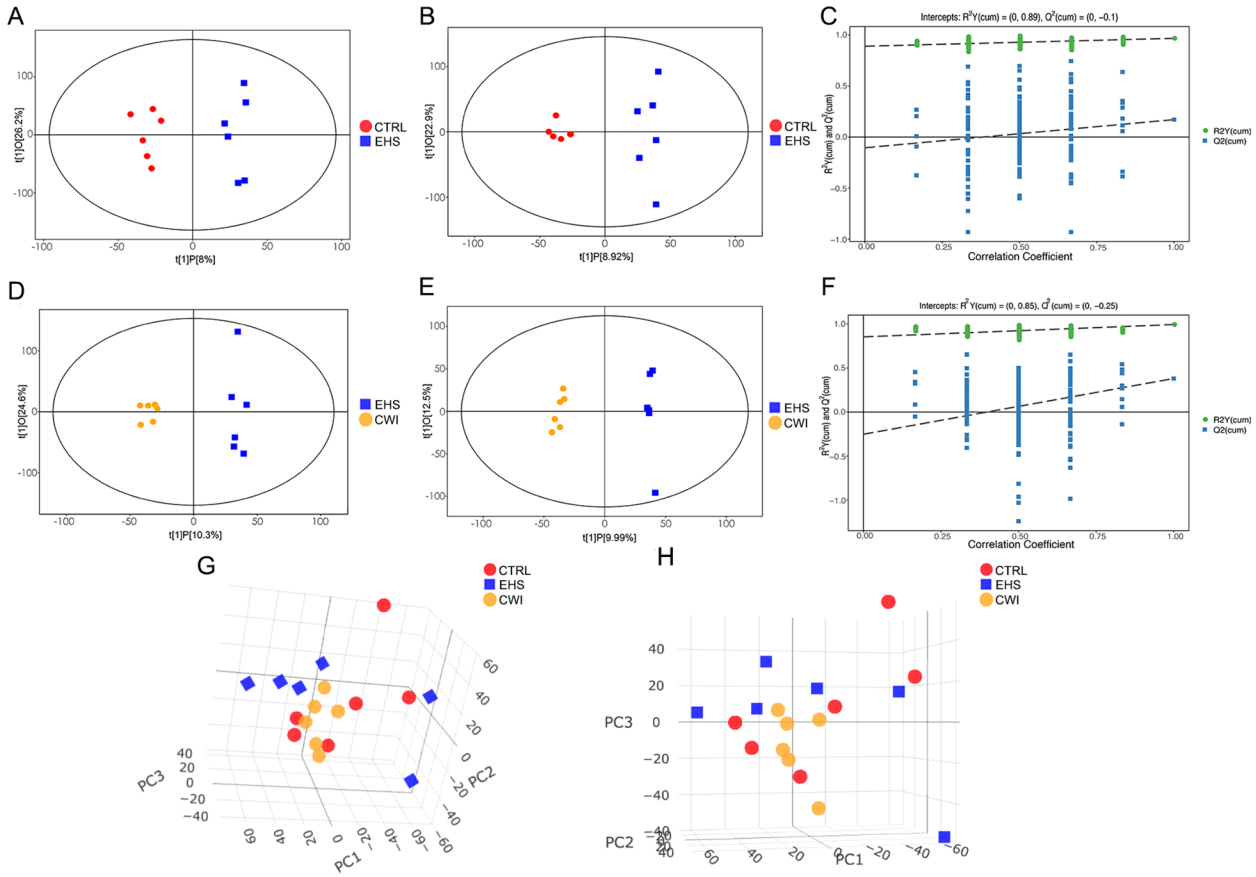

FIGURE 7
Metabolite distribution characteristics among the three groups.**(A–C)** Score scatter plot and permutation test of the orthogonal projection of potential structure discriminant analysis (OPLS-DA) model of the EHS and CTRL groups. **(D–F)** Score scatter plot and permutation test of the OPLS-DA model of the CWI and EHS groups. **(G, F)** PCA scores of experimental groups. **(A, D, G)** Positive ion mode. **(B, E, H)** Negative ion mode. Exertional heat stroke (EHS), Cold-water immersion (CWI), Normothermia control (CTRL).

P<0.05 as thresholds for differential metabolites. This method facilitated the detection of key metabolites and pathways affected by CWI, revealing 42 unique metabolites including nucleotides, nucleosides, analogs, lipids, lipid-like molecules, organic acids and derivatives. Among these, notable differences between the EHS and CWI groups were observed in metabolites such as inosine, hypoxanthine, guanosine, arabinosylhypoxanthine, anserine, taurine, and D-alanyl-D-alanine (Figure 8A). Specifically, the concentrations of inosine (10.0±4.68 vs. 1.54±0.54, P<0.01), hypoxanthine (0.40±0.19 vs. 0.07±0.06, P<0.01), guanosine (1.98±1.58 vs. 0.31±0.20, P<0.05), and arabinosylhypoxanthine (0.22±0.10 vs. 0.03±0.03, P<0.01) were lower in the EHS group but higher in the CWI group compared to the CTRL group (Figure 8B). Additionally, this experiment found metabolites related to Lipid Metabolites besides the aforementioned Purine Derivatives, including LysoPE(15:0/0:0), PC-M6, LysoPE(16:0/0:0), LysoPE(0:0/18:3(6Z,9Z,12Z)), and LysoPE(0:0/14:0). Conversely, levels of taurine (0.31±0.17 vs. 0.12±0.04, P<0.05) were elevated in the EHS group but reduced in the CWI group (0.12±0.03, P<0.05), and anserine (0.07±0.02 vs. 0.03±0.02, P<0.05) also showed a decrease in the CWI group from elevated levels in the EHS group, these Amino Acids and Derivatives related metabolites also include Methylguanidine, 2-Diethylaminoethanol, and D-Alanyldalanine. Furthermore, Small Molecule Antioxidants related metabolites include Vanillactic acid, 3-Oxooctadecanoic acid, L-Urobilin, and 4,5-Dimethyloxazole, while Microbial Metabolites related metabolites include Sandoricin and Tragopogonsaponin M.

3.8 Association analysis of microbial metabolites

To evaluate whether modifications in the gut microbiome serve as a mediator in the therapeutic impact of CWI, this study investigates the protective effects of CWI against intestinal damage caused by EHS (Figure 9). The integrated analysis of microbial genera and metabolite datasets indicated strong correlations, highlighted in Figure 9A. Notably, a positive link was found between taurine and its derivatives and specific species such as *Desulfovibrio fairfieldensis*, *Desulfotignum balticum*, and *Desulfococcus oleovorans* from the Proteobacteria phylum, as well as *Eubacterium* sp*14–2* from the Firmicutes phylum. Additionally, metabolites like hypoxanthine and inosine, along with their

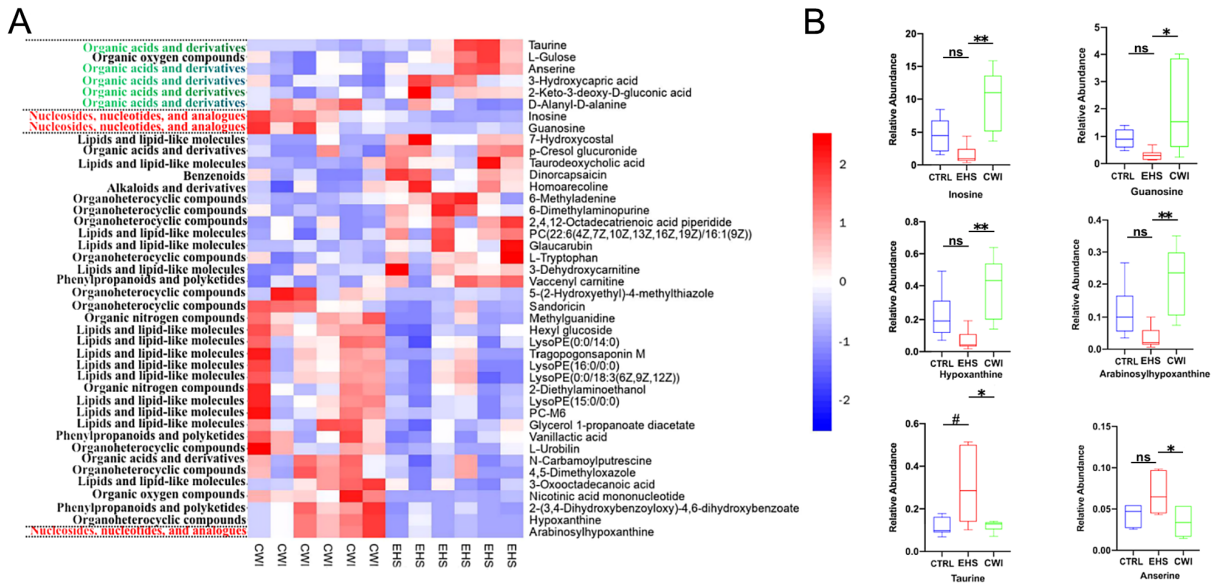

FIGURE 8
Differential metabolites between the CWI and EHS groups. **(A)** Heatmap of hierarchical clustering analysis based on metabolite z-normalized abundances. **(B)** Relative intensities of metabolites in the experimental groups. Benjamini-Hochberg method (FDR< 0.05) for balancing Type I error and statistical power in multi-omics data. #P<0.05 vs. CTRL group, *P<0.05 **P<0.01 vs. EHS group. Mann-Whitney ANOVA. Exertional heat stroke (EHS), Cold-water immersion (CWI), Normothermia control (CTRL).

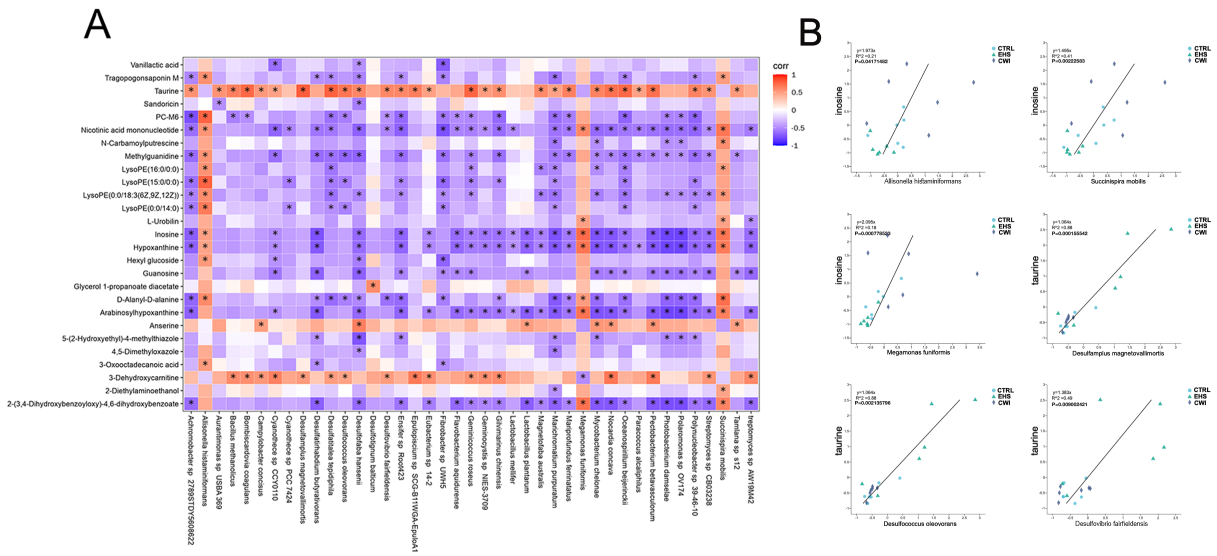

FIGURE 9
Analysis of metabolite correlation and enrichment pathways. **(A)** Correlation analysis of differential bacterial genera and metabolites between the EHS and CWI groups. **(B)** Correlation analysis of differential bacterial genera and metabolites between the EHS and CWI groups. Spearman analysis with FDR-adjusted P values (<0.05) for significance. Exertional heat stroke (EHS), Cold-water immersion (CWI), Normothermia control (CTRL).

derivatives, showed a positive correlation with species such as *Allisonella histaminiformans*, *Succinispira mobilis*, and *Megamonas funiformis* from the Firmicutes phylum (Figure 9B). These findings suggest that changes in the gut microbiome may underlie the metabolic alterations observed in rats subjected to CWI.

4 Discussion

EHS ranks as the third leading cause of death among athletes participating in physical activities, with its prevalence often underappreciated (Bouchama et al., 2022). EHS typically results in severe intestinal damage, primarily due to circulatory issues that

cause ischemia in the GI tract, which adversely affects the viability of intestinal cells and the permeability of cell walls during episodes of EHS (Tang et al., 2021). Recent studies suggest that dysbiosis of the gut microbiota plays a significant role in the pathophysiology of intestinal injuries.

The Dual Pathway Model (DPM) of heatstroke has identified two pathways: the 'heat sepsis' pathway, involves endotoxemia, systemic inflammation, and the 'heat toxicity' pathway, results from the thermolytic effects of heat, leading to damage in cellular structures and organs (Lim, 2018). Consequently, disturbances in intestinal flora due to heatstroke (HS) may contribute to multiple organ injuries. The established gold standard for treating athletes with EHS is to immerse the torso and lower limbs in water at 10°C, avoiding the neck and head, when Tcore exceeds 40°C and neurological symptoms are evident (Zhang et al., 2015). CWI has been shown to reduce Tcore and mitigate severe hyperemia and edema in intestinal structures, reducing damage to tight junctions in the colon and minimizing the effects of the 'heat toxicity' pathway (Tang et al., 2023). In models of EHS, CWI treatment has been shown to reduce severe hyperemia and edema in intestinal structures, and damage to the colon's tight junctions was observed, thereby reducing the effects of the 'heat toxicity' pathway. However, the 'heat sepsis' pathway, which involves the intestinal flora, has yet to be fully understood.

Elevated plasma lactate levels in EHS patients suggest systemic metabolic acidosis, indicating that intestinal epithelial cells produce lactate through local anaerobic metabolism when splanchnic blood flow decreases and tissues become hypoxic (Armstrong et al., 2018). This lactic acid crosses into the cytoplasmic membrane of gram-negative bacteria, triggering the release of LPS (Armstrong et al., 2018). While CWI treatment has shown some beneficial effects, other studies have observed no changes in blood metabolite levels or lactate concentrations post-CWI (Pointon et al., 2012). While rat models effectively mimic core features of EHS, human clinical trials are essential to validate CWI protocols, such as 10–15°C immersion for 20–30 minutes, to ensure their safety and efficacy in real-world clinical settings (Comp et al., 2025). Furthermore, future research should explore the potential of combining CWI with probiotic adjuvants to enhance therapeutic outcomes, as emerging studies suggest that probiotics may support intestinal integrity and mitigate systemic inflammation associated with heat stress (Li Y. et al., 2021). Severe hyperthermia can significantly compromise enterocyte membrane integrity, which promotes the translocation of LPS into the bloodstream, triggering a systemic immune response characterized by the release of pro-inflammatory cytokines (Zuhl et al., 2014). Tight junctions play a role in this process, exhibiting increased permeability to bacterial LPS as temperatures rise, thus allowing larger molecules to pass through (Vanuytsel et al., 2014). The presence of LPS, derived from gram-negative bacteria in the mucosal lining, serves as a powerful agonist for cytokine release, exacerbating systemic inflammation in severe cases of H_2S (Bouchama et al., 2005). A study found that levels of both pro- and anti-inflammatory cytokines were elevated following EHS, associated with exercise-induced endotoxemia due to compromised intestinal epithelial integrity (Gill et al., 2015). In models of EHS, there was a notable increase in Tcore and markers of intestinal permeability for LPS and lactate, which were effectively reversed by CWI treatment. It is hypothesized that the disruption of the intestinal microenvironment caused by EHS may exacerbate intestinal infections, leading to damage to the intestinal mucosal barrier. The metabolites produced by pathogenic bacteria could potentially disrupt the structure of the intestinal mucus layer, either directly or indirectly, leading to epithelial cell damage and accelerating the progression towards 'heat sepsis', ultimately resulting in damage to multiple organ functions.

Unlike prior studies focusing on probiotics (Li Y. et al., 2021), which explored the effects of probiotics on heat stroke by maintaining gut barrier integrity and modulating gut microbiota, or endotoxemia (Fuke et al., 2019), which focused on the role of gut microbiota in regulating endotoxins, we uniquely link cold-water immersion (CWI) to sulfur-metabolite regulation, highlighting its impact on the sulfur-containing metabolic bacteria in EHS rats. Sequencing results indicated that Bacteroidetes, Firmicutes, and Proteobacteria were the predominant flora, representing over 70% of the total microbial population. No differences were observed in the top 15 abundances at the phylum and genus levels among the experimental groups. However, significant variances were found in 18 genera and an additional 38 species between the EHS, CWI, and CTRL groups. It was noted that the sulfur-containing metabolic bacteria genera and strains in the EHS group were significantly disordered, and these disturbances were found to be reversible with CWI treatment. Sulfate-reducing bacteria (SRB) from the *Desulfovibrio* genus, which can be abundant in fecal matter, have been linked to ulcerative colitis. Numerous cases have associated *Desulfovibrio* with bacteremia, including sepsis, liver abscesses, acute cerebral infarction, and ulcerative colitis. Among the species, *Desulfovibrio desulfuricans* and *Desulfovibrio fairfieldensis* are frequently implicated (Singh et al., 2023). *Desulfovibrio fairfieldensis*, *Desulfotignum*, and *Desulfococcus oleovorans*, as predominant SRB, show a significant increase in abundance in the EHS groups, suggesting a potential role for SRB in exacerbating inflammation and compromising tight junction barriers in rats (Supplementary Figure S2). However, CWI treatment appears to restore the balance within the intestinal microecology. Additionally, alterations in small molecule metabolites within the EHS group were examined, revealing the presence of sulfur-containing taurine and indicating that CWI disrupted taurine production. Previous reports have shown a significant increase in taurine levels in patients with Inflammatory Bowel Disease (IBD) (Franzosa et al., 2019), indicating that elevated taurine concentrations may promote microbial degradation in the gut (Walker and Schmitt-Kopplin, 2021). This process leads to the production of sulfur-containing metabolites, entering the dissimilatory sulfate reduction pathway and resulting in the synthesis of H_2S (Walker and Schmitt-Kopplin, 2021). An overproduction of H_2S by gut bacteria has been linked to decreased mucosal integrity, attributed to reduced mucosal disulfide bonds and inhibition of colonocyte butyrate oxidation via cytochrome-c inhibition (Blachier et al., 2021). In addition, the metabolites derived from inosine, hypoxanthine, and guanosine in the CWI groups showed an increase compared to the EHS group.

Inosine, a purine metabolism intermediate consisting of hypoxanthine and ribose, has been shown to suppress TNF-α in both laboratory settings and *in vivo* experiments (Lovászi et al., 2021). It also promotes the production of IL-β in macrophages activated by inflammasomes (Lovászi et al., 2021). Guanosine has been demonstrated to regulate cellular responses in T cells by reducing inflammatory cytokine production and inhibiting the NF-κB signaling pathway, thus acting as an effective anti-inflammatory agent (Luo et al., 2021). In this study, other metabolites were identified, including LysoPE(15:0/0:0), PC-M6, LysoPE(16:0/0:0), LysoPE(0:0/18:3(6Z,9Z,12Z)), and LysoPE(0:0/14:0). These compounds, which are derivatives of LysoPE and structurally similar lipid metabolites, play an important role in regulating intestinal barrier function. They enhance the stability of cell membranes, thereby mitigating intestinal barrier disruption and suppressing inflammation (Gasaly et al., 2021). Furthermore, small molecule antioxidant metabolites such as Vanillactic acid, 3-Oxooctadecanoic acid, L-Urobilin, and 4,5-Dimethyloxazole have the potential to protect the intestinal barrier by reducing oxidative stress and diminishing inflammatory responses (Gasaly et al., 2021). In addition, microbial metabolites, including Sandoricin and Tragopogonsaponin M, produced by the gut microbiota, may modulate intestinal immune responses, promote the growth of beneficial bacteria, and enhance the integrity of the intestinal barrier (Gasaly et al., 2021; Yoon et al., 2023). Consistent with these findings, there was a significant increase in the levels of inosine, hypoxanthine, and guanosine following CWI treatment in the present study, suggesting that inosine and its derivatives may act as bioactive compounds with distinct anti-inflammatory properties (Supplementary Figure S2). The mechanism through which CWI intervenes in the EHS model requires further study.

In this study, we identified significant perturbations in sulfur-containing microbiome-metabolites in rats from the EHS group, which were subsequently reversed following CWI treatment, restoring the microbial status to that of healthy rats. Notably, CWI treatment increased levels of inosine and its derivatives and predominantly influenced purine metabolism pathways. Interestingly, this study is the first to propose a sulfur-containing microbiome-metabolite response to disruption of intestinal tight junctions in EHS, highlighting the surprising effectiveness of CWI in reversing such intestinal damage. Although our data suggest that CWI restores microbial homeostasis, direct evidence linking specific bacteria (e.g., *Desulfovibrio*) to intestinal barrier dysfunction requires further investigation, such as fecal microbiota transplantation or gnotobiotic models.

In conclusion, we found that sulfur-microorganisms (*Desulfovibrio fairfieldensis*, *Desulfotignum*, and *Desulfococcus oleovorans*) and sulfur-containing metabolites (taurine) were significantly increased in the colons of rats in the EHS group. After CWI treatment, this upregulation was reversed, and the microbial levels were restored to levels similar to those in healthy rats. Notably, CWI treatment could lead to an increase in *in vivo* adenosine and its derivatives, and regulate the purine metabolic pathway. The results of this study provide a theoretical and experimental basis for further research on EHS-induced intestinal damage in humans and animals.

Limitations

While our rat model replicates key characteristics of human EHS, such as hyperthermia and intestinal ischemia, interspecies differences in thermoregulatory efficiency and gut microbiota composition may influence the effectiveness of CWI. Therefore, future clinical trials are necessary to determine the optimal CWI protocols, including appropriate duration and temperature, for human application. Furthermore, this research team plans to further investigate the protective effects of CWI on intestinal injury through methods such as immunofluorescence detection of tight junction proteins and ELISA-based analysis of inflammatory cytokines.

Data availability statement

The datasets presented in this study can be found in online repositories. The names of the repository/repositories and accession number(s) can be found in the article/Supplementary Material.

Ethics statement

The authors confirm that all procedures involving animals in this study were conducted in accordance with local regulations and institutional requirements, and comply with the relevant national ethical guidelines for the care and use of laboratory animals. The study was approved by the Ethics Committee of the Eighth Medical Center of the PLA General Hospital (approval number: 3092024105301321) and was reported in accordance with the ARRIVE guidelines.

Author contributions

LX: Conceptualization, Data curation, Formal analysis, Funding acquisition, Investigation, Methodology, Project administration, Resources, Software, Supervision, Validation, Visualization, Writing – original draft, Writing – review & editing. XS: Data curation, Formal analysis, Software, Writing – original draft. BW: Investigation, Validation, Writing – review & editing. FC: Conceptualization, Methodology, Project administration, Funding acquisition, Writing – review & editing. YY: Formal analysis, Methodology, Writing – review & editing. HM: Formal analysis, Project administration, Supervision, Validation, Writing – review & editing. YW: Data curation, Investigation, Project administration, Resources, Software, Validation, Writing – review & editing. GZ: Funding acquisition, Investigation, Methodology, Project administration, Writing – review & editing. JW: Conceptualization, Data curation, Formal analysis, Project administration, Resources, Supervision, Writing – review & editing. YZ: Conceptualization, Funding acquisition, Project administration, Resources, Software, Supervision, Validation, Visualization, Writing – review & editing.

Funding

The author(s) declare financial support was received for the research and/or publication of this article. This work was supported by Military Medical Innovation Projects (18CXZ023, 18CXZ033),

the Key Project of the Eighth Medical Center of Chinese PLA General Hospital (2018ZD-009) and Eighth Medical Center of Chinese PLA General Hospital major Project (2021ZD002), (2016ZD-008).

Conflict of interest

The authors declare that the research was conducted in the absence of any commercial or financial relationships that could be construed as a potential conflict of interest.

Generative AI statement

The author(s) declare that no Generative AI was used in the creation of this manuscript.

Any alternative text (alt text) provided alongside figures in this article has been generated by Frontiers with the support of artificial intelligence and reasonable efforts have been made to ensure accuracy, including review by the authors wherever possible. If you identify any issues, please contact us.

Publisher's note

All claims expressed in this article are solely those of the authors and do not necessarily represent those of their affiliated organizations, or those of the publisher, the editors and the reviewers. Any product that may be evaluated in this article, or claim that may be made by its manufacturer, is not guaranteed or endorsed by the publisher.

Supplementary material

The Supplementary Material for this article can be found online at: https://www.frontiersin.org/articles/10.3389/frmbi.2025.1531991/full#supplementary-material

References

Ahmad, R., Yu, Y. H., Hsiao, F. S., Su, C. H., Liu, H. C., Tobin, I., et al. (2022). Influence of heat stress on poultry growth performance, intestinal inflammation, and immune function and potential mitigation by probiotics. *Animals (Basel)* 17, 2297. doi: 10.3390/ani12172297

Armstrong, L. E., Lee, E. C., and Armstrong, E. M. (2018). Interactions of gut microbiota, endotoxemia, immune function, and diet in exertional heatstroke. *JJ. Sports Med. (Hindawi Publ Corp)* 2018, 5724575. doi: 10.1155/2018/5724575

Babak, M. F., Ziaaldini, M. M., and Reza, A. H. S. (2021). Experience of cold-water immersion on recovery efficiency after soccer match. *Tunisie. Medicale.* 99, 252–258. Available at: https://pmc.ncbi.nlm.nih.gov/articles/PMC8636972/pdf/tunismedv99i2-252-258.

Blachier, F., Andriamihaja, M., Larraufie, P., Ahn, E., Lan, A., and Kim, E. (2021). Production of hydrogen sulfide by the intestinal microbiota and epithelial cells and consequences for the colonic and rectal mucosa. *Am. J. Physiol. Gastrointest. Liver. Physiol.* 320, G125–G135. doi: 10.1152/ajpgi.00261.2020

Bouchama, A., Abuyassin, B., Lehe, C., Laitano, O., Jay, O., O'Connor, F. G., et al. (2022). Classic and exertional heatstroke. *Nat. Rev. Dis. Primers* 8, 8. doi: 10.1038/s41572-021-00334-6

Bouchama, A., Roberts, G., Al Mohanna, F., El-Sayed, R., Lach, B., Chollet-Martin, S., et al. (2005). Inflammatory, hemostatic, and clinical changes in a baboon experimental model for heatstroke. *J. Appl. Physiol.* 98, 697–705. doi: 10.1152/japplphysiol.00461.2004

Casa, D. J., DeMartini, J. K., Bergeron, M. F., Csillan, D., Eichner, E. R., Lopez, R. M., et al. (2015). National athletic trainers' Association position statement: exertional heat illnesses. *J. Athl. Train.* 50, 986–1000. doi: 10.4085/1062-6050-50.9.07

Chong, J., Soufan, O., Li, C., Caraus, I., Li, S., Bourque, G., et al (2018). MetaboAnalyst 4.0: toward more transparent and integrative metabolomics analysis. *Nucleic Acids Res.* 43, W459–W464. doi: 10.1093/nar/gky310

Comp, G., Pugsley, P., Sklar, D., Akhter, M., McElhinny, M., Erickson, E., et al. (2025). Heat stroke management updates: a description of the development of a novel in-emergency department cold-water immersion protocol and guide for implementation. *Ann. Emerg. Med.* 1, 43-52. doi: 10.1016/j.annemergmed.2024.07.013

Demartini, J. K., Casa, D. J., Stearns, R., Belval, L., Crago, A., Davis, R., et al. (2015). Effectiveness of cold water immersion in the treatment of exertional heat stroke at the Falmouth Road Race. *Med. Sci. Sports Exerc.* 47, 240–245. doi: 10.1249/MSS.0000000000000409

Douma, M. J., Aves, T., Allan, K. S., Bendall, J. C., Berry, D. C., Chang, W. T., et al. (2020). First aid cooling techniques for heat stroke and exertional hyperthermia: a systematic review and meta-analysis. *Resuscitation* 148, 173–190. doi: 10.1016/j.resuscitation.2020.01.007

Franzosa, E. A., Sirota-Madi, A., Avila-Pacheco, J., Fornelos, N., Haiser, H. J., Reinker, S., et al. (2019). Gut microbiome structure and metabolic activity in inflammatory bowel disease. *Nat. Microbiol.* 4, 293–305. doi: 10.1038/s41564-018-0306-4

Fuke, N., Nagata, N., Suganuma, H., and Ota, T. (2019). Regulation of gut microbiota and metabolic endotoxemia with dietary factors. *Nutrients* 10, 2277. doi: 10.3390/nu11102277

Gasaly, N., de Vos, P., and Hermoso, M. A. (2021). Impact of bacterial metabolites on gut barrier function and host immunity: A focus on bacterial metabolism and its relevance for intestinal inflammation. *Front. Immunol.* 12, 658354. doi: 10.3389/fimmu.2021.658354

Ghosh, S., Whitley, C. S., Haribabu, B., and Jala, V. R. (2021). Regulation of intestinal barrier function by microbial metabolites. *Cell. Mol. Gastroenterol. Hepatol.* 11, 1463–1482. doi: 10.1016/j.jcmgh.2021.02.007

Gill, S. K., Teixeira, A., Rama, L., Rosado, F., Hankey, J., Scheer, V., et al. (2015). Circulatory endotoxin concentration and cytokine profile in response to exertional-heat stress during a multi-stage ultra-marathon competition. *Exerc. Immunol. Rev.* 21, 114–128. Available online at: http://eir-isei.de/2015/eir-2015-114-article.pdf.

Gu, S., Fang, L., and Xu, X. (2013). Using SOAPaligner for short reads alignment. *Curr. Protoc. Bioinformatics* 44, 11.11.1-11.11.17. doi: 10.1002/0471250953.bi1111s44

Ihsan, M., Watson, G., and Abbiss, C. R. (2016). What are the physiological mechanisms for post-exercise cold water immersion in the recovery from prolonged endurance and intermittent exercise? Sports. *Med* 46, 1095–1109. doi: 10.1007/s40279-016-0483-3

Jing, Y., Yu, Y., Bai, F., Wang, L., Yang, D., Zhang, C., et al. (2021). Effect of fecal microbiota transplantation on neurological restoration in a spinal cord injury mouse model: involvement of brain-gut axis. *Microbiome* 9, 59. doi: 10.1186/s40168-021-01007-y

Johnson, C. H., Ivanisevic, J., and Siuzdak, G. (2016). Metabolomics: beyond biomarkers and towards mechanisms. *Nat. Rev. Mol. Cell. Biol.* 17, 451–459. doi: 10.1038/nrm.2016.25

Knapik, J. J., and Epstein, Y. (2019). Exertional heat stroke: pathophysiology, epidemiology, diagnosis, treatment, and prevention. *J. Spec. Oper. Med.* 19, 108–116. doi: 10.55460/5P2Q-1MBQ

Krautkramer, K. A., Fan, J., and Backhed, F. (2021). Gut microbial metabolites as multi-kingdom intermediates. *Nat. Rev. Microbiol.* 19, 77–94. doi: 10.1038/s41579-020-0438-4

Leyk, D., Hoitz, J., Becker, C., Glitz, K. J., Nestler, K., and Piekarski, C. (2019). Health risks and interventions in exertional heat stress. *Dtsch. Arztebl. Int.* 116, 537–544. doi: 10.3238/arztebl.2019.0537

Li, K., Abdelsattar, M. M., Gu, M., Zhao, W., Liu, H., Li, Y., et al. (2023). The effects of temperature and humidity index on growth performance, colon microbiota, and serum metabolome of ira rabbits. *Anim. (Basel)* 13, 1971. doi: 10.3390/ani13121971

Li, Z., McKenna, Z. J., Kuennen, M. R., Magalhaes, F. C., Mermier, C. M., and Amorim, F. T. (2021). The potential role of exercise-induced muscle damage in exertional heat stroke. *Sports Med.* 51, 863–872. doi: 10.1007/s40279-021-01427-8

Li, L., Wang, M., Chen, J., Xu, Z., Wang, S., Xia, X., et al. (2021). Preventive effects of bacillus licheniformis on heat stroke in rats by sustaining intestinal barrier function and modulating gut microbiota. *Front. Microbiol.* 12, 630841. doi: 10.3389/fmicb.2021.630841

Lim, C. L. (2018). Heat sepsis precedes heat toxicity in the pathophysiology of heat stroke—a new paradigm on an ancient disease. *Antioxidants (Basel)* 7, 149. doi: 10.3390/antiox7110149

Liu, Y., Kang, W., Liu, S., Li, J., Liu, J., Chen, X., et al. (2022). Gut microbiota-bile acid-intestinal Farnesoid X receptor signaling axis orchestrates cadmium-induced liver injury. *Sci. Total. Environ.* 849, 157861. doi: 10.1016/j.scitotenv.2022.157861

Lovászi, M., Németh, Z. H., Gause, W. C., Beesley, J., Pacher, P., Haskó, G., et al. (2021). Inosine monophosphate and inosine differentially regulate endotoxemia and bacterial sepsis. *FASEB. J.* 35, e21935. doi: 10.1096/fj.202100862R

Luo, Y., Chen, H., Huang, R., Wu, Q., Li, Y., and He, Y. (2021). Guanosine and uridine alleviate airway inflammation via inhibition of the MAPK and NF-κB signals in OVA-induced asthmatic mice. *Pulm. Pharmacol. Ther.* 69, 102049. doi: 10.1016/j.pupt.2021.102049

Nguyen Thanh, H., Zhao, L., and Liu, Q. (2014). De novo transcriptome sequencing analysis and comparison of differentially expressed genes (DEGs) in Macrobrachium rosenbergii in China. *PLoS One* 10, e109656. doi: 10.1371/journal.pone.0109656

Pointon, M., Duffield, R., Cannon, J., and Marino, F. E. (2012). Cold water immersion recovery following intermittent-sprint exercise in the heat. *Eur. J. Appl. Physiol.* 112, 2483–2494. doi: 10.1007/s00421-011-2218-3

Proulx, C. I., Ducharme, M. B., and Kenny, G. P. (2003). Effect of water temperature on cooling efficiency during hyperthermia in humans. *J. Appl. Physiol.* 94, 1317–1323. doi: 10.1152/japplphysiol.00541.2002

Qiang, W., Xuan, H., Yu, S., Hailun, P., Yueli, Z., Zhiguo, P., et al. (2021). Impact of the gut microbiota on heat stroke rat mediated by Xuebijing metabolism. *Microb. Pathog.* 155, 104861. doi: 10.1016/j.micpath.2021.104861

Singh, S. B., Carroll-Portillo, A., and Lin, H. C. (2023). Desulfovibrio in the gut: The enemy within? *Microorganisms* 11, 1772. doi: 10.3390/microorganisms11071772

Smith, C. A., O'Maille, G., Want, E. J., Qin, C., Trauger, S. A., Brandon, T. R., et al. (2005). METLIN: a metabolite mass spectral database. *Ther. Drug Monitoring* 27, 747–751. doi: 10.1097/01.ftd.0000179845.53213.39

Tang, J., Xu, L., Zeng, Y., and Gong, F. (2021). Effect of gut microbiota on LPS-induced acute lung injury by regulating the TLR4/NF-kB signaling pathway. *Int. Immunopharmacol.* 91, 107272. doi: 10.1016/j.intimp.2020.107272

Tang, Z., Yang, Y., Wu, Z., and Ji, Y. (2023). Heat stress-induced intestinal barrier impairment: Current insights into mechanisms and interventions. *J. Agric. Food Chem.* 71, 2673–2688. doi: 10.1021/acs.jafc.3c00798

Vanuytsel, T., Van Wanrooy, S., Vanheel, H., Vanormelingen, C., Verschueren, S., Houben, E., et al. (2014). Psychological stress and corticotropin-releasing hormone increase intestinal permeability in humans by a mast cell-dependent mechanism. *Gut* 63, 1293–1299. doi: 10.1136/gutjnl-2013-305690

Varet, H., Brillet-Guéguen, L., Coppée, J. Y., and Dillies, M. A. (2016). SARTools: A DESeq2- and EdgeR-Based R pipeline for comprehensive differential analysis of RNA-seq data. *PLoS One* 11, e0157022. doi: 10.1371/journal.pone.0157022

Walker, A., and Schmitt-Kopplin, P. (2021). The role of fecal sulfur metabolome in inflammatory bowel diseases. *Int. J. Med. Microbiol.* 311, 151513. doi: 10.1016/j.ijmm.2021.151513

Wang, J., Sun, Z., Jiang, L., Xuan, L., Ma, Y., Wang, J., et al. (2024). Activation of Pink1/Parkin-mediated mitochondrial autophagy alleviates exertional heat stroke-induced acute lung injury in rats. *Clin. Hemorheol. Microcirculation* 88, 1–19. doi: 10.3233/CH-242100

Wishart, D. S., Feunang, Y. D., Marcu, A., Guo, A. C., Liang, K., et al. (2018). HMDB 4.0: the human metabolome database for 2018. *Nucleic Acids Res.* 46, D608–D617. doi: 10.1093/nar/gkx1089

Yoon, J. H., Do, J. S., Velankanni, P., Lee, C. G., and Kwon, H. K. (2023). Gut microbial metabolites on host immune responses in health and disease. *Immune Netw.* 24, 23, e6. doi: 10.4110/in.2023.23.e6

Zhang, Y., Davis, J. K., Casa, D. J., and Bishop, P. A. (2015). Optimizing cold water immersion for exercise-induced hyperthermia: A meta-analysis. *Med. Sci. Sports Exerc.* 47, 2464–2472. doi: 10.1249/MSS.0000000000000693

Zuhl, M. N., Lanphere, K. R., Kravitz, L., Mermier, C. M., Schneider, S., Dokladny, K., et al. (2014). Effects of oral glutamine supplementation on exercise-induced gastrointestinal permeability and tight junction protein expression. *J. Appl. Physiol.* 116, 183–191. doi: 10.1152/japplphysiol.00646.2013

Frontiers in Microbiology

Explores the habitable world and the potential of microbial life

The largest and most cited microbiology journal which advances our understanding of the role microbes play in addressing global challenges such as healthcare, food security, and climate change.

Discover the latest Research Topics

See more →

Frontiers

Avenue du Tribunal-Fédéral 34
1005 Lausanne, Switzerland
frontiersin.org

Contact us

+41 (0)21 510 17 00
frontiersin.org/about/contact